CJJC2022

The 11th China-Japan Joint Conference on Material Recycling and Waste Management

Nov, 17-18 2022, Online

Organizer:

Kyushu University

Tongji University

University of Science and Technology Beijing

九州大学
KYUSHU UNIVERSITY

同濟大學
TONGJI UNIVERSITY

北京科技大学
University of Science and Technology Beijing

PROCEEDINGS of CJJC2022 CONTENTS

3. Leaching behavior and harmless treatment

4. Landfill management (15:20-17:10)

5. Landfill monitoring, IoT utilization, plastic waste

6. Leachate treatment (1)

7. Leachate treatment (2)

8. Organic waste treatment and recycling (1)

9. Organic waste treatment and recycling (2)

10. Biogas recovery and GHG reduction

Air bubble-assisted tar removal in polyvinylchloride pyrolysis

Yanlei Chen[1], Hao Xu[1], and Fumitake Takahashi[1]

1 Department of Transdisciplinary Science and Engineering, School of Environment and Society, Tokyo Institute of Technology, G5-601, Tokyo Institute of Technology, Suzukake, 4259, Nagatsuta, Midori-ku, Yokohama 226-8503, Japan

INTRODUCTION

With increase of social and industrial importance of plastic-based products, plastic waste recycles have been concerned more seriously. According to the Ministry of the Environment Japan, the cumulative plastic waste generation in the world is expected to increase 5 times larger than that in 2020. 70% of collected plastic wastes were actually exported to China and other ASEAN countries before legal regulation of plastic waste import by China government. In real recycle processes, the 67% of plastic processing residues were incinerated and 8% of the residue was landfilled. Only 25% was used for direct recycles.

Of three major pathways of plastic waste recycles, chemical recycle is considered the best way owing to its large potential to generate energy resources such as syngas, oil and activated carbon products comparing to serious limitations of material recycle and relatively low efficiency of thermal recovery.

However, tar, which is by-products produced from chemical recycle processes like pyrolysis-oil generation and gasification for syngas production, will cause serious problems due to its high toxicity and damages to process equipment, human bodies, and the environment. The purpose of the study is to develop a new tar removal method using air bubble assistance for plastic pyrolysis.

MATERIALS AND METHODS

Materials

Polyvinylchloride (PVC) was used as feedstock in this study according to its high market-share, high contents of the additives and plasticizers. PVC and magnesium sulfate made by Fujifilm Wako Pure Chemical Corporation, Japan were used. Distilled water were from Monota RO,Co.,Ltd.(Japan). Nitrogen (G3 grade: purity=99.9995%) was used as pyrolysis medium gas purchased from TAIYO NIPPON SANSO Corporation, Japan. Air stone GX-63 was purchased from AS ONE Corporation, Japan. All reagents were used as received.

Methods

Proximate analysis and ultimate analysis for PVC sample were performed using a muffle furnace TMF-3000 (TOKYO RIKAKIKAI Co.,Ltd. Japan), constant temperature dryer (EIP-600B, AS ONE Corporation, Japan) and CHN corder JM10 (J-Science Lab Co.,Ltd. Japan). The contents of hydrogen, oxygen, carbon, sulfur and contents of moisture, volatiles, ash and fixed carbon were measured. Lab-scale fixed bed pyrolysis experiments were performed with the air bubble-assisted tar removal. Temperature controller AGC-1P and tubular furnace ARF series (Asahi Rika Factory. Ltd. Japan.) and Multi Air Station MSA-1 (AS ONE Corporation. Japan) were used for all pyrolysis experiments. Air flow rate ranged from 0 to 10L/min in the pyrolysis experiments for air bubble injection. Tar collected from the pyrolysis experiments was analyzed by Gas Chromatograph Mass Spectrometer QP2010 (Shimadzu Corporation, Japan) in order to identify the composition of organic compounds in collected tar. Before the analysis, tar needed dehydration treatment using magnesium sulfate. Octanol-Water partition coefficients and diffusion coefficients of these common organic compounds analyzed in this study were used to discuss the trend of hydrophilicity and hydrophobicity among the tar collected at different air flow rates.

RESULTS AND DISCUSSIONS

The results of proximate analysis and ultimate analysis were listed in Table 1. The results of collected tar at different air flow rates are shown in Fig. 1. As shown in Fig.1, when air flow rate is 5 L/min or less, the amount of tar collection decreased compared with that without air injection. On the other hand, when air flow rate increases to 6 L/min or more, tar collection increased with increase of air flow rate. When air flow rate is 10 L/min, tar collection exceeds that without air injection. It should be noted that tar collection was partially affected by air stone for bubble generation.

Table.1 Proximate analysis and ultimate analysis (wt%)

Sample/ Contents	Moisture	Volatile	Ash	Fixed Carbon
PVC	NA	92.33	1.20	6.47
	H	C	N	O
PVC	4.54	38.37	0.07	0.64

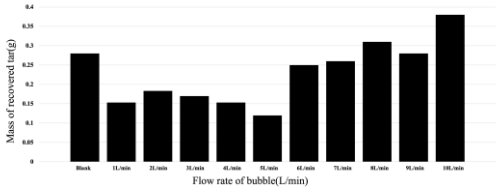

Fig.1 Tar recovery assisted by air bubble injection

The amount of tar adsorbed onto air stone might reach to 0.15 to 0.22 g. Further experiments are necessary to evaluate the impact of tar adsorption onto the air stone.

The compositions of tar are shown in Fig. 2 and 3. Fig.2 shows the compositions of organic groups like aliphatic, monocyclic aromatics, PAHs, and others. Fig.3 shows the compositions of tar categorized by carbon numbers like C6-9, C10-13, C14-17, and C18-more. Fig 2 shows that aliphatic tars were collected more with increase of air injection rate. On the other hand, PAHs tars were collected less at higher air injection rate. Fig.3 shows that more amount of small carbon tars (C6-9 fractions) was also trapped with increase of air injection. On the other hand, tars with larger carbon numbers was collected less with increase of air injection. Therefore, air injection affected not only tar removal efficiency but also collected tar characteristics.

The effects of air injection rate on tar collection performance and tar characteristics are discussed focusing on tar hydrophobicity and hydrophilicity. Fig.4 shows the average of Octanol-Water partition coefficients of major tar components. Fig.5 shows the average of gaseous diffusion coefficients of the major tar components. Fig.4 shows negative correlation between air flow rates and the average Octanol-Water partition coefficients. As shown in Fig.2 and Fig.3, higher air injection increased the collection of aliphatic tars and small carbon-number tars dramatically. These results are consistent with negative correlation between

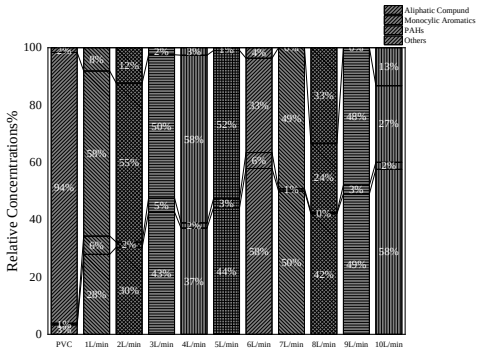

Fig.2 Tar compositions categorized by organic groups

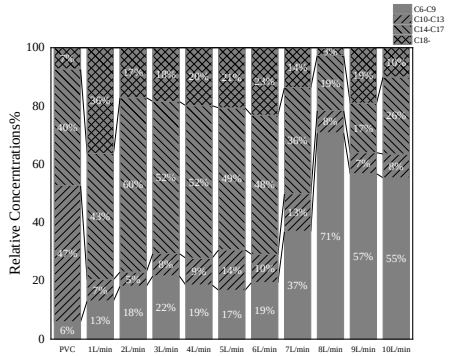

Fig.3 Tar compositions categorized by carbon number

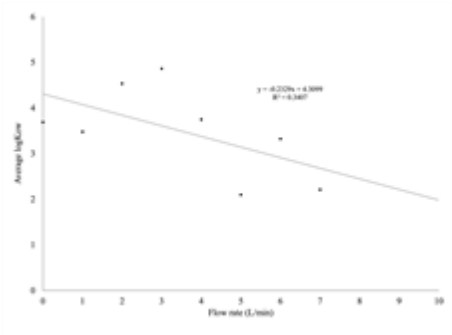

Fig.4 Comparison between air flow rate and average Octanol-Water partition coefficients

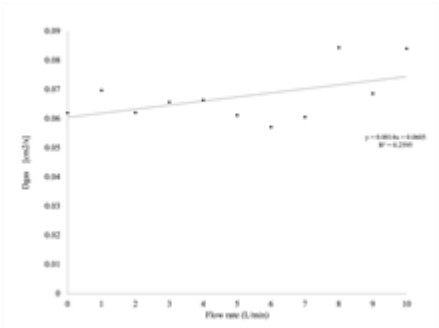

Fig.5 Comparison between air flow rate and average gaseous diffusion coefficients

air flow rate and the average Octanol-Water partition coefficients. Higher air flow rate helped the collection of hydrophilic, aliphatic, and small carbon number tars. The increase of tar collection at 6 L/min or larger injection rate is derived from promoted collection of aliphatic tars. A positive correlation between air flow rates and the average diffusion coefficients is also consistent with the other results. In general, smaller molecule tars will have larger diffusion coefficient. When air is injected at higher flow rate, more amount of air bubbles would be generated. It means that syngas bubble would have more contacts with air bubbles at water scrubbing stage (tar collection). When tar has larger diffusion coefficient, tar would transfer from syngas bubble to air bubble more and it results in more efficient transfer of tars to the scrubbing water. It would result in larger tar collection.

CONCLUSIONS

This study found that air bubble-assistance was helpful to promote tar collection in PVC pyrolysis when air flow rate exceeded 10 L/min. The promotion effect of air injection on tar collection was derived from the increase of hydrophilic, aliphatic, and small carbon-number tars. Further researches are necessary to investigate tar removal mechanisms. Gaseous tar transfer from syngas to air bubble might play an important role.

Application results of a dosage controller for acid gas neutralizing chemical

Takeshi Yamasaki, Hirotaka Fujiwara
Environment Technology, Technical Support Department 2, Solution Business Group,
Japan Sales Business Division Business Division,
Kurita Water Industries Ltd.
Nakano Central Park East, 4-10-1 Nakano, Nakano-Ku, Tokyo, Japan

Abstract

Slaked lime is mainly used in Japan to treat acid gases such as HCl and SOx generated from waste incineration facilities. In order to stably treat acid gas, it is necessary to change the amount of slaked lime added according to the load fluctuation of acid gas, and usually PID control is performed according to the acid gas concentration at the stack.

On the other hand, if the properties of the acid gas change due to changes in the quality of waste, the control settings also need to be changed. However, there are many cases in which the control setting is not adjusted, and the dosage amount is an excess or deficiency. To deal with these issues, we have developed a control device "S.sensing™HP" that is easy to install and highly responsive to fluctuations in acid gas concentrations. This time, we will introduce an application example of this device.

1. Features of S.sensing™HP

Figure1 shows the installation flow of S.sensing™HP.

The signal of the acid gas analyzer measured at the stack is branched and input to this device, and the necessary addition amount of slaked lime is calculated in the device. The calculated addition amount can be used as an output signal and input to an acid gas neutralizing agent addition device. In this way, the device can be easily installed.

In addition, there are many cases where conventional PID control is performed only for the instantaneous value of acid gas, but with this device, it is possible to perform more stable control by considering load fluctuations. Furthermore, it has a function to vary the dosage according to the 1-hour moving average value, eliminating the need for manual intervention by the operator even when the concentration rises.

2. Application example

An application example at the A industrial waste incineration facility shown in Table 1 is introduced.

Table 1 Facility overview

Incinerated matter	Industrial waste（Plastic, acid, alkali, sludge, etc.）
Incinerator model	Full continuous kiln furnace
Incineration capacity	45 tons/day
HCl control target value	60 ppm
Slaked lime consumption	55 tons/month

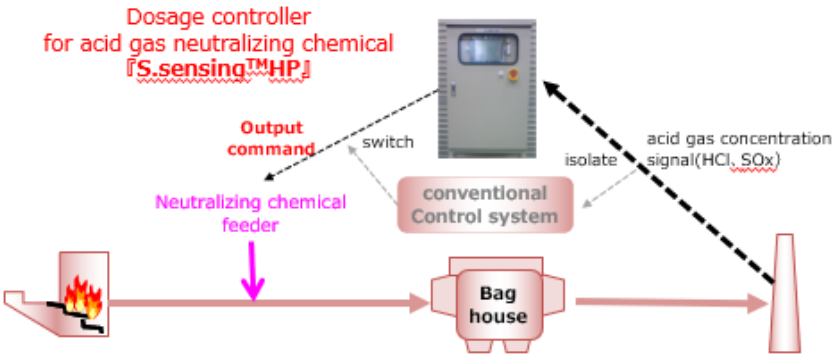

Fig.1 the installation flow of S.sensing™HP

As shown in Fig. 2(a), the fluctuation of acid gas load derived from waste was large, and although the conventional control was performed, the instantaneous value fluctuated greatly.

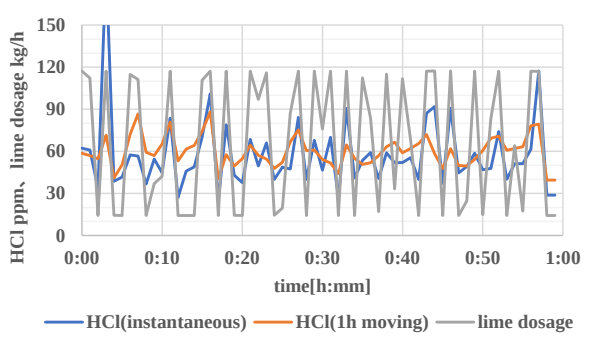

Fig.2(a) conventional control

Fig.2(b) shows the results of applying S.sensing^{TM}HP to this facility. The acid gas concentration was able to become more stable by controlling the injection amount by high responsivity.

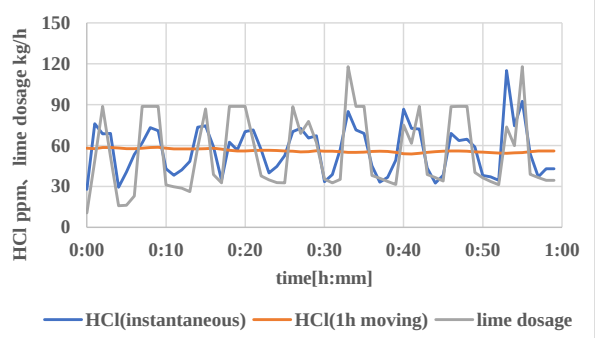

Fig.2(b) S.sensingHP control

Fig.3(a) and Fig.3(b) show the results of long-term data acquisition at this facility.

Even in continuous operation for 20 days, it was demonstrated that the treatment using S.sensing^{TM}HP(Fig.3(b)) was able to treat acid gas

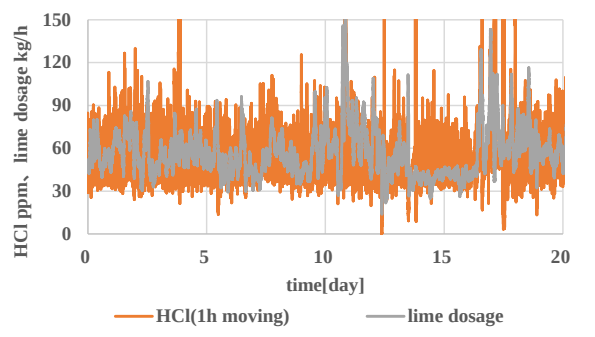

Fig.3(a) conventional control

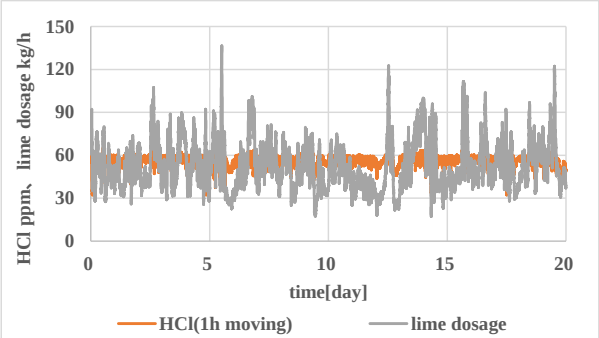

Fig.3(b) S.sensingHP control

concentrations more stably than the conventional control(Fig.3(a)).

Table 2 shows the analysis results of fly ash collected during the test period.

Compared to the conventional control, when S.sensing^{TM}HP was used, the Cl/Ca ratio was higher, suggesting that the effective utilization of Ca was increased.

Table 2 Examples of ash analysis

	Ca	Cl	Cl/Ca
	mg/kg	mg/kg	-
Conventional control	312,311	304,067	0.97
S.sensing^{TM}HP control	271,800	306,600	1.1

3. Summary and Future Considerations

As shown above, it was found that by reviewing the conventional control and using S.sensing^{TM}HP, slaked lime can be used more effectively, contributing to a reduction in the amount and stable treatment.

Reducing the amount of slaked lime used leads to a reduction in the unreacted alkali content remaining in the fly ash. The reduction of the unreacted alkali content increases the applicability of inorganic heavy metal immobilizing agent and is expected to replace organic heavy metal immobilizing agent, which have been facing price increases and supply instability in recent years.

We will continue to work to reduce the amount of waste generated by reducing the amount of slaked lime and reduce the load on final disposal sites due to organic matter.

Performance of Biochar Supported Multi-Metal Nano-Catalysts for Pyrolysis Tar Removal

Jun Zhang*, Lu Liu, Junjie Chen, Linlin Yin, Yu Tian

State Key Laboratory of Urban Water Resource and Environment (SKLUWRE), National and Local Joint Engineering Research Center of Biomass Energy Development and Utilization, Harbin Institute of Technology, Harbin, 150090, China.

Abstract

The by-product tar produced in the biomass pyrolysis production process not only severely limits the efficiency of biomass resource utilization, but also has the risk of polluting the environment and endangering human health. This study uses activated biochar as a carrier to prepare multi-metal nanocatalysts for in-situ tar removal, which is of great significance for the further development of tar steam catalytic reforming technology and biomass pyrolysis gasification technology. In this study, a series of multi-component metal nanocatalysts were prepared by citric acid sol-gel method, and the steam catalytic reforming of tar model compound toluene and toluene/naphthalene/phenol mixture was investigated in a self-made two-stage biomass catalytic pyrolysis fixed bed reactor. performance. The effects of activation temperature and activation time on the physicochemical properties of biochar were investigated, and a series of multi-component metal nanocatalysts were prepared using activated biochar as a carrier. The effects of reaction temperature, promoter metals and their loadings on the steam catalytic reforming performance of tar model compound toluene were investigated. The anti-deactivation performance and mechanism of the modified binary metal nanocatalyst 6% Ni-4% Co/char were studied in depth from the service life, carbon deposition amount, reduction performance, and carbon deposition microstructure and types. The anti-deactivation performance and mechanism of catalysts were further studied.

Keywords: Biochar; Nanocatalyst; Tar; Steam Catalytic Reforming; Carbon deposition

CARBON AND SULFUR CONVERSION OF HIGH-SULFUR ORGANIC WASTE IN THE ENHANCED CHEMICAL LOOPING GASIFICATION

Lulu Wang[1], Laihong Shen[2], Yuyang Long[1] and Dongsheng Shen [1]
1 Zhejiang Provincial Key Laboratory of Solid Waste Treatment and Recycling, School of Environmental Science and Engineering, Zhejiang GongshangUniversity, Hangzhou, China
2 Key Laboratory of Energy Thermal Conversion and Control of Ministry of Education, School of Energy and Environment, Southeast University, Nanjing, China

ABSTRACT
When sulfur in petroleum coke (petcoke) converts to H_2S instead of SO_2, it is the resource which can be recovered by Claus process. Chemical looping gasification (CLG) is capable of achieving petcoke conversion and sulfur recovery. To simultaneously overcome the obstacles of low gasification reactivity and improve H_2 and H_2S production, hematite modified by K as oxygen carrier (OC) was involved in the high-sulfur system to investigate the effect on sulfur conversion via batch fluidized bed in petcoke CLG process. K enhanced H_2 generation beyond expectation because K not only improved the petcoke gasification but also enhanced the steam oxidation of deep reductive OC. Especially when using 10%KNO_3-hematite, H_2 yield increased by 3.9 times as compared to 0%K, with the carbon conversion efficiency of 99.92% in the 22nd minute. The sulfur fate had been originally studied using K-modified hematite OC. H_2S was the main phase of sulfur release and the high H_2 yield also assisted H_2S production. Introducing K contributed to in-situ sulfur capture forming K-Fe-S compounds in the OCs due to the deep reduction of Fe. 10%KNO_3-hematite exhibited excellent cyclic stability with a H_2 volume fraction more than 65% in 21 cycles.

INTRODUCTION

Petroleum coke (petcoke) is the main by-product of industrial coking process, and its production has been dramatically increasing along with the over-exploitation and the poor quality of crude oil. Fuel-grade petcoke is considered as an alternative to coal due to high cost-effectiveness, little ash, and heating value [1]. However, high-sulfur content contributes to environmental degradation due to the sulfur pollutant, which is also a limit to petcoke utilization. Therefore, it is necessary to innovate the technology of petcoke usage environmentally and economically to provide the market with opportunities for demand growth.

Gasification is a cleaner method of carbonaceous material conversion to generate syngas with less heavy metal and SO_x pollution, as compared to combustion. Syngas with abundant H_2 and CO can be used for industrial chemicals. H_2 is widely known as a potential energy and the amount of H_2 also determines the further applications of the gaseous products and the calorific value of syngas. Moreover, petcoke mainly generates H_2S instead of SO_2 during the gasification atmosphere, which is widely used as feedstock to recover sulfur by mature Claus process with a substantial economic income. If the sulfur-containing gas product is H_2S, sulfur is no longer pollution, but resource. But the reactivity of petcoke gasification is dampened by its high graphitization structure, low porosity, and little alkali/alkaline earth metal (AAEM) content [2]. AAEM was always employed to enhance the gasification reactivity of petcoke and H_2 yield, and H_2 ratio was up to 60% of syngas especially at just 750 ^oC in steam gasification by prompting char gasification and water-gas shift reactions [3-6]. But K vaporization significantly limited the increase of reaction rate [7]. The alkali and transition metal such as K and Fe had synergistic catalytic effects on char gasification [8, 9] as well as H_2 yield [2] at the presence of steam. However, the dispersion of Fe on carbon surface caused agglomeration and sulfur poisoning during gasification, which was the primary reason of catalyst deactivation [9-11]. The application of expensive catalysts brought out some unfeasible problems in practice [12].

Chemical looping gasification (CLG) is a promising and green technology for solid fuel conversion in which oxygen carrier (OC) substitutes molecular oxygen sources with less SO_x and NO_x, originated from Chemical looping combustion [13]. Metal oxide as OC supplies lattice oxygen instead of pure oxygen to achieve the operating cost reduction [14]. Furthermore, OC as catalyst circulates between gasification reactor and air reactor, so the waste of expensive catalysts and equipment corrosion caused by

catalysts such as K, may be averted, compared with catalyzed gasification. Meanwhile, OC also acts as the heat source at the expense of combustible gases and provides heat during OC regeneration in AR. CLG could provide more extra heat to obtain the heat balance by contrast, when catalyzed gasification has the similar conditions.

In terms of the advantages of CLG, the investigation of OC becomes particularly important. Fe-based OCs were generally adopted for different chemical looping technologies due to the non-toxicity and abundant source [15-19]. However, Fe-based CLG process also encountered two difficulties, consisting of the low reaction rate between OC and solid fuel [20]. Potassium with movability between char and OC increased the reactivity of iron oxides as well as char gasification synergistically, thus improving the reduction rate [17, 21-24]. The K-Fe-O composites in OC inhibited the volatilization of K. They proposed that the low-ash coal contributed to inhibiting the loss of K [20, 25]. Gu [26] prepared K_2CO_3-modified hematite to accelerate char gasification and water-shift reaction. Besides, the iron oxides system had low tendency to generate sulfide or sulfate at any sulfur-containing gas concentration or operation temperature [27, 28]. In conclusion, considering the advantages and behaviors of catalysts in traditional gasification and OCs in CLG as described above, introducing K to Fe-based OC is an effective and economical approach to utilize the low-ash petcoke for enhancing the gasification rate, OC reactivity, and H_2 production. However, Fe-based OC modified by K has not been involved in the sulfur-containing system.

Accordingly, this research aimed at enhancing H_2 and H_2S production by promoting the reactivity of OC reduction and petcoke gasification during CLG process to improve the value-increment utilization. The performance based on K-modified hematite OC was detailed investigated in the sulfurous CLG via a batch fluidized bed, such as the enhancement of OC reactivity and petcoke gasification. The releases of SO_2 and H_2S were rival and intricate, so sulfur fate had been originally studied when K-modified hematite OC was employed. Furthermore, the multicycle operations were proposed to test the durability of OC. And the catalytic and competitive effects of K on petcoke gasification and OC reactivity were discussed.

MATERIAL AND EXPERIMENT

Material preparation

Wet-impregnation method was used to prepare several different K-modified hematite samples. A certain amount of KNO_3 was dissolved in deionized water. 100 g of dry hematite in the size range of 0.3-0.4 mm was accurately weighed and then was added to the prepared solution thoroughly. The addition amount of potassium was set to 0.3%, 3%, 10%, and 15% respectively, according to the mass ratio of metal atom mass to hematite. The mixture was vigorously stirred and evaporates in the water bath of 80 ^oC with a magnetic stirring rotor until the sample becomes slurry. After drying, the paste mixture was put in a muffle furnace to heat up to 950 ^oC in 4h, and calcined at this temperature for 4.5h. Finally, the OCs were screened to the size range of 0.3-0.4 mm for spare. The elemental contents of the bulk prepared OC samples were analyzed by X-ray Fluorescence Spectrometer (XRF-1800, SHIMADZU, Japan). The surface morphology and elemental analyses of the OC samples were examined by HITACHI SU3500 scanning electron microscopy combined with energy-dispersive X-ray spectroscopy (SEM-EDX).

Industrial high-sulfur petcoke from China Yangzi Petrochemical Co., Ltd was considered as fuel in the experiments. The proximate and ultimate analyses of petcoke were summarized in Table 1. Before the tests, the lumps of petcoke were crushed, and particles of 0.1-0.3 mm were screened out. The small size was favorable for increasing gasification rate of petcoke.

Table 1. Proximate and ultimate analyses of petcoke

Proximate analysis	(wt.%, ad)
M	0.76
V	12.98
FC	85.87
A	0.39
Ultimate analysis	(wt.%, ad)
C	85.24
H	3.82
O	2.44
N	1.29
S	6.06

Experiment procedure

In order to evaluate the performance of K-modified hematite OC in petcoke CLG, the experiments were conducted in a batch fluidized bed as illustrated in Fig.1. The reactor tube was made of quartz with an inner diameter of 32 mm and a height of 600 mm, in the middle of which the porous plate was settled. And the tube was heated up to the desired temperature of 900 ^oC by electric furnace. In the single test, before adding OC (36 g) from the top, the oxidation atmosphere was the mixture of O_2 (100 ml/min STP) and N_2 (2 L/min STP) to fully oxidize the synthetic OC. The gasification experiment started from introducing petcoke (0.75 g) when the bed materials were exposed to the stream of N_2 (1 L/min STP) and steam (1 ml/min) at 900 ^oC. Stable steam was transported by the constant flow pump (TBP-50 A) and generated by the heating tape of 120 ^oC. The conditional gases (CO, CO_2, CH_4 and O_2) were collected by sample bags after condensation, drying and filtration. The conditional

gases were analyzed by off-line gas analyzer (Emerson NGA2000), and the sulfurous gas products (H_2S and SO_2) were on-line analyzed by MRU Vario plus. The mass of fuel and OC were reduced by 1/3, and N_2 (5 L/min STP) diluted the outlet gases before the on-line analyzer to meet the range requirement of H_2S and SO_2 concentration when detecting sulfurous gases. The factors, including K adding amount, K source, which affect carbon and sulfur conversion were tested by the single experiment. Each single experiment was repeated for at least twice, and the average results were shown.

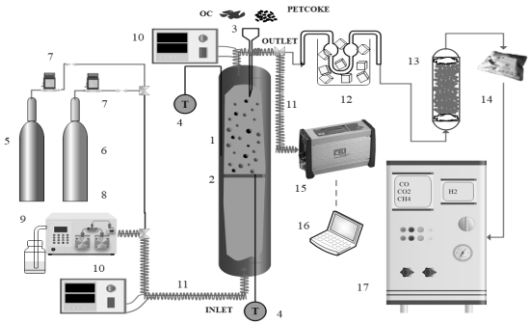

Fig.1 Scheme of batch fluidized bed experimental apparatus

Multicycle experiments were conducted under oxidizing and gasification atmosphere to simulate the actual situation of CLG. The reacted solid fuel petcoke and the reduced OC underwent complete oxidation. Between gasification and oxidation stage, the residual gas in the reactor was purged with N_2 (2 L/min STP). After the atmosphere alters to a mixture of N_2 and steam, petcoke was added from the hopper at the top of reactor by opening the valve once more, and the next cycle of reduction process started.

RESULTS

Effect of K on carbon and hydrogen conversion

The influences of hematite with different K amounts on gas generation rate in outlet gas and carbon conversion efficiency within 60 minutes of the petcoke CLG process were evaluated in Fig.2. The CH_4 product was low and the change was neglected, so it was omitted. H_2 was always the main gasification product of CLG based on petcoke. With the increase of K loading from 0% to 10%, H_2 production also increased from 0.81 Nm^3/kg to 3.18 Nm^3/kg; when the loading continued to increase to 15%, it slightly decreased to 2.74 Nm^3/kg because of the enhanced oxidation effect of OC modified by K. With the increase of potassium loading, CO decreased, and CO_2 became the second largest gas product only to H_2. The extremely small existence of K just promoted the generation rates of CO, CO_2 and H_2 slightly. When K loading increased from 3% to 15%, the yields of CO_2 and H_2 were opposite to CO. This was the competitive and combined effect of potassium promoting char gasification (R1), water-shift reaction (R2), reductive reactivity of OC (R3-R4). The change of gas products may be ascribed to the slight sintering when the potassium loading was 15%. In terms of the relative fraction of effective syngas (CO and H_2), it increased slightly when loading trace K, but it decreased by 9.61% with 3%K. The relative fraction of CO and H_2 increased with the K adding amount increasing from 3%K to 15%K. In the view of the comprehensive consideration of effective syngas concentration and gas generation rates, 10%K was the best K-modified hematite for petcoke CLG process in this work. The carbon conversion efficiency was presented in Fig.2(b) when using different K adding amount. The carbon conversion efficiency reached 73.44%, 77.42% and 97.02% respectively after the experiment lasted for 60 min when K loading was 0%, 0.3% and 3%. Petcoke was almost completely converted, and the carbon conversion efficiency sharply reached 99.92% at 36th minute and 22th minute in the case of 10%K and 15%K loading on hematite. As a conclusion, the increase of K adding amount accelerated the carbon conversion rate, effectively shortening the reaction time, and petcoke would be thermally converted to gas products sharply.

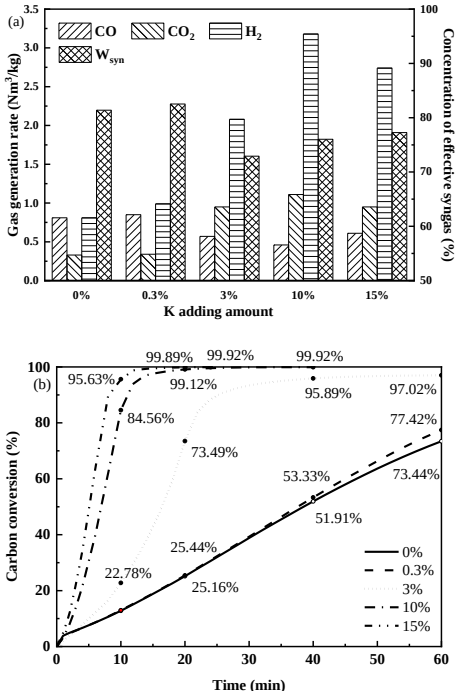

Fig.2 Effect of K adding amount to hematite on (a)gas generation and (b)carbon conversion at 900 °C

$$char + H_2O \leftrightarrow CO + H_2 \quad (R1)$$
$$CO + H_2O \leftrightarrow CO_2 + H_2 \quad (R2)$$
$$H_2 + 3Fe_2O_3 \rightarrow 2Fe_3O_4 + H_2O \quad (R3)$$
$$CO + 3Fe_2O_3 \rightarrow 2Fe_3O_4 + CO_2 \quad (R4)$$

To analyze the mechanism of CLG performance based on K-modified hematite, the X-ray diffraction (XRD) patterns of the fresh and reacted OC samples with 0%K, 0.3%K, and 10%K were shown in Fig.4. The main phase of fresh hematite and 0.3%K-hematite was Fe_2O_3, without obvious characteristic peak of K-containing phases. It verified the conclusion that the gas generation rate and carbon conversion rate were similar in the conditions of 0%K and 0.3%K. In the hematite with 10%K, some different phases besides Fe_2O_3 were found, mainly $K_2Fe_{22}O_{34}$. With the formation of various kinds of K_2O-xFe_2O_3, the reactivity of modified hematite was enhanced [29], along with the gas generation rates and carbon conversion efficiency in the CLG process of petcoke, which was consistent with the conclusion above. Fe_3O_4 and Fe_2O_3 were the main components in the reductive OCs of none and 0.3%K loading on hematite after reactions, while the peak of Fe_2O_3 could not be detected when hematite was loaded with 10%K. Although potassium ferrite had Fe_2O_3 after reaction, the peak intensity also implied the decreasing amount of Fe_2O_3, and K_3FeO_2 was detected which consisted of Fe in the valence state of +1. These indicated that the reduction degree of Fe_2O_3 in OCs was evidently deepened by introducing K. Therefore, it was speculated that $K_2O{-}xFe_2O_3$ were the main phases in OCs to promote the reactivity of OCs, thereby improving the performance of petcoke CLG process.

Sulfur fate in the petcoke CLG based on K-modified hematite

The impact factors such as K adding amounts and potassium sources were investigated to explore the sulfur conversion of the petcoke CLG based on K-modified hematite. Fig.4 showed the release of sulfur-containing gases (SO_2 and H_2S) with different K adding amounts (3%, 10%, and 15%) and different potassium sources (K_2CO_3 and KNO_3) when the CLG based on K-modified hematite lasted for 1200 s. SO_2 increased with K loading amount, because more K loading amount represented the high reactivity in gasification and more oxygen transformation capacity until the sintering endurance. Organic sulfur is the main form of sulfur in petcoke, which is usually combined with carbon matrix [30]. The effect of K on carbon conversion can be used for reference in the sulfurous CL system. The OC modified by K provided the lattice oxygen for char gasification [31], significantly promoting the conversion of carbon and sulfur. The K-Fe-O phases of superior catalytic activity was attributed to the weakened bonding strength and the elongated bonding length by the introduction of K. In the initial stage, there was a single SO_2 concentration peak with a value greater than 50 ppm. When 15%KNO_3 was added, the SO_2 concentration peak had already exceeded 100 ppm. When the potassium salt adding was 3%, 10% and 15%, the time without SO_2 observed was 36 s, 36 s, and 60 s, respectively. SO_2 was generated not only directly by volatile matter releasing, but also from the oxidation of H_2S and fresh K-modified hematite OC.

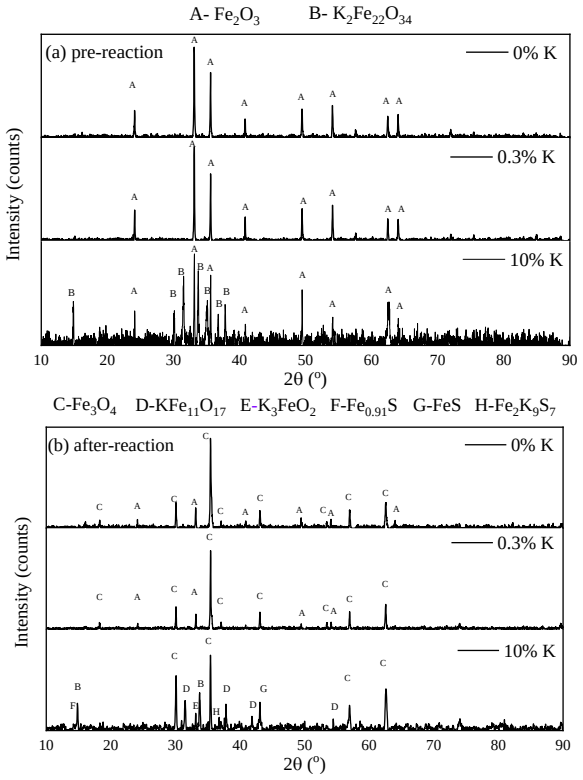

Fig.3 XRD patterns of (a) pre- and (b) after-reaction OC samples

In terms of H_2S releasing, it was always the main sulfurous component because the atmosphere of CLG including H_2 and H_2O was reductive and more conducive to producing H_2S instead of SO_2. The curves of H_2S appeared the two-bell shape obviously. The first peaks of H_2S appeared in approximately 10 s of the initial reaction, and the H_2S peak values above 800 ppm were much higher than those of SO_2. The H_2S peak value was even as high as 973 ppm using 15%KNO_3-hematite. For the case of 10%K and 15%K, the time observing the highest H_2S concentration in the char gasification stage was prior to the case of 3%KNO_3-hematite. H_2S and SO_2 generation both were improved by adding more K on hematite. The gasification reactivity of petcoke was enhanced by the

catalytic influence and the lattice oxygen supply amount. H_2 from the coke gasification played a decisive role on providing the ample hydrogen atmosphere, to react with organic sulfur and generate H_2S [32]. When the source of K changed from KNO_3 to K_2CO_3 with the same amount, SO_2 and H_2S in the case of K_2CO_3 released more intensely than using KNO_3-hematite. The above experimental data showed that the effect of promoting the release of SO_2 and H_2S using K_2CO_3 was better than KNO_3 during the reaction, and the reaction rate also became faster.

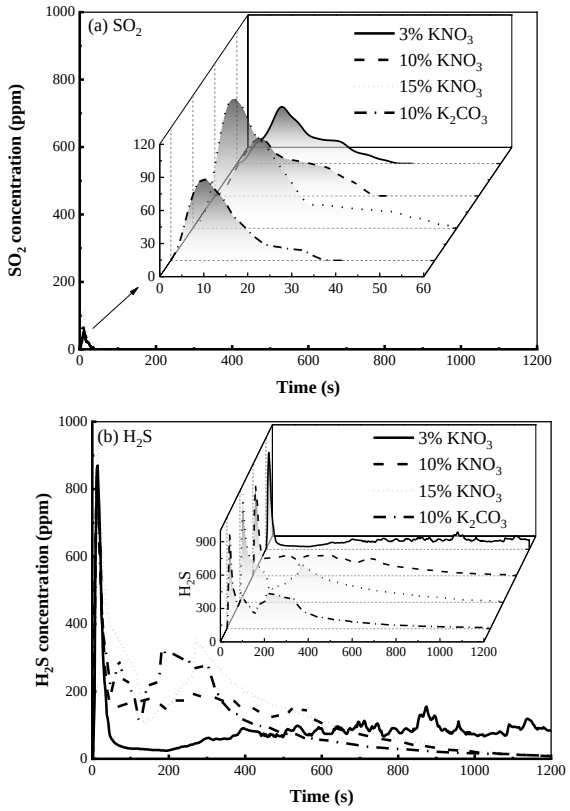

Fig.4 Effect of K amount and sources on (a) SO_2 and (b) H_2S concentration

The sulfur conversion of petcoke consisted of releasing in gas phases and capturing in solid phases of OC. The gases had been analyzed, and the sulfur-containing compositions in the reacted OC were detected by XRD (Table 2). It was found that no major phase of S-containing composition was detected, and just some trace phases such as Fe_xS_y were in the hematite OC without K and with 0.3%KNO_3. When the K adding amount reached 10%, Fe_xS_y and K-Fe-S were observed as major phases, and diverse minor phases including K-S, K-S-O and K-Fe-S were generated, thus K improving the sulfur adsorption on OC. Fe-based OC had been proven to be susceptible to sulfur after being reduced beyond Fe_3O_4 [33]. Moreover, the regeneration 10%KNO_3-hematite with Fe_2O_3, $K_2Fe_{22}O_{34}$, and some sulfur-containing phases such as $Fe_{0.91}S$, $KFe(SO_4)_2$ were also analyzed. Sulfate of K and Fe was detected in the major phases of regeneration OC besides Fe_xS_y. Sulfide could convert to sulfate in the oxidizing atmosphere and reductive Fe was easily sulfurized than Fe_2O_3 when K was added to hematite.

Table 2. Sulfur-containing phase composition in reacted OC

	Major phase	Minor/Trace phase
0K	-	Fe_3S_4, FeS
0.3%KNO_3	-	FeS, FeS_2
10%KNO_3	$Fe_{0.91}S$, FeS, KFe_2S_3	$Fe_2K_9S_7$, FeS_2, $K_3Fe_2S_4$, $KFe(SO_4)_2$, K_2S_5, $K_2S_4O_6$
R-10%KNO_3	$KFe(SO_4)_2$, $Fe_{0.91}S$	$K_2S_4O_6$, $K_2S_3O_{10}$, $K_3Fe_2S_4$, FeS_2, $Fe_2K_9S_7$

Cyclic performance of K-modified hematite in CLG process

From the results above, it was found that 10%KNO_3-hematite OC showed better performance in carbon conversion efficiency, gas generation rate and effective syngas ratio. It was significant to evaluate the OC stability of 10%KNO_3-hematite in a successive 21 redox cycles at high temperature 900 ºC and high sulfur atmosphere. Fig.5 demonstrated that the volume fraction of H_2 fluctuated between 65% and 67%. The volume fraction of CO_2 was just higher than 23% in the first two cycles, which decreased in oscillations and rebounded up to 22%. CO volume fraction was fluctuating upward following by a downward trend. In the early two cycles, the carbon conversion efficiency reached 99.9% in 30 minutes; with the increase of cycles, it decreased to 97.1% and showed a rebound growth from 15th cycle. But the difference of volume fraction was small, indicating the successive performance of 10%KNO_3-hematite OC was stable in CLG tests.

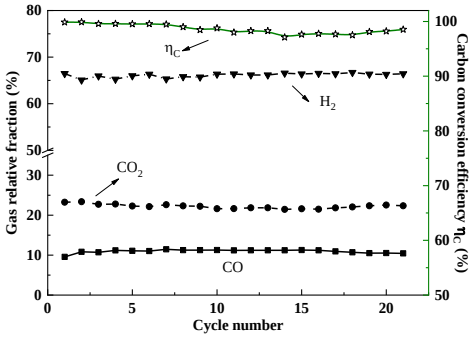

Fig.5 Redox performance of 10%KNO_3-hematite OC

DISCUSSIONS

H_2 not only is the vital gasification production, but also provides advantageous condition to H_2S. It is interesting to note that the H_2 production yield exceeded the theoretical yield of the complete gasification of carbon in the petcoke when using 10%K-hematite as OC. H_2 generation had two routes, one of which was from carbon gasification. The above results showed that the petcoke gasification was enhanced after introducing K to hematite, so higher H_2 yield generated when there was higher carbon conversion in the case of adding K. However, the excess portion of H_2 was from the reduction of H_2O by reductive state of iron [34, 35]. The adding of K deepened the reductive state of oxygen carrier, so more H_2 was generated according to the reactions (R5-R6). Consequently, H_2 yield was enhanced by the synergies of introducing K to hematite on carbon gasification and reductive OC, which could promote the competitiveness of petcoke CLG, as compared to the case of adding K to petcoke of a major effect on catalyzing the char gasification.

$$3FeO + H_2O \rightarrow H_2 + Fe_3O_4 \quad (R5)$$

$$Fe + H_2O \rightarrow FeO + H_2 \quad (R6)$$

The addition of K also had dual influences on sulfur fate: the sulfur conversion enhancement of petcoke due to driving the lattice oxygen and catalysis by K. Especially, HS or S radical was positive to form H_2S in the ample H_2 using K-modified hematite in petcoke CLG process. Another aspect was to absorb sulfur in OC through sulfides when Fe-based OC was deeply reduced after introducing K. Alkali was beneficial to in-situ sulfur capture through the formation of compounds containing K and S, which agreed with the finding of Furusjö [36]. For the large-scale OC production in the future, the most cost-effective and feasible method would be the utilization of natural hematite modified by potassium salts by mechanical mixing and impregnation [33, 37]. According to the performance of petcoke CLG based on K-modified hematite as OC, it was concluded that the adding of potassium promoted the fuel conversion including C, H and S. The tripartite mechanisms of K affecting the petcoke CLG performance was summarized in Fig.6.

CONCLUSION

- Introducing K had an evident enhancement on H_2 generation from improving petcoke gasification and partial oxidation of deepened reductive Fe by steam. Especially for the best case of 10%KNO_3-hematite, H_2 production increased by 3.9 times and carbon conversion efficiency dramatically increased by 26.48% with a sharp conversion rate in comparison with the iron ore.
- H_2S was the major sulfur-containing gas with the assistant of high H_2 yield using K-modified hematite. The dual functions of K to sulfur fate were accelerating the sulfur conversion via char-S gasification, and in-situ sulfur capture through the formation of K-Fe-S compounds in OCs.
- 10%KNO_3-hematite exhibited excellent cyclic stability with a H_2 volume fraction more than 66% and a carbon conversion efficiency over 98% after 21 cycles. The catalyzed char gasification due to migration of K to petcoke, the pores formation because of migration from surface to inner and the generation of K-Fe-O contributed to the enhancement of C, H, and S conversion during the sulfurous CLG process.

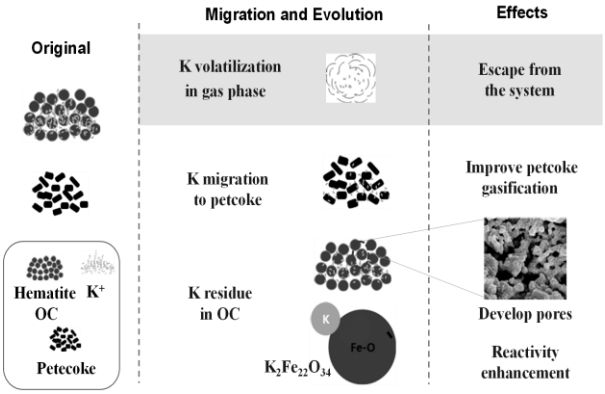

Fig.6 Schematic diagram of the mechanism of K to affect the CLG process

REFERENCES

[1] Cordoba, P., C. Ayora, and X. Querol, Evaluation of chemical stabilisation methods of coal-petcoke fly ash to reduce the mobility of Mo and Ni against environmental concerns. Ecotoxicol Environ Saf, 2020. 208: 111488.

[2] Huang, S., et al., Steam Cogasification of Petroleum Coke and Different Rank Coals for Enhanced Coke Reactivity and Hydrogen-Rich Gas Production. Energy & Fuels, 2014. 28(6): 3614-3622.

[3] Wu, Y., et al., Potassium-catalyzed steam gasification of petroleum coke for H2 production: Reactivity, selectivity and gas release. Fuel Processing Technology, 2011. 92(3): 523-530.

[4] Wang, J., et al., Steam gasification of coal char catalyzed by K2CO3 for enhanced production of hydrogen without formation of methane. Fuel, 2009. 88(9): 1572-1579.

[5] Fu, P., et al., Evolution of char structure during steam gasification of the chars produced from rapid pyrolysis of rice husk. Bioresour Technol, 2012. 114: 691-7.

[6] Wu, S.Y., et al., The Reactivity and H2 Production Characteristics of Petroleum Coke-steam Gasification Catalyzed by Potassium Salts. Energy Sources, Part A: Recovery, Utilization, and

Environmental Effects, 2013. 36(2): 184-190.
[7] Malekshahian, M. and J.M. Hill, Potassium catalyzed CO2 gasification of petroleum coke at elevated pressures. Fuel Processing Technology, 2013. 113: 34-40.
[8] Lee, W. and S. Kim, Catalytic activity of alkali and transition metal salt mixtures for steam-char gasification. Fuel, 1995. 74(9): 1387-1393.
[9] Zhou, Z., et al., Effect of iron species and calcium hydroxide on high-sulfur petroleum coke CO2 gasification. Energy & Fuels, 2012. 26(3): 1489-1495.
[10] Asami, K., et al., Gasification of brown coal and char with carbon dioxide in the presence of finely dispersed iron catalysts. Fuel Processing Technology, 1996. 47(2): 139-151.
[11] Kim, B.-c., et al., Effect of Thermal Treatment on Coke Reactivity and Catalytic Iron Mineralogy. Energy & Fuels, 2009. 23(7): 3694-3702.
[12] Li, J., et al., Experimental study on co-pyrolysis of petroleum coke and coals: Synergy effects and co-gasification reactivity. Fuel, 2020. 279: 118368.
[13] Liu, Y., et al., Effect of Coal Ash on Fe-Based Oxygen Carrier in Coal Char Chemical Looping Gasification. International Journal of Chemical Reactor Engineering, 2019. 17(8): 1-13.
[14] Hsieh, T.-L., et al., Chemical Looping Gasification for Producing High Purity, H2-Rich Syngas in a Cocurrent Moving Bed Reducer with Coal and Methane Cofeeds. Industrial & Engineering Chemistry Research, 2018. 57(7): 2461-2475.
[15] Fan, L., F. Li, and S. Ramkumar, Utilization of chemical looping strategy in coal gasification processes. Particuology, 2008. 6(3): 131-142.
[16] Guo, Q., et al., Coal Chemical Looping Gasification for Syngas Generation Using an Iron-Based Oxygen Carrier. Industrial & Engineering Chemistry Research, 2013. 53(1): 78-86.
[17] Wang, L., et al., Chemical Looping Hydrogen Generation Using Synthesized Hematite-Based Oxygen Carrier Comodified by Potassium and Copper. Energy & Fuels, 2017. 31(8): 8423-8433.
[18] Yu, Z., et al., Coal direct chemical looping hydrogen production with K-Fe-Al composite oxygen carrier. International Journal of Greenhouse Gas Control, 2018. 75: 24-31.
[19] Zhu, M., et al., Carbon formation on iron-based oxygen carriers during CH4 reduction period in Chemical Looping Hydrogen Generation process. Chemical Engineering Journal, 2017. 325: 322-331.
[20] Liu, T., et al., Interaction of coal ashes with potassium-decorated Fe2O3/Al2O3 oxygen carrier in coal-direct chemical looping hydrogen generation (CLHG). Journal of the Energy Institute, 2020. 93(5): 1790-1797.
[21] Yu, Z., et al., Reduction Rate Enhancements for Coal Direct Chemical Looping Combustion with an Iron Oxide Oxygen Carrier. Energy & Fuels, 2012. 26(4): 2505-2511.
[22] Cheng, X., et al., Modification of KNO3 on the reducibility and reactivity of Fe2O3-based oxygen carriers for chemical-looping combustion of methane. The Canadian Journal of Chemical Engineering, 2017. 95(8): 1569-1578.
[23] Liu, T., et al., Performance of potassium-modified Fe2O3/Al2O3 oxygen Carrier in coal-direct chemical looping hydrogen generation. International Journal of Hydrogen Energy, 2018. 43(42): 19384-19395.
[24] Bao, J., Z. Li, and N. Cai, Promoting the Reduction Reactivity of Ilmenite by Introducing Foreign Ions in Chemical Looping Combustion. Industrial & Engineering Chemistry Research, 2013. 52(18): 6119-6128.
[25] Liu, T., et al., Potassium migration and transformation during the deep reduction of oxygen carrier (OC) by char in coal-direct chemical looping hydrogen generation using potassium-modified Fe2O3/Al2O3 OC. Fuel, 2019. 256: 115883.
[26] Gu, H., et al., Iron ore as oxygen carrier improved with potassium for chemical looping combustion of anthracite coal. Combustion and Flame, 2012. 159(7): 2480-2490.
[27] Jerndal, E., T. Mattisson, and A. Lyngfelt, Thermal Analysis of Chemical-Looping Combustion. Chemical Engineering Research and Design, 2006. 84(9): 795-806.
[28] Keller, M., et al., Interaction of mineral matter of coal with oxygen carriers in chemical-looping combustion (CLC). Chemical Engineering Research and Design, 2014. 92(9): 1753-1770.
[29] Ge, H., et al., Effect of co-precipitation and impregnation on K-decorated Fe2O3/Al2O3 oxygen carrier in Chemical Looping Combustion of bituminous coal. Chemical Engineering Journal, 2015. 262: 1065-1076.
[30] Hussein, M.K., S.Z. El-Tawil, and M. Rabah, Desulphurization of high-sulfur Egyptian petroleum coke. J. Inst. Fuel, 1976. 49: 139-143.
[31] Yan, J., et al., Enhancing the performance of iron ore by introducing K and Na ions from biomass ashes in a CLC process. Energy, 2019. 167: 168-180 %@ 0360-5442.
[32] Wang, L., et al., Chemical looping gasification with potassium-catalyzed petroleum coke for enhanced production of H2 and H2S. Chemical Engineering Journal, 2020. 397: 124631.
[33] De Vos, Y., et al., Development of Stable Oxygen Carrier Materials for Chemical Looping Processes—A Review. Catalysts, 2020. 10(8): 926.
[34] Ge, H., et al., Experimental investigation on biomass gasification using chemical looping in a batch reactor and a continuous dual reactor. Chemical Engineering Journal, 2016. 286: 689-700.

[35] Wang, L., et al., Carbon and sulfur conversion of petroleum coke in the chemical looping gasification process. Energy, 2019. 179: 1205-1216.
[36] Furusjö, E., et al., Alkali enhanced biomass gasification with in situ S capture and novel syngas cleaning. Part 1: Gasifier performance. Energy, 2018. 157: 96-105.
[37] Hu, Q., et al., Chemical looping gasification of biomass with Fe2O3/CaO as the oxygen carrier for hydrogen-enriched syngas production. Chemical Engineering Journal, 2020. 379: 122346.

Preparing High-strength Ceramsite from Ferronickel Slag and Municipal Solid Waste Incineration Fly Ash

Xintao Wu[1], Foquan Gu[1,2], Chang Su[1], Wei Wang[1], Kai Pu[1], Dongsheng Shen[1,2], Yuyang Long[1,2]
1 Zhejiang Provincial Key Laboratory of Solid Waste Treatment and Recycling, School of Environmental Science and Engineering, Zhejiang Gongshang University, Hangzhou, Zhejiang 310012, China
2 Instrumental Analysis Center of Zhejiang Gongshang University, Hangzhou, Zhejiang 310018, China

ABSTRACT

This study investigated the feasibility of preparing ceramsites from ferronickel slag and municipal solid waste incineration (MSWI) fly ash by evaluating the effect of adding MSWI fly ash on the phase and microstructure transformations and properties of ceramsites. The theoretical calculations indicated that when the addition of MSWI fly ash ranges from 10 wt.% to 60 wt.%, the main phases in the system are diopside, feldspar, forsterite and merwinite, all of which contribute to the improvement of ceramsites properties. The XRD and SEM analyses revealed that the initial phase of ferronickel slag and MSWI fly ash can be transformed into ceramsite phases during the roasting process. Specifically, forsterite and enstatite produced by the decomposition of olivine in ferronickel slag will react with calcium oxide produced by the decomposition of fly ash to form diopside and merwinite. Additionally, the reaction product will gradually change from diopside to merwinite as the MSWI fly ash addition increases. An excellent ceramsite with the cylindrical compressive strength siginificantly exceeding the requirements of high strength lightweight aggregates could be obtained by roasting the ferronickel slag with addition of 20 wt.% MSWI fly ash at 800 °C for pre-roasting 15 min and 1275 °C for roasting 20 min, demonstrating its remarkable application prospects in concrete.

1. INTRODUCTION

Ferronickel slag is produced during the production of Ni-Fe. It was estimated that the annual output of ferronickel slag to be greater than 40 million tons in China [1]. However, only approximately 10% of ferronickel slag is utilized in the construction industry, with the remainder is stored in the open air [2], which not only consumes a lot of land resources but also poses a serious underlying risk to environmental pollution. Due to the massive amount of ferronickel slag and the presence of harmful components (such as Cr, and Ni) [3], proper treatment of ferronickel slag is a complex problem that needs to be addressed for the sustainable development of the Ni-Fe industry.

The researchers' study focused on the production of construction materials [4], geopolymers [5], glass ceramics and refractory materials [6-9], and recovering the valuable metals, i.e., Cr, Ni, Co etc. from ferronickel slag [10, 11]. Due to the low activity of ferronickel slag in construction materials, physical or chemical methods should be employed to activate the slag beforehand, although this pretreatment may limit the ferronickel slag dosage. Meanwhile, the high content of Cr in the slag significantly influences its dosage. The utilization of ferronickel slag to produce geopolymers and glass ceramics is hampered by disadvantages such as high cost and complex operation. It is feasible to prepare refractory materials from ferronickel slag, although the applications of the resulting refractory materials are rather limited. The cost of extracting valuable metals from ferronickel slag is considerably high since the slag's main components are MgO and SiO_2. Overall, resource utilization of ferronickel slag is still fraught with challenges.

In addition, municipal solid waste incineration (MSWI) has developed rapidly in China over the past decade. According to the National Bureau of Statistics, the total amount of municipal solid waste harmless treatment in China in 2020 was 0.23 billion tons, of which 0.15 billion tons were harmlessly treated by incineration [12], MSWI has gradually become the main method to treat municipal solid waste in major cities. Unfortunately, around 3% to 10% of MSWI fly ash was produced during the incineration process, which contains high levels of dioxins and heavy metal and is a hazardous waste [13-15]. China was estimated to generate about 4.5-15 million tons of waste incineration fly ash in 2020. With the increase in the annual generation of MSWI fly ash, the pressure on the disposal of waste incineration fly ash also increases.

For treatment of MSWI fly ash, many efforts have been spent. Some studies examined the feasibility of cement-based stabilization/solidification for disposal in landfill [16, 17], recycling into construction materials [17, 18], and resource recovery (such as Zn, Pb, Cu, and Cd recovery) [19-21]. Among them, stabilization prior to landfill and cement kiln co-processing are currently two major approaches for treating MSWI fly ash [22]. However, due to the compatibility of

solidification/stabilization, the MSWI fly ash landfill occupies a significant amount of land resources. Alarmingly, there is still the risk of heavy metals dissolution during long-term landfilling [23]. As for the cement kiln co-processing method, high temperature process promotes the removal of dioxins from MSWI fly ash. However, due to the the high Cl content in MSWI fly ash, additional dechlorination pretreatment [24], such as water washing, is necessary, however, the resulting effluent introduces secondary pollution problems. Meanwhile, in order to eliminate the influence of harmful elements such as Cl and heavy metals on cement-on-cement quality, the MSWI fly ash addition was strictly controlled in the cement kiln. In general, there are still numerous problems in the appropriate disposal of MSWI fly ash.

The main components of the ferronickel slag and MSWI fly ash are silica, magnesia, and calcium oxide, which have the potential to form ceramsite. Ceramsite has the advantages of high strength, good thermal insulation performance, excellent acid and alkali resistance, etc., and can be used as a good building aggregate [25-27]. Currently, the Chinese government restricts quarrying, advocates the use of solid waste as aggregate, and promotes comprehensive utilization of solid waste [28]. Therefore, the preparation of ceramsite from solid waste is expected to have promising future possibilities. Furthermore, during the process of ceramsite roasting, high temperatures can effectively solidify harmful substances such as heavy metals in MSWI fly ash [29-31], and the decomposition of organic matter in MSWI fly ash aids ceramsite in forming a porous structure. This strategy can not only eliminate the pollution concerns caused by ferronickel slag and MSWI fly ash, but it can also leverage the properties of ferronickel slag and MSWI fly ash to improve the performance of ceramsite.

In the present study, the phase and microstructure transformation behaviors of the ferronickel slag and fly ash systems were revealed based on the theoretical calculations, TG-DSC analysis, XRD analysis and SEM analysis under the condition of different MSWI fly ash additions, and the feasibility for preparing ceramsite from ferronickel slag and MSWI fly ash was verified. The findings are intended to provide an efficient and straightforward technological route for the resource utilization of ferronickel slag and MSWI fly ash.

2. EXPERIMENTAL

2.1. Materials

The ferronickel slag sample was a submerged arc furnace slag from the production of Ni-Fe alloy [32]. As showed in Table 1, the ferronickel slag was characterized by high contents of silica (48.29 wt.%) and magnesia (30.95 wt.%). The concentration of Zn, Pb, Cu, Cr, and Ni in ferronickel slag was 3023.09 mg/kg, 329.98 mg/kg, 528.57 mg/kg, 8135.65 mg/kg, and 909.38 mg/kg, respectively. The MSWI fly ash sample from flue gas treatment system of the municipal waste incineration plant. The MSWI fly ash contained 64.34 wt.% lime, 16.34 wt.% chlorine, 4.74 wt.% potassium oxide, 3.81 wt.% sodium oxide, 2.72 wt.% sulphur trioxide, and 2.50 wt.% silica. The concentration of Zn, Pb, Cu, Cd, Cr, and Ni in MSWI fly ash was 8558.58 mg/kg, 2039.57 mg/kg, 656.71 mg/kg, 292.14 mg/kg, 55.30 mg/kg and 17.25 mg/kg, respectively. The heavy metals leaching concentration of Pb, Zn, Cu, Cr, and Ni in MSWI fly ash was 18.91 mg/L, 3.07 mg/L, 0.02 mg/L, 0.36 mg/L and 0.14 mg/L, respectively. The heavy metals leaching concentration of Cr in ferronickel slag was 0.03 mg/L. The heavy metals leaching concentration of Pb in MSWI fly ash exceeds the limit of the Chinese national identification standards for hazardous wastes-identification for extraction toxicity (GB 5085.3-2007) [33]. The main phase of ferronickel slag was olivine, the main phase of MSWI fly ash was $CaCO_3$, CaOHCl, NaCl, $Ca(OH)_2$ and KCl.

2.2 Methods

2.2.1. Thermodynamic analysis: The FactSage 8.0 software was used to evaluate the influence of MSWI fly ash on the phase transformation of ferronickel slag by calculating the thermodynamic equilibrium phase content of the ferronickel slag and MSWI fly ash system under different temperature conditions.

2.2.2. Experimental procedure: At first, the ferronickel slag was ground to a particle size of less than 74 μm, and then mixed with MSWI fly ash according to the corresponding mass ratio. After adding suitable water, the mixture was granulated into pellets with a diameter of 12 mm. After dried at 105 °C for 12 h, the dried pellets were pre-roasted in an electric furnace at 800 °C for 15 min, and then roasted at 1275 °C for 20 min. After cooled down naturally in the furnace to 25 °C, the ceramsite was taken out for the subsequent analysis and performance characterization.

2.2.3. Instrumental analysis and performance characterization: The elemental composition of samples was analyzed by X-ray fluorescence (XRF; XRF-1800, Japan Shimadzu FEI Co., Ltd). The concentration of heavy metals in samples were determined by atomic absorption spectrometer (AAS, ICE 3500, USA Thermo Fisher Scientific Co., Ltd). The decomposition properties and thermodynamic characteristics of the samples during roasting were identified by a simultaneous thermal analyzer (DSC-TGA, SDT 650, TA Instruments Co., Ltd) in the temperature range from 25 °C to 1400 °C with a ramp rate of 10 °C/min in air. The phase compositions of the ceramsites were tested by an X-ray diffractometer (XRD, D8 Advance, Germany Bruker Co., Ltd) with a copper target. The microstructure and compositions of the ceramsites were analyzed by a scanning electron

microscope (SEM, FEI QUANTA 200, FEI Co., Ltd). The pore distribution of ceramsite were determined by an automatic mercury porosimeter (AutoPore 9620, USA Micromeritics Co., Ltd), and the sample size used for testing was 10 mm×10 mm×10 mm.

The properties of the obtained ceramsite were characterized according to the Chinese National Standard Test Methods (GB/T17431.2-2010) [34]. The leaching behavior of zinc, lead, copper, cadmium, chromium, and nickel in the MSWI fly ash and ceramsite samples was analyzed based on the Chinese Solid Waste Extraction Procedure for Leaching Toxicity- Sulphuric acid & nitric acid method (HJ/T 299-2007) [35].

3. RESULTS AND DISCUSSION

3.1. Thermodynamic analysis

The effect of MSWI fly ash addition on the phase evolution of ferronickel slag was revealed by evaluating the transformation behavior of the thermodynamic equilibrium phase content of ferronickel slag and MSWI fly ash system at 1275 °C. This can be seen from Fig. 1 that increasing MSWI fly ash addition, resulted in a significant difference in the phase content of the system presented a significant difference. Specifically, when the addition of MSWI fly ash of 10 wt.%, the system contained 28.15% forsterite, 28.09% diopside, 19.70% enstatite, 11.40% hematite and 12.66% feldspar. When the addition of MSWI fly ash of 20 wt.%, the liquid phase began to appear, and the system mainly included 33.30% forsterite, 30.35% diopside, 24.42% feldspar, 10.83% hematite, and 1.10% liquid. With the addition of MSWI fly ash increased to 30 wt.%-60 wt.%, the diopside and forsterite were gradually replaced by merwinite, with diopside disappearing at 30 wt.%, forsterite disappearing at 60 wt.%. With the addition of MSWI fly ash further increased to 70 wt.%-100 wt.%, merwinite disappeared and lime increased substantially, a large amount of free lime in the system will affect the stability of ceramsite. As the addition of MSWI fly ash reaches 100 wt.%, the system comprised 66.04% lime, 16.18% liquid, 8.45% Ca_2SiO_4, 5.39% $CaSO_4$, 3.94% $Ca_2Fe_2O_5$ and $Ca_3MgAl_4O_{10}$. It should be noted that as the percentage of MSWI fly ash increased from 20 wt.% to 100 wt.%, the content of liquid increased from about 1.10% to 16.20%. The formation of liquid in the system may promote roasting and increase the strength of ceramsite. In summary, the appropriate addition of MSWI fly ash is 20 wt.%-60 wt.%, however this must yet be determined by further experiments.

3.2. Phase and microstructure transformations of ferronickel slag and MSWI fly ash system during roasting

Phase and microstructure transformations of ferronickel slag and MSWI fly ash system during roasting was explored by XRD and SEM analyses.

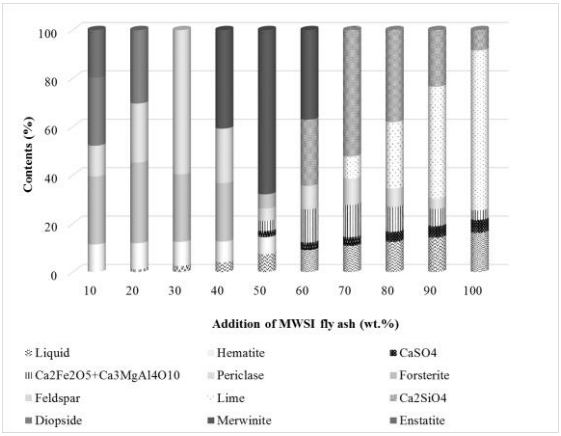

Fig. 1. Calculated contents of thermodynamic equilibrium phases in the ferronickel slag and MSWI fly ash system with different additions of MSWI fly ash.

3.2.2. XRD analysis The XRD results of the resulting ceramsite produced by roasting ferronickel slag with 10 wt.%-50 wt.% MSWI fly ash is shown in Fig. 2. The phases of the ceramsite obtained with 10 wt.% MSWI fly ash were diopside ($CaMgSi_2O_6$), feldspar, forsterite (Mg_2SiO_4), and enstatite ($MgSiO_3$). Increasing the MSWI fly ash addition to 20 wt.%, the intensity of the enstatite diffraction peaks decreased, and the main phases of the obtained ceramsite were diopside, feldspar and forsterite. With the MSWI fly ash addition increased to 30 wt.%, merwinite ($Ca_2MgSi_2O_7$) and quartz diffraction peaks appeared, while the intensity of diopside diffraction peaks decreased, diopside, merwinite, feldspar, forsterite and quartz were the main phases of the obtained cermsite. Futher increasing the MSWI fly ash addition to 50 wt %, the phase of the ceramsite remained unchanged, but the intensity of diopside and forsterite diffraction peaks gradually decreased, while the intensity of merwinite diffraction peaks increased dramatically. The transformation of the main phases agreed well with the calculate results in Fig. 3. It is apparent shows that the original phase undergoes a complex chemical reaction during the roasting process. The relevant reactions are depicted in Equations (1)-(9). At about 800 °C, the olivine in the ferronickel slag decomposed to Mg_2SiO_4, SiO_2, and Fe_2O_3 (Equation (1)). During the roasting process, the $CaCO_3$, $Ca(OH)_2$, and CaOHCl in MSWI fly ash decomposed to CaO (Equations (2)-(4)). The generated Mg_2SiO_4, SiO_2 and CaO further reacted to form $CaMgSi_2O_6$ and $Ca_2MgSi_2O_7$ (Equations (5)-(6)). In addition, Mg_2SiO_4 and SiO_2 can react to form $MgSiO_3$ (Equation (7)), and the resulting $MgSiO_3$, SiO_2, and CaO can also be further reacted to form $CaMgSi_2O_6$ and $Ca_2MgSi_2O_7$ (Equations (8)-(9)). As

the content of CaO in the system increases, the reaction product gradually changes from $CaMgSi_2O_6$ to $Ca_2MgSi_2O_7$ (Equation (10)), this explains the significantly increased merwinite diffraction peak intensity and the continuously decreasing diopside diffraction peak intensity in the ceramsites as the MSWI fly ash addition exceeds 40 wt.%. It was reported that during the diopside formation process, heavy metals (such as Zn, Cu, and Pb) could be substituted to magnesium (II) or calcium (II) to form the new components, thereby immobilizing the heavy metals in the crystal lattice of the new mineral. Besides, the calcium-containing mineral has been considered to be easy to form a high-strength structure [30]. As a result, ceramisites with diopside as the primary phase may characterize by high-strength and a great ability to immobilize heavy metals. In addition, unlike MSWI fly ash, no chlorine-containing minerals were found in the cermisites, because chlorine-containing compounds easily decompose and volatilize into gases during the high-temperature roasting process. It should be noted that, in contrast to the thermodynamic equilibrium phase calculation results, no Fe-bearing minerals were found in the cermisites as some iron may remain in the olivine phase formation of the iron-rich forsterite or substituted with Mg^{2+}/Ca^{2+} appeared in the diopside, merwinite, and feldspar phase.

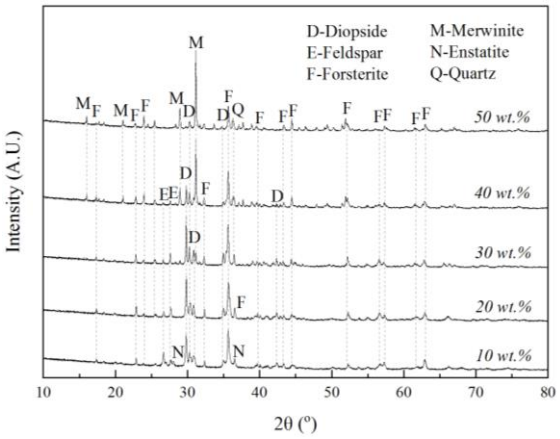

Fig. 2. XRD patterns of ceramsites roasted with different additions of MSWI fly ash.

$$2(Mg_{(1-x)}Fe_x)_2SiO_4+xO_2=(2-2x)Mg_2SiO_4+2xFe_2O_3+2xSiO_2 \quad (1)$$

$$CaCO_3=CaO+CO_2 \qquad \Delta_rG_m^{\Theta}=-0.15T+171.14\ kJ/mol \quad (2)$$

$$Ca(OH)_2=CaO+H_2O \qquad \Delta_rG_m^{\Theta}=-0.05T+77.61\ kJ/mol \quad (3)$$

$$CaOHCl=CaO+HCl \quad (4)$$

$$Mg_2SiO_4+2CaO+3SiO_2=2CaMgSi_2O_6 \qquad \Delta_rG_m^{\Theta}=0.0086T-231.09\ kJ/mol \quad (5)$$

$$Mg_2SiO_4+4CaO+3SiO_2=2CaMgSi_2O_7 \qquad \Delta_rG_m^{\Theta}=0.0499T-319.94\ kJ/mol \quad (6)$$

$$Mg_2SiO_4+SiO_2=2MgSiO_3 \qquad \Delta_rG_m^{\Theta}=0.0097T-5.69\ kJ/mol \quad (7)$$

$$MgSiO_3+CaO+SiO_2=CaMgSi_2O_6 \qquad \Delta_rG_m^{\Theta}=0.0092T-112.70\ kJ/mol \quad (8)$$

$$MgSiO_3+2CaO+SiO_2=Ca_2MgSi_2O_7 \qquad \Delta_rG_m^{\Theta}=0.0298T-157.12\ kJ/mol \quad (9)$$

$$CaMgSi_2O_6+CaO=Ca_2MgSi_2O_7 \qquad \Delta_rG_m^{\Theta}=0.0206T-44.43\ kJ/mol \quad (10)$$

3.2.2. SEM analysis Furthermore, the micro-morphologies of the ceramsites were analyzed using SEM. Fig. 3 shows SEM images of the ceramsite generated by roasting ferronickel slag with the addition of 10 wt.%-50 wt.% MSWI fly ash at 800 °C for 15 min pre-roasting and 1275 °C for 20 min roasting. As illustrated in Fig. 3, when the addition of MSWI fly ash was at 10 wt.%-20 wt.%, the ceramsites contained a modest amount of evenly distributed pores surrounded by a significant amount of crystal phases formed during the roasting process, with the majority of pores filled by the liquid phase generated during the roasting process. This not only helps to promote the roasting process and improve the strength of the ceramsite, but also reduces water absorption of the ceramsite and promotes the solidification of heavy metals. According to the mercury intrusion porosimetry results, the total pore area and average pore diameter of the ceramsite (MSWI fly ash addition of 20 wt.%) were 0.062 m^2/g and 4.26 μm. However, as the amount of MSWI fly ash addition increased, the pores gradually expanded and penetrated into wide open pores, which is harmful to the compressive strength and water absorption rate densification of the ceramsite.

3.3. Properties of ceramisites

The effect of MSWI fly ash on the bulk density, apparent density, cylindrical compressive strength and 1-h water absorption rate of the obtained ceramisite was investigated when the ferronickel slag was pre-roasted at 800 °C for 15 min and roasted at 1275 °C for 20 min with different MSWI fly ash additions. The results shown in Fig. 4 reveal that when 10 wt.%-20 wt.% of MSWI fly ash were added, the bulk density, apparent density, cylindrical compressive strength, and 1-h water absorption rate of the obtained ceramsite were similar, and exhibited extremely high cylindrical compressive strength (36.80 MPa-37.50 MPa). However, as the addition of MSWI fly ash increased, the cylindrical compressive strength of the obtained ceramsite declined significantly. In contrast, 1-h water absorption rate of the ceramsite increased rapidly, while the bulk density and apparent density showed a trend of first decreasing and then increasing. It is evident that the addition of MSWI fly ash leads to a significant decrease in bulk density and cylindrical compressive strength, which is due to the decomposition of carbonates, and the volatilization of heavy metal chlorides and salts in the MSWI fly ash during the roasting process [36]. At the

same time, the particles of ceramsite become smaller, due to the decomposition and volatilization of these substances, which was the reason for the ceramsite bulk density, apparent density starts to increase after the addition of MSWI fly ash exceeds 60%. It should be noted that the 1-h water absorption of ceramsite decreased when the addition of MSWI fly ash reaches 80 wt.%, which was due to the loose ceramsite structure and certain components being dissolved during the water absorption experiment. When the addition of MSWI fly ash reaches 90 wt.%, the dissolution phenomenon became more severe, and the ceramsite was entirely disintegrated in water.

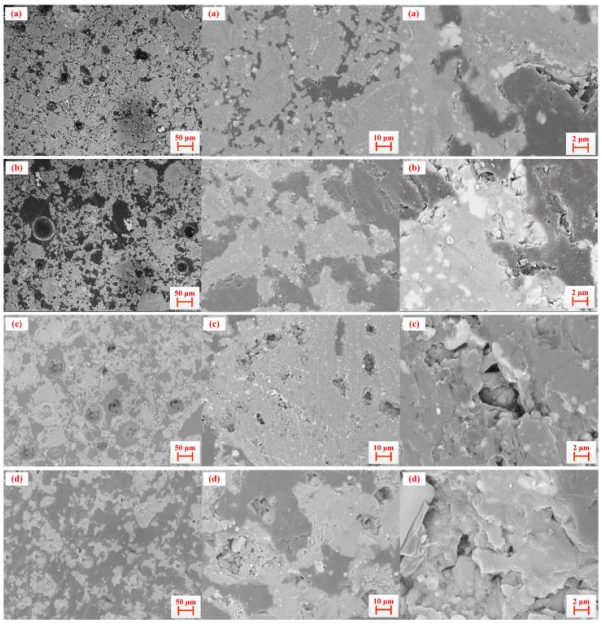

Fig. 3. SEM images of the ceramsites obtained with different additions of MSWI fly ash: (a) MSWI fly ash addition of 10 wt.%, (b) MSWI fly ash addition of 20 wt.%, (c) MSWI fly ash addition of 30 wt.%, and (d) MSWI fly ash addition of 50 wt.%.

Given the high Pb and Zn leaching concentrations and Cl content of MSWI fly ash, the Pb and Zn leaching concentrations and Cl content of ceramsites were examine to evaluate environmental safety. As shown in Table 3, the Zn leaching concentration in ceramsites was all below the detection limit with the MSWI fly ash addition reaches 10 wt.%-90 wt.%, indicating effective stabilization in ceramsites. When the MSWI fly ash addition reaches 10 wt.%-80 wt.%, the Pb leaching concentration in ceramsites remains low and can meets the requirements of the Chinese National Intefrated Wastewater Discharge Standard (GB 8978-1996) [37]. When the MSWI fly ash addition reaches 10 wt.%, no Cl was found in ceramsite. However, as the addition of MSWI fly ash increased, so did the content of Cl in ceramsites. When the addition of MSWI fly ash is below 40 wt.%, the Cl content can meet the requirements of pollution control [38].

Table 1. Pb and Zn leaching concentration and Cl content of the ceramsites.

Addition of MSWI fly ash (wt.%)	10	20	30	50	60	80
Pb leaching concentration (mg/L)	0.004	0.007	0.02	0.02	0.01	0.02
Zn leaching concentration (mg/L)	ND	ND	ND	ND	ND	ND
Cl content (wt.%)	ND	0.08	1.33	2.46	3.30	9.46

Based on the above analysis, a good ceramsite with bulk density of 1205 kg/m^3, apparent density of 2249 kg/m^3, cylindrical compressive strength of 36.80 MPa and 1-h water absorption rate of 6.15% can be obtained by roasting the ferronickel slag with the addition of 20 wt.% MSWI fly ash at 800 °C for pre-roasting 15 min and at 1275 °C for roasting 20 min. The obtained ceramsite basically met the quality standard of ceramsite products of GB/T17431.1-2010 [39], and the cylindrical compressive strength far exceeds the requirements of high strength lightweight aggregates, showing its great application potential in concrete.

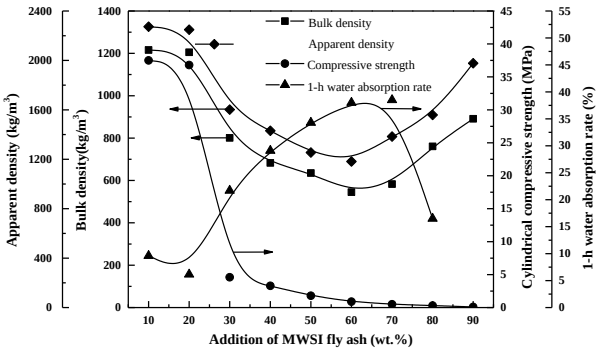

Fig. 4. Effect of addition of MSWI fly ash on the bulk density, apparent density, cylindrical compressive strength and 1-h water absorption rate of the ceramisite.

4. CONCLUSIONS

This study validated the feasibility of preparing ceramsites from ferronickel slag and MSWI fly ash was

verified in this study. The results of theoretical equilibrium phase content of ferronickel slag and MSWI fly ash system at 1275 °C revealed that with the MSWI fly ash addition of 10 wt.%-60 wt.%, the main phases in the system were diopside, feldspar, forsterite, and merwinite were, which contributed to improving the performance of ceramsites. With the addition of MSWI fly ash further increased to 70 wt.%-100 wt.%, a large amount of free lime generated in the system will impair the stability of ceramsite. The TG-DSC results indicated that the appropriate addition of MSWI fly ash contributed to decrease the smelting point of the ferronickel slag system, which is expected to promote the roasting process. XRD and SEM analyses indicated that the original phase of ferronickel slag and MSWI fly ash could be transformed to ceramsite phases during the roasting process. Specifically, forsterite and enstatite generated from the decomposition of olivine in ferronickel slag will react with calcium oxide produced by the decomposition of fly ash to form diopside and merwinite, and as the addition of MSWI fly ash increases, the reaction product will gradually change from diopside to merwinite. The experimental results exhibited that a great ceramsite with bulk density of 1205 kg/m3, apparent density of 2249 kg/m^3, cylindrical compressive strength of 36.80 MPa and 1-h water absorption rate of 6.15% could be obtained by roasting the ferronickel slag with the addition of 20 wt.% MSWI fly ash at 800 °C for 15 min pre-roasting and 1275 °C for 20 min roasting. In general, the proposed technological route has the characteristics of simple operation and high efficiency is expected to be widely adopted in the simultaneous utilization of ferronickel slag and MSWI fly ash.

ACKNOWLEDGEMENTS

This work was partially supported by the Key R&D Program of Zhejiang Province, China (2020C03086, 2022C03059), the Scientific Research Project of Zhejiang Provincial Department of Education (Y202147303), and the Undergraduate Training Program on Innovation and Entrepreneurship of Zhejiang Gongshang University (CX202223005, CX202223010).

REFERENCES

[1] F. Gu, Y. Zhang, Z. Peng, H. Tang, M. Lu, S. Liu, Z. Su, M. Rao, G. Li and T. Jiang. Recovery of chromium from ferronickel slag via alkaline roasting followed by water leaching: effect of roasting atmosphere, Z. Peng et al. (eds.), 11th International Symposium on High-Temperature Metallurgical Processing, The Minerals, Metals & Materials Series (2020) 359-367.

[2] Y. Huang, Q. Wang, M. Shi, Characteristics and reactivity of ferronickel slag powder, Constr. Build. Mater. 156 (2017) 773-789.

[3] F. Gu, Y. Zhang, Z. Su, Y. Tu, S. Liu, T. Jiang, Recovery of chromium from chromium-bearing slags produced in the stainless-steel smelting: A review, J. Clean Prod. 296 (2021) 126467.

[4] M. Nuruzzaman, J. C. Kuri, P. K. Sarker, Strength, permeability and microstructure of self-compacting concrete with the dual use of ferronickel slag as fine aggregate and supplementary binder, Constr. Build. Mater. 318 (2022) 125927.

[5] J.C. Kuri, P.K. Sarker, F.U.A. Shaikh, Sulphuric acid resistance of ground ferronickel slag blended fly ash geopolymer mortar, Constr. Build. Mater. 313 (2021) 125505.

[6] W. Shang, Z. Peng, F. Xu, H. Tang, M. Rao, G. Li, T. Jiang, Preparation of enstatite-spinel based glass-ceramics by co-utilization of ferronickel slag and coal fly ash, Ceram. Int. 47 (2021) 29400-29409.

[7] L. Yang, Z. Peng, Y. Huang, L. Wang, L. Zheng, M. Rao, G. Li, T. Jiang, Co-utilization of ferronickel slag and fly ash cenosphere for production of superior thermal insulation materials, Ceram. Int. 47 (2021) 10019-10026.

[8] H. Tang, Z. Peng, F. Gu, L. Yang, W. Tian, Q. Zhong, M. Rao, G. Li, T. Jiang. Chromium-promoted preparation of forsterite refractory materials from ferronickel slag by microwave sintering, Ceram. Int. 47 (2021) 10809-10818.

[9] F. Gu, Y. Zhang, Y. Tu, X. Wu, Y. Zhu, Y. Long, D. Shen, Assessing magnesia effect on preparing refractory materials from ferrochromium slag, Ceram. Int. 48 (2022) 13100-13107.

[10] Z. Peng, L. Wang, F. Gu, H. Tang, M. Rao, Y. Zhang, G. Li, T. Jiang, Recovery of chromium from ferronickel slag: A comparison of microwave roasting and conventional roasting strategies, Powder. Technol. 372 (2020) 578-584.

[11] F. Gu, Y. Zhang, Z. Peng, Z. Su, H. Tang, W. Tian, G. Liang, Joonho Lee, M. Rao, G. Li, T. Jiang, Selective recovery of chromium from ferronickel slag via alkaline roasting followed by water leaching, J. Hazard. Mater. 374 (2019) 83-91.

[12]https://data.stats.gov.cn/search.htm?s=%E5%9E%83%E5%9C%BE.

[13] C. Zhao, S Lin, Y Zhao, K Lin, L Tian, M Xie, T. Zhou, Comprehensive understanding the transition behaviors and mechanisms of chlorine and metal ions in municipal solid waste incineration fly ash during thermal treatment, Sci. Total. Environ. 807 (2022) 150731.

[14] P. Ren, T. Ling, K. Mo. CO_2 pretreatment of municipal solid waste incineration fly ash and its feasible use as supplementary cementitious material, J. Hazard. Mater. 424 (2022) 127457.

[15] Y. Mao, H. Wu, W. Wang, M. Jia, X. Che.

Pretreatment of municipal solid waste incineration fly ash and preparation of solid waste source sulphoaluminate cementitious material, J. Hazard. Mater. 385 (2020) 121580.
[16] C. Fan, B. Wang, T. Zhang. Review on cement stabilization/solidification of municipal solid waste incineration fly ash. Adv. Mater. Sci. Eng. 2018 (2018) 1-7.
[17] S. Zhao, F. Muhammad, L. Yu, M. Xia, X. Huang, B. Jiao, N. Lu, D. Li, Solidification/stabilization of municipal solid waste incineration fly ash using uncalcined coal gangue-based alkali-activated cementitious materials. Environ. Sci. Pollut. Res. 26 (2019) 25609-25620.
[18] J. Li, S. Zhang, Q. Wang, W. Ni, K. Li, P. Fu, W. Hu, Z. Li. Feasibility of using fly ash–slag-based binder for mine backfilling and its associated leaching risks. J. Hazard. Mater. 400 (2020) 123191.
[19] Y. Zhang, L. Wang, L. Chen, B. Ma, Y. Zhang, W. Ni, D.C.W. Tsang. Treatment of municipal solid waste incineration fly ash: State-of-the-art technologies and future perspectives. J. Hazard. Mater. 411 (2021) 125132.
[20] C. Geng, J. Liu, S. Wu, Y. Jia, B. Du, S. Yu. Novel method for comprehensive utilization of MSWI fly ash through co-reduction with red mud to prepare crude alloy and cleaned slag, J. Hazard. Mater. 384 (2020) 121315.
[21] K. Kurashima, K. Matsuda, S. Kumagai, T. Kameda, Y. Saito, T. Yoshioka. A combined kinetic and thermodynamic approach for interpreting the complex interactions during chloride volatilization of heavy metals in municipal solid waste fly ash, Waste Manag. 87 (2019) 204-217.
[22] Kanhar A. H., S. Chen, F. Wang, Incineration fly ash and its treatment to possible utilization: A review, Energies 13 (2020) 6681.
[23] X. Tian, F. Rao, C. Li, W. Ge, N.O. Lara, S. Song, L. Xia, Solidification of municipal solid waste incineration fly ash and immobilization of heavy metals using waste glass in alkaline activation system, Chemosphere 283 (2021) 131240.
[24] X. Wang, M. Wang, D. Zou, C. Wu, T. Li, M. Gao, S. Liu, Q. Wang, T. Shimaoka, Comparative study on inorganic Cl removal of municipal solid waste fly ash using different types and concentrations of organic acids, Chemosphere 261 (2020) 127754.
[25] T. Ji, D. Zheng, X. Chen, X. Lin, H. Wu, Effect of prewetting degree of ceramsite on the early-age autogenous shrinkage of lightweight aggregate concrete, Construct. Build. Mater. 98 (2015) 102-111.
[26] X. Zheng, T. Ji, S.M. Easa, B. Zhang, Z. Jiang, Tensile basic creep behavior of lightweight aggregate concrete reinforced with steel fiber, Construct. Build. Mater. 200 (2019) 356-367.
[27] X. Li, P. Wang, J. Qin, Y. Liu, Y. Qu, J. Liu, R. Cao, Y. Zhang, Mechanical properties of sintered ceramsite from iron ore tailings affected by two-region structure, Construct. Build. Mater. 240 (2020) 117919.
[28] L. Luo, X. Tu, Z. Peng, Preparation and heavy metals solidification of ceramsite from lake mud, Bull. Chin. Ceram. Soc. 38 (2019) 3397-3402 (In Chinese).
[29] Y. Long, J. Qiu, Q. Bao, F. Gu, Z. Wu, M. Wu, W. Guo, D. Shen, Effect of Fe_2O_3 on the leaching behavior of Cr in hazardous waste incineration fly ash after thermal treatment, Environ. Technol. Inno. 24 (2021) 102072.
[30] X. Zhan, L. Wang, L. Wang, J. Gong, X. Wang, X. Song, T. Xu, Co-sintering MSWI fly ash with electrolytic manganese residue and coal fly ash for lightweight ceramisite, Chemosphere 263 (2021) 127914.
[31] H. Mi, L. Yi, Q. Wu, J. Xia, B. Zhang, Preparation of high-strength ceramsite from red mud, fly ash, and bentonite, Ceram. Int. 47 (2021) 18218-18229.
[32] F. Gu, Z. Peng, Y. Zhang, H. Tang, L. Ye, W. Tian, G. Liang, M. Rao, G. Li, T. Jiang, Facile route for preparing refractory materials from ferronickel slag with addition of magnesia, ACS Sustainable Chem. Eng. 6 (2018) 4880-4889.
[33] China National Environmental Protection Administration and General Administration of Quality Supervision, Inspection and Quarantine of the People's Republic of China, Identification standards for hazardous wastes-identification for extraction toxicity, China Environmental Science Press, Beijing, 2007.
[34] General Administration of Quality Supervision, Inspection and Quarantine of the People's Republic of China and China Standardization Administration, Lightweight aggregates and its test methods—Part 2: Test methods for lightweight aggregates, Standards Press of China, Beijing, 2010.
[35] China National Environmental Protection Administration, Solid Waste Extraction Procedure for Leaching Toxicity Acetic Acid Buffer Solution Method, China Environmental Science Press, Beijing, 2007.
[36] M. Liu, C. Wang, Y. Bai, G. Xu, Effects of sintering temperature on the characteristics of lightweight aggregate made from sewage sludge and river sediment, J. Alloys Compd. 748(2018), 522-527.
[37] The State Bureau of Quality and Technical Supervision, Integrated wastewater discharge standard, Standards Press of China, Beijing, 1996.
[38] Ministry of Ecological Environment of the People's Republic of China, technical specification for pollution control of fly-ash from municipal

solid waste incineration, China Environmental Science Press, Beijing, 2020.
[39] General Administration of Quality Supervision, Inspection and Quarantine of the People's Republic of China and China Standardization Administration, Lightweight aggregates and its test methods—Part 1: Lightweight aggregates, Standards Press of China, Beijing, 2010.

THE LONG-TREM PERFORMANCE OF CONCRETE AMENDED WITH MUNICIPAL SEWAGE SLUDGE INCINERATION ASH

Zixiao Wu, Yumeng Jiang, Wenxin Guo, Junxun Jin, Minjin Wu, Dongsheng Shen, Yuyang Long*
Zhejiang Provincial Key Laboratory of Solid Waste Treatment and Recycling, School of Environmental Science and Engineering, Zhejiang Gongshang University, Hangzhou, 310012, China

ABSTRACT
Municipal sewage sludge incineration ash (MSSIA) is commonly used as a raw material in concrete, but few studies have focused on the long-term environmental tolerance of municipal sewage sludge incineration ash concrete (MSSIAC). In this study, acid rain leaching, salt erosion, and freezing-thawing tests were used to evaluate the long-term environmental behavior of the optimal MSSIAC formulation. One optimal MSSIAC formulation replaces 5% MSSIA, and results in a 7.2% increase in unconfined compressive strength (UCS), indicating that MSSIA-amended concrete can have enhanced UCS. Only Zn was released from the optimal MSSIAC formulations (replacing 5% or 10% MSSIA) in the acid rain leaching test, but only up to 0.071 mg Zn L-1, which was within the acceptable environmental range. No heavy metals were released at concentrations above the method detection limits in the salt erosion and freezing-thawing tests. The optimal MSSIAC formulations have excellent long-term environmental tolerance while meeting the requirement of UCS, and provide a valuable use for MSSIA.
Keywords: Concrete; Municipal sewage sludge incineration ash; Long-term; Environtal tolerance; Heavy meta

INTRODUCTION
With rapid economic development and increase in the standard of living, municipal sewage sludge generation is continuously escalating. According to the statistics, dry municipal sewage sludge produced in the municipal sewage treatment process in China exceeded 12 million metric tonnes in 2017 (Z. Chang et al., 2020; S. Ledakowicz et al., 2019), and only about 20% was disposed of in harmless ways such as the production of construction materials, thermal treatment (P. Das et al., 2020), agricultural application (M. Skowrońska et al., 2020), and sanitary landfill (A. Kelessidis and A.S. Stasinakis, 2012). Among them, incineration technology provides the advantages of volume reduction, sterilization, and electricity generation (O. Krüger and C. Adam, 2015); however, the municipal sewage sludge incineration ash (MSSIA) generated after incineration requires landfill disposal and can possibly cause secondary pollution such as the release of heavy metals. Therefore, MSSIA treatment merits global concern and research.
Unlike fly ash from the hazardous waste incineration process, MSSIA is a general industrial solid waste, although it contains certain heavy metals. Recently, MSSIA disposal methods have been reported, including landfills (S. Donatello et al., 2010), stabilization and solidification (R. Siddique, 2010), which can reduce the potential risks of MSSIA. However, MSSIA disposal will still require extensive land resources after treatment. MSSIA can also cause secondary pollution after long-term environmental exposure because of the limited immobilization of heavy metals. It still needs more thoughtful strategy for MMSIA disposal.
Concrete is in high demand for infrastructure construction. Because MSSIA has pozzolanic activity (L. Chen and D.-F. Lin, 2009), it can be used as raw material for concrete, which consumes the MSSIA and provides a valuable use for this waste product. This is a method that combines both waste management and resource utilization. Compared with other treatment methods, concrete prepared by ash incineration has obvious advantages in resource utilization. Therefore, this method has received extensive research and attention.
MSSIA has been used as cementitious material to replace about 10–20 % of cement in concrete, while having no significant impact on the concrete strength (G. Rutkowska et al., 2018; Z. Chen and C.S. Poon, 2017; Z. Chen et al., 2018). Municipal sewage sludge incineration ash concrete (MSSIAC) can meet strength requirements, and most published studies focus only on physical properties such as unconfined compressive strength (UCS) and flexural strength to characterize the effect of MSSIA on concrete (S. Chakraborty, 2017). Though some environmental tolerance studies on MSSIAC involve leaching test, these only reflect the short-term environmental effects, not long-term effects (J.-s. Li et al., 2017; C.J. Lynn et al., 2018). In some areas, high rainfall occurs, with a high frequency of acid rain, increasing the requirements for environmental

tolerance. Short-term leaching test cannot fully reflect the environmental performance of MSSIAC, and the long-term environmental behavior must be studied. In addition, the changing global climate may also increase the risk of release of pollutants from MSSIAC, and it is important to explore the long-term performance of MSSIAC under extreme environmental conditions.

In this study, MSSIA was introduced into concrete to find an optimal concrete formulation for MSSIA disposal. The MSSIAC was then evaluated in severe long-term environment exposure scenarios. It aims to provide a feasible and safe disposal strategy for MSSIA.

MATERIAOLS AND METOHDS

Materials and sample preparation

MSSIA (100 kg) was obtained from a municipal sewage sludge incineration plant located in Hangzhou, China. This incineration plant uses circulating fluidized bed sludge incineration at a capacity of 500 t d^{-1}.

Cement used in this study was P.O. 42.5. The sand and stone were purchased from a quarry in Hangzhou, China. The stone was sifted into five grain-grades: 16–19 mm, 13.2–16 mm, 9.5–13.2 mm, 4.75–9.5 mm, and 2.36–4.75 mm. Sand was sifted to 0.075–2.36 mm.

Concrete was prepared according to standard (EN 12390-2, 2000) by mixing cement, stone, sand, MSSIA (except in the controls), and water and curing the mixture for up to 28 d, either in a 100 mm × 100 mm × 100 mm cubic concrete form or a 60 mm × 60 mm × 150 mm cylindrical concrete form.

A simulated acid rain solution was prepared based on the acid rain chemistry in China, containing 3.10 mg L^{-1} $CaCl_2$, 2.80 g L^{-1} NH4Cl, 0.91 g L^{-1} NaCl, and 0.75 g L^{-1} KCl with a pH of 4.00 and a molar ratio of $SO4^{2-}$: NO^{3-} of 4.88: 1. These proportion and radio are some of the harsh conditions (not the harshest) seen many times in the acid rain in southern Chinese cities. We chose these conditions to verify the environmental tolerance of MSSIAC in harsh environments. A simulated seawater solution was prepared based on the actual salinity of offshore seawater, containing 3.5 % NaCl (w/w).

Experimental

The MSSIAC was set with reference to standard (EN 12390-2, 2000). The tested groups using MSSIA to replace sand were designed as shown in Table 1. Namely, seven groups of MSSIAC with different proportions of MSSIA were set. Each group of MSSIAC was cured in a 100 mm × 100 mm × 100 mm cubic concrete form. It is worth mentioning that, simply using MSSIA to replace sand without adding water will affect the fluidity of cement. Therefore, we added a certain proportion of water to keep the fluidity consistent. Four replicates were used for each group. All groups of MSSIAC were aged at room temperature. After 28 d, the UCS was calculated with reference to standard (EN 12390-3, 2001).

Table 1 Content of each component in MSSIAC tested groups

Groups	Water	Cement	Sand	Stone	MSSIA
C-0	9.0	22.4	22.0	46.7	0
C-5	9.2	22.4	20.9	46.7	0.84
C-10	9.5	22.4	19.8	46.7	1.68
C-15	9.7	22.4	18.7	46.7	2.52
C-20	10.0	22.4	17.6	46.7	3.36
C-25	10.2	22.4	16.5	46.7	4.2
C-50	11.5	22.4	11.0	46.7	8.4

Unit: w/w, %.

Based on the UCS results, the optimal MSSIAC formulation was selected for further tests of environmental tolerance under scenarios of simulated acid rain leaching, salt erosion, and freezing-thawing. According to the actual height of concrete pavement in China, 180 mm was selected as the height of the specimen for the simulated acid rain leaching test and salt erosion test.

The simulated acid rain leaching test were carried out in leaching columns (61 mm diameter, 180 mm height) with a spraying set-up that included a 25 L water tank and a drop filter. The optimal cylindrical MSSIAC was placed into the leaching columns, and simulated acid rain was continuously sprayed over the MSSIAC by controlling the drop filter. To mimic the most severe scenarios, the leaching experiment lasted for 60 d, which equaled 100 y of rainfall.

The salt erosion test was carried out in rectangular containers (80 mm length and width, 180 mm height). The optimal cylindrical MSSIAC was placed into the containers filled with simulated seawater, and sealed. The erosion experiment lasted for 42 d.

The freezing-thawing test was carried out in cylindrical containers (200 mm diameter, 110 mm height). The optimal cubic MSSIAC was placed into the containers filled with water. Each freezing-thawing cycle consisted of freezing at −20 °C for 12 h and thawing for 12 h at 25 °C, and the freezing-thawing experiment lasted for 42 cycles.

Analyses

The MSSIA moisture content and organic fraction was measured by standard methods (L. Hu et al., 2019). Heavy metals, including Cu, Pb, Cr, Cd, Ni, and Zn, were measured by atomic absorption spectroscopy (AAS, ZEEnit 700p, Germany) after acid (HCl-HNO_3-HF-$HClO_4$) digestion (J. Yao et al., 2017).

The MSSIA mineral and elemental compositions were determined by X-ray diffraction (XRD, Rigaku D/Max-Ⅲ A, Japan) and X-ray fluorescence (XRF, Axios-Advanced, Netherlands). The UCS of MSSIAC was measured according to standard EN 12390-3 using a hydraulic test machine. Each test was performed in triplicate, excluding the XRD and XRF.

Statistical analysis was performed with SPSS 22.0 software, and the standard deviation was obtained by descriptive statistics. A correlation analysis was performed using Tukey's test. Differences were considered to be statistically significant when $p < 0.05$.

RESULTS AND DISCUSSION

Characteristics of MSSIA and MSSIAC

The mineral and elemental compositions of MSSIA obtained from the XRD was shown in Fig. 1. The major mineral components in MSSIA were quartz and anhydrite, similar to coal ash and cement. The major components of MSSIA were SiO_2, Al_2O_3, Fe_2O_3, and CaO, with proportions of 10.3 %, 5.04 %, 15.4 %, and 34.1 %, respectively; these compounds are the main reactive components of pozzolan. It has been previously shown that MSSIA has pozzolanic activity, and the addition of MSSIA to concrete may increase concrete strength (Q. Wang et al., 2012).

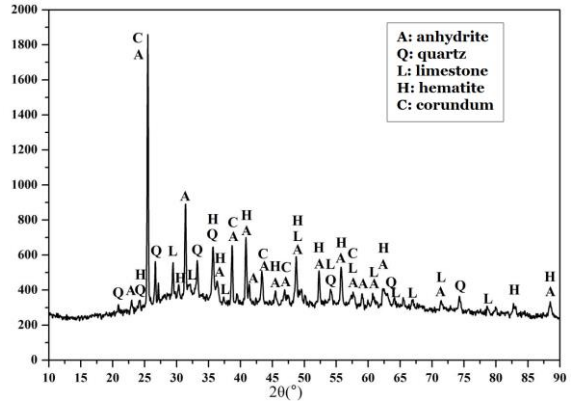

Fig. 1. XRD result of MSSIA.

In addition, decreasing the chloride and bromine contents in concrete can prevent damage caused by reinforcement corrosion (A.A. Naqvi et al., 2015; A.A. Naqvi et al., 2006). The contents of Cl and Br in MSSIA are 0.271 % and 0.026 % respectively, which indicates the MSSIA does not require pretreatment to reduce the corrosion risk. The results demonstrate that MSSIA not only has the mineral and elemental components similar to coal ash and cement and pozzolanic activity, but it also has low Cl and Br content and poses almost no corrosion risk to steel bars. Therefore, MSSIA has the potential to replace cement or aggregate raw materials and may be an ideal raw material for concrete.

With increasing amounts of MSSIA, the UCS increased then decreased (Fig. 2). With a MSSIA replacement rate of 5 %, sample C-5 has the highest UCS of 41.8 MPa, which is 7.2 % higher than the control sample, indicating that a small amount of MSSIA can increase UCS of concrete because of its pozzolanic activity (X. Xie et al., 2019; N. Saboo et al., 2019). With a MSSIA replacement rate of 10%, the UCS of C-10 was 32.7 MPa, 16.2 % lower than control sample, possibly because the increased proportion of MSSIA diluted the cement and hindered its normal cementation (M. Khan and M. Ali, 2019). However, the UCS of C-10 could still meet the requirements of commercial application. Higher proportions of MSSIA resulted in a further decrease in UCS, and at replacement rate greater than 15% (C-15 and above), the strength requirements for commercial applications were no longer met.

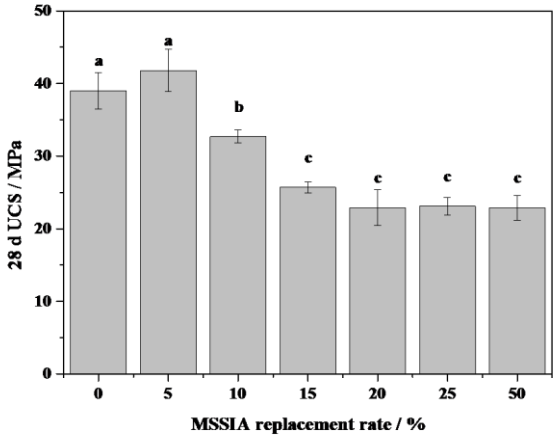

Fig. 2. UCS results of MSSIAC tested groups (The different letter indicates significant different at 0.05 level).

The sample C-5 has the highest UCS. Although the UCS of sample C-10 is hard compete with C-5, but it has a larger MSSIA capacity, which is good for the environment, and it maintains a commercially viable strength. Therefore, the samples C-5 and C-10 represented the optimal MSSIAC formulations. These samples balanced the required UCS and incorporation of some proportion of MSSIA, providing high application value.

Long - term environmental tolerance of optimal MSSIAC

To evaluate the long-term environmental tolerance of the optimal MSSIAC samples (C-5 and C-10), simulated acid rain leaching, salt erosion, and freezing-thawing were tested. C-0, containing no MSSIA, represented the control group. The Cu, Pb, Cr, Cd, Ni, and Zn contents of MSSIA were 4652 mg kg^{-1}, 600 mg kg^{-1}, 11.1 mg kg^{-1}, 0.00, 177 mg kg^{-1}, and 406 mg kg^{-1}, respectively. And the content of heavy metals in C-5 and C-10 are shown in Table 2.

Table 2 Content of heavy metals in C-5 and C-10

Heavy metals	Zn	Cr	Cd	Pb	Ni	Cu
C-5	39.1	5.04	0.093	0.00	1.49	3.41
C-10	78.2	10.1	0.186	0.00	2.97	6.82

Unit: mg kg^{-1}.

The content of heavy metals in the acid rain leaching tests of the control, C-5, and C-10 samples are shown in Fig. 3a, 3b, and 3c, respectively. No heavy metals except Zn were detected in the leachate representing 100 y of acid rain, which could be because MSSIA has a higher concentration of Zn compared with other heavy metals, but could also be a result of the solidification mechanism of cement (W. Ma et al., 2019). The cementitious components in cement can combine with heavy metals during solidification, and Zn is more reactive and more easily released under acidic conditions compared with other heavy metals. The results from the acid rain leaching test also show that MSSIAC can stabilize heavy metals, and the environmental risk of release of heavy metals from MSSIAC through acid rain leaching is low.

The concentration of released Zn reached maximum values of 0.066 mg L^{-1} on year 55 of the acid rain leaching test for C-0, 0.071 mg L^{-1} on year 5 for C-5, and 0.070 mg L-1 on year 5 for C-10. The experimental groups (C-5 and C-10) released the highest Zn concentrations at the first sampling point, which may be because some metal ions that were not completely solidified were released at the first sampling point. After this, the release of Zn slowed and the concentration fluctuated in a lower range. There was no significant difference in the concentration of Zn released by the three MSSIAC groups, and the concentration of Zn released was very low under all conditions and almost equal to that of normal surface water. These results demonstrate that acid rain will not threaten the stability of MSSIAC.

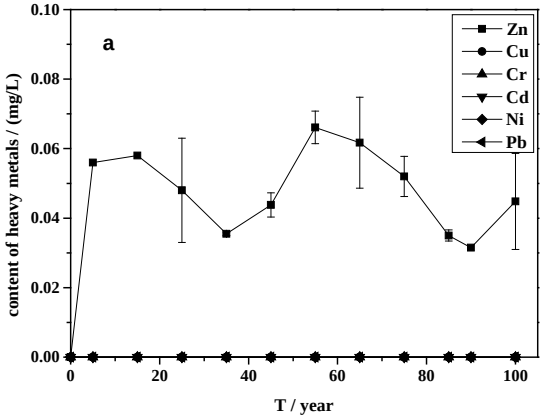

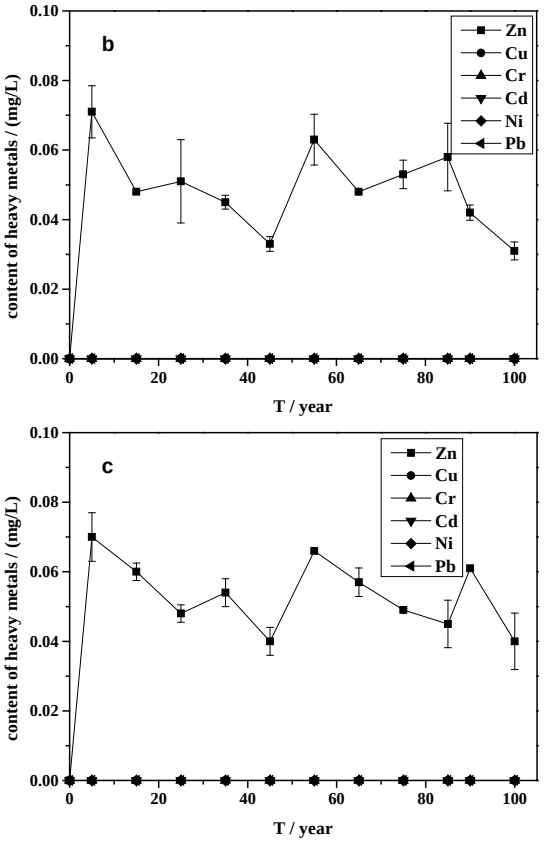

Fig. 3. The heavy metals contents in acid rain leaching test result of MSSIAC (a, b, and c mean the control, the C-5, and the C-10, respectively)

The accumulated Zn amounts for the three test groups is shown in Fig. 4a. There was no significant difference between the accumulated Zn amounts for the control and C-5 group, because of the low initial concentration of heavy metals and the stable solidification effect. C-10 group containing a higher amount of MSSIA so that C-10 had a higher accumulated Zn amount compared with the control. The source of the additional Zn is the MSSIA addition. Therefore, the ratio of the extra Zn released to the total C-10 content were calculated, and a linear curve was used to fit the cumulative ratio in Fig. 4b, which shows that it may take approximately 9,076 years for the Zn to be fully released. The service life of ordinary Portland concrete is about 120 years (S. Demis and V.G. Papadakis, 2019), and MSSIAC will have a low heavy metal release and excellent environmental safety during this period. Even after the approximate 9,076 years, after the Zn is fully released, the leachate concentration remains at a safe level, below the highest level of EU surface water quality standards. Therefore, MSSIAC has excellent long-term environmental tolerance under simulated acid rain leaching conditions.

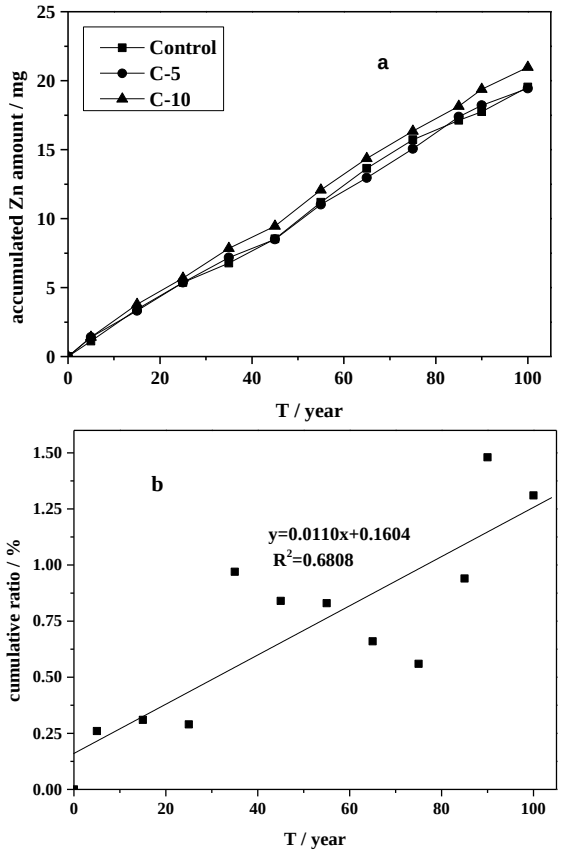

Fig. 4. a, the accumulated Zn amount from three MSSIAC groups; b, the cumulative ratio of the extra Zn released to total C-10 content.

The impact of salt erosion and freezing-thawing scenarios on MSSIAC results are shown in Table 3. The high salt content of seawater can erode the concrete structure, and the concrete may start to release heavy metals (V. Marcos-Meson et al., 2018). The freezing-thawing process freezes the free water in the pores of concrete, causing volume expansion and can damage the internal structure of concrete, also causing the concrete to release heavy metals (M.K. Ismail and A.A.A. Hassan, 2019). In this study, all heavy metal concentrations were below the method detection limit in both the salt erosion and freezing-thawing tests (Table 3). The heavy metals may have been immobilized in the concrete in very stable states, such as residual states. Salt erosion and freezing-thawing, which damage the physical structure of the concrete, may only release the heavy metals in less stable states, without affecting the heavy metals immobilized in stable states. These results indicate that MSSIAC can effectively stabilize heavy metals, and protect them from release under extreme environmental conditions such as salt erosion and freezing-thawing, adding MSSIA does not increase the risk of heavy metal release from concrete.

Table 3 Salt erosion and freezing-thawing test results

Salt erosion test						
Days	Zn	Cr	Cd	Pb	Ni	Cu
0	ND[a]	ND	ND	ND	ND	ND
7	ND	ND	ND	ND	ND	ND
14	ND	ND	ND	ND	ND	ND
21	ND	ND	ND	ND	ND	ND
28	ND	ND	ND	ND	ND	ND
35	ND	ND	ND	ND	ND	ND
42	ND	ND	ND	ND	ND	ND
Freezing-thawing test						
Days	Zn	Cr	Cd	Pb	Ni	Cu
0	ND	ND	ND	ND	ND	ND
7	ND	ND	ND	ND	ND	ND
14	ND	ND	ND	ND	ND	ND
21	ND	ND	ND	ND	ND	ND
28	ND	ND	ND	ND	ND	ND
35	ND	ND	ND	ND	ND	ND
42	ND	ND	ND	ND	ND	ND

a: ND means not detection.

CONCLUSIONS

As the proportion of MSSIA in concrete increased, the MSSIAC UCS first increased and then decreased. A replacement of 5% MSSIA resulted in a 7.2% increase in UCS (C-5), while a replacement of 10% MSSIA resulted in a 16.2% decrease in UCS (C-10). Only Zn was released from the optimal MSSIAC formulations (C-5 and C-10) in the acid rain leaching test, but at its highest concentration, only 0.071 mg L^{-1} was detected, within the acceptable range. No heavy metal release concentrations were above the method detection limit in both the salt erosion and freezing-thawing tests. The optimal MSSIAC has excellent long-term environmental tolerance while meeting the requirement of UCS, and represents a valuable use of MSSIA.

ACKNOWLEDGEMENTS

This work was funded by the Key R&D Program of Zhejiang Province (Number: 2020C03086), the Basic public research Plan Projects of Zhejiang Province (Number: LGC19E080001), National Undergraduate Training Program on Innovation and Entrepreneurship (Number: 201910353045, 202010353049), and Zhejiang Gongshang University students innovation and entrepreneurship training program (Number:

CX201923001, CX201923012).

REFERENCE

A.A. Naqvi, M. Maslehuddin, K. ur-Rehman, O.S.B. Al-Amoudi, 2015. Chlorine signal attenuation in concrete. Appl. Radiat. Isot. 105, 6-10.

A.A. Naqvi, M.M. Nagadi, O.S.B. Al-Amoudi, 2006. Prompt gamma analysis of chlorine in concrete for corrosion study. Appl. Radiat. Isot. 64, 283-289.

A. Kelessidis, A.S. Stasinakis, 2012. Comparative study of the methods used for treatment and final disposal of sewage sludge in European countries. Waste Manage. 32, 1186-1195.

C.J. Lynn, R.K. Dhir, G.S. Ghataora, 2018. Environmental impacts of sewage sludge ash in construction: Leaching assessment. Resour., Conserv. Recycl. 136, 306-314.

EN 12390-2, 2000 Testing hardened concrete - Part 2: Making and curing specimens for strength tests, 2000.

EN 12390-3, 2001 Testing hardened concrete - Part 3: Compressive strength of test specimens, 2001.

G. Rutkowska, P. Wichowski, J. Fronczyk, M. Franus, M. Chalecki, 2018. Use of fly ashes from municipal sewage sludge combustion in production of ash concretes. Constr. Build. Mater. 188, 874-883.

J.-s. Li, Q. Xue, L. Fang, C.S. Poon, 2017. Characteristics and metal leachability of incinerated sewage sludge ash and air pollution control residues from Hong Kong evaluated by different methods. Waste Manage. 64, 161-170.

J. Yao, Z. Qiu, Q. Kong, L. Chen, H. Zhu, Y. Long, D. Shen, 2017. Migration of Cu, Zn and Cr through municipal solid waste incinerator bottom ash layer in the simulated landfill. Ecol. Eng. 102, 577-582.

L. Chen, D.-F. Lin, 2009. Stabilization treatment of soft subgrade soil by sewage sludge ash and cement. J. Hazard. Mater. 162, 321-327.

L. Hu, W. Wang, Y. Long, F. Wei, Z. Nie, C. Fang, 2019. Fate and migration of arsenic in large-scale anaerobic landfill. Waste Manage. 87, 559-564.

M. Khan, M. Ali, 2019. Improvement in concrete behavior with fly ash, silica-fume and coconut fibres. Constr. Build. Mater. 203, 174-187.

M.K. Ismail, A.A.A. Hassan, 2019. Abrasion and impact resistance of concrete before and after exposure to freezing and thawing cycles. Constr. Build. Mater. 215, 849-861.

M. Skowrońska, E.J. Bielińska, K. Szymański, B. Futa, J. Antonkiewicz, B. Kołodziej, 2020. An integrated assessment of the long-term impact of municipal sewage sludge on the chemical and biological properties of soil. CATENA. 189, 104484.

N. Saboo, S. Shivhare, K.K. Kori, A.K. 2019. Chandrappa, Effect of fly ash and metakaolin on pervious concrete properties. Constr. Build. Mater. 223, 322-328.

O. Krüger, C. Adam, 2015. Recovery potential of German sewage sludge ash. Waste Manage. 45, 400-406.

P. Das, S. Khan, M. AbdulQuadir, M. Thaher, M. Waqas, A. Easa, E.S.M. Attia, H. Al-Jabri, 2020. Energy recovery and nutrients recycling from municipal sewage sludge. Sci. Total Environ. 715, 136775.

Q. Wang, J. Feng, P. Yan, 2012. The microstructure of 4-year-old hardened cement-fly ash paste. Constr. Build. Mater. 29, 114-119.

R. Siddique, 2010. Utilization of municipal solid waste (MSW) ash in cement and mortar. Resour., Conserv. Recycl. 54, 1037-1047.

S. Chakraborty, B.W. Jo, J.H. Jo, Z. Baloch, 2017. Effectiveness of sewage sludge ash combined with waste pozzolanic minerals in developing sustainable construction material: An alternative approach for waste management. J. Cleaner Prod. 153, 253-263.

S. Demis, V.G. Papadakis, 2019. Durability design process of reinforced concrete structures - Service life estimation, problems and perspectives. J. Build. Eng. 26, 100876.

S. Donatello, M. Tyrer, C.R. Cheeseman, 2010. EU landfill waste acceptance criteria and EU Hazardous Waste Directive compliance testing of incinerated sewage sludge ash. Waste Manage. 30, 63-71.

S. Ledakowicz, P. Stolarek, A. Malinowski, O. Lepez, 2019. Thermochemical treatment of sewage sludge by integration of drying and pyrolysis/autogasification. Renewable Sustainable Energy Rev. 104, 319-327.

V. Marcos-Meson, A. Michel, A. Solgaard, G. Fischer, C. Edvardsen, T.L. Skovhus, 2018. Corrosion resistance of steel fibre reinforced concrete - A literature review. Cem. Concr. Res. 103, 1-20.

W. Ma, D. Chen, M. Pan, T. Gu, L. Zhong, G. Chen, B. Yan, Z. Cheng, 2019. Performance of chemical chelating agent stabilization and cement solidification on heavy metals in MSWI fly ash: A comparative study. J. Environ. Manage. 247, 169-177.

X. Xie, Q. Feng, Z. Chen, L. Jiang, W. Lu, 2019. Diffusion and distribution of chloride ions in carbonated concrete with fly ash. Constr. Build. Mater. 218, 119-125.

Z. Chang, G. Long, J.L. Zhou, C. Ma, 2020. Valorization of sewage sludge in the fabrication of construction and building materials: A review. Resour., Conserv. Recycl. 154, 104606.

Z. Chen, C.S. Poon, 2017. Comparative studies on the effects of sewage sludge ash and fly ash on cement hydration and properties of cement mortars. Constr. Build. Mater. 154, 791-803.

Z. Chen, J.S. Li, C.S. Poon, 2018. Combined use of sewage sludge ash and recycled glass cullet for the production of concrete blocks. J. Cleaner Prod. 171, 1447-1459.

INFLUENCE OF SPECIFIC SURFACE RATE OF CEMENT SOLIDFIED FLY ASH ON LEACED AMAUNT OF SOLUBLE SUBUSTANCES

Yutaka Dote[1], Tomoo Sekito[1]
1 Faculty of Engineering, University of Miyazaki, Gakuen Kibanadai Nishi 1-1, Miyazaki, Japan

ABSTRACT
Tank leaching tests with different size of cubic solidified air pollution control residue (APCR) and cylindrical solidified APCR were conducted to evaluate the effect of size of solidified APCR on leaching rate and the applicability of leaching mode. it was found that increasing the specimen size could decrease the leaching rate per weight of solidified ARCP. It is suggested that the surface dissolution model might need to be improved.

INTRODUCTION
In Japan, the incineration rate of municipal solid waste (MSW) was reached to 80% in 2018[1)] and air pollution control residue (APCR) from MSW incineration contains highly soluble salts, causing high concentration of salts in leachate. The high concentration of soluble salts in leachate affects water quality and water use in receiving water body. Therefore, it is required to reduce the concentration of salts in leachate.

On the other hand, the stabilization of APCR is required because of hazardous heavy metals in APCR. Although solidification with cement is used for stabilizing APCR cannot insolubilize the salts, it can decrease the mobile speed of salts through the solidified APCR by its dense structure. Two mechanisms of salt leaching from solidified APCR have been reported: diffusion dissolution at the surface of solidified APCR. Both phenomena are affected by the surface area of solidified APCR. Therefore, it is expected that increase in volume of solidified APCR can decrease the leaching rate per weight of solidified APCR.

The objectives of this study were to evaluate the effect of volume of solidified APC residue on the leaching rate of salts per weight of solidified APC residue by tank leaching tests. And the applicability of the one-dimensional model to solidified APC residue was considered using cylindrical solidified APC residue.

EXPERIMENTAL
APC residue and solidified specimen
APC residue was sampled from an MSW incineration plant in Miyazaki city, Japan. This facility configured mechanical grate furnace, with flue gas treatment using activated carbon and $Ca(OH)_2$.

The solidified specimen was prepared with the APC residue(A), Portland cement(C) and water(W) according to the following ratio in duplicate: C/A, 20% and W/(A+C), 40%. The mixture was homogenized, poured into a cubic mold with 4, 6, or 8 cm each side or a cylindrical mold with 5 cm ϕ x10 cm long, and then rapped with a thin plastic film. After 7 days curing, one of the duplicates was used for tank leaching test, and the other was dried, ground, and then used for serial batch test. For a tank leaching test, the bottom and side of cylindrical solidified specimen were sealed with a water-proofing agent.

Tank leaching test
A tank leaching test was performed with distilled water: for cubic solidified specimen, 0.6 L for 4 cm specimen, 1.2 L for 6 cm specimen, and 2.3 L for 8 cm specimen; and for cylindrical solidified specimen, 1.5 L. The solution was renewed after 0.125, 0.25, 0.5, 1, 2, 4, 8, and 16 days. An aliquot of leachate was filtered with 0.45 μm membrane filters.

Serial batch test (SBT)
Serial batch test was performed with 10 g of samples and 400 mL of distilled water in a centrifugal tube. After shaking at 200 rpm for 6 hrs, it was centrifuged at 5,000 G, and then supernatant was recovered and filtered. Distilled water of 300 mL was added the centrifugal tube having the residuals, and the same leaching and separation was repeated for three times.

Analytical method
Concentrations of Na and K in solution were determined by atomic adsorption, concentration of Cl by colorimetry with mercury thiocyanate, and porosity of solidified PC residue by mercury porosimetry.

RESULTS AND DISUCUSSION
Characteristics of S/S samples
Table 1 shows the leaching amounts of salt by SBT. For each element, the leaching amounts were almost the same between the specimens.

Effect of specimen size

The leaching rate per specimen weight, LR (g/(kg･day) calculated by Equation 1, for cubic specimen, defined by Equation 1 are shown in Figure 1.

$$LR = \frac{M_i - M_{i-1}}{t_i - t_{i-1}} \quad \cdot\cdot (1)$$

where M_i is the cumulative leaching amount of salt at the i th sampling, and t_i is the elapsed time at the i th sampling. For each element, the LR decreased with increase in the specimen size. The effect of specimen size was clear especially at 0.124 day, and negligible after 4 days. It indicates that increasing the specimen size could decrease the concentration of salts in leachate. In addition, the highest LR appeared at the beginning of leaching test, which indicates that in actual landfill site, it is expected that the concentration of salts in leachate would become the highest at the beginning of landfilling the solidified APCR.

Applicability of the one-dimensional model

The following leaching model[2] was considered:

$$M = Q_0(1 - e^{-kt}) + 2SC_0\sqrt{\frac{D_e t}{\pi}} \quad \cdot\cdot (2)$$

where M was the cumulative leaching amount of salt (g/kg), Q_0 is the initial amount of salt content in solidified APCR (g/kg), k is a surface dissolution rate constant (1/s), S is the specific surface area of solidified APCR (m^2/kg), C_0 is the initial concentration of salt in solidified APCR (g/m^3), D_e is the effective diffusion coefficient of salt (m^2/s), and t is elapsed time (s). In this study, the leaching amounts of salt by SBT were used as the values of Q_0. The model parameters D_e and k, were determined by tank leaching tests using cylindrical solidified APCR to minimize the residual sum of squares between observed and calculated M. Obtained parameters are summarized in Table 2. The correlation coefficients (R^2) of Na, K, and Cl indicated that the experimental data could fit well into the model. Figure 2 shows the calculated and observed values of the fraction of the cumulative leaching amount calculated by M_i-M_{i-1}. At the beginning of leaching test, the calculated fraction was lower than the observed one for each element. It suggests that the surface dissolution model might need to be improved.

CONCLUSIONS

The tank leaching tests with different size of cubic solidified APCR showed increasing the specimen size could decrease the concentration of salts in leachate. The tank leaching tests with cylindrical solidified APCR suggested that the surface dissolution model used might need to be improved.

RERERENCES

1)Ministry of the Environment: Municipal solid waste emissions and disposal in FY2018

2)K. Suzuki, Y. Ono： Leaching characteristics of stabilized/solidified fly ash generated from ash-melting plant, Chemosphere, Vol.71, pp.922-932, 2008

Table 1 Leaching amounts of salt by SBT (g/kg)

Specimen	Na	K	Cl
Cubic-4cm	18.4	20.6	98.1
Cubic-6cm	19.1	21.4	106
Cubic-8cm	20.0	21.5	103
Cylinder	20.2	23.1	118

Table 2 Obtained parameters

	Na	K	Cl
k (1/s)	2.0×10^{-9}	2.8×10^{-9}	4.8×10^{-9}
D_e (m^2/s)	1.9×10^{-10}	2.7×10^{-10}	1.4×10^{-10}
R^2 (-)	0.9989	0.9993	0.9994

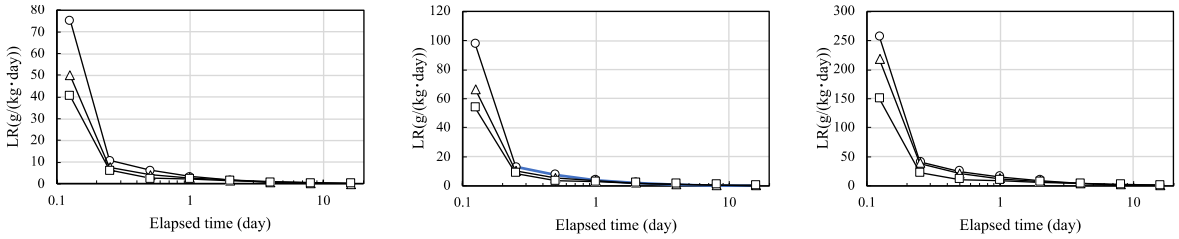

a) Na b) K c) Cl

Figure 1 Leaching rate per specimen weight from solidified PAC residue: ○, 4 cm; △, 6 cm; and □, 8 cm

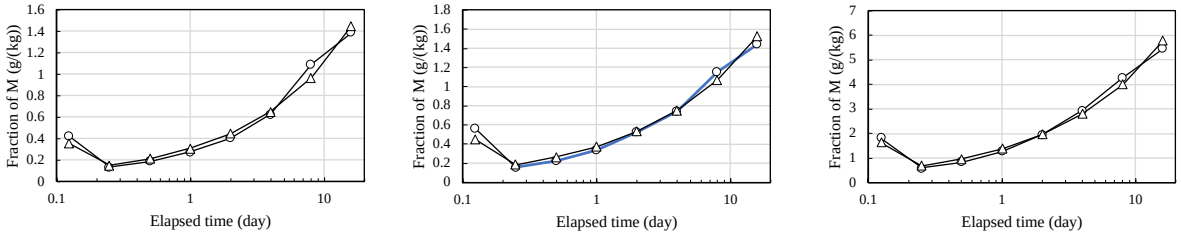

a) Na b) K c) Cl

Figure 2 Fraction of the cumulative leaching amount per specimen weight: ○, observed; and △, calculated

Incineration disposal of organic waste bio-residue via a deep dewatering process using refuse incineration bottom ash: moisture transfer and low calorific value improvement

Ran Wei[a], Ruina Zhang[b], Lijie Song[b], Xiong Zhou[c], Shunhong Lin[c], Youcai Zhao[a,d], Tao Zhou[a,d*]

a. The State Key Laboratory of Pollution Control and Resource Reuse, School of Environmental Science and Engineering, Tongji University, 1239 Siping Road, Shanghai 200092, China
b. Shanghai Environmental Sanitation Engineering Design Institute Co., Ltd, Shilong Road, Shanghai 200232, PR China
c. School of Mechanical and Power Engineering, Chongqing University of Science and Technology, 20 East Daxuecheng Road, Chongqing 401331, China
d. Shanghai Institute of Pollution Control and Ecological Security, 1515 North Zhongshan Rd. (No. 2), Shanghai 200092, PR China

Abstract: Bio-residue is a by-product from organic waste anaerobic digestion process with high moisture, high organic matter, low calorific value and poor biological stability, and may be incinerated after deep dewatering. The moisture existence forms of bio-residue were clarified firstly, finding that adsorbed water, capillary water and bound water occupied 75.61%, 23.81% and 0.58%, respectively. Furthermore, refuse incineration bottom ash was used as a typical deep dewatering reagent, while compared with calcium oxide (CaO), refuse incineration fly ash, and iron powder-potassium persulfate (Fe(0)-$K_2S_2O_8$). Results showed that the addition of bottom ash powder could decrease the bio-residue's moisture from 80.0% to 37.9% at the optimal dosage of 2.0%, and corresponding low calorific value reached to 10.5 MJ/kg at the 10^{th} d. It was suggested that $ZnCl_2$ and $ZnSO_4$ present in bottom ash powder could react with moisture in bio-residue, forming hydrates of inorganic salt and breaking the polyacrylamide colloid, and lead to the release of adsorbed water in the bio-residue.

Keywords: Anaerobic digestion; Organic residue; Moisture forms; Moisture release; Incineration waste; Dewatering mechanism

1 Introduction

Organic solid waste, with a huge quantity around the world, refers to solid waste contains organic components produced by human activities, and may include fruit peel, rotten vegetable leaves, eggshells, rice, flour, vegetable oil, animal oil, meat and bone, and so on. With the increase of world population, the generation of organic waste, such as food and kitchen waste, garden waste, crop residue and animal manures, is increased (Singh et al. 2014; Mata-Alvarez et al. 2000; Tella et al. 2013; Wei et al. 2021). Around 30%-40% of municipal solid waste in China consists of organic waste, with an annual quantity of around 110 million and possibly several billion of tons globally (Zhao 2020), which have caused a worldwide crisis (Arun and Sivashanmugam 2017; Guo et al. 2021).

The common organic waste treatment and disposal technologies include anaerobic digestion and aerobic composting. Anaerobic digestion is a highly effective technique for the disposal of agricultural residues, organic solid waste, food waste and sludge, and has been widely used as an ideal method for the waste disposal in recent years (Hu et al. 2022). In the anaerobic digestion process, anaerobic fermentation bacteria, hydrogen-producing acetic acid bacteria and hydrogen-consuming acetic acid bacteria are used to degrade complex organic matter into methane, carbon dioxide and other gases, achieving harmlessness and resource utilization (Yu et al. 2020). During anaerobic digestion process, biogas that is rich in methane and carbon dioxide is produced, which could be used as a fuel for combustion in transport or energy production, leaving the bio-residue for treatment further. Most organic substance in organic waste such as sugar, fat and protein has been decomposed and transferred into the biogas slurry, leaving the bio-residue with high moisture, high organic matter, low

calorific value and poor biological stability that should be properly treated.

In the current technological process of organic waste anaerobic digestion plant, bio-residue is treated by polyacrylamide (PAM) for dewatering. Polyacrylamide is a water-soluble polymer, and commonly used as the thickeners, viscosity modified reagents or flocculant (Li and Ni et al. 2020). Hundreds of millions of dollars per year on polyacrylamides are spent for the conditioning and dewatering of wastewater sludge. Polyacrylamide is also widely used in many industrial processes such as dewatering of sludge, treatment of wastewater and production of paper. After treated by polyacrylamide, the bio-residue will be disposed of by incineration along with municipal solid waste. However, because of the moisture holding capacity of polyacrylamide, the moisture of organic waste bio-residue can only be decreased to about 80%, which is still not suitable for incineration. Therefore, deep dewatering by certain reagents to reduce the moisture further and improve low calorific value is necessary before incineration. (Šyc et al. 2020; Chen et al. 2020; Wan et al. 2018).

To study the deep dewatering of bio-residue, it's necessary to research its moisture types. It is generally considered that the moisture in organic waste may be categorized into four types, i.e., free water, adsorbed water or surface water, interstitial water or capillary water, and cell water or bound water, as done for sewage sludge (Tsang and Vesilind 1990), and can be measured by thermal gravity - differential thermal analysis (TG-DTA) (Katsiris 1987; Willard 1988) and thermal drying method (Smollen 1986). Moisture content is the key factor influencing the performance of sludge incineration, including combustion completeness, energy recovery and pollutant emission (Xiao et al. 2015). Before mechanical dehydration of municipal sludge, some pretreatments are usually used to strengthen its dehydration property. The main pretreatment methods

include chemical conditioning (Mahmood 2007; Novak 2006), hydrothermal treatment (Neyens 2003; Jomaa 2003), and ultrasound treatment (Dewil 2006; Bien 1997).

There are many reagents that can be used for deep dewatering. Calcium oxide, a conventional dewatering reagent, is usually applied into municipal sludge for strengthening the process of dehydration and raise the thermal drying efficiency. General speaking, drying the sludge with 80% moisture content by adding CaO (sludge : CaO =10:3, w/w) can raise the drying rate by 20%, compared with sludge only. Persulfate is also used as oxidant for strengthening dehydration of sewage sludge. Persulfate salt is stable under the ordinary condition. However, under the condition of heating, irradiation with light and transition metal ions (Fe^{2+}, Cu^{2+}, Ag^{+}, Mn^{2+}), persulfate can be activated and produce SO_4-· and ·OH. Under the ordinary temperature and pH 3.0-8.5, persulfate is used to treat sludge activated by Fe^{2+}, and the dehydration performance of organic waste and sludge can be thus improved (Zhen 2012).

Bottom ash is a by-product from municipal solid waste incineration (Wiles 1995), mainly composed of slag, black and non-ferrous metals, ceramic chips, glass and other non-combustible organic matter (Zhu et al. 2020). Although the presence of heavy metals confines the use of bottom ash in further applications, some of it is used in applications such as road sub-base material, aggregate in concrete, clay brick and pavement, but most are currently landfilled (Loginova et al. 2021; Zhu et al. 2019). The incineration bottom ash of sludge was used with CPAM (cationic polyacrylamide) to dewater the sludge and the result showed that its effect of dehydration was better than any single reagent (Ning 2013). The effects of CaO, coal ash, diatomite, sodium dodecyl sulfate and municipal solid waste incineration fly ash on dehydration of sludge were compared, and it was found that the dehydration effect of CaO was the best and

next were coal ash, diatomite, sodium dodecyl sulfate and municipal solid waste incineration fly ash, respectively (Zhu 2012).

The purpose of this study was to research the deep dewatering of organic waste bio-residue for improvement of low calorific value, which was convenient for incineration. The moisture form of bio-residue was studied by thermal drying, vacuum filtration and thermal gravity analysis. The effects of CaO, Fe(0)-$K_2S_2O_8$, bottom ash and fly ash powder on deep dewatering of bio-residue were compared, and different dosages of bottom ash powder's influence on deep dewatering of bio-residue were analyzed in detail, combining with XPS analysis of bottom ash powder. Finally, the bio-residue treated with bottom ash powder was observed under the electron microscope after drying, for making the mechanism of deep dewatering clear. Meanwhile, economic analysis was given for estimating reagents' benefits.

2 Materials and methods

2.1 Materials

The original bio-residue is in slurry, and sent to the treatment process after treated by polyacrylamide. The bio-residue used in this study, which was black and smelly, was collected from the end centrifugal dehydrator of bio-residue treatment process line in an organic waste anaerobic digestion plant in *Shanghai, China*. The characteristics of original bio-residue treated by polyacrylamide are shown in **Table 1**. It can be seen that the moisture content of bio-residue was about 78.4% and the organic matter content of dried bio-residue was about 42.0%, with predominant elements C and O of 20.4% and 29.5%, respectively. The low calorific value of dried bio-residue was 13.32 MJ/kg, much higher than that required for incineration, and was increased much after drying.

Table 1 Characteristics of bio-residue used in this study

Item		Value
Moisture		78.40 %
Organic matter content (dry basis)		42.03 %
Low calorific value (wet basis)		0 MJ/kg
Low calorific value (dry basis)		13.32 MJ/kg
Element content	N	0.00 %
	C	20.41 %
	H	2.78 %
	S	0.34 %
	O	29.46 %

The main reagents, including calcium oxide (CaO), iron powder (Fe^0) and potassium persulfate ($K_2S_2O_8$) were purchased from Aladdin deposits in *Shanghai*, *China*. All reagents were of analytical grade and used without any pretreatment. Bottom ash and fly ash were taken from a municipal solid waste incineration plant and pretreated into powder (60-80 mesh) by the crusher.

2.2 Experimental design

2.2.1 Reagents comparison

The pre-experiment for bio-residue's deep dewatering was conducted in 1000 mL plastic containers, and each container contained 500 g of bio-residue. Four experiment groups with 2.0% dosage of different dewatering reagents were set for investigating each reagent's dewatering capacity. The bio-residue and reagents were mixed fully, and all the containers were placed in a calm place for 14 days, avoiding disturbed by wind. The treated bio-residue were sampled in two copies every other day, and one copy of the samples was dried in the oven with 101 ℃-105 ℃ until reaching a constant weight, with the weights recorded before and after drying. The other copy of the samples was used for low calorific value test. For avoiding reagents reacting directly, the iron powder and potassium persulfate were added in order, and their proportions were based on the reaction of Eq. (1):

$$Fe^0 + 2S_2O_8{}^{2-} \rightarrow 2SO_4 \cdot^- + Fe^{2+} + 2SO_4{}^{2-} \quad (1)$$

2.2.2 Bottom ash curing

The detailed curing experiments for bio-residue's deep dewatering by bottom ash powder were conducted on hollowing boards, which would not let the bio-residue leak through the hole. Five experiment groups were set with dosage of 1.0%, 2.0%, 3.0%, 4.0% and 5.0%, respectively. Each hollowing board loaded 100 g bio-residue, which was mixed fully with bottom ash powder, and the treated bio-residues were made into cubes (about 5 cm×5 cm×2 cm). Also, all the hollowing boards were placed above a vacant plastic container in a calm place for 14 days, avoiding disturbed by wind. The bio-residue were sampled in two copies every other day, and one copy of the samples was dried in the oven with 101 ℃-105 ℃ until reaching a constant weight, with the weights recorded before and after drying. The other copy of the samples was used for low calorific value test.

2.3 Analytical methods

Most of the moisture content in bio-residue was measured by the oven (DHG-9240A) with 101 ℃-105 ℃. In order to obtain the contents of different moisture forms, three steps were conducted: i) thermal drying was used for measurement of the whole moisture except for bound water. ii) vacuum filtration was used for measurement of capillary water. 100 g of bio-residue was compacted in the Büchner funnel in the form of pie. The vacuum pump (SHZ-D(III)) was connected with Büchner funnel and carried on until the vacuum degree of filtration container became zero; iii) thermal gravity analysis was used for measurement of bound water.

For evaluating the effect of reagents on bio-residue incineration performance, low calorific values were tested and analyzed. In this study, 1.0 g samples were taken to the automatic calorimeter (ZDHW-6L) for measurement. In order for comparison, the low

calorific value of original bio-residue treated by polyacrylamide was also tested and analyzed during the bottom ash powder curing experiment.

Organic matter content of bio-residue was measured by weighing method with the muffle furnace (SX2-5-12Y). After treated by bottom ash powder, the bio-residue was dried and observed for its micro structure by electron microscope (Phenom Pro). The X-ray photoelectron spectroscopy (XPS) characterizations of bottom ash and fly ash powder were done with a Kratos AXIS 165 electron spectrometer with monochromatic AlKa radiation at 100 W and high-resolution measurements in S 2p, Cl 2p, K 2p, Ca 2p, O 1s, F 1s, Zn 2p and Na 1s regions were used. Thermal analysis (TGA-DTG) of bio-residue was recorded on a thermal analysis system (Q600 SDT; TA Instruments, USA) over a temperature range of 25-600 °C with a heating rate of 5 °C/min in an N_2 stream. Elemental analysis of N, C, H, S and O of bio-residue was performed using an elemental analyzer (Vario EL III, Germany).

3 Results and Discussion

3.1 Moisture existence forms in bio-residue

The vacuum filtration experiments were conducted in triplicate, and the results are shown in **Table 2**. The weight of moisture removed by filtration was about 20 g, which cannot be removed easily by gravity. Drawing on the experience of sludge's moisture form, the capillary water in sludge could be removed by negative pressure (vacuum filter). Therefore, this part of moisture in bio-residue was identified as capillary water.

Table 2 Vacuum filtration experiment results (Unit: g)

No.	Initial weight	Weight of water removed by filtration (w_1)	Weight loss of drying (w_2)	w_1/w_2 (%)
1	100.0	20.5	84.3	24.32
2	100.0	19.3	85.1	22.68
3	100.0	20.6	84.3	24.44

For analyzing the moisture form in bio-residue, thermo-gravimetric analysis of dried bio-residue was conducted, and the result is shown in **Fig. 1**. When the temperature reached to 306.96 ℃, the $\frac{dw}{dT}$ reached to the maximum value and the dried bio-residue started to burn. The dewatering happened between 162.90 ℃ and 213.74 ℃, and the weight loss was about 3.16% of bio-residue (dry basis). According to the moisture content of bio-residue (wet basis), the weight loss between 162.90 ℃ and 213.74 ℃ was about 0.58% of the whole moisture in bio-residue. This part of moisture couldn't be removed by low-temperature thermal drying, which was identified as bound water. Bio-residue, coming from digested organic waste, was different from municipal sludge. Due to the utilization of polyacrylamide for dewatering, it can adsorb moisture and form colloid, which makes a large amount of moisture stored in the polyacrylamide colloid as adsorbed water. Therefore, the moisture in bio-residue could be classified into adsorbed water, capillary water and bound water, which occupied 75.61%, 23.81% and 0.58%, respectively.

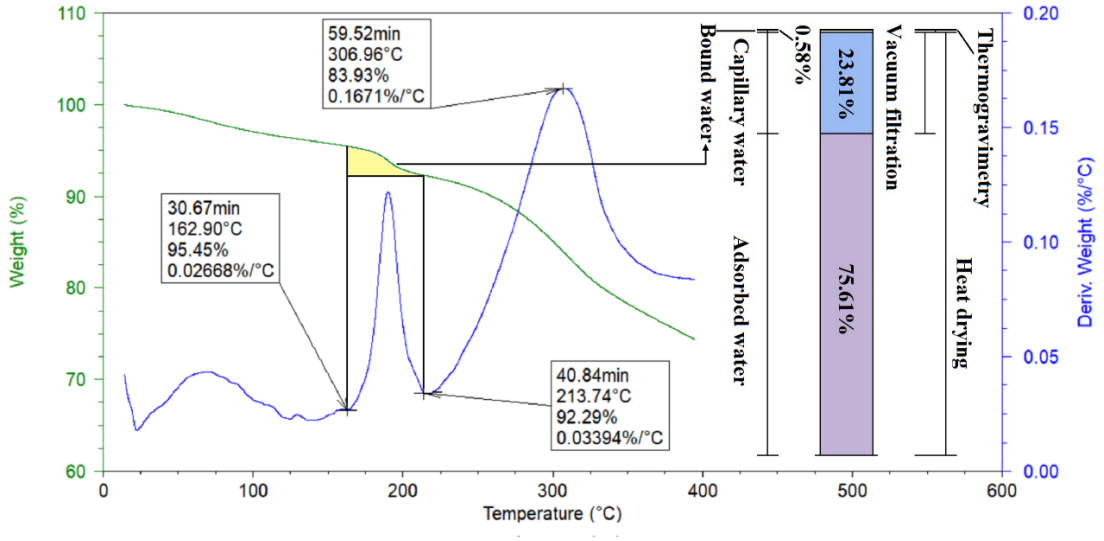

Fig. 1 Thermo-gravimetric analysis of dried bio-residue and moisture form definition of bio-residue

3.2 Dewatering capacity of different reagents

In bio-residue, the moisture was classified into adsorbed water, capillary water and bound water, which occupied 75.61%, 23.81% and 0.58%, respectively. Among these moisture types, adsorbed water had the largest proportion, which was the most possible moisture to be dewatered. The content of bound water was small, which could be ignored in practical engineering. The adsorbed water and capillary water were the main impediments for bio-residue's dewatering, and were removed hardly before treated by reagents.

The variations of moisture content and low calorific value with different dewatering reagents at the dosage of 2.0% were conducted. As shown in **Fig. 2(a)**, it can be seen that at the dosage of 2.0%, the moisture content decreased over the curing time. At the 4^{th} d, the moisture contents of four groups with CaO, bottom ash powder, fly ash powder and Fe(0)-$K_2S_2O_8$ were 69.17%, 61.34%, 72.00% and 65.39%, respectively, and bottom ash powder's excellent dewatering capacity was justified. After 8 days' curing, the moisture content of four groups decreased sharply, and reached to 67.94% (CaO), 66.20% (bottom ash powder), 71.50% (fly ash powder) and 68.84% (Fe(0)-$S_2O_8^{2-}$) at the 8^{th} d, respectively. Taking CaO group as example, the moisture content of bio-residue decreased from 78.4% to 43.3% after 14 days' treatment. The moisture loss was about 40.34 g, accounting for 51.5% of the whole moisture. According to the moisture proportion and characteristics of bio-residue, the dewatering treatment mainly removed the adsorbed water in bio-residue.

After CaO was mixed with bio-residue, which reacted with moisture in bio-residue, the calcium hydroxide ($Ca(OH)_2$) was generated. Both CaO and $Ca(OH)_2$ started to absorb carbon dioxide in the air over time, as shown in Eq. (2) and (3). Therefore, the

weight loss can only reflect a part of dewatering effect.

$$CaO + CO_2 = CaCO_3 \quad (2)$$

$$Ca(OH)_2 + CO_2 = CaCO_3 + H_2O \quad (3)$$

According to the XPS analysis, the fly ash powder used in pre-experiment mainly contained Na_3PO_4, Na_2SO_4 and $CaSO_4$, which could react with water by forming $Na_3PO_4 \cdot 12H_2O$, $Na_2SO_4 \cdot 10H_2O$ and $CaSO_4 \cdot 2H_2O$. These reactions are exothermic, shown as Eq. (4)-(6), and could help the evaporation of moisture. Although the fly ash powder was conducive to the release of moisture, most of which the existence form was bound water in the hydrates of inorganic salts and could not be dewatered by volatilization easily. The low calorific value of treated bio-residue was affected by the existence of hydrates, which was consistent with the results of low calorific value test.

$$CaSO_4 + 2H_2O = CaSO_4 \cdot 2H_2O \quad (4)$$

$$Na_3PO_4 + 12H_2O = Na_3PO_4 \cdot 12H_2O \quad (5)$$

$$Na_2SO_4 + 10H_2O = Na_2SO_4 \cdot 10H_2O \quad (6)$$

The dewatering effect of Fe(0)-$K_2S_2O_8$ ranged between the bottom ash powder and CaO. Persulfate is a strong and non-selective oxidant with a high redox potential of 2.01 V. It can be effectively activated by initiators, including heat, UV light, or transition metals (Me^{n+}) to generate sulfate free radicals ($SO_4^{-}\cdot$) which has an even higher redox potential estimated to be 2.60 V. Some of the reaction during activation of $S_2O_8^{2-}$ may be expressed as Eq. (7)-(10) (Yan et al. 2011; Oh et al. 2009; Oh et al. 2010; Zhen et al. 2012).

$$S_2O_8^{2-} + 2e^- \rightarrow 2SO_4^{2-} \qquad E^0 = 2.01\ V \quad (7)$$

$$S_2O_8^{2-} + heat/UV \rightarrow 2SO_4^{-}\cdot \quad (8)$$

$$S_2O_8^{2-} + Me^{n+} \rightarrow Me^{(n+1)+} + SO_4^{-}\cdot + SO_4^{2-} \quad (9)$$

$$SO_4^{-} \cdot + e^{-} \rightarrow SO_4^{2-} \qquad E^0 = 2.60\ V \tag{10}$$

Similar to fly ash powder, the dewatering capacity of bottom ash powder could be explained preliminarily that some inorganic salts in the bottom ash powder could react with moisture in bio-residue and achieve the transfer of moisture from bio-residue to inorganic salts. These reactions are exothermic, which can help the evaporation of moisture. However, different from CaO, bottom ash powder has little effect on low calorific value. Meanwhile, the inorganic salts in fly ash powder could bind more moisture than bottom ash powder, affecting its evaporation. The results suggested that bottom ash powder was a preferred dewatering reagent, and more mechanisms will be analyzed in detailed experiments.

The low calorific value is associated with moisture and organic contents. It can be seen from **Fig. 2(b)** that the low calorific value was related to moisture content and dewatering reagents greatly. With the decrease of moisture, the low calorific value increased. At the 4th d, the low calorific values of bio-residue with CaO, bottom ash powder, fly ash powder and Fe(0)-$K_2S_2O_8$ were 1872 kJ/kg, 1424 kJ/kg, 1066 kJ/kg and 976 kJ/kg, respectively. After treated for 8 days, the low calorific values increased gently, and at the 14th d, the low calorific values of bio-residue with CaO, bottom ash powder, fly ash powder and Fe(0)-$K_2S_2O_8$ were 9697 kJ/kg, 10544 kJ/kg, 10163 kJ/kg and 10873 kJ/kg, respectively. Although the low calorific value had a positive correlation with dosage at the 8th d, it was mainly affected by the moisture content, due to the dewatering effect of CaO. With the increase of dosage, the dewatering effect got better in the middle phase of treatment.

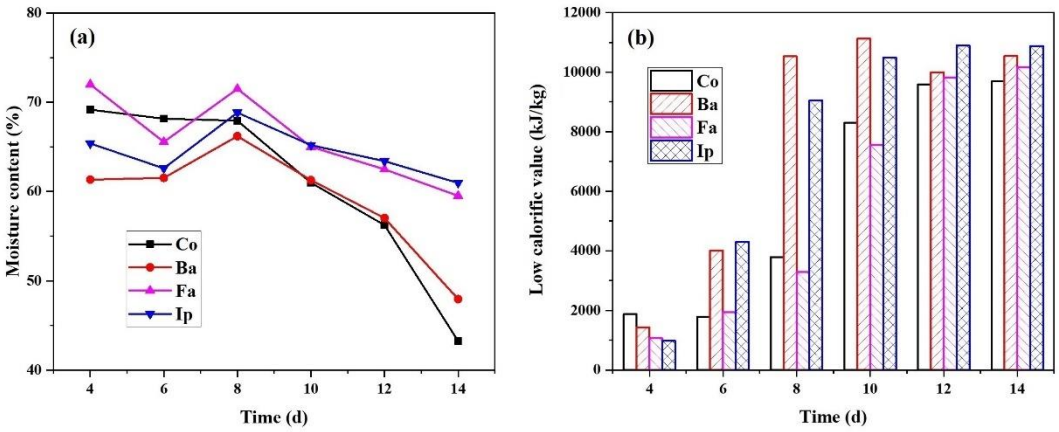

Fig. 2 Moisture content variation (a) and low calorific value (b) of bio-residue with the 2.0% dosage of CaO (Co), bottom ash (Ba), fly ash (Fa) and Fe(0)-$K_2S_2O_8$ (Ip)

3.3 Dewatering capacity of bottom ash with different dosages

The detailed curing experiments for bio-residue's deep dewatering by bottom ash powder with different dosages were conducted, and the variations of moisture content and low calorific value are shown in **Fig. 3**. During the curing experiments, there was no leakage of moisture.

Fig. 3(a-1) shows the dewatering performance of bio-residue without reagents. In the first 6 days of curing, the bio-residue's moisture content descended slowly, and its low calorific value maintained about 2.0 MJ/kg. With the decrease of moisture content, the low calorific value was increased obviously. After 14 days' treatment, the moisture content declined to about 30% and corresponding low calorific value raised to about 10.0 MJ/kg, which was suitable for incineration without affecting the operation of incineration plant. Combined with the dried bio-residue's combustion low calorific value (13.3 MJ/kg), the fitting curve of bio-residue' moisture content and low calorific value is given, shown in **Fig. 3(a-2)**, which fitted *Boltzmann Equation* and its image was like S-shaped curve. When the moisture content was over 45%, the low calorific value raised fast with the decrease of moisture content. With the moisture content going

down to 45%, the low calorific value raised slowly and reached a stable value when the moisture came to about 30%, over 10.0 MJ/kg.

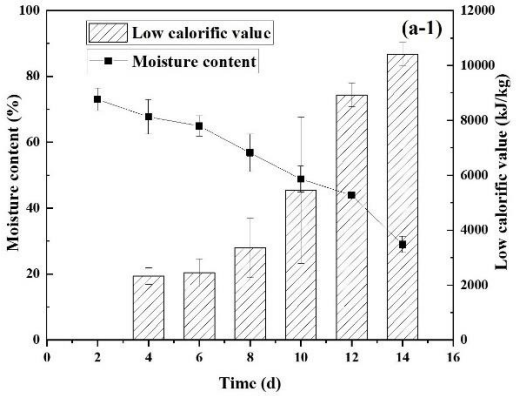

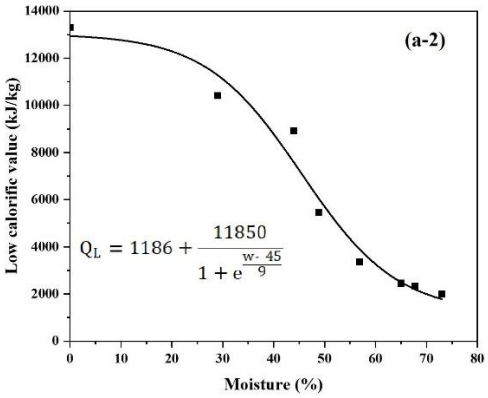

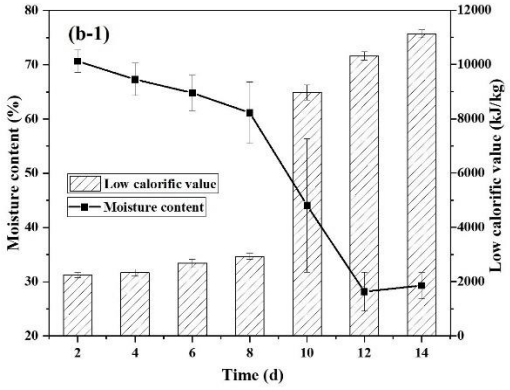

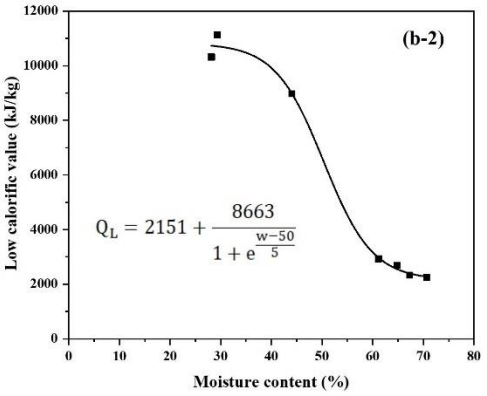

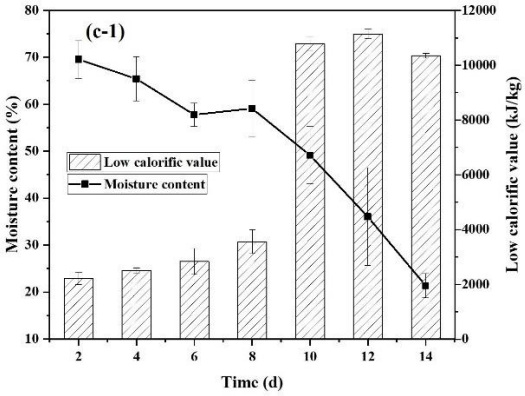

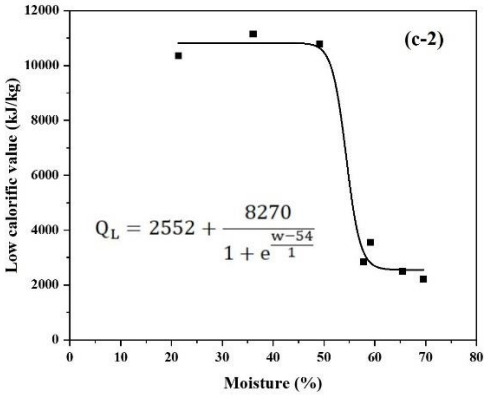

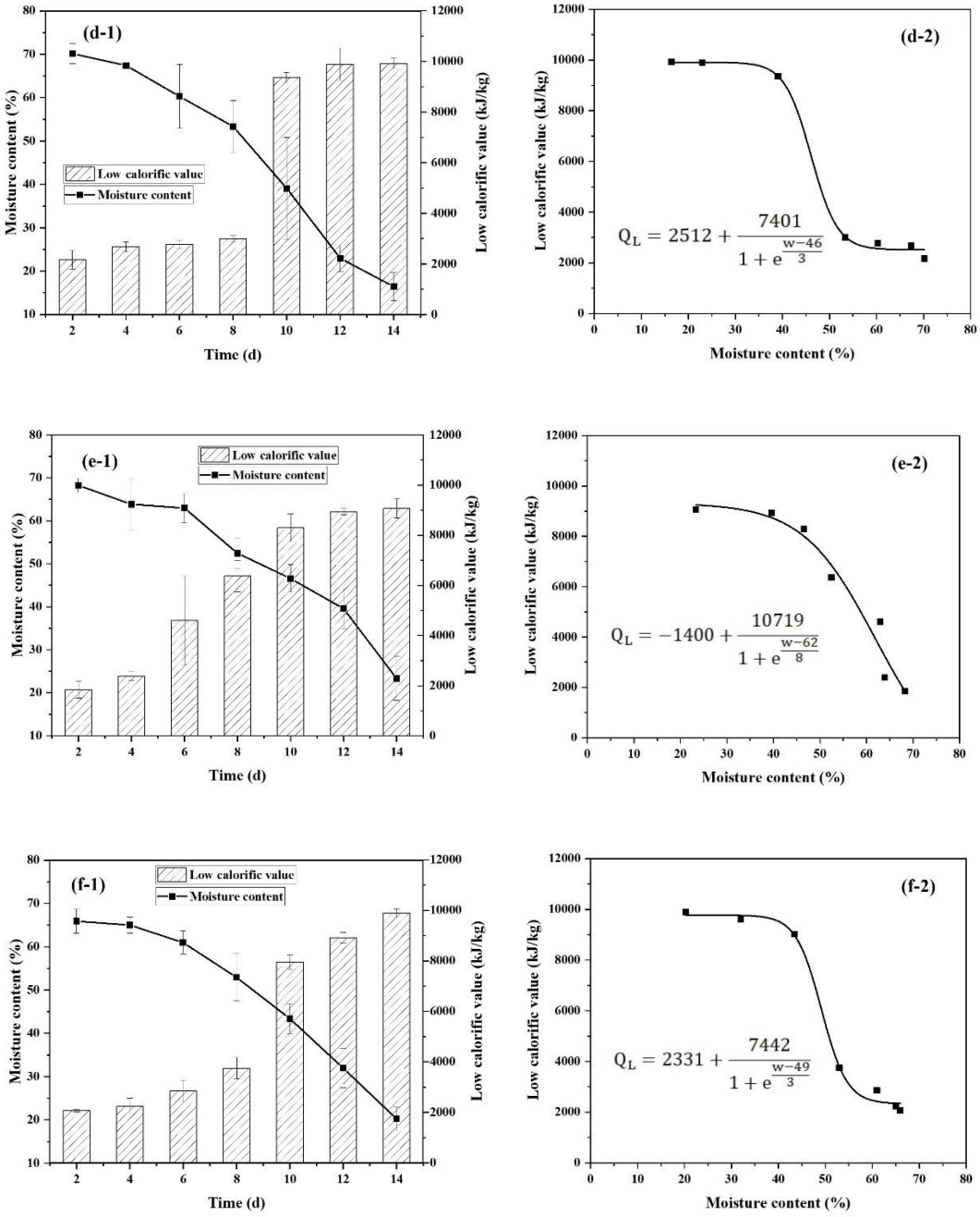

Fig. 3 Moisture content and low calorific value variation of bio-residue treated with different dosages of bottom ash powder (a, b, c, d, e and f represent the dosages of 0%, 1.0%, 2.0%, 3.0%, 4.0% and 5.0%; (a-1), (b-1), (c-1), (d-1), (e-1) and (f-1) represent the moisture content and low calorific value variations of bio-residue; (a-2), (b-2), (c-2), (d-2), (e-2) and (f-2) represent the fitting relation law of bio-residue' moisture content and low calorific value)

Fig. 3(b~f) confirms that bottom ash powder contributed to the deep dewatering of bio-residue in detail. After 10 days' curing, bio-residue's moisture content decreased to

about 40% and its low calorific value raised to over 8.0 MJ/kg. When the dosage of bottom ash powder was 2.0%, the final dewatering efficiency after 14 days was better than that of 1.0%, and its low calorific value maintained stably over 10.0 MJ/kg from the 10th d. When the dosage of bottom ash was 3.0%, the dewatering rate was accelerated as shown in **Fig. 3(d-1)**. Compared with the dosage of 1.0% and 2.0%, the final low calorific value declined because the bottom ash powder had no calorific value. With the increase of bottom ash powder dosage, low calorific value decreased at the same moisture content. The high dosage could promote the deep dewatering of bio-residue, but affect the final low calorific value more obviously. The fitting function is shown as Eq. (11) and their specific parameters of different dosages are shown in **Table 3**.

$$Q = \Delta Q + \frac{Q_0}{1+e^{\frac{w-\omega}{k}}} \tag{11}$$

where, Q, ΔQ, Q_0 – low calorific value, kJ/kg

w – moisture content, %

Table 3 Moisture content and low calorific value's fitting function and specific parameters with different dosages of bottom ash powder

Dosage	General Equation	Parameters			
		ΔQ	Q_0	ω	k
0%	$Q = \Delta Q + \frac{Q_0}{1+e^{\frac{w-\omega}{k}}}$	1186	11850	45	9
1.0%		2151	8663	50	5
2.0%		2552	8270	54	1
3.0%		2512	7401	46	3
4.0%		-1400	10719	62	8
5.0%		2331	7442	49	3

In Eq. (11), ω represents the critical point of *Boltzmann Equation*. When the value of moisture content was bigger than ω, low calorific value was relatively low, and raised fast with the decrease of moisture content. With the value of moisture content getting smaller than ω, low calorific value raised slowly and reached to a stable value gradually.

The sum of ΔQ and Q_0 represents the theoretical maximum low calorific value. It

can be seen from **Table 3** easily that with the increase of bottom ash powder dosage, the theoretical maximum low calorific value declined gradually.

With the increase of bottom ash powder dosage, the low calorific value at the 14^{th} d was declined, illustrating that bottom ash powder will affect incineration of bio-residue. When the dosage of bottom ash powder was 2.0%, the moisture of bio-residue could be decreased to about 50% and the corresponding low calorific value reached to 10.79 MJ/kg at the 10^{th} d from the original 0 MJ/kg. Based on the experiment above, 2.0% dosage of bottom ash powder addition indicated an excellent effect on deep dewatering of bio-residue.

3.4 Decoupling of moisture in bio-residue

3.4.1 Chemical composition of bottom ash powder

Fig. 4(a) shows the survey of XPS spectra for bottom ash powder, which exhibited S, Cl, C, K, Ca, O, F, Zn, and Na signals. **Fig. 4(b-i)** compiles the high-resolution surface spectra of S, Cl, K, Ca, O, F, Zn and Na recorded on bottom ash powder sample.

The high-resolution surface spectra of S included four peaks with binding energy of 169.5 eV, 170.7 eV, 169.1 eV and 170.3 eV. The binding energy of 169.5 eV and 170.7 eV represented S 2p3/2 peak and S 2p1/2 peak in $ZnSO_4$, and the binding energy of 169.1 eV and 170.3 eV represented S 2p3/2 peak and S 2p1/2 peak in K_2SO_4. The high-resolution surface spectra of Cl included four peaks. The binding energy of 198.5 eV and 200.1 eV represented Cl 2p3/2 peak and Cl 2p1/2 peak in NaCl, and the binding energy of 198.8 eV and 200.4 eV represented Cl 2p3/2 peak and Cl 2p1/2 peak in $ZnCl_2$. Two peaks were visible in the spectra of K 2p with the binding energy of 296.2 eV and 293.5 eV, which belonged to K 2p1/2 peak and K 2p3/2 peak in K_2SO_4. The high-resolution surface spectra of Ca included two peaks with binding energy of 351.1 eV

and 347.5 eV, which represented Ca 2p1/2 peak and Ca 2p3/2 peak in $CaCO_3$. The high-resolution surface spectra of F 1s included only one peak with binding energy of 685.1 eV, which represented ZnF_2. The high-resolution surface spectra of Zn 2p included six peaks. The binding energy of 1023.0 eV and 1046.0 eV represented Zn 2p3/2 peak and Zn 2p1/2 peak in $ZnSO_4$, the binding energy of 1021.9 eV and 1044.9 eV represented Zn 2p3/2 peak and Zn 2p1/2 peak in $ZnCl_2$, and the binding energy of 1022.2 eV and 1045.2 eV represented Zn 2p3/2 peak and Zn 2p1/2 peak in ZnF_2. The high-resolution surface spectra of Na 1s included only one peak with a binding energy of 1072.3 eV, which represented NaCl. The results confirmed that the bottom ash powder mainly contained NaCl, K_2SO_4, $CaCO_3$, $ZnSO_4$, ZnF_2 and $ZnCl_2$.

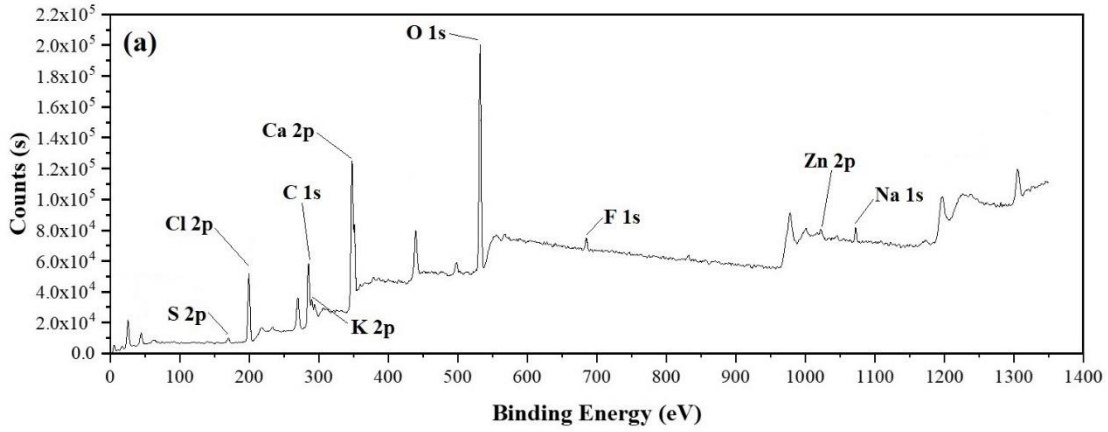

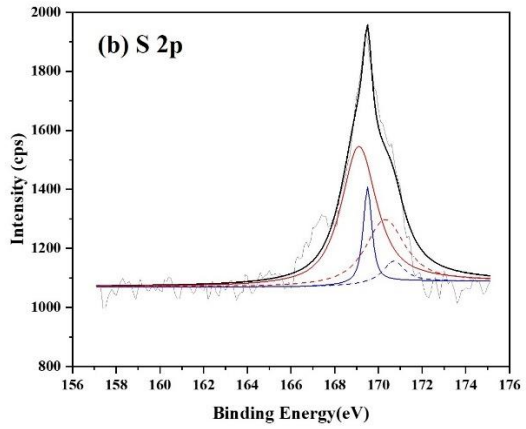

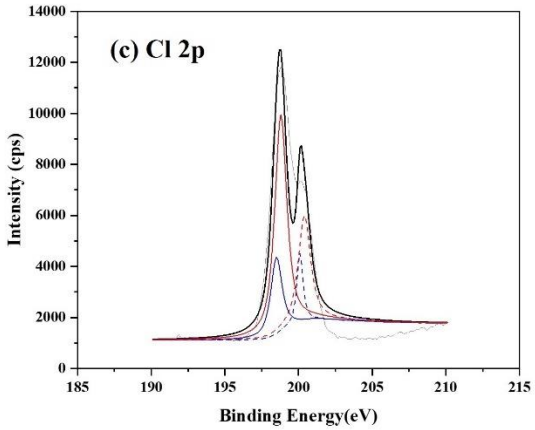

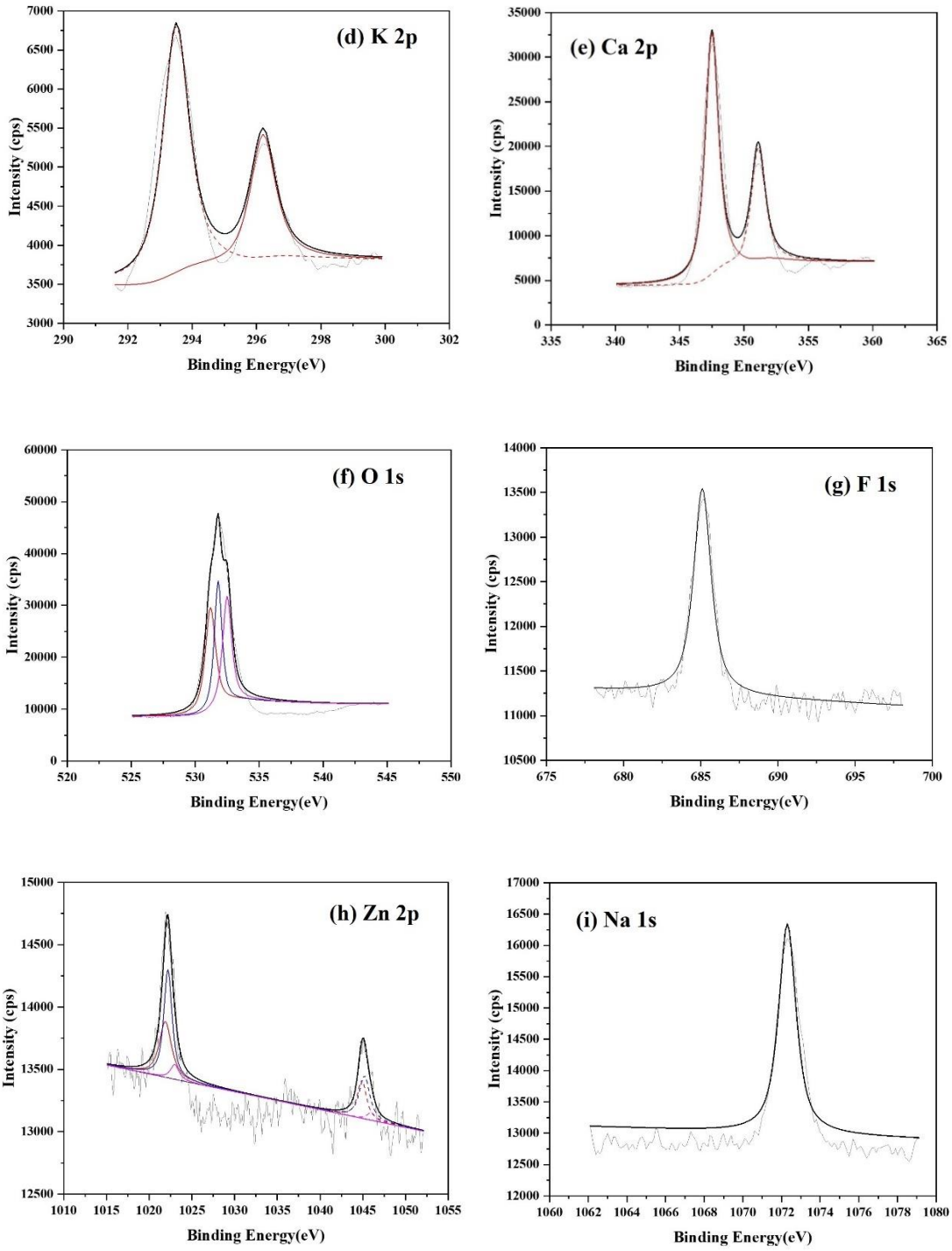

Fig. 4 X-ray photoelectron spectroscopy survey spectra of bottom ash powder(a) and high-resolution surface spectra of elements in bottom ash powder(b-i) (note: (b) S 2p, (c) Cl 2p, (d) K 2p, (e) Ca 2p, (f) O 1s, (g) F 1s, (h) Zn 2p, (i) Na 1s)

3.4.2 Dewatering mechanism

The dewatering mechanism was analyzed, combined with XPS analysis of the

bottom ash powder. $ZnCl_2$ in bottom ash powder can react with moisture in bio-residue and achieve the transfer of moisture from bio-residue to $ZnCl_2$, and the reaction is shown as Eq. (12).

$$ZnCl_2 + H_2O = Zn(OH)Cl + HCl \quad (12)$$

$ZnSO_4$ can also react with moisture by forming $ZnSO_4 \cdot 7H_2O$ and this reaction is exothermic, which can help the evaporation of moisture. The reaction is shown as Eq. (13). The bottom ash powder can react with moisture in bio-residue and realize the dewatering efficiently, and different from fly ash, the amount of moisture that bottom ash powder can react with was relatively limited, influencing low calorific value slightly.

$$ZnSO_4 + 7H_2O = ZnSO_4 \cdot 7H_2O \quad (13)$$

Fig.5 shows the micro-structure of treated bio-residue under the electron microscope, with the decoupling mechanism of moisture. It can be seen from **Fig. 5(a)** that after treated by polyacrylamide, the bio-residue was packed by polyacrylamide colloid and presented a steric reticular structure. After treated by bottom ash powder further, the packed polyacrylamide colloid began to spalling and the strip fiber structure could be observed clearly. This appearance got more obvious with the increase of bottom ash powder's dosage, which can be seen from **Fig. 5(b-f)**.

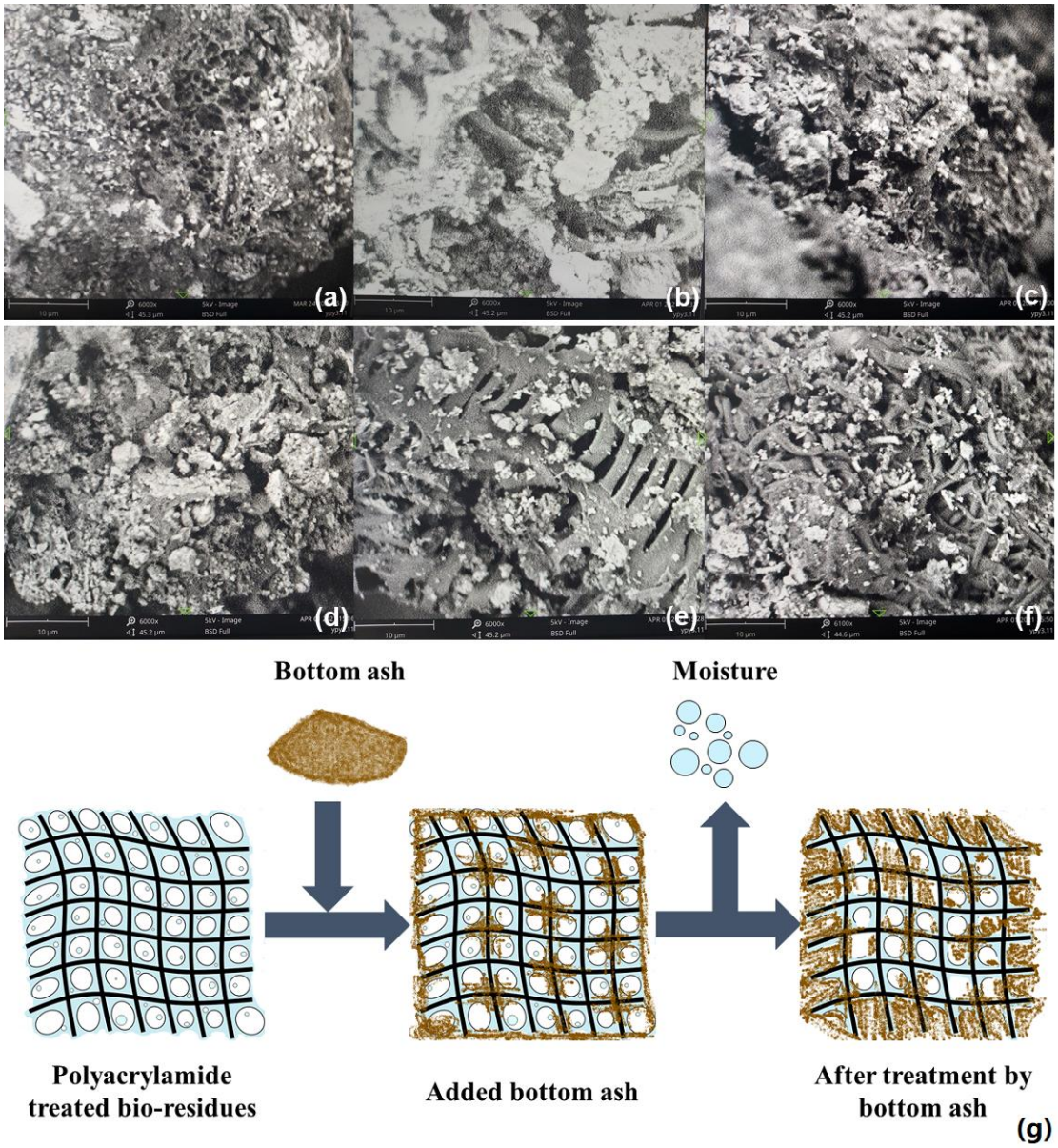

Fig. 5 Electron microscope observation of bio-residue treated by PAM and further treated with different dosages of bottom ash powder (a – bio-residue treated by PAM; b – 1.0% dosage; c – 2.0% dosage, d – 3.0% dosage; e – 4.0% dosage; f – 5.0% dosage) and decoupling mechanism of moisture (g)

The decoupling mechanism of moisture in bio-residue is shown in **Fig. 5(g)**. The decomposition of polyacrylamide colloid was related to the addition of bottom ash powder. As analyzed by XPS, the bottom ash powder mainly contained NaCl, K_2SO_4, $CaCO_3$, $ZnSO_4$, ZnF_2 and $ZnCl_2$. After adding bottom ash powder, the bio-residue treated by PAM were bound up and adhered with bottom ash powder. These inorganic

salts in bottom ash powder were electrolyte, which could accelerate the hydrolysis and destruction of polyacrylamide colloid with the moisture itself contained firstly. After the polyacrylamide colloid was broken, the moisture in colloid was exposed and began to release into the air by evaporation. Furthermore, it could be observed that when the dosage of bottom ash powder was over 2.0%, the spalling degrees of polyacrylamide colloid were similar, which meant 2.0% dosage of bottom ash powder was enough for the hydrolysis and destruction of polyacrylamide colloid, indirectly proving that 2.0% dosage of bottom ash powder has the best effect on deep dewatering of bio-residue.

3.5 Economic analysis of reagents

The conventional dewatering reagents include CaO and Fe(0)-$K_2S_2O_8$. Take the treatment with 2% dosage as example, different reagents' 10 days dewatering efficiencies are shown in **Table 4**. CaO had the best 10 days dewatering efficiency among four reagents, followed by bottom ash powder, about 21.84%. Fe(0)-$K_2S_2O_8$ has the worst 10 days dewatering efficiency among four reagents, followed by fly ash powder, about 17.08%. According to the cost of reagents and their dewatering efficiencies, the dewatering capacity cost can be calculated and the results are also shown in **Table 4**.

Table 4 Comparison between cost and dewatering efficiency of reagents (6.7 CNY = 1 US$ in June 2022)

Reagent (2% Dosage)	10 days dewatering efficiency (%)	Cost of reagents (CNY/ton)	Dewatering capacity cost (CNY/ton water)
CaO	22.22	500-1000	45-90
Fe(0)-$K_2S_2O_8$	16.85	2000-5000	237-593
Bottom ash powder	21.84	50-80	5-7
Fly ash powder	17.08	-	-

Compared with bottom ash and fly ash powder from municipal solid waste incineration plant, the dewatering capacity cost of CaO and Fe(0)-$K_2S_2O_8$ reagents

were higher. Although they had a certain dewatering efficiency, the high costs restricted their application in deep dewatering of bio-residue. On one hand, although the dewatering efficiency of fly ash powder was close to bottom ash powder, fly ash powder had greater impact on low calorific value of treated bio-residue, which was not convenient for the operation of incineration plant. As a consequence, municipal solid waste incineration (MSWI) fly ash categorized as a hazardous material must be managed and regulated more scientifically and effectively, which is not suitable for deep dewatering of treated bio-residue (Li et al. 2018). On the other hand, due to the source from municipal solid waste incineration plant, bottom ash has characteristics of huge yield and harmless. As estimated, the incineration of one-ton solid waste generates approximately 250-300 kg of bottom ash (Tan et al. 2022). Therefore, bottom ash powder is the best reagent for organic waste bio-residue's deep dewatering.

4 Conclusion

Organic waste bio-residue should be deep dewatered before incineration. The moisture existence forms of bio-residue were clarified as adsorbed water, capillary water and bound water, which occupied 75.61%, 23.81% and 0.58%, respectively. Furthermore, refuse incineration bottom ash powder was used as a typical deep dewatering reagent, while compared with CaO, refuse incineration fly ash powder, and Fe(0)-$K_2S_2O_8$. Results showed that the addition of bottom ash powder could decrease the bio-residue's moisture from 80.0% to 37.9% at the optimal dosage of 2.0%, and corresponding low calorific value reached to 10.5 MJ/kg at the 10^{th} d. The $ZnCl_2$, and $ZnSO_4$ present in bottom ash powder could react with moisture in bio-residue to form hydrates of inorganic salt and break polyacrylamide colloid, realizing the release of adsorbed water in bio-residue via water evaporation accelerated by exothermic process.

References

Arun C, Sivashanmugam P (2017) Study on optimization of process parameters for enhancing the multi-hydrolytic enzyme activity in garbage enzyme produced from preconsumer organic waste. Bioresour Technol 226:200-210.

Bien JB, Kempa ES, Bien JD (1997) Influence of ultrasonic field on structure and parameters of sewage sludge for dewatering process. Water Sci Technol 36:287–291.

Chen Y, Xu L, Tan SN, Sun X, Deng Y, Yang W (2020) Solidification and multi-cytotoxicity evaluation of thermally treated MSWI fly ash. J Hazard Mater 388:122041.

Dewil R, Baeyens J, Goutvrind R (2006) The use of ultrasonics in the treatment of waste activated sludge. Chinese J Chem Eng 14:105–113.

Guo H, Wu S, Tian Y, Zhang J, Liu H (2021) Application of machine learning methods for the prediction of organic solid waste treatment and recycling processes: A review. Bioresour Technol 319:124114.

Hu E, Li M, Tian Y, Yi X, Dai C, Shao S, Li C, Zhao Y (2022) Pyrolysis behaviors of anaerobic digestion residues in a fixed-bed reactor with rapid infrared heating. Environ Sci Pollut R https://doi.org/10.1007/s11356-022-19558-4.

Jomaa S, Shanableh A, Khalil W, Trebilco B (2003) Hydrothermal decomposition and oxidation of the organic component of municipal and industrial waste products. Advances in Environmental Research 7(3):647–653.

Katsiris N, Kouzeli-Katsiri A (1987) Bound water content of biological sludge in relation to filtration and dewatering. Water Res 21(11):1319-1327.

Li H, Ni D, Li L, Dong B, Chen Q, Gu L (2020). Insight into the role of polyacrylamide polymer powder on the cracking in plastic period of cement mortar. Constr Build Mater 260:119914.

Li J, Zeng M, Ji W (2018) Characteristics of the cement-solidified municipal solid waste incineration fly ash. Environ Sci Pollut R 25:36736-36744 https://doi.org/10.1007/s11356-018-3600-z.

Loginova E, Schollbach K, Proskurnin M, Brouwers H (2021) Municipal solid waste incineration bottom ash fines: Transformation into a minor additional constituent for cements. Resour Conserv Recy 166:105354.

Mahmood T, Elliott A (2007) Use of acid preconditioning for enhanced dewatering of wastewater treatment sludges from the pulp and paper industry. Water Environment Resource 79:168-176.

Mata-Alvarez J, Macé S, Llabrés P (2000) Anaerobic digestion of organic solid wastes. An overview of research achievements and perspectives. Bioresour Technol 74(1):3-16.

Neyens E, Baeyens J (2003) A review of thermal sludge pre-treatment processes to improve dewaterability. J Hazard Mater B98:51-67.

Ning X, Luo H, et al. (2013) Effect of tannery sludge incineration slag pretreatment on sludge dewaterability. Chem Eng J 221:1-7.

Novak JT (2006) Dewatering of sewage sludge. Dry Technol 24:1257–1262.

Oh SY, Kang SG, Chiu P (2010) Degradation of 2, 4-dinitrotoluene by persulfate activated with zero-valent iron. Sci Total Environ 408(16):3464–3468.

Oh SY, Kim HW, Park JM, Park HS, Yoon C (2009) Oxidation of polyvinyl alcohol by persulfate activated with heat, Fe^{2+}, and zero-valent iron. J Hazard Mater 168(1):346–351.

Singh R, Sharma B, Sarkar A, Sengupta C, Singh P, Ibrahim M (2014) Biological responses of agricultural soils to fly ash amendment. Rev Environ Contam T 232:45-60.

Smollen M (1986) Categories of moisture content and dewatering characteristics of biological sludges, in Proceeding of the 4th World Filtration Congress, Belgium, Ostend:22-25.

Šyc M, Simon FG, Hykš J, Braga R, Biganzoli L, Costa G, Funari V, Grosso M (2020) Metal recovery from incineration bottom ash: state-of-the-art and recent developments. J Hazard Mater 393:122433.

Tan J, Dan H, Li J (2022) Use of municipal waste incineration fly ashes (MSWI FA) in metakaolin-based geopolymer. Environ Sci Pollut R https://doi.org/10.1007/s11356-022-21580-5.

Tella M, Doelsch E, Letourmy P, Chataing S, Cuoq F, Bravin MN, Macary HS (2013) Investigation of potentially toxic heavy metals in different organic wastes used to fertilize market garden crops. Waste Manage 33(1):184-192.

Tsang K, Vesilind P (1990) Moisture distribution in sludges. Water Sci Technol

22(12):135-142.

Wan S, Zhou X, Zhou M, Han Y, Chen Y, Geng J, Wang T, Xu S, Qiu Z, Hou H (2018) Hydration characteristics and modeling of ternary system of municipal solid wastes incineration fly ash-blast bottom ash-cement. Constr Build Mater 180:154-166.

Wei Y, Wang N, Lin Y, Zhan Y, Ding X, Liu Y, Zhang A, Ding G, Xu T, Li J (2021) Recycling of nutrients from organic waste by advanced compost technology – A case study. Bioresour Technol 337:125411.

Wiles CC (1995) Municipal solid waste combustion ash: state of the knowledge. J Hazard Mater 3894:20.

Willard H, Merritt L, Dean JA (1988) Instrumental methods of analysis, in 7th Ed. Wadsworth Inc, Belmont Calif.

Xiao Z, Yuan X, Jiang L, Chen X, Li H, Zeng G, et al (2015). Energy recovery and secondary pollutant emission from the combustion of co-pelletized fuel from municipal sewage sludge and wood sawdust. Energy 91:441–50.

Yan J, Lei M, Zhu L, Anjum MN, Zou J, Tang H (2011) Degradation of sulfamonomethoxine with Fe_3O_4 magnetic nanoparticles as heterogeneous activator of persulfate. J Hazard Mater 186(2–3):1398–1404.

Yu Q, Feng L, Zhen X (2020) Effects of organic loading rate and temperature fluctuation on the microbial community and performance of anaerobic digestion of food waste. Environ Sci Pollut R 28:13176-13187 https://doi.org/10.1007/s11356-020-11548-8.

Zhao Y, Wei R (2020) <Biomethane Production from Vegetable and Water Hyacinth Waste>, Elsevier Publisher Inc. (Oxford OX5 1GB, United Kingdom and Cambridge, MA 02139, United States).

Zhen GY, Lu XQ, Hao YC, et al. (2012) Enhanced dewaterability of sewage sludge in the presence of Fe(II)-activated persulfate oxidation. Bioresour Technol 116:259-265.

Zhu F, Jiang H, et al. (2012) Research on drying effect of different additives on sewage sludge. Procedia Environmental Sciences 16:357-362.

Zhu W, Teoh PJ, Liu Y, Chen Z, Yang EH (2019) Strategic utilization of municipal solid waste incineration bottom ash for the synthesis of lightweight aerated alkali-

activated materials. J Clean Prod 235: 603-612.

Zhu Y, Zhao Y, Zhao C, Gupta R (2020) Physicochemical characterization and heavy metals leaching potential of municipal solid waste incineration bottom ash (MSWI-BA) when utilized in road construction. Environ Sci Pollut R 27:14184-14197 https://doi.org/10.1007/s11356-020-08007-9.

EVALUATION OF USING FLY ASH-SLAG-BASED MORTAR AS A MINE BACKFILLING MATERIALS PROPERTIES AND HYDRATION CHARACTERISTICS

Chutong Zhao[1], Chuanfu Wu[1], Xiaona Wang[1],Zhongli Luo[2] and Qunhui Wang[1]

1 School of Energy and Environmental Engineer, University of Science and Technology Beijing, 30 Xueyuan Road, Haidian District, Beijing 100083, China;

2 Organic Materials Research Laboratory, Tosoh Corporation,Shunan,746-8501, Japan

INTRODUCTION

Due to the tight land resources, incineration is considered the best means of domestic waste treatment, not only for the high degree of capacity reduction, which can reach more than 90%, but a large amount of MSWI Fly Ash, a by-product of the incineration process, is considered a hazardous waste due to its high content of heavy metals and organic pollutants(Yang and Ji et al., 2018; Li and Zhang et al., 2020). The heavy metals in MSWI FA cannot be removed and can only be transformed in different forms. Currently, S/S is an economical and widely used technology due to its physical and chemical fixation that can effectively trap toxic substances in MSWI FA in the solidified body(Kan and Shi et al., 2020; Xue and Liu, 2021). In this study, the mechanical properties of GGBS-SS-FGD mortar system and the leaching of heavy metals from mortar under different environments were evaluated by studying the incorporation of MSWI FA, so as to select the optimal amount of MSWI FA to be added to the GGBS-SS-FGD system.

MATERIALS AND METHODS

(1) Raw materials

GGBS, SS and FGD were obtained from Jingtaicheng Environmental Resources Co. Ltd in Hebei province, China. In order to facilitate adequate hydration reactions, the raw materials were dried and ground thoroughly in a ball mill after delivery to the laboratory. The MSWI fly ash was collected from a MSW incineration power plant located in Chengdu, China. The incinerator used in this domestic waste incineration plant is a grate furnace.

(2) Preparation of mortar samples

The designed composition of samples are listed in Table 1.The mortar samples were prepared at a water-to-binder of 0.5 and standard sand-to-binder ratio of 3, and samples were poured into a steel mould (40*40*160mm) .All samples were placed in a standard constant temperature and humidity cement curing box (humidity 95%±1%, temperature 20℃±5℃) for 1 days before mould removal. They were then placed in a curing box for curing to the corresponding age.

(3) Heavy metals leaching method

Mix concentrated sulfuric acid and concentrated nitric acid with a mass ratio of 2:1, adjust the pH of the leaching solution to 3.2, and carry out a tumbling and shaking test on the curing body according to the liquid-solid ratio of 10:1, adjusting the rotational speed to 30±2r/min and shaking for 18h.

Table. 1 The designed composition of samples

Sample number	Binders (g)				Standard sand (g)	Water (ml)
	fly ash	GGBS	SS	FGD		
FBM0	0	306	90	54	1350	225
FBM1	22.5	283.5	90	54	1350	225
FBM2	67.5	238.5	90	54	1350	225
FBM3	135	171	90	54	1350	225

The leaching amount of heavy metals is determined according to GB/T 30810-2014 test methods for leachable ions of heavy metals in mortar. The 10.0g mortar powders with particle size between 0.125 and 0.25mm were selected, which were added to 500 ml deionized water. The pH value of the suspension was titrating to pH 7.0±0.5 and remaining 2h by the mixed solution (the solution was prepared by mixing solution A and B, solution A: adding 100ml H_2SO_4 to 200 ml deionized water; solution B: adding 50 ml HNO_3 to 100 ml deionized water) while stirring. After filtration, the 500 ml deionized water was added to the residue, and the pH value of the suspension was titrating to pH 3.2±0.5 then remaining 7h while stirring. The filtrate from the above two steps was collected and diluted to 2L.

The pH dependent leaching test was conducted following EPA 1313. This method was designed to assess the pH leaching behaviour of inorganic

components in terms of equilibrium conditions at different pH values. In this work, 8 suspensions were prepared with pH values at 12、11、10、9、8、6、4 and 2. Each suspension was made of 30g samples and 300ml deionized water in 500ml HDPE vessels. The end-pH value was achieved by adding HNO_3 and NaOH solution.

RESULT AND DISCUSSION

Both the mechanical properties and the leaching of heavy metals from the mortar affect the practical use of fly ash slag base as backfilling material, and for underground backfilling in mining areas, the compressive strength is required to be between 1 and 4 MPa. In order to evaluate the safety performance of the mortar the total amount of leachable heavy metals in the mortar is evaluated. Considering that the backfilling material will not only be in contact with groundwater in practical application, but also the artificial roof may be in contact with acid rain, the leaching of heavy metals from the fly ash slag base under this environments needs to be evaluated. However, the HJ299 test standard only requires an initial pH of 3.2 for the leaching solution, while fly ash slag-based mortar is a strongly alkaline material. In order to evaluate the leaching of heavy metals from fly ash slag-based mortar under extreme pH environments, the mortar was tested for pH dependence.

(1) Mechanical property

After 3 d and 7 d of curing, the compressive strength of all groups with FA added was lower than that of FBM0 (Fig.1), which was due to the dispersed size of FA particles and their own low volcanic ash reactivity, which led to a decrease in the overall hydration reactivity and strength of the system(Liu and Hu et al., 2020; Fan and Wang et al., 2021; Gj and Xma et al., 2022). However, with the extension of the curing time, the release of OH^- from the dissolved FA particles promotes the breakage of [Si-O-Al] and [O-Si-O] bonds in GGBS and SS, which accelerates the hydration reaction(Xu and Ni et al., 2019). Thus when after 28 d of maintenance, the compressive strength of FBM2 is 32.62 MPa, which is almost the same as that of FBM0. This phenomenon also indicates that as the reaction proceeds more fly ash particles are dissolved to participate in the hydration reaction. Similar to the compressive strength, after 3 d curing, the flexural strength of all the added FA groups was lower than that of FBM0, but the flexural strength of FBM2 was comparable to that of FBM0 after 28 d curing, and the strength increased by 210.71%, which could reach 4.35 MPa. Similarly, this also indicates that although FA has poor hydration activity by itself, the strength of FA cured body increased significantly with the extension of curing time. The strength of FA cured body increased significantly with the increase of curing time. Therefore, it is considered that the mechanical properties of FA are best at 15% admixture.

(2) Heavy metals leaching \

According to the experimental results of GB/T 30810-2014 as shown in Figure 2.FA leaching of various heavy metals exceeded the limit, when the content of FA in FBM group was lower than 30%, the leaching content of various heavy metals was lower than the limit value in GB 30760-2014; however, when the content of FA was 30%, the leaching content of Zn was 1052ug/L, which exceeded the limit value, and the leaching content of Cd Although it is lower than the limit value of 30ug/L, but it is more dangerous. This is due to the fact that Zn is the most abundant among the various heavy metals in FA, which is still an order of magnitude lower than the leachable concentration of 47014 ug/L of Zn in FA. Although the leached content of Cr was not exceeded in any of the groups, it is noteworthy that the leached concentration of Cr in FB0 was higher when no FA was added, which was likely from SS. In general, the curing body cured the various heavy metals in FA better when the FA addition was less than 30%. A point of interest is that when the leaching method of HJ299 was used for SW, the leaching content of heavy metals in each group was extremely low (Table 2), and none of them exceeded the limit value. This is due to the fact that compared to the GB 30810 leaching method under fixed pH conditions (pH=7 maintained for 3h and pH=3.2 maintained for 3h), the HJ299 leaching method requires a fixed starting pH of 3.2, but the curing body is alkaline, as shown in Table 2, when the end pH of each group at the end of the leaching was in the alkaline range, indicating that probably most of the H+ was in the cured body. It has been extensively studied that the endpoint pH significantly affects the leaching of heavy metals from the curing body, which will be elaborated in the next section.

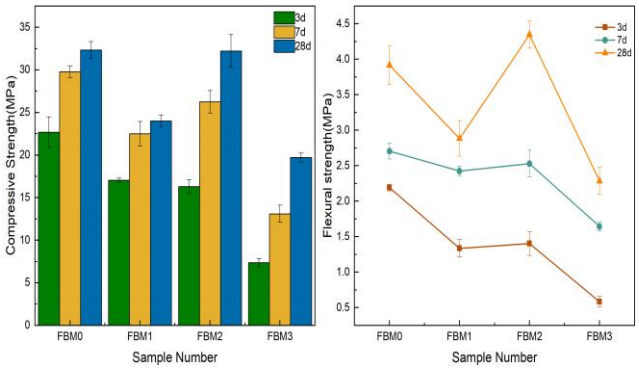

Figure 1. FBM mechanical properties;(a) compressive strength; (b) flexible strength

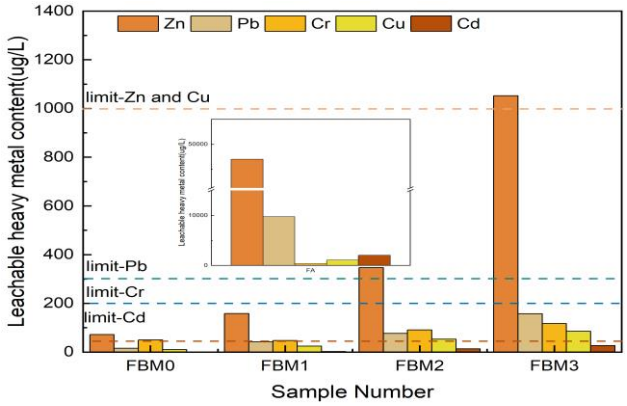

Figure 2. Total leachable heavy metals in FBM

Table. 2 HJ299 test the leaching of heavy metals in FBM

Samples number	Zn	Pb	Cd	Cu	Cr	Leaching end point pH
FBM0	NA	NA	NA	NA	0.06	9.71
FBM1	NA	NA	NA	NA	0.03	10.21
FBM2	NA	NA	NA	NA	0.02	10.52
FBM3	0.53	0.07	0.02	0.03	0.09	10.57

In order to investigate the effect of endpoint pH on the leaching of heavy metals and to evaluate the safety and stability of FBM, the leaching of heavy metals was studied in the pH range of 2-12 (Figure 5). In the solidified body, some heavy metals of FA are present in new mineral phases or immobilized by some hydration products, such as ettringite, C-S-H. It is interesting to note that both of these cases occur in a low alkaline environment (pH 8-11 range), so the leaching of various heavy metals is extremely low in the range of 8-11 as shown in Figure 3(Liang and Ysw et al., 2020; Xiang and Feng et al., 2020). Based on the leaching behavior of heavy metals, the heavy metals in the cured bodies can be classified into two categories, the first being amphoteric metals such as Pb, Zn and Cr; the other being Cu and Cd whose leaching concentration increases with decreasing pH. The leaching concentration of Pb in FA shows a V-shaped dependence on pH, and when FA is in a very basic and acidic environment, the leaching concentration of Pb is two orders of magnitude higher than that in a neutral environment. When the curing body is in the pH=12 environment, even FBM3 did not appear Pb leaching, while the leaching of Pb in FA was 10.54 mg/L; when in an acidic environment, at pH=6, the leaching concentration of Pb in all curing bodies can meet the standards of groundwater tertiary water, compared to FA at pH=4 has exceeded the hazardous waste identification standards (GB5085) The leaching concentration of Pb in the cured body group was two orders of magnitude lower than that of the FA, compared to the FA at pH=4, which already exceeded the limit value of Pb in the hazardous waste identification standard (GB5085). It is believed that the curing body cures Pb extremely well, especially for alkaline environments, mainly because the hydration product of the curing body, ettringite, is stable in alkaline environments, while when in acidic environments, the high presence of H^+ may lead to decomposition of ettringite decalcification, thus reducing the curing efficiency of Pb. The leaching behavior of Zn is similar to that of Pb , both exhibited obvious amphoteric metal leaching characteristics, and although the concentration of Zn in the original FA was high, for the cured body group, the leaching concentration of Zn was lower than the limits of GB16889 and GB5085 even in a very acidic environment with pH=2. Same as the leaching behavior of Pb in the cured body in a very alkaline environment, the leaching concentration of Zn remained undetected at pH=12. The leaching concentrations of Cr in the cured bodies in Figure 3(e) were low overall, but the difference between the leaching concentrations of Cr in the cured bodies and the original MSWI FA for each group at pH=2 was not significant due to the fact that Cr was mainly from SS. The leaching behavior of Cd and Cu was typical of the cationic leaching pattern, i.e., the leaching concentration increased with decreasing pH. At pH=4, the leaching concentrations of Cd in FBM1 and FBM2 were below the detection limit. According to the available studies on the mechanism of Cd curing is mainly in the form of Cd(OH)2 precipitation on the surface of C-S-H gel, but the reaction of C-S-H gels with H^+ in an acidic environment generates non-gel or soluble material, which in turn leads to the decomposition of C-S-H, and the increased porosity of the cured body also increases the risk of Cd leaching(Fei and Jian et al., 2021). As shown in Fig. 3(d), the S/S efficiency of the solidified body for Cu is so high that the leaching concentration of Cu in FBM1 is only 0.39 mg/L, which is lower than the standard for tertiary groundwater (1 mg/L), even in a pH=2 extremely acidic environment.

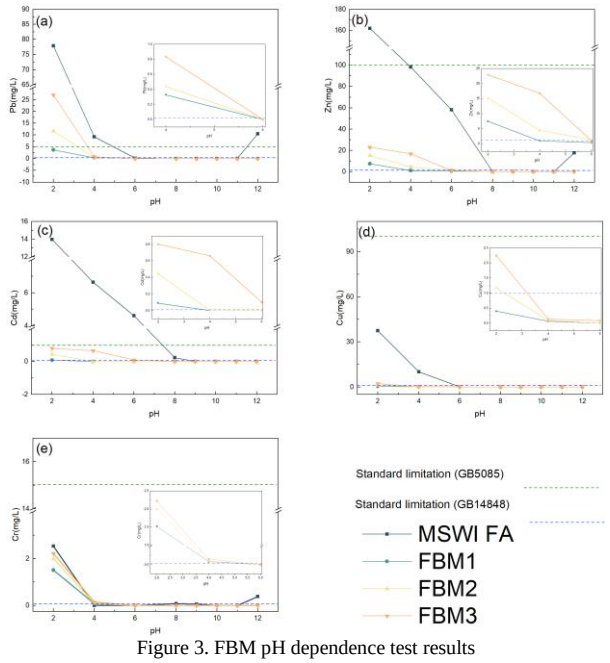

Figure 3. FBM pH dependence test results

CONCLUSION

According to the mechanical properties and the leaching of heavy metals, when the addition of fly ash is 15%, not only the compressive strength of fly ash slag-based mortar can reach the standard of OPC 32.5 cement, but also the content of heavy metals in the test method according to HJ299 are not exceeded, at this time fly ash slag-based mortars no longer belongs to hazardous waste. Moreover, in the pH dependence test of the mortars, the leaching of heavy metals of mortars under alkaline conditions was significantly reduced after the curing stabilization treatment, which is due to the stabilization of the hydration products in the curing body under alkaline conditions. In addition to this, fly ash slag-based mortars has a stronger resistance to acid attack compared to original fly ash, which substantially reduces the leaching of heavy metals under acidic conditions.

Therefore, it is concluded that the GGBS-SS-FGD system has an excellent curing and stabilizing effect on heavy metals in FA, and the mechanical properties of the mortars can also meet the standard, and it is considered that the fly ash slag-based mortar has the possibility of practical application as backfill material in mine extraction areas.

ACKNOWLEGEMENT

The study was supported by the National Key Research and Development Program of China
(2021YFE0112100).

REFERENCE

1.Fan, C. and B. Wang, et al. (2021). "A comparative study on solidification/stabilization characteristics of coal fly ash-based geopolymer and Portland cement on heavy metals in MSWI fly ash." Journal of Cleaner Production **319**: 128790-.

2. Fei, W. A. and X. B. Jian, et al. (2021). "Sustainable stabilization/solidification of the Pb, Zn, and Cd contaminated soil by red mud-derived binders." Environmental Pollution.

3.Gj,A. and B.Xma, et al. (2022). "Solidification/stabilization of highly toxic arsenic-alkali residue by MSWI fly ash-based cementitious material containing Friedel's salt: Efficiency and mechanism." Journal of Hazardous Materials.

4.Kan, L. and R. Shi, et al. (2020). "Feasibility study on using incineration fly ash from municipal solid waste to develop high ductile alkali-activated composites." Journal of Cleaner Production **254**: 120168.

5.Li, J. and S. Zhang, et al. (2020). "Feasibility of using fly ash–slag-based binder for mine backfilling and its associated leaching risks." Journal of Hazardous Materials **400**: 123191.

6.Liang, C. A. and A. Ysw, et al. (2020). "Stabilisation/solidification of municipal solid waste incineration fly ash by phosphate-enhanced calcium aluminate cement." Journal of Hazardous Materials **408**.

7.Liu, J. and L. Hu, et al. (2020). "Utilisation of Municipal Solid Waste Incinerator (MSWI) Fly Ash with Metakaolin for Preparation of Alkali-Activated Cementitious Material." Journal of Hazardous Materials 402(4): 123451.

8.oXiang, T. and R. Feng, et al. (2020). "Co-disposal of MSWI fly ash and spent caustic through alkaline-activation: Immobilization of heavy metals and organics - ScienceDirect." Cement and Concrete Composites 114.

9.Xu, C. and W. Ni, et al. (2019). "Hydration mechanism and orthogonal optimisation of mix proportion for steel slag–slag-based clinker-free prefabricated concrete." Construction and Building Materials 228(C).

10.Xue, Y. and X. Liu(2021). "Detoxification, solidification and recycling of municipal solid waste incineration fly ash: A review." Chemical Engineering Journal(11): 130349.

11.Yang, Z. and R. Ji, et al. (2018). "Recycling of municipal solid waste incineration by-product for cement composites preparation." Construction & Building Materials 162: 794-801.

Comparative study on the heavy metals stabilization performance of different organic chelating agents in municipal solid waste incineration fly ash

Ze Zhang[1], Chuanfu Wu [1], Xiaona Wang [1], Zhongli Luo[2] and Qunhui Wang[1]

1 School of Energy and Environmental Engineer, University of Science and Technology Beijing, 30 Xueyuan Road, Haidian District, Beijing 100083, China

2 Organic Materials Research Laboratory, Tosoh Corporation, Shunan, 746-8501, Japan

INTRODUCTION

Municipal solid waste (MSW) output is rising as urbanization is accelerating and people's quality of life is improving. Waste incineration technology has a high rate of weight and capacity reduction, and the heat generated from incinerator can be reused, it has gradually replaced other methods for handling domestic waste in Chinese cities[1].

Bottom ash (BA) and fly ash (FA) are the byproducts of incineration for solid waste[2]. Among them, FA contains a significant amount of hazardous wastes, including chlorides, persistent organic pollutants, and toxic heavy metals (Pb, Cr, Cd, As, Hg, etc.)[3]. It is worth noting that heavy metals in fly ash are the primary source of heavy metal pollution in China, with a high potential for leaching and pollution[4]. Therefore, to avoid secondary pollution, the fly ash has to be well treated before disposal.

At the present, the primary FA treatment methods are cement solidification, chemical agent stabilization, and heat treatment[5]. The chlorine content of FA is typically high, which devastates the cement hydration reaction, resulting in a greatly reduced treatment effect of cement solidification. Thermal treatment is typically associated with high energy consumption. Chemical agent stabilization, on the other hand, has the advantages of low compatibilization rate, low cost, and good effect, making it a very promising method for treating heavy metals in FA. Numerous studies have demonstrated that organic chelating agents have a better effect than inorganic stabilizers[6, 7].

In this study, FA was treated with three different organic chelating agents (CA), and the stabilization effects on the target heavy metal Pb were examined in order to determine the best organic chelating agent and the best addition ratio.

MATERIALS AND METHODS

(1) Materials

This study utilized MSWI FA from Chengdu Xingrong Group Co., Ltd. Grate type incinerators are the kind that are employed.

(2) Stabilization and heavy metal analysis

Different CA solution were applied to FA samples based on weight at 0.3 - 1.5% (water-FA ratio = 0.25). Mechanical stirring was carried out for 10 mins until a paste formed.

Microwave digestion method was used to determine the total heavy metal contents in raw FA. < The Solid Waste Leaching Toxicity Leaching Method Acetic Acid Buffer Solution Method > (HJ/T 300 - 2007) was used in this study to determine the leaching toxicity of heavy metals in FA. The modified BCR method is used to determine the heavy metal forms of FA (acid soluble, reducible, oxidizable, residue). Heavy metal concentrations were analyzed by inductively coupled plasma-atomic emission spectrometry (ICP-AES)

RESULT AND DISCUSSION

(1) Heavy metal analysis of raw FA

The amount of heavy metals leached from the raw FA and the total amount are shown in Table 1. The raw FA had the highest metal Zn content, but its leaching was limited, indicating that Zn is not easily leached and migrated in the environment. The HJ/T 300 leaching of raw FA showed that the leaching of Pb exceeded the limit value of the < pollution control standard for domestic waste landfills > (GB 16889-2008), so Pb was chosen as the target heavy metal for this study.

Table 1 Heavy metals leaching and total amount of raw FA

	HJ/T 300 (mg/L)	Total contents (mg/kg)
As	0.005	170
Zn	0.345	4770
Pb	0.461	740
Ni	0.004	350
Cd	0.013	220
Cr	0.021	10
Cu	0.030	405

(2) Comparison of leaching toxicity with different CA

The immobilization effects of Pb with different CA are shown in Fig. 1. The three chelating agents used at a 0.3%

concentration already have a lower leaching concentration of Pb than the standard limit value given in GB 16889-2008. The lowest leaching amount of TS300 was 0.009mg/L at 1.5% addition. Future thorough investigations on the variation of Pb leaching from chelator treatment between 0% and 0.3% of the dosage rate are planned in order to lower treatment costs and find the minimal dosing rate that satisfies the requirements.

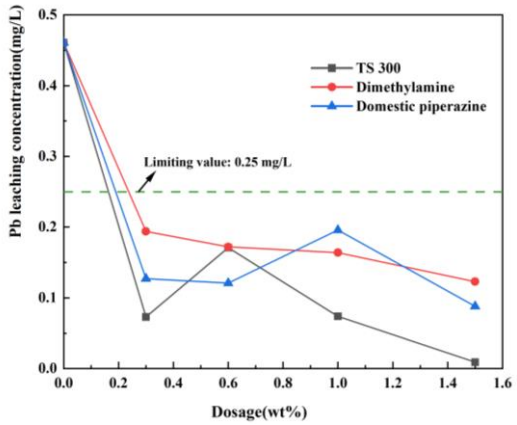

Fig.1 Pb leaching toxicity with different CA and dosages

(3) Variations in Pb speciation with different CA

As shown in Figure 2, the acid-soluble (F1) and reducible fraction(F2) of Pb in the original FA accounted for 10% and 41% of the total amount of Pb, respectively, which are unstable and easy to leach components.

The percentage of F1 and F2 fraction reduced by a combined 33% for TS300 when the addition amount was raised from 0.3% to 0.6%, indicating that the addition of TS300 enhanced the conversion of Pb to the stable state in FA. Although the acid soluble state of Pb in the FA treated with the other two chelating agents was reduced compared to the original ash, however, its F2 fraction was significantly increased, leading to an increase in the unstable fraction. Therefore, the chelating agent TS300 was relatively more effective in the treatment.

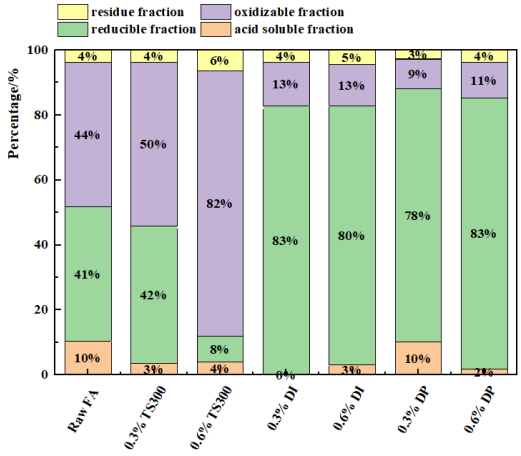

Fig 2 Speciation distribution of Pb with different CA

CONCLUSION

All three chelating agents in this study could meet the landfill limits at a 0.3% addition, and the leaching amount of TS300 is the lowest. By analyzing the proportion of four heavy metal forms of Pb, the F1 and F2 components of Pb treated with TS300 accounted for the least when the addition amounts were the same, indicating that the treatment effect of TS300 was better than the other two chelating agents.

ACKNOWLEGEMENT

The study was supported by the National Key Research and Development Program of China (2021YFE0112100).

REFERENCE

1.NBS, C. China Statistical Yearbook of 2021.

2.Mao, Y.; Wu, H.; Wang, W.; Jia, M.; Che, X., Pretreatment of municipal solid waste incineration fly ash and preparation of solid waste source sulphoaluminate cementitious material. Journal of Hazardous Materials 2020, 385, (Mar.5), 121580.1-121580.9.

3.Hongwei; Luo; Ying; Cheng; Dongqin; He; En-Hua; Yang, Review of leaching behavior of municipal solid waste incineration (MSWI) ash. The Science of the total environment 2019.

4.Dou, X.; Ren, F.; Nguyen, M. Q.; Ahamed, A.; Yin, K.; Chan, W. P.; Chang, W. C., Review of MSWI bottom ash utilization from perspectives of collective characterization, treatment and existing application. Renewable and Sustainable Energy Reviews 2017, 79, (nov.), 24-38.

5.Lu, Y.; Tian, A.; Zhang, J.; Ang, Y.; Huang, Y., Physical and Chemical Properties, Pretreatment, and Recycling of Municipal Solid Waste Incineration Fly Ash and Bottom Ash for Highway Engineering: A Literature Review. Advances in Civil Engineering 2020, 2020, (12), 1-17.

6. Ma, W.; Chen, D.; Pan, M.; Gu, T.; Zhong, L.; Chen, G.; Yan, B.; Cheng, Z., Performance of chemical chelating agent stabilization and cement solidification on heavy metals in MSWI fly ash: A comparative study. Journal of Environmental Management 2019, 247, (Oct.1), 169-177.

7. Luo, Z.; Tang, C.; Hao, Y.; Wang, Z.; Mu, Y., Solidification/stabilization of heavy metals and its efficiency in lead–zinc tailings using different chemical agents. Environmental Technology 2020, 1-11.

INSIGHTS INTO THE LANDFILL LEACHATE PROPERTIES AND BACTERIAL STRUCTURE SUCCESSION RESULTING FROM THE COLANDFILLING OF MUNICIPAL SOLID WASTE AND INCINERATION BOTTOM ASH

Ya-nan Wang[1], Han Shi[1], Qingzhao Wang[1]

1.Qingdao Solid Waste Pollution Control and Resource Engineering Research Center, Qingdao University of Technology, School of Environmental and Municipal Engineering, Qingdao, China

ABSTRACT

Four simulated bioreactors were loaded with only MSW, 5% BA+MSW, 10% BA+MSW and 20% BA+MSW to investigate the leachate property and bacterial community change trends during the colandfilling process. The results showed that with increasing BA addition proportion (5%~20%), the leachate oxidation–reduction potential (ORP) was lower, the leachate pH quickly entered the neutral stage, and the chemical oxygen demand (COD), volatile fatty acids (VFA), NH_4^+-N, Ca^{2+} and SO_4^{2-} presented faster downward trends. BA can quickly increase bacterial diversity, and the higher the addition proportion of BA, the more significant the change in microbial community structure during the landfilling process. The leachate pH and COD greatly influenced the bacterial community structure. A low BA proportion can increase metabolism pathway abundance during the initial stage, but a high BA proportion had an inhibitory effect on the metabolism pathway.

KEYWORDS: Municipal solid waste (MSW), bottom ash (BA), colandfilling, leachate property, microbial communit

1. INTRODUCTION

The increasing amount of municipal solid waste (MSW) has been one of the most serious environmental issues restricting economic and social development (Wijekoon et al., 2022). Landfilling is one of the main disposal methods for MSW due to its low construction cost, simple operation and wide applicability; however, it also poses numerous problems, such as the occupation of a large amount of land, the requirement of long stabilization times and secondary pollution problems (Cheng et al., 2020). Therefore, the long-term stabilization process and operation maintenance of landfills are bottlenecks that restrict landfill technology development. MSW incineration generates a large amount of bottom ash (BA), accounting for approximately 20~25% of the MSW amount (Al-Ghouti et al., 2021). To facilitate the final disposal of slag, the “Standard for Pollution Control on the Landfill Site of Municipal Solid Waste (GB 16889-2008)” stipulated that BA can be directly disposed of in MSW landfill sites in China.

BA has a strong acid-neutralizing capacity, and the release of alkaline substances, such as CaO and K_2O, can effectively improve the low pH value of the leachate, eliminate organic acid accumulation, and potentially accelerate methane production (He et al., 2017). MSW degradation is the result of the synergistic effects of different groups of microorganisms. The microorganisms in landfills utilize organic matter to continuously grow and multiply and accelerate the biodegradation of organic components, which plays a key role in the landfill stabilization process (Wei et al., 2017). An investigation of the bacterial communities in landfills and leachates showed that Firmicutes was predominantly present in all landfills, while

Actinobacteria and Proteobacteria also played important roles in refuse degradation. Wang et al. (2021c) investigated the succession of the bacterial community in refuse of landfills of different ages and found that the bacterial community compositions in the refuse of landfills of similar ages were highly similar, and bacterial community succession occurred continuously with landfill aging. Nevertheless, the effects of BA under different codisposal ratios on the microbial community and the relation between microbial and leachate properties during the landfilling process remain unclear.

In this study, simulated bioreactor landfills in which BA and MSW were mixed at different ratios were constructed. The effects of different codisposal ratios of BA on the variations in leachate properties as well as the leachate stabilization degree were explored. Moreover, the succession of the microbial community and the relationships between the microbial community and the leachate properties were illuminated. In addition, the effects of BA on the microbial function characteristics and metabolism pathways were illustrated. This research can help further understand the impacts of BA on refuse degradation and landfill stabilization.

2. MATERIALS AND METHODS

2.1 Experimental device

Four simulated anaerobic bioreactor landfill columns denoted A, B, C, and D were constructed. A was a control group that was loaded with only 11.25 kg MSW, while B, C, and D were loaded with BA and MSW at mass ratios of 1:20 (0.56 kg BA and 11.25 kg MSW), 1:10 (1.13 kg BA and 11.25 kg MSW), and 1:5 (2.25 kg BA and 11.25 kg MSW)

2.2 Experimental procedure

Before the experiment, 3 L of tap water was added to each column to maintain a suitable moisture content for the refuse biodegradation. During stage I (1~155 days), the bioreactors were operated anaerobically without leachate recirculation, and the leachate samples were collected through the leachate collection pipe every month. During stage II (156~365 days), a total volume of 3.0 L liquid (in order to avoid the long-term acidification of the system caused by leachate recirculation, a mixture of 2.5L leachate and 0.5L distilled water was used for recirculation) was recirculated into the column once a week by using a peristaltic pump, and the leachate samples were collected every week. After that, the leachate was recirculated, and then the columns were sealed until the next cycle.

2.3 Analytical methods

The physicochemical properties of the leachate during the landfilling process were determined. The pH was determined by using a pH meter. The EC was determined by using a conductivity meter. The ORP was determined by using an ORP meter. The alkalinity was determined by using an automatic potentiometric titrator. The chemical oxygen demand (COD) was determined by the potassium dichromate method. The Ca^{2+} and volatile fatty acids (VFA) were determined by ethylene diamine tetraacetic acid (EDTA) titration and distillation titration, respectively. NH_4^+-N was determined by spectrophotometry.

Solid samples (10 g) were collected at different degradation stages, including the initial stage (on Day 7), middle stage (on Day 176), late stage (on Day 267) and final stage (on Day 351), to analyze the microbial community.

2.4 Data analysis

Redundancy analysis (RDA) was performed using the Vegan package in R, based on KEGG annotation and PICRUSt software to analyze metabolic pathways. SPSS 22.0 was used to analyze the correlation between bacterial community structure and environmental factors.

3. RESULTS AND DISCUSSION

3.1 Changing leachate property trends during the colandfilling process

3.1.1 ORP, EC, pH and alkalinity

The leachate ORP, EC, pH and alkalinity change trend over time in each column is shown in **Fig. 1**. During stage I, the ORP change trend in column B was similar to that in column A, with values

fluctuating in the range of 0~-100 mV, while the ORP values in columns C and D were much lower than those in columns A and B. During stage II, the ORP values in columns C and D increased during Days 155~176 and then presented decreasing trends Overall, the order of the ORP values was D < C < B < A. The results showed that the columns loaded with BA and MSW had lower reduction potentials, which was conducive to the refuse entering the anaerobic biodegradation process. During stage I, the order of the EC values in each column was D > C > B > A, which was greatly related to the initial BA addition amount. During stage II, the EC values in all columns presented gradually decreasing trends, and the order of the corresponding decreasing rates was A < B < C < D. During stage I, the leachate pH in each column varied from 5.3 to 5.7, 5.3 to 6.1, 5.9 to 6.2, and 6.7 to 7.0, and the order of the leachate pH values in each column was A < B < C < D. During stage II, the leachate pH in column A was always acidic and significantly lower than that in columns B, C, and D. The results indicated that BA addition can effectively improve the system pH to prevent landfill system instability due to acid accumulation (He et al., 2017).During stage I, the leachate alkalinity in all columns showed increasing trends, and the values were in the order of A < B < D < C. During stage II, The increased alkalinity of the recirculated leachate played a buffering role and alleviated the initial acidification phenomenon, which further accelerated organic matter degradation (He et al., 2017; Wang et al., 2021b).

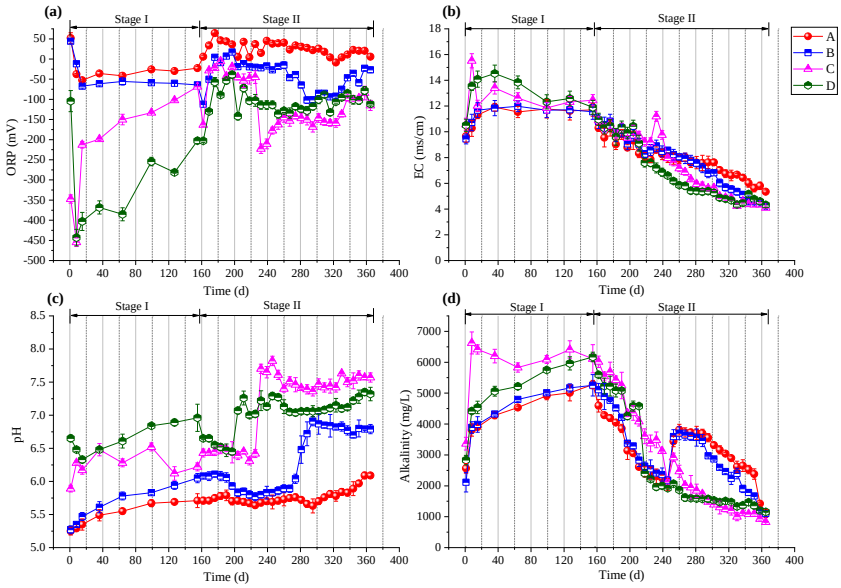

Fig. 1 The changing trends of leachate ORP (a), EC (b), pH (c), and alkalinity (d) in each column during the colandfilling of MSW and BA (A, B, C and D represented the columns that loaded with only MSW, 5% BA+MSW, 10% BA+MSW and 20% BA+MSW, respectively).

3.1.2 COD, VFA, Ca^{2+}, NH_4^+-N, SO_4^{2-} and S^{2-}

The leachate COD, VFA, Ca^{2+}, NH_4^+-N, SO_4^{2-} , and S^{2-} change trend in each column over time is shown in **Fig. 2**. During stage I, the leachate VFA increasing trends in all columns occurred because the complex organic matter in the refuse was hydrolyzed and fermented into soluble small-molecule organic matter under the action of hydrolysis and fermentation microorganisms (Luo et al., 2022). During stage II, the leachate VFA concentration in each column decreased because a large amount of acid was consumed by methanogens. In the late landfill period, the order of the leachate VFA concentration was D < C < B < A, which also indicated that the addition of slag can reduce the leachate VFA concentration and accelerate the refuse

stabilization process (Lo and Liao, 2007). During stage I, the leachate Ca^{2+} concentration in all columns showed increasing trends, and the peak concentrations in columns C and D of 5438 mg/L and 5410 mg/L were slightly higher than those in columns A and B. During stage II, the leachate Ca^{2+} concentration showed decreasing trends in all columns. The leachate Ca^{2+} concentration gradually decreased to 1400 mg/L and 900 mg/L in columns A and B, respectively, by the end of the experiment.

The decreasing leachate NH_4^+-N concentration was mainly ascribed to the dilution effect of recirculated leachate with 0.5 L distilled water every cycle. The decreasing trends in the other three columns were more obvious than that in column A, which was related to the absorption effect of BA (Yao et al., 2015). During stage I, the leachate SO_4^{2-} concentration in all columns increased rapidly to peak values during the first several days, after which it gradually decreased. During stage II, the leachate SO_4^{2-} concentration drastically fluctuated and presented sharp increases, with values of 483, 644, 759 and 379 mg/L in each column during Days 162~176. The leachate S^{2-} concentration was relatively low during the whole process.

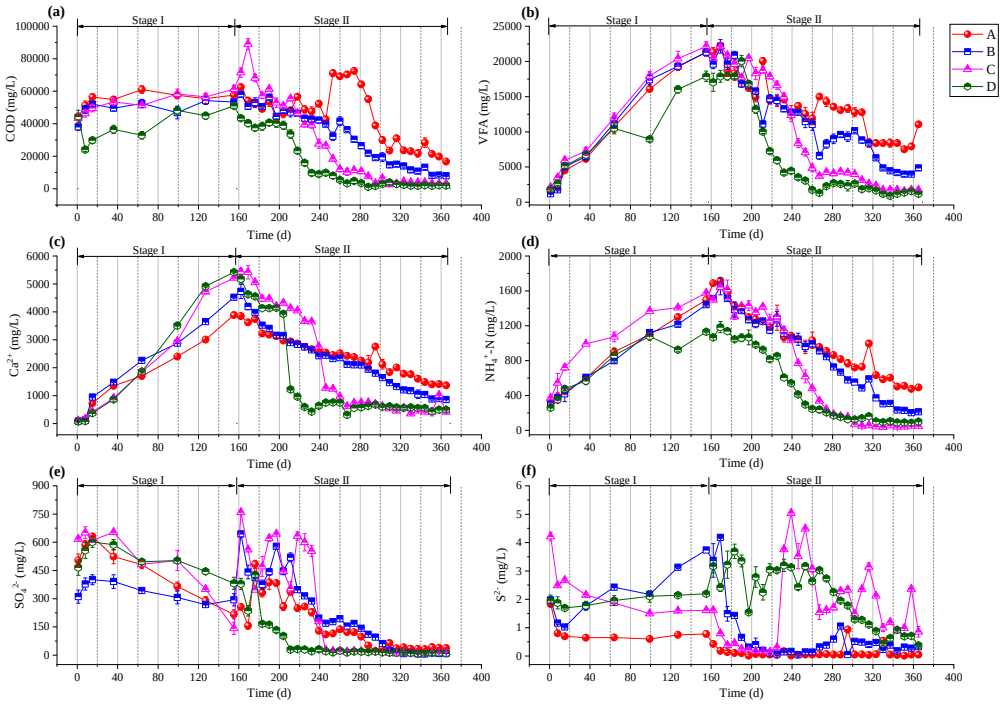

Fig. 2 The changing trends of leachate COD (a), VFA (b), Ca^{2+} (c), NH_4^+-N (d), SO_4^{2-} (e), and S^{2-} (f) in each column during the colandfilling of MSW and BA (A, B, C and D represented the columns that loaded with only MSW, 5% BA+MSW, 10% BA+MSW and 20% BA+MSW, respectively).

3.2 Bacterial community structure succession at the phylum and genus levels

(1) Phylum level

The bacterial community structure in each column at the phylum level during the colandfilling process is shown in **Fig. 3**. The structure of the dominant phyla in column A varied slightly during the whole landfilling process. The structure of the dominant phyla in column B showed obvious differences from that of column A during the initial stage, but it was similar to that of column A during the middle, late and final stages. For columns C and D, the structures of the dominant phyla showed significant differences from those of columns A and B, especially in the initial, late and final stages. These results indicated that BA addition can alter the

microbial community structure, and the higher the addition proportion is, the more significant the change in the microbial community structure in the landfilling process. During the waste degradation process, the predominant phyla were Firmicutes, Proteobacteria and Bacteroides, which was in accordance with previous studies reported by Liu et al. (2019) and Morita et al. (2020). Köchling et al. (2015) and Wang et al. (2021c) reported that Firmicutes and Proteobacteria were the dominant microbial communities associated with lignocellulosic and carbohydrate degradation during the early stage of a landfill, while with increasing landfill age, Bacteroidetes, which can degrade complex refractory organic compounds, began to play a dominant role.

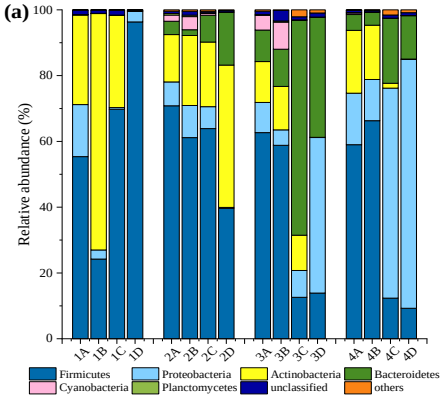

Fig.3 The bacterial community structure at the phylum levels in each column (1, 2, 3 and 4 represent the initial, middle, late and final stages of landfill process, respectively).

(2) Genus level

The changes in the bacterial community at the genus level in each column during different landfill stages are shown in **Fig. 4**. Overall, *Lactobacillus* and *Propionibacterium* were the major genera during the initial degradation stage, while over time, *Prevotella, Streptophyta, and Acinetobacter* were involved in the landfilling process, and *others* and *unclassified* accounted for high proportions in the late and final stages. Luo et al. (2020) pointed out that *Lactobacillus* is the dominant bacterium that secretes amylase. The presence of *Propionibacterium* can significantly increase the propionic acid concentration in VFAs (He et al., 2019), and the succession of *Propionibacterium* was greatly related to the variation of VFA (Wei et al., 2021).

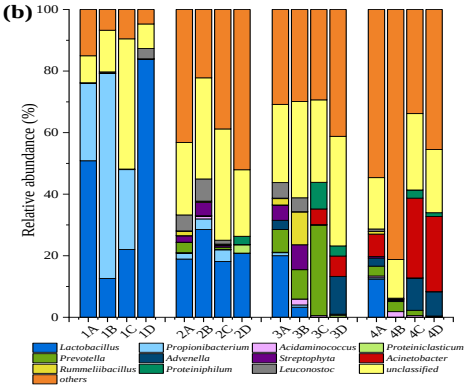

Fig.4 The bacterial community structure at the genus levels in each column (1, 2, 3 and 4 represent the initial, middle, late and final stages of landfill process, respectively).

3.3 Correlations between the bacterial community structure and the landfill environment

The RDA results of the bacteria and environmental factors at the genus level in the mixed landfilling process is shown in **Fig. 5**. The COD and EC are the main environmental factors affecting the microbial community structure in the early stage of waste degradation. The pH and alkalinity have great impacts on the microbial community in the middle and late stages of waste degradation. The COD and alkalinity were the main influencing factors of bacterial community structure in the MSW-alone system and 5%-BA system, while the pH, $E_{300/400}$ and ORP were the main influencing factors of bacterial community structure in the columns with higher BA proportions. The order of influence of the leachate properties on the bacterial community structure was pH > COD > EC >$E_{300/400}$ > alkalinity > ORP. Moreover, the genera *Lactobacillus* and *Propionibacterium* had strong positive correlations with COD and EC, while *Pseudomonas*, *Carnobacterium*,*Acinetobacter*, and *Corynebacterium* were positively correlated with pH. Wang et al. (2021c) and Zhao et al. (2021) reported that the effects of pH, organic matters, total Kjeldahl nitrogen

and EC were the major environmental factors that influencing the variation and distribution of bacterial community in landfills.

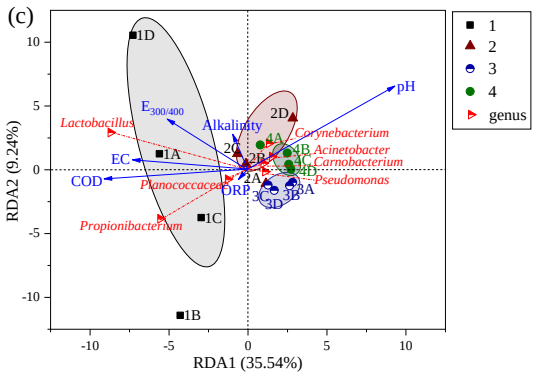

Fig.5 The redundancy analysis of bacteria and environmental factors at the genus level during the co-landfill process (1, 2, 3 and 4 represent the initial, middle, late and final stages of landfill process, respectively).

3.4 Functional characterization of the bacterial community

The functional properties of the bacterial communities in different landfill systems during waste degradation based on the KEGG pathway at levels I and II are shown in **Fig. 6**. The KEGG level I annotation of the bacterial community indicated that metabolism (Me), genetic information process (GIP) and environmental information process (EIP) were the main metabolic pathways. The KEGG level II annotation of the bacterial community showed that carbohydrate and amino acid metabolism were the dominant metabolic pathways in each system, followed by energy metabolism, coenzyme factor and vitamin metabolism, nucleic acid metabolism, and lipid compound metabolism. Overall, during the initial stage, a low BA addition proportion increased metabolism pathway abundance, but a high BA addition proportion had an inhibitory effect on the metabolism pathway. With refuse degradation, the metabolism abundance in each column increased, but the metabolism abundance in column A was higher than that in columns loaded with BA, which was in accordance with the variation in leachate COD.

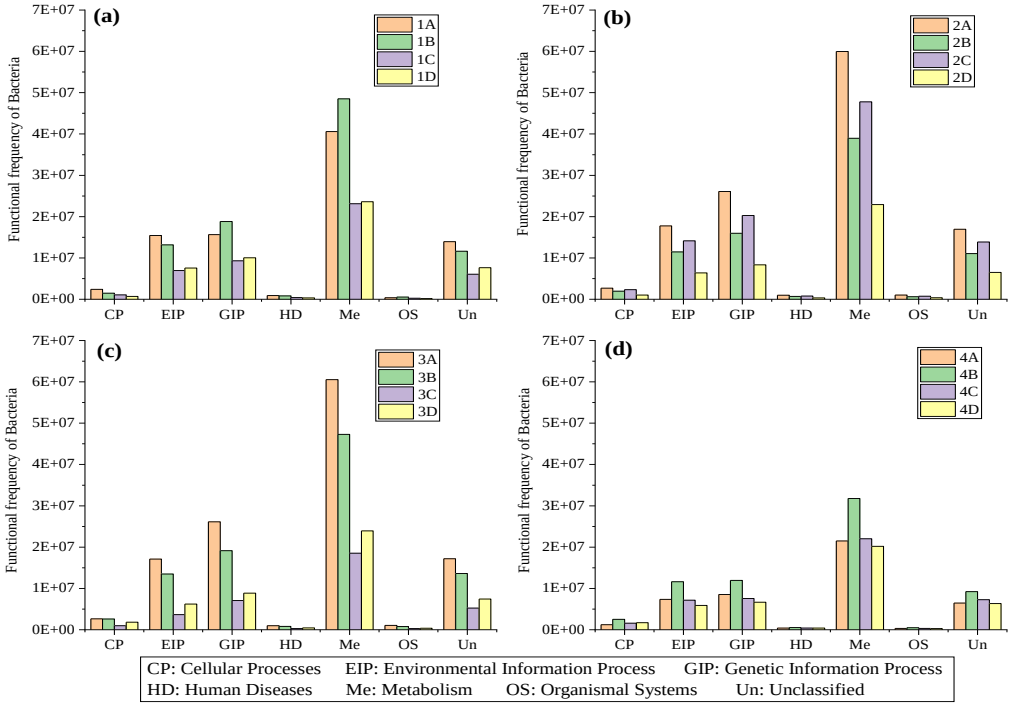

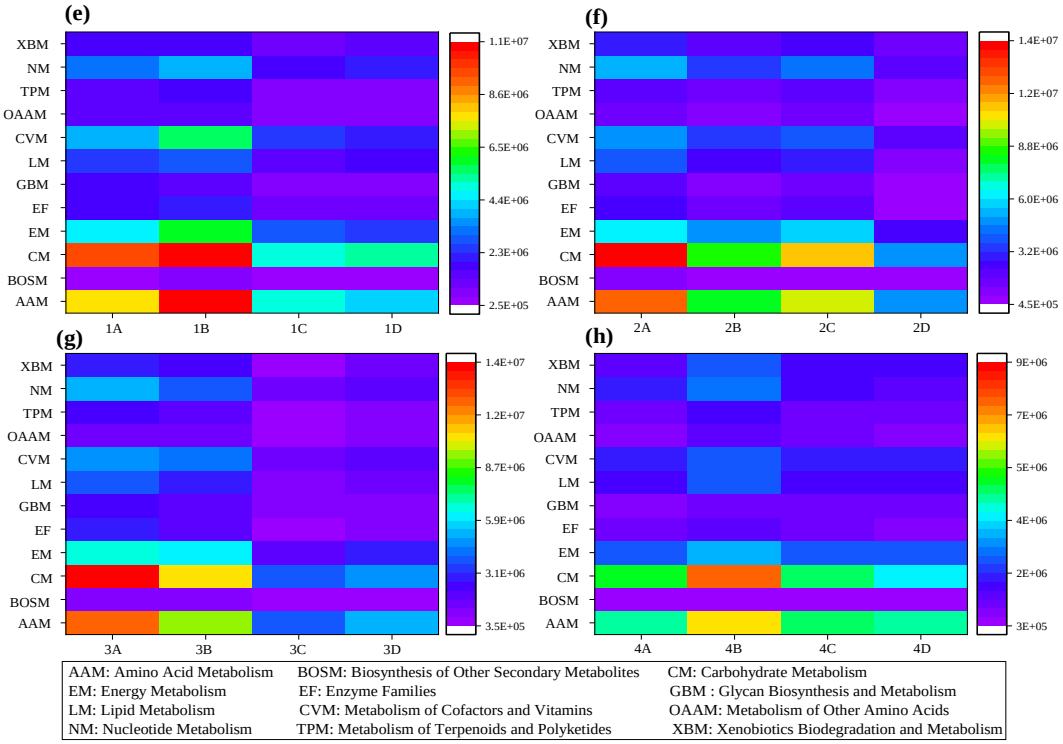

Fig. 6 The bacterial functional abundance based on KEGG level I (a, b, c, d) and level II (e, f, g, h) annotations in each column during the colandfilling of MSW and BA (1, 2, 3 and 4 represent the initial, middle, late and final stages of landfill process, respectively).

4. CONCLUSIONS

When incineration BA was codisposed with MSW during the landfilling process, the leachate pH could quickly enter the neutral stage, the COD, VFA, NH_4^+-N, Ca^{2+} and SO_4^{2-} presented faster downward trends. BA can quickly increase bacterial diversity, while the long-term selectivity of BA in the middle and late stages of the landfilling process resulted in a certain decrease in bacterial community diversity. *Lactobacillus* and *Propionibacterium* were the major genera during the initial degradation stage, while over time, *Prevotella*,*Streptophyta*, and *Acinetobacter* were involved in the landfilling process. Carbohydrate and amino acid metabolism were the dominant metabolic pathways in each system.

FUNDING

This work was supported by the National Natural Science Foundation of China [Grant numbers 51908304, 51978350 and 41907111], the China Postdoctoral Science Foundation [Grant number 2018M632642].

REFERENCES

Al-Ghouti, M.A., Khan, M., Nasser, M.S., Al-Saad, K., Heng, O.E., 2021. Recent advances and applications of municipal solid wastes bottom and fly ashes: Insights into sustainable management and conservation of resources. Environmental Technology & Innovation, 21: 101267.

Cheng, Z.W., Zhu, S.J., Chen, X.L., Wang, L.C., Lou, Z.Y., Feng, L.L., 2020. Variations and environmental impacts of odor emissions along the waste stream. Journal of Hazardous Materials, 384: 120912.

He, P.J., Pu, H.X., Shao, L.M., Zhang, H., 2017. Impact of co-landfill proportion of bottom ash and municipal solid waste composition on the leachate characteristics during the acidogenesis phase. Waste Management, 69: 232-241.

Köchling, T., Sanz, J.L., Gavazza, S., Florencio, L., 2015. Analysis of microbial community structure and composition in leachates from a young

landfill by 454 pyrosequencing. Applied microbiology and biotechnology, 99: 5657-5668.

Liu, S., Xi, B., Qiu, Z., He, X., Zhang, H., Dang, Q., Zhao, X., Li, D., 2019. Succession and diversity of microbial communities in landfills with depths and ages and its association with dissolved organic matter and heavy metals. Science of The Total Environment, 651: 909-916.

Lo, H.M., Liao Y.L., 2007. The metal-leaching and acid-neutralizing capacity of MSW incinerator ash co-disposed with MSW in landfill sites. Journal of Hazardous Materials, 142: 512-519.

Luo, J., Fang, S., Huang, W., Wang, F., Zhang, L., Fang, F., Cao, J., Wu, Y., Wang, D., 2022. New insights into different surfactants' impacts on sludge fermentation: focusing on the particular metabolic processes and microbial genetic traits. Frontiers of Environmental Science & Engineering, 16: 106.

Luo, K., Xie, X., Yang, Q., Chen, F., Zhong, Y., Xie, P., Wang, G., 2020. Multi-hydrolytic enzyme accumulation and microbial community structure of anaerobic co-digestion of food waste and waste-activated sludge. Environmental technology, 41: 478-487.

Morita, A.K.M., Sakamoto, I.K., Varesche, M.B. A., Wendland, E., 2020. Microbial structure and diversity in non-sanitary landfills and ass -ociation with physicochemical parameters. En -vironmental Science and Pollution Researc h, 27: 40690-40705.

Wang, Q., Ko, J.H., Liu, F., Xu, Q., 2021b. Leaching characteristics of heavy metals in MSW and bottom ash co-disposal landfills. Journal of Hazardous Materials, 416: 126042.

Wang, Y., Xu, R., Wang, H., Shi, H., Kai, Y., Sun, Y., Li, W., Bian, R., Zhan, M., 2021c. Insights into the stabilization of landfill by assessing the diversity and dynamic succession of bacterial community and its associated bio-metabolic process. Science of The Total Environment, 768: 145466.

Wei, H., Wang, J., Hassan, M., Han, L., Xie, B., 2017. Anaerobic ammonium oxidation-denitrification synergistic interaction of mature landfill leachate in aged refuse bioreactor: Variations and effects of microbial community structures. Bioresource Technology, 243: 1149-1158.

Wei, Y., Ren, B., Zheng, S., Feng, X., He, Y., Zhu, X., Zhou, L., Li, D., 2021. Effect of high concentration of ammonium on production of *n*-caproate: Recovery of a high-value biochemical from food waste via lactate-driven chain elongation. Waste Management, 128: 25-35.

Wijekoon, P., Koliyabandara, P.A., Cooray, A.T., Lam, S.S., Athapattu, B.C.L., Vithanage, M., 2022. Progress and prospects in mitigation of landfill leachate pollution: Risk, pollution potential, treatment and challenges. Journal of Hazardous Materials, 421: 126627.

Yao, J., Kong, Q., Zhu, H., Zhang, Z., Shen, D., 2015. Adsorption of ammonia on municipal solid waste incinerator bottom ash under the landfill circumstance. Korean Chemical Engineering Research, 53: 503-508.

Zhao, R., Liu, J., Feng, J., Li, X., Li, B., 2021. Microbial community composition and metabolic functions in landfill leachate from different landfills of China. Science of The Total Environment, 767: 144861.

LEACHING BEHAVIOR OF HEXAVALENT CHROMIUM FROM REFRACTORY BRICK UNDER HUMID ENVIRONMENT

Yasumasa Tojo[1], Kotone Matsui[1], In-Hee Hwang[1] and Takayuki Matsuo[1]
1 Division of Environmental Engineering, Graduate School of Engineering, Hokkaido University
N13W8 Kitaku, Sapporo, Japan

INTRODUCTION

In Japan, solid waste landfill is classified into three types. They are inert waste landfill, non-hazardous waste landfill, and hazardous waste landfill [1]. Among them, in hazardous waste landfill, hazardous waste which exceeds criteria for hazardous heavy metals leaching is disposed of. The hazardous waste landfill is required to be designed and constructed with robust concrete wall and base, and the top is capped. The concept of this landfill is containment of hazardous substance and eliminates the chance of reaction with water and air. In general, in non-hazardous waste landfill, various substances are subjected to many reactions and gradually stabilized. Even for hazardous heavy metals, it is known that their leaching potentials reduce due to the long-term weathering effect. But according to the concept of the hazardous waste landfill, these reactions cannot be expected. This means that the leaching potential of hazardous heavy metals will be kept forever. However, there is no guarantee that the container structure will be permanently maintained because of the impact of natural deterioration of structure or disaster.

In order to prevent sudden emission of hazardous substance due to these occasions in future, some measure must be taken. There are two candidates considered to be able to achieve it. The one is multi-barrier system. To surround the site by various barrier systems such as clay barriers, impact of heavy metal to the surrounding environment can be mitigated. The other is to reduce the leaching potential of hazardous substance itself from solid waste. For incineration residue, the aging phenomenon is known to be effective for reducing the mobility of heavy metals [2]-[4]. The aging or weathering of the incineration residue is occurred by the contact with rainwater and carbon dioxide in air. As mentioned above, the hazardous waste landfill is surrounded by concrete walls and roof. The waste inside the landfill is isolated from the outside environment. This means that active control of inside circumstance is necessary to create the condition preferable for aging or weathering.

In this study, the effect of inside circumstance of the hazardous waste landfill on the leaching behavior of harmful heavy metals was investigated. The refractory brick used in incinerator is major waste disposed of in hazardous waste landfill because of its high Cr(VI) leaching. Thus, the objective of the study is to elucidate suitable condition for reducing Cr(VI) leaching potential from the refractory brick disposed of in the hazardous waste landfill and to propose the active control method to achieve it.

MATERIALS AND METHODS

A used furnace refractory brick was obtained from a municipal solid waste melting facility and the leaching characteristics of hexavalent chromium was examined. Especially, influence of the internal circumstance of the hazardous waste landfill on its leaching was focused on. The obtained used refractory brick was rectangular parallelepipeds of about 10cm x 10cm x 20cm. It was reported that chromium in refractory bricks consists of trivalent chromium (Cr_2O_3) at the time of manufacture, but when used in the furnace, it reacts with CaO, which is the main component of slag produced by waste melting process, and changes to hexavalent chromium compound ($CaCrO_4$) [5]. This reaction can be expressed as;

$$Cr_2O_3 + 2CaO + 2/3O_2 \rightarrow 2CaCrO_4$$

After the refractory brick was pulverized into powder, the elemental composition, hexavalent chromium content, leaching concentration by leaching test of the Ministry of the Environment Notification No. 13 method (hereafter JLT-13), etc. were measured to grasp the characteristics of the refractory brick. However, detailed information such as elemental composition will not be shown in this paper because it will lead to product specification.

As a result of basic analysis mentioned above, it was found that trivalent chromium compound (Cr_2O_3), which is not harmful or leachable, was contained in large amounts in refractory brick. However, hexavalent chromium was generated from the reaction with slag components generated during the melting process, and this sample contained 30 mg/kg of Cr(VI). The

concentration of Cr(VI) obtained from the JLT-13 leaching test was 3 mg/L, exceeding the criteria (1.5 mg/L) for hazardous waste.

In order to prepare samples for the accelerated weathering experiment, a rectangular parallelepiped refractory brick was cut into 14 slices, and each slice was pulverized and mixed in a ball mill. This pulverizing and mixing pretreatment reduced the leaching concentration to 1/30 or less (Table 1).

Table 1. Leaching concentration of hexavalent chromium and pH before and after pulverizing and mixing

	Before	After
Cr(VI) mg/l	3	0.09
pH	8.6	7.1

This is thought to be caused by the fact that the refractory brick comes into contact with CO_2 in the atmosphere during the pulverizing and mixing process of the sample, resulting in a decrease in pH and a change in the leaching characteristics of chromium. The leaching test was also performed on each of the 14 slices, and there was little difference from the original sample. Therefore, it was suggested that a neutralization reaction progressed during mixing in the ball mill. As a result, the Cr(VI) leaching concentration was below the hazardous waste criteria, but it was subjected to the accelerated weathering experiment as it was. The pulverized refractory brick placed in a petri dish were placed in a desiccator adjusted to the circumstance that can be assumed as a hazardous waste landfill, and an accelerated weathering experiment was performed.

The four conditions shown in Table 2 were set as the circumstance conditions, including a humidified state, a completely dry state, and a gas atmosphere of air or nitrogen. Humidification conditions were achieved by placing a stainless steel tray containing water in a desiccator, and drying conditions were achieved by placing a tray containing silica gel. A sample was taken out every week, and the leaching concentration of hexavalent chromium was measured in accordance with JLT-13 method. Fig. 1 shows the status of accelerated weathering experiment. Each week, one tray of each was removed and analyzed.

Table 2. Circumstance condition set for accelerated weathering experiment

Wet/Dry	Gas condition	
Dry	N_2	Air
Wet (humid)	N_2	Air

RESULTS AND DISCUSSION

Fig. 2 shows the changes in the (a) pH and (b) leaching concentration of hexavalent chromium during the accelerated weathering test of the pulverized refractory brick conducted over 10 weeks.

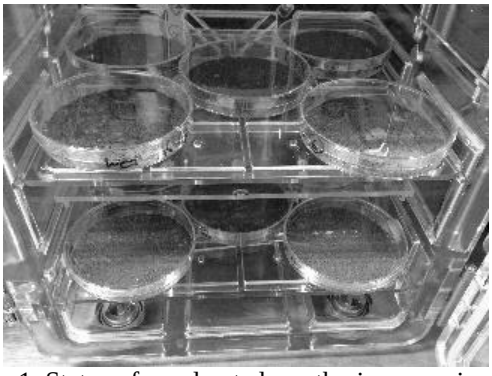

Fig. 1. Status of accelerated weathering experiment

As shown in (a), there was a significant difference in pH between dry and wet conditions. The dry conditions did not change significantly from the initial values, and the values at the start of the test were maintained within the range of 7 to 8, regardless of the gas atmosphere. On the other hand, under wet conditions, all of them were below 7, and especially under Wet (Air), they were below 6. Leaching concentration of hexavalent chromium shown in (b) also showed a significant difference between dry and wet conditions, and the leaching concentration of chromium decreased under wet conditions. In particular, under Wet (N_2) conditions, hexavalent chromium was no longer detected in all weeks after the second week.

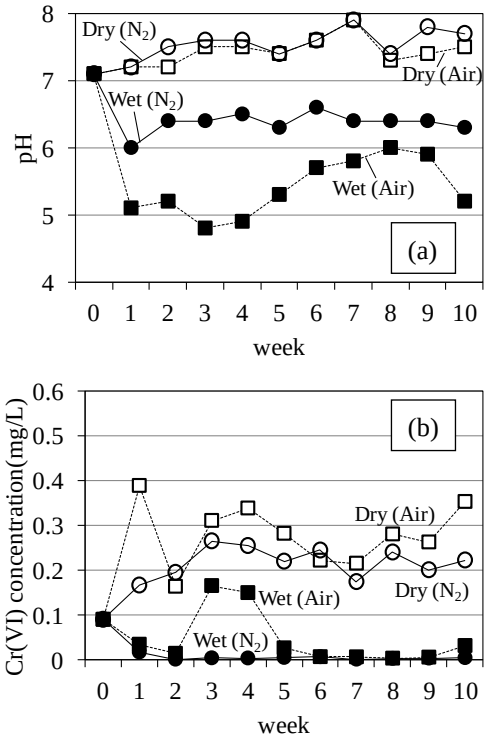

Fig. 2. Change in (a) pH and (b) hexavalent chromium

leaching concentration in accelerated weathering experiment

Although the results are not shown, pH dependent test was performed on the pulverized refractory brick to confirm whether the lowered pH reduced the leaching of hexavalent chromium. The initial addition method was adopted as the test method. As the result, no particular tendency was observed in the leaching concentration of hexavalent chromium in the pH range of 6-9. The used castable refractory (the leaching concentration of hexavalent chromium is two orders of magnitude higher than that of refractory brick) obtained at the same time from same facility was also subjected to the pH dependence test, and the leaching concentration was almost constant within the pH range of 2 to 5.

Therefore, the accelerated weathering experiment of the pulverized refractory brick was carried out again. Though the cause of the decrease in pH was not clear, tests were carried out at varying carbon dioxide concentration since it was confirmed that the leaching concentration of hexavalent chromium decreased significantly during the pulverizing and mixing process of the sample as mentioned in the experimental method. Both conditions (Table 3) were set at humid conditions, CO_2 concentrations were set at 50% and 100%, and the test period was set for 8 weeks.

Table 3. Condition of re-experiment

Run	Gas condition	Humidity
R-1	CO_2 50%, air 50%	Saturate
R-2	CO_2 100%	Saturate

The results are shown in Fig. 3. In this re-experiment as well, the leaching concentration of Cr(VI) tends to decrease with time as shown in Fig. 3(a). However, the change in pH (Fig. 3 (b)) was slight in this experiment. It was assumed that the neutralization would progress in the CO_2 atmosphere, but the pH was stabilized at around 9.5. On the other hand, the ORP (Fig. 3 (c)) decreased significantly from the first round under any CO_2 conditions. Although the results are not shown, a significant increase in ferrous ion concentration was confirmed under the condition of CO_2 = 100%. Since ferrous ion is known as reducer, it seems that leaching of ferrous ion into absorbed water on refractory brick work to reduce hexavalent chromium to trivalent chromium.

For the condition of CO_2 = 100%, Eh was calculated from the measured ORP, and the calculated Eh value and pH for each week were plotted on pH-Eh diagram of chromium [6] (Fig. 4) to examine the stable form of chromium in solution for each week. As can be seen in Fig. 4, Chromate ions (CrO_4^{2-}), which is hexavalent chromium compound, was in a stable form before the refractory was exposed to a moist environment. However, it was found that the stable form of

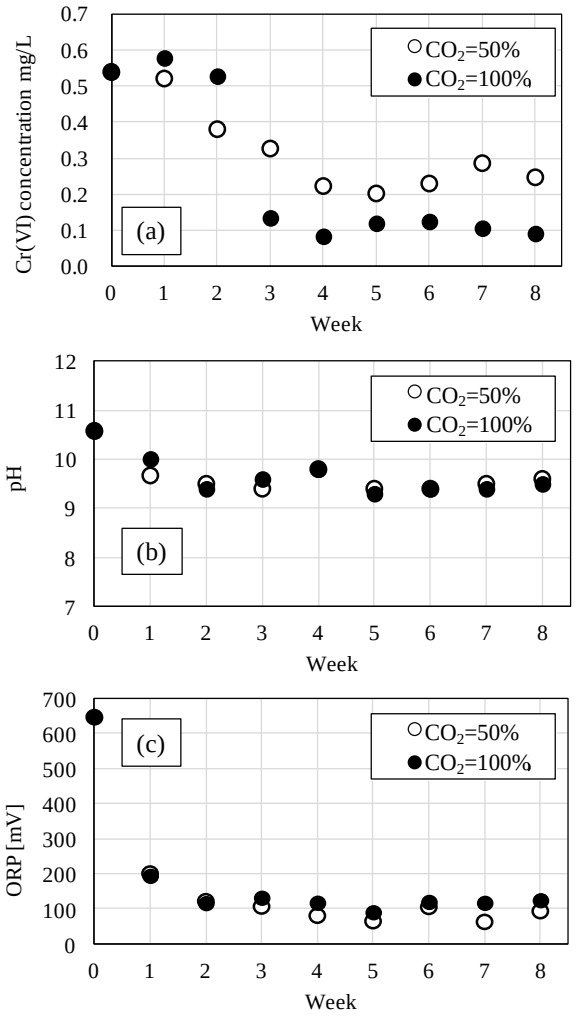

Fig. 3. Change of (a) Cr(VI) concentration, (b) pH, (c) ORP in accelerating weathering experiment done under wet condition

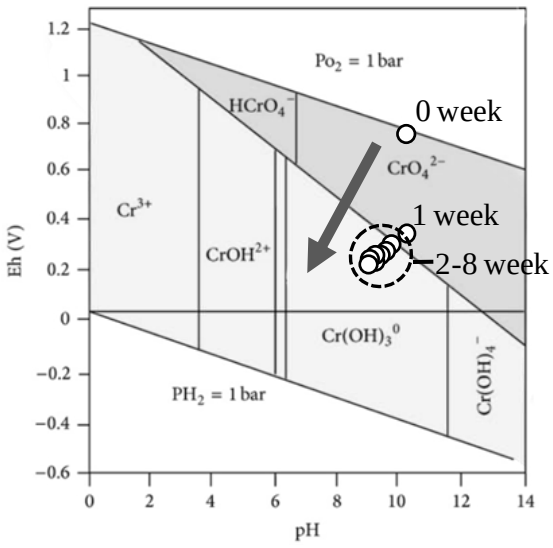

Fig. 4. Changes of chromium status at each week of weathering re-experiment

chromium after 2 weeks of exposure was chromium hydroxide ($Cr(OH)_3$), which is a trivalent chromium compound. From this, an environment in which ions can be leached out into surface adsorbed water around the pulverized refractory brick particle is created due to moisture absorption in a moist environment, and gas in the environment and metal ions (such as ferrous ion) in the refractory are leached there, causing a decrease in pH and Eh. As the results, the form of chromium changed from hexavalent chromium to trivalent chromium.

This suggests that to decrease leaching concentration of hexavalent chromium from refractory brick in hazardous waste landfill, wet (humid) environments may be preferable. Fortunately, the hazardous waste landfill site is insulated from the outside environment with a concrete structure. In other words, it is considered that a concrete realization measure is to keep the humidity of the internal environment high to some extent. However, since the generation of leachate is not permitted under this structural requirement, it is essential to limit to the extent that the amount of surface adsorbed water only occurs.

REFERENCES

[1] Ministry of Environment, Japan, Waste disposal and Recycling measures, https://www.env.go.jp/en/recycle/manage/waste.html

[2] Speiser, C., Baumann, T., Niessner, R., Morphological and Chemical Characterization of Calcium-Hydrate Phases Formed in Alteration Processes of Deposited Municipal Solid Waste Incinerator Bottom Ash, Environmental Science and Technology, 34, 2000, pp.5030-5037.

[3] Piantone, P., Bodenan, F., Chatelet-Snidaro, L., Mineralogical study of secondary mineral phases from weathered MSWI bottom ash: implications for the modeling and trapping of heavy metals, Applied Geochemistry, 19, 2004, pp.1891–1904.

[4] Meima, J. A., Comans, R. N. J., The leaching of trace elements from municipal solid waste incinerator bottom ash at different stages of weathering, Applied Geochemistry, 14, 1999, pp,159-171.

[5] Mizuhara, S., Urabe, T., Yamaguchi, A., Maeda, T., Fundamental Study on the Formation Mechanism of Hexavalent Chromium Compounds from Refractories Including Chromium Trioxide for Waste Melting Furnace, Journal of Japan society of material cycles and waste management, Vol.21, No.5, pp.170-177, 2010.

[6] Palmer, C. D., and Wittbrodt, P. R., Processes Affecting the Remediation of Chromium-Contaminated Sites, Environmental Health Perspectives, Vol. 92, pp. 25-40, 1991.

DEGRADATION OF CYANIDE CONTAMINANTS IN CTS BY ALKALI-HEAT CO-ACTIVATED PS: PERFORMANCE AND MECHANISM STUDY

Yunmei Wei*, Yi Wen, Lianying Chen, and Shuang Chen
Key Laboratory of Three Gorges Reservoir Region's Eco-Environment, Ministry of Education,
College of Environment and Ecology, Chongqing University, Chongqing, 400045, P.R. China

ABSTRACT:
Cyanide tailings (CTs) is hazardous waste and must be treated for cyanide degradation to meet the disposal requirements of the "Technical Specification for Pollution Control of Cyanide Leaching Residue in Gold Industry" (HJ 943-2018). Alkali-heat co-activated persulfate (PS) technology, a common Advanced Oxidation Process (AOP), was adopted for cyanide degradation, and the effect of NaOH to PS addition ratio and reaction temperature were emphasized in this study. The results showed that the cyanide removal rate reached 86.3% at conditions of 60℃ and NaOH:PS ratio 1:0.5. Leaching concentration of total cyanide after treatment was reduced to 0.2 mg/L, which could meet the requirement of HJ 943-2018.

KEYWORDS: Cyanide tailings; Persulfate; Resource recycling; Harmlessness treatment; Advanced oxidation

1 INTRODUCTION

CTs, with an annual production of roughly 100 million tons, were recently added to the "National Hazardous Waste List" in China. The cyanide concentration in the leachate of CTs far exceeded the disposal requirements in the "Technical Specifications for the Control of Cyanide Residue Pollution in the Gold Industry" (HJ 943-2018). The high concentration of cyanide in CTs is a key factor contributing to its environmental risk and inhibiting its deep resource utilization. The cyanides in the CTs mainly present as metal-cyanide complexes, and these complexes tend to show a high affinity with the mineral components in the CTs, which makes it difficult to be treated by conventional cyanide destruction methods. In this study, alkali-heat co-activated persulfate (PS) technology was used to decompose the cyanide pollutants in the CTs, in which alkali is used to promote desorption of cyanide from the solid matrix, and consequently the desorbed cyanide species were oxidized by the active species generated by PS activation.

2 MATERIAL AND METHODS

Cyanide tailings used in this study were collected from a gold smelter in Shandong, China. Chemical composition of CTs was determined by ARL PERFORM'X X-ray fluorescence spectrometer (XRF). The experimental operation is as follows: 1.00 g of CTs were accurately weighed into a 50 ml centrifuge tube, different masses of sodium persulfate and sodium hydroxide were added so that the mass ratios of sodium hydroxide to sodium persulfate were 0:1, 0.33:1, 0.4:1, 0.5:1, 0.67:1, 1:1. The reaction vessels were placed in a water bath shaker at 60°C during the whole experiment.

3 RESULTS AND DISCUSSIONS

3.1 Characterization of physical and chemical properties of the CTs

Physical and chemical properties of CTs are shown in Table 1. The leaching concentration of total cyanide was 11.7 mg/L, exceeding the 5 mg/L required in the "Technical Specifications for the Control of Cyanide Residue Pollution in the Gold Industry" (HJ 943-2018). Thus, the target contaminants in this study were total cyanide. Si, Fe, S and Al were the top four elements in CTs, with corresponding amounts of 33.70%, 28.46%, 16.47% and 6.56%. Additionally, the CTs also contains a little amount of K, Ca, Mg, Na, Zn, Pb, Cu, and Mn.

3.2 Effect of NaOH:PS ratio on cyanide degradation

Santos et al. [1] found that the activation effect of PS was greatest when the ratio of NaOH to PS was between 0.25:1 and 1:1. The addition ratios of NaOH to PS were studied at 0:1, 0.33:1, 0.4:1, 0.5:1, 0.67:1 and 1:1 at 10% PS dosage and the results are shown in Fig. 1. The highest cyanide removal rate of 86.3% was achieved after 72h when NaOH:PS was 0.67:1. The corresponding removal rates were 17.7%, 71.0%, 52.4%, 46.8% and 5.9% for the addition ratios of 1:1, 0.5:1, 0.4:1, 0.33:1 and 0:1.

3.3 Effect of activation temperature on cyanide degradation

The effect of different activation temperatures on cyanide degradation was investigated (NaOH: PS=0.5:1, PS addition =10%) and the results were shown in Fig.2a. When the temperature was 25°C, the cyanide was almost not decomposed. When the temperature was raised to 70 °C, the rate of cyanide elimination rose to 80.1%, indicating that more sulfate radicals were produced from PS as temperature rose[2-3]. From Fig. 2a, we can find

that higher temperature not only promoted cyanide removal but also accelerates the degradation process. By raising the temperature from 25°C to 70°C, the first-order reaction rate constant enhanced from 1.7×10^{-5} min^{-1} to 1.5×10^{-3} min^{-1}.

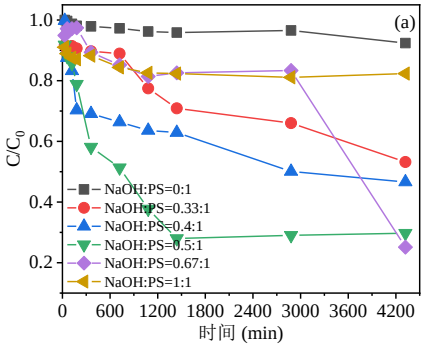

Fig. 1 Effect of NaOH to PS ratio on cyanide degradation

3.4 Leaching toxicity analysis of treated CTs

According to the "Technical Specifications for the Control of Cyanide Residue Pollution in the Gold Industry" (HJ 943-2018), The leaching concentration of total cyanide determined by the national standard leaching method decreased from 11.7 mg/L to 0.2 mg/L after treated by the alkali-heat co-activated persulfate method, which could meet the requirement of 5 mg/L in HJ 943-2018.

4 CONCLUSIONS

In this study, alkali-heat co-activated persulfate was used to degrade cyanide in CTs. The addition ratio of NaOH to PS and temperature had significant effect on cyanide degradation by activated PS. The best cyanide degradation was achieved when the NaOH:PS addition ratio was 0.67:1, with a removal rate of 86.3%. With the increase of activation temperature, the cyanide removal rate could be increased to 80.1%. The leaching concentration of total cyanide decreased from 11.7 mg/L to 0.2 mg/L under optimal conditions, satisfying the toxic leaching requirements of "Technical Specifications for Cyanide Residue Pollution Control in the Gold Industry".

Table 1 Physicochemical properties of cyanide tailings

items	Total cyanide(mg/kg)	WAD-cyanide(mg/kg)	SCN^- (mg/kg)	pH (1:1.25H_2O)	Water content (%)	Leaching toxicity of total cyanide (mg/L)
results	1580	16	2899	9.67	19.31	11.7

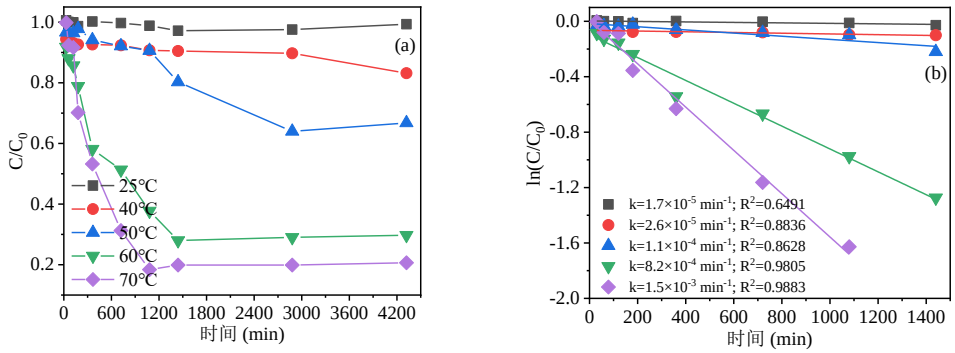

Fig. 2 Effect of different reaction temperatures on cyanide degradation (a) and fitting results by the first-order kinetic model (b). (Experimental conditions: NaOH to PS ratio is 0.5:1, PS dosage is 10%, and L/S ratio is 10:1)

REFERENCE

[1] A. Santos, J. Fernandez, S. Rodriguez, C.M. Dominguez, M.A. Lominchar, D. Lorenzo, A. Romero, Abatement of chlorinated compounds in groundwater contaminated by HCH wastes using ISCO with alkali activated persulfate, Science of The Total Environment. 615 (2018) 1070–1077. https://doi.org/10.1016/j.scitotenv.2017.09.224.

[2] X. Chen, M. Murugananthan, Y. Zhang, Degradation of p-Nitrophenol by thermally activated persulfate in soil system, Chemical Engineering Journal. 283 (2016) 1357–1365. https://doi.org/10.1016/j.cej.2015.08.107.

[3] C. Tan, N. Gao, Y. Deng, N. An, J. Deng, Heat-activated persulfate oxidation of diuron in water, Chemical Engineering Journal. 203 (2012) 294–300. https://doi.org/10.1016/j.cej.2012.07.005.

STABILITED MSWI FLY ASH CO-LANDFILLED WITH ORGANIC WASTE: EFFECT OF LEACHATE PROPERTIES ON THE LEACHING BEHAVIOR OF PCDD/Fs

Mingxue Xin [1], Weihua Li[1], Yingjie Sun[1,*]

1. Qingdao Solid Waste Pollution Control and Resource Engineering Research Center, School of Environmental and Municipal Engineering, Qingdao University of Technology, Qingdao 266520, Shandong, China

ABSTRACT

The leaching behavior and related influence factors of PCDD/Fs from stabilized fly ash were investigated during co-landfill of stabilized fly ash and municipal solid waste (MSW) with different co-landfill ways (layered co-landfill and mixed co-landfill). High leaching concentration of PCDD/Fs was observed at 14 – 56 d, and the fraction of high chlorinated PCDD/Fs exceed 80% in mass concentration of PCDD/Fs. However, the fraction of H_6CDF attained 43% – 73% of the I-TEQ concentration of PCDD/Fs in the period of high leaching concentration of PCDD/Fs. In addition to the various octanol/water partitioning coefficients of PCDD/Fs, characteristics of leachate as well as DOM composition and the content of PCDD/Fs in stabilized fly ash were crucial factor to affect leaching behavior of high chlorinated PCDD/Fs and low chlorinated PCDD/Fs, respectively. This study contributes to the understanding of leaching pattern of PCDD/Fs and environmental risk assessment for MSW landfills.

KEYWORDS

Municipal solid waste (MSW), Stabilized fly ash, Co-landfill, Dioxin (PCDD/Fs)

1.INTRODUCTION

Incineration is preferred as harmless municipal solid waste (MSW) treatment in China, due to advantage of volume reduction and energy recovery. As by-product of MSW incineration, many heavy metals and polychlorinated dibenzo-p-dioxins and dibenzofurans (PCDD/Fs) were enriched in fly ash (FA) and it is classified as hazardous waste. Thus, stabilized FA was landfilled in designated area of MSW landfill after stabilized pretreatment in China. However, the conflict between the rapidly increase of the FA production and practical problems such as shortage of land resources and difficulties in landfill management may causes stabilized FA was co-landfilled with raw MSW. The co-landfill may destroy the stability of toxic components in stabilized FA and cause them to enter the surrounding environment. Numerous studies have been conducted regarding the leaching risk of heavy metals, while little attention has been given to PCDD/Fs in stabilized FA **(Li et al., 2022)**. After MSW incineration, PCDD/Fs content in FA exceeds 80% of the total PCDD/Fs production **(Hsu et al., 2021)**. **Ren et al. (2020)** found that above 92% of highly toxic chlorinated aromatics in flue gas was enriched in FA with the improvement of flue gas control device. The existence of PCDD/Fs was observed in the leachate from different landfill site, which was considered as the result of the co-landfill of MSW and FA **(Choi et al., 2006; Ham et al., 2008; Osako et al., 2002)**. The leaching behavior for PCDD/Fs in FA was proved to significantly relevant for the variation of the concentration and composition of dissolved organic matter (DOM), as well as leachate characteristics **(Hsi et al., 2007; Yasuhara et al., 2007)**. In this study, two co-landfill columns were designed to simulate different co-landfill ways, and the leaching behavior of PCDD/Fs for co-landfill of MSW and stabilized FA in different co-landfill ways was examined during the hydrolysis and

acidogenesis phase. The results can help us better understand the leaching behavior of PCDD/Fs for co-landfill of MSW and stabilized FA, and provide theoretical references for evaluating potential risk during the operation of the landfill.

2. MATERIALS AND METHODS

2.1 Materials

FA was taken from reciprocating grate furnace of the MSW incineration power plant with incineration technology of mechanical grate-type incinerator, semi-dry purification, activated carbon, and bag filter in Qingdao City, China. The chelating agent (sodium diethyldithiocarbamate, industrial grade) derived from incineration power plant was used to prepare of stabilized FA. The stabilization treatment of FA was carried out by blending FA, chelating agent, and water in the proportion of 100:30:4 (mass ratio) via JJ-5 planetary type motar mixer in laboratory.

Raw MSW was collected from the canteen and dormitory on campus from Qingdao University of Technology, and MSW used in this study was synthesized based on the typical MSW composition in Qingdao City. The composition of the synthesized MSW by wet weight was as follows: kitchen waste (69.37%), paper (7.31%), plastics (11.08%), construction waste (6.18%), textile (2.76%), glass (2.94%), and metal (0.30%). Different components of MSW were broken into pieces less than 4 mm and were uniformly mixed. The water content of MSW was 63.2%, and the organic matter content was 28.4%.

2.2 Experimental device and operation

Two anaerobic bioreactor co-landfill columns were designed via thick acrylic pipe with height of 1800 mm and diameter of 300 mm. Details of the landfill columns were presented in Fig. 1. MSW and stabilized FA were landfilled in the landfill area of co-landfill columns at a ratio of 10:1 including 15 kg stabilized FA and 150 kg MSW. Different co-landfill ways including layered co-landfill way (column L) and mixed co-landfill way (column M) were simulated. For column L, 1600 mm landfill area was divided into 750 mm MSW layer, 100 mm stabilized FA and 750 mm MSW layer. For column M, stabilized FA and MSW were landfilled in the landfill area after well-mixing.

Two co-landfill columns were operated at room temperature to simulate the actual landfill environment. Before the operation, 8 L of distilled water was added to each column to attain optimum moisture content, which enhanced the MSW biodegradation. 4 L distilled water was injected weekly into each column with a peristaltic pump at a flow rate of 40 mL/min to accelerate the biodegradation process and ensure adequate leachate. Before injecting distilled water into each column weekly, leachate in leachate storage space was collected and stored at 4 ℃ for physicochemical analysis. Due to the 10 L leachate requirement for instrumental analysis of PCDD/Fs, the stored leachate is fully mixed and the volume of collected leachate weekly was determined during different co-landfill phase including 0 – 14 d, 14 – 28 d, 28 – 56 d, 56 – 84 d and 84 – 112 d, then the mass concentrations of PCDD/Fs homologues of different co-landfill phase were measured.

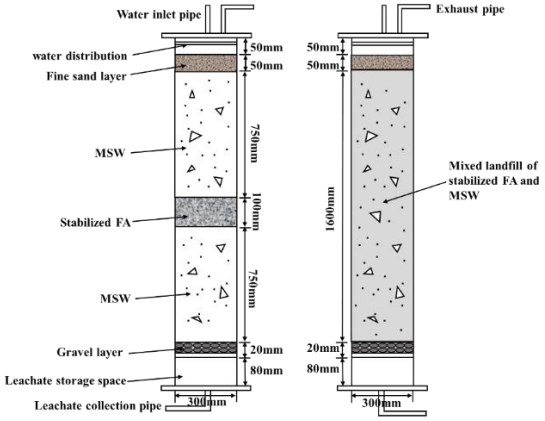

Fig. 1 Schematic diagram of the experimental device

3. RESULTS AND DISCUSSION

3.1 Variation of PCDD/Fs concentration in leachate

Fig. 2 a illustrates the mass concentrations and the I-TEQ concentration of PCDD/Fs in leachate for each column. For column L, the mass concentration of PCDD/Fs increased to 104.9 pg/L from 26.2 pg/L, and gradually decreased to 1.13pg/L. The similar trend was

observed in variation of the I-TEQ concentration of PCDD/Fs, which was evidently increased to 3.2 pg I-TEQ /L from 0.89 pg I-TEQ/L and gradually decreased to 0.0082 pg I-TEQ/L. The change trend of mass concentration and I-TEQ concentration of PCDD/Fs in the leachate for column M was approximately consistent with that of column L. The mass concentration of PCDD/Fs increased from15.2 pg/L to 43.9 pg/L and decreased to 10 pg/L, while the I-TEQ concentration increased from 1 pg I-TEQ/L to 1.6 pg I-TEQ/L and subsequently decreased to 0.083 pg I-TEQ/L. The similar leaching tendency under different co-landfill ways may be responsible for properties of stabilized FA, which was also observed in pervious study **(Hsi et al., 2007)**. The maximum leaching concentration of PCDD/Fs in leachate was observed in 14 ~ 28 days, which indicated that the initial stage of co-landfill was accompanied by high PCDD/Fs leaching risk. Although the leaching trend of PCDD/Fs is similar, the mass concentration and the I-TEQ concentration of PCDD/Fs in different landfill ways are quite different. Generally, the mass concentration and the I-TEQ concentration of PCDD/Fs for column M was significantly lower than that of column L. The discrepancy in leaching concentration of PCDD/Fs may resulted from distinct variation of leachate characteristics and composition of DOM for each column **(Osako et al., 2002)**.

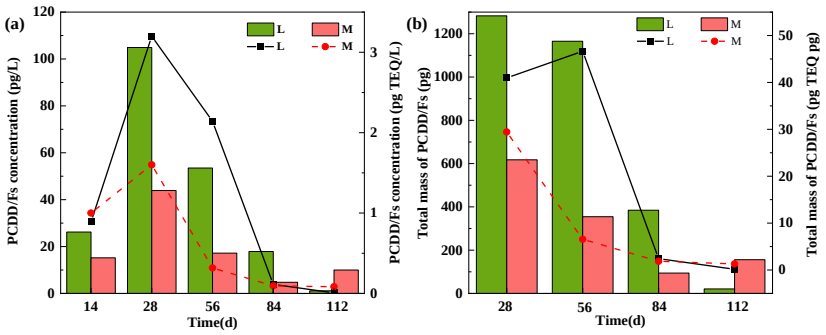

Fig. 2 The variation of (a) the mass concentration and I-TEQ concentration of PCDD/Fs and (b) cumulative mass amount and cumulative I-TEQ amount of PCDD/Fs in different co-landfill phase for each column (L and M represented the columns that layered co-landfill and mixed co-landfill, histogram represents the mass change of PCDD/Fs, and the dotted line chart represents the I-TEQ change of PCDD/Fs).

3.2 The mass distribution of PCDD/Fs homologous

The mass distribution of PCDD/Fs homologous in each column during the co-landfill process were displayed in **Fig. 3**. The highly chlorinated homologues were dominant and the total mass proportion of O_8CDD/Fs and H_7CDD/Fs exceeded 80%. Despite the contents of O_8CDD and H_7CDD in stabilized FA were similar, the mass proportion of O_8CDD was always higher than that of H_7CDD for both column L and column M. In addition, the content of H_7CDF in stabilized FA was 4.8 time higher than that of O_8CDF, whereas the fraction of H_7CDF in leachate was slightly higher than that of O_8CDF. The strong leachability shown by O_8CDD/Fs may be attributed to its high affinity for organic matter due to the abundant DOM in leachate. In the presence of DOM, solubility enhancement in highly chlorinated PCDD/Fs is higher than that in low chlorinated PCDD/Fs **(Kim et al., 2002)**. The high content of O_8CDD and H_7CDD in stabilized FA may also be another reason for the high mass concentration of leachate, while the high mass concentrations of O_8CDF and H_7CDF were still observed in leachate when total content of low chlorinated PCDFs exceed that of O_8CDF and H_7CDF. In addition to the characteristics of high chlorinated PCDD/Fs, DOM characteristic of leachate was considered as main factor for the high concentration of highly chlorinated homologues in leachate. Nevertheless, the content of

PCDD/Fs in stabilized FA has significant influence on the leaching behavior of low chlorinated homologues. In stabilized FA, the content of low chlorinated PCDFs is higher than that of low chlorinated PCDDs, which was also observed in previous paper **(Yao et al., 2012)**. The fraction of low chlorinated PCDFs in leachate was significantly higher than that of low chlorinated PCDDs, which is consistent with the content in stabilized FA. Low octanol/water partitioning coefficients of low chlorinated homologues results in weak affinity for organic matter compared with highly chlorinated homologues **(Chen et al., 2001)**. Leachability of low chlorinated homologues was not only controlled by DOM characteristics of leachate, but the availability of low chlorinated homologues in stabilized FA cannot be ignored. To sum up, the leaching behavior of PCDD/Fs during co-landfill process is related to the content of PCDD/Fs in stabilized FA and the physical-chemical parameters as well as DOM characteristics of leachate.

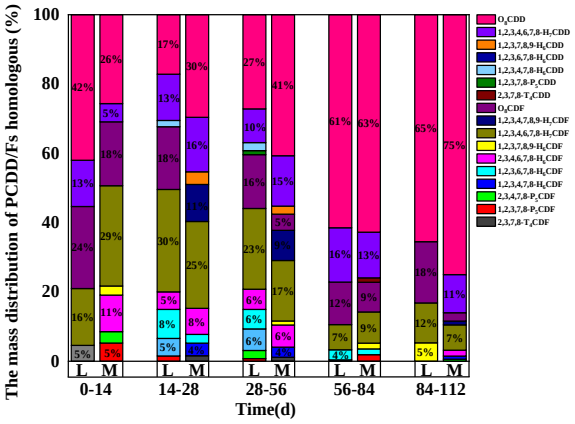

Fig. 3 The variation of mass distribution of PCDD/Fs homologous in different co-landfill phase for each column (L and M represented the columns that layered co-landfill and mixed co-landfill).

3.3 The I-TEQ contributions of PCDD/Fs homologous

The I-TEQ contributions of PCDD/Fs homologous during the co-landfill process were presented in **Fig. 4**. Although the highly chlorinated PCDD/Fs were the most abundant homologues detected in leachate, the low international toxicity equivalence factors of them resulted in low I-TEQ contributions for the total I-TEQ value. H_7CDD and H_7CDF were crucial proportions in total I-TEQ values, accounting for 5 – 25% and 4 – 20% of the total I-TEQ value, respectively. For low chlorinated PCDD/Fs, low chlorinated PCDFs were the dominant homologous for I-TEQ contributions due to the low mass concentration of low chlorinated PCDDs. H_6CDF represented a great fraction of the total I-TEQ value during the period of high I-TEQ concentration, and the proportion of H_6CDF was attained 43% – 73% at 14 – 56 d. However, the I-TEQ contribution of P_5DF in stabilized FA was largest, accounting for 41% of the total I-TEQ value. It is now acknowledged that bioavailability is a more significant key parameter than the total concentration to evaluate the environment risk. Obviously, it is difficult to determine the environmental risk of PCDD/Fs via calculating the I-TEQ contribution of PCDD/Fs homologues in stabilized FA. In addition, although the high chlorinated PCDD/Fs in the leachate showed low contribution to the total I-TEQ value, in the long-term landfill process, the microbial transformation of high chlorinated PCDD/Fs is an important hidden danger to aggravate the environmental risk of PCDD/Fs, and reductive dechlorination of microorganism has been found in sediment and compost **(Chen et al., 2016; Xu et al., 2016)**. High chlorinated PCDD/Fs may become the source of continuously exporting chlorinated PCDD/Fs to surrounding environment.

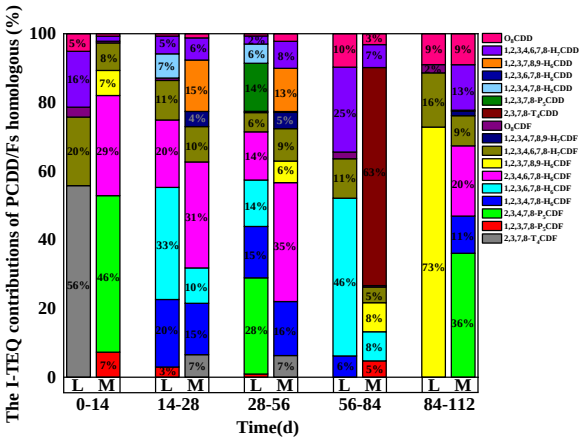

Fig. 4 The variation of I-TEQ contribution of PCDD/Fs homologous in different co-landfill phase for each column (L and M represented the columns that layered

co-landfill and mixed co-landfill).

4. CONCLUSION

Co-landfill of stabilized FA and MSW increased the leaching of PCDD/Fs during the hydrolysis and acidogenesis phase, and high leaching concentration of PCDD/Fs was observed at 14–56 d. Co-landfill ways had a significant impact on release of PCDD/Fs from stabilized FA, and layered co-landfill has higher leaching concentration of PCDD/Fs than mixed co-landfill. High chlorinated PCDD/Fs were dominant fraction of mass concentration of PCDD/Fs, and H6CDF represented a great fraction of the TEQ concentration of PCDD/Fs. However, P5CDF was the main contribution to the TEQ concentration of PCDD/Fs in stabilized FA, which indicated the content of different PCDD/Fs homologues in stabilized FA cannot effectively assess the environmental risk of PCDD/Fs. The leaching behavior of high chlorinated PCDD/Fs was controlled by DOM characteristic, and the content of PCDD/Fs homologues in stabilized FA was the crucial factor for leaching behavior of low chlorinated PCDD/Fs.

ACKNOWLEDGMENTS

This work was supported by the National Natural Science Foundation of China (Grant Nos. 51978350, 52000111). Thanks for the support of the Open Fund Project of Zhejiang Provincial Key Laboratory of Solid Waste Treatment and Recycling (Grant No. SWTR-2021-01), Shandong Postdoctoral Innovation Project Fund (Grant No. 202103026), and Qingdao Postdoctoral Applied Research Project.

REFERENCES

Chen, J., Quan, X., Yazhi, Z., Yan, Y., Yang, F., 2001. Quantitative structure–property relationship studies on n-octanol/water partitioning coefficients of PCDD/Fs. Chemosphere 44, 1369-1374.

Chen, W.Y., Wu, J.H., Lin, S.C., Chang, J.E., 2016. Bioremediation of polychlorinated-p-dioxins/dibenzofurans contaminated soil using simulated compost-amended landfill reactors under hypoxic conditions. J Hazard Mater 312, 159-168.

Choi, K.I., Lee, D.H., 2006. PCDD/DF in leachates from Korean MSW landfills. Chemosphere 63, 1353-1360.

Ham, S.Y., Kim, Y.J., Lee, D.H., 2008. Leaching characteristics of PCDDs/DFs and dioxin-like PCBs from landfills containing municipal solid waste and incineration residues. Chemosphere 70 (9), 1685-1693.

Hsi, H.C., Yu, T.H., 2007. Evaluation of the leachability of polychlorinated dibenzo-p-dioxins and dibenzofurans in raw and solidified air pollution control residues from municipal waste incinerators. Chemosphere 67, 1434-1443.

Hsu, Y.C., Chang, S.H., Chang, M.B., 2021. Emissions of PAHs, PCDD/Fs, dl-PCBs, chlorophenols and chlorobenzenes from municipal waste incinerator cofiring industrial waste. Chemosphere 280, 130645.

Kim, Y., Lee, D., 2002. Solubility enhancement of PCDD/F in the presence of dissolved humic matter. J Hazard Mater 91 (1-3), 113-127.

Li, W., Yu, Q., Gu, K., Sun, Y., Wang, Y., Zhang, P., Zheng, Z, Guo, Y., Xin, M., Bian, R., 2022. Stability evaluation of potentially toxic elements in MSWI fly ash during carbonation in view of two leaching scenarios. Science of The Total Environment, 803, 150135.

Ren, M., Lv, Z.Y., Xu, L., Lu, Q., Zhang, X., Yu, Y., Fan, Y., Gao, Y., Chen, J., Zhang, H., 2020. Partitioning and removal behaviors of PCDD/Fs, PCBs and PCNs in a modern municipal solid waste incineration system. Sci Total Environ 735, 139134.

Xu, Y., Gregory, K. B., VanBriesen, J. M., 2016. Microbial-catalyzed reductive dechlorination of polychlorinated biphenyls in Hudson and Grasse River sediment microcosms: determination of dechlorination preferences and identification of rare ortho removal pathways. Environ Sci Technol 50 (23), 12767-12778.

Yao, J., Li, W., Xia, F., Zheng, Y., Fang, C., Shen, D., 2012. Heavy metals and PCDD/Fs in solid waste

incinerator fly ash in Zhejiang province, China: chemical and bio-analytical characterization. Environ. Monit. Assess 184 (6), 3711-3720.

Yasuhara, A., Katami, T., 2007. Leaching behavior of polychlorinated dibenzo-p-dioxins and furans from the fly ash and bottom ash of a municipal solid waste incinerator. Waste Manage 27 (3), 439-447.

HEAVY METALS LEACHING BEHAVIOURS IN MSWI FLY ASH STABILIZED BY AN ORGANIC CHELATING AGENT

Yanyan Guan[1], Chuanfu Wu [1], Xiaona Wang [1], Zhongli Luo[2] and Qunhui Wang[1]
1 School of Energy and Environmental Engineer, University of Science and Technology Beijing, 30 Xueyuan Road, Haidian District, Beijing 100083, China
2 Organic Materials Research Laboratory, Tosoh Corporation, Shunan, 746-8501, Japan

INTRODUCTION

Municipal solid waste incineration fly ash (MSWIFA) is a secondary pollutant produced during municipal solid waste incineration and is classified as a hazardous waste because of its rich content of heavy metals (Quina et al., 2011). Considering the increasing production of fly ash leading to excessive pressure on safety landfills, the government stipulates that treated MSWI fly ash can enter sanitary landfill after meeting the requirements of the "Standard for pollution control on the landfill site of municipal solid waste" (GB16889-2008). Treatment technologies for fly ash include separation, solidification/stabilization, thermal treatment and reutilization (Wang et al., 2021). Stabilization is widely used in China by virtue of its simplicity of operation, high stabilization efficiency and no increase in fly ash volume (Li et al., 2019).

In sanitary landfills, fly ash is often landfilled separately from municipal solid waste. This means the fly ash entering the landfill is not exposed to the environment of organic acid leaching, but mainly rainwater leaching (Li et al., 2020). Therefore, in this study, in addition to the original provisions, the leaching behavior of stabilized fly ash in simulated acid rain was also investigated.

MATERIALS AND METHODS

MSWI fly ash used in this experiment was obtained from a waste incineration plant in Chengdu, Sichuan. The chelating agent used was piperazine chelating agent (TS300) from Tosoh, Japan. 100 g fly ash was mixed with 1%, 3%, 5%, 7% and 10% (w/w) of chelating agent, stirred for 10 min under a stirrer, stored in sealed bags, and sampled at 0d, 14d and 28d for leaching experiments. The leaching toxicity of stabilized fly ash entering the landfill under municipal solid waste leachate and acid rain was simulated using the acetic acid buffer solution method (HJ/T 300-2007) and the Sulphuric acid & nitric acid method (HJ/T 299-2007).

A modified four-step procedure sequential BCR extraction method was used to analyze heavy metal speciation in fly ash, namely, acid soluble fraction (F1), reducible fraction (F2), oxidizable fraction (F3), and residual fraction (F4). The acid soluble fraction and reducible fraction are considered as unstable speciation. the oxidizable fraction and residual fraction are considered as stable speciation.

RESULT AND DISCUSSION

Due to the imperfect classification and recycling system of municipal solid waste in China, municipal solid waste is mixed with some waste containing heavy metals, resulting in a large amount of Zn, Pb, Cd and other heavy metals in fly ash. In the acetic acid buffer solution method (HJ/T 300-2007), the leaching amounts of Pb and Cd in raw fly ash are 1.04 mg/L and 5.39 mg/L, which far exceed the limits of 0.25 mg/L and 0.15 mg/L specified in the GB16889-2008. So the raw fly ash needs to be treated and meet the standards before entering the sanitary landfill.

The leaching concentrations of Pb and Cd in acetic acid solution treated with different TS300 dosages are shown in Figure 1. With the increase of TS300 dosage, Pb and Cd are stabilized in fly ash, which leads to the decrease of their leaching in acetic acid solution. When the dosage of TS300 is 3%, the leaching concentrations of Pb and Cd in acetic acid leaching solution are 0.06 mg/L and 0.06 mg/L respectively, which are lower than the limit in GB16889-2008. However, there is still the possibility of re-dissolution of heavy metals in fly ash stabilized by chelating agents. After storage for 14 days, the leaching concentrations of Pb and Cd of fly ash stabilized are 0.10 mg/L and 0.17 mg/L, respectively, and increased to 0.23 mg/L and 0.62 mg/L, respectively, after storage for 28 days. Obviously, Cd exceeds the limit value in GB16889-2008 after 14d storage. Because the stabilized fly ash is oxidized by the air, which causes the decomposition of the stable heavy metal fraction, and the release of Pb and Cd leads to its easy transfer to the environment (Sakanakura, 2007).

The leaching concentration of Pb from raw fly ash in acid rain is 11.71 mg/L, which is much higher than that in acetic acid, and more than 46 times the limit value in GB16889-2008. Therefore, under the simulated acid rain scenario, Pb is a key heavy metal to dealt with. As shown in Figure 2, when the addition of chelating agent is 3%, the leaching concentration of Pb in simulated acid rain

(0.016 mg/L) can reach the limit value. With the extension of storage time, Pb has a tendency to be re-released, but it is not as obvious as in acetic acid leaching.

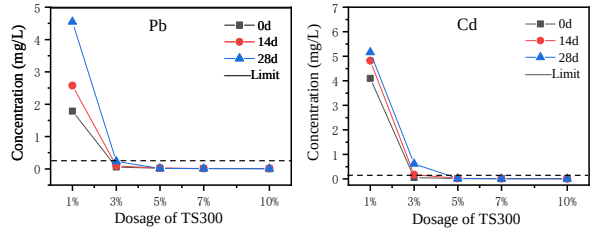

Figure 1. The leaching concentrations of Pb and Cd in acetic acid solution treated with different TS300 dosages

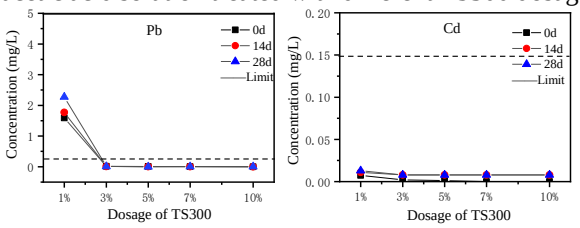

Figure 2. The leaching concentrations of Pb and Cd in acid rain solution treated with different TS300 dosages

As shown in Figure 3, the speciation of heavy metals (e.g. Pb, Cd) is changed after the addition of chelating agents. In raw fly ash, the speciation proportion of Pb follows the order of oxidizable fraction (42.66%) > reducible fraction (42.14%) > residual fraction (13.78%) > acid soluble fraction (1.41%). This is the reason why the large leaching of Pb from fly ash in acetic acid leachate and sulfuric acid nitric acid leachate. After the addition of chelating agent, the acid soluble fraction decreases to less than 1% and the reducible fraction also decreases. When the addition of chelating agent increases to 3%, the sum of acid soluble fraction and reducible fraction decreases to 0.64%, and most of Pb belong to the stable fraction and are not easy to leach. However, with the extension of storage time, the sum of acid soluble fraction and reducible fraction increases to 1.09%, and the leachable fraction increased. This is the same phenomenon as it showed in Figures 1 and 2.

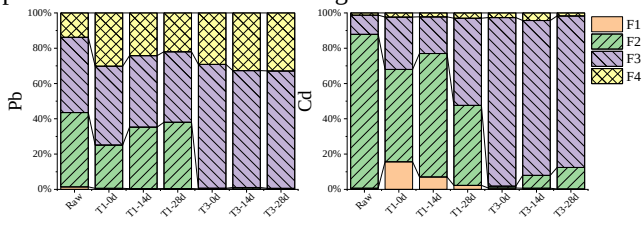

Figure 3. Proportion of Pb and Cd speciation in the FA sample determined by BCR

In raw fly ash, Cd mainly exists in the unstable reducible fraction (87.22%), while the oxidized fraction (10.86%) and residual fraction (1.24%) are very small. The addition of chelating agent has obvious stabilization effect on Cd. When the chelating agent dosage increases to 3%, the reducible state of Cd decreases from 87.22% to 1.07%. With the extension of storage time, the sum of acid soluble fraction and reducible fraction increases to 7.93% (14d) and 12.42% (28d). Therefore, chelating agents stabilize the heavy metals by combining the chelating groups with the heavy metals to reduce their mobility (Wang et al., 2015).

CONCLUSION

This study shows that when the chelating agent dosage is 3%, a large number of Pb and Cd in fly ash are stabilized, but with the increase of storage time, the stabilized Pb and Cd are re-released. According to the analysis of BCR method, chelating agent can change the speciation of heavy metal, and transformed it from unstable fraction (F1 and F2) to stable fraction (F3 and F4). Because chelating groups can effectively bind to heavy metals, reducing their mobility. Therefore, chelating agents have great potential in treating heavy metals in fly ash and reducing their toxicity.

ACKNOWLEGEMENT

The study was supported by the National Key Research and Development Program of China (2021YFE0112100).

REFERENCE

1.Li, W., Sun, Y., Huang, Y., Shimaoka, T., Wang, H., Wang, Y., Ma, L., Zhang, D., 2019. Evaluation of chemical speciation and environmental risk levels of heavy metals during varied acid corrosion conditions for raw and solidified/stabilized MSWI fly ash. Waste Manage., 87(407-416).

2.Li, W., Sun, Y., Xin, M., Bian, R., Wang, H., Wang, Y., Hu, Z., Linh, H.N., Zhang, D., 2020. Municipal solid waste incineration fly ash exposed to carbonation and acid rain corrosion scenarios: Release behavior, environmental risk, and dissolution mechanism of toxic metals. Sci. Total Environ., 744(140857).

3.Quina, M.J., Bordado, J.C.M., Quinta-Ferreira, R.M., 2011. Percolation and batch leaching tests to assess release of inorganic pollutants from municipal solid waste incinerator residues. Waste Manage., 31(2), 236-245.

4.Sakanakura, H., 2007. Formation and Durability of Dithiocarbamic Metals in Stabilized Air Pollution Control Residue from Municipal Solid Waste Incineration and Melting Processes. Environ. Sci. Technol., 41(5), 1717-1722.

5.Wang, F., Zhang, F., Chen, Y., Gao, J., Zhao, B., 2015. A comparative study on the heavy metal solidification/stabilization performance of four chemical solidifying agents in municipal solid waste incineration fly ash. J. Hazard. Mater., 300(451-458).

6.Wang, X., Gao, M., Wang, M., Wu, C., Wang, Q., Wang, Y., 2021. Removal of heavy metals in municipal solid waste incineration fly ash using lactic acid fermentation broth. Environ. Sci. Pollut. R., 28(44), 62716-62725.

LEACHING BEHAVIOR OF HEAVY METALS FROM BROKEN TON BAGS FILLED WITH FLY ASH IN ACID RAIN ENVIRONMENT

Qianwen Yu [1], Yingjie Sun[1], Weihua Li[1,*], Yan Wang[1]

1. Qingdao Solid Waste Pollution Control and Resource Engineering Research Center, School of Environmental and Municipal Engineering, Qingdao University of Technology, Qingdao 266520, Shandong, China

ABSTRACT: The column leaching experiment of landfill stabilized fly ash was established by simulating acid rain with "sulfuric acid + nitric acid" type extractant to study the influence of acid rain seepage path on the leaching behavior of heavy metals in fly ash under the condition that the fly ash ton bag in the landfill was damaged. The results showed that the six seepage paths all promoted the leaching of Pb, Zn, Cu, Cd, Cr, and Ni from landfill stabilized fly ash in varying degrees. Under the double influence of gravity potential energy and matrix potential, compared with the horizontal seepage path of "upper left inflow - lower right outflow", the vertical seepage path of "upper inflow - lower outflow" was more likely to promote the leaching of heavy metals in fly ash. Under the mode of "dynamic scouring + static soaking + dynamic scouring", the cumulative leaching amount of heavy metals was higher. Under the seepage path of "upper left inflow - upper right outflow", the fluctuation of pH value of leachate was the smallest, the cumulative leaching amount of heavy metals was the lowest, and the stability of heavy metals (especially Pb, Zn, and Cr) in stabilized fly ash matrix was the best. The research results can provide a scientific basis for the evaluation of the leaching behavior of heavy metals from landfill stabilized fly ash in extreme acid rain environment and the environmental risk management and control when the fly ash ton bag in the actual landfill was damaged.

KEYWORDS: fly ash landfill; broken ton bag; acid rain; seepage path; heavy metal leaching

INTRODUCTION

In China, more than 146.076 million tons of raw municipal solid waste (MSW) was incineration in 2020, accounting for 62.3% of the total harmless treatment. As the scale of municipal waste incineration grows, large amounts of fly ash rich in heavy metals and dioxin pollutants are generated. According to GB 16889-2008, fly ash can only be landfilled in domestic landfills alone after pretreatment to meet the standards. Dithiocarbamate (DTC) chelating agents can combine with heavy metals to form chelated products with high stabilization coefficients and solid environmental adaptability and thus have been widely used in the industry. However, due to the imperfect management system, fly ash ton bags are not strictly sealed in the actual operation of non-standard storage or landfills. Aging and breakage of the landfill fly ash pile cover and untimely maintenance can further increase the risk of exposure of fly ash in broken ton bags to the adverse external environment which increases the environmental risk of heavy metal leaching from landfill-stabilized fly ash. In addition, acid rain is one of the possible risks of environmental exposure for fly ash landfills—acid rainfall, often present south of the Yangtze River and in the southeastern coastal areas. Acid rain with "sulfuric acid + nitric acid" type is the primary type of acid rain

evolution in recent years.

In contrast to static batch leaching, the leaching column experiment is a dynamic scouring model of leachate based on realistic permeation conditions. Leaching column experiments can better simulate the dynamic scouring process of contaminants in wastes and thus have received more extensive attention from researchers [1-3]. The analysis found that the studies on metal leaching behavior in fly ash were based on the acid leachate in a single direction of vertical seepage path conditions. However, in the actual landfill process, the breakage of ton bags can significantly affect the seepage path of acid leachate in the landfill fly ash pile. Few relevant studies consider the effect of acid rain leachate seepage paths on the leaching behavior of heavy metals in landfill-stabilized fly ash based on the location of ton bag breakage. Based on this, this study investigates the effect of acid rain on the leaching behavior of heavy metals in landfill stabilized fly ash under diversified seepage path conditions by simulating acid rain with "sulfuric acid + nitric acid" type extractant. This study provides some theoretical references for the standardization of fly ash ton bag material, the landfill disposal operation process, and improving the management system in China.

MATERIALS AND METHODS

Experimental materials

Stabilized fly ash samples were taken from a large domestic waste incineration plant in Qingdao (750 $t \cdot d^{-1}$), and the chelating agent was DTC. The stabilized fly ash samples were crushed and sieved through 10 mesh sieves, mixed by quadratic method then kept in a sealed reserve, pH=12.34. The preparation of simulated acid rain was based on HJ/T 299-2007 standard. Sulfuric acid and nitric acid were mixed at 2:1 (mass ratio) and added to deionized water, adjusted pH=3.2±0.05.

Acid rain seepage path experiment

The experiments of six seepage paths were designed assuming the possible breakage of stabilized fly ash-filled ton bags (Table 1).

Table 1 Experimental design grouping of acid rain infiltration paths

NO.	Seepage path way
A1	upper inflow - lower outflow
A2	lower outflow - upper inflow
B1	upper left inflow - lower right outflow
B2	upper left inflow - upper right outflow
A3	After soaking, upper inflow - lower outflow
B3	After soaking, upper left inflow - lower right outflow

The experiment was performed using six PVC columns, which were external leachate collection bottles and simulated acid rain reservoirs. The experiments were conducted in a stage-feed mode, with each stage (S1 to S3) spaced 25 days apart, and each stage time of operation referred to the experimental design of EPA Method 1314 [4], in which the cumulative liquid-to-solid ratio (L/S) reached ten as the end point of the individual stage operation. The leachate sampling sites for the S1, S2, and S3 stages were set at cumulative L/S of 0.2/0.5/1.0/1.5/2.0/4.5/5.0/9.5/10, 0.2/0.5/1.0/2.0/5.0/10 and 0.2/2.0/10, respectively. At the end of each experiment phase, samples of residual landfill fly ash solids in the column were taken.

RESULTS AND DISCUSSION

pH, EC change

During the cleaning process of municipal solid waste incineration flue gas, excessive lime makes the fly ash matrix highly alkaline. Therefore, the fly ash matrix will rapidly neutralize the H+ introduced by the simulated acid rain when it comes in contact with it. As shown in Fig. 1 (a), the pH change increases in the leachate of each stage S1. For the B2 system, acid rain must flood the whole design before generating the leachate, B2 leachate pH=12. After

the cumulative L/S exceeded 2 in the S2 stage, all of them showed an increasing trend of pH. The seepage path was stabilized in phase S3, and each device showed a decreasing trend in leachate pH.

As shown in Fig. 1 (b), from S1 to S3, the acid rain invasion causes the soluble salts in the fly ash matrix to be continuously washed out and transferred to the leaching solution. Therefore, with the increase of cumulative L/S, the EC of each leachate path showed a tendency to increase, followed by a decrease, and gradually stabilized. At the beginning of the S2 stage, EC of the B2 leaching solution showed a transient upward trend. That's attributed to the B2 mode of operation, which allows full reconnection of the stabilized fly ash with acid rain resulting in increased EC. It decreases with increasing cumulative L/S when the seepage is stabilized in the path.

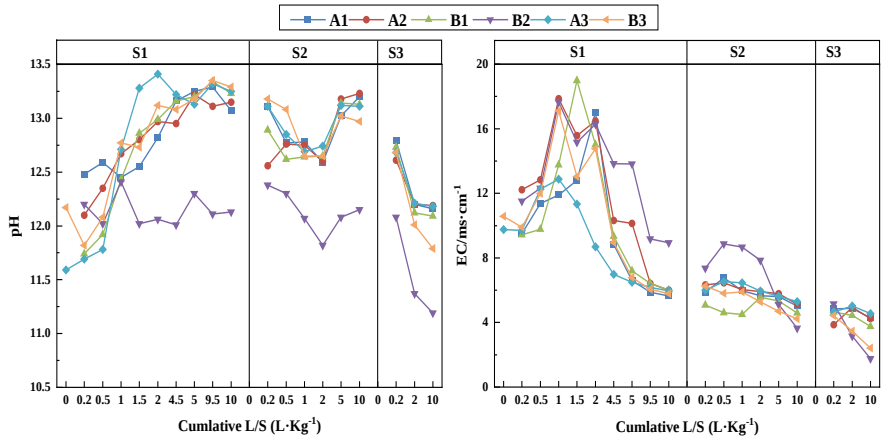

Fig. 1 Changes in pH and EC of fly ash leachate at each stage under different seepage path conditions

Changes in leaching behavior of major elements

Figure 2 shows the trend variation of the cumulative leaching amounts of Cl, K, Ca, Na and Mg in the stabilized fly ash leachate from the S1 to S3 stages. In this case, the cumulative leaching amount (M; mg·kg^{-1}) was calculated using equation (1), where is the sampling concentration (mg·L^{-1}) and is the sampling liquid-solid ratio (L·kg^{-1}).

$$M = \sum_{i=1}^{n} C_i \times (t_i - t_{i-1}) \qquad (1)$$

During the S1~S3 stage of acid rain invasion, soluble ions were flushed out in large quantities, and the cumulative leaching amounts of Cl, K, Ca, Na and Mg in the leachate of each device all increased with the increase of cumulative L/S. One of the most obvious trends was leaching in the S1 stage.

In stage S1, except B2, the cumulative leaching of major elements basically reached stability at L/S = 4.5. Ca increased significantly with cumulative L/S. B2 leached slowly in the early stage of S1, but the cumulative total leaching of Cl, K, and Na accounted for the highest in the stages of S2~S3. In general, the total leaching of major elements in A1 and A3 was relatively high. Furthermore, the contact area between A3 and B3 and the fly ash matrix was larger, which led to the rapid leaching of the major metal elements from the fly ash.

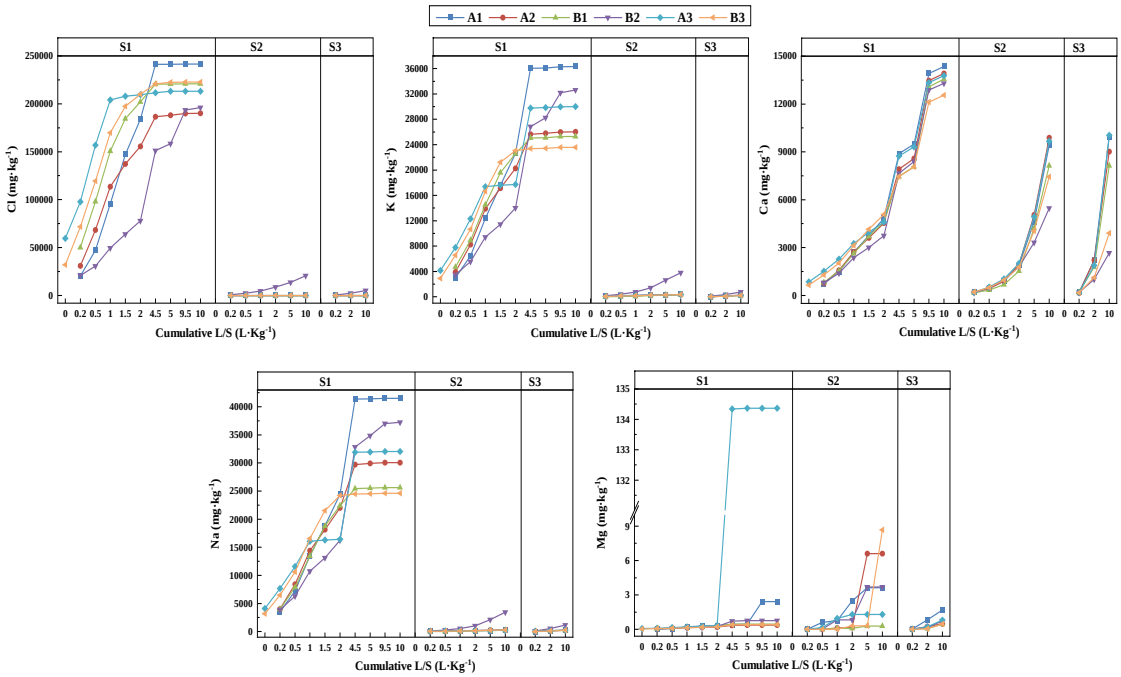

Figure 2 Cumulative leaching of significant elements (Cl, K, Ca, Na and Mg) from fly ash leachate at each stage under different seepage path conditions

Changes in leaching behavior of heavy metals

Calculating the cumulative leaching amount of each heavy metal (M; mg·kg^{-1}) in stages S1~S3 still used equation (1), and the variation of the results is shown in Figure 3.

The stage acid rain leaching process, early stage of acid rain leaching is a critical period for the leaching of heavy metals in landfill-stabilized fly ash. Among them, Pb was leached at the beginning of the S1 set, while the other heavy metals were leached slowly with the increase of cumulative L/S. A3 showed a significant jump in the cumulative Cd leaching at cumulative L/S=4.5. In addition, the leaching amount of Cd throughout the S1 phase was minimal. The leaching of heavy metals from the fly ash continues in the S2 and S3 phases.

Regarding acid rain infiltration paths, different infiltration paths significantly influence the cumulative leaching of heavy metals. S1 stage, A1 and A3 are more easily leached. S2 and S3 stages, the cumulative leaching of heavy metals from B1 and B3 leachate is significantly increased. In contrast, the long-term stability of heavy metals in landfill-stabilized fly ash is reduced under the transverse seepage path. A2 The whole process is only influenced by the acid rain matrix potential. It lacks the influence of gravitational potential energy, and the accumulated leaching of heavy metals is in a slowly activated release state throughout the stage. Therefore, heavy metal concentrations are lower in the S1 location while significantly higher in S2 and S3 steps. It is noteworthy that B2 has the lowest cumulative leaching of heavy metals of all seepage paths. In addition, the leaching of heavy metals is also affected by the " dynamic scouring " and "static soaking" of acid rain.

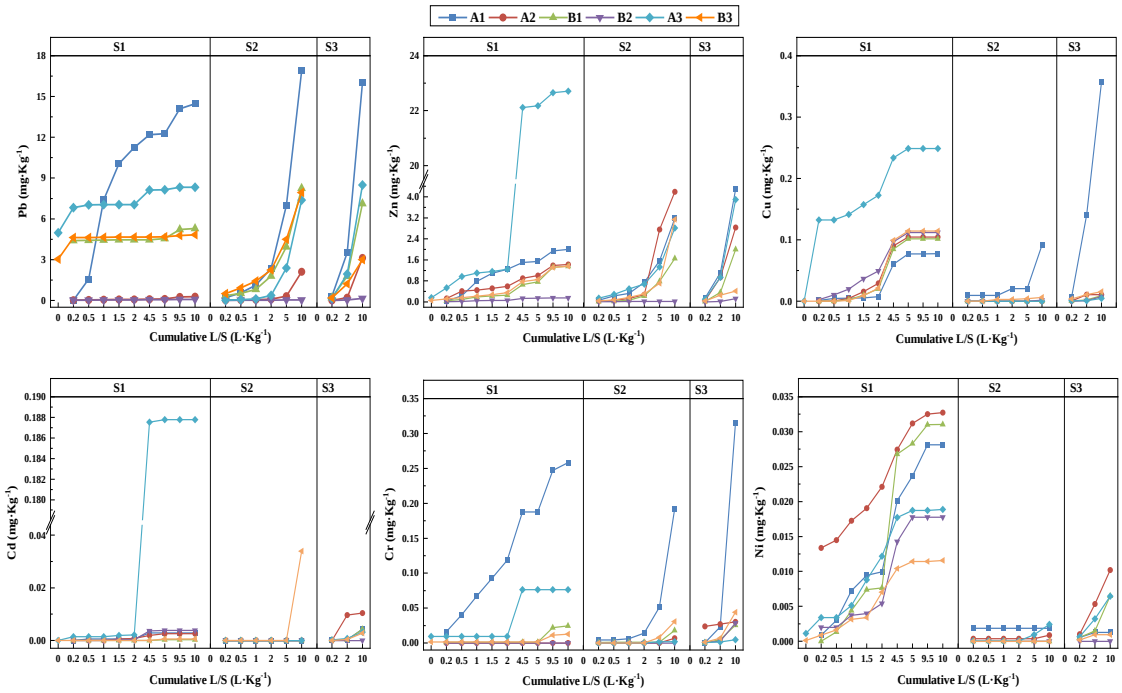

Figure 3 Cumulative leaching of heavy metals (Pb, Zn, Cu, Cd, Cr and Ni) from fly ash leachate at each stage under different seepage path conditions

CONCLUSION

S1~S3 phased acid rain intrusion can significantly affect the stability of heavy metals in landfill-stabilized fly ash. The initial acid rain leaching is the main period affecting the leaching of rich gold from landfill-stabilized fly ash.

A1 and A3 with " upper inflow - lower outflow ", heavy metals in fly ash are more likely to enter the leachate due to the influence of both gravitational potential energy and matrix potential at the early stage of acid rain invasion. Heavy metals in leaching cycles are longer than others because of B1 and B3 lack gravitational potential energy. The leaching of heavy metals and significant elements is mainly reflected in the S2 and S3 stages. Compared with the single acid rain dynamic scouring process, the total accumulated leaching of heavy metals is higher in the "dynamic scouring + static soaking + dynamic scouring" mode. The leachate pH was the lowest in B2 with a "upper left inflow - upper right outflow", and the leaching of heavy metals (especially Pb, Zn, and Cr) was the least affected.

Therefore , enhancing the anti-seepage capability of fly ash ton bags and standardizing the landfill operation process plays a vital role in reducing the leaching of heavy metals. Meanwhile, attention should be paid to the long-term stability of heavy metals in landfill-stabilized fly ash.

ACKNOWLEDGMENTS

This work was supported by the National Natural Science Foundation of China (Grant Nos. 52000111, 51978350). Thanks for the support of the Open Fund Project of Zhejiang Provincial Key Laboratory of Solid Waste Treatment and Recycling (Grant No. SWTR-2021-01), Shandong Postdoctoral Innovation Project Fund (Grant No. 202103026), and Qingdao Postdoctoral Applied Research Project.

REFERENCES

[1] MEZA S L, KALBE U, BERGER W, et al. Effect of contact time on the release of

contaminants from granular waste materials during column leaching experiments[J]. Waste Management, 2010, 30(04): 565-571.

[2] YIN K, CHAN W P, DOU X, et al. Cr, Cu, Hg and Ni release from incineration bottom ash during utilization in land reclamation–based on lab-scale batch and column leaching experiments and a modeling study[J]. Chemosphere, 2018, 197: 741-748.

[3] MEZA S L, GARRABRANTS A C, VAN DER SLOOT H, et al. Comparison of the release of constituents from granular materials under batch and column testing[J]. Waste Management, 2008, 28(10): 1853-1867.

[4] Method 1314, liquid-solid partitioning as a function of liquid-solid ratio for constituents in solid materials using an up-flow percolation column procedure[S]. USA. 2017.

Guideline for the end of aftercare of a closed landfill in Japan

Hideki YOSHIDA, Muroran Institute of Technology, gomigomi@mmm.muroran-it.ac.jp

Introduction

The Japan Society of Material Cycles and Waste Management published a report, ”Survey and evaluation method of landfill completion criteria for landfill sites” in 2002. “Landfill Completion Criteria” is recognized as the end of aftercare of a closed landfill in Japan. The standard for landfill gas (LFG) is set at "The generation of gas from the landfill site is scarcely observed, or that no increase of the generation of gas is observed over two years or more" in the Ordinance. This published report showed the exact evaluation methods in terms of landfill gas flux.

In this paper an old and closed landfill in Hokkaido, Japan is studied to examine LFG flux in terms of landfill stabilization related to the landfill completion criteria. A LFG monitoring well was installed for observing pressure difference between the atmosphere and inside waste body, temperature, gas components, and LFG flux rate since the end of landfilling in 2003. The observed data shows the stabilization process of this closed landfill. Then the standard for LFG is evaluated by numerical simulate with multi gas component transfer modelling.

Results in a monitoring well of a closed landfill

The surveyed landfill is located in Hokkaido, the northern part of Japan. Ambient temperature is 6.4°C and annual precipitation is 1090mm. Operation originally started in this landfill started in 1977, however, second stage of operation started in 1986 at the area. This landfill accepted mainly municipal wastes without incineration until 1996 (an incinerator operated from 1996), so large amount of biodegradable wastes like food, paper, wood, etc. was landfilled and closed in 2003. The monitoring well had been capped for observation of pressure difference and was temporarily opened for monitoring LFG gas component, LFG flux rate and temperature (4 times in a year).

LFG compositions and temperature in the well in this closed landfill is shown in Figure 1. LFG components showed high concentrations of CH_4 and CO_2 and low concentration of O_2 resulted from anaerobic biodegradation. The LFG temperature varied seasonally and the same trend of the atmosphere temperature. The maximum CH_4 concentration was 58% when the carbon dioxide concentration was 31%. The O_2 concentrations were nearly zero in the most monitoring period, so anaerobic biodegradation occurred inside the wells. Such anaerobic biodegradation resulted in the increased pressure inside waste body.

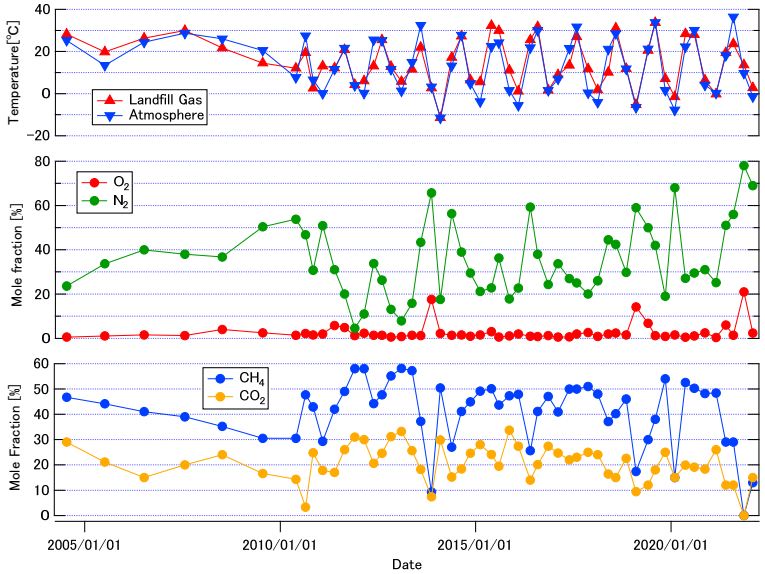

Figure 2. Observed landfill temperature and gas components in a monitoring well

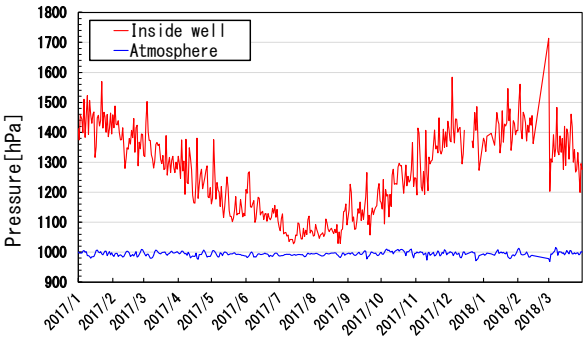

Figure 2. Observed pressure in atomosphere and a monitoring well

Pressure in the well and atmosphere pressure are shown in Figure 2. Significant pressure increase resulted from anaerobic biodegradation. The pressure difference between atmosphere and inside waste body was 50-500 hPa. Such pressure increase may represent the driving force for advective LFG flux.

Simulation of LFG flux around a monitoring well

LFG transfer in waste body and around a monitoring well is simulated by numerical simulation software, COMSOL Multiphysics®. Figure 3 shows the results of calculated pressure difference [hPa] and LFG velocity [m/s] inside waste body. LFG transfer is simulated by Darcy's low and multicomponent diffusion (Maxwell-Stefan diffusion).

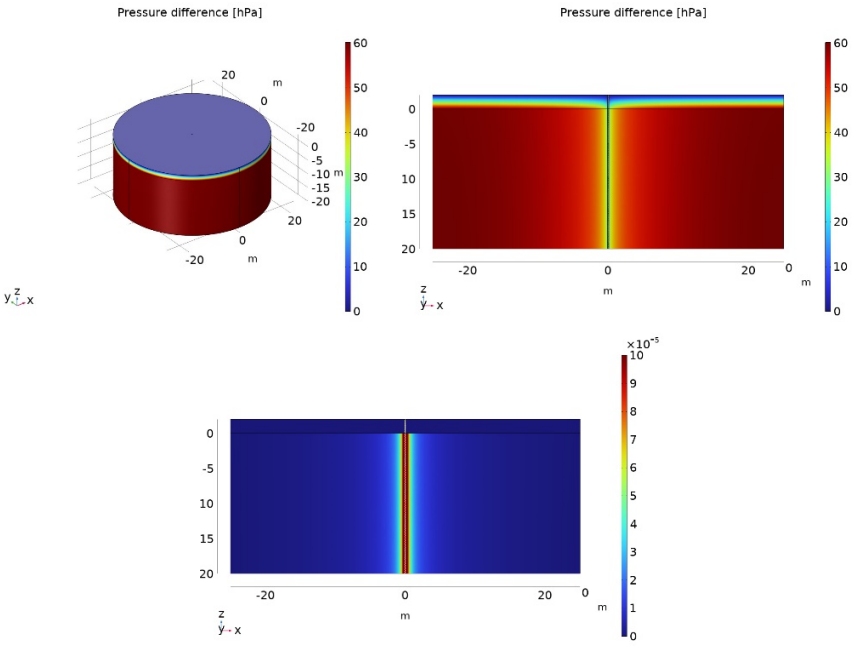

Figure 3. Simulation results of pressure difference [Pa] between waste body and atomosphere and velocity [m/s]

This simulation is based on LFG production scenario (3 m^3/m^3-waste body/y) in the published report. Maximum pressure diffrence is 60 hPa which is the same level of the observed pressure diffrence in a well. Maximum LFG velocity in a monitoring well is 0.06 m/s. This velocity is the same leve of the observed velocity in a well.
Finally an apporopriate revised standard relateded to "Landfill Completion Criteria" for evaluating landfill gas flux in a monitoring well is proposed.

HEAVY METAL LEACHING BEHAVIOUR OF CEMENT-SOLIDIFIED MUNICIPAL SOLID WASTE INCINERATION FLY ASH IN SANITARY LANDFILL

Chuanfu Wu [1], Xiaona Wang [1], Zhongli Luo [2], Qunhui Wang [1]

1 Department of Environmental Engineering, School of Energy and Environmental Engineering, University of Science and Technology Beijing, 30 Xueyuan Road, Haidian District, Beijing 100083, China

2 Organic Materials Research Laboratory, Tosoh Corporation, Shunan,746-8501, Japan

INTRODUCTION

With the increase of municipal solid waste (MSW) discharge and the development of the incineration technology, at least 10 million tons of MSW incineration fly ash (MSWIFA) is discharged annually in China (Wang and Fan, 2020). According to the 'Directory of National Hazardous Wastes' of China (Ministry of Ecology and Environment of the People's Republic of China, 2021), MSWIFA is categorized as a hazardous waste because it contains considerable amounts of heavy metals and toxic organic pollutants (e.g. dioxins). It may cause fatal harm to human health and ecological environment if MSWIFA is not disposed properly (Tong et al., 2020). In the light of the exemption list of 'National List of Hazardous Waste', an appropriately pre-treated MSWIFA can be disposed in sanitary landfills as a non-hazardous waste, thus providing an economical and practical scheme for MSWIFA disposal. However, notable, the pre-treated MSWIFA needs to meet the standard limits (e.g. heavy metals and dioxins content) before entering a sanitary landfill. In our pre-experiment, the dioxin content of MSWIFA we used was in a range of 0.23-0.89 ug/kg (data not shown), which is far below the limit set by GB 16889-2008 (i.e. < 3 μg/kg). Therefore, release of heavy metals is the main environmental risk for MSWIFA landfilled. Currently, pre-treatment technologies, especially cement solidification, have been widely used to reduce the mobility of heavy metals in MSWIFA to meet the regulation of sanitary landfill (GB 16889-2008, China) (Yu et al., 2005; Chen et al., 2021). Similar to TCLP, the 'Solid waste-extraction procedure for leaching toxicity acetic acid buffer solution method' (HJ/T 300-2007, China) is the standard in evaluating whether the leachable heavy metals in the solid waste can meet the threshold (i.e. GB 16889-2008). As per HJ/T 300, acetic acid (pH = 2.64) can be used as the leaching solvent to simulate the leaching behaviour of the solid waste in MSW sanitary landfill scenarios (i.e. mixed landfill). However, cement-solidified MSWIFA blocks is commonly transported to a separated area of the landfill (i.e. zoning landfill) in China. In this context, the cement-solidified MSWIFA blocks rarely comes in contact with the leachate generated in the sanitary landfill. Therefore, the reliability of the leaching toxicity and long-term environmental risk assessment of cement-solidified MSWIFA blocks in sanitary landfill following the HJ/T 300 leaching protocol is debatable.

At present, the environmental risk assessment for solid waste is mostly based on leaching tests. Technically, the accuracy of leaching toxicity and long-term environmental risk assessment of the solidified MSWIFA in sanitary landfill is mostly affected by the leaching protocols (including leaching solvents and methods) and evaluation methods. In a zoning landfill scenario, rainwater is the most typical leaching solvent encountered by cement-solidified MSWIFA blocks. Acid rainwater represents the worst condition of solvent leaching. Compared with acetic acid, acid rainwater would be a more appropriate leaching solvent for leaching toxicity and long-term environmental risk assessment. In addition to the leaching solvent, the leaching toxicity assessment results might vary greatly with the leaching method. Techniques for leaching can be divided into three categories according to purpose (Kosson et al., 2019). The first type is 'availability test', such as EA NEN7371. In this method, solid waste block is broken into tiny particles (i.e. <125 μm), and nitric acid is used as a leaching solvent to quickly determine (i.e. 6 h) the maximum leaching potential of heavy metals in the solid waste block. This index can provide a conservative estimate for maximum leaching to study the leaching characteristics of heavy metals in the solid waste block (Yang et al., 2011). The second method evaluates whether the solid waste block can meet the specific disposal threshold and determines the effect of influencing factors (e.g. pH (Yan et al., 2004; Quina et al., 2009; Leelarungroj et al., 2018), liquid–solid ratio (Van der Sloot, 2002; Xie et al., 2021) and dissolved organic matter (DOM) (Li et al., 2021). These indices

can determine the leaching of heavy metals in a short time (i.e. 18 h) with different leaching solvents [e.g. H_2SO_4, HNO_3 (HJ/T 299-2007, China) and acetic acid (TCLP and HJ/T 300-2007)] after crushing the solid waste block to medium particle size (i.e. <9.5 mm). The actual environmental risk evaluation for solid waste block is based on such leaching methods. However, these techniques only consider the short-term leaching behaviour of solid waste block under specific exposure scenarios but neglects the influence of time (Garrabrants et al., 2004; Shi et al., 2019) and therefore are not suitable for the long-term environmental risk evaluation of cement-solidified MSWIFA blocks in zoning landfill. The third method is static or dynamic leaching experiment (e.g. EA NEN7375) based on the principle of mass transfer control (i.e. interface diffusion) to analyse the leaching characteristics of inorganic components in solid waste block (i.e. particle size >4 cm). Under this leaching scenario, the leaching amounts of inorganic components in solid waste block are closely related to the leaching time. The leaching solvent is usually deionised water, and the experimental cycle is 64 days. Compared with those from the previous methods, the experimental results obtained by this leaching experiment are closer to the leaching characteristics of solid waste block in actual exposure scenarios, especially the leaching characteristics of heavy metals in solid waste block (Ogundiran et al., 2013; Taha et al., 2018). However, the use of a single leaching protocol for the environmental risk assessment of solidified MSWIFA in sanitary landfill is no longer adequate due to the diverse properties of the solid waste block and the complexity of disposal scenarios. Therefore, the development of a research framework combining different leaching protocols to investigate the leaching behaviours of cement-solidified MSWIFA blocks in sanitary landfill is the foundation of long-term environmental risk research.

Given the characteristics of these leaching tests (e.g. short-term experiment), their obtained results cannot be used directly for the long-term environmental risk assessment in a specific exposure scenario (Sanchez et al., 2000). Numerical simulations based on short-term leaching test results have been widely developed to describe the temporal-dependent leaching behaviours of contaminants in solid waste block and to obtain accurate reference data for long-term environmental risk assessment. Some of the typical models include first-order reaction kinetics, shrinking core and bulk diffusion (Zhang et al., 2021). The bulk diffusion model (BDM) based on Fick's second diffusion law is the most widely used and is particularly applicable when the heavy metal leaching in solid waste block is controlled by diffusion (Kim et al., 2020). However, this model is not applicable to all heavy metals and does not fit well when the heavy metal leaching is controlled by other mechanisms (Sanchez et al., 2003). Therefore, a BDM on the basis of the leaching characteristics of cement-solidified MSWIFA blocks under zoning sanitary landfill scenario must be constructed and calibrated for an accurate long-term environmental risk assessment.

Given that most of the studies on the cement-solidified MSWIFA were either focused on the process parameters optimization and the curing mechanism (Wang et al., 2015; Cerbo et al., 2017), or its environmental risk assessment based on the short-term leaching tests and the empirical models, the long-term environmental risk assessment of the cement-solidified MSWIFA in zoning sanitary landfill scenario was still unclear. Therefore, in this study, the heavy metal leaching behaviours of cement-solidified MSWIFA blocks following the EA NEN7375 leaching protocol were firstly investigated by laboratory batch-scale experiments. Acid rain comprising H_2SO_4 and HNO_3 (mass ratio of 2:1) was adopted as the leaching solvent to simulate the most severe exposure scenario of the zoning sanitary landfill. At the same time, deionized water was adopted as the leaching solvent to act as a control group. Additionally, the mechanistic model for a specific heavy metal on the basis of its leaching characteristics was developed and calibrated using the data from EA NEN7375 leaching test. Finally, the calibrated model was applied to evaluate the long-term environmental risk of cement-solidified MSWIFA blocks in acid rain scenarios. The obtained results and developed models might lay the foundation for the optimal design of zoning sanitary landfill and provide a scientific basis for further studies.

MATERIALS AND METHODS

Sampling and sample preparation

MSWIFA was obtained from a waste incineration plant in Beijing that adopts reciprocating mechanical grate incinerator to incinerate municipal waste. The flue gas purification of incinerator adopts the combined treatment facilities of 'dry deacidification + activated carbon adsorption + bag filter + SCR denitration'. The collected MSWIFA was dried to constant weight at 105 °C and then stored in sealed bags for later use. The basic physical and chemical properties of the MSWIFA are shown in Table 1.

Table 1. Basic properties of the MSWIFA.

Parameters	Value	Parameters	Value
Moisture content (%)	2.4	Na_2O (%)	7.47
pH (-)	13.84	SiO_2 (%)	3.67
CaO (%)	56.65	SO_3 (%)	2.79
K_2O (%)	8.51	Cl (%)	12.52

Cement-solidified MSWIFA blocks was prepared using the collected MSWIFA, benchmark cement (i.e.

ordinary Portland 32.5R cement sold in the market) and deionised water as follows. The MSWIFA and benchmark cement were poured into the mixing container according to the mass ratio of 4:1 and mixed evenly. It was well demonstrated that this mass ratio is applicable for MSWIFA solidification before landfilling (Du et al., 2019; Liu et al., 2019). Deionised water was then added according to the liquid–solid ratio of 0.5:1 for uniform mixing. This optimum liquid–solid ratio was determined in our preliminary experiment in terms of the solidification time and the flowability of the mixture. The mixture was then placed in a mould with dimensions of 5 cm × 5 cm × 5 cm and compacted with a vibrating plate. The cement-solidified MSWIFA blocks was cured in the curing box (temperature 20±2°C and relative humidity 95%±1%) for 24 hours (Berra et al., 2019). The hardened paste was demoulded and maintained for 28 days in the above ambiance. The prepared cement-solidified MSWIFA blocks was sealed in a bag and stored at room temperature for later use.

Leaching tests

The total amount of heavy metals, leaching toxicity of heavy metals, available leaching amounts of heavy metals and temporal-dependent leaching behaviours of the heavy metal in the cement-solidified MSWIFA blocks were measured to systematically study the leaching characteristics of heavy metals in the cement-solidified MSWIFA blocks. The total amount of heavy metals in the cement-solidified MSWIFA blocks was tested by using the microwave digestion method in 'Solid waste–Determination of 22 metal elements-Inductively coupled plasma optical emission spectrometry', and the obtained digestion solvent was used to determine the heavy metal content. The leaching toxicity of heavy metals in cement-solidified MSWIFA blocks and in cement blocks was determined according to 'Solid waste–Extraction procedure for leaching toxicity–Sulphuric acid & nitric acid method' (HJ/T 299-2007) and 'Solid waste–Extraction procedure for leaching toxicity–Acetic acid buffer solution method' (HJ/T 300-2007). The available leaching amounts of heavy metals in the cement-solidified MSWIFA blocks was measured according to EA NEN7371. Particularly, a certain amount of broken and ground cement-solidified MSWIFA blocks (diameter <125 μm) was placed in a beaker, added with deionised water with a liquid–solid ratio (L/kg) of 50:1, titrated with 1 mol/L nitric acid at pH=7±0.5 and maintaining for 3 hours. After filtration, a certain amount of filtrate was obtained. The residue was added with deionised water to a liquid–solid ratio (L/kg) at 50:1, titrated with 1 mol/L nitric acid at pH=4±0.5, and maintained for 3 hours. After filtration, the residue was mixed in the same amount of filtrate as before. The mixed solution was used to determine the content of heavy metals.

The temporal-dependent leaching behaviours of the heavy metals in the cement-solidified MSWIFA blocks was measured by using an improved version of EA NEN7375. The main component of acid rain in some parts of China is SO_4^{2-} and NO_3^- (Xie et al., 2009; Yang et al., 2018; Jia et al., 2021), and the pH of acid rain ranges from 3.2 to 5.6 (Zhou et al., 2017). According to the most unfavourable principle, HNO_3/ H_2SO_4 (mass ratio is 1:2) with pH value of 3.2±0.05 was selected as the leaching solvent (Yang et al., 2011), known as acid rain group. In addition, the group using deionized water as leaching solvent is designated as the control group. EA NENE7375 stipulated a liquid–solid ratio (L/m^3) of 2:1-5:1, and the most unfavourable principle stated a liquid–solid ratio (L/m^3) of 5:1 for this study. After the leaching solvent and liquid–solid ratio in the leaching experiment were set, a certain volume of cement-solidified MSWIFA blocks was continuously immersed in a specific volume of leaching solvent. According to the leaching protocols of EA NEN7375, the leaching solvent was replaced in eight steps, namely, 0.25 days, 1 day, 2.25 days, 4 days, 9 days, 16 days, 36 days and 64 days. At the end of each leaching step, a certain amount of leaching solvent was filtered through a 0.45 μm membrane filter and was immediately acidified with (1+1) nitric acid following filtration to pH <2. This leaching solvent was then stored in a refrigerator at 4 °C. According to the concentration of heavy metals in the leaching solvent obtained in different steps, the cumulative leaching amount (Formula (1) and Formula (2)) and leaching rate of heavy metals (Formula (3)) during the immersion of cement-solidified MSWIFA blocks were calculated.

$$E_i^* = (C_i \times V)/m \quad (1)$$

$$\varepsilon_n^* = \sum_{i=1}^{n} E_i^* \quad (2)$$

$$F_i = E_i^*/(t_i - t_{i-1}) \quad (3)$$

where ε_n^* is cumulative leaching amounts of heavy metals, mg/kg; E_i^* is the leaching amounts of heavy metals in step *i*, mg/kg; $C_i$is the concentration of heavy metals in the leaching solvent of step *i*, μg/L; *V* is Volume of leaching solvent, L; *m* is the weight of the MSWIFA, g; F_i is the leaching rate of heavy metals in step i, mg/kg/d; and t_i and $t_{i-1}$are the end time and start time of step i respectively, d.

Governing equations

When the leaching of heavy metals is controlled by diffusion, the bulk diffusion model (BDM) based on Fick's second diffusion law developed by Crank in 1975 (Lu et al., 2016) can fit the leaching amounts of heavy metals. The expression of this model is show in Formula (4).

$$M = 2\left(S/V\right)C_0\left[\left(D^{obs}t\right)/\pi\right]^{1/2} \quad (4)$$

When the leaching characteristics of heavy metals

under the control of surface wash-off can be described by first-order reaction model (FRM) (Formula 5), and its analytical solution is shown in Formula 6 (Zhang et al., 2021). Dissolution model (DIM) can be used to describe the leaching characteristics of heavy metals under dissolution, and the derivation process is shown in Formulas 7–9. Therefore, heavy metals controlled by diffusion and surface wash-off can be expressed as Formula 10, and heavy metals controlled by diffusion and dissolution can be expressed as Formula 11.

$$dQ/dt = -kQ \qquad Q|_{t=0} = Q_0 \tag{5}$$

$$Q = Q_0\left[1-\exp(-kt)\right] \tag{6}$$

$$U_{(t)} = U_0\left(1-C_t^l/C_{sat}^l\right) \tag{7}$$

For the simple case, C_t^l/C_{sat}^l is approximately 0, that is, $U_{(t)}=U_0$, then

$$M = C_0\left(S/V\right)U_0 t \tag{8}$$

Since C_0 and U_0 are constants in Equation (8), let $K=C_0U_0$, then

$$M = K\left(S/V\right)t \tag{9}$$

$$M = Q_0\left[1-\exp(-kt)\right] + 2\left(S/V\right)C_0\left[\left(D^{obs}t\right)/\pi\right]^{1/2} \tag{10}$$

$$M = 2\left(S/V\right)C_0\left[\left(D^{obs}t\right)/\pi\right]^{1/2} + K\left(S/V\right)t \tag{11}$$

where Q is the content of soluble heavy metals in the cement-solidified MSWIFA blocks at time t, mg/kg; Q_0 is the initial content of soluble heavy metals in the cement-solidified MSWIFA blocks (t = 0), mg/kg; k is the rate constant,1/d; $U_{(t)}$ is the dissolution rate of soluble heavy metals in the cement-solidified MSWIFA blocks at leaching time t, cm/d; U_0 is the maximum dissolution rate of soluble heavy metals in the cement-solidified MSWIFA blocks, cm/d; C_t^l is the concentration of heavy metals in the leaching solvent at leaching time t, mg/L; C_{sat}^l is the saturation concentration of heavy metals in the leaching solvent, mg/L; M is the cumulative leaching amounts of heavy metals per unit mass in the cement-solidified MSWIFA blocks at time t, mg/kg;C_0 is the available leaching amount of heavy metals per unit mass in the cement-solidified MSWIFA blocks, mg/kg; D^{obs} is the observed diffusion coefficient, cm^2/d; t is the leaching time, d. S is the surface area of the cement-solidified MSWIFA blocks, cm^2;V is the volume of the cement-solidified MSWIFA blocks, cm^3.

Analytical methods

X-ray fluorescence spectroscopy (PANalytical Axios) was used to determine Chemical composition (Zhang et al., 2021). pH was determined by A PHS-3C digital acidity detector (INESA Scientific Instrument Co., Ltd., Shanghai, China). Water content was determined by standard method (GB 7172-1987), and heavy metal concentration in the leaching solvent was determined by ICP-MS (NexLON350X, PerkinElmer, USA), each test was performed in triplicate (Wang et al., 2020).

RESULT AND DISCUSSION

Leaching toxicity of the cement-solidified MSWIFA blocks

According to the 'Standard for pollution control on the landfill site of municipal solid waste' (GB 16889-2008), solid waste block that can be disposed in a sanitary landfill must meet two basic requirements: (1) the solid waste block buried in the landfill should not be hazardous waste and (2) after pre-treatment, the leaching solvent of MSWIFA must meet the concentration limit of pollutants. Therefore, this study firstly evaluated whether the cement-solidified MSWIFA blocks meet the admission requirements of sanitary landfill according to the standard requirements.

The national standard GB 16889-2008 lists 11 heavy metals in the leaching solvent of solid waste, including Hg, Cu, Pb, As, Ni, Cr and Zn. Owing to its high environmental risk and easy leaching, the concentration limit of Cu, Cr, Pb, As and Ni in the leaching solvent is lower than the standard. Therefore, the five heavy metals mentioned above were selected as the investigation targets. The leaching toxicity of the cement-solidified MSWIFA blocks and cement blocks is shown in Table 2. Heavy metal leaching concentrations in cement blocks were substantially lower than in MSWIFA blocks that have been cement-solidified. As a result, the impact of heavy metals in cement could be overlooked in future studies. For the cement-solidified MSWIFA blocks, the leaching concentration of heavy metal Cu, Cr, Pb, As and Ni is lower than the concentration limit of heavy metal stipulated in GB 5085.3 and GB 16889, indicating that the MSWIFA is no longer classified as a hazardous waste after cement solidification, has met the admission standard of domestic solid waste block landfill and can be disposed in sanitary landfill. The leaching solvent prepared by HJ/T 300-2007 leaching protocol (using acetic acid as leaching solvent) has significantly higher As, Cu and Cr concentration but lower Ni and Pb than the leaching solvent prepared by HJ/T 299-2007 leaching protocol (using sulfuric acid and nitric acid as leaching solvent). Whether the leaching toxicity results of solid waste block prepared with the HJ/T 300-2007 leaching protocol can be used to evaluate the environmental risk of cement-solidified MSWIFA blocks in zonation landfill remains to be clarified. Given the complex and changeable composition of cement-

solidified MSWIFA blocks and landfill environment, further investigation must be conducted to determine whether the results of short-term leaching experiments (e.g. HJ/T 300-2007 and HJ/T 299-2007) can represent the long-term environmental safety of cement-solidified MSWIFA blocks in the zoned landfill.

Table 2. Leaching toxicity of heavy metals in cement-solidified MSWIFA blocks (ug/L).

Items	Leaching test protocol	Heavy metal (ug/L)				
		Cu	Cr	As	Ni	Pb
MSWIFA [a)]	HJ/T 299-2007	1.60 ± 0.45	9.96 ± 2.20	6.67 ± 1.42	56.83 ± 4.46	870.83 ± 89
GB5085.3-2007		100000	15000	5000	5000	5000
MSWIFA [a)]	HJ/T 300-2007	8.67 ± 0.74	62.40 ± 9.30	37.90 ± 0.75	35.67 ± 10.92	91.87 ± 13.
GB16889-2008		40000	5500	300	500	250

[a)] represents the mean and standard deviation values of the three parallel samples.

Heavy metals leaching behaviours of the cement-solidified MSWIFA blocks

(1) Total amount and available leaching of heavy metals

To reduce the time for the long-term environmental risk assessment of heavy metals in solid waste block, researchers estimate long-term stability according to the leaching amounts of heavy metals from solid waste block under extreme leaching environment (e.g. high temperature, low pH value, high liquid-solid ratio and small particle size). Particularly, the total amount of heavy metals and available leaching amount are the most common indicators. The total amount of heavy metal and available leaching amount of the cement-solidified MSWIFA blocks are shown in Fig. 1. The total amount of heavy metals in the cement-solidified MSWIFA blocks ranges 36–646 mg/kg, and the available leaching amount ranges 1–37 mg/kg. The total amount of heavy metals in cement-solidified MSWIFA blocks is higher than that their available leaching amount. When cement was used to solidify the MSWIFA, hydration occurred and prompted the heavy metals in MSWIFA to combine with silicate or be wrapped in C-S-H gel, thus preventing leaching (Wang et al., 2020). Although the total amount of Pb in cement-solidified MSWIFA blocks is the largest (i.e. 645.7 mg/kg), its available leaching amount and available leaching rate (i.e. ratio of available leaching amount to total amount of heavy metals) are only 22.8 mg/kg and 3.5%, respectively. The total amount of Ni is the smallest (i.e. 36.6 mg/kg), but its available leaching rate is as high as 22.2%. The above results show that the available leaching rate of different heavy metals in cement-solidified MSWIFA blocks are different. The leaching rate of heavy metals is related to cement solidification process, matrix characteristics, heavy metal species and leaching protocol. In specific exposure scenarios, the available leaching amounts of heavy metals in the cement-solidified MSWIFA blocks can better reflect its actual environmental risk than the total amount. This index will be used as a control parameter to study the leaching characteristics of heavy metals (Yang et al., 2009).

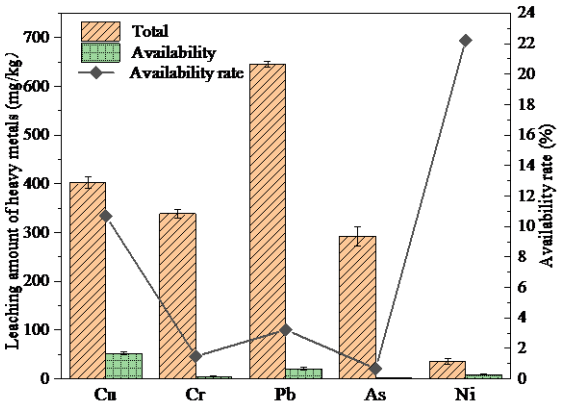

Fig. 1. Total, availability and availability rate of Cu, Cr, Pb, As and Ni in the cement-solidified MSWIFA blocks.

(2) Leaching characteristics of the heavy metals:

Heavy metal leaching from solid waste block is an unsteady process that varies with time. The leaching characteristics of heavy metals in the cement-solidified MSWIFA blocks are shown in Fig. 2. In acid rain group, the leaching rates of five heavy metals in the cement-solidified MSWIFA blocks follow the same pattern, with the rate being highest at the start and gradually decreasing Among the heavy metals, the leaching of Cu, Cr and Ni is similar. The cumulative leaching amounts of heavy metals increase rapidly in the first 16 days of leaching experiment and approach the maximum cumulative leaching amount on the 36th day. However, the cumulative leaching amount of As in the first 16 days of leaching experiment increases rapidly and approaches an equilibrium state. This phenomenon can be explained as follows. Firstly, the leaching control mechanism of As in the cement-solidified MSWIFA blocks is different from that of other heavy metals. Secondly, As has the lowest available leaching rate (i.e. Fig. 1) and thus reaches the leaching equilibrium point faster than other heavy metals. By contrast, the leaching control mechanism of Pb in the cement-solidified MSWIFA blocks is quite different from that of Cu, Cr, As and Ni. The cumulative leaching amount of Pb increases rapidly in the first 16 days of leaching experiment and maintains a high level at 16–64 days when the leaching rate is constant. This finding indicates that the cumulative leaching amount of Pb fails to reach the equilibrium state in this experimental period. On the other hand, the cumulative leaching levels of heavy metals in the control group have a comparable growth trend to those in the acid rain group, showing that each heavy metal has a similar leaching rate. The cumulative leaching levels of heavy metals were lower than in the acid rain group, owing to the fact that the leaching solvent, HNO_3/H_2SO_4 (mass ratio 1:2) with pH value of 3.2±0.05, stimulates heavy metal leaching more than deionized water. In acid rain group, during the 64-day leaching experiment, the cumulative leaching amounts of Cu, Cr, Pb, As and Ni

are 1.3, 1.1, 1.6, 0.3 and 0.5 mg/kg, respectively, which are only a percentage of its available leaching at 2.5%–22.0%. This result reveals that the leaching period of these five heavy metals in the cement-solidified MSWIFA blocks is longer than the experimental period of EA NEN7375 leaching protocol. Therefore, a set of mechanism models based on the leaching control mechanisms of different heavy metals were developed and used to predict the long-term stability of the cement-solidified MSWIFA blocks to effectively shorten the experimental period.

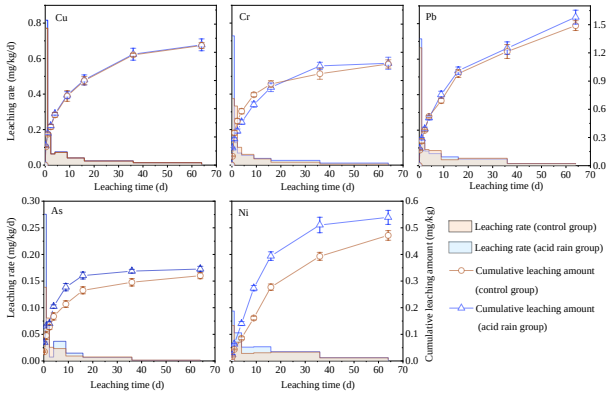

Fig. 2. Cumulative leaching amount and leaching rate of Cu, Cr, Pb, As and Ni in the cement-solidified MSWIFA blocks.

(3) Leaching mechanism and leaching model of heavy metals:

At present, the most recognised and widely used model to describe the leaching of pollutants from solid waste block is the BDM. In this study, BDM (Formula 4) was firstly used to fit the cumulative leaching amounts of heavy metals in the cement-solidified MSWIFA blocks. The observed diffusion coefficient D^{obs} in the formula is only related to leaching temperature (Song et al., 2013). At the same temperature, the square of accumulated leaching amounts (i.e. M^2) of heavy metals will show a linear relationship with leaching time *t*. BDM has the best fitting on Pb (R^2 = 0.98), followed by Ni (R^2 = 0.92). For the other heavy metals, the fitting effect of BDM is poor (i.e. R^2 <0.9). In the light of the result, BDM has the best fitting on Pb (i.e. R^2 = 0.97) and Ni (i.e. R^2 = 0.98). The fitting effect of BDM is likewise incorrect for other heavy metals (i.e. $R^2 \leq 0.9$). The above results indicate that the leaching control mechanism of some heavy metals (e.g. Cu, Cr and As) in the cement-solidified MSWIFA blocks is influenced by mechanisms other than diffusion control. Therefore, analysing the leaching control mechanism of different heavy metals is necessary to accurately predict their leaching law in the cement-solidified MSWIFA blocks.

According to the EA NEN7375 leaching protocol, the leaching control mechanism of inorganic components (e.g. heavy metal) in solid waste block includes surface wash-off, diffusion, dissolution, depletion and delayed diffusion. Surface wash-off refers to the dissolution of inorganic components in the solid–liquid interface when the leaching solvent contacts the block surface. Diffusion refers to the leaching of inorganic components due to molecular motion. Both of which are physical leaching control mechanisms. Dissolution refers to the leaching of inorganic components caused by the dissolution of some oxides in the block, and depletion means that the inorganic components is depleted in the block, these two are chemical leaching control mechanisms (Sun and Vollpracht, 2020). With this leaching protocol, the leaching control mechanism of heavy metals in solid waste block was identified by calculating (Formula 12) the leaching characteristics of different heavy metals at varying leaching intervals [i.e. leaching rate; Fig.2].

$$rc_{a-b} = \left(\log \varepsilon_a^* - \log \varepsilon_b^*\right) \Big/ \left(\log t_a - \log t_b\right) \quad (12)$$

Where $\varepsilon_a^*$and ε_b^* are the cumulative leaching of heavy metals in the leaching increment 1-a and 1-b, respectively, mg/kg; t_a and t_b are the completion time of leaching period a and b, respectively, d.

The heavy metal leaching rate and leaching control mechanism of the cement-solidified MSWIFA blocks at different leaching increments are shown in Table 3. Different heavy metals in the cement-solidified MSWIFA blocks are found to be controlled by varying leaching control mechanisms at different leaching increments. Pb is controlled by diffusion, which is also the reason why BDM can accurately fit its cumulative leaching data in the cement-solidified MSWIFA blocks. The leaching of Cu, Cr and As is controlled by diffusion, surface wash-off and depletion, and that of Ni is controlled by diffusion, dissolution and depletion. In a block solid, the proportion of heavy metal leaching caused by depletion control mechanism is extremely small and can be ignored (Tiruta-Barna et al., 2005). Therefore, the leaching of Cu, Cr and As in the cement-solidified MSWIFA blocks is mainly controlled by diffusion and surface wash-off, and that of Ni is mainly controlled by diffusion and dissolution. However, in the control group, BDM can also well fit the cumulative leaching amounts of Ni, possibly because the amount of Ni released by dissolution is very small.

Therefore, for acid rain group, formulas (10) and (11) were used to fit the accumulative leaching amounts of Cu, Cr, As and Ni (Fig. 2), and the fitting results and parameter values are shown in Table 3. Compared with those of BDM, the fitting results of FRDM and DDIM are closer to the actual test values. The correlation coefficients (R^2) of Cu, Cr, As and Ni obtained from BDM are 0.87, 0.89, 0.74 and 0.92, respectively, which increase to 0.98, 0.95, 0.97 and 0.95, respectively. For the control group, the accumulative leaching quantities of Cu, Cr, and As were fitted using formula (10); the fitting results and parameter values are provided in Table

Table 3. Slope of heavy metal Cu, Cr, Pb, As and Ni at different leaching increment and determination of leaching mechanism.

Increment	Cu		Cr		Pb		As		Ni	
a-b	1#	2#	1#	2#	1#	2#	1#	2#	1#	2#
2-7	Dif	Dif	Dif	Sur	Dif	Dif	Sur	Sur	Dif	Dif
5-8	Dep	Dep	Dep	Dep	Dif	Dif	Dep	Dep	Dep	Dif
4-7	Dif	Dif	Dif	Dep	Dif	Dif	Dep	Dep	Dif	Dis
3-6	Dif	Dif	Dif	Dep	Dif	Dif	Dif	Dif	Dis	Dis
2-5	Dif	Dif	Dif	Dif	Dif	Dif	Dep	Dif	Dis	Dif
1-4	Sur	Sur	Sur	Dif	Dif	Dif	Dif	Dif	Dif	Dif

Note: Dif-Diffusion; Dep-Depletion; Dis-Dissolution; Sur-Surface wash-off; 1# represents acid rain group; 2# represents control group

4. The correlation coefficients (R^2) of Cu, Cr, and As are enhanced from 0.90, 0.84, and 0.84, respectively, to 0.98, 0.99, and 0.98, respectively, using this formula. Therefore, the above corrected models can be used to predict the long-term leaching characteristics of heavy metals from the cement-solidified MSWIFA blocks during zonal landfill.

Table 4. Nonlinear regression parameters of different leaching models for Cu, Cr, Pb, As and Ni in cement-solidified MSWIFA blocks.

Heavy metals	Sample number	Model	Parameters				R^2 (-)
			D^{obs} (cm^2/d)	Q_0 (mg/kg)	k (1/d)	K (mg•cm/kg•d)	
Cu	1#	FRDM	2.72×10^{-6}	0.40	0.54	--	0.98
	2#	FRDM	2.65×10^{-6}	0.40	0.49	--	0.98
Cr	1#	FRDM	1.69×10^{-4}	0.45	0.33	--	0.97
	2#	FRDM	9.91×10^{-5}	0.56	0.50	--	0.99
Pb	1#	BDM	4.40×10^{-5}	--	--	--	0.98
	2#	BDM	3.94×10^{-5}	--	--	--	0.97
As	1#	FRDM	2.66×10^{-5}	0.25	0.37	--	0.95
	2#	FRDM	5.78×10^{-5}	0.17	0.41	--	0.98
Ni	1#	DDIM	4.43×10^{-5}	--	--	3.31×10^{-7}	0.95
	2#	BDM	2.71×10^{-5}	--	--	--	0.98

Note: 1# represents acid rain group; 2# represents control group

Long-term stability assessment

At present, GB 16889-2008 is the standard for identifying the environmental risk of solid waste block entering sanitary landfills in China. When the concentration of heavy metals in solid waste block leachate (preparation method: HJ/T 300-2007) is lower than the limit specified in this standard, the environmental risk of solid waste block in the landfill is acceptable. Although the cement-solidified MSWIFA blocks used in this experiment can meet the requirements of entry materials in China's sanitary landfills, the leaching concentration of Pb may exceed the limit specified in GB 16889-2008 under the exposure scenario of partition landfills (Table 2). In addition, the cumulative leaching amounts of heavy metals in cement-solidified MSWIFA blocks using HNO_3/H_2SO_4 (simulated acid rain) as the leaching solvent are greater than those using deionized water (Fig. 2), indicating that cement-solidified MSWIFA blocks pose a greater environmental risk under acid rain scenarios. Therefore, the corrected pollutant leaching model was used to predict the daily and cumulative leaching amounts of different heavy metals and to judge the long-term environmental risk of the zoned landfill of the cement-solidified MSWIFA blocks in acid rain scenarios (as shown in Fig.3).

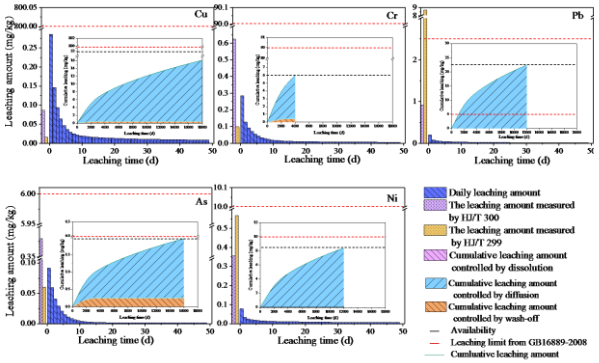

Fig. 3. Prediction of cumulative leaching amounts of heavy metals Cu, Cr, Pb, As and Ni in the cement-solidified MSWIFA blocks in acid rain scenarios.

Figure 3 shows that in the case of zoned landfill exposure, the daily leaching amounts of heavy metals in the cement-solidified MSWIFA blocks are maximised at the 1st day, then gradually decrease, and tend to balance after 10 days. Additionally, the maximum daily leaching of heavy metals in the cement-solidified MSWIFA blocks is lower than the leaching limit set by GB16889-2008, indicating that, in the zoned landfill, the leaching toxicity of the heavy metals in the cement-solidified MSWIFA blocks with high liquid-solid ratio or leaching solvent (i.e. acid rain) under short contact time is below the sanitary landfill environmental risk acceptable level. Moreover, according to the predicted leaching characteristics of heavy metals by the established model under the assumption that the leaching environment (e.g. temperature, pH, liquid-solid ratio and disregarded the bacterial effects) and the physicochemical properties (e.g. mineralogical phase particle size and porosity) of the test blocks remained constant, the cumulative leaching of Cu, Cr, As and Ni for the next 50 years is still lower than the leaching limit specified in GB16889.Therefore, cement solidification treatment has a good fixation effect on these four heavy metals and can significantly reduce the environmental risk of their landfill. Additionally, the leaching of these four heavy metals from surface wash-off control accounts for a low proportion of the total leaching of heavy metals (i.e. between 2.4% and 29%). According to the model prediction, the leaching of Pb is mainly controlled by diffusion, and the cumulative leaching amount in 718 d is higher than the limit in GB16889. When the liquid-solid ratio is low or the

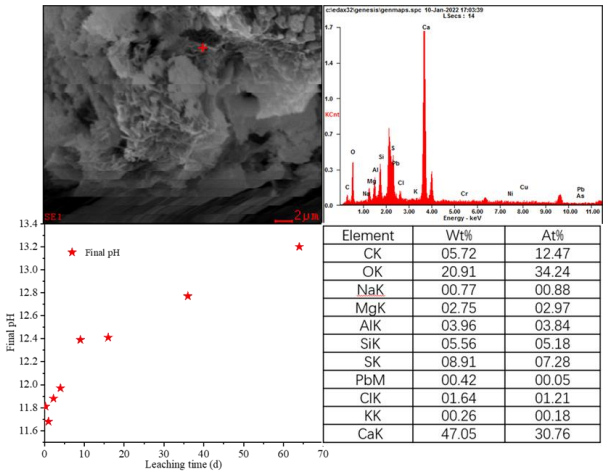

Element	Wt%	At%
CK	05.72	12.47
OK	20.91	34.24
NaK	00.77	00.88
MgK	02.75	02.97
AlK	03.96	03.84
SiK	05.56	05.18
SK	08.91	07.28
PbM	00.42	00.05
ClK	01.64	01.21
KK	00.26	00.18
CaK	47.05	30.76

Fig. 4. Final pH of the solvent after each leaching step and SEM-EDS of ettringite in cement-solidified MSWIFA blocks.

leachate discharge is not smooth in landfill (i.e. the cement-solidified MSWIFA blocks is in contact with leachate for a long time), Pb leaching toxicity may exceed the acceptable levels of environmental risk in sanitary landfills. The main reasons for the high environmental risk of Pb in cement-solidified MSWIFA blocks are as follows. Firstly, the content of Pb is high in the cement-solidified MSWIFA blocks (i.e. 645 mg/kg) and GB16889 stipulates a low concentration limit of Pb in the leachate of landfill materials due to the high environmental toxicity of Pb. Secondly, it was documented that the pore solution of cement-solidified MSWIFA blocks was highly alkaline which contained large amount of Ca^{2+}, Na^{+}, K^{+}, OH^{-} and SO^{2-}_{4} ions. Under this alkaline condition, Pb is mainly present in the form of $Pb(OH)_2$ and $PbSO_4$ in the blocks. However, given the Pb is a amphoteric metal, the $Pb(OH)_2$ and $PbSO_4$ precipitates can exist below a certain pH point (i.e. pH<12). When the pH of the solution rises above this point, the $Pb(OH)_2$ and $Pb(SO)_4$ precipitates will gradually dissolves into $[Pb(OH)_3]^{-}$, $[Pb(OH)_4]^{2-}$ and $[Pb(OH)_2SO_4]^{2-}$, increasing the solubility of Pb (Zhou et al., 2015; Wang, 2016). Although the hydration products of the cement-solidified MSWIFA blocks (e.g. ettringite; Fig. 4) could prevent partial Pb leaching out, the final pH of the leaching solvent was still mostly higher than 12 (Fig. 4), inducing large amount of Pb leaching out form the blocks. Therefore, the removal of partially soluble salts (e.g. Pb salts) from the freshly made cement-solidified MSWIFA blocks by water or natural rainwater washing in the initial landfilling stage (i.e. in this stage, the landfill is not capped with a final cover system and the leachate drainage system remains functional) is an effective countermeasure to reduce the environmental risk of cement-solidified MSWIFA blocks in zoning sanitary landfill.

CONCLUSION

This study tends to estimate the long-term environmental risk of cement-solidified MSWIFA in zoning sanitary landfill in terms of the leaching behaviours of five different heavy metals (i.e. Cu, Cr, Pb, As, Ni). The following conclusions was drawn.

(1) Under simulated acid rain scenarios, Pb leaching from cement-solidified MSWIFA was controlled by diffusion, whereas Cu, Cr and As were dominated by wash-off and diffusion. Ni leaching was mostly controlled by diffusion and dissolution. The established BDM, FRDM and DDIM could accurately described the leaching behaviours of the abovementioned heavy metals with different control mechanisms (R^2>0.95).

(2) The prediction results of the calibrated models indicated that the long-term environmental risk of Pb was high in acid rain scenarios, in terms of the cumulative leaching amount of Pb exceeded the limit issued in GB-16889 after 718 days' leaching. It could be attributed to the strong alkali environment of the cement-solidified MSWIFA (pH > 12) which might stimulate the dissolution of partial Pb salts (e.g. $Pb(OH)_2$ and $PbSO_4$).

(3) Removal of partially soluble Pb salts from freshly made cement-solidified MSWIFA is an effective countermeasure to reduce the environmental risks in zoning sanitary landfill.

ACKNOWLEGEMENT

The study was supported by the National Key Research and Development Program of China (2021YFE0112100).

REFERENCE

Berra, M., Ippolito, N.M., Mangialardi, T., Paolini, A.E., Piga, L., 2019. Leaching test procedure for assessing the compliance of the chemical and environmental requirements of hardened woody biomass fly ash cement mixtures. WASTE Manag. 90, 10–16.

Cerbo, A.A. V., Ballesteros, F., Chen, T.C., Lu, M.C., 2017. Solidification/stabilization of fly ash from city refuse incinerator facility and heavy metal sludge with cement additives. Environ. Sci. Pollut. Res. 24, 1748–1756.

Chen, L., Wang, Y.S., Wang, L., Zhang, Y., Li, J., Tong, L., Hu, Q., Dai, J.G., Tsang, D.C.W., 2021. Stabilisation/solidification of municipal solid waste incineration fly ash by phosphate-enhanced calcium aluminate cement. J. Hazard. Mater. 408, 124404.

Du, B., Li, J., Fang, W., Liu, J., 2019. Comparison of long-term stability under natural ageing between cement solidified and chelator-stabilised MSWI fly ash. Environ. Pollut. 250, 68–78.

Garrabrants, A.C., Sanchez, F., Kosson, D.S., 2004. Changes in constituent equilibrium leaching and pore water characteristics of a Portland cement mortar as a result of carbonation. Waste Manag. 24, 19–36.

Jia, M., Yu, J., Li, Z., Wu, L., Christie, P., 2021. Effects of biochar on the migration and transformation

of metal species in a highly acid soil contaminated with multiple metals and leached with solutions of different pH. Chemosphere 278, 130344.

Kim, M., Kim, H.G., Kim, S., Yoon, J.H., Sung, J.Y., Jin, J.S., Lee, M.H., Kim, C.W., Heo, J., Hong, K.S., 2020. Leaching behaviors and mechanisms of vitrified forms for the low-level radioactive solid wastes. J. Hazard. Mater. 384, 121296.

Kosson, D.S., Garrabrants, A.C., Thorneloe, S.A., Fagnant, D., Helms, G., Connolly, K., Rodgers, M., 2019. Leaching Environmental Assessment Framework (LEAF) How-To Guide, Appendices. U.S. Epa.

Leelarungroj, K., Likitlersuang, S., Chompoorat, T., Janjaroen, D., 2018. Leaching mechanisms of heavy metals from fly ash stabilised soils. WASTE Manag. Res. 36, 616–623.

Li, W.H., Gu, K., Yu, Q.W., Sun, Y.J., Wang, Y., Xin, M.X., Bian, R.X., Wang, H.W., Wang, Y.N., Zhang, D.L., 2021. Leaching behavior and environmental risk assessment of toxic metals in municipal solid waste incineration fly ash exposed to mature landfill leachate environment. WASTE Manag. 120, 68–75.

Liu, J., He, L., Luo, C., Song, K., 2019. Dynamic leaching rule of heavy metals in solidified body of fly ash from MSW incineration. China Environ. Sci. 39, 1087–1093.

Lu, H., Wei, F., Tang, J., Giesy, J.P., 2016. Leaching of metals from cement under simulated environmental conditions. J. Environ. Manage. 169, 319–327.

Ogundiran, M.B., Nugteren, H.W., Witkamp, G.J., 2013. Immobilisation of lead smelting slag within spent aluminate-fly ash based geopolymers. J. Hazard. Mater. 248–249, 29–36.

Quina, M.J., Bordado, J.C.M., Quinta-Ferreira, R.M., 2009. The influence of pH on the leaching behaviour of inorganic components from municipal solid waste APC residues. WASTE Manag. 29, 2483–2493.

Sanchez, F., Barna, R., Garrabrants, A., Kosson, D.S., Moszkowicz, P., 2000. Environmental assessment of a cement-based solidified soil contaminated with lead. Chem. Eng. Sci. 55, 113–128.

Sanchez, F., Garrabrants, A.C., Vandecasteele, C., Moszkowicz, P., Kosson, D.S., 2003. Environmental assessment of waste matrices contaminated with arsenic. J. Hazard. Mater. 96, 229–257.

Shi, H., Ni, J., Zheng, T., Wang, X., Wu, C., Wang, Q., 2019. Remediation of wastewater contaminated by antibiotics . A review. Environ. Chem. Lett.

Song, F.Y., Gu, L., Zhu, N.W., Yuan, H.P., 2013. Leaching behavior of heavy metals from sewage sludge solidified by cement-based binders. Chemosphere 92, 344–350.

Sun, Z., Vollpracht, A., 2020. Leaching of monolithic geopolymer mortars. Cem. Concr. Res. 136, 106161.

Taha, Y., Benzaazoua, M., Edahbi, M., Mansori, M., Hakkou, R., 2018. Leaching and geochemical behavior of fired bricks containing coal wastes. J. Environ. Manage. 209, 227–235.

Tiruta-Barna, L., Rethy, Z., Barna, R., 2005. Release dynamic process identification for a cement based material in various leaching conditions. Part II. Modelling the release dynamics for different leaching conditions. J. Environ. Manage. 74, 127–139.

Tong, L.Z., He, J.Y., Wang, F., Wang, Y., Wang, L., Tsang, D.C.W., Hu, Q., Hu, B., Tang, Y., 2020. Evaluation of the BCR sequential extraction scheme for trace metal fractionation of alkaline municipal solid waste incineration fly ash. Chemosphere 249.

Van der Sloot, H.A., 2002. Characterization of the leaching behaviour of concrete mortars and of cement-stabilized wastes with different waste loading for long term environmental assessment. Waste Manag. 22, 181–186.

Wang, B., Fan, C., 2020. Hydration behavior and immobilization mechanism of MgO–SiO2–H2O cementitious system blended with MSWI fly ash. Chemosphere 250, 126269.

Wang, C.P., 2016. Study on Solidification/Stabilization of Cement on MSWI Fly Ash and the Leaching Mechanism of Pb and Cd.Chinese. Wang, C.P., Li, F.Z., Zhou, M.K., Chen, Y., Chen, X., 2015. Effect of cement-MSWI fly ash hydration on the stabilisation/solidification of Pb and Cd. Mater. Res. Innov. 19, S51161–S51166.

Wang, X.N., Wang, M.L., Zou, D.Z., Wu, C.F., Li, T., Gao, M., Liu, S., Wang, Q.H., Shimaoka, T., 2020. Comparative study on inorganic Cl removal of municipal solid waste fly ash using different types and concentrations of organic acids. Chemosphere 261, 127754.

Wang, Y., Ni, W., Zhang, S., Li, J., Suraneni, P., 2020. Optimal mixture designs for heavy metal encapsulation in municipal solid waste incineration fly ash. Appl. Sci. 10, 1–21.

Xie, B.X., Qin, J., Sun, H., Wang, S., Li, X., 2021. Leaching behavior of polycyclic aromatic hydrocarbons (PAHs) from oil-based residues of shale gas drill cuttings. Environ. Pollut. 288, 117773.

Xie, Z., Du, Y., Zeng, Y., Li, Y., Yan, M., Jiao, S., 2009. Effects of precipitation variation on severe acid rain in southern China. J. Geogr. Sci. 19, 489–501.

Yan, J.H., Peng, W., Li, X.D., Li, J.X., Cen, K.F., 2004. Leaching behavior of heavy metals from MSWI fly ash. Ranliao Huaxue Xuebao/Journal Fuel Chem. Technol. 32, 65.

Yang, J.Z., Yang, Y., Li, Y., Chen, L., Zhang, J., Die, Q., Fang, Y., Pan, Y., Huang, Q., 2018. Leaching of metals from asphalt pavement incorporating municipal solid waste incineration fly ash. Environ. Sci. Pollut. Res. 25, 27106–27111.

Yang, Y.F., Huang, Q.F., Zhang, X., Yang, Y., Wang, Q.H., 2009. Release amount of heavy metals in cement product from co-processing waste in cement kiln.

Huanjing Kexue/Environmental Sci. 30, 1539–1544.

Yang, Y.F., Yu, Y., Wang, Q.H., Huang, Q.F., 2011. Release of heavy metals from concrete made with cement from cement kiln co-processing of hazardous wastes in pavement scenarios. Environ. Eng. Sci. 28, 35–42.

Yu, Q.J., Nagataki, S., Lin, J.M., Saeki, T., Hisada, M., 2005. The leachability of heavy metals in hardened fly ash cement and cement-solidified fly ash. Cem. Concr. Res. 35, 1056–1063.

Zhang, B.X., Gao, M., Geng, J., Cheng, Y., Wang, X.N., Wu, C.F., Wang, Q.H., Liu, S., Ming, S., 2021. Catalytic performance and deactivation mechanism of a one-step sulfonated carbon-based solid-acid catalyst in an esteri fi cation reaction. Renew. Energy 164, 824–832.

Zhang, H., Chen, G., Cai, X., Fu, J., Liu, M., Zhang, P., Yu, H., 2021. The leaching behavior of copper and iron recovery from reduction roasting pyrite cinder. J. Hazard. Mater. 420, 126561.

Zhang, W.L., Zhao, L., Yuan, Z., Li, D.Q., Morrison, L., 2021. Assessment of the long-term leaching characteristics of cement-slag stabilized/solidified contaminated sediment. Chemosphere 267, 128926.

Zhou, X.D., Xu, Z.F., Liu, W.J., Wu, Y., Zhao, T., Jiang, H., 2017. Progress in the Studies of Precipitation Chemistry in Acid Rain Areas of Southwest China. Huanjing Kexue/Environmental Sci. 38, 4438–4446.

Zhou, M.K, Wang, C.P, Chen, Y., Chen, X., 2015. Leaching behavior and mechanism of cement solidified heavy metal Pb in acid medium. J. Wuhan Univ. Technol. Mater. Sci. Ed. 30, 781–786.

Stochastic approach of location-independence earthquake disaster risk estimation for mercury waste landfill

Fumitake Takahashi[1]
1 Department of Transdisciplinary Science and Engineering, School of Environment and Society, Tokyo Institute of Technology
G5-13, 4259, Nagatsuta, Midori-ku, Yokohama, 226-8503 Japan

INTRODUCTION

Mercury has unique characteristics like liquid under ambient condition and has been used in industry and society. Due to high toxicity and hazards to human bodies and the environment, international efforts to regulate and decrease mercury use has been paid [1]. In this context, the Minamata convention on mercury was agreed in 2013 and made effective on 16th Aug. 2017. The collection of mercury used in industry and society is requested and long-term safe storage of collected mercury is also necessary in near future. Mercury storage in engineered landfill sites is one option in terms of cost and environmental safety. However, environmental risk of mercury landfill disposal should be carefully assessed, in particular earthquake regions like Japan. Seismic impact on landfill site safety or durability has been concerned [2]. For example, earthquake-induced displacement of landfilled wastes were affected by the amplitude (peak acceleration) and frequency content (mean period) of the design rock motion and the dynamic response characteristics of the landfilled wastes [3]. In addition, local geological condition of a landfill site might also play a significant role in the seismic response of a landfill [4]. In this sense, site selection of landfill sites is important and should be socially concerned [5]. Landfill site selection is a complex task in which various factors should be considered [6]. One of important factors for site selection or screening is Not-In-My-Backyard (NIMBY) syndrome, in other word, public opposition toward landfill site construction [7-8]. According to strongly negative attitude toward site screening, pre-assessment of environmental risk for mercury final disposal in specific candidate sites might cause public confusion and/or miscommunication. On the other hand, geological information of potential landfill sites is necessary for appropriate assessment of earthquake-induced environmental risk of mercury landfill disposal. In order to overcome this paradoxical problem, this study developed a new method for environmental risk estimate of location-independence earthquake disaster risk. The purpose of this work is to test a stochastic approach to build a methodological framework for location-independence risk estimation. As the first step, this study considered mercury temporal storage on the ground near the final landfill site because mercury stabilization before landfill disposal is necessary.

METHODS

Risk scenario of mercury release to the environment caused by big earthquake

This study considered a risk scenario of mercury release event to the environment. In this scenario, mercury storage facility on the ground will be hit by a big earthquake. Owing to facility destruction, mercury containers will be transferred unintentionally to the environment. Owing to container damages, mercury will be emitted from the containers by rain water penetration. In this article, the amount of released mercury from the containers would be reported.

Stochastic approach to estimate the probability of big earthquake hit to mercury storage facility

As mentioned in Introduction section, this work does not take any site-specific scenario for mercury risk estimation. According to USGS Earthquake Catalog database [9], earthquake event with magnitude more than 6.5 were screened and then the event data (location, hypocentral depth, and magnitude) were extracted in the area at 130-135 degrees east longitude and 30.5-40.1 degrees north latitude. Time period of data extraction was 120 years from Jan 1900 to Mar 2020. The locations of screened earthquake event are shown in **Fig 1**. Appropriate statistical distributions of hypocentral depth, magnitudes, and distances from hypocentral location to capital cities of all prefectures in Japan were determined based on Bayesian

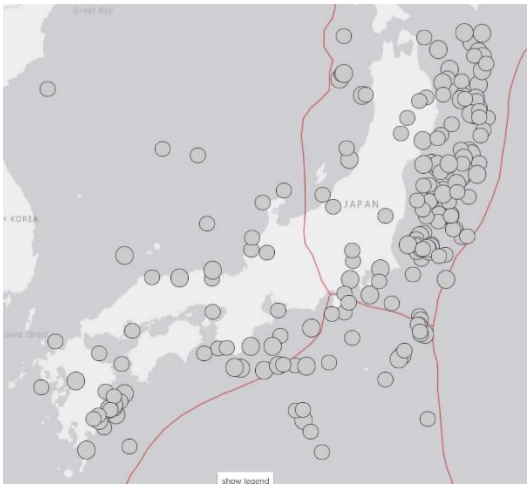

Fig. 1 Locations of earthquake events with more than M6.5 extracted from Jan 1900 to Mar 2020

information criterion (BIC). Using these statistical distributions, the probability of a earthquake event at specific time and location can be predicted stochastically as well as the earthquake magnitude and distances to specific location. According to the earthquake magnitude and distance data, peak ground acceleration (PGA), peak ground velocity (PGV), and their distance attenuations [11] were also possible to predict stochastically. To validate predicted PGV, database of J-SHIS earthquake hazard station [10] were used. PGVs with 3 % and 6 % of 30-year exceedance probabilities and PGVs with 2 %, 5 %, 10 %, and 39 % of 50-year exceedance probabilities for all prefectural capital cities in Japan were extracted from J-SHIS database and local averages of these PGVs were calculated. These averages were compared with those predicted by this method for validation.

Stochastic approach to estimate the destruction probability of mercury storage facility caused by big earthquake hit

This work used empirical response spectrum with 5 % distance attenuation, proposed by Umemura [12], of each earthquake event. Even when acceleration response spectrum of an earthquake event exceeds maximum durable acceleration response spectrum determined by limit horizontal strength calculation, it does not result in inevitable destruction of mercury storage facility. According to destruction survey of houses and buildings hit by Southern Hyogo earthquake in 1995, building destruction ratio followed normal distribution of earthquake strength, which was described as the ratio of PGA to gravity acceleration [13]. This statistical distribution was used to predict the probability of facility destruction by an earthquake hit in this study.

Stochastic approach to estimate mercury release from storage containers to the environment via rain water penetration

135-year precipitation data in Tokyo from 1880 to 2015 were used for the Stochastic approach to estimate mercury release from storage containers to the environment. Data shows that the precipitation follows normal distribution as shown in **Fig. 2**. When mercury sulfide in the storage containers contacts with water penetrated from cracks on container surface, which was caused by the earthquake hit, mercury is dissolved in water and transfers to outside along with water flow and finally reached to the environment. The cumulative amount of released mercury and its probability were calculated for mercury risk assessment. In this article, however, mercury risk will not be reported due to page limitation.

RESULTS AND DISCUSSIONS

Optimum statistical distributions of earthquake hypocentral depth, magnitudes, and distances from hypocentral location to capital cities of all prefectures in Japan

This study tested three statistical distributions, lognormal, gamma, and Weibull distributions, to find the most appropriate distributions based on BIC. The results are shown in **Fig. 3** for hypocentral depth, **Fig. 4** for magnitude, and **Fig. 5** for distances to prefectural

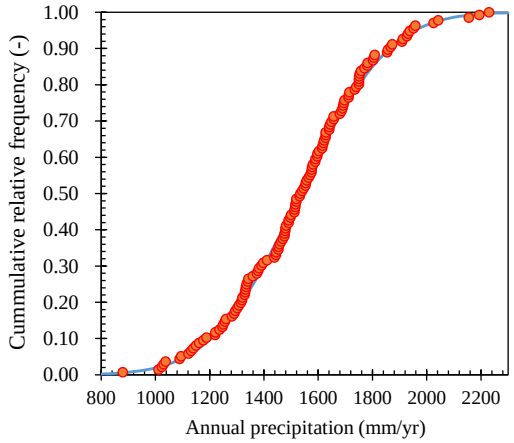

Fig. 2 Cumulative relative frequency of the annual precipitation for 135-year from 1880 to 2015

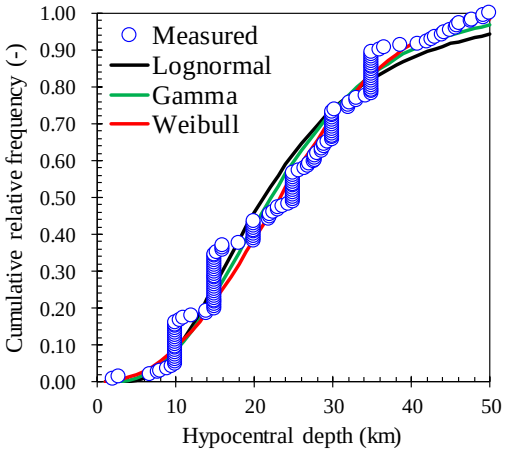

Fig. 3 Statistical distributions of hypocentral depth

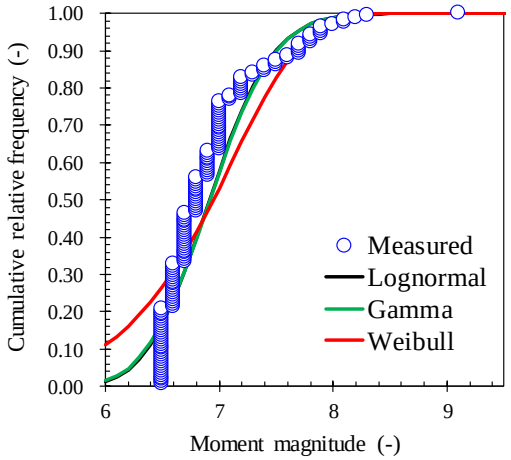

Fig. 4 Statistical distributions of moment magnitude

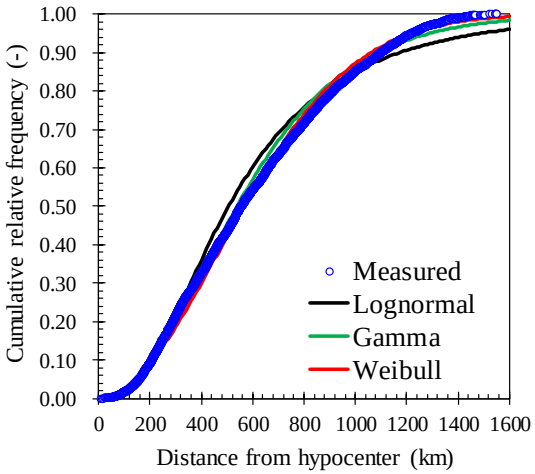

Fig. 5 Statistical distributions of distance to the hypocenter

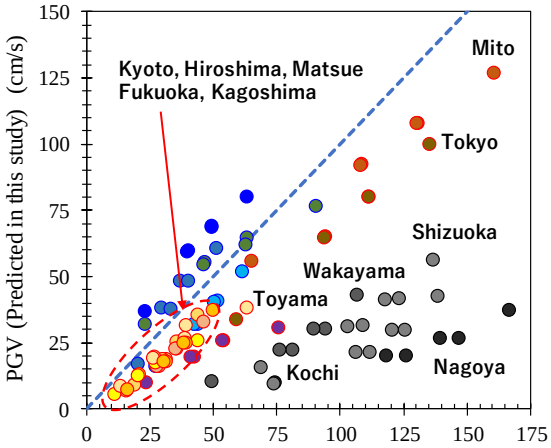

Fig. 6 Comparison of peak ground velocity between the predictions of this study and J-SHIS database [10]

capital city, respectively. The most appropriate statistical distribution of hypocentral depth and magnitude was identified lognormal distribution. Weibull distributions was the best for the distances to prefectural capital cities.

The validation results using PGVs with 3 % and 6 % of 30-year exceedance probabilities and PGVs with 2 %, 5 %, 10 %, and 39 % of 50-year exceedance probabilities are shown **Fig. 6**. Although predicted PGVs at many prefectural capital cities agree with those referred from J-SHIS database [10], large underestimation of PGVs by this method are found in some cities near pacific oceans. These cities are expected to be hit by Nankai and Tokai Trough Earthquakes in the future due to periodical earthquake events. As mentioned in Methods section, this study used earthquake event data since 1900, not included periodical earthquake events before 1900. It might have caused this underestimation. Therefore, the stochastic approach developed in this study needs further improvement to include highly-probable periodical earthquake events like Nankai and Tokai Trough Earthquakes.

Stochastic estimation of 100-year exceedance probabilities of earthquake events with seismic intensity class of 5 or more.

When mercury storage facility is built anywhere in Japan, 100-year exceedance probabilities of earthquake events with seismic intensity class of 5 or more are shown in **Fig. 7**. In particular, class 7 earthquake event is concerned due to its high probability of facility destruction. This study estimated that 25-year exceedance probabilities of class 7 earthquake events was 0.83 %. It was increased to 1.7 % for 50-year exceedance probability and 3.3 % for 100-year exceedance probability. It is considered that 25 years or longer use of mercury storage facility on the ground was not realistic because this facility would be used for mercury stabilization (conversion to mercury sulfide) and temporal storage before final disposal in the landfill site. In this sense, 3.3 % for 100-year exceedance probability might not be necessary to consider facility destruction risk. On the other hand, the stochastic model of this study also suggests that 0.83 % probability of class 7 earthquake hit should be concerned when the facility is used for 25 years.

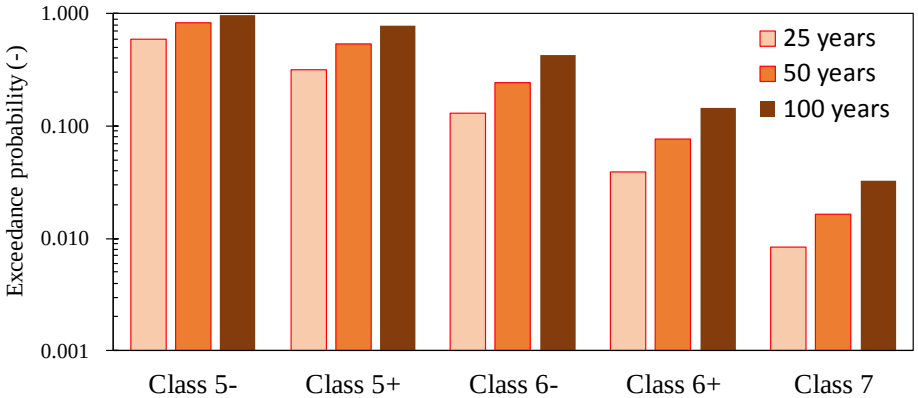

Fig. 7 Exceedance probabilities of earthquake events with seismic intensity class of 5 to 7

100-year mercury release from storage containers to the environment via rain water penetration

When mercury containers are transferred unintentionally to the environment after the destruction of mercury storage facility, mercury will be released from the container for long term. This study considered 100 years mercury release. Cumulative relative frequency of expected total release of mercury for 100 years is shown in **Fig. 8**. 75 percentile range of mercury release is 0.138-41.5 mg-Hg. The median is 13.3 mg-Hg. When 95 percentile range is considered, the maximum is only 50.4 mg-Hg. Because the stochastic model of this study seems to overestimate the destruction probability of mercury storage facility, even 50.4 mg-Hg release might be overestimated. Therefore, this study concludes that accidental mercury release from mercury storage facility by large earthquake hit gives negligible risk to the environment. However, it should be noted that this study assumed that mercury sulfide, in containers transferred out of the facility, was stable in the environment. When mercury sulfide is converted to other mercury species like mercury oxide by chemical or biological reactions, several orders of magnitude larger leaching rate of mercury to penetrated rain water is expected. Further researches are necessary to conclude mercury risk more appropriately.

CONCLUSIONS

This study developed the stochastic model of location-independence earthquake disaster risk estimation for mercury ground storage before final landfill disposal. This study concludes that accidental 100-year cumulative release of mercury by the destruction of mercury storage facility hit by a large earthquake is 50.4 mg-Hg or less. Although it might be negligible in terms of environmental risk, further research is necessary for more reliable estimation.

ACKNOWLEDGEMENT

This study was supported financially by Environment Research and technology development grant (3-1701 and JPMEERF20S20602), funded by Ministry of the Environment, Japan. The authors appreciate the support greatly.

REFERENCES

1. Mercury report
2. Krinitzsky E.L., Hynes M.E., Franklin A.G. (1997) Earthquake safety evaluation of sanitary landfills, *Engineering Geology*, 46(2), 143-156.
3. Bray J.D. Rathje E.M. (1998) Earthquake-induced displacements of solid-waste landfills, *Journal of Geotechnical and Geoenvironmental Engineering*, 124(3), 242-253.
4. Psarropoulos P.N., Tsompanakis Y., Karabatsos Y. (2007) Effects of local site conditions on the seismic response of municipal solid waste landfills, *Soil Dynamics and Earthquake Engineering*, 27(6), 553-563.
5. Yesilnacar M.I., Cetin H. (2005) Site selection for hazardous wastes: A case study from the GAP area, Turkey, *Engineering Geology*, 81(4), 371-388.
6. Aksoy E., San B.T. (2019) Geographical information systems (GIS) and Multi-Criteria Decision Analysis (MCDA) integration for sustainable landfill site selection considering dynamic data source, *Bulletin of Engineering Geology and the Environment*, 78(2), 779-791.
7. Simsek C., Elci A., Gunduz O., Taskin N. (2014) An improved landfill site screening procedure under NIMBY syndrome constraints, *Landscape and Urban Planning*, 132, 1-15.
8. Kontos T.D., Komilis D.R., Halvadakis C.P. (2003) Siting MSW landfills on Lesvos island with a GIS-based methodology, *Waste Management and Research*, 21(3), 262-277.
9. USGS: Search Earthquake Catalog, Web site: https://earthquake.usgs.gov/earthquakes/search/
10. National Research Institute for Earth Science and Disaster Prevention (Japan) J-SHIS earthquake hazard station database, Web site: http://www.j-shis.bosai.go.jp/
11. Midorikawa S., Ohtake M (2003) Empirical analysis of variance of ground motion intensity in attenuation relationships, *Journal of Japan Association for Earthquake Engineering*, 3(1), 59-70. *In Japanese*
12. Umemura K., Osawa Y., Matsushima Y. (1966) Analysis of response spectra for a variety of ground, Annual report of the Engineering Research Institute, School of Engineering, University of Tokyo, 24(2).
13. General Insurance Rating Organization of Japan (2006) A survey of earthquake hazard estimation methods of local authorities in Japan, *Earthquake Insurance Research*, 8, Chapter III.

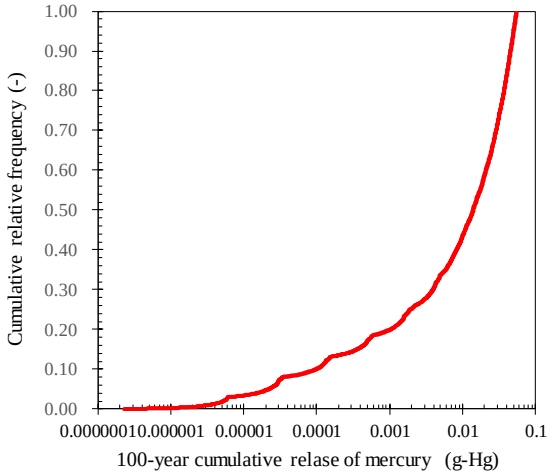

Fig. 8 100-year cumulative release of mercury

NEUTRALIZATION OF INCINERATOR ASH LANDFILL LAYER BY HIGHLY CO_2 DISSOLVED WATER

Kentaro Miyawaki[1]
1 School of Science and Engineering, Meisei University,
Hodokubo 2-1-1, Hino-city, Tokyo,191-8506, Japan

INTRODUCTION

Incinerator ash is the main landfilled waste at landfill for municipal solid waste in Japan. Therefore, the landfill layer remains alkaline for a very long time. At some disposal sites, leachate has a high pH for a long period of time, and the pH does not reach the wastewater standard (<8.6). There are many cases of studies on neutralization of incinerator ash and u insolubilization of heavy metals using carbon dioxide, and certain effects have been reported in Japan. The problem is that CO_2 does not reach the inside of the incinerator ash particles and sufficient carbonation does not proceed. At the covered landfill, moisture control is carried out by artificial watering.

In this study, a CO_2 highly dissolved solution using ultrafine bubbles (UFB) was supplied to the glass bead layer and incinerator ash layer. CO_2 abundance in water and the promotion of the neutralization reaction were investigated.

METHODS

Carbon dioxide (CO_2) dissolved water

The device for generating high dissolved CO_2 solution (hereafter referred to as CO_2 dissolved device) consisting of a UFB generating loop flow type OK nozzle (OK Engineering Co. Ltd) and pump were used (Photo.1)

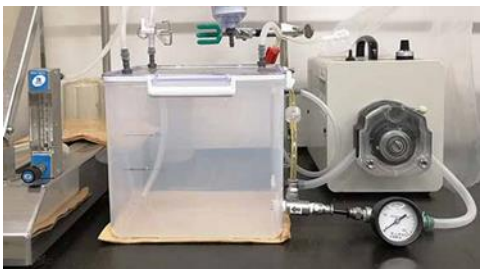

Photo 1 CO_2 dissolved device

Dissolved CO2 in the glass bead layer

The column packed with glass beads (inner diameter 42.5 mm, 1mm diameter glass beads, layer thickness of 50mm or 150mm) was used for measuring of CO_2 dissolved condition. (Photo2).

CO_2 dissolved water was dripped from the top of the glass bead layer at a flow rate of 2.37 mL/min (100 mm/h in terms of rainfall) and 4.73 mL/min, and the IC concentration of the effluent was measured.

Neutralization of incinerated ash layer with CO_2 dissolved water

The column packed with incinerator ash (inner diameter of 53.8 mm and a layer thickness of 150 mm, ash weight 270g) was used for investigating as neutralization condition). (Photo 3)

CO_2 dissolved water and pure water were dripped at 5 mL/min (132 mm/h in terms of rainfall), which is assumed to be the maximum amount of permeation possible. The pH, EC, ORP and IC of the leachate discharged from the column were measured.

At end test, leaching test (JLT13) was done for incinerator ash at top, middle, bottom layer.

Photo2 Glass bead packed column

Photo3 Incinerator ash packed column

RESULTS AND DISCUSSION

Dissolved CO_2 in the glass bead layer

Figure 1 shows the IC concentration at 50mm and 150mm glass bead layers.The supply water IC concentration of the CO_2 dissolved device has a range

of about 120-180mg-C/L.
The outflow rate (outflow IC/inflow IC) at a layer thickness of 150mm was 62.8-67.1%.

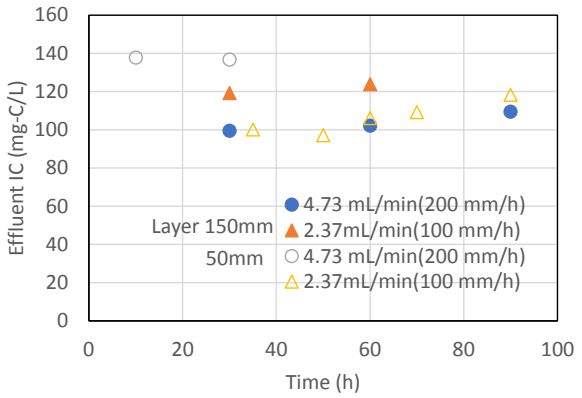

Figure 1 Change in IC concentration (glass bead layer)

Neutralization of incinerated ash layer with CO_2 dissolved water

Figure 2 shows the pH of leachate from the incinerator ash layer. When CO_2 dissolved water (UFB-CO_2 water in the figure) was introduced into the incinerator ash layer, the pH of the leachate was lower than that of pure water. From this, it was inferred that the incinerator ash was neutralized.

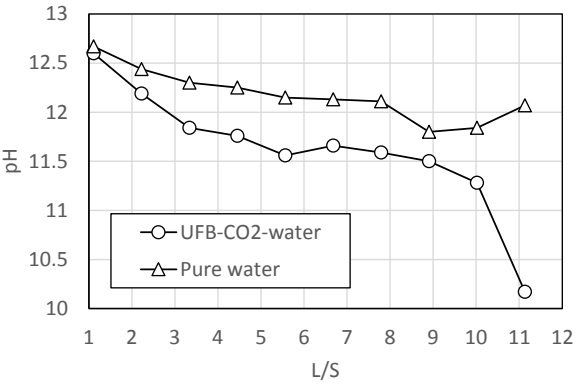

Figure 2 Leachate pH (CO_2 dissolved water, pure water)

Figure 3 shows the electrical conductivity (EC) of leachate from the incineration ash layer. There was no difference between passing CO_2 dissolved water (UFB-CO_2 water in the figure) and pure water, and EC decreased rapidly. It was considered that the effect of CO_2 was not observed in washing out the salts contained in the incinerator ash.

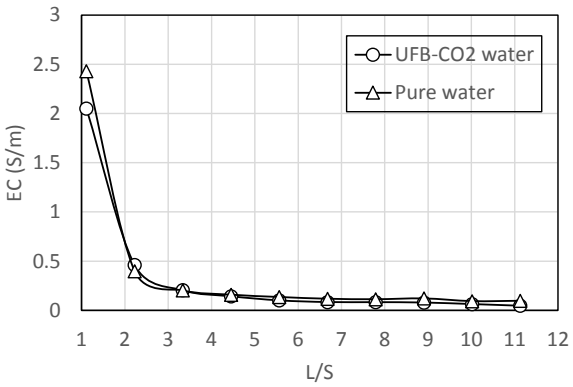

Figure 3 Electrical conductivity of leachate

Figure 4 shows the pH in the leaching test by depth. The eluate pH with CO2 was lower than that with pure water. From this, neutralization of incinerator ash was confirmed.

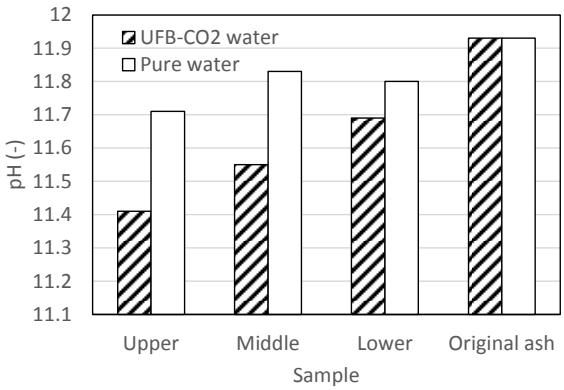

Figure 4 Packed incineration ash elution pH (in column)

SUMMARY

When CO_2 dissolved water was passed through a 150mm incinerator ash layer, the pH of leachate was lower than that of pure water.
From the results of the leaching test of the incineration ash, the neutralization of the incineration ash progressed slowly due to the CO_2 dissolved water flowing down.

ACKNOWLEDGMENT

This work was supported by KAKENHI Grant-in-Aid for Scientific Research(C) (20K12227). I would like to express my appreciation to Ms. Hishiyama, Mr.Ouchi and all members of working of these investigations.

HETEROGENEITY OF OXYGEN CONSUMPTION IN ORGANIC SOLID WASTES

[1] Tadis DILLON, [2] Takayuki SHIMAOKA, [3] Teppei KOMIYA
[1,2,3] Department of Urban and Environmental Engineering, Kyushu University, Japan
[1] dillon.tadis.488@s.kyushu-u.ac.jp,[2] shimaoka@doc.kyushu-u.ac.jp, [3] komiya-t@doc.kyushu-u.ac.jp

Abstract*— In many developing countries a vast majority of the solid waste is disposed, untreated, to landfill sites. As much as 70% of these wastes are considered as some form of easily degradable organic matter. The presence of available organic matter creates a constant demand for oxygen from aerobic, heterotrophic microorganisms which affects the diffusion and distribution of oxygen in waste. While oxygen intrusion into soils is usually studied in the context of its utilization by plants in agriculture or other similar applications, this study attempted to visualize the distribution and consumption of soil oxygen in landfill environments where respiration by microfauna becomes the dominant oxygen sink. Further the study investigated the effect of varying organic content on oxygen distribution and consumption dynamics. Immature waste bodies were observed to produce highly variable oxygen consumption and distribution due to unpredictable microfauna proliferation. Increasing organic content elevates oxygen consumption but the increased consumption is not proportional to the increase in organic availability. These factors suggest that the oxygen consumption rate in immature, highly organic, waste is not simply predicted based solely on time. It may be acceptable to assign a generalized, fixed rate of oxygen consumption for landfills rich in organics matter.

Index Terms— *aerobic biodegradation,* solid waste, organic waste, oxygen consumption

I. INTRODUCTION

According to the World Bank, in developing countries in Latin America and the Caribbean (LAC), as much as 95% waste generated in these countries is treated by some form of in-situ land disposal on a spectrum ranging from planned sanitary landfills to ad hoc open dump sites [1]. Regardless of the location or condition of these disposal sites, they share an important characteristic; as much as 70% of the waste they contain can be considered as some form of easily degradable organic matter (kitchen waste, paper products, wood). With the high organic composition of the wastes of these landfills the introduction of oxygen into these waste bodies is expected to greatly accelerate the stabilization of these sites. While there has been research into understanding the mechanisms affecting the influx of oxygen into soils [2],[3,[4], the research has been primarily focused the role of flora on oxygen demand. Landfills in LAC and other developing regions pose a different facet to the soils in these studies due to the expected difference in organic concentration. Studies on understanding and modelling the transport and consumption of oxygen specifically within waste bodies has been previously undertaken [5],[6]. These studies demonstrated the link between oxygen consumption and oxygen diffusion into solid waste. However, the conditions replicated mirrored that of the present municipal solid waste of a developed nation composed predominantly of incineration residues. This waste composition does not reflect the waste composition of the developing world. To understand the oxygen dynamics of organic waste additional work is required. The aim of the current research is to focus on waste of high organic content. Column experiments were performed to analyze the oxygen profile of highly organic waste and the associated oxygen consumption rate.

II. MATERIALS AND METHODOLOGY

A. Samples

Proxy materials were utilized to represent the target waste stream. Easily degradable organic matter in the form of compost (CP) generated from food waste was selected as the organic fraction as it was deemed a close approximate to the kitchen waste. The inorganic and not easily degraded fraction of waste was replicated utilizing waste incineration bottom ash (BA) sieved for the fraction under 10mm then air dried before use.

B. Materials

Figure 1 shows the layout of the materials utilized for the study. The columns used were composed of acrylic material of dimensions 0.1m (Diameter)x 2m (Height) consisting of two layers; a. Drainage layer, b. Waste Layer.

The drainage layer consisted of glass beads to facilitate separation and removal of leachate from the waste mass. The waste layer spanned a depth of 187cm and was constructed utilizing CP and BA. BA and CP were subjected to analysis including particle size distribution, moisture content (ω [%]), ignition loss [LOI (mg [g-dry solid (DS)], oxygen consumption and leachability

characteristics. The methodologies utilized for these analyses were referenced from [5]. A total of three (3) columns were constructed with the proportions of 0%CP:100%BA in column 1; 10%CP:90%BA in column 2 and 20%CP:80% BA in column 3. The mixture was placed into the columns in 10cm layers at a time to ensure uniform compaction to an average density of approximately 1100 kg/m3. The columns were purged of oxygen by opening all ports and applying a positive pressure of pure nitrogen gas (N2) to displace oxygen. The addition of Nitrogen was terminated and all ports and openings, including the leachate collection port, closed and the baseline oxygen levels determined. Once baseline levels were obtained, the top of each column was opened to allow unrestricted gas exchange.

C. Sampling

Closed gas sampling ports were established at every 0.1m height intervals for the first meter of the column and subsequently at 0.2m intervals for the remaining meter for

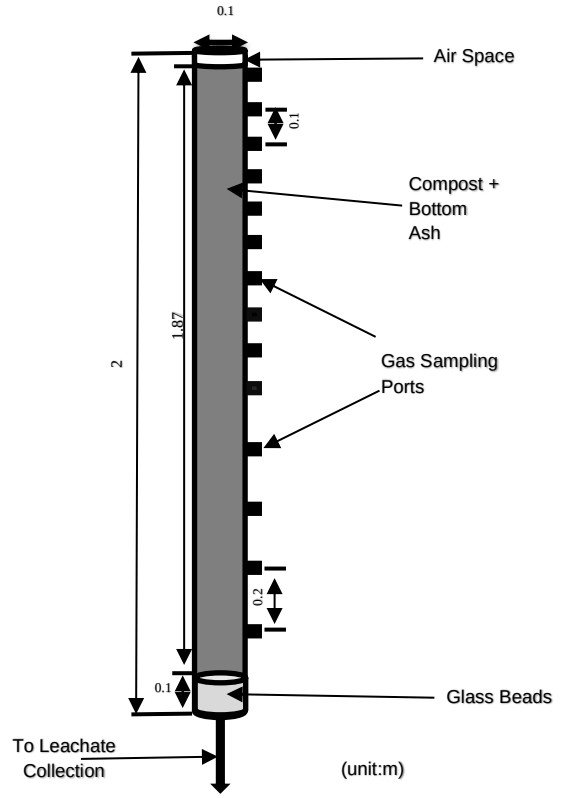

Figure 1: Column Layout

a total of fourteen (14) points. Each sampling port was protected by a ball valve. The mouth of each valve was sealed by a plastic sleeve and capped with a rubber cork to isolate the sampling ports from the outside air, when the samples were being removed. Samples were removed utilizing a needle affixed to a 6ml syringe via a 3-way stopcock. Before samples were taken the residual air within each sample port was first withdrawn utilizing the syringe to create a vacuum within the sample port. The needle was then reinserted into the vacuum before the valve was opened. The air within the cavity was then mixed by pumping the syringe repeatedly approximately 10 times. A sample, not exceeding 2-3ml was extracted and kept for analysis utilizing a SHIMADZU GC-2014. Gas samples were obtained from the column initially every two days for the first week, after which they were taken at 5–7-day intervals.

Leachate was collected via collection bottles attached to the column via hoses. When leachate was not being collected, the hoses were sealed to prevent gas entering the column. A leachate head was maintained within the collection system to prevent entry of air when leachate was collected. Leachate was removed on an as needed basis as the drainage layer approached capacity. Collected leachate was recirculated back into the columns.

Moisture was supplied to the columns initially in the form of distilled water at a rate of 40ml per day to simulate an average daily rainfall of 5mm, typical of tropical climates.

III. RESULTS

A. Waste Characteristics

Table I- Loss on Ignition Test

	Moisture Content (%)	Loss on Ignition (%)
BA	11.88	0.78
CP	11.37	60

Table II-Leaching Test Analysis

COLUMN	TOC (mg/L)	IC (mg/L)	TC (mg/L)	TN (mg/L)
(0%CP: 100%BA)	19.70	N.D	19.7	3.20
(10%CP: 90%BA)	383.3	0.6	383.9	49.9
(20%CP: 80%BA)	1411	7.0	1418	178

(N.D – Not Detectable)

Tables I-II show results of analysis undertaken on the waste materials utilized. The CP utilized as the organic fraction contained around 60% volatile organics based on loss on ignition tests (I). BA utilized contained less than 1% volatile organic matter. Leaching tests (II) further

demonstrate the low levels of readily available carbon available in BA as compared the elevated levels in CP.

B. Oxygen Distribution

Figures 2-4 present the oxygen distribution profiles for the experiment. The first graphic (a) maps the oxygen concentration measured at each sampling point (vertical axis) vs time (horizontal axis). The oxygen concentration at the intervals which were not measured were interpolated based on the measured data. Blue represents areas of low oxygen concentration with red representing atmospheric concentration. Graphic (b) represents the change in oxygen concentration (vertical axis) with time (horizontal axis) at selected sampling ports. Graphic (c) highlights the vertical oxygen distribution within the column on selected days. After air was introduced, it rapidly diffused to the lower levels driven by the large diffusion gradient between the atmosphere and the waste mass created by the oxygen purging at the start of the experiment. In pure BA oxygen penetrates slowly and continuously driven primarily by the diffusion gradient with resistance to the diffusive movement defined by the diffusion coefficient of oxygen in BA. Within 100 days the diffusion gradient became minimal with no significant difference in oxygen levels between the column surface and the base. In the presence of organic matter the effect on the oxygen profile is readily observed. After initial replenishment of the oxygen concentration to the 12-14% range the subsequent 30 days saw the oxygen levels in both columns begin to decrease. The reduction in oxygen in the columns with high organic matter as opposed to no reduction in bottom ash was thus attributed to oxygen consumption from bacterial respiration utilizing the available substrates. The oxygen distribution profile of organic waste however produced an irregular structure where the oxygen consumption appeared adhoc and oxygen concentration was not linearly distributed as observed in bottom ash. This was attributed to the tendancy of microrganisms in soils ,even though being present at 10^6 ->10^{12} individual cells per gram of soil, to mainly associate into colonies which in turn develop into respiration hotspots.[7]. These hotspots are defined as small pockets within the soil which display accelerated microbial process as compared to the surrounding areas[8]. These hotspots become active during what are termed hot moments; triggers which spur microorganisms moment. Bearing similar characteristics to soils, the waste mass was believed to be subject to a similar process. One dominant factor which is proposed as the catalyst for the promulugation of the hot moments observed in the simulated waste mass was temperature. Due to the columns being composed of acrylic material into action. As such the introduction of any factor, which previously limited microbial growth, can trigger a hot

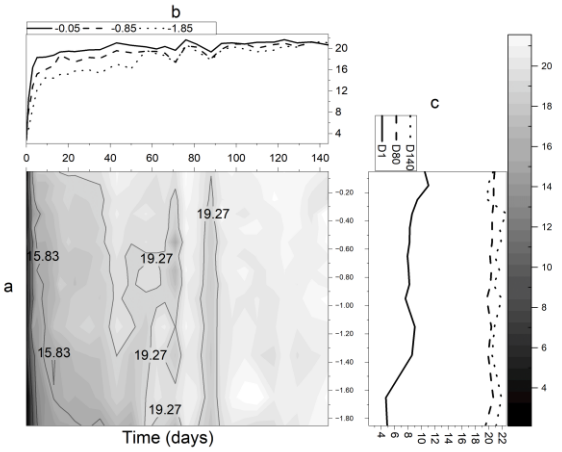

Figure 2:Oxygen Distribution 100%BA

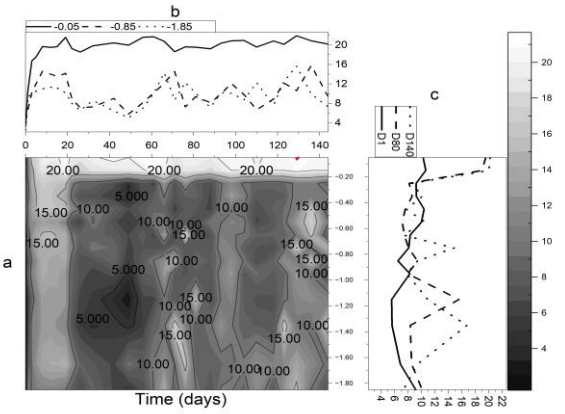

Figure 3:Oxygen Distribution 90%BA: 10%CP

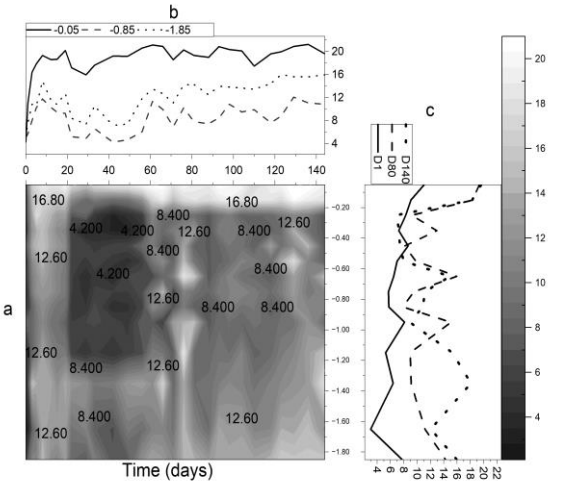

Figure 4:Oxygen Distribution 80%BA: 20%CP

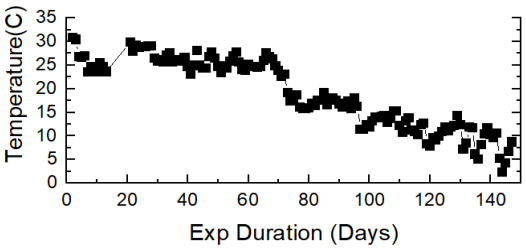

Figure 5: Atmospheric Temperature during experiment

there was no thermal insulation and as such the column temperatures were influenced by the external conditions. When the atmopheric temperature is considered, as seen in figure 5, a 5^{o}C rise in temperature was observed between days 10 – 21. This temperature increase coincided with the observed hotspots in figures 3a+4a .With the subsequent reduction in the atmostpheric temperature consistently below 25^{0}C, after 70 days it was observed that, while some hotspots re-emerge their expanse and duration were reduced . The presence of temperatures above 25^{0}C were therefore interpreted as being a common factor impacting the oxygen profile in organic waste due to its importance in promoting microbial activity.

C. Oxygen consumption

From the oxygen distribution profiles the greatest oxygen debt, post column opening, was observed with 20%CP where the minimum oxygen level recorded was as low as 4.3%. However, this value is not significantly lower than the minimum recorded in the presence of 10% CP of 4.7%. Initial high oxygen consumption in low oxygen soils has been shown to be initially driven by oxidation of ions into oxides e.g. Fe_2^+, NH_4^+ combined with consumption by soil microorganisms [9]. The low oxygen levels observed with 1*0%* CP and 20% CP after 20 days compared to the absence of additional organic matter shows the significant role of microorganisms in the consumption of oxygen in waste containing readily available substrates. Four separate areas, spanning the expanse of the columns, were selected as the points for the determination of maximal oxygen consumption rate. The rate was calculated utilizing the Crank–Nicolson form of the diffusion differential equation as referenced from [6]

$$\frac{(x)_k^{t+\Delta t}-(x)_k^t}{\Delta t}=\frac{1}{2}\frac{D}{\xi}\left(\begin{array}{c}\dfrac{(x)_{k-1}^t-2(x)_k^t+(x)_{k+1}^t}{\Delta y^2}\\ +\\ \dfrac{(x)_{k-1}^{t+\Delta t}-2(x)_k^{t+\Delta t}+(x)_{k+1}^{t+\Delta t}}{\Delta y^2}\end{array}\right)-\rho_d\frac{RT}{\varepsilon P}R_1{}^t \quad (1)$$

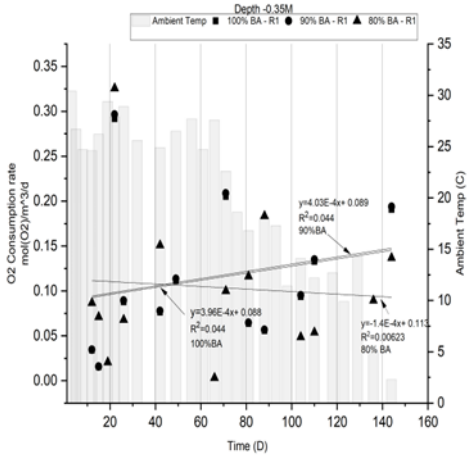

Figure 6:Calculated Oxygen Consumption Rate(-0.35M)

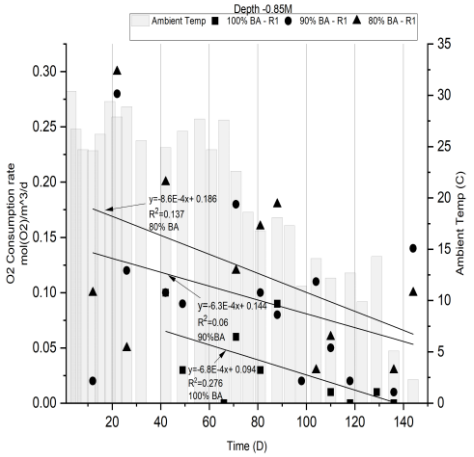

Figure 5:Calculated Oxygen Consumption Rate(-0.85M)

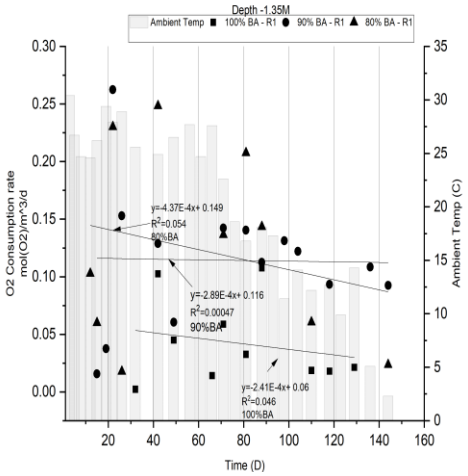

Figure 7: Calculated Oxygen Consumption Rate(-1.35M)

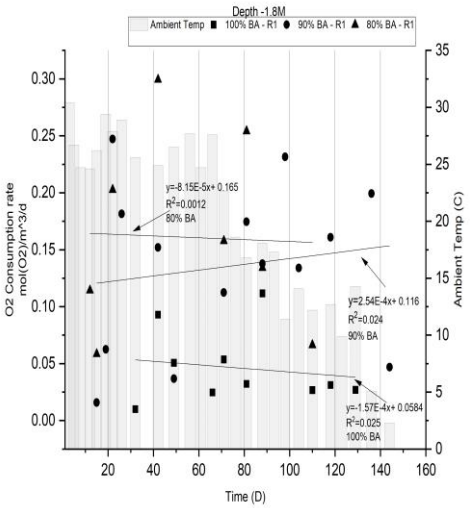

Figure 8:Calculated Oxygen Consumption Rate(-1.8M)

Where x is measured oxygen mole fraction *(–)*, t is elapsed experimental time (days), k is sampling depth (m), D is the diffusion coefficient of oxygen (m^2/day), ξ is tortuosity*(–)*, y is the distance between sampling points(m), P is the total pressure (Pa) , R is the universal gas constant (m^3 Pa mol^{-1} K^{-1}), ρ_d is the dry density T is temperature (K) and R_1 is the oxygen consumption rate.
Due to the discontinuity of the data, interpolation was conducted so that y=0.1m. Utilizing the Crank–Nicolson equation on this dataset resulted in days where there was no calculated positive oxygen consumption. Only days where net *o*xygen consumption was positive, were plotted and presented in Figures 6-9. These figures show the change in the calculated oxygen consumption rate with time with the first figure representing the consumption profile close to the soil-atmosphere boundary at -0.35m depth with the last figure representing the consumption at the deepest point. In terms of the depth calculated consumption rates determined at the hotspot near to the 0.85M displayed the clearest trend in all columns with highest consumption occurring during the initial periods with a gradual decrease with time. This trend was consistent to that observed in [5] in previously landfilled wastes. However, this trend was not clearly discernable at each depth analyzed. In terms of the time the high scatter of the calculated oxygen consumption rates as well as low predictability of the consumption rate with time given by the low R^2 values of the line functions derived further demonstrate the highly variable nature of oxygen consumption in organic waste in the near term. Longer term investigations are thus needed to determine the oxygen consumption function of highly organic waste.

IV. CONCLUSION

Landfills are by their nature very heterogeneous masses, and this is reflected in the tendency of respiration hotspots developing. These areas are characterized as 'pockets' where oxygen is utilized at accelerated rates compared to the surrounding areas due to favorable conditions being present for bacterial proliferation. This results in a variable oxygen profile where the oxygen concentration, at any given depth, is not simply and accurately predicted as a function of time in the short term. It may be therefore more applicable to utilize generalized consumption rates for mature and stabilized wastes with high organic content to account for hotspot activity in areas with subsurface temperatures averaging above 20°C. Further experimentation over an extended period at constant temperatures is recommended to create a general oxygen consumption function for organic wastes.

REFERENCES

[1] Silpa, K., Yao, L. C., Bhada-Tata, P., & Van Woerden, F. (2018). What a Waste : Global Snapshot To 2050. Washington: World Bank Publications.

[2] Cook, F. J. (1995). One-dimensional oxygen diffusion into soil with exponential respiration: analytical and numerical solutions. Ecological Modelling, 78(3), 277–283. https://doi.org/10.1016/0304-3800(94)00179-L

[3] Cook, F. J., & Knight, J. H. (2003). Oxygen transport to plant roots: Modeling for physical understanding of soil aeration. Soil Science Society of America Journal, 67(1), 20–31. https://doi.org/10.2136/sssaj2003.2000

[4] Neira, J., Ortiz, M., Morales, L., & Acevedo, E. (2015). Oxygen diffusion in soils: Understanding the factors and processes needed for modeling. Chilean Journal of Agricultural Research, 75(August), 35–44. https://doi.org/10.4067/S0718-58392015000300005

[5] Kallel, A., Matsuto, T., & Tanaka, N. (2003). Determination of oxygen consumption for landfilled municipal solid wastes. Waste Management and Research, 21(4), 346–355. https://doi.org/10.1177/0734242X0302100407

[6] Kallel, A., Tanaka, N., Tojo, Y., Matsuto, T., & Hanada, S. (2006). Oxygen intrusion into waste in old landfills of low organic content. Waste Management and Research, 24(3), 242–249. https://doi.org/10.1177/0734242X06064209

[7] Schlüter, S., Zawallich, J., Vogel, H. J., & Dörsch, P. (2019). Physical constraints for respiration in microbial hotspots in soil and their importance for denitrification. Biogeosciences, 16(18), 3665–3675. https://doi.org/10.5194/bg-16-3665-2019

[8] Kuzyakov, Y., & Blagodatskaya, E. (2015). Microbial hotspots and hot moments in soil: Concept & review. Soil Biology and Biochemistry, 83, 184–199. https://doi.org/10.1016/j.soilbio.2015.01.025

[9] Reddy, K. R., Rao, P. S. C., & Patrick, W. H. (1980). Factors Influencing Oxygen Consumption Rates in Flooded Soils. *Soil Science Society of America Journal*, *44*(4), 741–744. https://doi.org/10.2136/sssaj1980.03615995004400040016x

[10] Esener, A. A., Roels, J. A., & Kossen, N. W. F. (1981). The influence of temperature on the maximum specific growth rate of Klebsiella pneumoniae. Biotechnology and Bioengineering, 23(6), 1401–1405. https://doi.org/10.1002/bit.260230620

BEHAVIOR OF HEAVY METALS IN LANDFILLED FLY ASHES FOR 27 YEARS

Jamie Tan Mae Chee[1], Takayuki Shimaoka[2], and Amirhomayoun Saffarzadeh[2]

1 Department of Urban and Environmental Engineering, Graduate School of Engineering, Kyushu University, 744 Motooka, Nishi-ku, Fukuoka 819-0395, Japan
2 Department of Urban and Environmental Engineering, Faculty of Engineering, Kyushu University, 744 Motooka, Nishi-ku, Fukuoka 819-0395, Japan

Abstract - Municipal Solid Waste Incineration (MSWI) produces a substantial amount of fly ash (FA) and bottom ash (BA), which contains harmful heavy metals such as Pb, Cd, and Cr. Generally, FA has relatively higher heavy metals content than that of BA. Thus, MSWI FA needs to be pre-treated before landfill disposal. This paper discusses about the behavior of heavy metals in landfilled fly ash by different treatment method in a simulated environment for the past 27 years. X-ray fluorescence (XRF), column experiment, and Japan Leaching Test (JLT-13) were conducted on untreated, chelate treated, phosphate stabilized and slag treated FA. After 27 years, the discussed heavy metals Pb, Cd, Cr, Zn, and Cu from column experiment have stabilized, and the leached Pb and Cd from leaching test fell way below the Japanese regulatory criteria for landfilling of 0.3mg/L. [1] Even though Zn is stabilized, the result of leached Zn is heavily dependent on the pH value of the sample at the time.

1. INTRODUCTION

Due to economic development and population growth, significant amount of municipal solid wastes (MSW) is generated annually in Japan. Incineration has played an important role in solving the scarcity of available land to accommodate the accumulated MSW. Solely in year 2020, 41,670,000 tons of MSW was generated and 79.1% of which were incinerated into 3,640,000 tons landfill waste. [2] MSWI produces a substantial amount of fly ash (FA) and bottom ash (BA), which contains harmful heavy metals such as Pb, Cd, Cr, Zn, and Cu. Generally, FA has relatively higher heavy metals content than that of BA. [3] Thus, MSWI FA fly ash needs to be pre-treated before landfill disposal according to the Waste Disposal and Public Cleansing Law in Japan. [4]

Furthermore, there are far more landfill sites in mountainous areas than in other areas in Japan, and the long-term stabilization of treated fly ash in mountainous landfills has not been clarified. [5] The study investigates the behavior of fly ash from simulated mountainous landfill model tanks for untreated, chelate treated, phosphate treated fly ash, and slag. With chelating treatment being the most commonly used treatment in Japan, XRF, column experiment, and JLT-13 were conducted to evaluate the behavior of fly ash for the past 27 years.

2. MATERIALS AND METHODS

In 2002, two separate research of similar objectives from Fukuoka University were merged into one. [5] [6] Ten landfill model columns were filled with fly ash that has undergone pre-treatment (Table 1). The top end of the column is exposed to natural rainfall, whereas the leachate is collected at the bottom of the column. (Fig.1)

Table 1. Types of ash mix and treatment method corresponding to the column number.

Column No.	Sample Name	Abbreviation
1	Untreated Bottom Ash, Fly Ash, Compost, Crushed Garbage	BAFA CG(U)
2	Chelate treated BAFA CG	BAFA CG(C)
3	Phosphoric acid treated BAFA CG	BAFA CG(P)
4	Untreated Bottom Ash	BA (U)
5	Untreated Fly Ash	FA (U)
6	Untreated Bottom Ash + Fly Ash	BAFA (U)
7	Surface Melting Slag	SMS
8	Plasma Melting Slag	PMS
9	Chelate treated Fly Ash	FA (C)
10	Phosphoric acid treated Fly Ash	FA (P)

The BAFA CG ash mix has a 60:20:15:5 ratio corresponding to BA: FA: Garbage: Compost. BAFA (U) and SMS has a 3:1 ratio for BA:FA whereas PMS has a 4:1 BA to FA ratio. The rest of the samples are purely 100% FA and BA respectively.

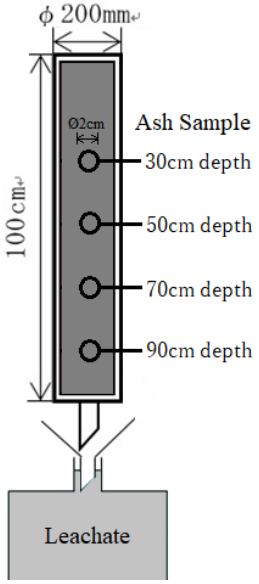

Fig. 1. Column sketch of Lysimeter

Sample Collection

For ash collection, 2cm hole was drilled on 4 collection points, at the depth of 90cm, 70cm, 50cm, and 30cm. (Fig. 1) 80g of ashes were collected from every point. 30g of ash samples were oven dried at 105 °C for 24h to remove moisture for XRF. To prepare for JLT-13, 500mL of super pure water were mixed with 50g ash sample to achieve a liquid to solid (L/S) ratio of 10, and shaken horizontally for 6h at 200 oscillations per minute. The samples were then filtered through a glass-fiber filter, followed by separating 50mL of the filtered sample for analyzing. For column experiment, 500mL of leachate samples were collected from all ten columns. Similarly, the leachate was filtered through a glass-fiber filter and 50mL were separated for analyzing.

Sample Preparation

For XRF test, 10g of oven-dried ash samples were further heated at 600 °C for 2h to calculate the Loss on Ignition (LOI). For column experiment and leaching test, 5mL of 61% nitric acid (HNO_3) was added to the 50mL of filtered sample prepared in a conical flask, which was left to evaporate until 10mL of solution remains using the HPR-4030 hot plate that was pre-heated to 150°C. Another 5mL of 61% HNO_3 was subsequently added to the 10mL solution. Glass lids were placed onto every conical flask before evaporating the solution again until 5mL remains. The 5mL solution was diluted with 1% HNO_3 in a 50mL volumetric flask.

Analytical Method

The chemical composition of MSWI fly ash were determined by using XRF spectrometer (Rigaku RIX3100). 4g of oven-dried ash samples were formed into pressed pellets by pulverization with a 4:1 ash sample to binder ratio.

The concentration of heavy metals leached were determined by using Inductively Coupled Plasma Optical Emission Spectroscopy (720 ICP-OES). The prepared samples were tested against standard solutions of 0.005 mg/L, 0.01mg/L, 0.02 mg/L, 0.05 mg/L, 0.1 mg/L, 0.5 mg/L, and 1 mg/L.

3. RESULTS AND DISCUSSION

Bulk Chemical Composition Analysis

XRF was conducted to determine the constituents present in the ash samples. According to Table 2, the MSWI ash samples comprises mainly of SiO_2, Al_2O_3, Fe_2O_3, and CaO. Interestingly, samples with consisting of only pure FA: FA (U), FA (C), and FA (P) have higher CaO weight percentage (wt%) than that of SiO_2. Inversely, samples with BA have higher SiO_2 content.

These three trace constituents - Pb, Cu, and Zn particularly displayed significant concentrations. Cd and Cr have a smaller ppm in comparison, but as both Cd and Cr are considered harmful heavy metals, these five trace constituents are selected for this study.

Generally, the amount of insoluble Pb, Cd and Zn present in the 10 samples decreased in year 2000 from year 1996 as shown in Table 3. Contrastingly, apart from BAFA CG ash mix samples, the amount of insoluble Cr increases. Chelate treatment causes the amount of Cu to decrease, whereas phosphate treatment results in Cu to increase. The amount of trace constituent in 2022 has a random pattern when compared to previous results. Some increased drastically, while some showed very little changes. When the two research were merged, only a small fraction of ash were randomly extracted from 8m height by 1m diameter model column and stored in the current column of 1m height by 0.2m diameter. The huge reduction in amount of non-homogeneous ash samples transferred may have resulted in the inconsistent results.

Table 2. Bulk Compositional Analysis (XRF)

Sample Name			BAFA CG (U)	BAFA CG (C)	BAFA CG (P)	BA (U)	FA (U)	BAFA (U)	SMS	PMS	FA (C)	FA (P)
Major Constituent (mass%)	SiO2	[%]	25.5	33.9	34.5	29.3	18.7	25.9	33.8	40.2	20.6	11.7
	Al2O3		16.2	16.4	16.3	18.6	8.8	17.4	17.7	19.4	10.1	6.5
	Fe2O3		7.6	7.7	7.8	17.4	2.1	15.1	11.4	3.6	2.3	1.7
	CaO		23.3	20.9	20.9	19.5	38.0	24.7	26.5	30.3	40.0	33.6
	Sub Total		72.5	78.9	79.6	84.8	67.7	83.1	89.4	93.6	73.0	53.5
Minor Constituent (mass%)	TiO2	[%]	1.26	1.26	1.24	1.47	0.79	1.18	1.24	1.34	0.88	0.61
	MnO		0.11	0.10	0.12	0.21	0.07	0.17	0.17	0.17	0.07	0.06
	P2O5		2.59	2.86	3.74	1.97	0.72	1.49	2.66	0.16	0.80	25.1
	MgO		2.86	2.79	2.79	2.50	2.17	2.47	2.69	2.56	2.47	1.08
	Na2O		1.30	1.43	1.60	1.09	0.67	0.90	1.85	0.67	0.70	4.54
	K2O		0.52	0.56	0.58	0.37	0.02	0.27	0.48	0.11	0.05	0.23
	Cl		0.13	0.14	0.11	0.08	0.13	0.10	0.24	0.44	0.12	0.70
	S		0.05	0.05	0.05	0.10	1.49	0.14	0.04	0.39	1.13	0.47
	F		0.03	0.03	0.03	0.01	0.19	0.09	0.00	0.03	0.24	0.21
	Sub Total		8.84	9.22	10.26	7.80	6.25	6.81	9.37	5.87	6.45	32.95
Trace Constituent (ppm)	Zn	[ppm]	5865	5034	5497	4511	16188	7444	4650	496	16776	5907
	Cu		2388	2536	1847	3507	822	2342	1341	207	831	650
	Pb		3865	4871	4364	1729	2414	2826	715	49	4130	1941
	Cr		243	228	231	782	304	601	1182	715	294	215
	Ni		103	106	97	311	83	188	162	26	81	77
	Ba		851	791	756	1235	339	1014	1100	1460	468	362
	Sb		0	0	0	106	0	0	0	0	0	1
	Sn		139	157	162	305	289	235	101	49	317	227
	Sr		359	316	324	292	59	251	392	502	93	134
	As		26	33	29	12	16	19	5	0	28	13
	V		3	3	3	4	2	3	4	3	2	2
	Cd		107	102	102	98	174	120	95	79	199	105
	Co		7	6	6	3	1	3	7	13	2	3
	Sub Total	[%]	1.40	1.42	1.34	1.29	2.07	1.50	0.98	0.36	2.32	0.96
	LOI (%)		9.8	10.4	8.9	6.1	24.0	8.5	0.3	0.2	18.3	12.6
	Total	[%]	82.75	89.58	91.15	93.93	75.97	91.47	99.75	99.85	81.73	87.45

Table 3. Comparison of Chemical Composition in Ash Samples in Year 1995/1996, 2000, and 2022 (XRF)

No.	Sample	Trace Constituents																					
		Pb (mg/kg)						Cd (mg/kg)						Cr (mg/kg)						Zn (mg/L)						Cu (mg/L)					
1	BAFA CG (U)	1995	2640	2000	2123	2022	3865	1995	25	2000	27.5	2022	107	1995	40	2000	25.0	2022	243	1995	2835	2000	3570	2022	5865	1995	1455	2000	1640	2022	2388
2	BAFA CG (C)		2435		2358		4871		10		25.0		102		40		27.5		228		3030		448		5034		1515		578		2536
3	BAFA CG (P)		2695		2293		4364		25		27.5		102		40		17.5		231		2855		558		5497		1475		1503		1847
4	BA (U)	1996	3100	2000	1750	2022	1729	1996	20	2000	4.7	2022	98	1996	810	2000	1300	2022	782	1996	6000	2000	2950	2022	4511	1996	2300	2000	2500	2022	3507
5	FA (U)		3300		2550		2414		190		110.0		174		270		255		304		17000		10850		16188		650		570		822
6	BAFA (U)		4700		2400		2826		45		26.5		120		680		855		601		6800		4600		7444		4000		3600		2342
7	SMS		610		545		715		9.9		0.2		95		890		1100		1182		4800		4000		4650		2600		1550		1341
8	PMS		210		60		49		0.2		0.2		79		430		515		715		410		320		496		130		245		207
9	FA (C)		2800		2850		4130		180		125.0		199		250		265		294		17000		10800		16776		600		595		831
10	FA (P)		3300		2200		1941		160		125.0		105		210		290		215		14000		7450		5907		470		635		650

Behavior of FA Leachate from Column Experiment

In a simulated environment where the ashes are exposed to natural rainfall, leachate was collected every month for the first 5 years, then annually for the following 22 years. The most common pattern seen in all the graphs below, from Fig. 2 to Fig 5, is that by year 2005, all heavy metals discussed have concentrations of less than 0.5mg/L. Furthermore, leached harmful heavy metals Pb, Cd, and Cr were already below detection limit by year 2000, hence the consistent overlapping of data points is visible on the graphs from 7 years onwards.

Fig 2a. shows that Pb leached out of BA (U) decreased gradually throughout the 27 years from 0.2mg/L to 0.01mg/L. Initially (Year 1995), 3300mg/L of Pb was leached out of FA (U), which decreased to 1800mg/L in the 2nd year. The concentration of Pb gradually

decreased from then on for the next 4.5 years, before arriving at a constant value of 0.01mg/L up until year 2022 due to the limitations of ICP-OES equipment. As for BAFA (U), the amount of Pb leached was between BA (U) and FA (U) at 1100mg/L in the beginning, before reducing to 0.05mg/L in less than 3 years, which is quicker than FA, as anticipated. As for Cd (Fig. 2b), the samples with raw FA have more leached Cd in comparison to samples without FA. The Cr results from the column experiment shows that only FA (U) had high amount of Cr leached in 1st year at 4mg/L. (Fig. 2c) All the other samples showed very low leached Cr values. (Fig 3c; 4c; 5c)

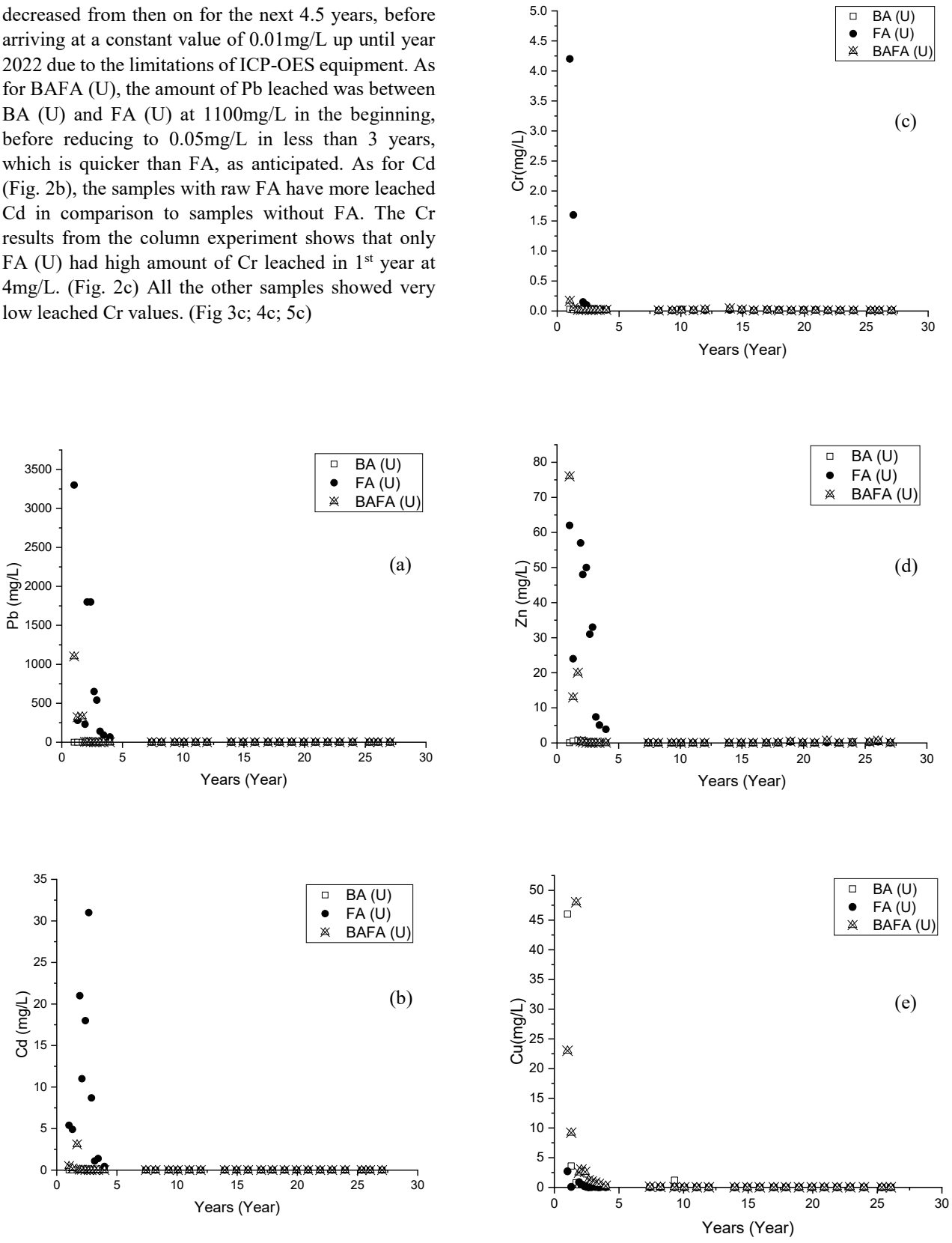

Fig 2. Leached heavy metals for untreated raw BA and FA: (a) Pb; (b) Cd; (c) Cr; (d) Zn; (e) Cu

The leached Pb in BAFA CG mixed ash samples (Fig. 3a) had a peak value of 0.69mg/L, 0.45mg/L, and 0.43mg/L for sample 1 to 3 respectively. As for Cd, there was very little Cd detection throughout 27 years for BAFA CG (U). The leached Pb meets standard landfill criterion of 0.3mg/L in less than a year. [7] Contrastingly, in Fig. 3b, Cd detection was initially low in the first quarter of the 1st year for BAFA CG (C) and BAFACG (P), but the leached Cd spiked to 0.33mg/L and 0.4mg/L respectively before decreasing to less than 0.1mg/L, which remained unchanged until today. This particular ash mix has a larger proportion of BA compared to FA. According to the leached Pb and Cd results (Fig. 2a and 2b), BA has significantly lower leached Pb and Cd value. Thus, the ash mix ratio affects leached concentration of Pb and Cd.

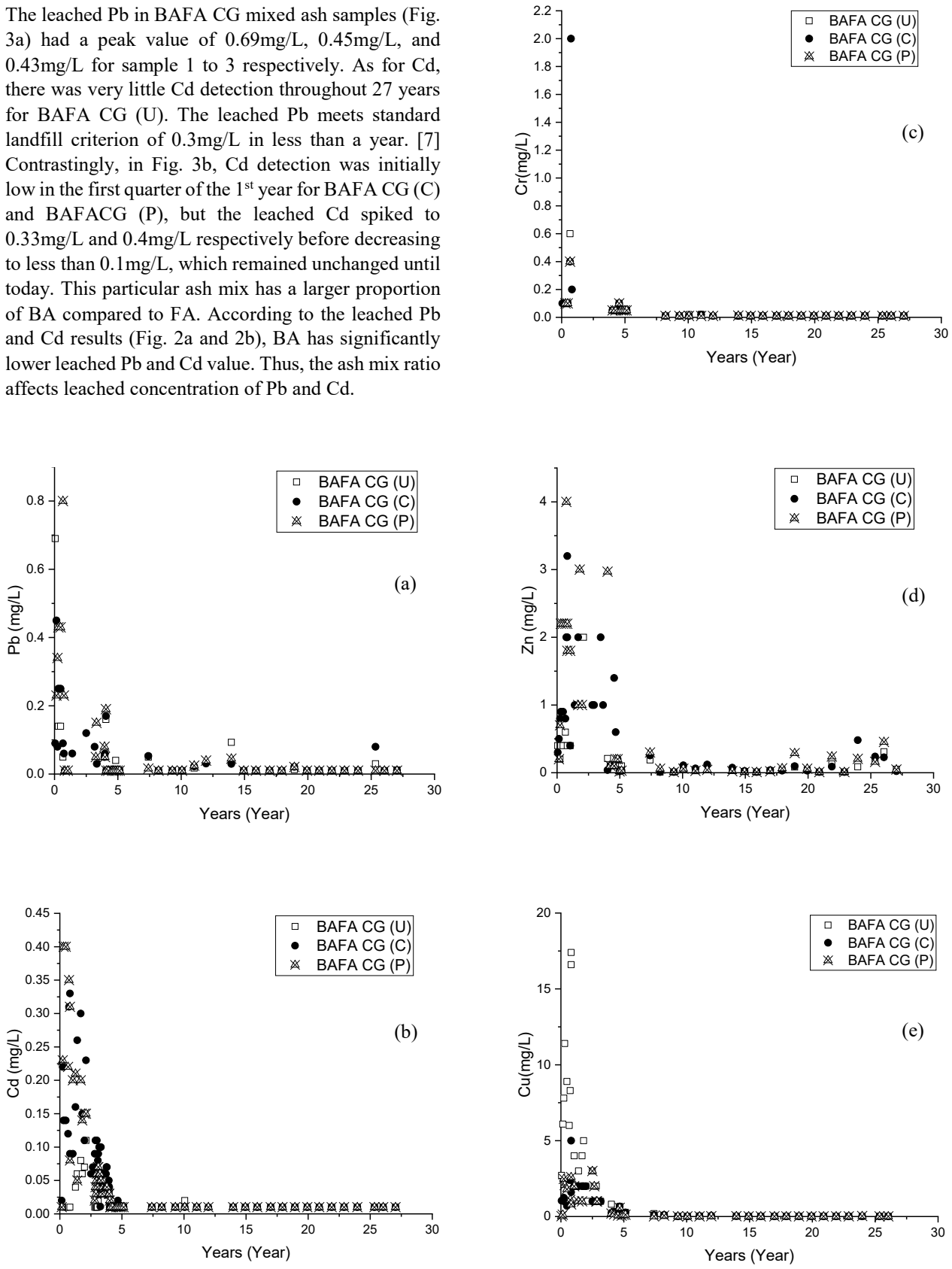

Fig 3. Leached heavy metals for BAFA CG ash mix: (a) Pb; (b) Cd; (c) Cr; (d) Zn; (e) Cu

The samples with slag treatment in this study consists of BA and FA mix. Both SMS and PMS displayed stable and safe amount of leached heavy metals (Pb, Cd, Cr, Zn, and Cu) throughout the 27 years. Most of the leached heavy metals are below detectable limit and does not exceed the concentration of 0.09mg/L as shown in the graphs in Figure 4.

According to the results from column experiment in Figure 4 and leaching test in Table 4, slag treated MSWI FA and BA should be classified as general non-hazardous waste, that meets the effluent standards. In view of the fact that MSWI FA and BA slag will not cause pollution due to the leaching of heavy metals, it is possible to reuse MSWI FA and BA.

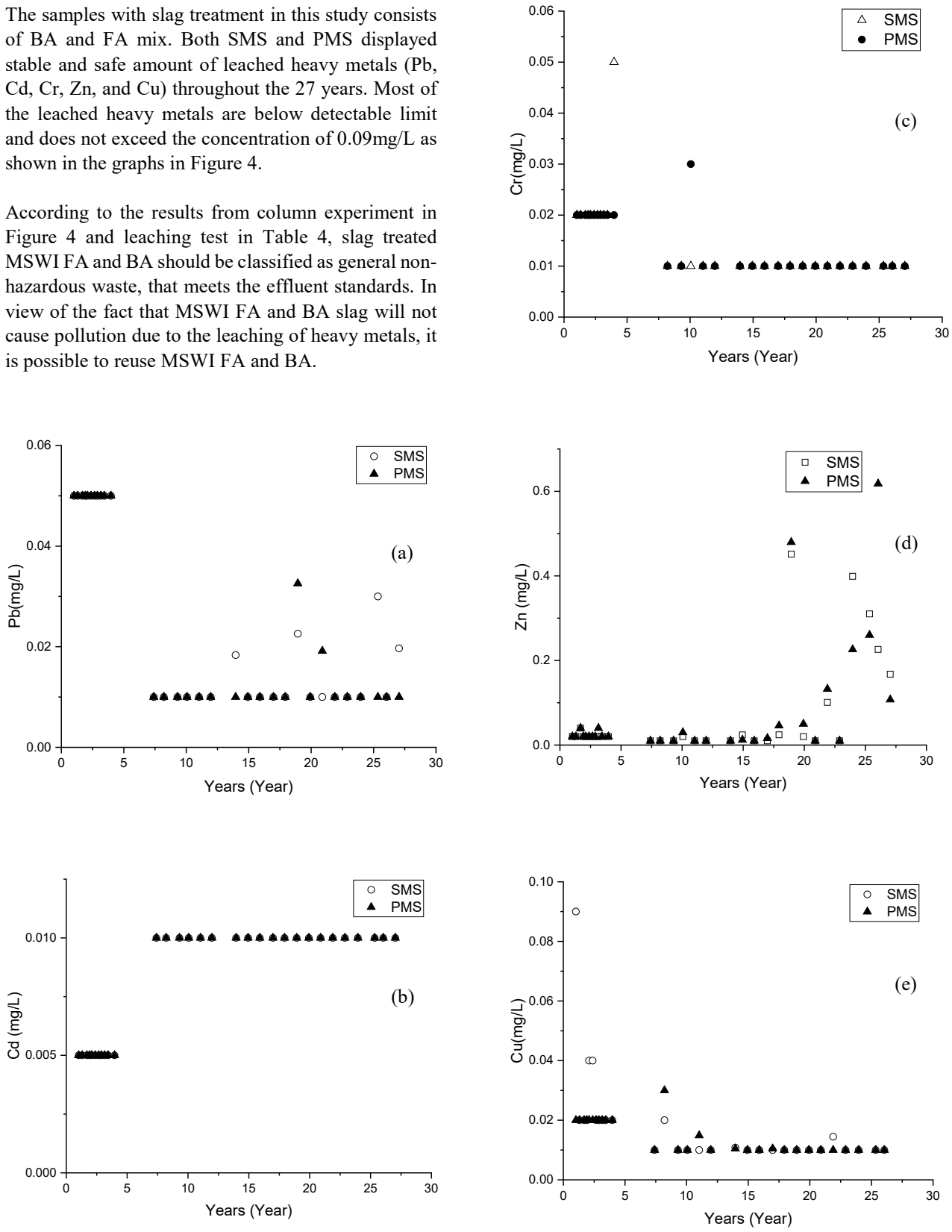

Fig 4. Leached heavy metals for slag treated FA and BA: (a) Pb; (b) Cd; (c) Cr; (d) Zn; (e) Cu

Phosphate stabilization is very effective at reducing the leachability of heavy metals, particularly on Pb, over the entire pH range in comparison to chelate treatment. [1] This is supported by the results in Fig. 5a. FA (P) had a significantly larger leached amount of Pb as compared to chelate treated FA (C) at peak value of 6600mg/L and 110mg/L respectively. However, FA (P) stabilized in approximately 3.5 years, twice the speed of FA (C) which stabilized in 7 years. Similarly for FA (P) on Cd (Fig. 5b), the concentration leached was very high in comparison with FA (C) at 210mg/L, and also stabilized in 3.5 years. Contrastingly, the leached Cd in FA (C) fluctuated between 0.1mg/L 0.3mg/L for 4 years before arriving at a constant value of 0.01mg/L. However, even though phosphate stabilization is a quicker method, chelate treatment displayed a significantly lower leached amount of Pb and Cd and is more consistent and gradual method in comparison.

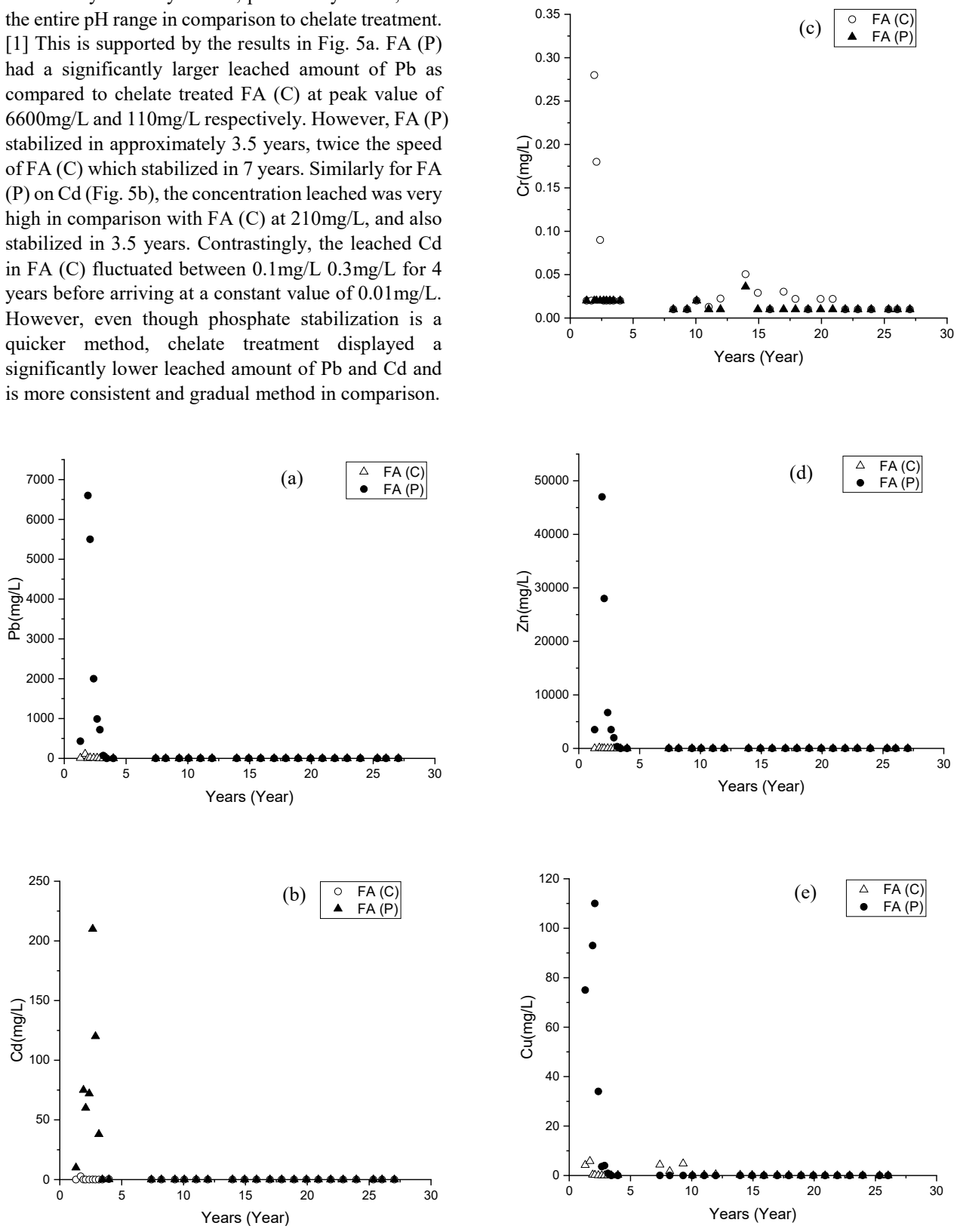

Fig 5. Leached heavy metals for treated FA: (a) Pb; (b) Cd; (c) Cr; (d) Zn; (e) Cu

Leaching Behavior of BA and FA (Leaching Test)

JLT-13 conducted three times: year 1995 for sample 1 to 3, year 1996 for sample 4 to 10, year 2000 and year 2022, as shown on Table 4. The BAFA CG (U), BAFA CG (C), BAFA CG (P), and FA (C) exhibits the trend of increased leached Pb in year 2000 before decreasing to meet the landfill disposal criteria of 0.3mg/L. [7] The increase in amount of leached Pb may be caused by the non-homogeneous ash sample. Contrastingly, BA (U), FA (U), BAFA (U), and FA (P) showed decrement in leached Pb throughout the three tests.

Slag is the only treatment method that displayed stable, safe and consistent amount of leached heavy metals for both leaching tests. Almost all of the leached Cd are below detection limit. BAFA CG (U), BAFA CG (C), BAFA CG (P) has the same amount of leached Cr in year 1995 and 2000, followed by a below detection limit value in year 2022. Thus, as mentioned in the discussion for the leaching behavior of heavy metals from the leachate, slag treated MSWI FA and BA is safe for reuse.

In year 1996, BA (U), FA (U), BAFA (U), and BAFA CG (P) initially leached relatively high concentration of Cu at 1.50mg/L, 0.26mg/L, 1.50mg/L and 0.40mg/L respectively. These four samples exhibit a decrement trend over time. BAFA CG (U) and BAFA CG (C) on the other hand has an increased in leached Cu in year 2000, while SMS, PMS, FA (C), and FA (P) exhibited

Table 4. Leached Heavy Metals from Leaching Test (JLT-13):
(a) Harmful Heavy Metals (b) Not Harmful Heavy Metals

(a)

No.	Sample	Heavy Metals															
		Pb (mg/L)						Cd (mg/L)						Cr (mg/L)			
1	BAFA CG (U)	1995	0.06	2000	0.07	2022	0.04	1995	>0.01	2000	0.01	2022	>0.01	1995	0.20	2000	0.20	2022	>0.01
2	BAFA CG (C)		0.05		0.49		0.04		>0.01		>0.01		>0.01		0.20		0.20		>0.01
3	BAFA CG (P)		0.05		0.37		0.02		>0.01		0.02		>0.01		0.20		0.20		>0.01
4	BA (U)	1996	0.36		0.05		>0.01	1996	>0.01		>0.01		>0.01	1996	0.02		>0.02		>0.01
5	FA (U)		95		23.5		0.02		>0.01		>0.01		>0.01		0.03		0.02		0.02
6	BAFA (U)		6.6		0.05		0.01		>0.01		>0.01		>0.01		0.02		>0.02		>0.01
7	SMS		>0.05		>0.05		0.02		>0.01		>0.01		>0.01		0.02		>0.02		>0.01
8	PMS		>0.05		>0.05		0.01		>0.01		>0.01		>0.01		0.02		>0.02		>0.01
9	FA (C)		0.09		0.16		0.01		>0.01		>0.01		>0.01		0.02		>0.02		>0.01
10	FA (P)		0.05		>0.05		0.01		>0.01		>0.01		>0.01		0.02		>0.02		>0.01

(b)

No.	Sample	Heavy Metals															
		Zn (mg/L)									Cu (mg/L)						
1	BAFA CG (U)	1995	0.10	2000	0.28	2022	0.05	1995	0.53	2000	0.64	2022	0.03				
2	BAFA CG (C)		0.10		0.25		0.05		0.10		0.18		0.02				
3	BAFA CG (P)		0.10		0.34		0.05		0.40		0.17		0.02				
4	BA (U)	1996	0.05		0.02		0.03	1996	1.50		0.06		0.02				
5	FA (U)		9.80		1.11		0.04		0.26		0.02		0.01				
6	BAFA (U)		2.20		0.02		0.03		1.50		0.28		0.01				
7	SMS		0.02		0.02		0.06		0.02		0.02		0.04				
8	PMS		0.17		0.03		0.04		0.17		0.02		0.01				
9	FA (C)		0.02		0.58		0.05		0.02		0.02		0.03				
10	FA (P)		0.02		6.03		0.03		0.02		0.02		0.01				

Table 5. Comparison between In-House Laboratory and External Laboratory Test

Sample		BAFA CG (U)	BAFA CG (C)	BAFA CG (P)	BA (U)	FA (U)	BAFA (U)	SMS	PMS	FA (C)	FA (P)
pH	In-House Laboratory	8.0	8.0	8.2	8.7	11.7	8.9	8.2	8.1	10.1	8.5
	External Laboratory	8.9	8.8	9.0	9.2	11.8	9.0	8.6	8.2	9.6	8.5
Zn	In-House Laboratory	0.06	0.05	0.03	0.03	0.06	0.04	0.05	0.05	0.03	0.03
	External Laboratory	0.025	0.022	0.006	0.005	0.005	0.005	0.039	0.014	0.007	0.005

low leached Cu values. As time elapsed, the leached Cu results of all ten samples gradually shifted towards a low and stabilized range of 0.01mg/L and 0.04mg/L.

To ensure the accuracy of the leaching test results. A set of ash samples were sent to an external laboratory to conduct the same test. After data comparison, all the heavy metals have very similar values except for Zn. A comparison of the pH value and Zn for all ten samples are shown in Table 5.

Fig. 6 is a simulation of the relationship between Zn and pH plotted using data from column experiment on Visual Minteq. In the recent 10 years, the leached Zn from column experiment for all samples have been fluctuating between below detection limit and 1.2mg/L. These irregular fluctuation patterns can be explained by Fig 6. The leached Zn corresponds to the pH value of the sample. These samples have the pH value between 8.0 and 9.0, which is the range where a slight change in pH value will result in a large difference in the amount of Zn leached.

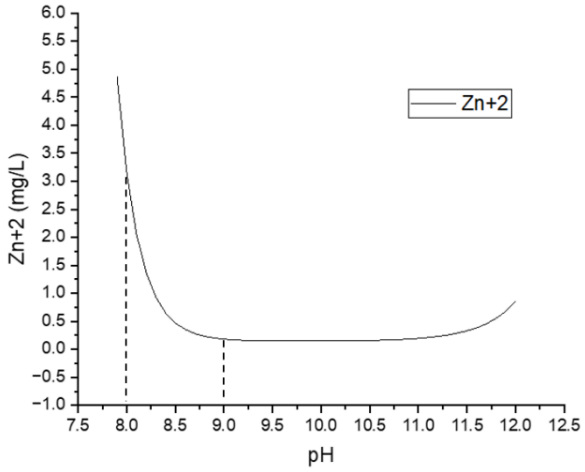

Fig 6. Relationship between Zn and pH

Overall, all heavy metals discussed in the ten samples have either very low leached value or value below the detection limit. Therefore, along with the results from column experiment, it can be concluded that the heavy metals in these ten samples have stabilized.

4. CONCLUSION

In conclusion, leached Pb and Cd from the leaching test fell way below the Japanese regulatory criteria for landfilling of 0.3mg/L. After 27 years, it is safe to say that the heavy metals in all ten samples are stabilized. Among all the heavy metals tested, the value of leached Zn is heavily dependent on the pH of the ash sample. Among the three treatment methods, slag treatment stabilized the harmful heavy metal the quickest and is the most consistent throughout the 27 years. Phosphoric acid treated FA stabilizes water-leachable Pb and Cd in approximately 3.5 years, which is almost twice as fast in comparison to chelate treated FA that took 7 years. Even though phosphate stabilization is a quicker method, chelate treatment displayed a significantly lower leached amount of Pb and Cd and is a more consistent and gradual method.

References

[1] S.-Y. Kim, T. Matsuto and N. Tanaka, "Evaluation of pre-treatment methods for landfill disposal of residues from municipal solid waste incineration," *Waste Management and Research,* vol. 21(5), pp. 416-423, 2003.

[2] Ministry of the Environment, Government of Japan, "Municipal Solid Waste Generation and Disposal in FY2020," March 2022. [Online]. Available: https://www.env.go.jp/en/headline/2595.html.

[3] Y. Lu, A. Tian, J. Zhang, Y. Ang, P. Shi, Q. Tang and Y. Huang, "Physical and Chemical Properties, Pretreatment, and Recycling of Municipal Solid Waste Incineration Fly Ash and Bottom Ash for Highway Engineering: A Literature Review," *Hindawi,* vol. 2020, p. 17, 2020.

[4] S.-i. Sakai, "Municipal Solid Waste Management in Japan," *Waste Management,* Vols. 16(5-6), pp. 395-405, 1996.

[5] M. Hirokawa and S. Fukuda, "Behavior of Chemically Treated Fly Ash in Mountainous Landfills (in Japanese)," Fukuoka, 2000.

[6] M. Tanaka, T. Naganuma and M. Uchikawa, "Study on Leaching Characteristics of Heavy Metals from Landfilled Treated Fly Ash," Fukuoka University, Fukuoka, 2000.

[7] M. Ksibi, A. Ghorbal, S. Chakraborty, H. I. Chaminé, U. Förstner, W. H. Rulkens and W.

Salomons, Recent Advances in Environmental Science from the Euro-Mediterranean and Surrounding Regions (2nd Edition), Tunisia: Springer, 2019.

[8] E. P. S. Environment Canada, "Compendium of waste leaching tests," Wastewater Technology Centre, Canada, 1990.

[9] M. K. Tiwari, S. Bajpai, U. Dewangan and R. K. Tamrakar, "Suitability of Leaching Test Methods for Fly Ash and Slag: A Review," *Journal of Radiation Research and Applied Sciences,* pp. 1-15, 2015.

Effect of Heavy Metals on Cement Solidification of Municipal Solid Waste Incineration Residues

Kazuki Nakamura[1], Teppei Komiya[2], Takayuki Shimaoka[2], Takahiro Aoki[3], Hiroyuki Akita[3], Isamu Sandanbata[3] and Fuminori Hirosue[3]
1 Department of Civil Engineering, Graduate School of Engineering, Kyushu University
(E-mail: nakamura-k@doc.kyushu-u.ac.jp, TEL: Phone: +81-92-802-3431)
2 Faculty of Engineering, Kyushu University
3 Hazama Ando corporation

1. INTRODUCTION

In light of the current situation in Japan, incineration residue (bottom ash and fly ash) accounts for about 80% of the landfill waste at final disposal sites for general waste[1)]. Therefore, the authors aim to establish a "waste solidification disposal system[2)]" that reduces landfill capacity consumption, improves environmental safety, and stabilizes landfill sites quickly while taking advantage of the characteristics of incineration residues. Specifically, this reclamation method applies coal ash solidification technology[3)] and mixes incineration residue with cement and water, then compresses it by applying high-frequency vibration to form a solidified ground. During the study, it was confirmed that incineration residue causes differences in the strength development of cement-mixed solidified products[4)] (hereafter referred to as "solidified incineration residues"). Reclaimed ground with delayed strength development in solidified landfills creates reclamation construction management problems, such as avoiding heavy equipment travel over these areas. The reason for this was thought to be the high heavy metal content and leaching of the solidified incineration residues. In this study, in order to clarify the effect of heavy metals on the strength development of solidified incineration residues, we added heavy metals to solidified mixture samples and conducted strength tests and physical property analysis of specimens prepared by varying the amount of heavy metal addition. Then, we determined the relationship between uniaxial compressive strength and the concentration of eluted heavy metals.

2. SAMPLES AND METHODS

2-1 Samples

The samples were bottom ash and fly ash collected from the R incineration plant in F City. The bottom ash (wet ash), from which coarse grains were removed (hereafter referred to as incineration ash), and the fly ash, from which chelated fly ash (hereafter referred to as fly ash).

2-2 Selection of heavy metals to be added

We selected three heavy metals (copper, lead, and zinc) with the highest percentage in the incineration residues and the highest retarding effect on cement solidification[5), 6)]. A solution of chloride compounds of the three heavy metals was added because lead and zinc are particularly chloride-rich in fly ash[7)].

Table 1. Moisture content and properties of incineration residue

Samples	Water content ratio		Remarks
	Bottom ash	Fly ash	
FR	27.4	19.9	Incinerator ash is from the bottom of a 40 mm sieve

2-3 Preparation of solidified incineration residues

Each incineration residue solidified product material was prepared under the conditions shown in Table 2. Incineration ash and fly ash were mixed at a dry mass ratio of 3:1 (hereafter referred to as "incineration residue"). Blast furnace cement Type B was added to the incineration residue at a dry mass ratio of 10%. Tap water in which each heavy metal was dissolved was added so that the water content ratio was 27%. The target elution concentrations were determined based on the general effluent standard values (Copper: 3.0 mg/L, Lead: 0.1 mg/L, Zinc: 5.0 mg/L) specified in the Japanese Water Pollution Control Law. The amount of each heavy metal added was calculated from these values. Each heavy metal was added to the sample as an aqueous solution of a chloride compound for uniform addition. After kneading, the mixture was placed in a cylindrical formwork with an inner diameter of 10 cm and a height of 20 cm, vibrated, and compacted for 150 seconds at a vibration frequency of 75Hz and an amplitude of approximately 0.5 mm using a small table vibrator (TV500 x 500 manufactured by Exen). The mold was then sealed and cured indoors (10–18 °C) for 28 days. After that, they were demolded and subjected to uniaxial compression tests.

Table 2. Kneading conditions for each incineration residue solidifier

Samples	Bottom ash (wet) [kg]	Fly ash (wet) [kg]	cement [kg]	water [kg]	added heavy metals	Measured elution concentration [mg/L]			Measured elution concentration [mg/L]		
						Cu	Pb	Zn	Cu	Pb	Zn
A-1	19.1	6.00	2.22	1.17	-	-	-	-	-	-	-
A-2					Cu	1.00	-	-	0.273	-	-
A-3						2.00	-	-	0.556	-	-
A-4						3.00	-	-	0.820	-	-
B-1					Pb	-	0.03	-	-	0.683	-
B-2						-	0.07	-	-	1.376	-
B-3						-	0.10	-	-	2.059	-
C-1					Zn	-	-	1.67	-	-	0.014
C-2						-	-	3.33	-	-	0.027
C-3						-	-	5.00	-	-	0.041

3. RESULTS AND DISCUSSION

3-1 Relationship between uniaxial compressive strength of solidified incineration residues and heavy metal leaching concentration of incineration residue

Figure 1 shows the relationship between uniaxial compressive strength (7, 28, and 91 days of age) and heavy metal leaching concentrations of copper, lead, and zinc in solidified incineration residue. The uniaxial compressive strength was measured for three specimens under each condition, and the maximum, minimum, and average values are shown in Figure 1. For the 7-day intensity, no change in intensity was observed with changes in the elution concentrations of the three heavy metals. For the 28-day-old specimens, the strength of copper decreased as the leaching concentration increased. On the other hand, the decrease in strength for lead and zinc was slightly above the certain leaching concentration, and the strength can be considered almost constant. As for the 91-day strength, it was confirmed that the rate of decrease in strength with heavy metal addition was lower than that of the 7-day and 28-day strengths.

3-2 Relationship between uniaxial compressive strength of solidified incineration residue and heavy metal content of incineration residue

Figure 2 shows the relationship between uniaxial compressive strength (7, 28, and 91 days of age) and copper, lead, and zinc content in solidified incineration residue. No significant strength changes were observed for the 7-day-old specimens with increasing heavy metal content. For the 28-day-old specimens, the strength of copper decreased with increasing content. On the other hand, the decrease in strength for lead and zinc is insignificant when the content exceeds a certain value, and the strength can be considered almost constant. The difference in the strength of the 91-day-old specimens was smaller than that of the 28-day-old specimens, suggesting that the effect of inhibition of strength development was smaller. The relationship between the heavy metal content in the incineration residue and the uniaxial compressive strength of the specimens was similar to the relationship between the heavy metal leaching concentration in the incineration residue and the uniaxial compressive strength.

3-3 Time Dependence of Uniaxial Compressive Strength of Incineration Residue Solidified with Heavy Metals

Figures 1 and 2 show that the strength of each specimen had the highest loss at 28 days of age, with a lower rate of strength loss at 91 days of age. Therefore, Figure 3 summarizes the time variation of the uniaxial compressive strength of solidified incineration residue with the addition of heavy metals and the time required to reach the target strength for developing solidification-type disposal systems (5 N/mm^2). A significant decrease in strength with increasing addition was observed for the copper-added solidified products at 28 days of age. When zinc was added, the strength decreased in small amounts for solidified products. The decrease in strength with the increasing amount of heavy metal additions was the decrease in strength with increasing heavy metal additions. For the solidified product with lead added, a decrease in strength was observed at small amounts, but no significant decrease in strength was observed with increasing amounts of the heavy metal added. However, no significant decrease in strength was observed with increasing the amount of heavy metal. The strength loss rate of the specimens with the three heavy metals was the largest at 28 days, while the strength loss rate was the smallest at 91 days. The strength loss rate of the specimens with the three heavy metals was the largest at 28 days, while the strength loss rate was the smallest at 91 days. In addition, focusing on the time to reach the development target, it became clear that the target

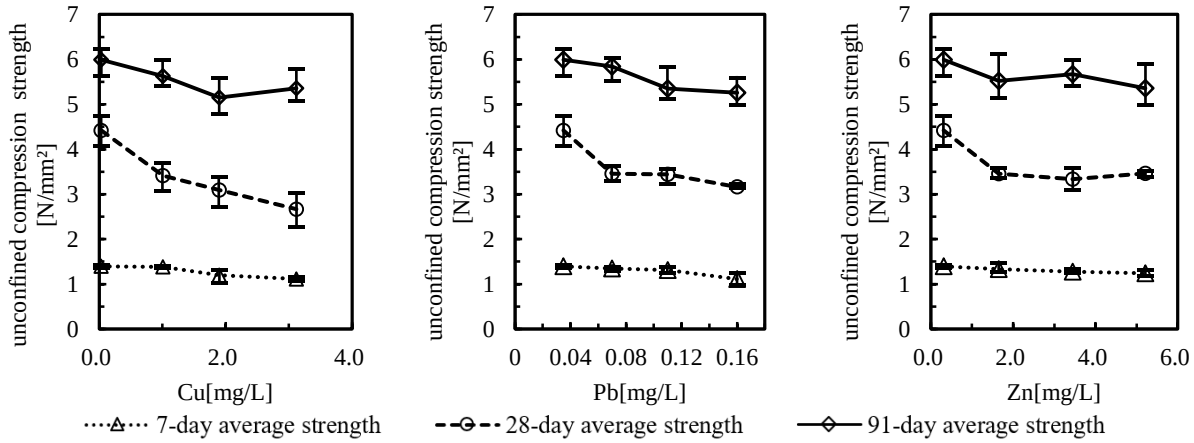

Figure 1. Relationship between heavy metal leaching concentration of incineration residue and uniaxial compressive strength of solidified incineration residue.

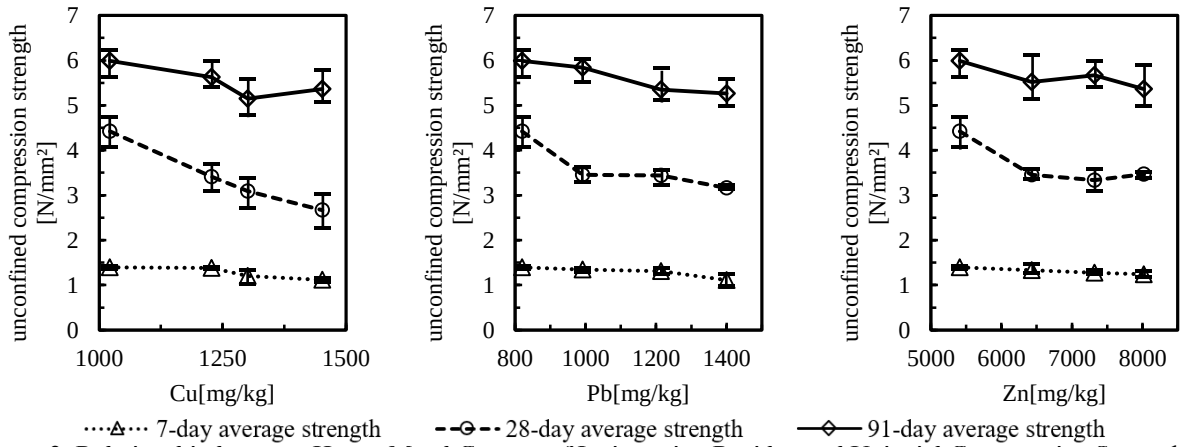

Figure 2. Relationship between Heavy Metal Content of Incineration Residue and Uniaxial Compressive Strength of Solidified Incineration Residue.

strength was fully met, although the cement solidification delay was occurring. The effect of solidification inhibition by heavy metals as a delay in cement solidification significantly affects the initial stage of cement solidification reactions. Simultaneously, it has a negligible impact on long-term strength. As a possible mechanism of inhibition of cement solidification by heavy metals, copper and lead react with hydroxyl ions to form compounds with lower solubility than calcium hydroxide, inhibiting the formation of calcium hydroxide necessary for the reaction in the aluminate phase (C_3A) [8]. It is also known that metal chlorides of Cu and Zn may interact with cement silicates and aluminates to form complex substances that may affect strength development[9]. As for lead, insoluble lead salts form a gelatinous film over the main component of the cement, acting as an anti-diffusion agent against water. This slows the rate of hydration and consequently the rate of curing[10]. In addition, with regard to zinc, it is believed that calcium zincate, which is formed by the reaction of calcium and zinc in cement, forms over C-S-H and causes delayed solidification[11].

4. CONCLUSIONS

For the 7-day-old specimens, no significant change in strength was observed with increasing the amount of the three heavy metals (copper, lead, and zinc). However, for the 28-day-old specimens, the higher the leached concentration of heavy metals in the incineration residue, the lower the strength of the solidified incineration residue. On the other hand, the effect was more negligible for the 91-day-old specimens. The highest rate of strength loss was observed at 28 days for the specimens with the three heavy metals, while the rate of strength loss was lower at 91 days of age. Therefore, the effects of each heavy metal can be summarized as follows. As for copper, a significant decrease in the strength of the solidified product was observed at the 28-day age of the material as the added amount of copper increased. Moreover, the effect of delaying solidification was the most significant. Finally, as for lead, no increase

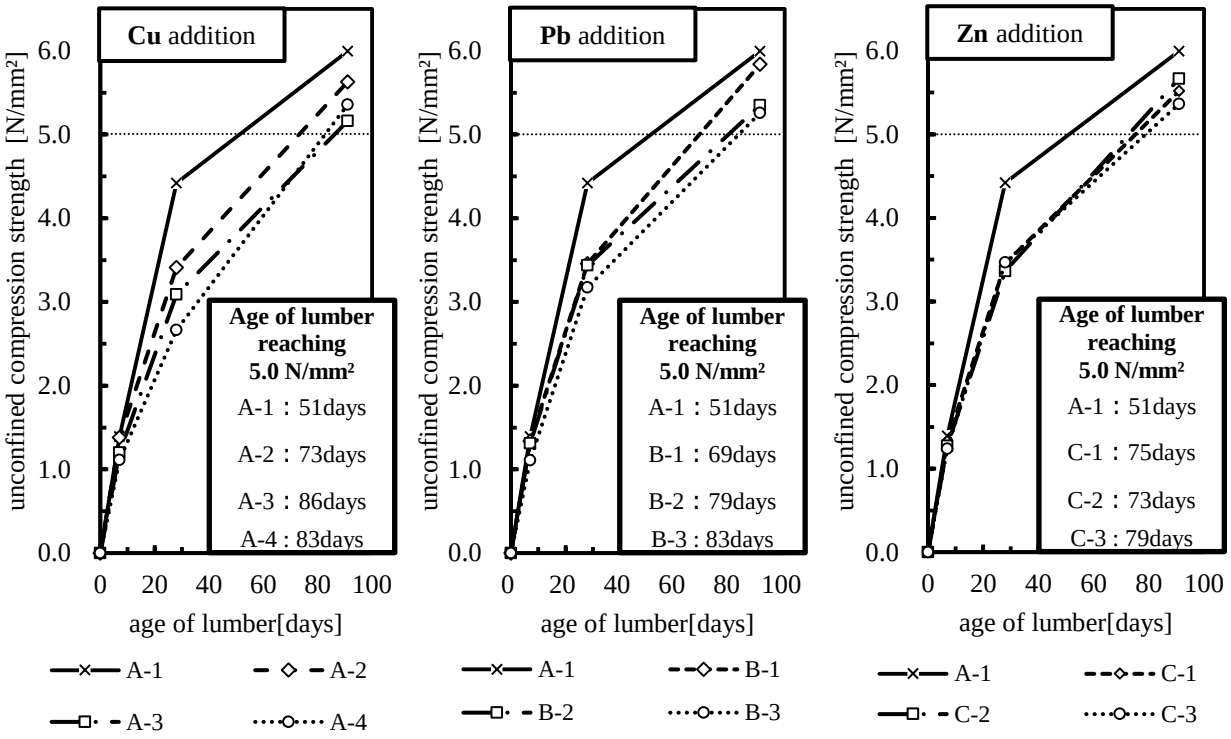

Figure 3. Time Dependence of Uniaxial Compressive Strength of Incineration Residue Solidified with Heavy Metals.

was observed in the retardation effect of solidification with increasing heavy metal additions. However, a decrease in strength was observed with small additions. It became clear that within the range of conditions in this study, the effect of heavy metals on long-term strength is negligible and fully meets the development target (5.0 N/mm²). However, some delay in strength development occurs due to heavy metals.

5. REFERENCES

1) Ministry of the Environment (2022). Results of the Survey on General Waste Disposal in Fiscal Year 2022, https://www.env.go.jp/recycle/waste_tech/ippan/r1/index.html (accessed 2022-06-25)

2)Shimaoka, T (2016). On the development of a solidification-type disposal system for incineration residue, Urban Cleaning, Vol. 69, No. 333, pp. 419-425

3) Hazama Ando Corporation (2016). Development and Deployment of Ashcrete Technology, Ando Hazama Research Annual Report, Vol. 4

4) Nakamura, K. et al. (2021). Fundamental Study on Inhibition of Cementation by Heavy Metals in Cementation of Incineration Residue, Western Branch of JSCE 2021

5) Takahashi, H. et al. (1973). Basic Study on Solidification of Industrial Wastes Containing Heavy Metals with Cement, Onoda Research Report, Vol. 25, No. 3, No. 90, pp. 1-10

6) Cement Association of Japan. Encyclopedia, pp. 62-64

7) Facun Jiao et al (2016). Study on the species of heavy metals in MSW incineration fly ash and their leaching behavior, Fuel Processing Technology, Vol.52, pp.108-115

8) Tashiro, C. and Oba, J. (1980). The effect of $Cu(OH)_2$ on the hydration of C_3A in Proceedings of the seventh international congress on chemistry of cement, 2, 59-63.

9) David Cocke et al (1989). A Model for Lead Retardation of Cement Setting, Vol. 19, No. 1, 156-159

10) N.L. Thomas, D.A. Jameson and D.D. Double (1981). Cem. Conc. Res. 11, 143

11) Hazama Ando Corporation (2021). Causes and Countermeasures for Cement Hardening Failure in Ground Improvement: Negishi et al, Annual Report of Hazama Ando Research Vol. 9

RESEARCH ON DEVELOPMENT OF POWER SOURCE FOR IOT DEVICES USING LANDFILL LEACHATE

Rintaro MURAKAMI[1], Hirofumi NAKAYAMA[2], Takayuki SHIMAOKA[2] and Haruichi KANAYA[3]
1 Dept. of Faculty of Engineering, Kyushu University
West3 room916 744 Motooka, Nishi-ku, Fukuoka City, Japan
2 Dept. of Urban and Environmental Engineering, Faculty Engineering, Kyushu University
West3 room916 744 Motooka, Nishi-ku, Fukuoka City, Japan
3 Dept. of Information Science and Electrical Engineering, Kyushu University
West2 room456 744 Motooka, Nishi-ku, Fukuoka City, Japan

1 INTRODUCTION

In solid waste landfill sites, it is required to monitor landfill waste properties, leachate quality, the composition of gas generated, temperature, and the deterioration and damage of facilities to prevent environmental pollution. It is expected to build an advanced environmental monitoring system by utilizing IoT sensors, whose technological development has been advancing dramatically in recent years. Under such circumstances, securing a power source for wireless communication and installing IoT sensors that do not use a power line has become an urgent issue. Water in landfill waste is highly alkaline and has high electrical conductivity due to the dissolution of soluble salts and alkaline substances in incineration residues in rainwater. Therefore, a battery circuit is formed when metals with different ionization tendencies are immersed in the leachate. Therefore, this study aims to (1) design a garbage battery design that can be buried in landfill waste and (2) create a multilayered prototype for voltage enhancement.

2 METHODS

2.1 GARBAGE BATTERY DESIGN

Figure 1 shows the design of the garbage battery. There are slits in the case, and the leachate seeps into the battery through these slits. The advantages of this structure are (1) the retained water flows through the slits, and the electrolyte circulates, and (2) it prevents the electrodes from coming into direct contact with incineration residues, thereby reducing corrosion. The structure comprises a water holder sandwiched between a positive and negative electrode. The amount of water retained is adjusted according to the material and shape of the water holder. In the case of a pair of positive and negative electrodes, the electromotive force is approximately 1.3V. To make the voltage of the garbage battery reach the operating voltage of the microcontroller (3.3–5V), the positive and negative electrodes are stacked in layers.

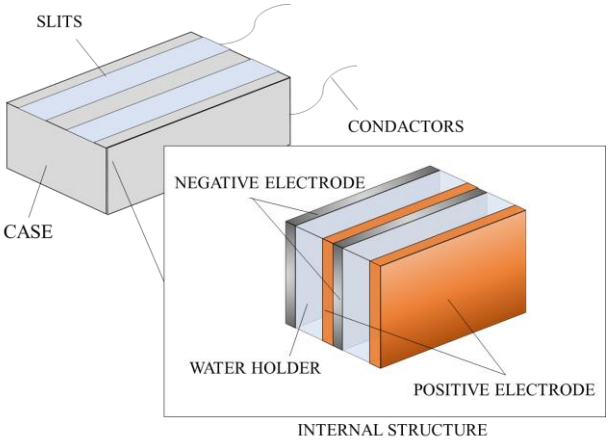

Figure 1. The design and internal structure of the garbage battery case.

2.2 MULTILAYERED PROTOTYPE

This experiment used a copper plate for the positive electrode and a magnesium plate (45 mm × 15 mm × 0.5 mm) for the negative electrode. A mixture of gypsum and diatomaceous earth, with high water absorption and water retention properties, was used as the water holder. The mass ratio of gypsum and diatomaceous earth and the amount of water added were determined based on Hakiri (2019)[1)] and Li et al. (1991)[2)], with the mass ratio of gypsum: diatomaceous earth = 10:3 and the amount of water added being 90% of the solid mass fraction. Diatomaceous earth was mixed with pure water to form a paste, poured into an acrylic case, assembled into a rectangular shape, and hardened in a drying oven at 60 °C for one day. A silicon sealant was used as a shield between the positive and negative electrodes to prevent short circuits. Prototypes with multilayer structures ranging from 2 to 4 layers with 10 mm interelectrode distance were created. Figure 2 shows the prototype of the created garbage battery.

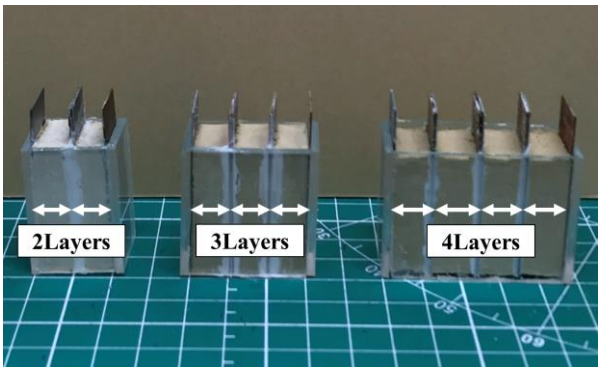

Figure 2. Multilayered prototypes.

2.3 EXPERIMENTAL PROCEDURES

Figure 3 shows the diagram of the experimental apparatus. Leachate from the incineration residue was prepared by eluting the soluble components contained in the incineration residue. Incineration residues (bottom ash: fly ash = 3:1) were sieved using a 4.75-mm sieve in a 250-ml polyethylene container, and pure water was added to bring the liquid-solid ratio to 10. The residue was shaken at 200 rpm for 6 hours using a shaker, and then solid-liquid separation was performed using a centrifuge at 2000 rpm for 20 minutes. A membrane filter with a pore diameter of 0.1 μm was used for filtration, and the resulting filtrate was used as a simulation solution. The metal plates used for the electrodes were polished with water-resistant paper before immersion to account for the effect of voltage drop due to the oxide film. Next, 4 ml of the prepared leachate solution was gently dripped onto the water retention body, and the voltage and current were measured with a digital tester when four different resistors (1 kΩ, 4.7 kΩ, 10 kΩ, and 20 kΩ) were incorporated.

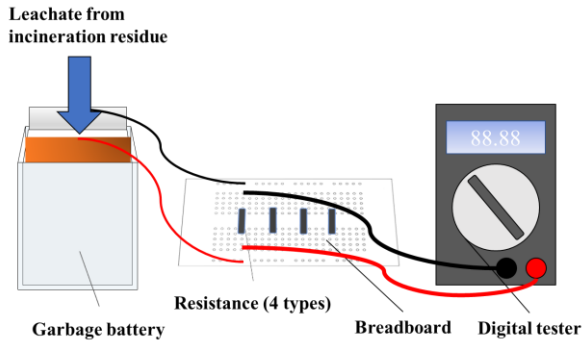

Figure 3. Experimental equipment.

3 RESULTS

Figure 4 shows the relationship between current and voltage for each case. The intercept of the regression line in Figure 4 is E (electromotive force), and the slope is -r (internal resistance). From the voltage V = E − rI, the

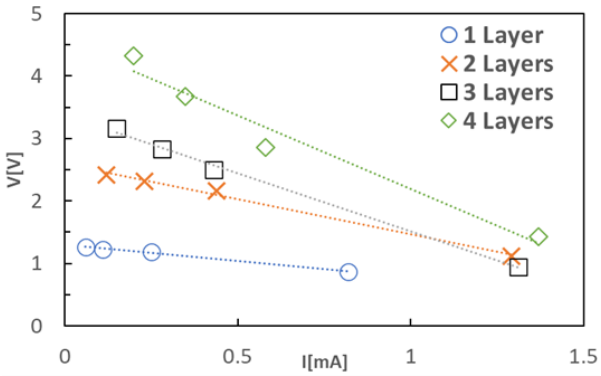

Figure 4. Relationship between voltage and current in a multilayered prototype.

Table 1. Electromotive force, internal resistance, and maximum power for each number of layers

	1 Layer	2 Layers	3 Layers	4 Layers
Electromotive Force[V]	1.29	2.59	3.37	4.55
Internal Resistance[Ω]	510	1,120	1,860	2,350
Maximum Pawer[mW]	0.82	1.50	1.53	2.20

electromotive force and internal resistance were determined. The maximum power $P_{MAX} = E^2 / 4r$ [W] that the power source could supply was obtained from the magnitudes of the electromotive force and internal resistance obtained in the experiment. Table 1 shows the emf, internal resistance, and maximum power for each case. It was observed that the electromotive force and internal resistance increased in proportion to the number of layers. Since the operating voltage of the microcomputer envisioned for IoT monitoring of landfill sites is 3.3 V or higher, we believe that three or more layers can generate sufficient electromotive force to power the microcomputer. It was found that the multilayer structure increased internal resistance, hindering maximum power increase.

4 CONCLUSIONS

In this study, we designed and fabricated a "garbage battery" prototype that can be buried in landfill sites and obtained the following findings:

(1) We designed the housing of a refuse battery and fabricated a prototype using a mixture of gypsum and diatomaceous earth as the water-holding material.

(2) We fabricated a prototype with a multilayer structure that could satisfy the microcomputer operating voltage with three or more layers.

5 REFERENCES

1) Masahide H. et al.: Water absorbent material made from gypsum and diatomaceous earth (2019)

2) Lee et al.: The relationship between the pore characteristics and the suctionability of a Gypsum Mold (1991)

APPLICABILITY OF OPTICAL FIBER SENSOR ON TEMPERATURE DISTRIBUTION ESTIMATION AND LEAKAGE DETECTION OF IMPERMEABLE LINER IN SOLID WASTE LANDFILL

Teppei KOMIYA [1], Rion HAMADA [2], Takayuki SHIMAOKA [1], Michio IMAI [3] and Kazuki OZAWA [3]
1 Faculty of Engineering, Kyushu University, Fukuoka, Japan
2 Department of Civil Engineering, Graduate School of Engineering, Kyushu University, Fukuoka, Japan
3 Kajima Corporation, Tokyo, Japan

1. INTRODUCTION

In Japan, Basic Act on Establishing a Sound Material-Cycle Society has promoted the recycling of waste, and the volume of final waste disposal has been greatly reduced. However, technological and economic constraints inevitably result in the generation of waste that is difficult to recycle. Solid waste landfills will continue to be an indispensable social capital to receive such waste.

11 criteria must be met when decommissioning general waste landfills and industrial waste managed landfills[1]. One of the items listed is that "the interior of the landfill is not abnormally hot compared to the temperature of the surrounding area.

The methods proposed for monitoring the temperature inside the landfill include measuring the temperature inside the gas vent pipe and the temperature of leachate, and measuring the temperature of a pore hole drilled about 1 m deep from the ground surface as a method that is not affected by air temperature[2]. However, all of these temperature measurements were taken at limited points on the landfill site. It is not easy to properly select representative points in a landfill with a large area, huge landfill capacity, and heterogeneous landfill waste. It is desirable to determine the temperature inside the landfill in area and even in three dimensions.

Optical fiber sensors are capable of measuring the distribution of temperature, strain, etc. in the linear direction of an optical fiber by using the optical fiber itself as the measuring section, utilizing the fact that the intensity, frequency, etc. of scattered light incident on the optical fiber varies with the temperature, strain, etc. of the optical fiber[3) 4) 5) 6)].

In the temperature monitoring of landfill sites, it is thought that by wiring optical fibers to the impermeable liner at the boundary between the landfill site and the surrounding ground in a mesh pattern or at regular intervals, the temperature distribution at the boundary of the landfill site can be grasped from an areal perspective, and is expected to contribute to the determination of the abandonment of landfill sites. It is also expected to estimate the three-dimensional temperature distribution inside a landfill by inverse analysis based on the temperature distribution at the bottom and on the slope of the landfill.

Given that temperature distribution can be measured by optical fiber sensors, there is a possibility that leachate leakage due to the breakage of the impermeable liner can be detected as an abnormal temperature distribution by wiring optical fibers under the impermeable liner.

In this study, optical fibers were wired to a model of the slope of a landfill with an impermeable liner, and the reproducibility of the temperature distribution of the impermeable liner and the possibility of detecting water leakage were examined using temperature measurement data from the optical fiber sensor.

2. METHODS

2-1 Optical Fibers and Measuring Instruments

In this study, general-purpose single-mode optical fibers coated with resin were used for optical fiber (0.9 SM(PAPB)-NH, Sumitomo Electric Industries, Ltd., 0.9 mm outside diameter). This optical fiber is capable of distribution measurement and can act as a measurement section at any position along the entire length of the optical fiber.

An optical fiber sensor was formed by connecting an optical fiber to an instrument to measure temperature. Temperature was measured in two ways. A method for measuring temperature from the amount of frequency shift of Brillouin scattered light（Brillouin Optical Correlation Domain Analysis (BOCDA)）[3)] and a method for measuring temperature from the intensity of Raman scattered light（Raman Optical Time Domain Reflectometry (ROTDR)）. For the former measurement, a Brillouin instrument (custom-made, Yokogawa Electric Corp., 5 cm spatial resolution, 2.5 cm measurement interval) was used, and for the latter, a

Raman instrument (OPTHERMO FTR3000X, Sumitomo Electric Industries, Ltd., Spatial resolution 100 cm, measurement interval 25 cm) was used. The measurement interval is the distance between the temperature measurement points, and the spatial resolution is the average value of the temperature over a length of meters centered on the temperature measurement point.
In the Brillouin measurement, the amount of frequency shift of Brillouin scattered light depends on changes in strain and temperature. In this study, however, no external force was applied to the optical fiber, and the temperature was determined assuming that the amount of frequency shift depends only on changes in temperature.

2-2 Experimental Device

Two impermeable liners and two nonwoven geotextile were laid alternately on the slope using an impermeable liner laying trestle (W272cm×D300cm×H150cm) consisting of concrete panels with a slope of 1:2. Figure-1 shows a photograph of a slope model with impermeable liners laid.
Figure-2 shows a schematic cross-section of the slope where the impermeable liner was laid. On the upper surface of the lower nonwoven geotextile, a rubber heater was placed as a heat source and an aluminum plate was placed for heat diffusion and fixed with curing tape. Optical fiber cables were placed on the top surface of the upper nonwoven geotextile and fixed with curing tape. Two optical fiber cables were placed in parallel adjacent to each other to enable simultaneous temperature measurement at the same position by the Brillouin and Raman instruments.
Figure-3 shows a wiring diagram of an optical fiber cable. The upper end of the figure is the shoulder and the lower end is the butt of the cable. The fiber optic cable routing started at the left end of the slope shoulder and was routed in a single stroke, with longitudinal wires running from left to right at 50 cm intervals, followed by horizontal wires running from top to bottom at 50 cm intervals, then crossing the center of the slope from right to left and returning to the left end of the slope shoulder. The total length of one fiber optic cable on the slope was 41,360 mm.
The surface temperature distribution of the upper impermeable liner was photographed by a thermal infrared camera.

2-3 Experimental Conditions

Two experiments were conducted: Experiment 1 and Experiment 2.
The objective of Experiment 1 was to understand the reproducibility of the two-dimensional temperature distribution of the impermeable liner using the measurement data from the optical fiber sensor. First, temperatures were measured at room temperature by

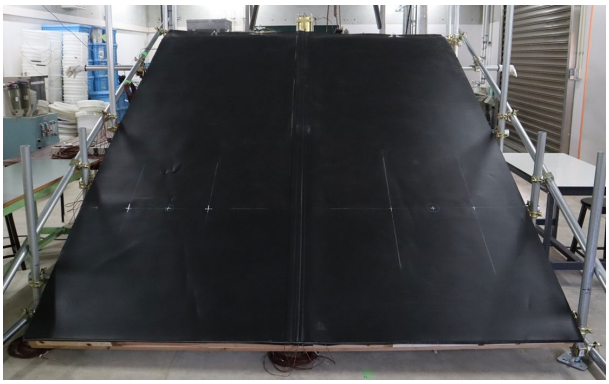

Figure-1 Slope Model with Impermeable Liner Laid

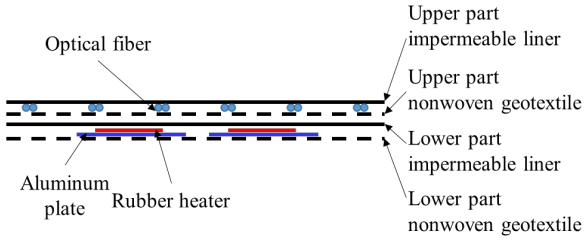

Figure-2 The Structure of The Impermeable Liner and The Fiber Optic Cable and Location of Heat Sources

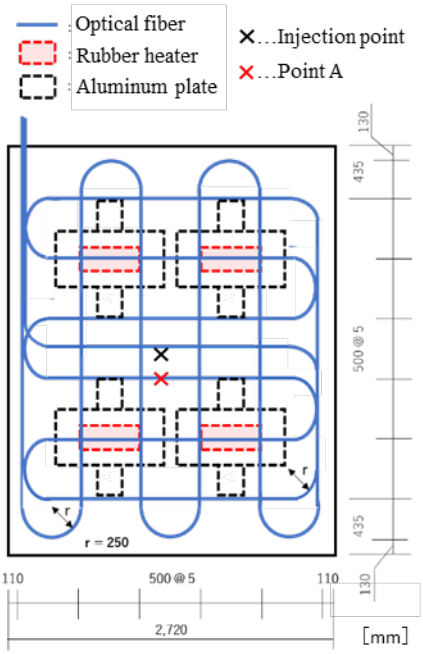

Figure-3 Arrangement of Fiber Optic Cables, Heat Sources and Water Injection point

optical fiber sensors using Brillouin and Raman instruments and a thermal infrared camera. After that, the temperature of the rubber heater was set to 80°C, and the temperature distribution of the upper impermeable liner was confirmed to be normal by a thermal infrared camera, and then the temperature was measured by an optical

fiber sensor using Brillouin and Raman instruments and a thermal infrared camera. The two-dimensional temperature distribution of the impermeable liner was created using the measurement data from the optical fiber sensor, and compared with the two-dimensional temperature distribution of the impermeable liner captured by the thermal infrared camera.

The objective of Experiment 2 was to understand the possibility of detecting water leakage using an optical fiber sensor. First, in order to simulate water leakage due to damage of the upper impermeable liner, a hose nipple was drilled through the upper impermeable liner in the center of the slope to enable water injection using a metering pump. The water injection points are shown in Figure-3. Next, temperatures were measured at room temperature using optical fiber sensors with Brillouin and Raman instruments and a thermal infrared camera. After that, pure water adjusted to 27.0°C in a thermostatic bath was continuously injected for 56 minutes using a micro volume metering pump. Immediately after the water was injected, temperatures were measured seven times at 8-minute intervals using optical fiber sensors with Brillouin and Raman instruments and a thermal infrared camera. The air temperature was 19.7°C, and the temperature of the injected water was approximately 7°C higher than the air temperature. The flow rate of the injected water was 17.1 mL/min.

2-4 Temperature Calibration

Since the optical fiber is placed in contact with the underside of the upper impermeable liner, the temperature of the optical fiber is considered to be approximately equal to the temperature of the upper impermeable liner directly above it. Therefore, we calibrated the temperature measured by the optical fiber sensor using the temperature of the upper impermeable liner directly above the optical fiber cable, which was measured by a thermal infrared camera.

2-5 Creation of Two-Dimensional Temperature Distribution

A two-dimensional temperature distribution was created from the temperature distribution data measured by the optical fiber sensor. The temperature distribution data from the optical fiber sensor consists of the distance from the starting point of the optical fiber and the temperature. The two-dimensional coordinates of each point were obtained from the wiring diagram of the optical fiber and the distance, and the two-dimensional temperature distribution was created using the data set of the two-dimensional coordinates and temperature. Contour plotting software（Visualizer Pro，Malloc Code）was used to create the two-dimensional temperature distribution.

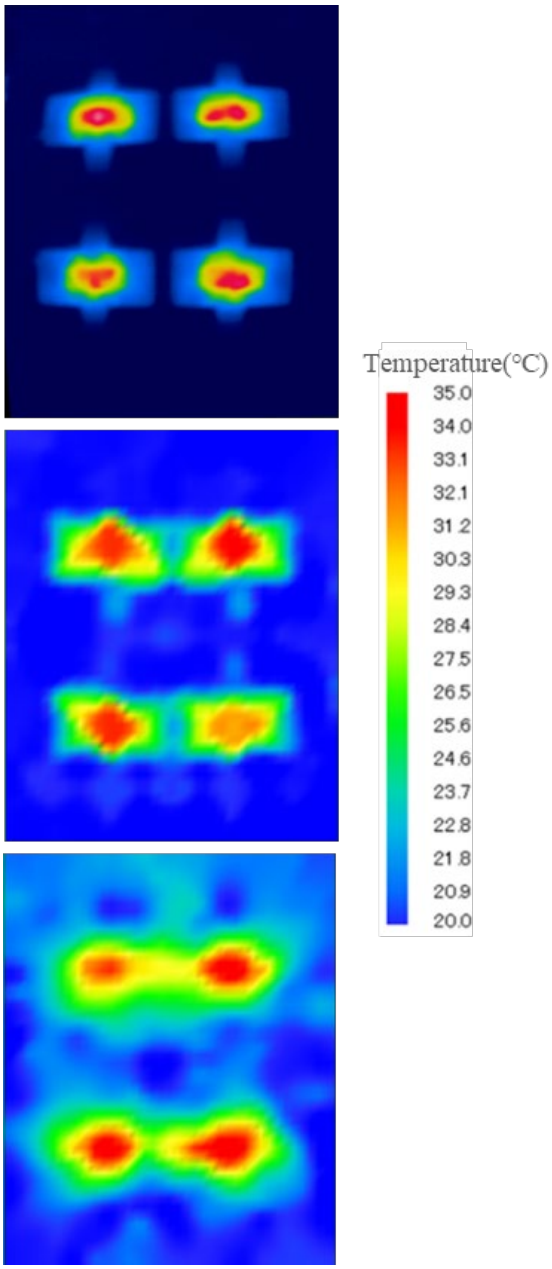

Figure-4 Two-Dimensional Temperature Distribution in Experiment 1 (Top: Thermal infrared camera, Middle: Brillouin measurement, Bottom: Raman measurement)

3. RESULTS AND DISCUSSION

3-1 Applicability to The Estimation of Two-Dimensional Temperature Distribution of Impermeable Liners

Figure-4 shows the temperature distribution of the impermeable liner taken by the thermal infrared camera in Experiment 1 and the two-dimensional temperature distribution generated from the data measured by the optical fiber sensor using Brillouin and Raman instruments.

The set temperature of the rubber heaters was 80°C,

whereas the maximum temperature of the upper impermeable liner was about 35°C. The rubber heaters were installed between the lower impermeable liner and the lower nonwoven geotextile, and the upper nonwoven geotextile existed between the rubber heaters and the upper impermeable liner. The high porosity of the nonwoven geotextile and the heat insulation effect of the air prevented the heat from the rubber heater from being transferred to the upper impermeable liner, which is thought to have caused the large temperature difference between the upper impermeable liner and the rubber heater.

There were four heat sources, and their presence was clearly identified by the thermal infrared camera. In the two-dimensional temperature distribution generated from the Brillouin data, the four heat sources were clearly identified, although not as clearly as with the thermal infrared camera. On the other hand, the two-dimensional temperature distribution generated from the Raman data showed four peaks in the temperature distribution, but the left and right heat sources appeared to be connected.

This is largely due to the difference in spatial resolution. The Brillouin measurement cannot capture temperature differences within a narrower range than the spatial resolution. The higher spatial resolution of 5 cm for the Brillouin measurement allows for a finer temperature distribution to be captured. However, in the Raman measurement, where the spatial resolution is as low as 100 cm, it would be difficult to distinguish the left and right rubber heaters separately in this experiment, where the distance between the left and right rubber heaters is 50 cm.

Although Brillouin measurement has better reproducibility in estimating temperature distribution, considering the actual size of the landfill and the size of the heat source, a spatial resolution of 100 cm is sufficient, and Raman measurement data is considered applicable in estimating the two-dimensional temperature distribution of the impermeable liner.

3-2 Applicability for Detecting Water Leakage from Impermeable Liner Damaged Areas

Figure-5 shows the change over time of the temperature measured by Brillouin measurements at two locations in Experiment 2: point A, which is the optical fiber sensor measurement point nearest the water injection point (hereinafter referred to as "water injection point"), and a point far from the water injection point and unaffected by the water injection (hereinafter referred to as "ambient temperature point"). Point a is located approximately 20 cm below the point of water injection in the direction of the slope gradient. The plots in the figure show data from seven measurements taken at eight-minute intervals, each plot being the value of an eight-minute measurement and plotted at the center of an eight-minute period.

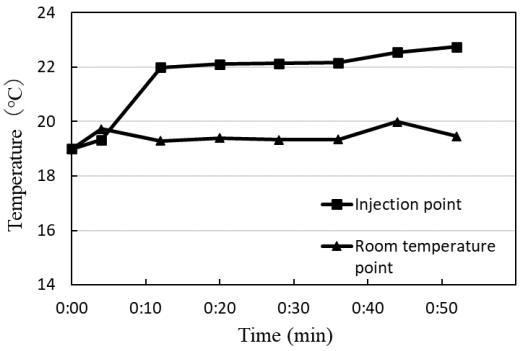

Figure-5 Temperature Change During Water Injection (Brillouin measurement)

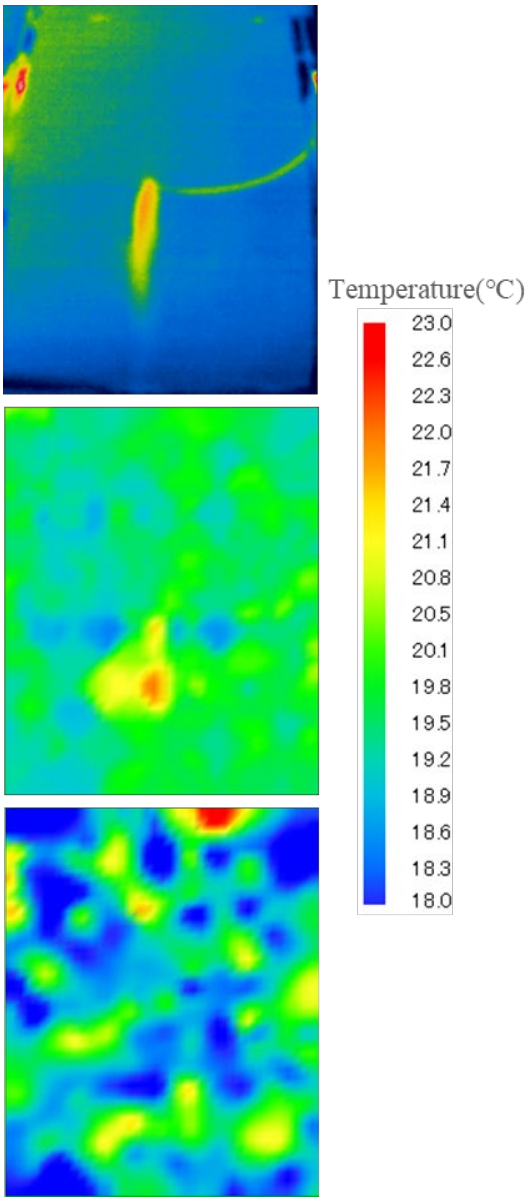

Figure-6 Two-Dimensional Temperature Distribution in Experiment 2 (Top: Thermal infrared camera, Middle: Brillouin measurement, Bottom: Raman measurement)

The temperature at the water injection position was continuously 2 to 3°C higher than that at the room temperature position from 8 minutes after the start of water injection. The reason for the delay in the measured temperature increase from the point of water injection is considered to be that point a, which is called the water injection position, is about 20 cm away from the water injection point, and it took about 8 minutes for the water injection to reach the point. The temperature of the injected water was about 7°C higher than the room temperature, but the temperature difference between the injection point and the room temperature point was smaller than that, suggesting that the injected water was cooled in the process of reaching the injection point from the injection point to the injection point.

When such a leak causes a sudden temperature change that can be detected by an optical fiber sensor, it is considered to be an abnormal temperature fluctuation that could be detected by an optical fiber sensor.

Figure-6 shows the temperature distribution of the impermeable liner taken by the thermal infrared camera 48 minutes after the start of water injection in Experiment 2, as well as the two-dimensional temperature distribution generated from the data measured by the optical fiber sensor using Brillouin and Raman instruments.

The thermal infrared image shows that the water injection was flowing down the slope in the direction of the slope gradient. The maximum temperature in the thermal infrared image was 21.5°C, while the temperature of the injected water was 27.0°C.

The two-dimensional temperature distribution generated from the Brillouin measurement data showed hot areas similar in shape to the hot areas seen in the thermal infrared image associated with water injection. The hot area in the Brillouin measurement was located slightly below the hot area in the thermal infrared image. This is because the optical fiber was not located directly below the water injection point, and the optical fiber whose temperature changed with water injection was located below the water injection point. Thus, the Brillouin measurement indicated that leakage can be detected if a large area with a temperature about 2°C higher than the normal temperature is generated in association with the leakage.

The two-dimensional temperature distribution generated from the Raman data did not clearly identify the temperature increase associated with water injection. In the case of Raman measurements, the spatial resolution is 100 cm, and the temperature is the average of a 100 cm interval centered at the measurement point. In other words, if the anomalous temperature associated with the leakage does not occur in the same section as the spatial resolution, there will be no change in the average temperature. When considering water leakage on a slope, it is assumed that the leakage flows down the slope direction and does not spread widely in the direction perpendicular to the slope direction. Therefore, Raman measurements with coarse spatial resolution are considered unsuitable for leak detection on slopes.

Next, focusing on the Brillouin measurement data from Experiment 2, we examined the effective routing of optical fibers for leak detection on a slope. In order to compare the case where the optical fibers are laid parallel (longitudinal) and perpendicular (transverse) to the slope direction, we created two-dimensional temperature distributions using only the longitudinal data and the transverse data from the Brillouin measurement data in Experiment 2.

The results are shown in Figure-7. In the longitudinal wiring, the optical fiber was not located directly under the point of water injection, and the water injection did not spread widely in the horizontal direction, so the temperature change of the optical fiber due to water injection was limited and the water injection could not be clearly captured. On the other hand, in the lateral wiring, the optical fiber was located in the penetration area of the water injection, and the temperature change caused by the water injection could be clearly captured. The results showed that the lateral wiring of optical fibers is effective in detecting water leakage on a slope.

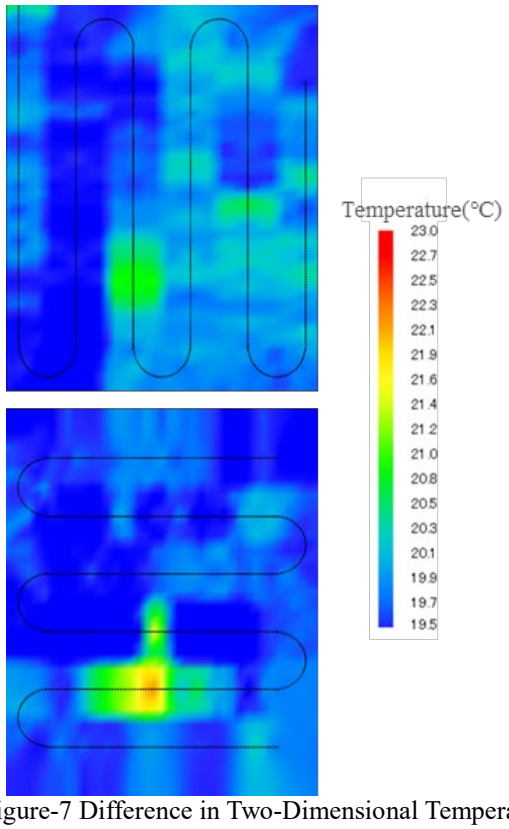

Figure-7 Difference in Two-Dimensional Temperature Distribution between Wiring Parallel and Perpendicular to The Direction of Slope Gradient (Brillouin measurement)

4. CONCLUSIONS

In this study, single-mode optical fibers were wired to a model of a reclaimed land slope with an impermeable liner to investigate the applicability of an optical fiber sensor in estimating the temperature distribution of the impermeable liner and detecting water leakage. The following is a summary of the findings obtained. The findings are as follows.

1) Brillouin measurement is more reproducible than Raman measurement in terms of temperature distribution. However, considering the actual size of the landfill and the size of the heat source, a spatial resolution of 100 cm is sufficient, and the Raman instrument is considered sufficient for estimating the temperature distribution of the impermeable liner.
2) If a temperature change that can be captured by an optical fiber sensor occurs with a leak, leak detection is considered possible.
3) For leak detection on slopes, it is effective to route optical fiber cables orthogonally to the slope direction.

As future issues, it is necessary to study the durability of optical fiber cables against impact, loading, and cyclic loading, and the long-term chemical durability of optical fiber cables for landfill disposal. It is also necessary to consider the installation method of optical fiber cables to the impervious sheet, appropriate wiring intervals, and leakage conditions under which leakage can be detected.

ACKNOWLEDGMENTS

The authors would like to thank Toyobo Corporation and Mitsuboshi Belting Co. Ltd. are gratefully acknowledged.

REFERENCES

1) Ministry of the Environment : Outline of Criteria for Decommissioning Solid Waste Landfill, https://www.env.go.jp/recycle/kosei_press/h980616a/h980616a-3.html (Date viewed: July 28, 2022)
2) The Waste Management Society of Japan : Survey and Evaluation Methods for Waste Final Disposal Site Decommissioning Criteria, 2002.
3) Song, K. Y., He, Z., & Hotate, K. : Brillouin Optical Correlation Domain Analysis Based on Millimeter-Order Spatial Resolution with Distributed Strain Measurement, Optics Letters, 31(17), 2526-2528, 2006.
4) Association for The Advancement of Fiber Optic Sensing : Introduction to Fiber Optic Sensors, 2012.
5) Kengo Koizumi, Hitoshi Murai, and Tokuro Yamaguchi : Distributed Fiber Optic Sensing Technology to Support Social Infrastructure, Journal of The Institute of Electrical Installation Engineers of Japan, 37(10), 736-739, 2017.
6) Imai, M., Hironaka, Y., Sasaki, T., Fujiwara, K., Waki, J., Terada, K., Suyama, Y., and Mizunari, M. : Experimental Study for Application of Distributed Optical Fiber Sensor to Monitoring of Radioactive Waste Disposal Facilities, Journal of Japan Society of Civil Engineers F2, 77(1), 60-74, 2021.

MICROPLASTICS IN A SOLID WASTE LANDFILL IN JAPAN : THEIR CONCENTRATION IN LANDFILLED WASTE, COVERSOIL, RAINWATER AND LEACHATE

Hirofumi Nakayama[1], Atsuki Fukuda[2] and Takayuki Shimaoka[1]
1 Faculty of Engineering, Kyushu University
744, Motooka, Nishi-ku, Fukuoka, 819-0395 Japan
2 Graduate School of Engineering, Kyushu University
744, Motooka, Nishi-ku, Fukuoka, 819-0395 Japan

Abstract

In this study, focusing on the material flow of MPs at a landfill site in Japan, a survey with the aim of understanding the material flow of MPs at a municipal solid waste landfill site in Fukuoka city has been investigated. MPs were found in the samples collected from different places in the landfill site such as landfilled waste, intermediate cover soil, final cover soil, sediment in rainwater reservoir pond, although MPs were not found from the samples collected from the discharged water after leachate treatment. In the landfill site MPs were confirmed to be removed during the leachate treatment process.

1. INTRODUCTION

Among landfilled waste in municipal solid waste landfill sites in Japan, there are wastes containing Microplastics (MPs), such as recycling residues from crushing and sorting facility. The non-woven fabric used as a light-shielding protective mat on geomembrane liners at the slope of the landfill site is made of chemical fiber and there is a possibility that part of the chemical fibers are detached and becomes MPs. It is thought that the MPs carried into the landfill site and the MPs generated within the site move together with the rainwater discharged laterally and reach the rainwater reservoir pond. Also, part of it may have moved to the leachate treatment facility together. However, research on material flow in landfill sites is insufficient. The purpose of this study is to understand the material flow of MPs in a municipal solid waste landfill site in Fukuoka city, Japan.

2. Survey of MPs in a municipal solid waste landfill site

In this study, landfilled waste, cover soil, rainwater, and leachate were collected from a municipal solid waste landfill site in Fukuoka city. MPs density was measured by counting the number of MPs in the collected samples. We also tried to identify the components of MPs by FTIR.

2.1 Sampling methods

About 2 kg of recycling residue generated at a crushing and sorting facility was collected. About 3 kg of cover soil was collected at a section under landfilling and a section where the landfilling has been completed. About 10 kg of sediment was collected from a drain at slope of the site. In rainwater reservoir basins and ponds, submersible pump were used to suck up surface water, and after 1,000 L of water was passed through a plankton net with a mesh size of 100 μm, the remaining residue in the net was collected. The bottom sediment in the rainwater reservoir basin and pond were collected with an Ekman barge mud sampler, then the sample. 1,000 L of raw leachate flowing through the leachate collection pipe was passed through a plankton net with a mesh size of 100 μm, and the remaining residue in the net was collected. At the leachate treatment facility, about 40L of coagulated sedimentation sludge was passed through a plankton net, and the sample remaining in the net was collected. About 100L of discharged water after leachate treatment was passed through a plankton net, and the remaining residue in the net was collected.

2. 2 Method for MPs extraction

In this study, MPs were extracted and analyzed according to the procedure shown in Fig. 1, referring to the method of Alfonso et al(2021).

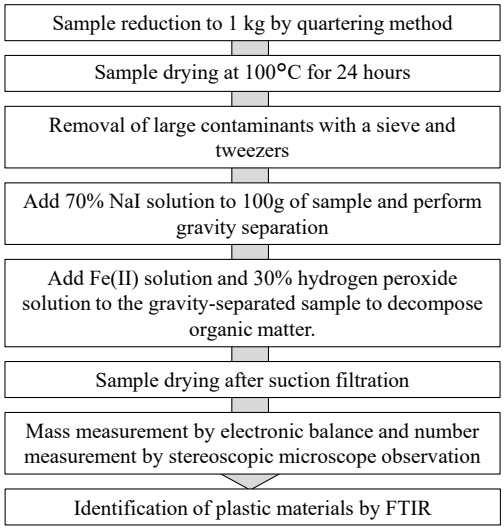

Fig.1 MPs extraction and analysis method

2.3 Analysis results

Table 1 shows the MPs density in the samples collected at each location and the composition of plastic materials identified by FTIR. 920 MPs/kg-dry were found in the residue from a crushing and sorting facility which is sent to the landfill site. The main components were PET, polynosic, and ethylene propylene rubber. PET, polynosic, and polyethylene were also main components of MPs in the intermediate covering soil. MPs in the deposits in the slope drain were PET. Since the material of the light-shielding protective mat installed on the slope was also PET, it was thought that the detached MPs accumulated in the deposits. Only 6 MPs/m^3 were found in the surface water of rainwater reservoir pond, but 201 MPs/kg-dry were found in bottom sediments. Since no MPs were found in the treated leachate, it was confirmed that MPs were removed during the leachate treatment process.

Table 1 MPs density and composition in samples taken at different places in a landfill site

Place of samling	Sample	MPs density	Composition
Crushing and sorting facility	Residue after crushing and sorting	920 pieces/kg-dry	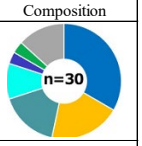
Slope of landfill site	Sediment in drain	18 g/kg-dry	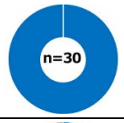
Section under landfilling	Intermediate cover soil	120 pieces/kg-dry	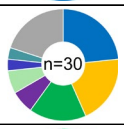
Section landfilling has been completed	Final coversoil	47 pieces/kg-dry	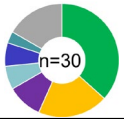
Rainwater reservoir basin	Surface water	0 piece/m3	-
	Sediment	249 pieces/kg-dry	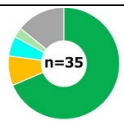
Rainwater reservoir pond	Surface water	6 pieces/m3	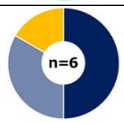
	Sediment	201 pieces/kg-dry	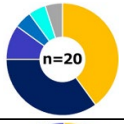
Leachate treatment facility	Raw leachate	3 pieces/m3	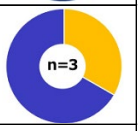
Leachate treatment facility	Coagulation sedimentation sludge	0 piece/kg-dry	-
Leachate treatment facility	Discharged water after treatment	0 piece/m3	-

PET
Polynosic
Ethylene propylene rubber
Nylon
Polypropylene
Polyethylene
Vinylon
Polynorbornene
PVC
Rayon
Cupra
Unknown

3. CONCLUSION

In the landfill site investigated in this study, MPs were found in the samples collected from different places such as landfilled waste, intermediate cover soil, final cover soil, sediment in rainwater reservoir pond, though MPs were not found from the samples collected from the discharged water after leachate treatment. In the landfill site MPs were confirmed to be removed during the leachate treatment process.

REFERENCES

1) Alfonso, M. B., K. Takashima, S. Yamaguchi, M. Tanaka, and A. Isobe: Microplastics on plankton samples: multiple digestion techniques assessment based on weight, size, and FTIR spectroscopy analyzes, Marine Pollution Bulletin, Vol.173, pp.1-10, 2021.

SULFATE REDUCTION BEHAVIOR IN PRESSURE-BEARING LEACHATE SATURATED ZONE

Dongsheng Shen[1] , Haomin Zhou[1] , Zhiyuan Jin[1] , Wenyi Yang[1] , Manting Ci[1] , Yuyang Long[1,*] , Lifang Hu[2,*]
1 Zhejiang Provincial Key Laboratory of Solid Waste Treatment and Recycling, School of Environmental Science and Engineering, Instrumental Analysis Center, Zhejiang Gongshang University, Hangzhou, 310012, China
2 College of Quality and Safety Engineering, Institution of Industrial Carbon Metrology, China Jiliang University, Hangzhou, 310018, China

ABSTRACT
Attention should be paid to the sulfate reduction behavior in a pressure-bearing leachate saturated zone. In this study, within the relative pressure range of 0–0.6 MPa, the ambient temperature with the highest sulfate reduction rate of 50°C was selected to explore the difference in sulfate reduction behavior in a pressure-bearing leachate saturated zone. The results showed that the sulfate reduction rate might further increase with an increase in pressure; however, owing to the effect of pressure increase, the generated hydrogen sulfide (H_2S) could not be released on time, thereby decreasing its highest concentration by approximately 85%, and the duration extended to about two times that of the atmospheric pressure. Microbial community structure and functional gene abundance analyses showed that the community distribution of sulfate-reducing bacteria was significantly affected by pressure conditions, and there was a negative correlation between DsrB gene abundance and H_2S release rate. Other sulfate reduction processes that do not require DsrA and DsrB may be the key pathways affecting the sulfate reduction rate in the pressure-bearing leachate saturated zone. This study improves the understanding of sulfate reduction in landfills as well as provides a theoretical basis for the operation and management of landfills.
Keywords: Landfill, Pressure, Leachate saturated zone, Sulfate reduction, Odors, Microbial community

INTRODUCTION

Landfills have always been pertinent solutions for the final disposal of municipal solid wastes because of their advantages of simple construction and management, large processing capacity, and low treatment cost (Meyer-Dombard et al., 2020). With the continuous improvement of technical means and operation management levels, landfill sanitation level has significantly improved, but the odor pollution caused by landfill gas emissions continues to cause serious harm to the surrounding environment. Hydrogen sulfide (H_2S) has the characteristics of low odor threshold and high toxicity and is often considered as one of the main pollutants causing landfill odor pollution (Long et al., 2016). Similarly, volatile organosulfur compounds (VOSCs), such as dimethyl sulfide (DMS) and methyl mercaptan (MM), are considered the main pollutants of landfill odor pollution (Zhang et al., 2017). The above sulfur-containing odorous gases are often found in the odorous pollution of landfills (Jin et al., 2020b). Notably, H_2S, DMS, and MM discharged from landfills come from the sulfate reduction behavior that occurs inside landfills.

Previous studies have shown that active sulfate reduction behavior exists in landfills, mainly due to the high sulfate content of landfills, as well as the anaerobic environment and widespread presence of sulfate-reducing bacteria (SRB) in landfills (Long et al., 2017). Our studies found that as the depth of landfill deepens, there were significant differences in internal water content (Ying et al., 2019), temperature (Jin et al., 2020a), and other environmental factors, affecting SRB to an extent, leading to an impact on sulfate reduction behavior.

In addition, there are shreds of evidence that because of the internal structure as well as material migration and transformation factors, the pressure field in the deep layer of a landfill is formed inside the landfill, making the pressure inside the landfill significantly higher than that on the surface (Giri and Reddy, 2014; Kadambala et al., 2011; Zhang et al., 2021). For the internal pressure field of landfills, there are three main sources of pressure, namely, landfill waste accumulation and extrusion (weight of solid matter) (Benson et al., 2012), leachate silting (pore water pressure) (Tupsakhare et al., 2020), and long-term detention of landfill gas (pore gas pressure) (Ma et al., 2019), which are influenced by multiple factors. First, owing to the accumulation and burial of landfill wastes in the landfill process, the pressure in the bottom layer of a landfill is significantly higher than that of the surface layer, whereas the surface layer's pressure is similar to the atmosphere. With an increase in depth, the pressure on a landfill waste and microorganism changes sequentially (Tupsakhare et al., 2020). Further, owing to the influence of factors, such as the high moisture content of deposited wastes and

landfill management, there is a widespread phenomenon of high leachate production in landfills, leading to the deposition of landfill leachate and formation of leachate saturation zone. Owing to the vertical migration of leachate, pore water pressure in a landfill also increases with an increase in depth (Ma et al., 2019). Finally, by measuring the gas production pressure of landfill gas well, the relative pressure of the gas production is generally less than 0.5 MPa, whereas, if the leachate is retained, the relative pressure of the gas production is between 0.7 and 1.6 MPa (Jafari et al., 2017), attributable to the accumulation of landfill gas due to the clogging of a gas-well pipeline, and the local pressure increases (Zhang et al., 2021). Therefore, the internal pressure field of landfills is common, and the pressure increases gradually in the longitudinal direction. We can assume that a sulfate reduction process dominated by SRB in an actual landfill is affected by a specific pressure field for a long time. Pressure as a physics and thermodynamics parameter, has been proven to have a certain impact on SRB and sulfate reduction behavior in various pressure-bearing environments, such as oceans (Bhattarai et al., 2018; Fichtel et al., 2015), lakes (Cassarini et al., 2019), and reservoirs (Williamson et al., 2018). Unfortunately, to the best of our knowledge, studies on sulfate reduction in pressure-bearing leachate saturated zones are inadequate.

In this study, the sulfate reduction behavior in a landfill leachate saturated zone was simulated under different pressures, especially at a high temperature (50°C), where sulfate reduction behavior was found to be extremely active in previous studies (Jin et al., 2020a). H_2S, MM, and DMS production were investigated, and microbial diversity and functional gene abundance were analyzed. We aim to elucidate the sulfate reduction behavior in landfills as well as provide a reliable theoretical basis for landfill gas management and control strategies.

1. MATERIAOLS AND METOHDS

1.1. Materials

Mineralized wastes used in our experiment were collected from a real landfill site in Beijing, an anaerobic municipal solid waste landfill site. Two parallel sampling points were selected in a closed landfill cell, which was strictly operated based on the landfill process from historical records. Waste samples of different ages were collected at various depths from the two points at the same pace using the well-sampling method (Hu et al., 2019). Holes were drilled at the two sampling points. Subsamples of landfilled wastes from the same depth in each hole were mixed to obtain representative samples. The mineralized wastes were collected at 12 and 15 m and fully mixed.

The inert components, including stone, plastic, glass, and fabric, were removed, and the remaining mineralized wastes were cut into fragments of no more than 1 cm in diameter. All mineralized wastes after crushing were collected and fully mixed, sealed in a ziplock bag, and stored in a refrigerator at 0°C. Because it is difficult to collect landfill leachate and mineralized wastes simultaneously in an actual landfill site, simulated leachate prepared according to actual leachate is used in the experiment. Table 1 lists the main characteristics of landfills and simulated leachate.

Table 1 The main characteristics of landfill waste and configured leachate.

Components	SO_4^{2-}	$S_2O_3^{2-}$	S^0	S^{2-}
Mineralized waste (mg/kg)	2584.3	/	/	131.4
leachate (mg/L)	1032.2	/	/	/
Components	DOC	NH_4^+	NO_3^-	NO_2^-
Mineralized waste (mg/kg)	1425.7	2021.5	44.9	/
leachate (mg/L)	1212.6	4.42	2.10	/

1.2. Experimental design

Pressure-bearing leachate saturated zone tests were simulated by stainless steel pressure tank reactors. Meanwhile, the normal atmospheric pressure tests were performed in glass tank reactors. All reactors' volumes were 1 L. The lid of the pressure reactor tanks was designed as four connecting ports, connecting pressure gauge, pressure-reducing valve, safety valve, and spherical exhaust valve (Fig. 1).

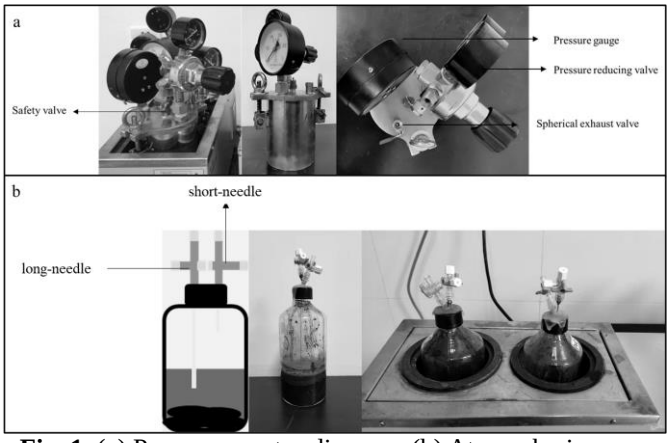

Fig. 1. (a) Pressure reactor diagram; (b) Atmospheric pressure reactor diagram.

The tank lid was sealed with two spiral valves. A pretreated mineralized waste sample (100 g) and 300-mL leachate were added to each reactor, and the initial headspace volume was recorded. The pressure condition of an atmospheric pressure reactor was simulated by

purging nitrogen to the headspace. The relative pressures of the reactors were set to 0.0, 0.2, 0.4, and 0.6 MPa, corresponding to landfill depths of about 0, 20, 40, and 60 m, respectively. The atmospheric pressure reactor used a butyl rubber plug and plastic cap to seal the bottle, and two three-way valves were arranged, connecting long and short-needle tubes, which were connected to each bottle through a bottle cap, and the long needle tube could reach the leachate surface. Meanwhile, the short-needle tube was used to connect the Schiller fermenter to the three-way valve to obtain gas production (Jin et al., 2020a).Two parallel groups were set for each pressure. Pressure reactor sampling, relying on the pressure-reducing valve-fixed release of 0.01 MPa gas, employed a gas collection bag and the same method to restore the pressure in the reactor. Gas-phase samples in the atmospheric pressure reactor are collected via a syringe through a short-needle three-way valve. To make SRB achieve a high sulfate reduction ability in this reaction system and conform to the actual internal landfill temperature, the experimental temperature was set to 50°C (Jin et al., 2020a) and heated in a constant temperature water bath. The test was completed when odor-containing sulfur could not be detected in the reactors.

1.3. Analyses

During the tests, the headspace H_2S, MM, and DMS concentrations of all reactors were determined using a gas chromatograph equipped with a flame photometric detector (GC 7890A, Agilent Technologies, USA) (Zhang et al., 2017).

At the beginning and end of the tests, landfill waste and leachate samples were analyzed for sulfate (SO_4^{2-}), sulfite (SO_3^{2-}), thiosulfate ($S_2O_3^{2-}$), sulfur (S^0), sulfide (S^{2-}), nitrate (NO_3^-), nitrite (NO_2^-), and dissolved organic carbon (DOC) after the samples were passed through a 0.22-μm filter. The methods used to determine the concentrations were in accordance with previous studies (Fang et al., 2016; Ying et al., 2019). The abovementioned analyses were performed in triplicate.

DNA was extracted from each landfill waste sample (0.1–0.6 g per sample) using a FastDNA Spin kit (MP Biomedicals, USA) according to the manufacturer's instructions. After extraction, the DNA concentration was determined using a NanoDrop2000 ultraviolet–visible (UV − Vis) spectrophotometer (Wilmington, USA). 16S rRNA gene was amplified via polymerase chain reaction (PCR) using 515FmodF (5′-GTGYCAGCMGCCGCGGTAA-3′) and 806RmodR (5′-GGACTACNVGGGTWTCTAT-3′) primers, and the PCR reaction was in accordance with a previous study (Liu et al., 2018).

In this study, Mothur (Version: 1.30.2) software was used to calculate the α-diversity of microorganisms in samples based on the OTU level. Principal coordinate analysis (PCoA) was employed to analyze the similarity or difference in microbial community compositions of samples treated with different pressures. We adopted the Bray–Curtis distance algorithm. Microbial β-diversity was analyzed on the basis of the phylum level.

DNA isolation, detection, and PCR amplification were in accordance with Section 2.4. The PCR primers for DsrA and DsrB were DsrA_F (5′-ACSCACTGGAAGCACG-3′) and DsrA_R (5′-CAACATCGTYCAYACCCAGGG-3′), respectively. Finally, the abundance of the amplified genes was quantified via real-time quantitative PCR (ABI7500, Applied Biosystems, USA), as previously reported (Hu et al., 2021).

2. Results and discussion

2.1 Release behavior of H_2S and VOSCs under pressure

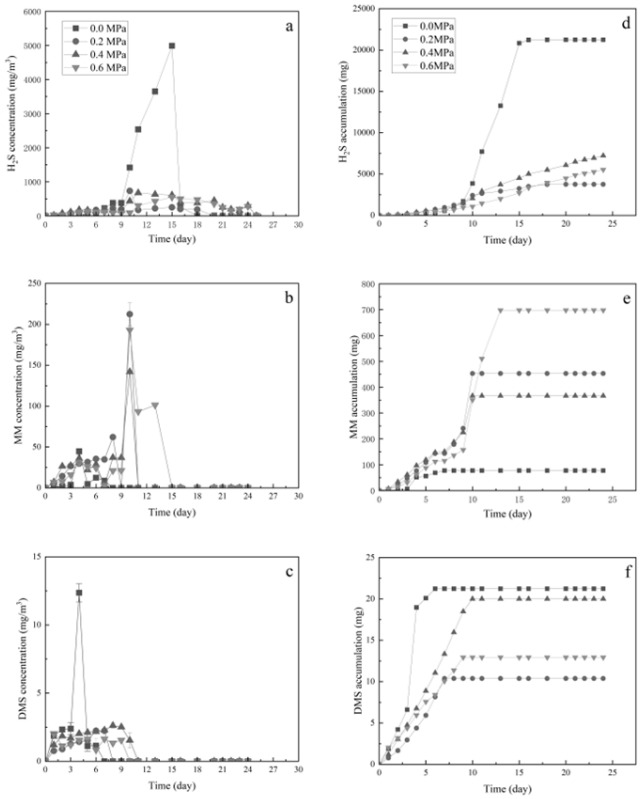

Fig. 2. Emission of (a) hydrogen sulfide (H_2S), (b) methyl mercaptan (MM), and (c) dimethyl sulfide (DMS) under various pressures and accumulation of (d) H_2S, (e) MM, and (f) DMS under various pressures.

The pressure environment in the pressure-bearing leachate saturated zone is harsher than that that in the surface saturated zone. The release behaviors of H_2S,

MM, and DMS under the influence of pressure are shown in Fig. 2. From Fig. 2 (a), H_2S release behavior was significantly inhibited under high pressure. When it was atmospheric pressure, the highest H_2S concentration was in the same order of magnitude as that of the surface saturated zone, which was 4,991.0 mg/m^3 on the 15th day. The highest H_2S concentration decreased with an increase in pressure. When the ambient pressure was in the range of 0.2–0.6 MPa, the highest concentration of H2S was 733.9, 674.1, and 546.2 mg/m^3, on the 10th, 11th, and 15th days, respectively, proving that the H_2S release rate would increase in a pressure environment of 0.2–0.4 MPa, but would decrease under higher pressures. In addition, when the pressure was higher than the atmospheric pressure, H_2S concentration maintained the same order of magnitude range for about 10 days after reaching the peak and then decrease to below the detection limit. The decrease rate also showed a downward trend with an increase in pressure, and the decrease process only lasted for two days at 0 MPa, probably due to the increase in the headspace pressure, which limited the release of H_2S and kept it at a relatively low and constant concentration for a long time (Huttenhuis et al., 2008).

Figs. 1 (b) and (c) show the MM and DMS release behaviors, respectively. Unlike with H_2S, the release rates of MM and DMS did not decrease significantly when the pressure was 0 MPa. The highest MM concentration occurred on the 4th day, but the concentration was only 44.7 mg/m^3. The highest DMS concentration of 12.4 mg/m^3 also appeared on the 4th day. When the pressure was in the range of 0.2–0.6 MPa, the highest MM concentration appeared on the 10th day, corresponding to 62.1, 141.9, and 192.9 mg/m^3. The DMS concentration peaked at 2.2 and 2.3, and 1.6 mg/m^3 on days 6–7. The highest MM and DMS concentrations generally occurred earlier than the highest H_2S concentration. The releases of H_2S, MM, and DMS were not synchronous, confirming that the main sources of H_2S and VOSCs differed. During microbial activation, some microorganisms that could degrade amino acids were activated first, releasing MM, DMS, and a small amount of H_2S through the degradation process (Jin et al., 2020b). After SRB was fully activated, H_2S began to dominate. This view can be verified by the change in DOC content. Compared with the release behavior of sulfur-containing odorous gas in the leachate saturated zone at different temperatures in the surface layer (Jin et al., 2020a), the DOC content in the landfill waste samples decreased, and some amino acids were decomposed in the preservation process, decreasing the highest MM and DMS concentrations.

Because the H_2S concentration remained at the highest for a long time under high pressure, to eliminate the influence of pressure difference on the apparent concentration value, we analyzed the release capacity of sulfur-containing odorous gas at various pressures from the cumulative release amount of gas.

The results of significance analysis showed that the cumulative release amounts of H_2S and MM differed significantly when the pressure was 0 MPa compared with other pressure conditions ($P < 0.05$). There was no significant difference between the cumulative release of DMS under 0 and 0.4 MPa pressure environments ($P > 0.05$), significantly different from 0.2 to 0.6 MPa ($P < 0.05$). When the pressure was in the range of 0.2–0.6 MPa, there was no significant difference in H_2S accumulation ($P > 0.05$). According to the above results, when the ambient pressure was higher than the atmospheric pressure, the release of sulfur-containing odorous gas would be immediately affected, the release capacity of H_2S and DMS would decrease, and the release capacity of MM would increase. From the accumulation result of H_2S, the accumulation amount was the lowest at 0.2 MPa. However, while the sulfate reduction behavior was affected, the subsequent transformation of H_2S, including dissolution, oxidation, and precipitation, might also be affected.

As shown in Fig. 2, we can obtain an early indication of the concentration change. When the pressure was 0.2 MPa, H_2S would immediately decline after the peak, but it did not directly return to zero, proving that the phenomenon of concentration decline was due to the increase in the H_2S conversion rate. Combined with the conclusion that the H_2S release rate was fast at 0.2 MPa, the H_2S conversion rate was also higher at higher pressure.

2.2 Sulfate reduction behavior discrepancy

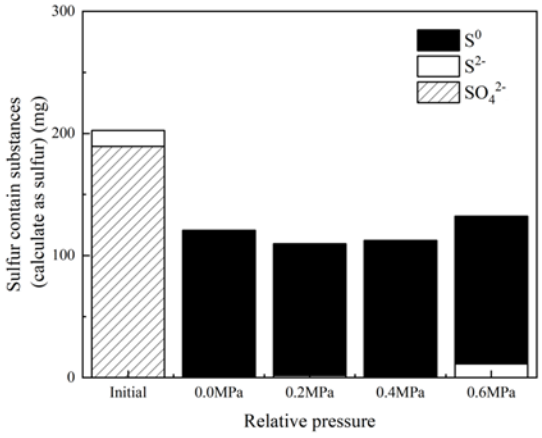

Fig. 3. Sulfate fate under various pressures (calculated as sulfur) after sulfate reduction.

These results proved that there was no difference in the cumulative release amount of H_2S at a pressure higher than the atmospheric pressure. Similar to the sulfate

reduction behavior at different temperatures in the surface saturated zone (Jin et al., 2020a), the reduction product was dominated by sulfur. The accumulation of sulfur in each reactor was 120.1, 107.9, 111.4, and 120.0 mg, with no significant difference ($P > 0.05$) (Fig. 3). The accumulation amount of sulfide was 0.5, 1.8, 0.9, and 11.2 mg, and there was more sulfide accumulation in a 0.6-MPa environment.

Further analyses of the contribution rate of sulfate to sulfide and sulfur are shown in Fig. 3. The analyses showed that it is not difficult to find that the contribution rate of sulfate exceeded 50% under all tested pressures and reached over 60% under the 0.6 MPa pressure. The results showed that pressure did not significantly affect the reducing ability of sulfate and could only fluctuate within a certain range.

Accordingly, wastes under low pressure, in the leachate saturated environment, could release more sulfur-containing odorous gas, increasing the highest concentration of odorous gas. However, for wastes under high pressure, the odorous gas concentration was diluted on the time scale, but it could maintain the odor pollution for a long time; at this pollution level, all sulfates would be reduced.

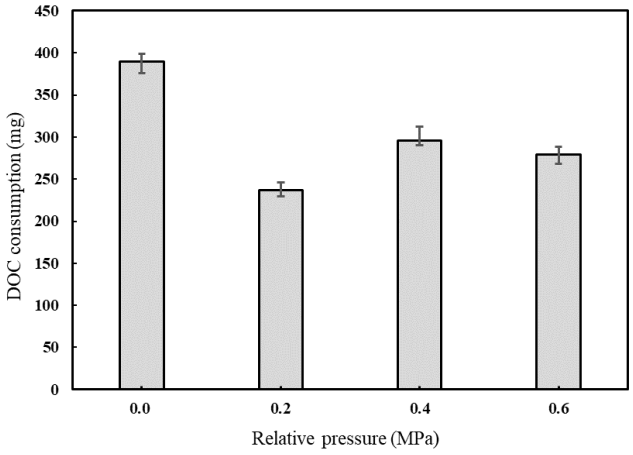

Fig. 4. Dissolved organic carbon (DOC) consumption under various pressures.

Fig. 4 shows DOC consumption under various pressures. Although microorganisms need a certain time to be activated, DOC consumption did not significantly decrease at 0 MPa and was still about 400 mg. However, under higher pressure, DOC consumption decreased to different degrees, and the DOC consumption of 0.2–0.6 MPa was 236.5, 296.1, and 279.1 mg. We found that only DOC consumption at 0 MPa had significant difference ($P < 0.05$). The results showed that high pressure influenced the activity of microorganisms, but the influence degree was not correlated with pressure. That is, the total activity of microorganisms was similar under high pressure. Combined with the difference of sulfate reduction behavior, we could infer that the difference in microbial community structure under higher pressure was not less obvious than other pressure conditions.

2.3 Functional microbial community structure under different pressures

PCoA was employed to investigate the variation in microbial β-diversity in the pressure environments. After dimension reduction, the explanatory rate of variables was 81.4%, and that of main axes 1 and 2 were 20% and 61.4%, respectively (Fig. 5). The results showed that under different pressure conditions, the microbial community structure in the saturated leachate zone presented three conditions: 0.0 (unpressured), 0.2 (micropressure), 0.4–0.6 MPa (high pressure). Under the high-pressure condition, the distance between quadrats was almost the same as the distance within quadrats, indicating that the change in pressure had little influence on the microbial community structure under the high-pressure condition.

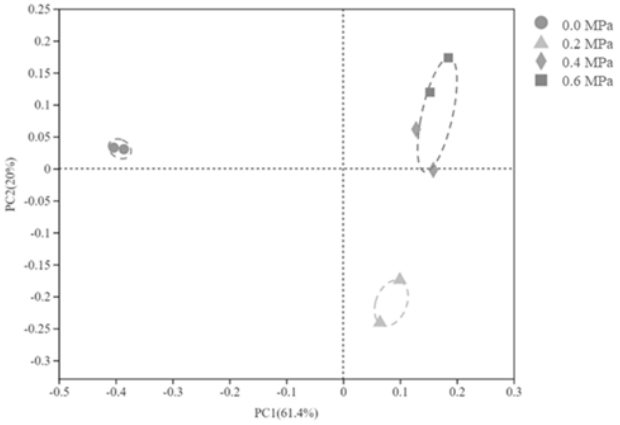

Fig. 5. PCoA analysis on OTU level of samples from various pressures.

Thus, under high pressure, microorganisms in the leachate saturated zone have a strong ability to adapt to pressure, so that pressure cannot affect their community structure. Therefore, in a follow-up study of this study, 0.4 and 0.6 MPa were combined as high-pressure groups, and the mechanism of microbial-mediated sulfate reduction under different pressures was discussed under the unpressured and micropressure conditions.

From the viewpoint of microbial community distribution characteristics, the microbial community structure of the landfill leachate saturated zone under different pressures was further analyzed (Fig. 6). Firmicutes were the dominant microorganisms in the landfill leachate saturated zone, and the abundance of Firmicutes decreased with an increase in environmental pressure. The relative abundance of Firmicutes was as high as 80% in an unconfined environment, but it decreased to 66% and 72% in the micropressure and high-pressure

environments, respectively. The abundance of Proteobacteria increased significantly, reaching 17% under the micropressure condition, and decreased to 6% under the high-pressure condition, approximately 1/3 of that under the micropressure condition. The variation trend of Chloroflexi was similar to that of Proteobacteria, and its growth was inhibited by pressure. Thus, microorganisms in different phyla have different abilities to adapt to pressure. Firmicutes have a strong ability to adapt to the high-pressure environment; the SRB of *Desulfitibacter*, *Dethiobacter*, and *Desulfotomaculum* belong to Firmicutes.

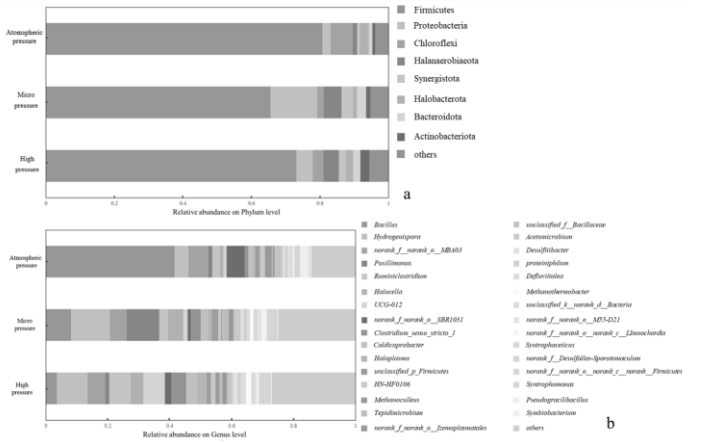

Fig. 6. Microbial community of all the microorganisms at (a) Phylum level and (b) Genus level.

At the genus level, in the unpressured environment, *Bacillus* replaced *Lentimicrobiaceae* as the dominant bacterium in the saturated zone of the surface layer found in previous studies (Jin et al., 2020a) and became the dominant bacterium in the leachate saturated zone. Its relative abundance was close to 40%, indicating that *Bacillus* had good adaptability to temperature. However, *Bacillus* had a low ability to adapt to pressure, its abundance was significantly reduced in the micropressure environment, and its relative abundance was even reduced to less than 5% in the high-pressure environment. In addition, the relative abundance of *Hydrogenispora* and *Pusillimonas* increased in the micropressure environment, and *Hydrogenispora* could still maintain a relative abundance of 11% in the high-pressure environment, showing high adaptability to pressure. In addition to *Hydrogenispora*, the relative abundance of many microbial genera, including *Ruminiclostridum*, increased under the high-pressure condition. Notably, the relative abundance of *MBA03* genus remained between 5% and 10% at different pressures.

2.4 Key SRB under various pressures

According to the Dsr function, SRB screened in GenBank, DDBJ, EMBL, and other databases and confirmed by literature reports mainly include *Desulfitibacter*, *Dethiobacter*, *Desulforudis*, *Desulfovibrio*, *Desulfosporosinus*, *Desulfitobacterium*, *Desulfotomaculum*, and *Desulfovibrio* (Melton et al., 2017; Nielsen et al., 2006; Sorokin et al., 2013; Vatsurina et al., 2008). Pressure significantly influenced SRB distribution in the leachate saturated zone (Fig. 7). *Desufitibacter* was the main SRB genus, and its abundance accounted for 50%–67% of SRB. *Desufitibacter* had the lowest abundance under the micropressure condition. However, it still accounted for about half of SRB in the leachate saturated zone. The abundance of *Dethiobacter* decreased significantly compared with that in the saturated zone study of surface leachate (Jin et al., 2020a). The correlation between SRB distribution and sulfate reduction factors showed that *Dethiobacter* was positively correlated with the peak occurrence time of H_2S under different pressures (Fig. 8). Although the abundance of *Dethiobacter* decreased, it still contributed to sulfate rates. At 0.6 MPa, the relative abundance of *Dethiobacter* decreased, indicating that it was also poorly adapted to the high-pressure environment.

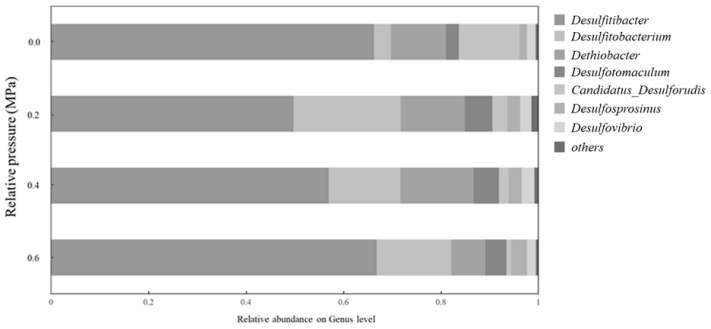

Fig. 7. Microbial community of sulfate-reducing bacteria (SRB) at Genus level.

Previous studies had proven that DsrA and DsrB abundances were positively correlated, and both exist continuously (Geets et al., 2006; Zeleke et al., 2013). The DsrB gene is a commonly used indicator gene. Therefore, this study only analyzed the differences in the DsrB functional gene content under different pressures (Fig. 9). At 0.0 MPa, the DsrB gene abundance reached 1.15×10^7 copies·g^{-1}, 57 times higher than that at 50°C in the shallow saturated zone and even higher than the maximum value at 30°C (4.0×10^6 copies·g^{-1}) (Jin et al., 2020a). However, the highest concentration of H_2S did not appear earlier but was delayed to the 15th day. At 0.2–0.6 MPa, the DsrB gene abundance was less than 4.0×10^6 copies·g^{-1}, indicating that SRB containing DsrB decreased in abundance at high pressures.

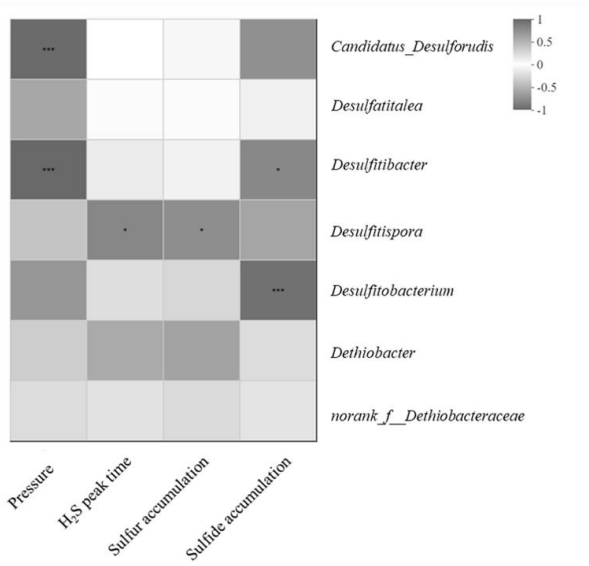

Fig. 8. Correlation analysis of environmental factors and SRB. * and *** denote significant correlation at $P < 0.05$ and $P < 0.001$, respectively (Student's t test); Red and blue respectively indicate the positive and negative correlation between environmental factors and SRB. The darker the color, the higher the correlation.

The abundance of the DsrB gene was negatively correlated with the H_2S release rate, confirming the conclusion in the shallow saturated zone. The direct relationship between the abundance of DsrB related to sulfite and sulfate reduction rates was not obvious. However, DsrA and DsrB were not completely unrelated to the sulfate reduction rate. Studies had shown that within a certain range, the sulfate reduction rate was positively correlated with DsrA abundance; however, when DsrA abundance continues to increase, the sulfate reduction rate did not increase further (Chin et al., 2008). Thus, some other pathway in the saturated zone increased the sulfate reduction rate.

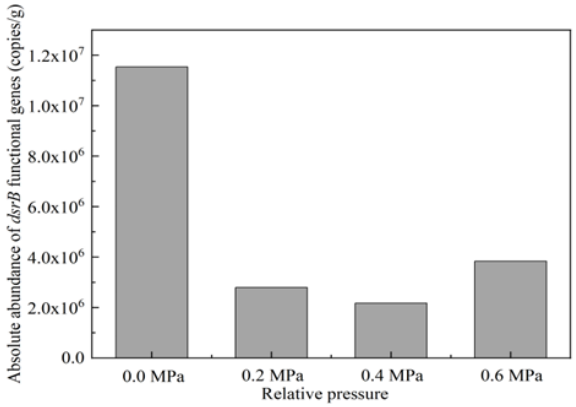

Fig. 9. Quantity DsrB in the samples from reactors under various pressures.

Notably, although the sulfate reduction behavior of the pressure-bearing leachate saturated zone might be performed by various SRB, some key SRB still play a paramount role in rate regulation, and pressure disturbance can change the dominant SRB, significantly affecting its reduction rate. *Dethiobacter* is a key SRB that affects the sulfate reduction rate. *Dethiobacter* can maintain a certain relative abundance in the unpressed and micropressure environments; however, in the high-pressure environments, the abundance of *Dethiobacter* decreased significantly, whereas *Desulfitibacter* had a constant abundance, which may be the main influencing factor.

3. CONCLUSIONS

Sulfate reduction behavior differs with respect to the pressure-bearing condition in a landfill leachate saturated zone. When the relative pressure is 0.0 MPa, the concentration of H_2S decreases rapidly within two days from the peak. In the range of 0.2–0.6 MPa, the highest concentration of H_2S can be further advanced, but its highest value decreases significantly, which may cause persistent odor pollution. The sequencing results of microbial community and functional genes showed that the SRB community structure differed significantly from that of other pressure environments under a relative pressure of 0.0 MPa, whereas the SRB community structure was similar under different pressures of 0.2–0.6 MPa. The content of SRB and the DsrB functional genes of *Dethiobacter* were positively and negatively correlated with the sulfate reduction rate, respectively. Other sulfate reduction processes without DsrA and DsrB enzymes may be the key microorganisms affecting the sulfate reduction rate in the leachate saturated zone. Finally, sulfate reduction behavior in pressure-bearing leachate saturated zone, which is the focus of this study, further indicates the long-term risk of odor contamination in the landfill leachate saturated zone. Therefore, strengthening the management of landfill gas collection and landfill leachate drainage and considering the elevation of landfill may provide some help to the source control of landfill odor pollution.

REFERENCES

Benson, C.H., Edil, T.B., Wang, X., 2012. Evaluation of a final cover slide at a landfill with recirculating leachate. Geotext. Geomembr. 35, 100-106.

Bhattarai, S., Zhang, Y., Lens, P.N.L., 2018. Effect of pressure and temperature on anaerobic methanotrophic activities of a highly enriched ANME-2a community. Environ. Sci. Pollut. Res. Int. 25, 30031-30043.

Cassarini, C., Zhang, Y., Lens, P.N.L., 2019. Pressure selects dominant anaerobic methanotrophic phylotype and sulfate reducing bacteria in coastal marine Lake Grevelingen sediment. Front. Environ. Sci. 6, 162.

Chin, K.J., Sharma, M.L., Russell, L.A., O'Neill, K.R.,

Lovley, D.R., 2008. Quantifying expression of a dissimilatory (bi) sulfite reductase gene in petroleum-contaminated marine harbor sediments. Microb. Ecol. 55, 489-499.
Fang, Y., Zhong, Z., Shen, D., Du, Y., Xu, J., Long, Y., 2016. Endogenous mitigation of H_2S inside of the landfills. Environ. Sci. Pollut. Res. Int. 23, 2505-2512.
Fichtel, K., Logemann, J., Fichtel, J., Rullktter, J., Cypionka, H., Engelen, B., 2015. Temperature and pressure adaptation of a sulfate reducer from the deep subsurface. Front. Microbiol. 6, 1078.
Geets, J., Borremans, B., Diels, L., Springael, D., Vangronsveld, J., van der Lelie, D., Vanbroekhoven, K., 2006. DsrB gene-based DGGE for community and diversity surveys of sulfate-reducing bacteria. J. Microbiol. Methods 66, 194-205.
Giri, R K, Reddy, K R, 2014. Slope stability of bioreactor landfills during leachate injection: Effects of heterogeneous and anisotropic municipal solid waste conditions. Waste Manag. Res. 32, 186-197.
Hu, L.F., Nie, Z.Y., Wang, W.J., Zhang, D.C., Long, Y.Y., Fang, C.R., 2021. Arsenic transformation behavior mediated by arsenic functional genes in landfills. J. Hazard. Mater. 403, 123687.
Huttenhuis, P.J.G., Agrawal, N.J., Versteeg, G.F., 2008. The solubility of hydrogen sulfide in aqueous N-methyldiethanolamine solutions. Int. J. Oil. Gas. Coal. T. 1, 399-424.
Jafari, N.H., Stark, T.D., Thalhamer, T., 2017. Spatial and temporal characteristics of elevated temperatures in municipal solid waste landfills. Waste Manage. 59, 286-301.
Jin, Z., Ci, M., Yang, W., Shen, D., Hu, L., Fang, C., Long, Y., 2020a. Sulfate reduction behavior in the leachate saturated zone of landfill sites. Sci. Total Environ. 730, 138946.
Jin, Z.Y., Zhang, S.Y., Hu, L.F., Fang, C.R., Shen, D.S., Long, Y.Y., 2020b. Effect of substrate sulfur state on MM and DMS emissions in landfill. Waste Manage. 116, 112-119.
Kadambala, R, Townsend, T G, Jain, P, Singh, K, 2011. Temporal and Spatial Pore Water Pressure Distribution Surrounding a Vertical Landfill Leachate Recirculation Well. Int. J. Environ. Res. Public Health 8(5), 1692-1706.
Liu, W.J., Long, Y.Y., Fang, Y., Ying, L.Y., Shen, D.S., 2018. A novel aerobic sulfate reduction process in landfill mineralized refuse. Sci. Total Environ. 637, 174-181.
Long, Y., Fang, Y., Shen, D., Feng, H., Chen, T., 2016. Hydrogen sulfide (H_2S) emission control by aerobic sulfate reduction in landfill. Sci. Rep. 6, 38103.
Long, Y., Zhang, S., Fang, Y., Du, Y., Liu, W., Fang, C., Shen, D., 2017. Dimethyl sulfide emission behavior from landfill site with air and water control. Biodegradation 28, 327-335.
Ma, P., Ke, H., Lan, J., Chen, Y., He, H., 2019. Field measurement of pore pressures and liquid-gas distribution using drilling and ERT in a high food waste content MSW landfill in Guangzhou, China. Eng. Geol. 250, 21-33.
Melton, E.D., Sorokin, D.Y., Overmars, L., Lapidus, A.L., Pillay, M., Ivanova, N., del Rio, T.G., Kyrpides, N.C., Woyke, T., Muyzer, G., 2017. Draft genome sequence of Dethiobacter alkaliphilus strain AHT1(T), a gram-positive sulfidogenic polyextremophile. Stand. Genom. Sci. 12, 57.
Meyer-Dombard, D.R., Bogner, J.E., Malas, J., 2020. A review of landfill microbiology and ecology: A call for modernization with 'next generation' technology. Front. Microbiol. 11, 1127.
Nielsen, M.B., Kjeldsen, K.U., Ingvorsen, K., 2006. Desulfitibacter alkalitolerans gen. nov., sp. nov., an anaerobic, alkalitolerant, sulfite-reducing bacterium isolated from a district heating plant. Int. J. Syst. Evol. Microbiol. 56, 2831-2836.
Sorokin, D.Y., Tourova, T.P., Muyzer, G., 2013. Isolation and characterization of two novel alkalitolerant sulfidogens from a Thiopaq bioreactor, Desulfonatronum alkalitolerans sp nov., and Sulfurospirillum alkalitolerans sp nov. Extremophiles 17, 535-543.
Tupsakhare, S., Moutushi, T., Castaldi, M.J., Barlaz, M.A., Luettich, S., Benson, C.H., 2020. The impact of pressure, moisture and temperature on pyrolysis of municipal solid waste under simulated landfill conditions and relevance to the field data from elevated temperature landfill. Sci. Total Environ. 723, 138031.
Williamson, A.J., Carlson, H.K., Kuehl, J.V., Huang, L.L., Iavarone, A.T., Deutschbauer, A., Coates, J.D., 2018. Dissimilatory sulfate reduction under high pressure by Desulfovibrio alaskensis G20. Front. Microbiol. 9, 1465.
Ying, L.Y., Long, Y.Y., Yao, L.H., Liu, W.J., Hu, L.F., Fang, C.R., Shen, D.S., 2019. Sulfate reduction at micro-aerobic solid-liquid interface in landfill. Sci. Total Environ. 667, 545-551.
Zeleke, J., Sheng, Q., Wang, J.G., Huang, M.Y., Xia, F., Wu, J.H., Quan, Z.X., 2013. Effects of spartina alterniflora invasion on the communities of methanogens and sulfate-reducing bacteria in estuarine marsh sediments. Front. Microbiol. 4, 243.
Zhang, S., Long, Y., Fang, Y., Du, Y., Liu, W., Shen, D., 2017. Effects of aeration and leachate recirculation on methyl mercaptan emissions from landfill. Waste Manage. 68, 337-343.
Zhang, X., Wang, J., Bao, S., Zhang, X., 2021. Impact of internal conditions on the gas flow path in semi-aerobic landfill reactors. Sci. Total Environ. 770, 144673.
Zhang, T, Shi, J Y, Wu, X, Lin, H, Li, X L, 2021. Simulation of gas transport in a landfill with layered new and old municipal solid waste. Sci. Rep. 11(1), 9436.

APPLICATION OF COUPLING PARTIAL NITRIFICATION WITH ANAMMOX IN LANDFILL LEACHATE：A REVIEW

Xueshuang Lu[1, 2], Xiaojie Sun[1, 2*]

1. Guangxi Key Laboratory of Environmental Pollution Control Theory and Technology, Guilin University of Technology, Guilin 541004, China

2. Guangxi Collaborative Innovation Center for Water Pollution Control and Water Safety in Karst Area, Guilin University of Technology, Guilin 541004, China

Abstract: Leachate with high ammonia nitrogen and low carbon to nitrogen ratio (C/N) was produced by waste landfill. Furthermore, nitrogen removal in leachate has been always a hot research area all over the world. The traditional nitrogen removal technology in wastewater has always been occurred the consumption of resources, resulting in the increased cost. However, partial nitrification anammox (PN/A) has been used for removing the nitrogen due to the advantage of organic carbon source and reducing the cost, etc. Although numerous studies claimed nitrogen removal via PN/A process was able to achieve, few studies summarized the application and feasibility analysis of nitrogen removal in leachate by the process. Therefore, the latest research in landfill leachate via PN/A process was explained. Besides, influence factors in PN/A system and how to achieve stable nitrogen removal under inappropriate environment is described in the paper. The review provides a theoretical basis for the PN/A application.

INTRODUCTION

The environmental issue has garnered attention with the high speed of urbanization and industrialization. And the nitrogen removal of wastewater has already become an important problem. The traditional methods of biological nitrogen removal involves aerobic nitrification and anaerobic denitrification (Zanetti et al., 2012). However, the conventional denitrification process has always been drawbacks (Gao et al., 2023). For example, large amounts of aeration and organic carbon sources (methanol etc.) need to be consumed resulting in increased operating costs, etc (Wang et al., 2017). Considering these drawbacks, many researchers have begun to focus on developing the new biological denitrification techniques. The anaerobic ammonium oxidation process (anammox) was first verified (Mulder et al., 1995). Anammox bacteria (AnAOB) converted ammonia nitrogen (NH_4^+-N) into nitrogen (N_2) using NO_2^--N as electron acceptor in an anaerobic or hypoxia environment (Ren et al., 2022). ANAMMOX has gradually attracted the attention of people due to the process with avoiding nearly all carbon source supplementation, less greenhouse gas emission (N_2O) generated (Gonzalez-Martinez et al., 2017), 60% energy savings (Wanget al., 2022) and less sludge production (Z. Guo et al., 2022). It was regarded as an innovative and environmentally friendly process in biological nitrogen removal (Ni et al., 2010). As previously reported, at least over 300 anaerobic ammonia oxidation plants have been put into operation worldwide, and the amount will increase continuously in the future (Kumwimba et al., 2020; Wang et al., 2022).

NO_2^--N as electron acceptor is obtained by other means because it was hardly taken from the general natural water body (Singhet al., 2021). Thus, to obtain stable NO_2^--N is the main goal to reach. In practical applications, partial nitrification (PN) was used in order to get sufficient NO_2^--N, coupled with anammox process

(PN/A) have been applied to remove the biological nitrogen (Wang et al., 2017). PN/A has always been a hot spot in the areas of nitrogen removal of wastewater at the domestic and foreign research (Chen et al., 2021; Yang et al., 2022). PN/A includes two types of processes: the single-stage process of the same reactor and the two-stage process of multiple reactors. The influent NH_4^+-N about 50% under aerobic conditions was oxidized to NO_2^--N by AOB, and AnAOB use NO_2^--N from PN as the terminal electron acceptor to oxidize the remaining NH_4^+-N to N_2 (Kartal et al., 2011). The single-stage process mainly includes aerobic deammonification (DEMON), and the two-stage process mainly include Single reactor High activity Ammonium Removal Over Nitrite (SHARON)-anammox process (Ren et al., 2022). Compared to the conventional nitrogen removal process, PN/A has plenty of advantage, which is no need for organic carbon by 100% due to ammonia-oxidizing bacteria (AOB) and AnAOB belonging to chemoautotrophic (Kosgey et al., 2022), reduce oxygen delivery (Cao et al., 2017) and better nitrogen removal effect (Zhang et al., 2020).

Currently, it is reported that the stable PN/A process have been successfully implemented in various wastewater. The research (Xiao et al., 2021) used a novel two-stage PN/A reactor for wastewater treatment, which was successfully achieved and the nitrogen removal efficiency (NRE) was 92.3%. Another (Wang et al., 2022) investigated the nitrogen removal efficiency (NRE) of the PNA process in SBR could be more than 90%. However, the application in landfill leachate and the encountered difficulty in operating conditions was rarely summarized. Therefore, varieties of factors in PN/A system and the application of landfill leachate are described in the paper. Meanwhile, applicability in others wastewater was also listed. The review provides a theoretical basis for the PN/A application.

INFLUENCE FACTORS

NO_2^--N is an important intermediate for the successful linking of the PN and anammox process. In the PN/A process, NH_4^+-N is oxidized to NO_2^--N by AOB, then NH_4^+-N and NO_2^--N are converted to diatomic nitrogen by AnAOB. The accumulation of NO_2^--N is advantageous for the activity of AnAOB (Gao et al., 2021). However, NOB competes with AnAOB to oxidation NO_2^--N, resulting in decreasing the removal of nitrogen and inhibition proliferation of AnAOB (Di et al., 2022). Therefore, AOB and AnAOB are enrichment and becomes the dominant species, and NOB is washed out in the system, which has been mainly goal and it is necessary to for implementing highly efficient nitrogen removal (Liu et al., 2021). According to previous reports, the activity of bacteria in PN/A process depend on various environmental factors. And dissolved oxygen (DO), pH, temperature, free ammonia (FA) and free nitrite acid (FNA) have been regarded as important parameters. Therefore, it is particularly important to identify the optimum range for microbial and the following is a detailed introduction.

DO

AOB is aerobic bacteria and AnAOB is strictly anaerobic bacteria. The environments of aerobic and anaerobic is usually provided by aeration and is one of the most common strategies. However, compared to continuous aeration, researchers proposed that intermittent aeration was more beneficial to wash out NOB due to NOB had no sufficient O_2 to oxidize NO_2^--N, which contributed to improve the nitrite accumulation efficiency. Therefore, DO as one of the critical parameters have been widely applied for the successful initiation of the PNA process, and it was increasingly regarded as effective for NO_2^--N accumulation. Wiesmann et al. confirmed that DO concentrations >1.8mg/L contributed to the survival of NOB (Wiesmann, 1994). However, previous study documented (Ma et al., 2017) that AOB had significantly sensitivity to low concentration of DO than that of NOB and NOB was easily suppressed, and it was due to the half-saturation constants of AOB less than that of NOB ($K_{AOB}<K_{NOB}$). Tong also found that AOB represented a

significantly larger affinity to DO and had stronger ability of enrichment than that of NOB (Jia et al., 2022). However, in the one-stage PN/A process, the effect of AnAOB by DO was taken into consideration because the survival environment of AOB in the two-stage PN/A system was always under strict anaerobic conditions (Kumwimba et al., 2020). Strauss et al. found that the inhibition of AnAOB activity was reversibly by DO in 1997 (Strous et al., 1997). Therefore, by controlling the DO concentration in one-stage PN/A system have been used to inhibit NOB, it is not only less effect on the activity of AnAOB but assured high-performance nitrogen removal by the cooperation between AOB and AnAOB.

Researchers (Blackburne et al., 2008) controlled the concentration of DO at 0.4mg/L and successfully removed NOB to obtain enrichment of AOB in SHARON. The concentration of DO ranges from 0.2 to 0.4mg/L, the accumulation amount of AOB far greater than NOB, and it is consistent with the above results (Le et al., 2020). However, studies had reported that NOB is more sensitive to oxygen under long-term low DO condition (Liu et al., 2013). The researchers found that species of NOB like Nitrospira can adapt to low DO concentrations (the concentration is generally less than 0.5 mg/L) (Singh et al., 2022). The result was also confirmed in the Singh's experiment when DO concentrations is increased to 0.4-0.5mg/L. (Lei et al., 2021) found that the gene encoding hydroxylamine oxidation was affected because of DO concentrations in the range 0.30-0.43 mg/L, which reduced the activity of AOB. The PN run stably again and the accumulation of NO_2^--N was restored when adjusted to 0.90-1.30mg/L. Although the situation did happen, the research shows that the activity of AnAOB was effected by DO concentrations >0.6mg/L and nitrogen removal is achieved in one-stage system at a DO concentrations 0.2-0.4mg/L (Liu et al., 2017). The presence of NOB did not limit AOB activity when the concentrations of DO was 0.6±0.1mg/L and nitrogen removal was the best under the conditions (Zou et al., 2018). It was illustrated that both AOB and NOB were affected by low DO concentrations but the activity of NOB was not easily recoverable (Li et al., 2011). (Chen et al., 2021) controlled DO concentration at 0.1-0.2 mg/L, and the PNA reaction was able to successfully remove nitrogen at about 70% effective. Based on above, although the data varied from researchers, the PN/A process was stable operation usually under DO concentration < 0.6 mg/L.

FA and FNA

FA and FNA played an important parameter for the accumulation of NO_2^--N, the calculation of FA and FNA concentrations was following by the formula (Qiao et al., 2010). The appropriate concentration of FA and FNA were considered as a inhibited for the activity of NOB to achieve the enrichment of AOB in PN (Gong et al., 2021). As reported in a previous study, FA concentration had an inhibitory impact on the activity of AOB and NOB in ranges of 10-150 mg/L and 0.1-1.0 mg/L, respectively, whereas FNA concentration ranged from 0.2 to 2.8 mg/l had an inhibitory impact on the activity of NOB (Anthonisenet al., 1976). (Vadiveluet al., 2007) proposed that the activity of NOB could be completely inhibited when the concentrations of FA and FNA were 6 mg/L and 0.02 mg/L respectively. The result was evidenced, along with the operation of A/O reactor, the final concentrations of FA and FNA were 1.23 mg/L and 0.095 mg/L respectively, which achieved the accumulation of NO_2^--N and stable PN process (Wang et al., 2016).

However, some researchers proposed that the activity of NOB under above conditions could not be completely inhibited due to NOB in the long-term operation acclimated to the changes of FA and FNA, resulting in NOB still existed in the system (Villaverde, et al., 2000). The similar situation was found and demonstrated in Bin et al. research (Ma et al., 2017). Thus, the adaptive capacity of NOB in PN/A system become the crucial issue. Some approaches have been investigated to overcome the adaptive ability of NOB to provide sufficient NO_2^--N for anammox process. An effective strategy was applied to suppress the activity of

NOB, which was adopted by FNA shock sludge led to several communities of NOB was unable to acclimate and wash out in the system (D. Wang et al., 2016). Similar thought have been adopted in PN/A reactor, the sludge was respectively treated by FA and FNA (four hours in a week) which the stable PN/A process was obtained (Peng et al., 2020). Although several studies showed NOB suppression by return sludge was capable of occurring under FA and FNA, few studies have been conducted to reach a sufficient amount of NO_2^--N. Therefore, it is still needed to find the optimum approach by experimental exploration.

Temperature

Temperature had also a great influence on microbial activity. According to an Arrhenius-type equation (Hao et al., 2002), the risk of inactive for bacteria was increased due to high temperature but low temperature will inhibit activity. The adaptability and the maximum relative generation rate of AOB was stronger than that of NOB at elevated temperature, and the optimum temperature of AOB was approximately between 30 and 40 ℃ (Hellinga et al., 1998). Besides, the suitable temperature for the growth of AnAOB growth has been documented from 30 to 35 ℃ and it have a strong sensitivity to the temperature descending condition (Jetten et al., 2001). (Balmelle et al., 1992) found that the maximum accumulation of NO_2^--N was obtained at temperature 35℃. Previous studies have shown that the conversion rate of NH_4^+-N to NO_2^--N in PN process was successfully 81% at the temperature 37 ℃ (Cho et al., 2011). Wiśniewska et al. (Banachet al., 2021) confirmed that the NRE reached 80% in anammox process when temperature was maintained at 30 ℃. By controlling the temperature at 32-35℃ in stage 1 and 2, the NRE could achieve 94.5%, in contrast, the NRE in stage 3 was declining at temperature decreasing from 35 to 24℃ (Leet al., 2022). (Isanta et al., 2015) showed that the efficient of nitrogen removal had significantly decreased with increased temperature (from 35 to 46℃). Therefore, the data showed that the stable PN/A process and increased the efficiency of nitrogen removal are achievement under the optimum temperature between 30 and 35 ℃.

Nevertheless, the fluctuation in the seasonal temperature has an effect on the PN/A process and it is an obstacle hindering the efficiency of nitrogen removal, resulting in the microorganisms of PN/A system vulnerable. (Wanget al., 2014) also recorded the activity of microbial community structure and the NRE decreased as temperature drops. When temperature decreased from 22.2℃ to 15℃, the decrease of NRR from the initial to the end was observed (Gong et al., 2020), which was consistent with the above finding. To address the mainly bottleneck at low temperature, controlling the nitrogen load (NLR) by adjusting the concentration of NH_4^+-N in the PN/A system was proposed to reach the increased efficiency of nitrogen removal, and the NRE achieved more than 96% in Li's study when the temperatures at 13±2℃ (Liet al., 2021). (Li et al., 2022) proposed carrier biofilms under the temperature changes from 29.1℃ to 16.3℃ was inoculated in the PN system to apply for treating low C/N sewage, and the result showed that the PN/A process was relatively stable and the NRE was maintain about 80%. (Ishimotoet al., 2021) proposed that the stable PN/A system was implemented in treating swine wastewater by controlling anammox granules to acclimate low temperature.

RESEARCH APPLICATION

Landfill leachate

Leachate with high ammonia nitrogen and low carbon to nitrogen ratio (C/N) was produced by waste landfill (Wanget al., 2022). Leachate has a complex composition and can have an impact on the environment (Qiuet al., 2022). The C/N of leachate will lead to increased treatment costs (Gabarró et al., 2012; Renouet al., 2008). And the problem of nitrogen removal from leachate in landfills has become the focus of work. The PN/A is attracting attention for its ability to solve the

problem of increased operating costs due to low C/N in the treatment of waste leachate, and the process is highly effective in nitrogen removal of leachate (Nhatet al., 2014). (Wu et al., 2020) studied the PNA treatment of leachate at low temperatures. Nitrogen removal was successfully achieved by a combination of four processes (UASB-A/O-ANAOR-ASBR). The removal rate of NH_4^+-N is more than 97%, and the removal rate of TN is about 94%. (Yan et al., 2022) used a fictional method to treat mature waste leachate. Ozone pretreatment is first applied to mature waste leachate, and granular sludge is used in a two-stage system of the PN/A process. The PN process can occur without controlling the exact amount of dissolved oxygen (DO) in the study. It also provides a new idea for future research work on PN/A. (Jiang et al., 2020) introduced aerobic biofilm combined with PNA. The reactor had the best effect on mature leachate treatment when the DO concentration was around 4.03mg/L by constantly adjusting. Compared with the traditional PNA process, the highest NRE was 96.7% in the reactor with biofilm. (Wang et al., 2022) designed a novel gas-rising reactor. An integrated PNA reaction is implemented in a new reactor to treat waste leachate. The reactor received a fast start-up and NRR was 1.54 kg $N/m^3 \cdot d$.

Other sewage

(Wanget al., 2017) used a medium-scale PN/A reactor to treat sludge digestate. The PN process was started up because of the effectively controlled concentration of FA and FNA by adjusting the environmental factors. The process provided a stable substrate for anammox. Eventually, the PN/A reactor was in stable operation and NRR was 1.23 kg $N/m^3/d$ at 148 days. (Silveiraet al., 2021) addressed the nitrogen removal in slaughterhouse wastewater by combining suspended biomass reactors and settling tanks for PN and Upflow Anaerobic Sludge Blanket (UASB) reactors for anammox. The COD/N was maintained at 0.4-0.6 mg COD/N. throughout the experiment. Studies have shown that PNA can successfully solve slaughterhouse wastewater and the NRE ranged from 74.4% to 94%. (Lin et al., 2020) applied the PNA process to artificial wetlands to achieve the nitrogen removal of low ammonium wastewater. The optimal idle time and reaction time of the PN reactor were found to be 7.5 h and 16 h through trial. The ratio of nitrite to ammonia nitrogen in the effluent is close to the theoretical value of 1.32. (Daverey et al., 2013) added nitrite total auto-nitrification (CANON) to SBR to achieve an integrated PNA process for treating wastewater in the photovoltaic industry. By adjusting the NLR and HRT, the reactor was able to achieve 89% and 98% removal of TN and NH_4^+-N, respectively. (Y. Guo et al., 2022) studied the PNA process to treat anaerobic membrane bioreactor filtrate under low temperature conditions, and was eventually able to perform denitrification as well.

CONCLUTION

Compared with the traditional technology, the advantage in PNA process is obvious, which has been used for full-scale application in the treatment of landfill leachate and other wastewater. At present, Combination of PN/A process and technology has attracted many researches to remove nitrogen in wastewater due to the high nitrogen removal efficiency. However, the accumulation of nitrite has been a problem. Furthermore, AnAOB was also a bottleneck because of hard to remain stable. Therefore, how to enhance the stability of PNA in nitrogen removal under the above difficulties is still priority and need more experimental exploration to find appropriate strategy.

ACKNOWLEDGEMENTS

This work was financially supported by Guangxi innovation research team project (2018GXNSFGA281001) and Guangxi major science and technology projects (GuikeAA18118013).

References:

Anthonisen, A. C., Loehr, R. C., Prakasam, T., & Srinath, E. G. (1976). Inhibition of nitrification by ammonia and nitrous acid. Journal (Water Pollution Control Federation), 835-852

Balmelle, B., Nguyen, K. M., Capdeville, B., Cornier, J. C., & Deguin, A. (1992). Study of factors controlling nitrite build-up in biological processes for water nitrification. Water Science and Technology, 26(5-6), 1017-1025

Banach-Wiśniewska, A., Ćwiertniewicz-Wojciechowska, M., & Ziembińska-Buczyńska, A. (2021). Effect of temperature shifts and anammox biomass immobilization on sequencing batch reactor performance and bacterial genes abundance. International Journal of Environmental Science and Technology, 18(7), 1719-1730

Blackburne, R., Yuan, Z., & Keller, J. (2008). Partial nitrification to nitrite using low dissolved oxygen concentration as the main selection factor. Biodegradation, 19(2), 303-312

Cao, Y., van Loosdrecht, M., & Daigger, G. T. (2017). Mainstream partial nitritation–anammox in municipal wastewater treatment: status, bottlenecks, and further studies. Applied microbiology and biotechnology, 101(4), 1365-1383

Chen, H., Wang, H., Chen, R., Chang, S., Yao, Y., Jiang, C.,... Li, Y. (2021). Unveiling performance stability and its recovery mechanisms of one-stage partial nitritation-anammox process with airlift enhanced micro-granules. Bioresource Technology, 330, 124961.

Chen, H., Wang, H., Yu, G., Xiong, Y., Wu, H., Yang, M.,... Li, Y. (2021). Key factors governing the performance and microbial community of one-stage partial nitritation and anammox system with bio-carriers and airlift circulation. Bioresource Technology, 324, 124668.

Cho, S., Fujii, N., Lee, T., & Okabe, S. (2011). Development of a simultaneous partial nitrification and anaerobic ammonia oxidation process in a single reactor. Bioresource Technology, 102(2), 652-659.

Daverey, A., Su, S., Huang, Y., Chen, S., Sung, S.,... Lin, J. (2013). Partial nitrification and anammox process: A method for high strength optoelectronic industrial wastewater treatment. Water Research, 47(9), 2929-2937.

Di Capua, F., Iannacone, F., Sabba, F., & Esposito, G. (2022). Simultaneous nitrification–denitrification in biofilm systems for wastewater treatment: Key factors, potential routes, and engineered applications. Bioresource Technology, 361, 127702.

Gabarró, J., Ganigué, R., Gich, F., Ruscalleda, M., Balaguer, M. D.,... Colprim, J. (2012). Effect of temperature on AOB activity of a partial nitritation SBR treating landfill leachate with extremely high nitrogen concentration. Bioresource technology, 126, 283-289

Gao, R., Peng, Y., Li, J., Zhang, Q., Li, X., Deng, L.,... Kao, C. (2021). Improving performance and efficiency of partial anammox by coupling partial nitrification and partial denitrification (PN/A-PD/A) to treat municipal sewage in a step-feed reactor. Bioresource Technology, 341, 125804.

Gao, X., Zhang, L., Peng, Y., Ding, J., & An, Z. (2023). The successful integration of anammox to enhance the operational stability and nitrogen removal efficiency during municipal wastewater treatment. Chemical Engineering Journal, 451, 138878.

Gong, Q., Wang, B., Gong, X., Liu, X., & Peng, Y. (2021). Anammox bacteria enrich naturally in suspended sludge system during partial nitrification of domestic sewage and contribute to nitrogen removal. Science of The Total Environment, 787, 147658.

Gong, X., Wang, B., Qiao, X., Gong, Q., Liu, X.,... Peng, Y. (2020). Performance of the anammox process treating low-strength municipal wastewater under low temperatures: Effect of undulating seasonal temperature variation. Bioresource Technology, 312, 123590.

Gonzalez-Martinez, A., Muñoz-Palazon, B., Rodriguez-

Sanchez, A., & Gonzalez-Lopez, J. (2018). New concepts in anammox processes for wastewater nitrogen removal: recent advances and future prospects. FEMS microbiology letters, 365(6), y31

Guo, Y., Sanjaya, E. H., Rong, C., Wang, T., Luo, Z., Chen, H.,... Li, Y. (2022). Treating the filtrate of mainstream anaerobic membrane bioreactor with the pilot-scale sludge-type one-stage partial nitritation/anammox process operated from 25 to 15 °C. Bioresource Technology, 351, 127062.

Guo, Z., Ahmad, H. A., Tian, Y., Zhao, Q., Zeng, M., Wu, N.,... Ni, S. (2022). Extensive data analysis and kinetic modelling of dosage and temperature dependent role of graphene oxides on anammox. Chemosphere, 308, 136307.

Hao, X., Heijnen, J. J., & Van Loosdrecht, M. C. M. (2002). Model-based evaluation of temperature and inflow variations on a partial nitrification–ANAMMOX biofilm process. Water Research, 36(19), 4839-4849.

Hellinga, C., Schellen, A. A. J. C., Mulder, J. W., van Loosdrecht, M. C. M., & Heijnen, J. J. (1998). The sharon process: An innovative method for nitrogen removal from ammonium-rich waste water. Water Science and Technology, 37(9), 135-142.

Isanta, E., Bezerra, T., Fernández, I., Suárez-Ojeda, M. E., Pérez, J.,... Carrera, J. (2015). Microbial community shifts on an anammox reactor after a temperature shock using 454-pyrosequencing analysis. Bioresource Technology, 181, 207-213

Ishimoto, C., Waki, M., & Soda, S. (2021). Adaptation of anammox granules in swine wastewater treatment to low temperatures at a full-scale simultaneous partial nitrification, anammox, and denitrification plant. Chemosphere, 282, 131027.

Jetten, M. S., Wagner, M., Fuerst, J., van Loosdrecht, M., Kuenen, G.,... Strous, M. (2001). Microbiology and application of the anaerobic ammonium oxidation ('anammox') process. Current opinion in biotechnology, 12(3), 283-288

Jia, T., Li, X., Jiang, H., Dan, Q., Sui, J., Wang, S.,... Peng, Y. (2022). Advanced nitrogen removal from municipal sewage via partial nitrification-anammox process under two typical operation modes and seasonal ambient temperatures. Bioresource Technology, 363, 127864.

Jiang, H., Peng, Y., Li, X., Zhang, F., Wang, Z.,... Ren, S. (2020). Advanced nitrogen removal from mature landfill leachate via partial nitrification-Anammox biofilm reactor (PNABR) driven by high dissolved oxygen (DO): Protection mechanism of aerobic biofilm. Bioresource Technology, 306, 123119.

Kartal, B., Maalcke, W. J., De Almeida, N. M., Cirpus, I., Gloerich, J., Geerts, W.,... Francoijs, K. (2011). Molecular mechanism of anaerobic ammonium oxidation. Nature, 479(7371), 127-130

Kosgey, K., Zungu, P. V., Kumari, S., & Bux, F. (2022). Critical review of process control strategies in anammox-mediated nitrogen removal systems. Journal of Environmental Chemical Engineering, 10(4), 108068.

Kumwimba, M. N., Lotti, T., Şenel, E., Li, X., & Suanon, F. (2020). Anammox-based processes: How far have we come and what work remains? A review by bibliometric analysis. Chemosphere, 238, 124627

Le, L., Jeon, J., Dang, B., Bui, X., & Jahng, D. (2022). Influence of temperature on anammox reaction and microbial diversity in a bio-carriers reactor under mainstream conditions. Environmental Technology & Innovation, 25, 102178.

Le, L., Lee, S., Bui, X., & Jahng, D. (2020). Suppression of nitrite-oxidizing bacteria under the combined conditions of high free ammonia and low dissolved oxygen concentrations for mainstream partial nitritation. Environmental Technology & Innovation, 20, 101135.

Lei, Z., Wang, L., Wang, J., Yang, S., Hou, Z., Wang, X. C.,... Chen, R. (2021). Partial-nitritation of low-strength anaerobic effluent: A moderate-high dissolved oxygen concentration facilitates ammonia-oxidizing bacteria disinhibition and nitrite-oxidizing bacteria suppression. Science of The Total Environment, 770, 145337.

Li, H., & Tao, W. (2017). Efficient ammonia removal in recirculating vertical flow constructed wetlands: complementary roles of anammox and denitrification in simultaneous nitritation, anammox and denitrification process. Chemical Engineering Journal, 317, 972-979

Li, J., Li, J., Wang, B., Wang, Z., Li, X., Wang, S.,... Peng, Y. (2022). Stable enhanced nitrogen removal from low COD/N municipal wastewater via partial nitrification-anammox in the traditional continuous anoxic/oxic process through bio-augmentation of partial nitrification sludge under decreasing temperatures. Bioresource Technology, 363, 127953.

Li, X., Lu, M., Huang, Y., Yuan, Y., & Yuan, Y. (2021). Influence of seasonal temperature change on autotrophic nitrogen removal for mature landfill leachate treatment with high-ammonia by partial nitrification-Anammox process. Journal of Environmental Sciences, 102, 291-300.

Lin, Z., Xu, F., Wang, Y., Huang, W., Zhou, J., He, Q.,... Zhou, J. (2020). Autotrophic nitrogen removal by partial nitrification-anammox process in two-stage sequencing batch constructed wetlands for low-strength ammonium wastewater. Journal of Water Process Engineering, 38, 101625.

Liu, G., & Wang, J. (2013). Long-term low DO enriches and shifts nitrifier community in activated sludge. Environmental science & technology, 47(10), 5109-5117

Liu, T., Jia, G., Xu, J., He, X., & Quan, X. (2021). Simultaneous nitrification and denitrification in continuous flow MBBR with novel surface-modified carriers. Environmental Technology, 42(23), 3607-3617

Liu, T., Ma, B., Chen, X., Ni, B., Peng, Y.,... Guo, J. (2017). Evaluation of mainstream nitrogen removal by simultaneous partial nitrification, anammox and denitrification (SNAD) process in a granule-based reactor. Chemical Engineering Journal, 327, 973-981.

Ma, B., Yang, L., Wang, Q., Yuan, Z., Wang, Y.,... Peng, Y. (2017). Inactivation and adaptation of ammonia-oxidizing bacteria and nitrite-oxidizing bacteria when exposed to free nitrous acid. Bioresource technology, 245, 1266-1270

Ma, W., Han, Y., Ma, W., Han, H., Zhu, H., Xu, C.,... Wang, D. (2017). Enhanced nitrogen removal from coal gasification wastewater by simultaneous nitrification and denitrification (SND) in an oxygen-limited aeration sequencing batch biofilm reactor. Bioresource Technology, 244, 84-91.

Mulder, A., van de Graaf, A. A., Robertson, L. A., & Kuenen, J. G. (1995). Anaerobic ammonium oxidation discovered in a denitrifying fluidized bed reactor. FEMS Microbiology Ecology, 16(3), 177-183.

Nhat, P. T., Biec, H. N., Tuyet Mai, N. T., Thanh, B. X., & Dan, N. P. (2014). Application of a partial nitritation and anammox system for the old landfill leachate treatment. International Biodeterioration & Biodegradation, 95, 144-150.

Ni, S., Lee, P., & Sung, S. (2010). The kinetics of nitrogen removal and biogas production in an anammox non-woven membrane reactor. Bioresource technology, 101(15), 5767-5773

Peng, L., Xie, Y., Van Beeck, W., Zhu, W., Van Tendeloo, M., Tytgat, T.,... Vlaeminck, S. E. (2020). Return-sludge treatment with endogenous free nitrous acid limits nitrate production and N2O emission for mainstream partial nitritation/Anammox. Environmental Science & Technology, 54(9), 5822-5831

Qiao, S., Matsumoto, N., Shinohara, T., Nishiyama, T., Fujii, T., Bhatti, Z.,... Furukawa, K. (2010). High-rate partial nitrification performance of high ammonium containing wastewater under low temperatures. Bioresource Technology, 101(1), 111-117.

Qiu, J., Li, X., Peng, Y., & Jiang, H. (2022). Advanced nitrogen removal from landfill leachate via a two-stage combined process of partial nitrification-Anammox (PNA) and partial denitrification-Anammox (PDA). Science of The Total

Environment, 810, 151186.

Ren, Z., Wang, H., Zhang, L., Du, X., Huang, B.,... Jin, R. (2022). A review of anammox-based nitrogen removal technology: From microbial diversity to engineering applications. Bioresource Technology, 363, 127896.

Silveira, N. C., Oliveira, G. H. D., Damianovic, M. H. R. Z., & Foresti, E. (2021). Two-stage partial nitrification-Anammox process for nitrogen removal from slaughterhouse wastewater: Evaluation of the nitrogen loading rate and microbial community analysis. Journal of Environmental Management, 296, 113214.

Singh, V., Ormeci, B., Mishra, S., & Hussain, A. (2021). Simultaneous partial Nitrification, ANAMMOX and denitrification (SNAD)–A review of critical operating parameters and reactor configurations. Chemical Engineering Journal, 133677

Singh, V., Ormeci, B., Mishra, S., & Hussain, A. (2022). Simultaneous partial Nitrification, ANAMMOX and denitrification (SNAD) – A review of critical operating parameters and reactor configurations. Chemical Engineering Journal, 433, 133677.

Villaverde, S., Fdz-Polanco, F., & Garcıa, P. A. (2000). Nitrifying biofilm acclimation to free ammonia in submerged biofilters. Start-up influence. Water Research, 34(2), 602-610

Wang, D., Wang, Q., Laloo, A., Xu, Y., Bond, P. L.,... Yuan, Z. (2016). Achieving stable nitritation for mainstream deammonification by combining free nitrous acid-based sludge treatment and oxygen limitation. Scientific reports, 6(1), 1-10

Wang, F., Jin, X., Yang, S., Liu, Y., & Chen, X. (2014). A control strategy for promoting the stability of denitrifying granular sludge in upflow sludge blankets. Environmental technology, 35(1), 52-59

Wang, G., Xu, X., Zhou, L., Wang, C., & Yang, F. (2017). A pilot-scale study on the start-up of partial nitrification-anammox process for anaerobic sludge digester liquor treatment. Bioresource Technology, 241, 181-189.

Wang, H., Dan, Q., Du, R., Li, J., Wang, S., Li, X.,... Peng, Y. (2022). Enhanced nitrogen removal in partial nitrification-anammox (PNA) suspended sludge system for real municipal wastewater treatment at extremely low carbon to nitrogen ratio. Chemical Engineering Journal, 139256.

Wang, J., Liang, J., Ning, D., Zhang, T., & Wang, M. (2022). A review of biomass immobilization in anammox and partial nitrification/anammox systems: Advances, issues, and future perspectives. Science of The Total Environment, 821, 152792. doi: https://doi.org/10.1016/j.scitotenv.2021.152792

Wang, S., Teng, Z., Li, Y., Chen, F., Liu, X., Liu, S.,... Wang, W. (2022). A novel vertical dual-loop limited oxygen reactor for rapid start-up of simultaneous partial nitritation and anammox process: Performances and mechanisms of efficient nitrogen removal from landfill leachate. Bioresource Technology, 127947.

Wang, Y., Wang, D., Yang, Q., Zeng, G., & Li, X. (2017). Wastewater Opportunities for Denitrifying Anaerobic Methane Oxidation. Trends in Biotechnology, 35(9), 799-802.

Wang, Y., Zhang, R., Lei, Y., & Song, L. (2022). Antibiotic resistance genes in landfill leachates from seven municipal solid waste landfills: Seasonal variations, hosts, and risk assessment. Science of The Total Environment, 853, 158677.

Wang, Z., Liu, X., Ni, S., Zhang, J., Zhang, X., Ahmad, H. A.,... Gao, B. (2017). Weak magnetic field: A powerful strategy to enhance partial nitrification. Water Research, 120, 190-198.

Wang, Z., Peng, Y., Miao, L., Cao, T., Zhang, F., Wang, S.,... Han, J. (2016). Continuous-flow combined process of nitritation and ANAMMOX for treatment of landfill leachate. Bioresource Technology, 214, 514-519.

Wang, Z., Zheng, M., Duan, H., Yuan, Z., & Hu, S. (2022). A 20-Year Journey of Partial Nitritation and Anammox (PN/A): from Sidestream toward Mainstream. Environmental Science & Technology

Wiesmann, U. (1994). Biological nitrogen removal from wastewater. Biotechnics/wastewater, 113-154

Wu, L., Yan, Z., Huang, S., Li, J., Su, B., Wang, C.,... Peng, Y. (2020). Rapid start-up and stable maintenance of partial nitrification–anaerobic ammonium oxidation treatment of landfill leachate at low temperatures. Environmental Research, 191, 110131.

Xiao, H., Peng, Y., Zhang, Q., & Liu, Y. (2021). Pre-anaerobic treatment enhanced partial nitrification start-up coupled with anammox for advanced nitrogen removal from low C/N domestic wastewater. Bioresource Technology, 337, 125434.

Yan, Z., Li, A., Shim, H., Wang, D., Cheng, S., Wang, Y.,... Li, M. (2022). Effect of ozone pretreatment on biogranulation with partial nitritation - Anammox two stages for nitrogen removal from mature landfill leachate. Journal of Environmental Management, 317, 115470.

Yang, E., Chen, J., Jiang, Z., Deng, Z., Tu, Z., Wang, H.,... Chen, H. (2022). Insights into rapidly recovering the autotrophic nitrogen removal performance of single-stage partial nitritation-anammox systems: Reconstructing granular sludge and its functional microbes synergy. Bioresource Technology, 361, 127750.

Zanetti, L., Frison, N., Nota, E., Tomizioli, M., Bolzonella, D.,... Fatone, F. (2012). Progress in real-time control applied to biological nitrogen removal from wastewater. A short-review. Desalination, 286, 1-7.

Zhang, D., Wang, G., & Dai, X. (2020). Operation of pilot-scale nitrification-anammox reactors for the treatment of reject-water produced from the anaerobic digestion of thermal hydrolysis-treated sludge. Bioresource Technology, 314, 123717.

REMOVAL EFFICIENCY AND MECHANSIM OF REFRACTORY ORGANIC MATTER FROM LANDFILL LEACHATE MBR EFFLUENT BY THE MoS_2-RNHANCEG Fe^0/H_2O_2 SYSTEM

Jing Yang1, Xiaoqin Zhang2, Jia Tang3, Jinlan Li4, Aiping Zhang*
College of Chemistry and Materials Science, Sichuan Normal University, Chengdu 610066, China

ABSTRACT

In this study, molybdenum disulfide (MoS_2) was used to enhance a zero-valent iron/hydrogen peroxide (Fe^0/H_2O_2) Fenton-like system, which was able to remove refractory organic matter from the effluent produced during the treatment of landfill leachate by a membrane bioreactor (MBR). The $MoS_2/Fe^0/H_2O_2$ system could efficiently remove refractory organic matter (i.e., fulvic acid-like substances and humic-like substances) from the MBR effluent and also exhibited a strong synergistic effect. Under the conditions of initial pH=3, H_2O_2=40 mmol/L, Fe^0=0.4 g/L, MoS_2=0.1 g/L, and t=30 min, compared with a Fe^0/H_2O_2 system, the absorbance UV_{254}, chroma (CN), and total organic carbon (TOC) removal rates in MBR effluent treated with $MoS_2/Fe^0/H_2O_2$ increased to 48.68%, 63.85%, and 35.85%, respectively. Through the identification of reactive oxygen species (ROS), the hydroxyl radical ($HO^{\bullet}$) concentration and an analysis of the effective utilization rate of H_2O_2, as well as an analysis of the morphology of the material, the distribution of Fe compounds, valence changes, and the Fe ion concentration, it was proven that MoS_2 promoted the cycling of Fe^{3+}/Fe^{2+} in the Fe^0/H_2O_2 process. The addition of MoS_2 promoted the Fe^{3+}/Fe^{2+} cycling reaction through the exposed Mo^{4+} active center, significantly promoting the decomposition of H_2O_2 and the formation of $HO^{\bullet}$. The $MoS_2/Fe^0/H_2O_2$ system was able to remove a wide range of aromatic organics, indicating the wide applicability of the system. This study developed a new method for the efficient removal of refractory organic matter from landfill leachate.

1 TNTRODUCTION

In recent years, with the rapid development of China's economy and the continuous improvement of living standards, the production of urban household waste has grown. According to the *China Statistical Yearbook,* the total output of urban domestic waste in 2020 was 235 million tons. To satisfy the growing need for waste disposal, the number of landfills and incineration plants has increased in recent years. However, a large amount of secondary effluent, i.e., landfill leachate, will inevitably be produced in the treatment of sanitary landfill or incineration effluent. Landfill leachate is a special wastewater that is extremely difficult to treat. It usually contains high concentrations of refractory organic matter, ammonia nitrogen, inorganic salts, and heavy metal ions. With the prolongation of landfill life and the stabilization of municipal solid waste (MSW), the molecular composition of organic matter in landfill leachate will become more complex, and its chemical structure will stabilize, inhibiting biodegradation. If landfill leachate is discharged without strict treatment, it will cause considerable pollution to the surrounding environment.

In practical applications, due to the low cost of biological treatment technologies, a biological treatment is usually applied to remove most of the organic matter in landfill leachate. However, further treatment methods are required to fully treat the biologically treated leachate and satisfy the strict discharge requirements. Currently, the most commonly used treatment methods include multistage membrane treatment, advanced oxidation processes (AOPs), and other combined systems.

The application of membrane treatment to landfill leachate can produce wastewater that satisfies discharge requirements, but this technology is controversial because of the other issues it raises (e.g., membrane contamination and production of leachate concentrate).

Advanced oxidation processes are chemical oxidation methods that use reactive oxygen species (ROS) with a high redox potential to degrade and even mineralize organic matter.

In recent years, zero-valent iron (Fe^0) has attracted much attention as an environmentally sustainable and cost-effective material for the removal of various environmental pollutants, especially as a promising alternative source of the Fe^{2+} activator in heterogeneous Fenton reactions. Thus, a zero-valent iron-hydrogen peroxide combined system (Fe^0/H_2O_2) has been developed as a Fenton-like system for treating organic wastewater. Under acidic conditions, Fe^{2+} can be gradually released from Fe0 (Eq. (1)) to activate H_2O_2. In addition, Fe0 can be oxidized by H_2O_2 to produce Fe^{2+}; thus, contributing to the degradation of organic matter. In addition, iron (hydrogen) oxides generated on the surface of Fe^0 can also heterogeneously activate H_2O_2, further promoting the degradation of organic matter.

$$Fe^0+2H^+\rightarrow Fe^{2+}+H_2 \quad (1)$$

$$Fe^0+H_2O_2\rightarrow Fe^{2+}+2OH^- \quad (2)$$

$$Fe^{2+}+H_2O_2\rightarrow Fe^{3+}+HO^{\bullet}+OH^-,\ k1=76\ M^{-1}s^{-1} \quad (3)$$

$$Fe^{3+}+H_2O_2\rightarrow Fe^{2+}+HO^{\bullet}{}_2+H^+,\ k2=0.02\ M^{-1}s^{-1} \quad (4)$$

$$Fe^{3+}+HO^{\bullet}{}_2\rightarrow Fe^{2+}+O_2+H^+,\ k3=2\times10^{-3}\ M^{-1}s^{-1} \quad (5)$$

The rate-limiting step of Eq. (4) determines the overall efficiency of the reaction. Even under the action of the activator, the efficiency of this reaction is still very low, requiring excessive amounts of H_2O_2 and activator, which makes the large-scale application of AOPs uneconomical in wastewater treatment. In addition, the activity of the Fe^0 activator is affected by the formation of a passivation layer of iron oxide on the surface, and the Fe^{2+}/Fe^{3+} cycle reaction (Eq. (4) and (5)) is not fast enough, which greatly reduces the removal efficiency of Fe^0/H_2O_2 systems for landfill leachate treatment. There is an urgent need to improve this system to overcome the inefficient conversion between Fe^{2+} and Fe^{3+} ions.

Promoting the Fe^{3+}/Fe^{2+} redox cycle has the potential for further developing AOPs, and studies of AOPs in this field have focused on the use of organic acids as Fe chelators to complex Fe^{3+} and provide electrons to promote the Fe^{3+}/Fe^{2+} redox cycle. However, the above methods can also cause secondary pollution and make it difficult to completely mineralize organic molecules.

It has been proven that metal sulfides (molybdenum disulfide (MoS_2), tungsten disulfide (WS_2, etc.) are excellent materials for improving the efficiency of H_2O_2 decomposition and will significantly reduce the amount of H_2O_2 and Fe^{2+} needed. According to previous studies, the surface of MoS_2 contains unsaturated S atoms, and will capture protons to form H_2S; thus, exposing the reductive metal active center Mo^{4+} to promote the rate-limiting reaction of the Fe^{3+}/Fe^{2+} redox cycle and the formation of Mo^{6+}. After the Fenton reaction, Mo^{6+} is further reduced to Mo^{4+} with the help of H_2O_2, ensuring the cycling of MoS_2 (Eq. (6) and (7)).

$$Mo^{4+}+2Fe^{3+}\rightarrow Mo^{6+}+2Fe^{2+} \quad (6)$$

$$Mo^{6+}+2H_2O_2\rightarrow Mo^{4+}+2O^{\bullet-}{}_2+4H^+ \quad (7)$$

Using an Fe^0/H_2O_2 system, in this study MoS_2 was applied as an additive to degrade the effluent produced during the treatment of landfill leachate by a membrane bioreactor (MBR). The aims of the study were: (1) to study the synergistic effect of the $MoS_2/Fe^0/H_2O_2$ system for the removal of MBR effluent; (2) to study the effect of important factors controlling the degradation of MBR effluent; (3) to propose a possible degradation pathway of organic matter in the $MoS_2/Fe^0/H_2O_2$ process and identify the mechanism by which MoS_2 is enhanced in a heterogeneous Fenton reaction.

2 MATERIALS AND METHODS

2.1 The MBR effluent used in the experiment

The leachate samples used in this study were collected from the MBR effluent of a large anaerobic landfill located in southwest China. The landfill was built in 1992 and had been in operation for 28 years at the time of sampling. The leachate was yellow–brown with no obvious odor, pH=8.27, total organic carbon (TOC)=189.70 mg/L, absorbance (UV_{254})=5.69 cm^{-1}, and chroma (CN)=0.3577. After the leachate was collected in a 25 L blue polyethylene plastic bucket, it was immediately sealed and stored in a cool dry place in the laboratory away from light.

3.RESULTS AND DISCUSSION

3.1 The performance of the $MoS_2/Fe^0/H_2O_2$ system

To investigate the effectiveness of the $MoS_2/Fe^0/H_2O_2$ system on refractory organic matter in MBR effluent, the removal effect, and the structure and humus content of refractory organic matter in MBR effluent treated by different systems (Fe^0 alone, H_2O_2

alone, MoS_2 alone, H_2O_2/MoS_2, MoS_2/Fe^0, and Fe^0/H_2O_2) were compared in controlled experiments.

3.1.1: Removal rate of refractory organic matter

As shown in Fig. 1(a), when pH=3 and the reaction time was 30 min, the leachate was hardly degraded under the conditions of Fe^0 alone, H_2O_2 alone, and MoS_2 alone. The decolorization rates of the MBR effluent in the MoS_2 alone, H_2O_2/MoS_2, and Fe^0/MoS_2 systems were 30.60%, 21.04%, and 21.74%, respectively. This may be related to the adsorption of MoS_2, mainly due to the van der Waals forces and electrostatic attraction between MoS_2 and organic matter. A relatively lower treatment efficiency of H_2O_2/MoS_2 was observed comparing to that of MoS_2, it could be attributed to that MoS_2 cannot activate H_2O_2 and instead MoS_2 could be oxidized by H_2O_2, affecting the adsorption effect of MoS_2 as well as the oxidation effect of H_2O_2. The UV_{254}, CN, and TOC removal rates from the MBR effluent by Fe^0/H_2O_2 were 36.2%, 51.83%, and 27.94%, respectively. The heterogeneous Fenton reaction based on Fe^0/H_2O_2 (Eq. (2) and (3)) produced a large amount of $HO^{\bullet}$. Because $HO^{\bullet}$ can react with biological macromolecules, as well as different types of organic and inorganic matter, and has a high reaction constant and negative charge electrophilicity, it attacks organic pollutant molecules by hydrogen extraction, electrophilic addition, and electron transfer. However, under conditions with the same oxidant and Fe^0, the UV_{254}, CN, and TOC removal rates in the $MoS_2/Fe^0/H_2O_2$ system were 48.68%, 63.85%, and 35.85%, respectively, within 30 min, which were higher than in the other systems. In addition, compared with the Fe^0/H_2O_2 system, the reaction rate in the $MoS_2/Fe^0/H_2O_2$ system increased from 1.30 to 2.02 min^{-1} (Fig. 1(b)), indicating that the addition of a small amount of MoS2 may accelerate the Fe^{3+}/Fe^{2+} redox cycle (Eq. (3) and (6)). Therefore, Fe^{2+} activated H_2O_2, producing more $HO^{\bullet}$ to react with organic pollutant molecules.

3.1.2: Changes in the structure of organic matter

The MBR effluent contained a large amount of organic matter with complex structures. The presence of these compounds was confirmed by the absorbance at 200–600 nm in the UV–vis spectrum of the leachate, as shown in Fig. S1. The leachate after treatment had no obvious absorption peak, indicating that it contained a large amount of dissolved organic matter.

The overall absorbance of the MBR effluent treated by the $MoS_2/Fe^0/H_2O_2$ system was lower than that in the other systems. This indicated that the $MoS_2/Fe^0/H_2O_2$ system was effective for breaking down the complex structures of refractory organic matter. Specific absorbances at 254 and 280 nm (A_{254} and A_{280}, respectively) are commonly used to characterize the degree of aromatization of organic matter. The A_{300}/A_{400}, A_{240}/A_{420}, and A_{250}/A_{365} ratios are used to characterize the degree of polymerization, the structuralization of humic acid, and the molecular weight of organic matter, respectively. The higher the ratio, the lower the degree of polymerization, structuralization, and molecular weight of the organic matter. The absorbance at wavelengths of 226–400 nm was mainly caused by the structure of benzene rings in a variety of conjugated compounds, and the integration of absorbance in this range was used to analyze the variation in aromatic compounds. As shown in Table S1, the $MoS_2/Fe^0/H_2O_2$ system effectively degraded aromatic organic matter containing benzene rings in the leachate, and the system also effectively reduced the molecular weight, as well as the degree of polymerization and structuralization of the organic matter.

3.1.3: Changes in the humus

The 3D-EEM spectra were used to analyze the changes in the humus in the leachate during the treatment by different systems. As shown in Fig. 1(c-j), there were two maximum fluorescence peaks in the 3D fluorescence of the MBR effluent. Peak A (Ex/Em = 250/460 nm, intensity=3625 au, humic acid-like fluorescence in the UV region) was mainly caused by low molecular weight organic matter with a high fluorescence frequency. Peak C (Ex/Em = 325/410 nm, intensity=2578 au, humic acid/fulvic acid-like fluorescence in the visible region) was mainly caused by relatively stable large molecular weight aromatic organic matter. Therefore, the leachate used in this study was difficult to degrade.

It can be clearly observed in Fig. 1(i) and (j) that the 3D-EEM fluorescence in the Fe^0/H_2O_2 and $MoS_2/Fe^0/H_2O_2$ systems weakened after 30 min of reaction compared with the other systems. Table S2 shows that the intensities of peaks A and C in the $MoS_2/Fe^0/H_2O_2$ system were weaker than those in the Fe^0/H_2O_2 system, with the lowest intensities reaching 1001.0 and 1091.0 au. The humus removal rate of this system in the UV and visible regions was 72.4% and 57.7%, respectively.

The peak A/peak C fluorescence peak intensity ratios for the H_2O_2 alone, Fe alone, MoS_2 alone, Fe^0/MoS_2, and H_2O_2/MoS_2 systems did not differ much

from those of the MBR effluent raw water. The peak A/peak C ratios for the Fe^0/H_2O_2 and $MoS_2/Fe^0/H_2O_2$ systems were much lower than those of the MBR effluent raw water, and there was an obvious blueshift of peak A, indicating a degree of molecular condensation and molecular weight decomposition. Additionally, the organic matter content of the leachate was greatly reduced, which was due to the nonselective oxidation property of HO•. It also had a strong effect on organic matter with a low molecular weight and high fluorescence frequency. The $MoS_2/Fe^0/H_2O_2$ system significantly improved the degradation of humus in leachate.

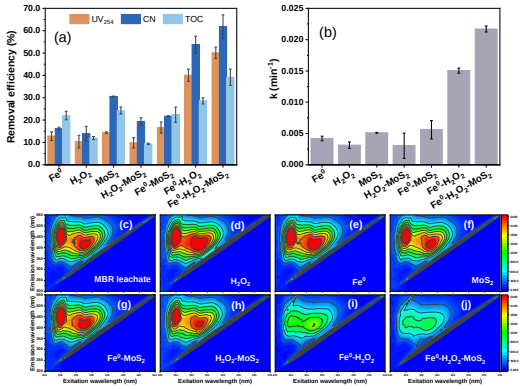

Fig 1 The influence of different treatment systems on organic matter removal efficiency (a) and reaction rate (b). (c-j) The 3D-EEM spectra of MBR effluent treated by different systems

3.1.4: Quantitative analysis of HO• and effective utilization of H_2O_2

Tert-Butanol (TBA) is an efficient HO• scavenger with reaction rate constants ranging from 3.8 to 7.7 × 108 $M^{-1}s^{-1}$. Because TBA affected the TOC concentration of the MBR effluent, but had no effect on the absorbance in the UV region, UV_{254} was used as the evaluation index of the refractory organic matter content of the MBR effluent. As shown in Fig. 2(a), after adding TBA to the $MoS_2/Fe^0/H_2O_2$ system, the UV_{254} of the MBR effluent decreased to different degrees. When the mole ratio of TBA to H_2O_2 was 20:1, the UV_{254} removal rate decreased from 42.2% to 19.4%, i.e., a 22.8% decrease. The main ROS in the $MoS_2/Fe^0/H_2O_2$ system was HO•, with HO• being essential for the degradation of refractory organic matter.

Fig.2(b) shows the formation of HO• in the H_2O_2 alone, H_2O_2/MoS_2, Fe^0/H_2O_2 and $MoS_2/Fe^0/H_2O_2$ systems from 0 to 60 min. The results showed that the HO• concentration did not increase significantly with time in the systems with H_2O_2 addition (H_2O_2 alone, H_2O_2/MoS_2, Fe^0/H_2O_2, and $MoS_2/Fe^0/H_2O_2$). The HO• concentrations in the H_2O_2 alone and H_2O_2/MoS_2 systems at 60 min were 0.26 and 0.30 mmol/L, respectively. The self-decomposition of H_2O_2 in these two systems was slow, which further indicated that MoS_2 hardly activated H_2O_2 in the absence of Fe^0. The HO• concentration in the Fe^0/H_2O_2 and $MoS_2/Fe^0/H_2O_2$ systems increased rapidly with time. At 60 min, the HO• concentration (3.69 mmol/L) in the $MoS_2/Fe^0/H_2O_2$ system was 1.31 times that (2.81 mmol/L) of the Fe^0/H_2O_2 system. The HO• was generated more efficiently in the Fe^0/H_2O_2 heterogeneous Fenton system with MoS_2 added.

To investigate the role of H_2O_2 in the $MoS_2/Fe^0/H_2O_2$ system, the residual H_2O_2 concentration in the different systems was determined by a spectrophotometric determination using potassium titanium oxalate, and the unit effective utilization of H_2O_2 in the different systems was calculated. The results are shown in Fig. 2(c) and (d). In the $MoS_2/Fe^0/H_2O_2$ system, H_2O_2 was significantly decomposed, while the decomposition of H_2O_2 in the H_2O_2 alone, H_2O_2/MoS_2, and Fe^0/H_2O_2 systems was limited. The decomposition of H_2O_2 in the $MoS_2/Fe^0/H_2O_2$ system was the fastest among the different systems investigated. This was consistent with the fastest oxidation and mineralization of refractory organic matter in the MBR effluent occurring in the $MoS_2/Fe^0/H_2O_2$ system. In terms of the amount of H_2O_2 consumed by TOC per unit mass, the effective utilization rate of H_2O_2 was highest in the $MoS_2/Fe^0/H_2O_2$ system, and the ratio of H_2O_2 to TOC was 8.1, which highlighted the potential degradation of pollutants in the $MoS_2/Fe^0/H_2O_2$ system.

3.1.5: Comparison of the Fe ion concentration and homogeneous activation in the system

As shown in Fig. 2(e), with the prolongation of reaction time, the Fe^{2+} and total Fe concentrations in the two systems increased, with higher concentrations in the $MoS_2/Fe^0/H_2O_2$ system than in the Fe^0/H_2O_2 system. The Fe^{3+} concentration was calculated by the difference between the total Fe and Fe^{2+} concentrations in Fig. 2(e). The Fe^{3+} concentration in both the Fe^0/H_2O_2 and $MoS_2/Fe^0/H_2O_2$ systems increased gradually with time, while the Fe^{2+} concentration increased slowly with time between 0 and 20 min. When the reaction time was prolonged to 30 min, the Fe^{2+} concentration decreased from 11.62 and 10.23 mg/L to 10.86 and 7.80 mg/L in the two systems, respectively. The reaction rate of HO• and Fe^{3+} generated by the reaction of Fe^{2+} and H_2O_2 was

too fast, while the rate of Fe^{3+} reduced to Fe^{2+} was too slow (Eq. (3) and (4)), resulting in a lack of Fe^{3+} recovery. However, for the same reaction time, the Fe^{2+} concentration in the $MoS_2/Fe^0/H_2O_2$ system was always higher than that in the Fe^0/H_2O_2 system. It was confirmed that the presence of MoS_2 could accelerate the transformation of Fe^{3+} to Fe^{2+} (Eq. (6)); thus, improving the transformation rate of Fe^{3+} to Fe^{2+}.

To study the effect of the slow release of Fe^0 on organic matter removal in the $MoS_2/Fe^0/H_2O_2$ system, the Fe^0 was replaced with different Fe^{2+} concentrations (5, 10, and 20 mg/L), as shown in Fig. 2(f). When the Fe^{2+} concentration was 5 mg/L, the UV_{254} and CN removal rates from the refractory organic matter in the MBR effluent were low. When the dosage of Fe^{2+} was increased to 10 mg/L, the UV_{254} removal rate increased to 20%. However, a further increase in the Fe^{2+} dosage to 10 mg/L did not significantly improve the UV_{254} removal rate. In addition, the overall organic matter removal efficiency of the $Fe^{2+}/H_2O_2/MoS_2$ system was almost 30% lower than that of the $MoS_2/Fe^0/H_2O_2$ system. The $MoS_2/Fe^0/H_2O_2$ system was a long-acting oxidation system with high reactivity.

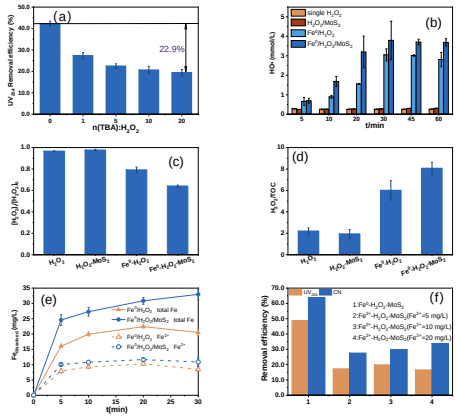

Fig. 2. (a) Effect of a HO• quencher on MBR effluent treated in the $MoS_2/Fe^0/H_2O_2$ system. (b) The HO• concentration in different treatment systems. The H_2O_2 residual concentration (c) and unit effective efficiency of H_2O_2 (d) in different treatment systems. A comparison of the Fe ion leaching concentration (e) and organic matter removal efficiency (f)

3.2 Factors influencing the degradation of refractory organic matter in MBR effluent by $MoS_2/Fe^0/H_2O_2$

3.2.1: The H_2O_2 dosage

As shown in Fig. 3(a), when the H_2O_2 dosage increased from 1 to 40 mmol/L, the UV_{254} and CN removal efficiency increased significantly from 18.10% and 29.27–46.92% and 61.34%, respectively. However, when the H_2O_2 dosage continued to increase to 60 mmol/L, the organic matter removal rate decreased slightly. Increasing the H_2O_2 dosage in the $MoS_2/Fe^0/H_2O_2$ system increased the yield of HO• to a certain extent; thus, improving the organic matter removal efficiency. However, when the H_2O_2 concentration was too high, it operated as a HO• quencher (Eq. (12)).

$$HO^{\bullet} + H_2O_2 \rightarrow H_2O + HO_2^{\bullet} \quad (12)$$

3.2.2 The MoS_2 dosage

As shown in Fig. 3(b), the addition of MoS_2 enhanced the performance of the Fe^0/H_2O_2 system in degrading the refractory organic matter in the leachate. When the MoS_2 dosage was in the range of 0–0.1 g/L, with the increase in MoS_2, the UV_{254} and CN removal rates increased from 30.58% and 43.77–48.68% and 63.26%, respectively, and k increased from 0.012 to 0.024 min^{-1}. This was attributed to the action of MoS_2 and Fe^0 (Eq. (6) and (7)), which accelerated the rate limiting step of Fe^{3+} to Fe^{2+} transformation in the heterogeneous Fenton process. The UV_{254} and CN removal rates decreased slightly when the MoS_2 dosage continued to increase (from 0.1 to 0.2 g/L), and therefore, the surplus MoS_2 had an inhibitory effect on the leachate degradation process. This was probably because some free Mo^{4+} eliminated HO• and inhibited degradation.

3.2.3: The Fe^0 dosage

As a heterogeneous activator, Fe^0 played an important role in the degradation of pollutants in the $MoS_2/Fe^0/H_2O_2$ system. As shown in Fig. 3(c), when the Fe^0 dosage increased from 0.05 to 0.4 g/L, the UV_{254} and CN removal efficiency in the leachate increased from 15.29% and 36.56–44.29% and 60.43% after 30 min of reaction, and the corresponding reaction rate increased from 0.006 to 0.020 min^{-1}. The increase in Fe^0 dosage increased the release of dissolved Fe^{2+}; thus, promoting the decomposition of H_2O_2 to HO•. In contrast, the UV_{254} and CN removal efficiencies in leachate at an Fe^0 dosage greater than 0.4 g/L tended to level off. At a higher Fe^0 dosage, the degradation of organic matter in the leachate may be due to the HO• consumed by Fe^{2+} (Eq. (13)).

$$Fe^{2+} + HO^{\bullet} \rightarrow Fe^{3+} + OH^- \quad (13)$$

3.2.4: The initial pH

The initial pH significantly affected the release of Fe^{2+} and influenced the interaction of MoS_2 with Fe^0. The effect of different initial pH values (3-11) on the degradation of organic matter in the effluent was studied. As shown in Fig. 3(d), the UV_{254} and CN removal rates at an initial pH=3 were 50.09% and 61.58%, respectively. However, when the initial pH was increased to 5–11, the removal rate of UV_{254} was less than 20%. Under acidic conditions, the generation of Fe^{2+} was promoted due to the corrosion of Fe^0, which was beneficial for the generation of HO• to degrade the pollutants. On the other hand, the activity of MoS_2 was affected in this pH range. Under acidic conditions, the edge S atoms on the MoS_2 surface may separate and then be captured by H^+. However, when the pH value increased, the S atoms cannot be captured; thus, hindering the exposure of Mo^{4+}.

3.2.5： The reaction time

As shown in Fig. 3(e), when the initial pH=3, H_2O_2=40 mmol/L, Fe^0=0.4 g/L, and MoS_2=0.1 g/L, with the prolongation of reaction time, the UV_{254} and CN removal rates in the MBR effluent increased from 18.54% and 35.32% at 5 min to 55.18% and 65.12% at 60 min, respectively. Correspondingly, with the prolongation of reaction time, due to the limitation of oxidizer and reaction substrate, the organic matter removal rate increased slowly. In addition, the UV_{254} removal conformed to pseudo first-order kinetics, and the fitting results are shown in Fig. 3(f). The kUV_{254} was 0.0105 min^{-1}, indicating that the HO• produced a faster removal rate for macromolecules and aromatic organic matter. Fig. S2 and Table S3 also show that the humus in leachate decreased substantially with the prolongation of reaction time, with humus removal rates in the ultraviolet and visible regions reaching 74.21% and 61.40%, respectively, at 60 min. However, with a reaction time from 30 to 60 min, the UV_{254} removal rate increased by less than 10%.

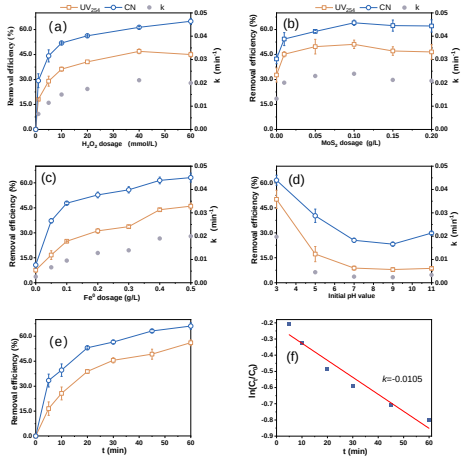

Fig. 3. Effect of different experimental conditions on the organic matter removal rate of the Fe^0/H_2O_2 system enhanced by MoS_2: (a) H_2O_2, dosage, (b) MoS_2, dosage, (c) Fe^0 dosage, (d) different initial pH values, and (e)

3.3 Enhancement of the Fe^0/H_2O_2 system by MoS_2

3.3.1： Analysis of the Fe^0 characteristics before and after the reaction

Scanning electron microscopy and EDS were used to study the surface morphology and elemental composition of Fe^0 before and after the reaction in the Fe^0/H_2O_2 and Fe^0/H_2O_2 systems enhanced by MoS_2. The results are shown in Fig. 4. The Fe^0 surface before the reaction was uneven (Fig. 4(a)), with a specific pore structure and metallic luster, and the Fe content of the material before the reaction was 100%. Many amorphous crystalline substances were generated on the surface of the Fe material after 30 min of reaction in the two systems, resulting in a rough Fe^0 surface after the reaction. In addition, it was observed that the surface of the Fe^0 material in the $MoS_2/Fe^0/H_2O_2$ system (Fig. 4(c)) was relatively smoother than that in the Fe^0/H_2O_2 system (Fig. 4(b)), which may have been caused by the generation of more nanoscale metal oxides (Fe_2O_3, CaO, MgO, etc.) on the material surface. The Fe content (53.41%) decreased and the O content (42.53%) increased in the $MoS_2/Fe^0/H_2O_2$ system. This indicated that Fe^0 was susceptible to O absorbing corrosion under acidic conditions, and iron oxides formed on the surface during the oxidation in the $MoS_2/Fe^0/H_2O_2$ system.

3.2.3： The Fe^{3+}/Fe^{2+} redox cycle and MoS_2 conversion mechanism

To study the change in phase composition before and after the reaction of Fe^0, Fe^0 before and after the reaction in the two systems was characterized by XRD. As shown in Fig. 4(d), the characteristic crystallographic planes of Fe^0 appeared in the X-ray maps of Fe^0 before the reaction, i.e., (110), (200), and (211), which corresponded to the diffraction peaks at 44.6°, 65.0°, and 82.3° in the plots, respectively, in agreement with Fe^0 (Joint Committee on Powder Diffraction Standards (JCPDS) standard card PDF#06–0696). The diffraction peak at 2θ=44.6° in the $MoS_2/Fe^0/H_2O_2$ system clearly weakened after the reaction, but the overall diffraction peak was consistent with that before the reaction. This may be because only a small amount of iron oxide or iron hydroxide formed on the Fe^0 surface after the reaction, and it could not be detected by XRD. We then used XPS to analyze the elemental components of the materials after the reactions in the Fe^0/H_2O_2 and $MoS_2/Fe^0/H_2O_2$

systems.

From the full XPS spectrum (Fig. S3) it was apparent that there were three strong photoelectron lines of Fe (2p), O (1s), and Mo (3d) in the XPS spectrum. This indicated the presence of the three elements, Fe, O, and Mo, on the surface of the material. To further study the valence changes of Fe, O, and Mo during the reaction, an XPS-peak differentiation analysis was conducted for Fe, O, and Mo, and the specific peak differentiation results are shown in Table S4. Fig. 4(e) is a high-resolution XPS optical map of O1 s. Two peaks were identified at 530.2 and 531.6 eV, corresponding to the Fe-O and Fe-OH bonds in the material, respectively. This indicates that during the reaction process in the Fe^0/H_2O_2 and $MoS_2/Fe^0/H_2O_2$ systems some iron (hydrated) oxides (such as Fe_2O_3, Fe_3O_4, and FeOOH) formed and were present on the surface of Fe^0 as mixtures, but Fe^0 was still the main component, which was consistent with the SEM–EDS results.

The fitting results for Fe and Mo are shown in Fig. 4(f) and (g), respectively. The value 719.3 and 733.1 eV in the Fe 2p curves represent the oscillatory satellite energies of Fe 2p3/2 and Fe 2p1/2, respectively. The XPS spectra of Fe^0 before and after the reaction in Fe^0/H_2O_2 were similar to those in the $MoS_2/Fe^0/H_2O_2$ system, with the main difference lying in the different proportions of Fe ions in each system. According to previous studies, Fe^0 also had two main peaks of Fe2p 3/2 and Fe2p 1/2 after the reaction. The binding energies of 712.4 and 726.0 eV indicated the presence of Fe^{3+}, while the binding energies of 710.7 and 724.3 eV were attributed to Fe^{2+}. The fitted peak areas according to Fe2p are shown in Table S4. The Fe^{2+} and Fe^{3+} in the Fe^0/H_2O_2 system accounted for 42.9% and 57.1% of the Fe ions, respectively, and Fe^{2+} accounted for 47.5% of the Fe ions in the $MoS_2/Fe^0/H_2O_2$ system. This indicated that the presence of MoS_2 increased the conversion rate of Fe^{3+} to Fe^{2+}.

From Eq. (6), as Fe^{3+} was reduced to Fe^{2+}, Mo^{4+} was oxidized to Mo^{6+}. According to previous studies, unsaturated S atoms on the surface of MoS_2 could be removed by capturing protons in the solution. Therefore, Mo^{4+} exposed on the surface of MoS_2 became very active. This was conducive to the transformation of Fe^{3+} into Fe^{2+}. The XPS results confirmed the oxidation of the exposed Mo^{4+}. In Fig. 4(g), the Mo3d peak of MoS_2 before and after the reaction moved slightly in the direction of the high binding energy. This was attributed to the reduction of the electron cloud of Mo3d. As Mo^{4+} was oxidized to Mo^{6+}, the electrons of Mo^{4+} were captured by Fe^{3+} in the reaction solution, which resulted in a decrease in the electron cloud density of Mo^{4+}, and the XPS peak of Mo^{4+} moved in the direction of the high binding energy. In addition, the Mo3d XPS spectrum after the MoS_2 reaction had a new peak at 235.7 eV, corresponding to Mo^{6+}, which further proved that Mo^{4+} was oxidized to Mo^{6+}. The characteristic peak of Mo^{6+} was very weak, which may be due to the reduction of Mo^{6+} to Mo^{4+} in the presence of H_2O_2. These results further confirm that Eq. (6) and (7) can be used for the degradation and even mineralization of refractory organic matter in MBR effluent in the $MoS_2/Fe^0/H_2O_2$ system.

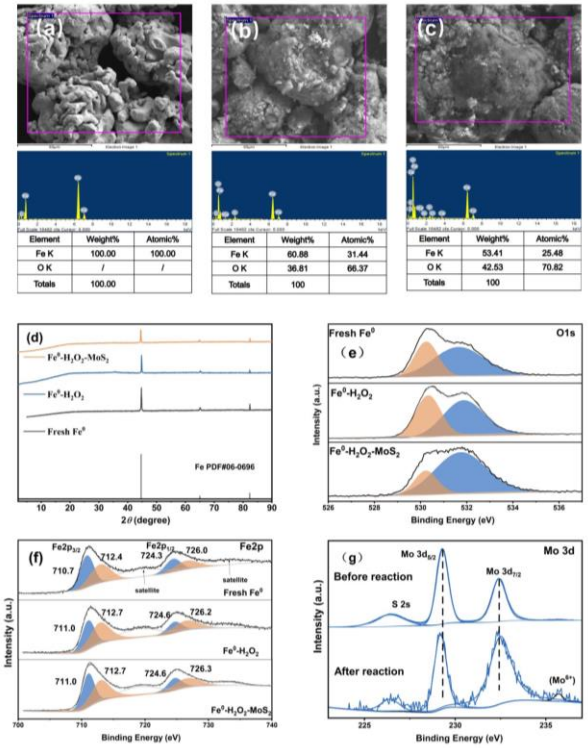

Fig. 4. Scanning electron microscope images and energy dispersive spectrometer spectra of Fe^0 before the reaction in the Fe^0/H_2O_2 system (a), $MoS_2/Fe^0/H_2O_2$ system, (b), and after the reaction (c). (d) The XRD patterns of Fe^0 before and after the reaction in the Fe^0/H_2O_2 and $MoS_2/Fe^0/H_2O_2$ systems. (e–f) The XPS patterns of O, Fe, and Mo before and after the reaction in the Fe^0/H_2O_2 and $MoS_2/Fe^0/H_2O_2$ systems.

3.4 The application of the $MoS_2/Fe^0/H_2O_2$ system to several aromatic model pollutants

3.4.1 : The degradation efficiency of aromatic model pollutants in the $MoS_2/Fe^0/H_2O_2$ system

Bisphenol A (BPA), IBU, and CIP are typical constituents of the refractory organic matter in leachate. To prove the effectiveness of the $MoS_2/Fe^0/H_2O_2$ system in the degradation of these aromatic pollutants, their degradation efficiencies in the Fe^0/H_2O_2 and $MoS_2/Fe^0/H_2O_2$ systems were compared. Considering that the composition of the model pollutants was not as complex as that of leachate, the dosage of oxidant and activator in the system was adjusted correspondingly. The results are shown in Fig. 5(a).

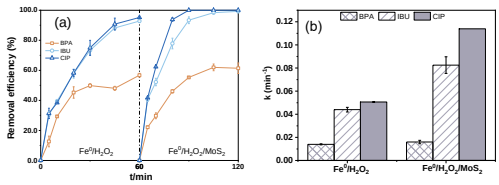

Fig. 5. Removal efficiency (a) and reaction rate (b) of IBU, BPA, and CIP in the Fe^0/H_2O_2 and $MoS_2/Fe^0/H_2O_2$ systems (reaction conditions: initial pH = 3, [BPA] = [IBU] = [CIP] = 40 mg/L, H_2O_2 = 5 mmol/L, Fe^0 = 0.2 g/L, MoS_2 = 0.02 g/L).

The IBU and CIP removal rates in the $MoS_2/Fe^0/H_2O_2$ system were in excess of 99% after 30 min, while IBU and CIP were completely removed after 60 min, with degradation rate constants (Fig. 5(b)) of 0.082 and 0.113 min^{-1}, respectively. The degradation rate of BPA was only 62%. The biphenyl structure of BPA requires the continuous oxidation of HO• to break bonds and open rings. The removal of IBU and CIP in the $MoS_2/Fe^0/H_2O_2$ system was 1.1 times that in the Fe^0/H_2O_2 system, and CIP could be completely eliminated in the $MoS_2/Fe^0/H_2O_2$ system within 30 min. In addition, the removal rate constant of IBU in the $MoS_2/Fe^0/H_2O_2$ system (0.082 min^{-1}) was 1.9 times higher than that in Fe^0/H_2O_2 (0.044 min^{-1}). The removal of CIP in the $MoS_2/Fe^0/H_2O_2$ system (1.13 min^{-1}) was 2.2 times higher than in the Fe^0/H_2O_2 system (0.051 min^{-1}). This indicates that the $MoS_2/Fe^0/H_2O_2$ system was faster than the Fe^0/H_2O_2 system for the removal of the two aromatic model pollutants.

3.4.2. : The degradation pathways of IBU, BPA, and CIP

The degradation of aromatic organic matter is usually accompanied by the formation of intermediate byproducts. These intermediates have strong toxic effects and may present a risk to the environment. Several intermediates produced by IBU, BPA, and CIP in the $MoS_2/Fe^0/H_2O_2$ system were identified by LC-TOF-MS. The possible degradation pathways of IBU, BPA, and CIP in the $MoS_2/Fe^0/H_2O_2$ system were proposed as follows.

(1) The degradation pathways of the nonsteroidal anti-inflammatory drug IBU.

Based on the data from this and related studies, three possible degradation pathways of IBU were speculated, as shown in Fig. 6(a). Pathway I: Due to the large special steric hindrance of the 2-methylpropyl group on the side chain of IBU, HO• preferentially attacks the para-position to form the corresponding hydroxylation product (P2 *m/z* 220) and forms 1-[4-(2-methylpropyl) phenyl] ethenone (P3 *m/z* 176) under the continuous attack of HO•. Pathway II: HO• attacks the lipid chain alkyl group of IBU to form an intermediate product (P4 *m/z* 220), and the acyl group is then oxidized to the carboxyl group to form 2-(4-methylphenyl) propanoic acid (P5 *m/z* 164). Pathway III: HO• simultaneously attacks the two groups in the para position on the benzene ring of IBU and forms the corresponding hydroxylated intermediate (P6 *m/z* 237). After oxidation-dehydration, the small organic acid 4-acetyl benzoic acid (P7 *m/z* 164) is formed. Finally, with the continuous attack of HO•, some intermediates of these aromatic molecules can form short chain small molecules through ring-opening reactions, such as 5-methylhexan-2-one (P8 *m/z* 114) and (P9 *m/z* 171).

(2) The degradation pathway of the endocrine disruptor BPA.

Fig. 6(b) shows the possible degradation pathway of BPA. First, the electrophilic group (HO•) will preferentially attack the densest part of the electron cloud of BPA. Therefore, C2 and C5 are more vulnerable to HO•. Then, P2 is produced after hydroxylation, and is converted to carbonyl to form P3 by HO• continuous oxidation and further cleavage to small organic acids 2-(3,4-Dioxyidenecyclohex-1,5-dienyl) acetic acid (P4 *m/z* 164). The C-C bond connection between isopropyl and the benzene ring is cleaved by a HO• attack, which can be coupled with phenol in solution to form 4-(4-Hydroxyphenyl) benzene-1,2-dione (P5 *m/z* 200). Under the continuous attack of HO•, these aromatic compounds gradually split into straight chain compounds, such as hexa-1,5- diene-3,4-diol (P7 *m/z* 114) and methyl 3-hydroxyheptanoate (P8 *m/z* 160).

(3) The degradation pathway of the antibiotic CIP.

As shown in previous studies, the degradation of quinolones may occur on the piperazine ring and quinolone ring structures. Combined with information from previous studies and the intermediates detected by LC-TOF-MS, a possible pathway of oxidation of CIP in the $MoS_2/Fe^0/H_2O_2$ system was proposed, as shown in Fig. 6(c). Because of the high electron affinity of $OH^{\bullet}$, it will readily attack the piperazine and quinolone rings on CIP. With the opening of the piperazine and quinolone rings of CIP, a series of oxidation and decarboxylation reactions take place, and the small organic molecule 4-fluoroaniline (P8 *m/z* 112) is formed. The piperazine and quinolone structures of CIP molecules could be completely destroyed in the $MoS_2/Fe^0/H_2O_2$ system.

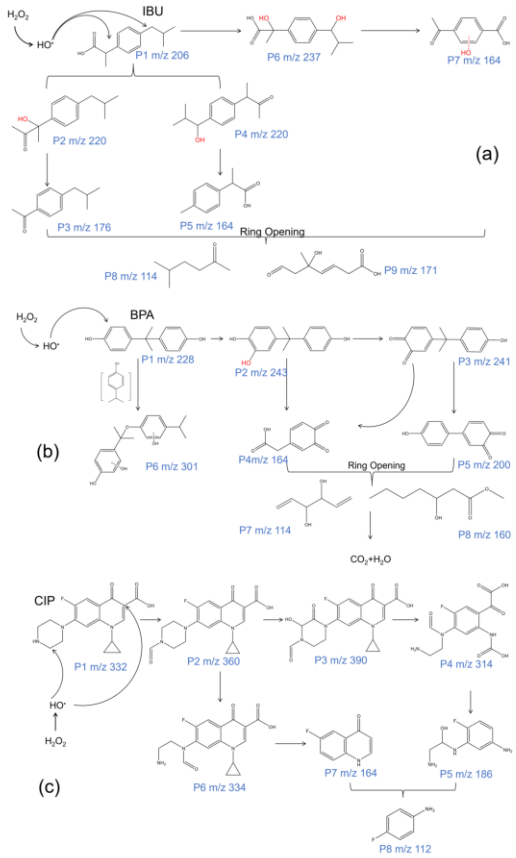

Fig. 6. Degradation pathways of IBU, BPA, and CIP in the $MoS_2/Fe^0/H_2O_2$ system (a)–(c).

3.4.3: Degradation mechanism

Based on the above results, a possible mechanism for the degradation of refractory organic matter in MBR effluent in the $MoS_2/Fe^0/H_2O_2$ system was proposed. As shown in Fig. 7, H_2O_2 was decomposed by the Fe^{2+} released from Fe^0 to generate $OH^{\bullet}$ and Fe^{3+} in the solution at the same time. In the $MoS_2/Fe^0/H_2O_2$ system, the presence of MoS_2 helped to convert Fe^{3+} into Fe^{2+}. First, MoS_2 captured protons, generating H_2S in solution and forming unsaturated S atoms on the surface of MoS_2. Then, the Mo^{4+} exposed on the MoS_2 surface promoted the transformation of Fe^{3+} to Fe^{2+} through a redox reaction and generated Mo^{6+}. Finally, under the action of H_2O_2 in solution, Mo^{6+} was reduced to Mo^{4+} to realize its own cycle. The circulation of Fe ions led to an increase in the Fe^{2+} concentration in the solution and further increased the $HO^{\bullet}$ concentration in the system. Finally, due to the characteristics of $HO^{\bullet}$ nonselective oxidation, a series of additions, substitutions, bond breaking, ring opening, and other reactions could occur with pollutants, with the result that macromolecular organic matter with a stable structure or that is difficult to biodegrade was transformed into small molecules that were easy to degrade or even mineralize. In addition, the iron oxides generated on the surface of Fe0 had certain adsorption and precipitation effects. To reduce the Fe ion concentration following treatment by the oxidation method in the wastewater, the pH of the effluent in the $MoS_2/Fe^0/H_2O_2$ system was adjusted to 9. Because a large number of Fe ions were converted into Fe-based colloids or other flocculants under alkaline conditions, the leached Fe ion concentration was effectively controlled after precipitation and flocculation, and the pollutants were removed by flocculation to a certain extent. In summary, the mechanism of the refractory degradation of organic pollutants in MBR effluent in the $MoS_2/Fe^0/H_2O_2$ system could be attributed to the homogeneous and heterogeneous Fenton reaction and the adsorption and precipitation of organic matter by Fe-based colloids.

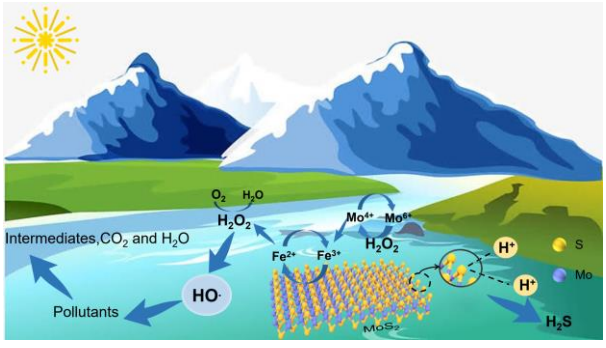

Fig. 7. Mechanism of refractory organic pollutant removal in the effluent produced during the treatment of landfill leachate by an MBR in the $MoS_2/Fe^0/H_2O_2$ system.

4 CONCLUSIONS

This study analyzed the ability of the $MoS_2/Fe^0/H_2O_2$ system to oxidize refractory organic matter in the effluent produced during the treatment of landfill leachate by an MBR, and assessed the synergistic effect of MoS_2 on the mineralization of organic matter and degradation of humic-like organic matter in different systems. The mechanism of the $MoS_2/Fe^0/H_2O_2$ system was proposed through the identification of ROS and a system comparison of the $HO^{\bullet}$ concentration, the effective utilization rate of H_2O_2, the morphology of the materials, and the results of an XRD and XPS analysis. The degradation rate of aromatic organics (e.g., nonsteroidal and quinolones) in the $MoS_2/Fe^0/H_2O_2$ system was approximately twice that in the Fe^0/H_2O_2 system. Because MoS_2 accelerated the Fe^{3+}/Fe^{2+} redox cycle, the system had a higher reactivity and oxidation performance. It was concluded that the $MoS_2/Fe^0/H_2O_2$ system was an effective method for the removal of refractory organic matter from MBR effluent following the treatment of landfill leachate.

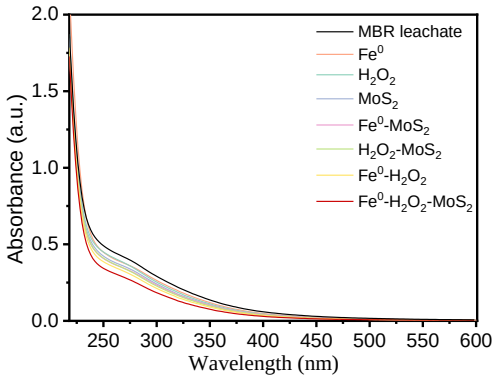

Figure S1. The UV-Vis spectra of MBR effluent treated by different processes.

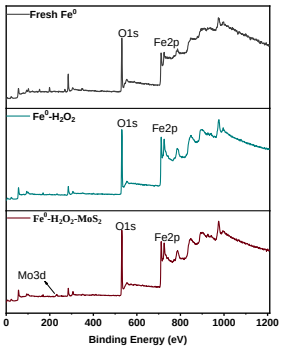

Figure S3. A full-range scan of the XPS spectra of Fe^0 in the Fe^0/H_2O_2 and $MoS_2/Fe^0/H_2O_2$ processes before and after the reaction.

Table S1. Specific absorbance value of MBR effluent treated by different processes.

Type	A_{254}	A_{280}	A_{300}/A_{400}	A_{240}/A_{420}	A_{250}/A_{365}	$A_{226\text{-}400}$
MBR leachate	0.4807	0.3853	4.9144	13.2302	4.6991	52.1834
Fe^0	0.4285	0.3430	5.5378	15.5362	5.1187	46.3047
H_2O_2	0.4407	0.3469	5.7444	16.7209	5.4495	46.4678
MoS_2	0.4135	0.3283	6.1207	17.8904	5.5909	44.0284
Fe^0-MoS_2	0.3984	0.3169	5.7422	16.3654	5.3706	42.6049

H_2O_2-MoS_2	0.4007	0.3131	6.0000	18.1762	5.6970	42.1956
Fe^0-H_2O_2	0.3780	0.2945	6.0722	18.3783	5.8446	39.7701
Fe^0-H_2O_2-MoS_2	0.3353	0.2575	6.3377	20.1915	6.1901	35.2513

Table S2. Variations of peak intensity and peak position of Peak A and Peak C of MBR effluent before and after treatment by different processes.

Type	Peak A	(a u)	efficiency	Peak C	(a u)	efficiency	Peak A/ Peak C
MBR	250.0/460.0	3625.0	/	325.0/410.0	2578.0	/	1.41
H_2O_2	250.0/455.0	3857.0	0	325.0/410.0	2844.0	0	1.36
Fe^0	250.0/450.0	3712.0	0	330.0/415.0	2707.0	0	1.37
MoS_2	250.0/460.0	3450.0	4.8%	315.0/435.0	2341.0	9.2%	1.47
Fe^0/MoS_2	250.0/455.0	3627.0	0	325.0/405.0	2630.0	0	1.38
H_2O_2/MoS_2	250.0/455.0	3396.0	6.3%	325.0/415.0	2488.0	3.5%	1.36
Fe^0/H_2O_2	245.0/410.0	1311.0	63.8%	320.0/405.0	1502.0	41.7%	0.87
Fe^0/H_2O_2/MoS_2	250.0/420.0	1001.0	72.4%	315.0/410.0	1091.0	57.7%	0.91

Table S4. Peak differentiation results of Fe 2p, O 1s, and Mo 3d.

BE/eV	Peak area	Ratio %

		Fresh	Fe^0/H_2O_2	$Fe^0/H_2O_2/MoS_2$	Fresh	Fe^0/H_2O_2	$Fe^0/H_2O_2/MoS_2$	Fresh	Fe^0/H_2O_2	$Fe^0/H_2O_2/MoS_2$
O1s		530.2	530.3	530.2	6554	17103	4895	34.4	45.7	23.5
		531.6	531.8	531.7	12479	20287	15957	65.6	54.3	76.5
Fe2p		712.4	712.7	712.7	6362	21364	11046			
	Fe^{3+}							45.5	57.1	52.4
		726.0	726.2	726.3	3181	10682	5523			
		724.3	724.6	724.6	3799	9672	4078			
	Fe^{2+}							54.42	42.9	47.5
		710.7	711.0	711.0	7598	19345	8157			
Mo3d		232.4	\	232.4	66815	\	1031	34.1	\	57.6
		229.2	\	229.1	90777	\	478	46.3	\	26.7
		226.5	\	226.3	38221	\	226	19.5	\	12.6
		\	\	235.7	\	\	54	\	\	0.3

EFFECT OF DIFFERENT AERATION RATES ON THE BIODRYING OF BIOGAS RESIDUE WITH HIGH MOISTURE CONTENT

Mingyue Xu[1], Min Yang[1], Jie Meng[1], Haishu Sun[1] and Qunhui Wang[1]
1 School of Energy and Environmental Engineer, University of Science and Technology Beijing, 30 Xueyuan Road, Haidian District, Beijing 100083, China

INTRODUCTION

Anaerobic digestion is widely used in the treatment of agricultural and municipal waste, and it is regarded as a cost-effective and efficient method of dealing with organic solid waste (Ren et al., 2018; Ma et al., 2020). However, it generates a large quantity of residue, which has a negative impact on the environment. The high moisture content of waste (74%-90%), bad odour, pathogens, plant toxins, and high quantities of heavy metals all constitute a significant environmental burden (Ma et al., 2021; Bai et al., 2020). As a result, resource utilization and reduction of biogas residue must be realized.

Biodrying is an energy-saving approach for successfully recovering organic solid waste with a high moisture content (Hao et al., 2018). However, the use of BR, particularly BR with a high moisture content, as a raw material for biodrying has received little attention. Moisture content is a key metric for assessing the effectiveness of biodrying, and the degree of maturation assures that biodrying products are nontoxic and helpful. As a result, the current study concentrated on biodrying performance and maturation impact, and investigated the effect of varied aeration rates on biodrying and maturity of BR with a high moisture content.

MATERIALS AND METHODS

In this investigation, BR with a high moisture of 91.1% was collected from the Dongcun Comprehensive Garbage Treatment Plant in Beijing, which used wet anaerobic technique to handle food waste. All of the reactors were laboratory-scale and self-designed. Pump, gas flowmeter (LZB-3,0.1-1.0L/min), biodrying reactor, and gas absorption bottle were all incorporated in the system. The aeration rate was 0.6、0.8、1.0、1.2、1.5 L/min•kg for the T1、T2、T3、T4、T5 names, respectively. The auxiliary heat temperature was kept at 50°C, and the stack rotating operation was done at the same time every day. Dates of sampling: 0, 2, 4, 5, 6, 7, 8, 9, 10, 11, 12.

RESULT AND DISCUSSION

(1) Biodrying performance

Water regulates the temperature, dissolves organic matter, and aids in microbial metabolism. As a result, water content has a significant impact on biodrying and is one of the key indicators for assessing drying effect (Mohammed et al., 2017). The change in the moisture content of BR during biodrying was shown in Fig.1.

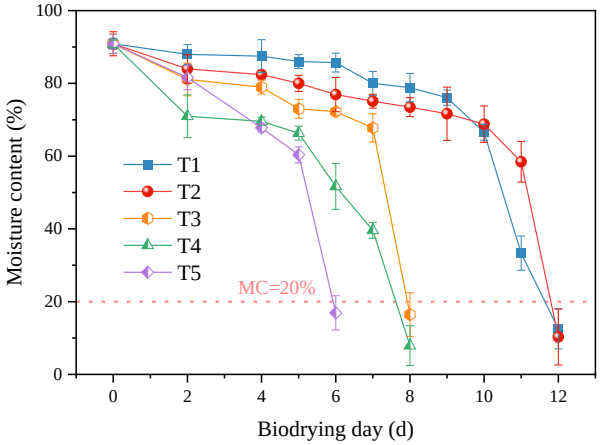

Figure 1. Changes in water content of different samples.

Aeration not only supplied the oxygen needed for microbial activity, but it also removed water from the biogas residue in time. As shown in Fig.1, the aeration greater, the rate of water content reduction turned quicker, and the reduction tended to be gradual at first, then fast. The biodrying process took 12 days when the aeration rate was 0.6 and 0.8 L/min·kg. The biodrying process took 8 days when the aeration rate was raised to 1.0 and 1.2 L/min·kg. When the aeration rate raised to 1.5 L/min·kg, the water content of BR reduced to less than 20% in only 6 days.

(2) Evaluation of germination index and pH

The germination index (GI) was used to determine if the dried product could be utilized as organic fertilizer for agriculture by evaluating the degradation and phytotoxicity of hazardous chemicals (Li et al., 2020). Material with a GI of 70% or greater was thought to be highly degraded and non-toxic to plant germination and growth. With an initial GI value of 14.7%, it was discovered that BR exhibited considerable phytotoxicity (Fig. 2) and was thus unsuitable for direct agricultural and non-agricultural uses. The GI of the T1 and T2 groups grew slowly at initially and significantly after day 9 of the drying experiment, as shown in Fig. 2. The GI of group T1 reached a maximum on day 12 (105.8%).

The group T2 had a GI of over 70% on day 9, meeting the standard set by NY525-2021 of China, and a maximum GI on day 11 (107.3%). However, groups T3, T4 and T5 had a GI below 40% and were toxic to plants and did not meet the criteria for decomposition.

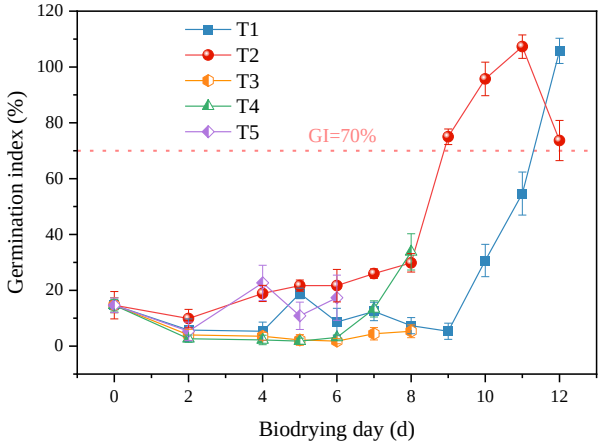

Figure 2. Dynamic changes in GI.

pH was a crucial element influencing microorganism development. It influenced not just mineral dissolution but also the level of microbial activity (Bai et al., 2020). Because bacterial metabolism decreased the pH of organic waste, pH may be used to indicate bacterial activity.

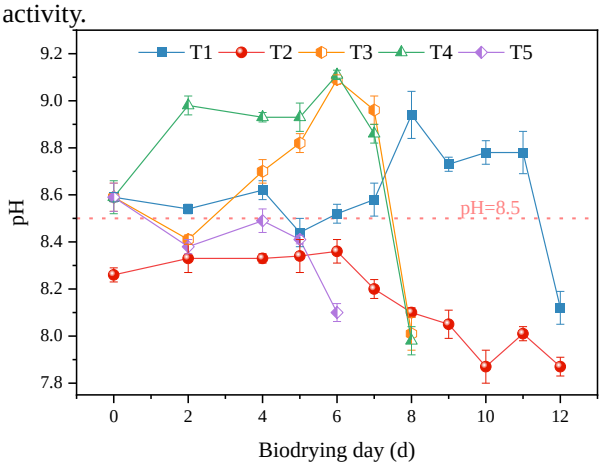

Figure 3. Dynamic changes in pH.

The pH of all the groups showed an overall trend of firstly increasing and then decreasing. The increase in pH may be related to the degradation of protein followed by the generation of ammonia gas with the increase in temperature at the initial stage of biodrying. Except for T2, the pH values of all the groups did not meet the standard of pH 5.5–8.5 stipulated in NY 525-2021, China. High pH, which was not conducive to plant growth, could potentially be the cause of low GI.

CONCLUSION

The aim of this study was to investigate the optimum aeration rate for the BR with high moisture content in biodrying process. An aeration rate of 0.8 L/min·kg resulted in a product with a high GI value and stable pH. This study provided a new solution for the treatment and disposal of high water content BR.

ACKNOWLEGEMENT

This work was supported by the National Key R&D Program of China (Grant NO. 2018YFC1900904 and Grant NO. 2019YFC1906302), the National Environmental and Energy Base for International Science & Technology Cooperation.

REFERENCE

1. Bai, L., Deng, Y., Li, J., Ji, M., Ruan, W., 2020. Role of the proportion of cattle manure and biogas residue on the degradation of lignocellulose and humification during composting. Bioresour. Technol. 307, 122941. https://doi.org/10.1016/j.biortech.2020.122941

2. Hao, Z., Yang, B., Jahng, D., 2018. Combustion characteristics of biodried sewage sludge. Waste Manag. 72, 296–305. https://doi.org/10.1016/j.wasman.2017.11.008

3. Li, Yinchao, Liu, Y., Yong, X., Wu, X., Jia, H., Wong, J.W.C., Wu, H., Zhou, J., 2020. Odor emission and microbial community succession during biogas residue composting covered with a molecular membrane. Bioresour. Technol. 297, 122518. https://doi.org/10.1016/j.biortech.2019.122518

4. Ma, J., Mu, L., Zhang, Z., Wang, Z., Kong, W., Feng, S., Li, A., Shen, B., Zhang, L., 2021. Influence of thermal assistance on the biodegradation of organics during food waste bio-drying: Microbial stimulation and energy assessment. Chemosphere 272, 129875. https://doi.org/10.1016/j.chemosphere.2021.129875

5. Ma, X., Yu, M., Song, N., Xu, B., Gao, M., Wu, C., Wang, Q., 2020. Effect of ethanol pre-fermentation on organic load rate and stability of semi-continuous anaerobic digestion of food waste. Bioresour. Technol. 299, 122587. https://doi.org/10.1016/j.biortech.2019.122587

6. Mohammed, M., Ozbay, I., Karademir, A., Isleyen, M., 2017. Pre-treatment and utilization of food waste as energy source by bio-drying process. Energy Procedia 128, 100–107. https://doi.org/10.1016/j.egypro.2017.09.021

7. Ren, Y., Yu, M., Wu, C., Wang, Q., Gao, M., Huang, Q., Liu, Y., 2018. A comprehensive review on food waste anaerobic digestion: Research updates and tendencies. Bioresour. Technol. 247, 1069–1076. https://doi.org/10.1016/j.biortech.2017.09.109

8. Shao, L.M., Ma, Z.H., Zhang, H., Zhang, D.Q., He, P.J., 2010. Bio-drying and size sorting of municipal solid waste with high water content for improving energy recovery. Waste Manag. 30, 1165–1170. https://doi.org/10.1016/j.wasman.2010.01.011

THE PERFORMANCE OF ORIENTED LACTIC ACID FERMENTANTION BROTH FROM FOOD WASTE AS EXTERNAL CARBON SOURCE FOR DENITRIFICATION

Feng Liu[1, 2], Ming Gao[3], Beiping He[2], Qunhui Wang[3, *], Leiyu Feng[1], Yinguang Chen[1, *]

1 State Key Laboratory of Pollution Control and Resources Reuse, School of Environmental Science and Engineering, Tongji University, 1239 Siping Road, Shanghai 200092, China

2 Tus-Environmental Technology Development Co., LTD. Haidian District, Beijing100084, China

3 Department of environmental engineering, University of Science and Technology Beijing

30 Xueyuan Road, Haidian District, Beijing 100083 P. R.China

*Corresponding author: yinguangchen@tongji.edu.cn (**Yinguang Chen**); wangqh59@ustb.edu.cn **(Qunhui Wang**)

INTRODUCTION

The problem of water environment pollution has been attached of great importance all over the world. In 2019, the Ministry of Housing and Urban-Rural Development and other ministries and commissions issued the 'Three-year Action Plan for Improving the Quality and Efficiency of Urban Sewage Treatment (2019-2021)'. The pollutant discharge standards of China's urban sewage treatment plants were gradually raised from Grade I B standard to Grade I A standard, and even proposed to meet the grade IV water standards of the Surface Water Environmental Quality Standard (GB3838-2002). The introduction of these policies put forward higher requirements for the total nitrogen concentration of effluent from sewage treatment plants. At the same time, with the proposal of carbon peak, and carbon neutrality in China, new challenges have been put forward for exogenous carbon source and other drugs in the sewage treatment process. At present, commercially available carbon sources for enhancing biological denitrification efficiency were expensive and had many drawbacks. For example, methanol was a class A dangerous chemical commonly used, which had toxic effects and great potential safety risks in the process of storage and appliance. Glucose was easy to cause the microbe growth and reproduction drastically, resulting in sludge expansion. The COD equivalent of sodium acetate was low, whose dosage was relatively high with great mud yield, etc[1-3]. Therefore, alternative carbon sources, cheaper and more efficient, were extremely urgent for sewage treatment. The high content of organic matter in food waste (FW) could theoretically be used as raw material for alternative carbon source[4,5]. However, due to the complex composition of FW and various fermentation products, it was necessary to investigate the denitrification effect and stability of the carbon source generated from FW. Therefore, in this paper, by comparing with the traditional chemical carbon sources, we investigated the denitrification effect of the oriented lactic acid (LA) fermentation broth from FW as a denitrification supplementary carbon source (FW-LA) in the SBR reactor. Further, Microbial community analysis in SBR system was performed. Here, we would like to provide theoretical support for an efficient liquid composite carbon source for sewage treatment, which was obtained from oriented LA fermentation of FW.

MATERIALS AND METHODS

Feedstock and inocula

FW was obtained from a kitchen waste treatment plant in Anhui Province, China. The collected FW was pretreated as follows: high-pressure extrusion→ impurity removal→boiling for oil removal→ three-phase separation. In detail, the original FW with total solids (TS) 15%, was firstly treated with high-pressure extrusion (12 MPa) to remove the impurities and mix slurry, with an extruder filter hole diameter of 8 mm, and with 10% dry impurities (TS 50%) removed; after the stock was sieved through the screening machine with hole diameter 5 mm, and 5% small slag (TS 40%) was removed; then, the organic material was mixed with 160℃ saturated steam within the boiling tank, where the temperature was kept at 75-80℃ for 1.5 h. The boiled material was extracted by a three-phase separator to extract crude oil, and the remaining organic slurry was the FW substrate taken in this experiment. Sodium acetate (NaAc), chemical grade, was directly purchased.

Experimental Methods

Preparation of FW-LA: *Enterococcus mondii* was used as inoculum, and the fermentation temperature was carried out at 43℃ with continuously pH control at 6.8

by using 10 M NaOH as a neutralizer in an open system for 7 days. Subsequently, the fermentation broth was filtered through a 0.45 μm membrane to produce FW-LA.

Denitrification and nitrogen removal effect test: Two SBR reactors with a working volume of 8 L were operated in AOA mode, and the operation cycle was 8 h (anaerobic 50 min, aerobic 120 min, anoxic 180 min, and static sedimentation 60 min). The initial sludge concentration MLSS in SBR reactors was 3800-4200 mg/L, the temperature was 23-25℃, the influent pH was 6.5-7.0, and the aeration volume was 3.5 L/min. The influent ammonia nitrogen concentration was 35 mg/L, and the initial COD concentration was adjusted to 200, 300, and 400 mg/L, respectively. Carbon sources were NaAc and FW-LA prepared above.

Microbial community analysis: In this paper, 16SrRNA high-throughput gene sequencing molecular biology technology was used to analyze the community of the initial sludge of WWTP, the sludge with FW-LA as carbon source (COD=200 mg/L), and the sludge with NaAc as carbon source (COD=200 mg/L).

Analysis method

The fermentation broth was sampled periodically and centrifuged, then the supernate was filtered through a 0.45 μm membrane for COD analysis regarding 'HJ/T399-2007', and further filtered through a 0.22 μm membrane for LA and acetate measurement by High-Performance Liquid Chromatography (HPLC, LC-20A, Shimadzu, Japan). TN 'HJ636-2012', NH_4^+-N 'HJ535-2009', NO_3^--N 'HJ/T346-2007', NO_2^--N 'GB7493-1987', and MLSS were determined by standard methods. Microbiological analysis was performed based on 16SrRNA high-throughput gene sequencing.

RESULTS AND DISCUSSION

The performance of SBR reactors with different carbon sources

By comparing the changes of COD and nitrides in two different systems, we found that when NaAc was used as the carbon resource, the COD removal rate was 63%-80% (average 74.0%), and the TN removal rate was 55%-73% (average 64.7%), 78%-88% (average 77.8%), 50%-60%(average 57.0%) under different influent COD 100, 200, 300 mg/L, respectively (Fig.1). The COD removal rate of the reactor with FW-LA as carbon source ranged from 65% to 82%, with an average removal rate of 72.13%. The TN removal rate was 45.2%-68.1% (average 52.3%), 75.1%-91.9% (average 83.8%), and 74.3%-84.1% (average 78.2%) under different intake COD 100, 200, 300 mg/L, separately (Fig.2). On the whole, the performance of denitrification with FW-LA as carbon source was better than that with NaAc, especially at higher influent COD concentration.

Furthermore, we focused on the variation of sludge settling performance during each cycle in the SBR system and got some interesting findings. In the reactor with FW-LA as the carbon source, MLSS was 4209, 4460, 4216 mg/L, separately under the influent COD 200, 300, and 400 mg/L. In NaAc reactor, MLSS was 4129, 4223, 4339 mg/L respectively under influent COD 200, 300, 400 mg/L. With the growth of sludge, the phenomenon of sludge swelling gradually occurred, especially in the FW-LA system, accompanied by sludge floating. Under inlet COD 400 mg/L, the sludge of both reactors could swell and rise above obviously. After the reaction tended to be stable, SV30 of the FW-LA reactor ranged from 47% to 51%, which was 43%-48% in the NaAc reactor, and the sludge settling performance decreases greatly. So, slashes with FW-LA as carbon sources showed obvious swelling and sludge upwelling. This reminded us that we should pay much more attention to the system stability and sludge bulking when using FW-LA as a carbon source in practical engineering.

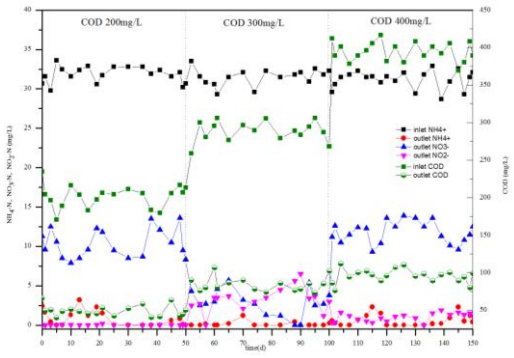

Fig. 1. The variation of COD and nitrides of the SBR reactor with NaAC as carbon source

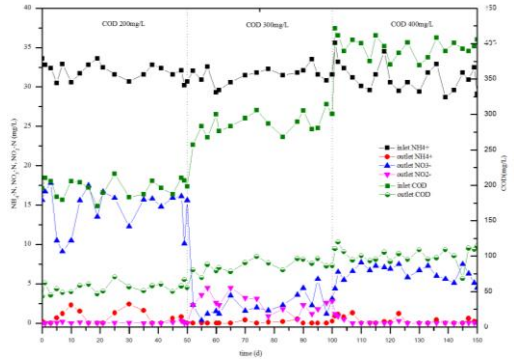

Fig. 2. The variation of COD and nitrides of the SBR reactor with FSFW-lactic acid as carbon source

Comparison of nitrogen removal effect between two carbon sources

As was shown in Table1, the nitrosation and nitrification rate with the FW-LA was much lower than that of NaAc. When the influent COD was 200 mg/L, the denitrification rate, TN remove rate, and Nitrogen removal load (NRR) with FW-LA as the carbon resource was inferior to that with NaAc. Whereas with the increase of COD concentration, the advantages of the FW-LA carbon source became more obvious, and it was worth stating that the denitrification yield, TN remove rate, and NRR in the FW-LA system was approximately 1.6, 1.4, 1.3 times higher than that in NaAc reactor when the COD inlet was 400 mg/L. In the SBR system with FW-LA as carbon source, the denitrification efficiency of inlet COD 400 mg/L, on which high organic loading inhibited the nitrification process with NH_4^+ incompletely nitrated, was weaker than that of 300 mg/L. When the influent COD concentration was 300 mg/L, there was little difference in the TN removal rates between the two carbon sources. When COD was 400 mg/L, FW-LA had little influence on the nitrification process and was more easily utilized by denitrifiers, which displayed obvious advantages over NaAc in the TN removal rate. On the other hand, the SBR system supplementing NaAc as a carbon source was more likely to cause the accumulation of NO_2^-N.

Table 1 Comparison of nitrogen removal effect between two carbon sources

Carbon source	Inlet COD (mg/L)	removal ratio COD (%)	nitrosation rate (NO_2^-/ NH_4^+)	nitrification rate (NO_x^-/ NH_4^+)	Denitrification yield ($\Delta NO_3^-/NO_3^-$max)	TN remove rate (ΔTN/NH_4^+ inlet)	Nitrogen removal load (NRR) (ΔTNg/ΔCODg)
FW-LA	200	71.86	0.48	68.26	30.61	51.44	0.11
	300	66.73	9.61	68.70	86.82	85.73	0.15
	400	74.97	0.65	48.77	65.69	78.75	0.08
NaAc	200	75.32	15.37	82.93	49.61	64.45	0.14
	300	71.36	29.39	67.63	79.67	83.04	0.13
	400	74.77	6.51	51.09	40.66	56.51	0.06

Microbial community analysis

Based on the species-abundance curve analysis (Fig.3), the population diversity of the sludge with FW-LA addition was close to that of the sludge with stable operation and good reaction effect retrieved from the municipal sewage works. On the contrary, the diversity of the sludge population with NaAc as carbon source changed significantly. Therefore, the operation effect of FW-LA as carbon source was more stable. In Fig.4, the main microorganisms in the reaction system were *Gammaproteobacteria*, *BacteroidiaAnaerolineae*, *Alphaproteobacteria*, *Actinobacteria*, etc. *Gammaproteobacteria* was the most abundant group in class level. The distribution of the raw sludge group, FW-LA group, and NaAc group were 33.08%, 31.97%, and 7.12% respectively. Some *Gammaproteobacteria* contained the *Nosz* enzyme gene in denitrification, which always played an important role in the nitrogen transfer process. *Bacteroidia* had the function of nitrogen and phosphorus removal, whose distribution in the original sludge group, FW-AL group, and NaAc group were 16.42%, 25.92%, and 15.84%, respectively. The results indicated that FW-LA as carbon source was more conducive to the growth of this class of bacteria and the nitrogen cycle process. *Anaerolineae* was one of the main bacterial groups to remove COD and NH_4^+-N in WWTP, and the distribution of the three groups were 19.87% (original), 17.95% (FW-LA), and 16.43% (NaAc) respectively, which was slightly affected by carbon sources. NirK sequences were found in some *Alphaproteobacteria*, and some NirK-type denitrifiers had both denitrification and DNRA pathways, which were highly correlated with nitrogen cycling. The distributions of *Alphaproteobacteria* in the three groups were 9.80% (original), 8.97% (FW-LA), and 6.64% (NaAc), respectively. From the second genus-related population abundance map（Fig.5）, *Ca.competibacter* showed a significant difference between the two reactors with the intake of COD 200 mg/L was *Candida polygonatum*, which was a class of glycan bacteria, that could make the sludge easier to form condensed structures. However, the content of *Candida polygonatum* in the reactor with FW-LA as the carbon source was significantly lower than that in

the reactor with NaAc, which also explained the obvious phenomenon of sludge bulking in the reactor with FW-LA as the carbon source in the experiment. This issue should be addressed emphatically in actual application. Another species with notable differences in content was Rank-F-Saprospiraceae, the genus Saprospiraceae, a primary key contributor to sludge bulking in SBR reactor, which was obviously higher in FW-LA group than in NaAc. Ferruginibacter was shown in relevant studies that it could release relevant signaling factors to promote the self-cleaning of EPS, thus promoting the denitrification process. And fortunately, it was found the FW-LA reactor contained a high amount of functional microbes, which could bring about its better denitrification effect.

CONCLUSIONS

When the oriented LA fermentation broth of FW pretreated with 'high-pressure extrusion→impurity removal→crude oil removal→three-phase separation' was used as the carbon source for sewage treatment, the denitrification efficiency was comparable to that of NaAc in SBR system. The FW-LA carbon source exhibited a higher denitrification capacity with increasing to a higher inlet COD. The denitrification and TN removal rates could reach over 87% and 85% respectively when the influent COD was 300 mg/L. Analysis of the microbial community indicated the operation was relatively stable with FW-LA as carbon source, illustrating that FW-LA was of great significance in the recycling of FW, energy saving, and consumption reduction of sewage. Certainly, since LA carbon source has not yet been applied in the projects, its long-time operating impact on the sewage treatment system needed to be further studied.

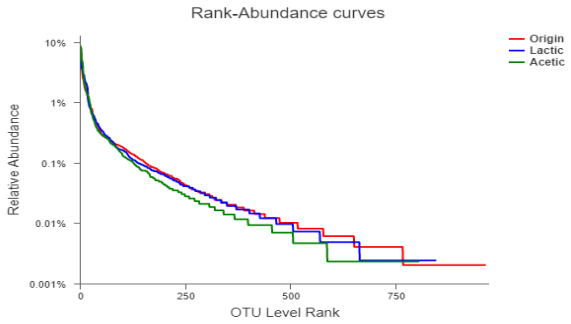

Fig. 3. Relative abundance curves of the sludge with FW-LA reactor, NaAc reactor, and origin sewage plant (COD inlet 200 mg/L)

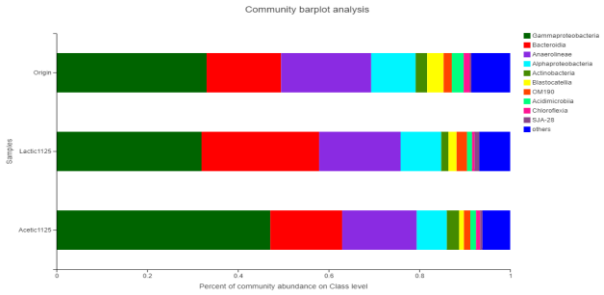

Fig. 4. Percent of community abundance on the class level in FW-LA group, NaAc group, and origin sewage plant (COD inlet 200 mg/L)

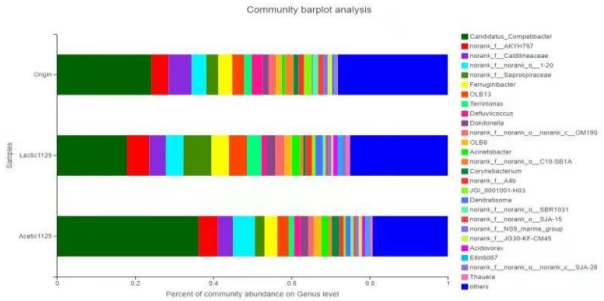

Fig. 5. Percent of community abundance on the genus level in FSFW-Lactic acid reactor, NaAc reactor, and origin sewage plant (COD inlet 200 mg/L)

REFERENCES

1. Wang D.M. Study on the characteristics and application of food waste fermentation with high lactic acid [D]. Xi 'an University of Architecture and Technology, 2016.

2. Yang Q.L, Xi XY et al. Enhanced nitrogen removal efficiency of external carbon source during abnormal influent in municipal waste water treatment plant[J]. China Water & Wastewater, 2011, 27(3):106-108.

3. Hu X.Y, Zhu JP. Biological denitrification efficiency of three single and mixed carbon sources[J]. Technology of water treatment, 2020, 46(01):57-61.

4. Tang J, Pu Y, Wang X. C, et al. Effect of additional food waste slurry generated by mesophilic acidogenic fermentation on nutrient removal and sludge properties during wastewater treatment[J]. Bioresource Technology, 2019, 294: 122218.

5. Hu H, Ma S, Zhang X, et al. Characteristics of dissolved organic nitrogen in effluent from a biological nitrogen removal process using sludge alkaline fermentation liquid as an external carbon source [J]. Water Research, 2020, 176: 115741.

RESEARCH TREND ANALYSIS OF HIGH-VALUE PRODUCTS BY ANAEROBIC FERMENTATION BASED ON THE WEB OF SCIENCE DATABASE

Yuanchun Zhang[1], Wenbin Zhu[1], Na Song[2], Ming Gao[1] and Qunhui Wang[1]
1 School of Energy and Environmental Engineer, University of Science and Technology Beijing, 30 Xueyuan Road, Haidian District, Beijing 100083, China
2 Tianjin College, University of Science and Technology Beijing, 1 Zhujiang North Ring East Road, Baodi District, Tianjin 301830, China

INTRODUCTION

Organic solid waste (OSW) is a type of organic matter produced by human activities, about 2.01 billion tons of OSW are produced globally each year, and the yield of OSW has been on an upward trend due to the rapid development of modern society and the continuous growth of the global population [1]. OSW is rich in biodegradable organic matter (such as proteins, carbohydrates and lipids) and phytonutrients (nitrogen, phosphorus and potassium) that can be reused as inexpensive and readily available raw materials in green energy production [2]. Anaerobic fermentation (AF) is an efficient and economical method for the treatment of organic solids, from which a large number of renewable resources can be obtained. AF can achieve efficient organic solid waste treatment and contribute to the development of a low-carbon economy and the replacement of clean energy. The synthesis, preparation, processing and application of AF products have enormous potential for large-scale development, and their market demand is rapidly increasing. Because of differences in physical and chemical properties, as well as microbiological composition, the pretreatment process, fermentation process, and composition of fermentation products differ between organic solid wastes.

In this paper, a bibliometric method was used to study the research of anaerobic fermentation from 2001 to 2021, and different kinds of indicators were analyzed. We combined the results of the current study of anaerobic fermentation, and also can provide a guiding role for future development.

MATERIALS AND METHODS

The ISI Web of Science and Science Citation Index Expanded (SCIE) database were the primary data source. The Web of Science of the Institute of Scientific Information is an internationally recognised major retrieval tool for scientific statistics and evaluation, and a major platform for exchanges between international scholars [3]. In this study, (anaerobic ferment*) was used as a search phrase to search topics in SCIE for the period from 2001 to 2021. Furthermore, the Web of Science offers intelligent tools for data analysis in various forms, making it possible to approximate the trend in the field of AF for a specific raw material/product by searching for the keyword 'anaerobic fermentation' combined with that raw material/product.

For the research on anaerobic fermentation, all the analysis were all count using Microsoft Excel 2016.

RESULT AND DISCUSSION

2896 publications related to anaerobic fermentation from 2001 to 2021, research articles are the most important form of literature output, with a total of 2380 articles, accounting for about 82.2% of the total statistical literature.

(1) Characteristics of publication outputs

The top five countries with the largest number of publications are China, the United States, Germany, India and Japan (Fig.1).

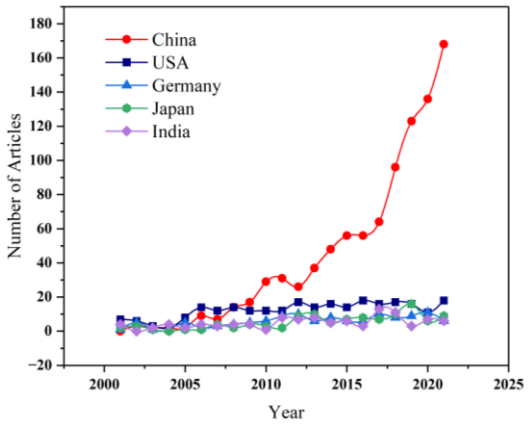

Figure 1. Published articles on AF related research from 2001 to 2021

After 2008, China ranked first in terms of the number of published documents than other countries, mainly because the Chinese government began to pay attention to the recycling of food waste. In addition, the number of countries/regions participating in AF research has increased from 32 in 2001 to 380 in 2021, which shows

that AF-related research has attracted worldwide attention, and the cooperation trend of various scientific research institutions has also significantly enhanced, the technology of using AF to treat solid waste has been widely used.

(2) Distribution of journals and subject categories

According to the analysis of discipline categories in the Journal Citation Report based on ISI, the number of discipline categories exceeding 10% of the total number of articles is 6. Amongst them, Biotechnology & Applied Microbiology contributed the most with 803 articles, followed by Energy Fuels, Engineering, Environmental Sciences Ecology, Agriculture and Chemistry. Microbiology also ranked in the top eight, which is consistent with the fact that the AF process mainly relies on the action of microorganisms. In addition, AF products have been gradually applied in the energy field in recent years, and this technology has made significant contributions to the treatment of agricultural organic wastes, such as straw, weeds, fallen leaves, fruit shells, and etc.

(3) Research hotspots in AF

By analysing the keywords of AF-related papers, we can understand the research trend information and identify research hotspots [4]. Amongst the top 30 keywords in the search frequency, there are fermentation substrates such as waste activated sludge; food waste; microalgae and crude glycerol; and fermentation products such as hydrogen, biogas, ethanol, butanol, VFAs, lactic acid and succinic acid, which also reflect the research hotspots in this field.

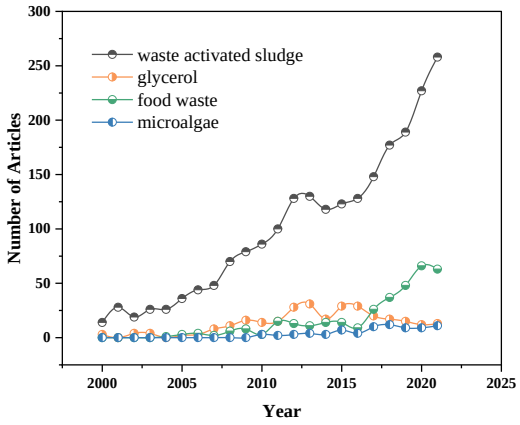

Figure 2. The trend of the relevant articles of different substrates over time from 2001 to 2021

The production of platform chemicals and fuels from renewable resources is a major focus of circular economy. Hot research products of AF include energy substances such as biohydrogen, biogas, bioethanol, and biobutanol, and liquid chemicals such as VFAs, succinic acid and lactic acid.

The analysis of keywords revealed that the valorisation of cheap and easily available raw materials with high organic matter content and the production of clean energy substances and high value-added platform products will continue to become global research hotspots in future research.

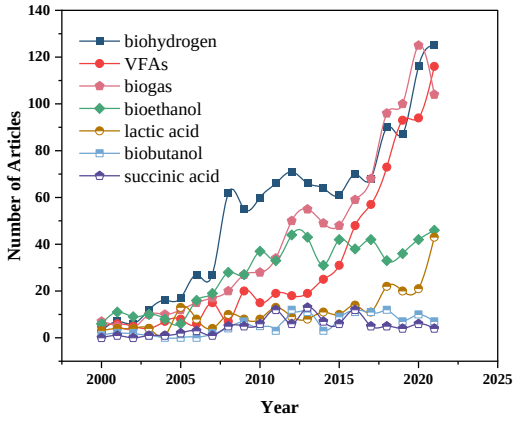

Figure 3. Growth trend of different AF products from 2001 to 2021

CONCLUSION

Based on the articles in the SCI database, this study used bibliometrics to conduct a statistical analysis of the relevant articles on AF from 2001 to 2021. The analysis of keywords shows that biomass wastes with low price, easy availability and high organic matter content (such as waste activated sludge, food waste, microalgae and crude glycerol) have good potential for resource utilisation. The production of clean energy substances such as hydrogen, biogas, ethanol and butanol through AF will continue to be the focus of attention.

ACKNOWLEGEMENT

This work was supported by the National Key R&D Program of China (Grant NO. 2019YFC1906302 & 2019YFC1906304) and Tianjin Education Commission Scientific Research Planning Project (2021KJ064).

REFERENCE

1. Wainaina S, Awasthi MK, Sarsaiya S, Chen H, Singh E, Kumar A, et al. Resource recovery and circular economy from organic solid waste using aerobic and anaerobic digestion technologies. Bioresour Technol 2020;301:122778.
2. Ma Y, Liu Y. Turning food waste to energy and resources towards a great environmental and economic sustainability: An innovative integrated biological approach. Biotechnol Adv 2019;37:107414.
3. Ho Y-S. The top-cited research works in the Science Citation Index Expanded. Scim 2012;94:1297-312.
4. Hou Q, Mao G, Zhao L, Du H, Zuo J. Mapping the scientific research on life cycle assessment: a bibliometric analysis. The International Journal of Life Cycle Assessment 2015;20:541-55.

UNVEILING THE TECHNOLOGY AND MECHANISMS OF MEDIUM-CHAIN FATTY ACIDS PRODUCTION FROM WASTE ACTIVATED SLUDGE FERMENTATION LIQUOR

Shu-Lin Wu[1,2], Yuyang Long[1,2] and Dongsheng Shen[1,2]
1 School of Environmental Science and Engineering, Zhejiang Provincial Key Laboratory of Solid Waste Treatment and Recycling, Zhejiang Gongshang University Hangzhou 310012, China
2 China Zhejiang Engineering Research Center of Non-ferrous Metal Waste Recycling, Hangzhou 310012, China

ABSTRACT
Chain elongation (CE) with open-culture microbiomes has been demonstrated to be an effective biotechnological platform to produce valuable medium chain fatty acids (MCFAs). Herein we reported a new biotechnological process for producing MCFAs by using waste-activated sludge alkaline fermentation liquor as feedstock and electron acceptors (EAs) with ethanol as electron donor (ED). Under three different carbon-molar ratios of ED to EAs (i.e., 1:2, 1:1 and 2:1), three different types of MCFAs (i.e., n-caproate, n-heptanoate and n-caprylate) were produced. Thermodynamic analysis showed the higher amount of ethanol was more favorable for MCFAs production. Microbial community revealed that the ethanol participation caused microbes shift in the favorable direction for CE process. Metagenome analysis showed both reverse β-oxidization and fatty acid biosynthesis pathways simultaneously enhanced and occurred in the CE process.

BACKGROUND AND RELEVANCE
Large quantities of waste activated sludge (WAS) were produced due to the wide application of the activated sludge process for the biological treatment of wastewater. It has been estimated that, in China only, WAS production would increase from around 40 million tons to more than 60 million tons from 2015 to 2020 posing serious threats to the natural environment (Li et al. 2018, Sun et al. 2019). Thus, effective sludge treatment, especially the implementation of renewable technologies, is of great importance for sludge disposal.

Recently, a newly developed carboxylate platform to produce medium chain fatty acids (MCFAs) via chain elongation (CE) may provide a promising solution for bioenergy or resource recovery from WAS (Cavalcante et al. 2017, Ge et al. 2015, Lonkar et al. 2016). MCFAs, such as n-caproate (C6), n-heptanoate (C7), and n-caprylate (C8), have higher caloric value than short chain fatty acids (SCFAs) due to their higher carbon/oxygen ratios. They are high monetary value products and can be adopted as superior precursors for further processing to biofuels or directly as industrial commodity (Agler et al. 2012, Ge et al. 2015). Moreover, MCFAs have superior separation characteristics due to their hydrophobic carbon chains (Steinbusch et al. 2011). The separation of MCFAs from fermentation broth could be relatively easily achieved through physical extraction with much less energy consumption compared to SCFAs (Angenent et al. 2016).

In the CE process, MCFAs could be produced by anaerobic microorganisms using SCFAs as electron acceptors (EAs). The alkaline fermentation of WAS could produce significant quantities of SCFAs. It has been reported that the SCFA yield could reach ~250 mg COD per gram of volatile suspended solids, with acetate, propionate, butyrate and valerate being the main products (Yuan et al. 2006). Thus, the high SCFA concentration in the WAS alkaline fermentation liquor (WASAFL) suggested it could work as an emerging source of EAs for the production of MCFAs. However, so far, the feasibility of upgrading WASAFL into MCFA has not been demonstrated.

Therefore, in this study, we explored the feasibility of upgrading WASAFL into MCFA using ethanol as electron donor. The MCFAs production was investigated at increasing carbon-molar ratios of ED to EA, i.e., 1:2, 1:1 and 2:1. Thermodynamic analysis was conducted for assessing the potential spontaneity and competition in the CE processes. In addition, the high-throughput sequencing and metagenomic analyses were also performed to elucidate the taxonomic composition and functional genes in the culture, with the goal of identifying the key metabolic pathways in the CE process for upgrading WASAFL into MCFAs. The results of this study are expected to provide a new insight into the bioenergy and resource recovery from WAS.

MATERIAL AND METHODS

Waste activated sludge alkaline fermentation liquid (WASFL) was cultivated under alkaline condition (pH=10) with waste activated sludge from secondary sedimentation tank of municipal waste water treatment plant. After reaching the steady state, different levels of ethanol were added into fermenters as electron donor (ED). To investigate a wide range of carbon molar ratio of ED to EA on the CE process and to avoid the toxicity of ethanol and produced MCFAs on microorganisms, CE experiments were carried out with ethanol as the ED under three different carbon molar ratios of ED to EA, i.e., 1:2 (R1), 1:1 (R2), and 2:1 (R3). Thermodynamic analysis was applied to explore the spontaneity of the CE process with WASFL as EA and ethanol as ED. Illumina Miseq sequencing was applied to explore the shift of microbial communities and functional microbes in CE process. Metagenomic analysis was applied for figuring out the pathway participated in CE process.

RESULT AND DISSCUSSION

MCFAs Production from WASFL via CE Process

The MCFAs (i.e., n-caproate, n-heptanoate, n-caprylate) could be obtained with different carbon molar ratio of ED (ethanol) to EA (WASFL). As shown in Figure 1, the concentration of MCFAs significantly increased with ratios of ED to EA increasing from 1:2 to 2:1. The total cumulative MCFAs yield increased from 2.88 ± 0.01 g COD/L to 5.19 ± 0.42 g COD/L with respect to the ED: EA ratio of 1:2 to 1:1 and then further increased slightly to 5.28 ± 0.18 g COD/L at the ED: EA ratio of 2:1. However, the proportion of total MCFAs (C6, C7 and C8) was highest at ED: EA ratio of 1:1, accounting for 72.9 % of the total carbon content, followed by those at ED: EA ratios of 2:1 and 1:2, each accounting for 60.2% and 65.9%, respectively.

It should also be noted that two higher alcohols, i.e., n-butanol and n-hexanol were produced when the highest ED:EA ratio is applied (2:1). The n-butanol concentration reached 0.49 ± 0.02 g COD/L and the hexanol was 0.30 ± 0.02 g COD/L at the end of the experimental period, respectively. The n-butanol and n-hexanol could be generated through the reduction of butyrate and n-caproate, respectively (Gomez and Cantero, 2007). Besides, they could also be produced through the CoA-dependent pathway.

Thermodynamic calculations

The thermodynamic calculation results were shown in Figure 2. All calculated Gibbs free energy values for n-caproate, n-heptanoate and n-caprylate were negative and numerically higher than the minimum amount of energy (-20kJ per reaction) required for the survival of living cells, confirming that all of the experimental carbon molar ratio of ethanol to WASFL combinations were thermodynamically feasible in the CE processes.

Effect of ethanol on functional microbial communities in CE process

The microbial compositions at genus level in different sludge sample were exhibited in Fig. 3. The relative abundance of *Clostridium sensu stricto*, a major member of *Clostridia*, was increased with the addition of ED, with average abundances being 0.17%, 0.73%, 0.85% and 2.85% for R0, R1, R2 and R3, respectively. Blasting the OTUs belonged to *Clostridium sensu stricto* on National Central for Biotechnology Information (NCBI) database, some of them were belonged to *Clostridium Kluyveri* (Identity >99%), which is by far the best-studied species known to produce MCFAs (Angenent et al. 2016, Spirito et al. 2014). The relative abundance of *C. Kluyveri* was positively related to the ethanol addition in the studied system, which increased from 0 in R0 (without ethanol addition) to 0.44% in R3 (ethanol 74 mM). This indicated that *C. Kluyveri* also played an important role in CE process using WASAFL. Other species which also have been reported capable of MCFA production through CE, such as *Clostridium sp. BS-1*, *Eubacterium pyruvativorans* and *Eubacterium limosum* were absent in the studied system (Angenent et al. 2016). However, the relative low abundance of *C. Kluyveri* suggested that other unreported species might also be responsible for CE process in the studied system.

The relative abundance of other genera such as *Oscillibacter*, *Leptolinea* and *Exilispira* were also increased with the ethanol addition and MCFA production. These microorganisms are known as anaerobic fermenters. The increase of the abundance of *Oscillibacter* with MCFAs production has also been reported previously (Wu et al. 2018). Although there is no evidence of directly carrying out CE process by these fermenters, the positive correlation between their abundance and MCFA production indicated that they might be beneficial to the CE process when using ethanol as ED.

Pathway in CE process revealed by metagenomic analysis

All the functional genes identified by the metagenomics analysis were annotated against the Kyoto Encyclopedia of Genes and Genomes (KEGG) database (http://www.genome.jp/kegg/pathway. html) to carry out enzyme assays for further investigation of the CE pathways. Potential functional enzymes involved in CE processes were specifically studied. Accordingly, two cyclic pathways, i.e., the reverse b-oxidization (RBO) pathway and fatty acid biosynthesis (FAB) pathway were constructed (Figure 4). Most enzymes involved in the above two pathways were clearly more abundant in CE sludge sample than that in original inoculum, suggested that RBO and FAB pathway were enhanced and played important role in CE process.

FIGURES/ PHOTOGRAPHS

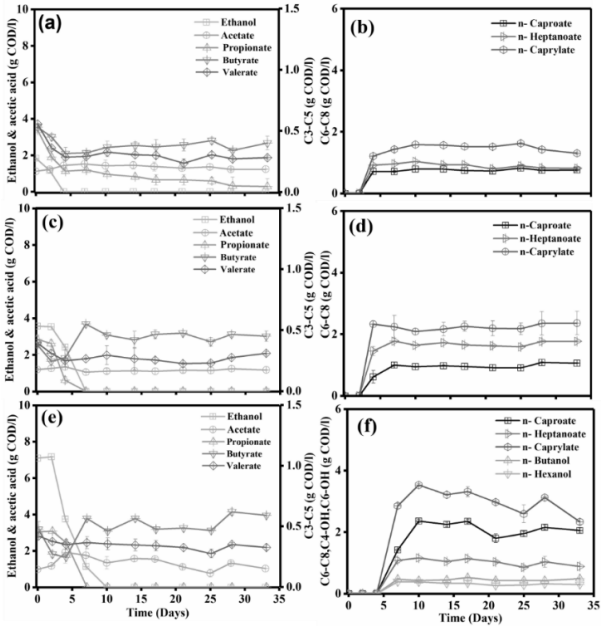

Figure 1. Concentrations evolution of ethanol and SCFAs (acetate, propionate, butyrate and valerate) as well as MCFAs (n-caproate, n-heptanoate and n-caprylate) in three sets of CE experiments using ethanol as ED and WAS alkaline fermentation liquid as EA: (a-b) the ED to EA ratio was 1:2; (c-d) the ED to EA ratio was 1:1; and (e-f) the ED to EA ratio was 2:1.

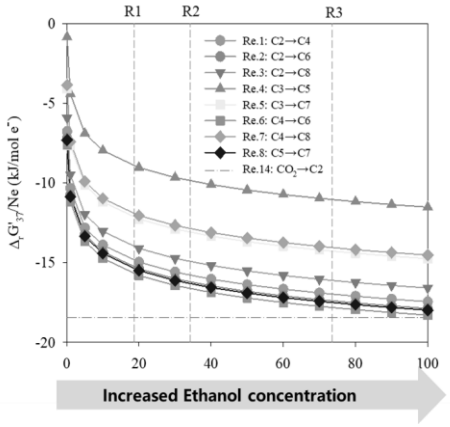

Figure 2 Thermodynamics calculation in three sets of ED to EA ratios.

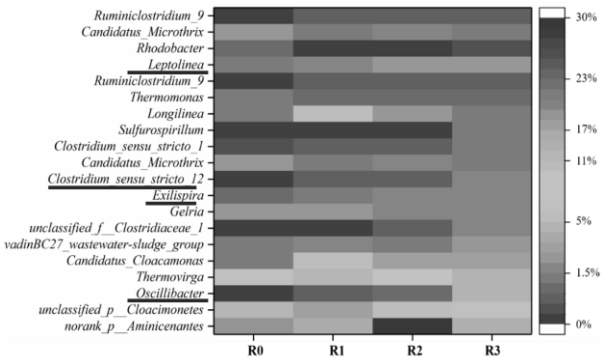

Figure 3. Composition of relative species at genus level for the initial inoculum (R0) and the three CE sludge samples (R1, R2 and R3)

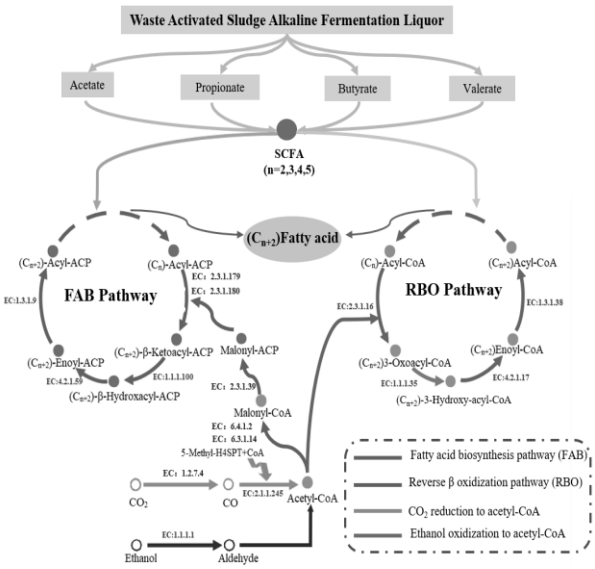

Figure 4. Potential metabolic chain elongation pathways with ethanol as ED and WASFL as EA in this work.

REFERENCE

Agler, M.T., Spirito, C.M., Usack, J.G., Werner, J.J. and Angenent, L.T. (2012) Chain elongation with reactor microbiomes: upgrading dilute ethanol to medium-chain carboxylates. Energy Environ Sci 5(8), 8189.

Angenent, L.T., Richter, H., Buckel, W., Spirito, C.M., Steinbusch, K.J., Plugge, C.M., Strik, D.P., Grootscholten, T.I., Buisman, C.J. and Hamelers, H.V. (2016) Chain Elongation with Reactor Microbiomes: Open-Culture Biotechnology To Produce Biochemicals. Environ Sci Technol 50(6), 2796-2810.

Cavalcante, W.d.A., Leitão, R.C., Gehring, T.A., Angenent, L.T. and Santaella, S.T. (2017) Anaerobic fermentation for n-caproic acid production: A review. Process Biochemistry 54, 106-119.

Ge, S., Usack, J.G., Spirito, C.M. and Angenent, L.T. (2015) Long-Term n-Caproic Acid Production from Yeast-Fermentation Beer in an Anaerobic Bioreactor with Continuous Product Extraction. Environ Sci Technol 49(13), 8012-8021.

Li, X., Chen, L., Mei, Q., Dong, B., Dai, X., Ding, G. and Zeng, E.Y. (2018) Microplastics in sewage sludge from the wastewater treatment plants in China. Water Res 142, 75-85.

Lonkar, S., Fu, Z. and Holtzapple, M. (2016) Optimum alcohol concentration for chain elongation in mixed-culture fermentation of cellulosic substrate. Biotechnol Bioeng 113(12), 2597-2604.

Spirito, C.M., Richter, H., Rabaey, K., Stams, A.J. and Angenent, L.T. (2014) Chain elongation in anaerobic reactor microbiomes to recover resources from waste. Curr Opin Biotechnol 27, 115-122.

Steinbusch, K.J.J., Hamelers, H.V.M., Plugge, C.M. and Buisman, C.J.N. (2011) Biological formation of caproate and caprylate from acetate: fuel and chemical production from low grade biomass. Energy Environ. Sci. 4(1), 216-224.

Sun, J., Dai, X., Wang, Q., van Loosdrecht, M.C.M. and Ni, B.J. (2019) Microplastics in wastewater treatment plants: Detection, occurrence and removal. Water Res 152, 21-37.

Wu, Q., Guo, W., Bao, X., Meng, X., Yin, R., Du, J., Zheng, H., Feng, X., Luo, H. and Ren, N. (2018) Upgrading liquor-making wastewater into medium chain fatty acid: Insights into co-electron donors, key microflora, and energy harvest. Water Res 145, 650-659.

Yuan, H., Chen, Y., Zhang, H., Jiang, S., Zhou, Q. and Gu, G. (2006) Improved bioproduction of short-chain fatty acids (SCFAs) from excess sludge under alkaline conditions. Environ Sci Technol 40(6), 2025.

CONDITION OPTIMIZATION AND ECONOMIC ANALYSE OF ULTRASONIC-ALKALI CRACKING OF EXCESS SLUDGE

XINBO YUE, SHEN Tingting, ZHANG Guangming*, and ZHANG Jie
School of Energy and Environmental Engineering, Hebei University of Technology, Tianjin, China

China's sewage treatment plants are generally insufficient carbon sources, often by adding external carbon sources (methanol, acetic acid, glucose, etc.) to solve(Tao et al., 2021), may bring about an increase in the output of excess sludge, and cost a lot of operating costs (Feng et al., 2015)。Excess sludge hydrolysis is an important way to solve the shortage of carbon source for biological denitrification and phosphorus removal in wastewater treatment plants and to achieve sludge minimization.Reduce operating costs for sewage treatment plants. The main methods of sludge cracking are microwave treatment(Lin et al., 2020), ultrasound (Xu et al., 2019) and heat treatment (Wang et al., 2009), Acid/alkaline treatment (Li et al., 2017; Xie et al., 2014)et al. Among them, the ultrasonic-alkali combination method has certain advantages, ultrasonic waves can promote the release of cellular organic matter in a short period of time, alkalil crack can promote the hydrolysis of organic matter (Gao et al., 2021), and the synergistic effect of the two is better than that used only.

Most of the existing studies have focused on the release of SCOD in the sludge, and have not noticed that the return of N and P released at the same time may make C/N and C/P low, not conducive to nitrogen and phosphorus removal, and have not noticed economic cost analysis. Therefore, in this study, the changes of C/N and C/P are paid attention to at the same time as obtaining high carbon-containing supernatants, so as to avoid excessive nitrogen and phosphorus in the return carbon source. The orthogonal test optimizes the required ultrasound-alkaline crack conditions of high SCOD and high C/N and C/P, and compares this technique with other cracking techniques.

The following conditions were recommended: Power density = 1.5 W/ml, pH = 10, ultrasound time = 15 min, alkali time = 1.5 h, SCOD > 7 600 mg/L, C/N > 30, C/P > 60, which can prepare sludge supernatant with high carbon and low nitrogen and phosphorus, and save cost than the way of external carbon source. VSS removal rate reaches about 35%, which can reduce the sludge disposal VSS removal rate of about 35% can reduce the cost of sludge disposal. The economic cost is about 38.7 RMB/t sludge when the technology is applied on a large scale.

Table. 1 Results of different parameter combinations

	Power density（W/ml）	pH	Ultrasound Time（min）	Alkali Time（h）	Crack rate（%）	C/N	C/P
1	1	10	15	1	2.9	80.16	55.19
2	1	11	25	1.5	3.5	59.97	54.67
3	1	12	35	2	9.5	38.11	56.32
4	1.5	10	25	2	3.0	58.83	70.86
5	1.5	11	35	1	2.8	44.33	51.03
6	1.5	12	15	1.5	12.8	34.80	61.36
7	2	10	35	1.5	5.0	31.18	60.46
8	2	11	15	2	4.9	23.85	46.08

	Power density（W/ml）	pH	Ultrasound Time（min）	Alkali Time（h）	Crack rate（%）	C/N	C/P
9	2	12	25	1	13.1	34.23	60.42

Reference:

Feng, L., Luo, J., Chen, Y., 2015. Dilemma of Sewage Sludge Treatment and Disposal in China. Environ. Sci. Technol. 49, 4781–4782. https://doi.org/10.1021/acs.est.5b01455

Gao, J., Wang, Y., Yan, Y., Li, Z., 2021. Ultrasonic-alkali method for synergistic breakdown of excess sludge for protein extraction. J. Clean Prod. 295, 126288. https://doi.org/10.1016/j.jclepro.2021.126288

Li, X., Peng, Y., Li, B., Wu, C., Zhang, L., Zhao, Y., 2017. Effects of alkali types on waste activated sludge (WAS) fermentation and microbial communities. Chemosphere 186, 864–872. https://doi.org/10.1016/j.chemosphere.2017.08.017

Lin, K.-H., Zeng, J.-Y., Chiang, H.-L., 2020. Microwave pyrolysis of sludge for potential use as land application and biofuel. J. Chem. Technol. Biotechnol. 95, 975–984. https://doi.org/10.1002/jctb.6055

Tao, Z., Jing, Z., Wang, Y., Tao, M., Luo, H., 2021. Higher nitrogen removal achieved in constructed wetland with polyethylene fillers and NaOH-heating pre-treated corn stalks for advanced treatment of low C/N sewage. Environ. Sci. Pollut. Res. 28, 13829–13841. https://doi.org/10.1007/s11356-020-11652-9

Wang, Z., Wang, W., Zhang, X., Zhang, G., 2009. Digestion of thermally hydrolyzed sewage sludge by anaerobic sequencing batch reactor. Journal of Hazardous Materials 162, 799–803. https://doi.org/10.1016/j.jhazmat.2008.05.103

Xie, S., Wu, Y., Wang, W., Wang, J., Luo, Z., Li, S., 2014. Effects of acid/alkaline pretreatment and gamma-ray irradiation on extracellular polymeric substances from sewage sludge. Radiation Physics and Chemistry 97, 349–353. https://doi.org/10.1016/j.radphyschem.2013.07.026

Xu, X., Cao, D., Wang, Zonghua, Liu, J., Gao, J., Sanchuan, M., Wang, Zhenjun, 2019. Study on ultrasonic treatment for municipal sludge. Ultrasonics Sonochemistry 57, 29–37. https://doi.org/10.1016/j.ultsonch.2019.05.008

CURRENT SITUATION OF MUNICIPAL SLUDGE PRODUCTION AND DISPOSAL IN GUANGXI

Muxi Zhang[1,2,3], Xiaojie Sun[1,2,3*]

1.Guangxi Key Laboratory of Environmental Pollution Control Theory and Technology, Guilin University of Technology, Guilin 541004, China

2.Guangxi Collaborative Innovation Center for Water Pollution Control and Water Safety in Karst Area, Guilin University of Technology, Guilin 541004, China

3. Guangxi Key Laboratory of Environmental Pollution Control Theory and Technology for Science and Education Combined with Science and Technology Innovation Base, Guilin University of Technology, Guilin 541004, China

Abstract: With the acceleration of urbanization in China, the sewage treatment capacity and scale continue to rise, and the production of municipal sludge is also more and more. This paper summarizes and analyzes the current situation of sludge generation and disposal in Guangxi region and each city in 2019, and puts forward suggestions for sludge disposal in Guangxi region, which is of great significance for planning the future development of municipal sludge in Guangxi region. Taking into account factors such as area, carbon emission, sludge composition and calorific value in Guangxi region, the sludge in Guangxi region is suitable for disposal by anaerobic digestion + land use and aerobic fermentation + land use; when the sludge is not suitable for land use and incineration and building materials utilization conditions are not available locally, landfill disposal will be considered. In the long run, Guangxi sludge should be disposed in a multi-form and multi-channel way.

INTRODUCTION

Along with the speeding up of industrialization and urbanization and the tightening of environmental policy, urban sewage treatment capacity has been improved rapidly and the scale of sewage treatment has surged in recent years[1]. In 2019, there were 2,471 sewage treatment plants in China, with a total sewage treatment volume of 53.7 billion m^3 and a sewage treatment capacity of 180 million m^3/d[2]. With the improvement of sewage treatment capacity, sludge as a by-product of sewage treatment continues to increase. According to the calculation of 5 ~8 t per 10,000 m^3 domestic sewage production (in moisture content 80%)[3], the annual output of sludge in our country is more than 40 million t, with an annual growth rate of 10%, is expected to break through 60 million t (in moisture content 80%) in 2020 to 2025[4]. According to the 2020 Urban and Rural Construction Statistical Yearbook, the output of dry sludge from municipal sewage treatment plants at the prefecture level and above in 2020 is 1.163×107 t, and the dry sludge yield of county-level cities is 1.7×106 t. Based on the wet sludge with 80% moisture content, the wet sludge yield in counties and above cities is 6.664×107 t [5].

Sewage sludge is a semi-solid waste produced from wastewater treatment plants (WWTPs) after a series of physical, chemical and biological wastewater treatment. Sludge is a heterogeneous complex mixture, mainly composed of fibers, animal and plant residues, microorganisms, pathogens, parasites and heavy metals. If the sludge is not properly treated and disposed of, it may cause serious secondary environmental pollution problems[6-10]. According to the 13th Five-Year Plan, the disposal of sludge generated by sewage treatment will be one of the main directions of environmental protection and pollution control in China in the future, so it can be seen that the disposal of sludge will be elevated to a new

historical height [11]. In the 14th Five-Year Plan for Urban Sewage Treatment and resource Utilization, it is pointed out that sludge treatment facilities should be included in the construction plan of local sewage treatment facilities, requiring that the harmless disposal rate of urban sludge should reach more than 90% by 2025, and the harmless disposal of sludge should be fully realized by 2035 [5]. Although 90% of sewage treatment plants in China have realized sludge dewatering and reduction treatment, the proportion of sewage treatment plants that realize biological stabilization treatment of sludge is less than 3%. Most of the sludge is directly landfill without stabilization treatment, and less than 20% of the sludge has been safely treated and disposed of [12]. Therefore, further efforts are needed to meet the requirements of the program.

Sludge disposal is an important link in sewage treatment process[13]. However, there is a serious phenomenon of "heavy water and light mud" in the construction of sewage treatment plants, and the lack of subsequent supporting treatment facilities leads to a large amount of sludge backlog, which has not been reasonably and safely treated and disposed of, and has brought a lot of impacts on the normal operation of sewage treatment plants [14,15]. The sludge from Nanning sewage treatment plant is concentrated and dehydrated to 80% water content and then transported to an agricultural compound fertilizer company to make biological compound fertilizer. However, fertilizer companies cannot guarantee long-term and stable acceptance of sludge due to seasonal and sales conditions. As a result, sludge accumulates inside the treatment plant, increasing the environmental safety risk around the plant and affecting the normal operation of each sewage treatment plant [16]. Therefore, how to properly and safely dispose the sludge with huge output and complex composition, so as to reduce, harmlessly and recycle it, has become an urgent environmental problem to be solved in Guangxi.

This paper summarizes and analyzes the current situation and disposal of sludge in Guangxi region and cities in 2019, and further analyzes the harmless disposal method of sludge in Guangxi. It is necessary to fully understand the current situation of sludge generation and disposal in Guangxi region, provide decision-making reference and policy measures for relevant departments, and plan the future development of municipal sludge in Guangxi region.

SLUDGE PRODUCTION STATUS

According to the data released by the Ministry of Housing and Urban-Rural Development, there were 56 sewage treatment plants in Guangxi in 2019, with a total sewage treatment volume of 126.72 million m^3 and a sewage treatment capacity of 3.918 million m^3/d[5]. Guangxi dry sludge production capacity of 120,000 t, dry sludge treatment capacity of 90,000 t, the treatment rate is only 75.51%. Figure 1 shows the dry sludge production volume of urban sewage treatment plants in Guangxi in 2019. Nanning, Liuzhou and Guilin were the major cities with sludge production volume exceeding 10,000 t/a, with a total sludge production volume of 92,000 t, accounting for 74.1% of the total production volume in the whole region.

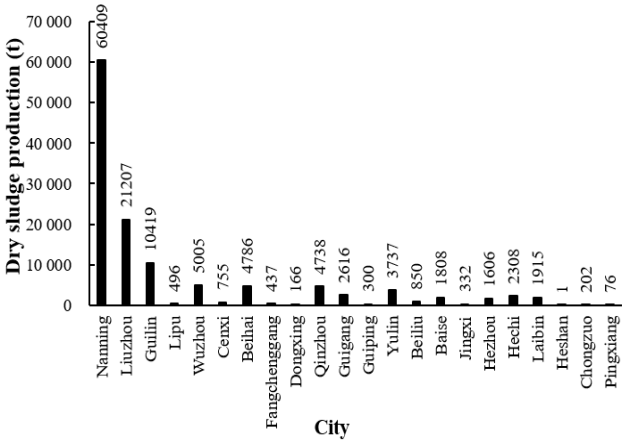

Figure 1 Dry sludge production of Guangxi Municipal Sewage Treatment Plant in 2019

CURRENT SITUATION OF SLUDGE DISPOSAL

At present, the main sludge disposal methods are sanitary landfill, incineration, building materials utilization and land utilization [17]. In terms of final destination, landfill is still the main destination of urban sludge in our country at present. The second is land use and building materials use [18]. More than 52.89% of the sludge generated by sewage treatment plants in China is treated and disposed in the way of sanitary landfill, and 14.97% is land utilized [1]. During the 13th Five-Year Plan period, the capacity of harmless treatment and disposal facilities for sludge (measured by wet sludge with 80% moisture content) was 60,100 tons per day nationwide, and Guangxi reached 1,921 tons per day. Among them, Guangxi has 1,622 tons/day for cities, 122 tons/day for counties and 177 tons/day for towns [19]. The proportion of municipal sludge land utilization in Guangxi reached 54.2%, landfill 27.8%, incineration 2%, and others 16% [13]. Harmless sludge disposal facilities in the region are mainly concentrated in Nanning, Liuzhou and other major cities, Guilin, Beihai, Guigang, Hezhou, Hexi and Laibin are mainly landfill, Wuzhou, Qinzhou and other parts of the sludge landfill disposal method, a considerable number of cities have not been equipped with harmless disposal facilities [20].

Landfill

Sludge landfill can be divided into two ways: single landfill and mixed landfill with municipal solid waste. However, the addition of household garbage and sludge will significantly increase the concentration of total suspended solids in the leachate and the proportion of particles with large particle size in the filtrate, which will accelerate the physical blockage process of the drainage system at the bottom of the landfill. Therefore, from the perspective of blockage of the drainage system, it is extremely unfavorable to mix sludge with municipal solid waste for landfill [21]. Landfill has the advantages of simple operation, large processing capacity, low investment and remarkable effect [22]. However, landfill will occupy a large amount of land, resulting in a waste of resources, and also cause a large amount of greenhouse gas emissions, which is not conducive to the realization of carbon neutrality goals [23,24]. It costs a lot in seepage prevention and leakage prevention, and it needs to be equipped with the treatment of leachate and waste gas in the later stage [25]. More mountains and less land are the main characteristics of land resources in Guangxi. The area of mountains, hills and stone mountains accounts for 69.7% of the total area, and there are no landfill sites that can sustainably accept sludge. Therefore, landfill is not suitable for long-term as the main sludge disposal method in Guangxi.

Land utilization

Sludge land utilization is an effective disposal method that can realize the recycling of sludge resources. Land use of sludge includes agricultural use, green space use, forest use and land restoration. Sludge contains a large amount of nitrogen, phosphorus, organic matter and other nutrients, so the application of sludge can increase soil nutrients, promote plant growth, and provide favorable conditions for sludge land use. Guangxi encourages sludge products that meet standards and have controllable risks to be used for land use, especially for forestland, land improvement and landscaping [26]. When the sludge meets the requirements of "Sludge for Landscaping in sludge Disposal of Urban Sewage treatment Plant" (GB/T23486-2009), it can be used in the construction and maintenance process of urban green space system or suburban forest land. It is generally used as cultivation medium soil, soil improvement material, and can also be used as raw material for making organic fertilizer. When the mud conforms to the provisions of "Mud for Land Improvement of Sludge Disposal in Urban Sewage Treatment Plant" (GB/T 24600-2009), it can be used for soil improvement in saline-alkali land, desertified land and abandoned mining site [27].

Yang Jianlao[28] to Guangxi District towns and disposal of the sludge characteristics in the direction of research shows that Guangxi towns of total nitrogen, phosphorus and potassium content in sludge, within the

range 4.19% ~ 13.62% higher than that of agricultural and forest land use and landscape with the nutrient requirements of three kinds of argillaceous standards, especially the passengers, the total nitrogen, phosphorus and potassium content of Guilin, the sludge is high (> 10%), Therefore, the reclamation potential of sludge land use in Guangxi area is very large. Cd is the main contributor to the potential ecological risk of heavy metals in urban sludge in Guangxi, and there are potential ecological risks in the sludge for agricultural use [29]. However, Xue Wanlai et al. [30] studied the impact of sludge land use on soil ecological environment, and showed that short-term land use of sludge did not significantly increase soil heavy metal content, which was safe for soil ecological environment. Huang Xingfa et al. [31] showed that the heavy metal content of sludge in Nanning met the standard requirements of landscaping, land improvement and national and Guangxi local agricultural A-grade sludge, and sludge could be used for landscaping, soil improvement, forestland and agriculture. The organic matter and total nutrient content of sewage sludge in Guilin city are high, and the heavy metal content is low. All pollutant control indexes can meet the agricultural characteristics of various soil properties. From the perspective of technical and economic analysis, the sewage sludge in Guilin city should be selected for land use [32]. However, limited to relevant national standards, sludge cannot be directly used for land.

At present, the basic building of adjust measures to local conditions, variety, and the argillaceous feature matching dispose and resource utilization of sludge treatment technology system, has formed four mainstream dispose and resource utilization of sludge safe disposal technology route: anaerobic digestion + land use, aerobic fermentation + land use, dry incineration + ash landfill or building materials utilization, deep dehydration + emergency landfill[33]. According to the characteristics of sludge in Guangxi, the methods of anaerobic digestion + land use and aerobic fermentation + land use are suitable for Guangxi.

Building materials using

The construction material utilization of sludge is mainly to make bricks by mixing sludge with inorganic materials such as fly ash or waste clay after deep dehydration, or to use cement kiln exhaust gas to dry sludge and then add raw material for clinker calcination [34]. The building materials utilization of sludge has the forms of making bricks, making cement, making light aggregate and making biochemical fiberboard. The product of sludge building materials utilization is a material product that can be used in construction projects, so it does not need to rely on land as the carrier of its final consumption, and can also replace part of the raw materials used to manufacture building materials [35]. Sludge preparation of ceramsite is conducive to reducing the leaching amount of heavy metals in raw materials, and the leaching level of heavy metals does not exceed the safety standard limit [36], which can be safely used in engineering construction and water treatment fields. Sludge brick solidify heavy metals in sludge, which is safe and feasible. Zhang Yu et al. [37] determined through leaching experiment that the amount of harmful heavy metals dissolved from sludge brick is very low, and it can be used as external wall material without causing harm to environmental safety.

The utilization of sludge building materials can effectively reduce energy consumption and solve the problem of sludge stacking occupying land resources, which is conducive to promoting the virtuous cycle of economic development, but also effectively reducing environmental pollution and realizing ecological sustainable development. It has good economic, social and environmental benefits [38]. The ash content of sludge in Guangxi is 56.46%, more than twice that of 27.18% of coal, and the inorganic mineral components in the ash can be used in the production of building materials, which indicates that the utilization value of sludge is very high [39]. Liuzhou also has large cement production enterprises in Lionan District, which can use existing facilities for sludge disposal according to local conditions [40]. Therefore, Guangxi should actively study

the use of sludge to make building materials in order to achieve the purpose of resource recovery.

Incineration

Incineration technology can reduce a large amount of sludge and effectively convert it into energy [41]. Sludge incineration process mainly includes semi-dry incineration and mixed combustion power generation [42]. Sludge incineration gasifies water, mineralizes sludge, kills pathogens, and minimizes sludge volume [43]. Sludge incineration is to treat itself by using its own calorific value, which reflects the concept of energy recycling and sustainable development. In view of the advantages of sludge incineration reduction and harmless treatment, it is likely to become the mainstream process of sludge treatment [44]. However, sludge drying incineration is faced with the problems of high energy consumption and high operating cost, which limits its promotion and application in Guangxi [45].

In addition to the reduction and capacity reduction of sludge mixed firing power generation, the steam generated can also be used for power generation, and the flue gas can be basically discharged up to standard. The ash and slag after mixed firing can be used as cement clinker or raw material for brick making to realize the resource utilization of sludge [42]. However, at the same sludge to coal blending mass ratio, with the decrease of sludge energy quality, the calorific value of mixed fuel per unit mass decreases, and the power generation decreases, and more coal energy needs to be consumed for sludge drying, thus reducing the power generation efficiency. The elemental composition of sludge in Guangxi is quite different from that of coal. For example, the C content is 20.648%, which is only one third of the coal, and the estimated calorific value of sludge is 7 423.34 kJ/kg, which is only one third of the coal [39]. There is no comprehensive and systematic study on the control of carbon emission and pollutant emission by incineration. In general, Guangxi does not have the conditions to carry out extensive incineration disposal.

SUGGEST

Sludge treatment and disposal technology should first achieve harmlessness, and then consider the maximum degree of resource utilization. In the Technical Specification for Land Use of Sludge Products of Guangxi Urban Sewage Treatment Plant, it is required to strictly control the concentration of toxic and harmful substances such as heavy metals and organic pollution of sludge products, and prohibit the sludge without harmless treatment to be directly absorbed in the land by mixing with soil or covering soil and other simple ways, so as to prevent secondary pollution. Land use is also prohibited for the sludge products that fail to meet the standard after harmless treatment of toxic and harmful sludge products and fail to reach the sludge stabilization and harmless technology.

With the promotion of carbon neutrality, future sludge treatment and disposal should aim at energy saving and consumption reduction and energy resource recovery. The energy conversion technology of sludge is mainly based on the existence of organic components in sludge. The average content of organic matter and total nutrients in sludge of major cities in Guangxi is 34.63% and 87.11 g/kg, which has high agricultural value. The total land area of Guangxi is 237,600 square kilometers, accounting for 2.5% of the total land area of China, and the cultivated land area reaches 4,385,900 hectares (the number of land use change surveys in 2018). At the end of 2016, the per capita cultivated land is about 0.08 hectares (1.20 mu). Conditions for sludge land use. Therefore, under the premise of controlling the risk of heavy metals, land use of treated sludge is a sludge disposal technology in line with the current situation in Guangxi. When the sludge is not suitable for land use and the local incineration and building materials utilization conditions are not available, landfill disposal can be adopted.

The sludge disposal process consumes energy on the one hand and emits a large amount of greenhouse gases on the other hand. Typically, 400 to 600 kg CO_2

equivalent direct carbon emissions can be generated per ton of wet sludge. The carbon emission level of other typical disposal schemes is lower than that of direct sludge landfill. It is estimated that landfill can emit 500 kg CO_2 equivalent GHG per ton of wet sludge, while incineration has direct CO_2 emissions of 74 kg and indirect CO_2 emissions of 119 kg per ton of wet sludge, and land use increases carbon emissions in the short term. However, in the long run, soil carbon sinks can be increased by increasing plant carbon sinks and promoting CH_4 oxidation. Land use has the lowest carbon emissions, while sanitary landfill has a large carbon emission. Therefore, anaerobic digestion + land use and aerobic fermentation + land use can be considered as the best methods for sludge disposal, followed by sludge incineration and building materials utilization, and finally sanitary landfill.

CONCLUSION

Sludge disposal needs to choose the appropriate disposal method according to local conditions. Based on the main characteristics of the land resources of Guangxi, there is no landfill site that can accept sludge sustainably, so landfill is not suitable for the main sludge disposal method in Guangxi for a long time. Based on the economic situation of Guangxi and the characteristics of low heating value of sludge, the incineration treatment technology with high energy consumption and high treatment cost is not suitable for promotion and application in Guangxi. The heavy metal and nutrient contents of municipal sludge in Guangxi district basically meet the requirements of land use, and the fast-growing eucalyptus, sugarcane, rice, corn and banana crops are planted in a large area in Guangxi district, so there are conditions for sludge land use. Therefore, under the premise of controlling the risk of heavy metals, land use of sludge is a sludge disposal technology in line with the current situation in Guangxi. Taking into account factors such as area, carbon emission, sludge composition and calorific value in Guangxi region, the sludge in Guangxi region is suitable for disposal by anaerobic digestion + land use and aerobic fermentation + land use; when the sludge is not suitable for land use and incineration and building materials utilization conditions are not available locally, landfill disposal will be considered. In the long run, Guangxi sludge should be disposed in a multi-form and multi-channel way.

ACKNOWLEDGEMENTS

This work was financially supported by Guangxi innovation research team project (2018GXNSFGA281001) and Guangxi major science and technology projects (GuikeAA18118013).

REFERENCES

[1] Zhang, T., Liu, Y. & Wang, N. et al. Research progress on sludge reduction technology and mechanism in wastewater treatment process [J]. Water Treatment Technology, 2020, 46(08): 6-12. (In Chinese)

[2] Liu Xin, Hui Xiujuan, Tang Fengde. Current situation and economic trend analysis of sludge treatment and disposal in typical cities of our country [J]. Environmental Protection and Circular Economy, 2021, 41(04): 88-93. (In Chinese)

[3] Dai Xiaohu. Consideration on the necessity and urgency of sludge stabilization treatment in urban sewage treatment plant [J]. Water Supply and Drainage, 2017, 53(12): 1-5. (In Chinese)

[4] Wang Jie, Xiong Z. & Shi Mingyan. Research progress of sludge energy conversion technology [J]. Modern Chemical Industry: 1-4. (In Chinese)

[5] Ministry of Housing and Urban-Rural Development of the People's Republic of China. Statistical yearbook of construction [EB/OL].

[6] G. Yang, G. Zhang, H. Wang, Current state of sludge production, management, treatment and disposal in China, Water Res. 78 (2015) 60–73.

[7] H. Huang, X. Yuan, The migration and transformation behaviors of heavymetals during the hydrothermal treatment of sewage sludge, Biores. Technol. 2015.

[8] A. Passuello, M. Mari, M. Nadal, M. Schuhmacher, J. Domingo, POP
accumulation in the food chain: Integrated risk model for sewage sludge
application in agricultural soils, Environ. Int. 36 (2010) 577–583.
[9] B. Clarke, N. Porter, R. Symons, J. Blackbeard, P. Ades, P. Marriott, Dioxin-like compounds in Australian sewage sludge – review and national survey, Chemosphere 72 (2008) 1215–1228.
[10] W. Rulkens, Sewage sludge as a biomass resource for the production of energy:overview and assessment of the various options, Energy Fuels 22 (2008) 9–15.
[11] Liu X J, Zhu H Y, Yang S S. Current situation research and suggestion analysis of sludge treatment and disposal in Wuhan city [J]. Industrial Safety and Environmental Protection, 2020, 46(06): 93-96.
[12] Liao, K., Yang, H. & Wang, H. Current situation and suggestions of municipal sludge treatment and disposal in Guangdong Province [J]. Guangdong Chemical Industry, 2019, 46(04): 126-127+129.
[13] YU R. Analysis on operation status and characteristics of sewage treatment plant in Guangxi Zhuang Autonomous Region [J]. Environmental Engineering, 2017, 35(08): 25-28.
[14] Wang, X., Zhang, R., Yan, B. et al. Analysis of sludge characteristics and resource utilization potential in Tibet Autonomous Region [J]. Chinese Journal of Environmental Engineering, 2019, 13(11): 2753-2769.
[15] Dai, X. Current situation and consideration of urban sludge treatment and disposal in our country [J]. Water SUPPLY and Drainage, 2012, 48(02): 1-5.
[16] Wang, Y., Xu, Q., Zhang, Y. et al. Analysis and discussion on the process route of urban sludge treatment and disposal in Nanning [J]. Water Supply and Drainage, 2019, 55(03): 31-34+41.
[17] Huang, L., Feng, L. Du, Z. et al. Bottleneck analysis and countermeasure research of urban sludge land use in China. China Water Supply and Sewerage, 2019, 35(20): 31-36.
[18] Li, X., Li, J., Li, C. et al. Application status and development trend of sludge treatment and disposal technology in China [J]. China Water Supply and Drainage, 2016, 32(16): 26-30+35.
[19] Ministry of Housing and Construction. National Construction Plan for Urban Sewage Treatment and Recycling Facilities during the 13th Five-Year Plan Period.
[20] Pan, Z., Liang, Z., Tian, D. et al. Analysis of sludge production and disposal status in Guangxi Municipal sewage treatment plant. Energy and Environmental Protection, 2020, 34(02): 105-108.
[21] Sun, W., Liu, Y. & Liu, J. Effect of mixed landfill of sludge and household waste on blockage of leachate drainage system [J]. Chinese Journal of Environmental Engineering, 2018, 12(12): 3490-3497.
[22] Wei, L., Jin, X., Ma, L. Research progress on treatment and disposal technology of residual sludge from sewage plant [J]. Agriculture and Technology, 2021, 41(08): 8106-8108.
[23] Liu, Z. & Zhang, Z. Selection of sludge treatment and disposal technology in Guangxi sewage treatment plant [J]. Environmental Protection Technology, 2014, 20(04): 34-37.
[24] Li B J, Zhan J, Lu X Y, et al. Discussion ON SLUDGE TREATMENT and DISPOSAL SCHEME of Nanchang Municipal Sewage Treatment Plant. Environmental Engineering, 2016, 34(05): 104-107.
[25] Lin Huanjia. Technology and practice of sludge disposal in urban sewage treatment plant [J]. Resource Conservation and Environmental Protection, 2020(09): 101-102.
[26] Standard of sludge treatment in Guangxi [J]. Juye, 2015(16): 148.
[27] He, Q., Ji, F. & Li, J. Treatment and disposal of sludge and new technologies [J]. Water Supply and Sewerage, 2016, 52(02): 1-3.
[28] Yang, J., Liu, H., Chen, T. et al. Characteristics and disposal direction of urban sludge in Guangxi Zhuang Autonomous Region [J]. China Water Supply and Drainage, 2013, 29(03): 87-89.
[29] Zhang, J., Zhang, Z., Wang, D. et al. Analysis of SLUDGE and potential ecological risk assessment of land use in Guangxi Municipal Sewage Treatment Plant.

Environmental Engineering, 2014, 32(01): 108-112.
[30] Xue, W. & Li, F. Effects of different utilization forms and utilization rates of sludge on soil ecological environment [J]. Ecological Science, 2018, 37(04): 130-137.
[31] Huang, X., Huang, Y., He, S. et al. Research on recycling and energy treatment of urban sludge in Nanning City [J]. Environmental Protection and Circular Economy, 2019, 39(07): 5-8+25.
[32] Liu, L. & Lu, D. Current situation and prospect of sludge disposal in Guilin sewage treatment Plant [J]. Guangxi Urban Construction, 2013(09): 128-131.
[33] Qu J H, Dai X H, Hu H Y, et al. Emerging trends and prospects for municipal wastewater management in China [J]. ACS ES & T Engineering, 2022, 2(3): 323–336
[34] Xie, K., Yin, J. & Chen, X. Research progress on sludge disposal technology of urban sewage treatment projects in China [J]. Industrial WATER TREATMENT, 2020, 40(07): 18-23.
[35] Tu, X., Zhu, N. & Yuan, H. Utilization approach and evaluation of sludge building materials [J]. Water Purification Technology, 2014, 33(04): 30-35.
[36] Hanxi W., Jianling X., Yunqing L., et al. Preparation of ceramsite from municipal sludge and its application in water treatment: A review[J]. Journal of Environmental Management, 2021, 287.
[37] Zhang, Y., Tao, M. & Shen, D. et al. Toxicity leaching from sludge containing heavy metals for brick production [J]. Chinese Journal of Environmental Engineering, 2015, 9(04): 1984-1988.
[38] Zhang, W., Lin, M., Yu, Z. et al. Analysis and research on the utilization of sludge from sewage plant in Yuhang District, Hangzhou [J]. Resource Conservation and Environmental Protection, 2021(03): 118-119.
[39] Yang, H., Xian, P. & Yang, L. et al. Analysis of composition characteristics of urban sludge mixed firing utilization in Guangxi [J]. Chinese Journal of Environmental Engineering, 2015, 9(03): 1440-1444.
[40] Meng, X., Peng, Y. Yang, M. et al. Selection and practice of sludge disposal in Liuzhou Municipal Sewage treatment Plant [J]. China Water Supply and Sewerage, 2015, 31(04): 18-21
[41] An D., Rourou Z., Hao N. H., et al. Life cycle assessment of sewage sludge treatment and disposal based on nutrient and energy recovery: A review[J]. Science of The Total Environment, 2021.
[42] Yuan, Y., Huang, Y., Zhang, D. et al. Research on energy utilization and pollutant discharge characteristics of sludge incineration [J]. Chinese Journal of Power Engineering, 2016, 36(11): 934-940.
[43] office. Analysis of sludge treatment and disposal status of urban sewage plant and demonstration of engineering scheme [J]. Water Purification Technology, 2018, 37(05): 93-96.
[44] Hu, W. & Zhou, Y. Study on mechanism of sludge incineration process in urban sewage treatment plant [J]. China Water Supply and Sewerage, 2019, 35(10): 15-20.
[45] Wang, L., Lyu, G., Wang, F. et al. Research on energy saving and consumption reduction of sludge drying and incineration system [J]. China Water Supply and Sewerage, 2021, 37(04): 29-36.

RESEARCH PROGRESS ON ANAEROBIC DIGESTION OF CELLULOSE WASTE BASED ON BIBLIOMETRIC ANALYSIS

Pan Zhao, Xiaona Wang, Shuang Zhang, Yan Guo and Qunhui Wang
School of Energy and Environmental Engineer, University of Science and Technology Beijing, 30 Xueyuan Road, Haidian District, Beijing 100083, China

INTRODUCTION

Lignocellulosic waste as an important component of organic waste is more productive and more difficult to treat. Lignocellulosic waste is a huge biomass resource when disposed of rationally, so it is vital that lignocellulosic waste is disposed of in a rational way[1]. Relying on incineration and landfill for waste disposal can create secondary pollution and is not economically viable[2]. Studies have demonstrated that lignocellulosic biomass has a significant potential for biomass fuel production[3]. Anaerobic digestion of organic waste can produce clean energy and other organic products while efficiently degrading organic waste, reducing human dependence on fossil energy and greenhouse gas emissions, with environmental, economic and social benefits[4]. However, the crystalline and reticulate structure formed by the lignin, cellulose, and hemicellulose increases the difficulty of anaerobic digestion[5]. Therefore, the hydrolysis rate of cellulose waste is slow and the methane yield is low[6]. Scholars have conducted extensive research to improve the methane yield of cellulose waste. To study the progress of the anaerobic digestion of cellulose waste and the future development trend, this paper conducted a literature search and bibliometric analysis based on the Web of science database, and reviewed the current hot areas to improve the anaerobic digestion of cellulose waste.

MATERIALS AND METHODS

Information Summarized from the ISI Web of Science published by Thomson Reuters [7] and Science Citation Index Expanded (SCIE) database were the primary data source. In this study, (cellulos* waste* or fiber* waste* or fibre* waste or garden waste* or paper* waste* or straw* waste* or agricutur* residue* or yard* waste* or lignocellulosic biomass or forests waste or grass) and (anaerob* digest* or biogas or methane) was used as a search phrase to search topics in SCIE for the period from 2002 to 2021. The 2021 Journal Citation Report (JCR) is also add in the study as a data source.

All the analysis were all count using Excel 2019, Bibliometrix(in R) and VOSviewer.

RESULT AND DISCUSSION

Fig. 1 displays the overall publications as well as the number of articles from the top 5 countries for the period 2002-2021. Research on the anaerobic digestion of cellulose waste has developed rapidly in this century, which may be related to the emphasis placed by the Food and Agriculture Organisation of the United Nations (UN) on bioenergy, agroenergy, wood energy, etc The results of a bibliometric analysis of articles published between 2002 and 2021 by countries and institutions are shown in Fig. 2 which shows that anaerobic digestion of cellulose waste has been actively explored and studied in many countries around the world.

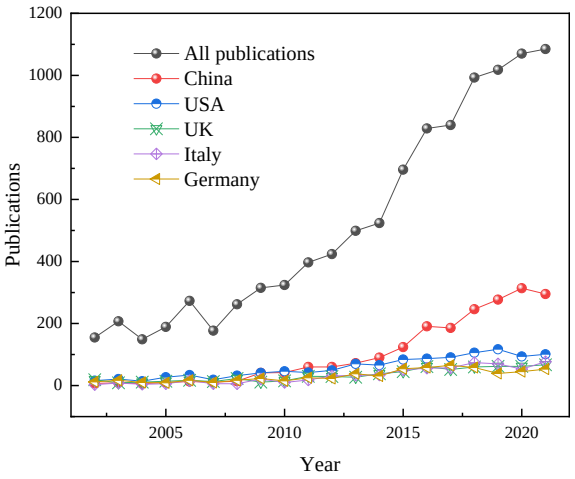

Figure 1. Number of SCI publications on -related research and trends in the top 5 countries with the highest numbers of publications in 2002-2021

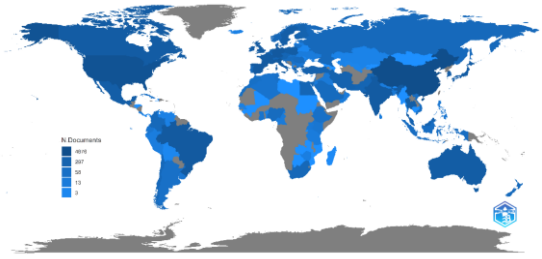

Fig. 2 Research in various countries around the world

Statistical analysis is often performed on author keywords to understand the research trends and frontiers. Words with the same meaning need to be combined before processing. This result indicates that pretreatment

and co-digestion play an important role in improving the efficiency of anaerobic digestion of cellulose waste. The microbial community is valued during anaerobic digestion.

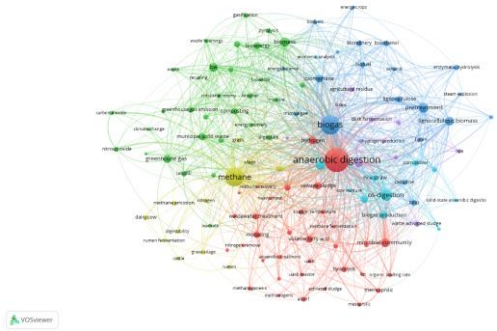

Fig. 3 Clustering analysis of author keywords occurring more than 40 times

TREATMENT TO IMPROVE THE ANAEROBIC DIGESTION EFFICIENCY

Pretreatment is an initial treatment to modify the structure of lignocellulose waste for increased efficiency before anaerobic digestion The pretreatment is varied and the conditions are complex, so it has a wide range of effects on methane production. The improper selection of conditions may not promote increased methane production. The mechanism of physical pretreatment to enhance the methanogenic capacity of cellulose waste varies. Crushing destroys the cell wall of the plant and increases the specific surface area to enhance biodegradability. Microwave, ultrasound, electron beam and γ-ray treatments can destroy the structure of lignocellulose. Physical pretreatment may lead to the loss of components. Microwave and thermal pretreatments may produce furfural, melanoid and other substances due to the temperature rise that may inhibit the methane production process. Two main principles of chemical pretreatment to enhance anaerobic digestion exist. One is to break chemical bonds, i.e. break down esters or glucoside side chains to improve the biodegradability of waste. The other is using the substances generated from the reaction process as catalysts for 'autocatalysis' to promote anaerobic digestion. Biological pretreatment has low energy consumption and no pollution and mild operating conditions. This pretreatment needs no additional chemical substances. From the perspective of energy, biological pretreatment has certain advantages. Cellulose waste such as agricultural wastes often have a high C/N ratio, so the degradation rate is usually slow and the stability of the system is poor when anaerobic digestion is performed alone. Co-digestion can not only improve the process stability by regulating the C/N ratio but also reduce the cost of biogas purification and fermentation residue processing. The most common substrates for co-digestion are kitchen waste, livestock manure and sludge. Anaerobic digestion is a complex, multi-process metabolic pathway carried out by various microorganisms acting together in an anaerobic environment. With the development of molecular biology technology, increasing studies on microbial community structure are being conducted. The microorganisms of the anaerobic digestion process are often divided into bacteria and archaea.

CONCLUSION

Based on the articles from SCIE, this bibliometric study provided an overview of research in anaerobic digestion of cellulose waste and identified some significant points in this field throughout the investigation period. China was the most productive country. The results show that the overall research related to the anaerobic digestion of cellulose waste is increasing. Pretreatment, co-digestion and microbial communities of cellulose waste are hotspots of research.

ACKNOWLEGEMENT

This research was financially supported by National Key R&D Program of China [2018YFC1900903] and the National Environmental and Energy Base for International Science & Technology Cooperation.

REFERENCE

1.Xu M, Yang M, Xie D, Ni J, Meng J, Wang Q, Gao M., Wu C, 2021. Research trend analysis of composting based on Web of Science database. Environmental Science and Pollution Research 28:59528-59541.

2. Gao Z, Ma YQ, Liu Y, Wang QH, 2022. Waste cooking oil used as carbon source for microbial lipid production: Promoter or inhibitor. Environmental Research 203:111881.

3 Guo MX, Song WP, Buhain J, 2015. Bioenergy and biofuels: History, status, and perspective. Renewable and Sustainable Energy Reviews 42 (712-725).

4 Shane A, Gheewala SH, 2017. Missed environmental benefits of biogas production in Zambia. Journal of Cleaner Production 142 (1200-1209).

5 Abraham A, Mathew AK, Park H, Choi O, Sindhu R, Parameswaran B, Pandey A, Park JH, Sang BI, 2020. Pretreatment strategies for enhanced biogas production from lignocellulosic biomass. Bioresour Technol 30 (1122725).

6 Mothe S, Polisetty VR, 2021. Review on anaerobic digestion of rice straw for biogas production.Environ Sci Pollut Res Int 28 (24455-24469).

7.Zheng T, Wang J, Wang Q, Nie C, et al., 2015. A bibliometric analysis of industrial wastewater research: current trends and future prospects, Scientometrics, 105 (863-882).

INVESTIGATION ON THE VEGETATION DISTRIBUTION LANDFILL COVER, METHANE OXIDATION CAPACITY OF VARIOUS RHIZOSPHERE SOIL, AND RHIZOSPHERIC MICROBIAL METABOLISM IN THE PROCESS OF MSW LANDFILL

Shangjie Chen[1], Zhilin Xing[1]*, Baozhong Mou[1], Chunyu Zhu[1], Li Dong[1], Cairong Hu[1], Lin Cheng[1], Tiantao Zhao[1]*

1 School of Chemistry and Chemical Engineering, Chongqing University of Technology, Chongqing 400054, China

*Correspondence to Zhilin Xing and Tian-tao Zhao, e-mail: xingzhilin@cqut.edu.cn and zhaott@cqut.edu.cn

Abstract: In the process of the landfill, landfills naturally grow a variety of vegetation, which has higher tolerance and anti-toxicity, and plays an important role in controlling disordered landfill gas emissions with microorganisms. In this study, the natural growth vegetation and the soil methane oxidation ability of the dominant vegetation roots were investigated for the landfills in Chongqing, and the rhizosphere microecological diversity and microbial metabolic characteristics were analyzed by multi-group techniques. It is found that in the process of the landfill, there is a large area of vegetation growing in the covered soil area and garbage corruption area, and more than 22 kinds of vegetation grow well in the landfill, among which there are the most species of herbs, including *Rumex Acetosa*, *Mugwort*, *Cynodon Dactylon* and so on. The results of the methane oxidation capacity analysis showed that the methane oxidation capacity of rhizosphere soil of all vegetation was higher than that of non-rhizosphere soil, and the methane oxidation capacity of *Rumex Acetosa* root soil was the highest, which was 8.45 mg/(mL·d), which was 20 times higher than that of non-rhizosphere soil. The methane oxidation ability of *Mugwort* and *Cynodon Dactylon* roots was the second, which was 7.09 mg/(mL·d) and 6.37 mg/(mL·d), respectively. The results of plant diversity sequencing showed that compared with the non-rhizosphere soil, the microbial diversity and evenness in the rhizosphere of vegetation were higher, and the difference in dominant bacteria was obvious. Under the action of vegetation, methane-oxidizing bacteria such as *Methylomicrobium*, *Methylobacter,* and *unclassified_f_Methylomonadaceae* could significantly promote the microdomain enrichment of methane-oxidizing bacteria in the rhizosphere, which was of great significance in cooperation with other bacteria for methane bio-oxidative degradation. The results of the metabonomic analysis showed that Lemonic acid and Nicotinic were the dominant metabolites in rhizosphere soil with high oxidative activity. As nutrients enhance the activity of rhizosphere microorganisms and regulate the specific metabolic pathway produced by microorganisms, it may be an important way to promote microorganisms to enhance the degradation of pollutants.

Keywords: Landfills, Natural vegetation, Metabonomics, Rhizosphere microorganisms, Rhizosphere effects

1 INTRODUCTION

Sanitary landfill is one of the main treatment methods for solid waste. During the stabilization operation of landfill waste, complex biochemical reactions take place and a large amount of landfill gas is produced. The main components are methane CH_4 (55 ~ 60 vol%), carbon dioxide CO_2 (40 ~ 45 vol%), and non-methane organic compounds (NMOCs < 1%, containing sulfur compounds, halogenated hydrocarbons, aromatic hydrocarbons, aliphatic hydrocarbons, terpenes, and oxidizing compounds, etc.). CH_4 is considered to be the second largest greenhouse gas in the world, its warming potential is 27.9 times that of CO_2, and its contribution to the Greenhouse Effect of the world is more than 30% [1,2]. In addition, as the main source of odor in landfills, NMOCs have many kinds of pollutants, complex components, and strong toxicity, and many components have a "three-cause" effect and genetic toxicity, which pollute the overlying soil and its surrounding environment for a long time, seriously endangering human health and ecological safety [3]. Therefore, the effective control and removal of disordered landfill gas discharge from landfills have always been a hot spot in the field of solid waste.

Under landfill gas acclimation, a variety of functional microorganisms are derived from the overburdened soil, which plays an important role in landfill gas removal. At the same time, the establishment of cover vegetation can enhance the degradation of landfill gas by functional microorganisms, which has important application potential in effectively controlling landfill gas emissions. A study on the synergistic degradation of methane by vegetation and microorganisms in landfill cover has been carried out. Xiaoli Chai et al. [4] investigated the types of vegetation in closed landfills and their effects on methane emission reduction and found that the methane concentration in the covered soil near the rhizosphere of *Phragmites Australis* was significantly lower than that in bare soil. Thomas G. et al. [5] found that the methane oxidation effect under the combined action of *Medicago sativa Linn* and *Zizania Latifolia* was the best, which was significantly higher than that of *Populus tomentosa Carr* and *Miscanthus*. Bian Rongxing et al. [6] found that the CH_4 emission from the vegetation cover area in the landfill is only 1/2 of that in the bare area. Stralis-Pavese et al. [7] found that the CH_4 oxidation capacity of bare soil was less than 18 g/($m^2 \cdot$ d), while that of CH4 was higher than 35 g/($m^2 \cdot$ d) under *Zizania Latifolia* and *Medicago sativa Linn* cover. These studies fully proved that vegetation has a significant effect on the methane oxidation capacity of landfill cover soil, and vegetation roots and rhizosphere microorganisms play an important role in controlling methane emissions.

At present, almost all studies have only carried out root microbial-enhanced CH4 degradation for one or several limited vegetation, and no effective vegetation selection list has been obtained. Under the influence of climatic environment and tolerance, many problems have not been solved, such as the complex growth of vegetation in the natural state of landfill soil, which vegetation has stronger adaptability in landfill, and which vegetation has better control effect of landfill gas pollution. The artificial establishment of landfill cover vegetation has become an important means of landfill gas control in closed landfills, and the optimization of vegetation is an important prerequisite for artificial planting. At present, many studies are based on closed landfills, and during the operation of landfills, naturally growing vegetation is constantly stressed by landfill gas, and continuously domesticated plants can tolerate pollutants and degrade [8-12]. The application of natural vegetation in landfill closure has important potential for methane emission reduction. However, few studies are focusing on the synergistic action of vegetation and microorganisms to control methane emissions, and there are few reports on vegetation species information, rhizosphere microecological characteristics, bio-oxidation capacity, and metabonomic characteristics during landfill operation.

Based on this, this study systematically investigated the vegetation of unclosed landfills under the subtropical monsoon humid climate in Chongqing, China, and sampled and analyzed the roots and rhizosphere soil of different vegetation. The root characteristics, rhizosphere microecological characteristics, methane-oxidizing bacteria community composition, microbial community distribution, and root depth of different vegetation were investigated, and based on the methane oxidation ability of rhizosphere soil, the effects of different vegetation on the utilization of microbial methane in the rhizosphere were investigated, and the metabolites composition and distribution of typical vegetation rhizosphere soil were investigated by metabonomics technology. Finally, the relationship between vegetation type, rhizosphere microecological characteristics, and biological oxidation capacity was established systematically, and the primary vegetation with high methane degradation efficiency was selected, which is expected to provide theoretical guidance for plant establishment in situ restoration project to control methane emission.

2 MATERIALS AND METHODS

2.1 Landfill investigation and rhizosphere soil sampling

The municipal solid waste landfill in Rongchang District of Chongqing (106°34′25″N，29°23′38″E) is located in Qibaoyan Village, Yuanzhen Town, Rongchang District, with an effective landfill capacity of $19.847 \times 10^6 m^3$, a daily treatment capacity of 260 t and a service life of 15 years. The structure diagram is shown in Figure 1. The landfill is located in the subtropical monsoon climate region, with an annual average temperature of 7~12 ℃ and a relative humidity of 87%. Vegetation investigation and soil sampling are carried out in the cover layer of the landfill for more than 2 years to avoid the contingency of the survey results.

The vegetation cover characteristics of the landfill were investigated, and the plants with good

growth were selected for plant sampling and rhizosphere soil collection. Under the condition of ensuring the integrity of the plant root as much as possible, dig the plant, remove a large piece of soil from the root, and measure the root length of different vegetation. The rhizosphere soil was carefully extracted, placed on ice, and transported to the laboratory for immediate treatment. The soil samples were stored in a -80 ℃ refrigerator for DNA extraction and soil physical and chemical properties detection.

Fig. 1 Schematic diagram of a municipal solid waste landfill site in Rongchang District, Chongqing

2.2 Determination of methane oxidation capacity of vegetation rhizosphere soil

15g soil samples of vegetation roots were put into a series of 100 mL clean serum bottles, sealed with aluminum lid and lined with polytetrafluoroethylene silica gel gasket, and the air in the bottle was replaced by 20 ml CH_4 (about 2080 ppmv). All samples were in triplicate. The serum bottle system was cultured in a 30 ℃ biochemical incubator, and the change in methane concentration was determined continuously.

2.3 Rhizosphere soil microbial DNA extraction and diversity sequencing

Soil samples of the root system of cover vegetation were stored in an environment of -80 ℃ for microbial diversity analysis. The total genomic DNA of microorganisms was extracted by Mobio PowerSoil ®DNA Isolation Kit, and the DNA sample was purified by Mobio PowerClean ®DNA Clean-Up Kit. The purified DNA products were detected by 1% agarose gel electrophoresis.

The 16s DNA hypervariable region sequence was sequenced, and the sequencing region was V3+V4. Use Trimmomatic and FLASH software to process the Miseq sequencing data to obtain clean data: (1) filter the bases with a quality value of less than 20 in the read tail, set the window of 50 bp, if the average value in the window is less than 20 bp, truncate the back base from the window, and filter the read; below 50 bp after quality control. (2) according to the overlapping relationship between PE reads, the paired reads will be merged into a sequence, and the minimum overlap length is 10 bp. (3) the maximum mismatch ratio of the overlap region of the splicing sequence is 0.2, and the screening does not conform to the sequence; (4) detect the box sequence at the end of the sequence, the minimum mismatch number is 0, reverse complement the sequence including box at the beginning, and remove the barcode from the box; (5) detect the sequence and distinguish the sample, the barcode mismatch number is 0, and the maximum primer mismatch number is 2.

The data error and correlation were analyzed by SPSS Statistics 21 software, and the principal component analysis and diversity data were analyzed by the i-sanger platform (http://www.i-sanger.com/).

2.4 Sequencing of microbial metabonomics in rhizosphere soil

The soil samples of different vegetation roots were measured and analyzed by LC-MS non-targeted metabonomics, and the original data were imported into metabonomics processing software Progenesis QI (Waters Corporation, Milford, USA). At the same time, the MS information was matched with the metabolic common database HMDB (http://www.hmdb.ca/) and Metlin (https://metlin.scripps.edu/) database.

The preprocessed data is uploaded to the Meiji Biological Cloud platform (https://cloud.majorbio.com) for data analysis. The R software package ropes (Version1.6.2) carries out principal component analysis (PCA) and orthogonal least square discriminant analysis (OPLS-DA) and uses 7 cycles of interactive verification to evaluate the stability of the model. In addition, students' t-tests and multiple different analyses were performed. The selection of significant differential metabolites was based on the variable weight value (VIP) obtained by the OPLS-DA model and the p-value of the student's t-test. The metabolites with VIP>1 and $p<0.05$ were significant differential metabolites. By constructing the volcano map of differential metabolites, the number of metabolites was significantly up-regulated, and down-regulated, and no significant change.

Then, the metabolic pathways of all the differential metabolites were analyzed, and the KEGG (https://www.kegg.jp/kegg/pathway.html) metabolic pathways of the differential metabolites were constructed. At the same time, the metabolic pathways involved in the metabolites were visually analyzed by iPath3.0 (http://pathways.embl.de) to view the metabolic pathway information of the whole biological system.

Sample preparation method: take 50 mg solid sample or 100 μL liquid sample into 1.5 ml centrifuge tube, add 400 μ l extract (acetonitrile: methanol = 1:1), after vortex mixing for 30 s, extract 30 min (5 ℃, 40 kHz) by low-temperature ultrasonic extraction, place the sample in-20 ℃, 30 min,4 ℃, 13000 g centrifuge 15 min, remove the supernatant, dry with nitrogen, and re-dissolve in 120 μ l resolution (acetonitrile: water = 1:1). The samples were extracted by low-temperature ultrasonic extraction with 5 min (5 ℃, 40 kHz), 4 ℃ and 13000 g centrifugation for 5 min. The supernatant was removed from the injection vial with intubation and analyzed on the machine.

The LC-MS analysis instrument platform is Semefeld's ultra-high-performance liquid chromatography-tandem Fourier transform mass spectrometry UHPLC-Q Exactive HF-X system.

The chromatographic conditions were as follows: ACQUrTY UPLC HSS T3 (100mm × 2.1mm i.d., 1.8 um; Waters, Milford, USA); mobile phase An is 95% water + 5% acetonitrile (containing 0.1% formic acid), mobile phase B is 47.5% acetonitrile + 47.5% isopropanol + 5% water (containing 0.1% formic acid), the injection volume is 2 μL, and the column temperature is 40 ℃.

3 RESULTS AND DISCUSSION

3.1 Vegetation distribution and community characteristics of landfill site during landfill

In the process landfill, the environment of the landfill is bad, the garbage is constantly in landfills and compacted, the garbage is placed in the open before the soil and film are covered, and the landfill gas produced by natural fermentation continues to spread to the surrounding area. The vegetation growth environment of the whole landfill is complex and bad so the vegetation coverage of the cover is low and the plant grows slowly and naturally. The vegetation cover during the operation of the Chongqing Rongchang Municipal solid waste Landfill site in western China was investigated. Samples were taken in winter and summer every year, and the growth of vegetation (Figure S1-S6) was observed for three consecutive years. Almost no vegetation grows in all the garbage dumps, and most of the vegetation grows in the soil cover around the garbage dumps. The vegetation coverage is higher in summer, the vegetation height is lower, the growth cycle is longer, the vegetation coverage is lower in winter, the plant height is higher, and the life cycle is shorter. In addition, the composition of typical vegetation communities is investigated, and the results are shown in Figure 2. The air and soil where the natural vegetation grows are stressed by malodorous landfill gas and landfill leachate for a long time, and the vegetation community evolves to herbaceous vegetation that is easy to survive, and there are few trees and shrubs. A total of 22 species were found, of which herbaceous vegetation such as *Goosegrass Herb*,

Cynodon Dactylon, *Zizania Latifolia*, *Mugwort*, *Miscanthus Floridulus*, *Wild Chrysanthemum*, *Canna Indica L.* and *Cyperus Glomeratus L.* are growing well (Table S1).

The physical and chemical properties of rhizosphere soils with different vegetation are shown in Table S2. The results show that the pH value of the rhizosphere soil of each vegetation is between 6.16 and 7.42, and the pH value of the rhizosphere soil of most vegetation is lower than that of bare soil; the water content of the rhizosphere soil of each vegetation is between 9.24% and 35.82%, and the moisture content of bare soil is 23.69%, which will significantly affect the water content of rhizosphere soil under the action of vegetation. The secretory components of the rhizosphere are related to plant species and the growth stage, in which acid ions and hydrogen ions can change the pH value of the soil rhizosphere environment. The soil under acidic condition is more conducive to organic matter desorption and promote the absorption of pollutants by plant roots [13]. The effect of soil moisture content on the degradation of pollutants in rhizosphere soil is more complex. Soil water can inhibit the adsorption of pollutants on the surface of soil particles and promote bioavailability. However, too much water will inhibit plant nutrient transport in the rhizosphere. Affect plant growth and degradation ability [14,15]. Thus it can be seen that vegetation varieties and root characteristics are important factors to change the physical and chemical properties of rhizosphere soil.

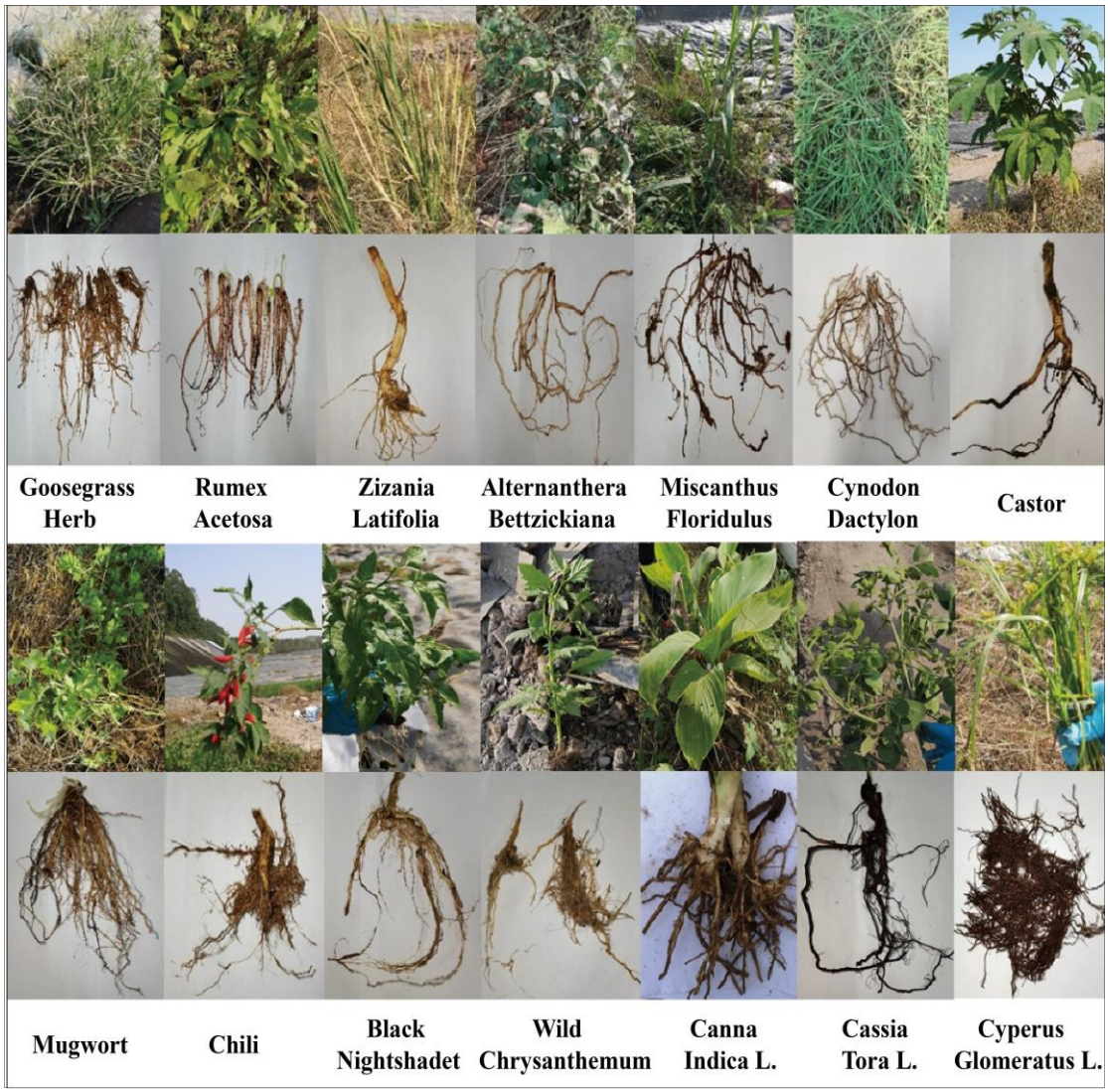

Fig. 2 Different vegetation and root structure of landfill cover

3.2 Analysis of methane oxidation ability of rhizosphere soil under different vegetation

Based on the ability of methane oxidation, the microbial activities in the rhizosphere of different vegetation were investigated, and the results are shown in Figure 3. Overall, the average methane degradation ability of the rhizosphere soil of each vegetation was higher than that of non-rhizosphere soil. The methane oxidation efficiency of the rhizosphere soil of *Reed*, *Amaranthus Spinosus*, *Cassia Tora L.,* and *Black Nightshade* decreased gradually after 48 h, while that of other vegetation increased continuously. The methane oxidation efficiency of Rumex rhizosphere soil was the highest at 72 h, which was 90.32%. The rate of methane oxidation in the rhizosphere soil of *Reed* and *Goosegrass Herb* was the lowest, which was 0.0133 $g_{CH4}/(kg_{soil}\cdot h)$ and 0.0113 $g_{CH4}/(kg_{soil}\cdot h)$. These vegetation were not suitable for enhancing methane oxidation in landfills, while those of *Rise*, *Black Nightshade*, *Broussonetia Papyrifera,* and *Cassia Tora L.* rhizosphere soil were further enhanced, which were 0.0556 $g_{CH4}/(kg_{soil}\cdot h)$, 0.0459 $g_{CH4}/(kg_{soil}\cdot h)$, 0.0305 $g_{CH4}/(kg_{soil}\cdot h)$ and 0.0355 $g_{CH4}/(kg_{soil}\cdot h)$. The methane oxidation rate of *Rumex Acetosa* rhizosphere soil was the strongest, which was 0.0800 $g_{CH4}/(kg_{soil}\cdot h)$, which was nearly 20 times higher than that of non-rhizosphere soil. According to the methane oxidation rate, the promoting effect of vegetation on methane oxidation in rhizosphere soil can be divided into three grades: "slight promotion" (0.0000-0.0200 $g_{CH4}/(kg_{soil}\cdot h)$), "general promotion" (0.0200-0.0600 $g_{CH4}/(kg_{soil}\cdot h)$) and "strong promotion" (0.0600-0.1000 $g_{CH4}/(kg_{soil}\cdot h)$). The above results show that plant root exudates can promote methane biological oxidation to a certain extent, and the methane oxidation ability of rhizosphere soil of different vegetation is quite different. "strong promotion" vegetation such as *Rumex Acetosa*, *Mugwort,* and *Chili* is beneficial to enhance methane oxidation in landfills.

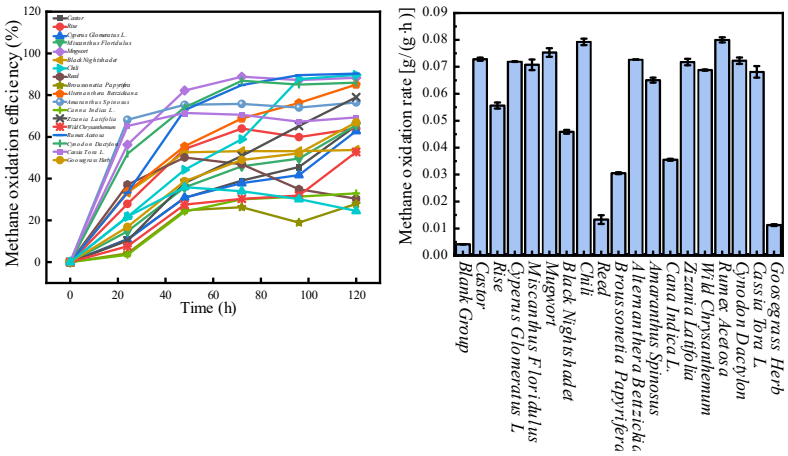

Fig. 3 methane bio-oxidation ability of rhizosphere soil of different vegetation.

3.3 Analysis of microbial diversity in the rhizosphere of different vegetation

3.3.1 Analysis of microbial diversity in the rhizosphere of vegetation: The diversity of soil microorganisms in the rhizosphere of typical vegetation was sequenced, and the results of Alpha diversity were shown in Table S3. A total of 1130239 sequences were obtained from all samples, and 49431 to 64394 sequences were obtained from a single sample (Average = 56511.95). Except for *Reed*, *Cynodon Dactylon*, *Goosegrass Herb,* and *Black Nightshade*, the microbial abundance in the rhizosphere soil of other vegetation was higher than that in non-rhizosphere soil, and the Chao index of *Zizania Latifolia* and *Miscanthus Floridulus* rhizosphere soil was the highest, 3964.40 and 3897.03, respectively. In addition, the Shannon index of rhizosphere microorganisms of each plant was higher than that of non-rhizosphere soil (Shannon=4.45), and *Miscanthus Floridulus* had the largest Shannon index (Shannon=6.83). Thus it can be seen that the landfill cover soil under the action of vegetation can enrich a variety of microorganisms and effectively improve the uniformity and diversity of the microbial community. Some studies have shown that vegetation root exudates and oxygen transport in the rhizosphere can change the physical and chemical properties of soil, provide a suitable growth environment for some functional microorganisms, enhance the activity of functional microorganisms, and induce microbial enrichment in plant rhizosphere microdomains[16,17].

3.3.2 Analysis of microbial Community composition in Rhizosphere soil of different vegetation: Bray-Curtis clustering and the microbial community at the rhizosphere soil gate level are shown in Figure S7. The results showed that the microbial community structure of *Black Nightshade* and *Goosegrass*

Herb rhizosphere soil was the most similar to that of non-rhizosphere soil. *Wild Chrysanthemum*, *Canaa Indica L.*, *Castor*, *Rumex Acetosa*, *Mugwort*, *Amaranthus Spinosus*, *Cyoerus Glomeratus L.*, *Chili*, *Cassia Tora L.*, *Zizania Latifolia*, *Rise*, *Miscanthus Floridulus*, *Broussonetia Papyrifera,* and *Alternanthera Bettzickiana* plant rhizosphere microbial community cluster distance is closer, *Cynodon Dactylon* and *Reed* have the same cluster tree. Under the action of vegetation, the microbial community structure of the covered soil was quite different, and the dominant bacteria were Proteobacteria, Acidobacteriota, Chloroflexi, Actinobacteria, Acidobacteriota, Gemmatimonadota, and Bacteroidota. The maximum relative abundance of Proteobacteria appeared in the non-rhizosphere soil (50.79%), the maximum relative abundance of Acidobacteriota in the rhizosphere soil of *Cynodon Dactylon* (32.76%), the maximum relative abundance of Chloroflexi in the rhizosphere soil of *Reed* (18.99%), the maximum relative abundance of Actinobacteria in *Castor* rhizosphere soil (16.02%), and the maximum relative abundance of Acidobacteriota in the rhizosphere soil (32.76%). The maximum relative abundance of Gemmatimonadota and Bacteroidota in the rhizosphere soil of *Reed* and *Black Nightshadet* was 18.49% and 22.57% respectively. The relative abundance of Acidobacteriota, Chloroflexi, and Actinobacteriota can be increased under the action of vegetation.

The structure of the horizontal microbial community is shown in Figure 4A. The dominant bacteria in non-rhizosphere soil was *Methylocaldum*, accounting for 28.94%. Under the action of vegetation, the dominant bacteria in each rhizosphere soil changed one after another, and the evenness increased significantly. The dominant bacteria in the rhizosphere soil of *Cynodon Dactylon* were *norank_f_norank_o_Vicinamibacterales, YC-ZSS-LKJ147* and *norank_f_norank_o_Subgroup_7*; and the dominant bacteria in *Mugwort* rhizosphere soil were *Sphingomonas, unclassified_o_Rhizobiales,* and *Steroidobacter*. The dominant bacteria in *Castor* rhizosphere soil were *unclassified_f_Methylomonadaceae*, *norank_f_Gemmatimonadaceae,* and *Sphingomonas*; The dominant bacteria in *Rumex Acetosa* rhizosphere soil were *Methylomicrobium*, *unclassified_f_Methylomonadaceae* and *Methylocaldum*. Many studies have found that *Methylomicrobium*, *unclassified_f_Methylomonadaceae*, *Methylocaldum,* and other strains are the key microorganisms in the process of methane bio-oxidation in soil, and play an important role in the transformation of pollutants. In addition, there are some interaction effects between the dominant bacteria such as *norank_f_norank_o_Vicinamibacterales* and *Dongia* and the corresponding vegetation, which indirectly promote the methane use efficiency of rhizosphere soil, but the specific interaction mechanism needs to be further explored.

3.3.3 Analysis of enrichment effect of methane-oxidizing bacteria community: Methane oxidizing bacteria is considered to be one of the most critical functional strains in the mulch layer. The characteristic methane-oxidizing bacteria community in the rhizosphere of vegetation was analyzed, as shown in Figure 4B. The total abundance of methane-oxidizing bacteria community in non-root soil was significantly higher than that in rhizosphere soil samples. *Methylophilaceae*, as the dominant methane-oxidizing bacteria in non-rhizosphere soil, had a relative abundance was as high as 28.94%. After the induction of *Rumex Acetosa* vegetation, the dominant methane-oxidizing bacteria in rhizosphere soil was transformed into *Methylomicrobium*, and the relative abundance was 6.27%. According to the methane bio-oxidation ability of the rhizosphere soil of each vegetation, it was inferred that some vegetation induced the dominant methane-oxidizing bacteria to colonize in the rhizosphere microdomain, and enhanced the methane bio-oxidation ability of the rhizosphere soil under the effect of vegetation-microbial interaction. *Rumex Acetosa*, *Castor*, and *Mugwort* rhizosphere soil can significantly enrich *unclassified_f_Methylomonadaceaehe*, *Methylomicrobium*; *Rice*, *Miscanthus Floridulus* rhizosphere soil can effectively enrich *Methylobacter*; *Goosegrass Herb* rhizosphere soil can significantly enrich *Methylobacillus*; *Amaranthus Spinosus* and *Broussonetia Papyrifera* can effectively enrich *Methylocystis*; *Black Nightshade* rhizosphere soil can significantly enrich *Methylococcus*. Thus, it can be seen that the inducing effect of vegetation on rhizosphere microorganisms is specific, and the difference in the composition of vegetation's root exudates may be the main reason for inducing the colonization of methane-oxidizing bacteria in the rhizosphere. Previous studies have shown that *Methylomicrobium* can efficiently assimilate methane through the Embden-Meyerhof-Parnas pathway [18]. The comprehensive genome-scale metabolic model of Villada J C et al have proved that *Methylomicrobium* has a variety of methane utilization strategies [19]. Therefore, *Methylophilaceae* is not the main function of methane-oxidizing bacteria in the covered soil. Under the action of vegetation, it can improve the diversity and

uniformity of methane-oxidizing bacteria in the covered soil, strengthen the cooperation between a variety of microorganisms and methane-oxidizing bacteria, and effectively promote the biotransformation of pollutants.

3.3.4 Changes of microbial community structure with vegetation root depth: The root length of vegetation affects the process of gas mass transfer in the covered soil, which in turn affects the distribution of functional strains. Based on the root characteristics of *Rumex Acetosa* and *Mugwort*, the microbial community structure at different root depths was investigated, and the results are shown in Figure 4D. The results showed that the average length of the *Rumex Acetosa* root system was 15.4cm. The relative abundance of Proteobacteria and Chloroflexi was the highest in the 15cm *Rumex Acetosa* root system, in which the relative abundance of Proteobacteria was as high as 22.6%. The structure of the microbial community in the rhizosphere of *Mugwort* root was significantly different between 5cm and 10cm, and the dominant phylum changed from Proteobacteria, Acidobacteria, Chloroflexi to Proteobacteria, Bacteroidota, and Acidobacteria. In addition, Firmicutes was only detected in 15 cm and 20 cm *Mugwort* rhizosphere soil and 20cm *Rumex Acetosa* rhizosphere soil. Combined with the investigation of root length, it was speculated that root oxygen transport increased oxygen concentration in the rhizosphere microdomain, the biological activity of anaerobes Firmicutes was inhibited and the abundance was low. Many scholars have also done some research on Firmicutes. Christian et al [20] isolated Firmicutes from anaerobic biomass hydrolysis; Subirats J et al [21] have proved that Firmicutes are more suitable for an anaerobic environment.

In addition, there were significant differences in the community structure of methane-oxidizing bacteria under different root depths between *Rumex Acetosa* and *Mugwort*. *Methylomicrobium* can be enriched in the rhizosphere microdomain of 5-10cm *Mugwort* and 5-15cm *Rumex Acetosa*, while the enrichment effect of methane-oxidizing bacteria is not strong in other root depths. It is speculated that *Methylomicrobium* is the main functional bacteria that can enhance the ability of methane oxidation in rhizosphere soil[22,23]. Combined with the physical and chemical properties of rhizosphere soil, *Rumex Acetosa* root exudates promote the acidity of rhizosphere soil, and the enrichment of methane-oxidizing bacteria is beneficial to the removal of organic pollutants.

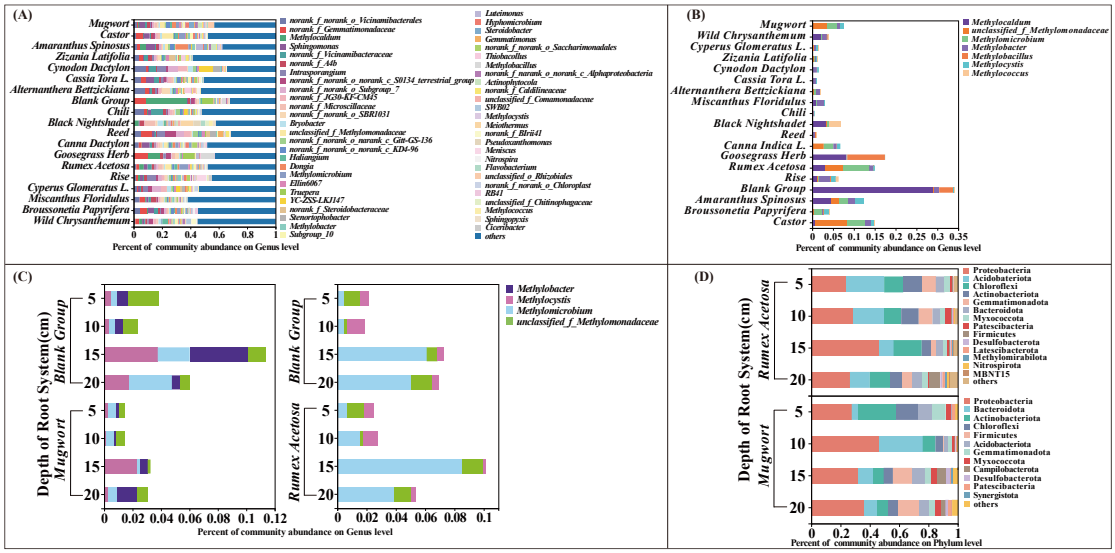

Fig. 4 Microbial community structure in the rhizosphere of natural vegetation in landfill cover. A: Relative abundance of rhizosphere microorganisms of each vegetation; B: Relative abundance of methane-oxidizing bacteria in rhizosphere microorganisms of each vegetation; C: Distribution of methane-oxidizing bacteria under different root depths of *Rumex Acetosa* and *Mugwort* vegetation; D: Gate-level microbial diversity under different root depths of *Rumex Acetosa* and *Mugwort*.

3.4 Metabolomics analysis of microorganisms in the rhizosphere of vegetation

3.4.1 Analysis of microbial metabonomics data: *Rumex Acetosa*, *Amaranthus Spinosus*, *Broussonetia Papyrifera,* and *Goosegrass Herb* rhizosphere soil were selected as typical samples to carry out LC-MC non-targeted metabonomic analysis to explore the metabolic map differences among the samples. A total of 6253 positive ion mode peaks and 5579 negative ion mode peaks were selected to complete the follow-up screening. The quality control (QC) samples were clustered in the center, indicating the good reproducibility and stability of the equipment in the whole study. To determine the possible discrete points, the overall distribution trend of all samples was studied by PCA analysis (Figure 5A). All groups showed changes in positive and negative ion patterns respectively, and there were significant differences among the four groups of samples. This shows that the type of vegetation is an important reason for the difference in metabolites in different rhizosphere soils. The verification results of the PLS-DA model (Figure S8) show that there is no over-fitting phenomenon in the model. Compared with the Venn map, the number of microbial metabolites in the rhizosphere of four kinds of vegetation was obtained, as shown in Figure S9. A total of 499 rhizosphere microbial metabolites were obtained from the rhizosphere soil samples of four kinds of vegetation, of which the total number of metabolites was as high as 388. The specific rhizosphere microbial metabolites of *Rumex Acetosa*, *Amaranthus Spinosus*, *Broussonetia Papyrifera,* and *Goosegrass Herb* were 14, 7, 19, and 3 respectively.

3.4.2 Qualitative and quantitative analysis of microbial metabolism in the rhizosphere: According to HMDB 4.0database (http://www.hmdb.ca/), 596 metabolites were identified in ESI+ and ESI- mode. The chemically classified number of certain HMDB metabolites accumulated at the highest frequency in each rhizosphere microbiome is shown in Figure S10. 596 metabolites are chemically classified into 239 lipids and lipid molecules, 83 organic acids and derivatives, 71 organic oxides, 71 organic heterocyclic compounds, 64 phenyl propionic acids and polyketones, 28 benzene compounds, 22 nucleosides, nucleotides and analogs, 6 organic nitrogen compounds, 5 alkaloids and derivatives, 3 hydrocarbons, 2 lignans, neolignans, and related compounds One organic sulfide and 1 metal/non-metal mixed compound. The clustering of metabolites in the sample is shown in Figure 5F. The main metabolites enriched in *Rumex Acetosa* rhizosphere soil are Fluvoxamino acid, 1-Formyl neogrifolin, 3-[3,4-dihydroxy-2-(8-hydroxy-3,7-dimethylocta-2,6-dien-1-yl) phenyl]propanoicae, Limonexic acid, Lucidenic acid A, Trigoforin. The main metabolites enriched in the rhizosphere soil of *Broussonetia Papyrifera* were2-Hydroxycinnamic acid, 6-[(2-carboxyethyl)oxy]-3, 4,5-trihydroxyoxane-2-carboxylic acid, Cinnamic acid; the clustering of metabolites in the rhizosphere soil of *Broussonetia Papyrifera* and *Amaranthus Spinosus* was not significant. Yang L [24] used Cinnamic acid as autotoxin to investigate the effect of Cinnamic acid on microbial community structure in the rhizosphere of vegetation under salt stress. The results showed that Cinnamic acid aggravated the effect of salt stress at high concentrations, but reduced it at low concentrations. A cinnamic acid concentration of 50 $mg \cdot kg^{-1}$ could effectively alleviate the effect of salt stress on the bacterial community. Therefore, the microorganisms in the rhizosphere of *Broussonetia Papyrifera* resist salt stress in the overlying soil by secreting Cinnamic acid and its derivatives, but their inhibitory effect on the biological process of methane-oxidizing bacteria [25], reduces the abundance of methane-oxidizing bacteria in the rhizosphere soil of *Broussonetia Papyrifera*. As a result, the ability of methane oxidation in the rhizosphere soil is low. In contrast, *Rumex Acetosa* rhizosphere microorganisms promote their own TCA cycle through Limonexic acid in root exudates and promote the metabolic efficiency of microorganisms in the rhizosphere environment. Microbial metabolites can further induce the biosynthesis of plant secondary metabolites and plant hormones [26,27], which is beneficial to vegetation synthesis of nicotine and other alkaloids while promoting the carbon sequestration process of prokaryotes [28]. To improve the methane oxidation ability of rhizosphere soil [29].

Compared with the microbial metabolites in the rhizosphere of *Goosegrass Herb* with low methane oxidation ability, the specific metabolites of *Rumex Acetosa*, *Amaranthus Spinosus* and *Broussonetia Papyrifera* rhizosphere microbial communities are mainly Lipids, Organic acids and their derivatives, Organic oxides, Phenylpropionic acids, and polyketones, while there are little differences in metabolites such as metal/non-metallic compounds, organic nitrogen compounds, alkaloids and derivatives (Figure S11). A total of 327 differentially expressed proteins were identified in the rhizosphere soil of four kinds of vegetation ($P < 0.05$, $Vip > 1$, as shown in Figure 5B-5D). It was found that there were three substances with the most significant differences in metabolites, which were 11alpha,17beta-Dihydroxy-1,4-androstadienone-3-one, Neopetasitenine and 3,11,12-Trihydroxy-1(10)-spirovetiven-2-one.

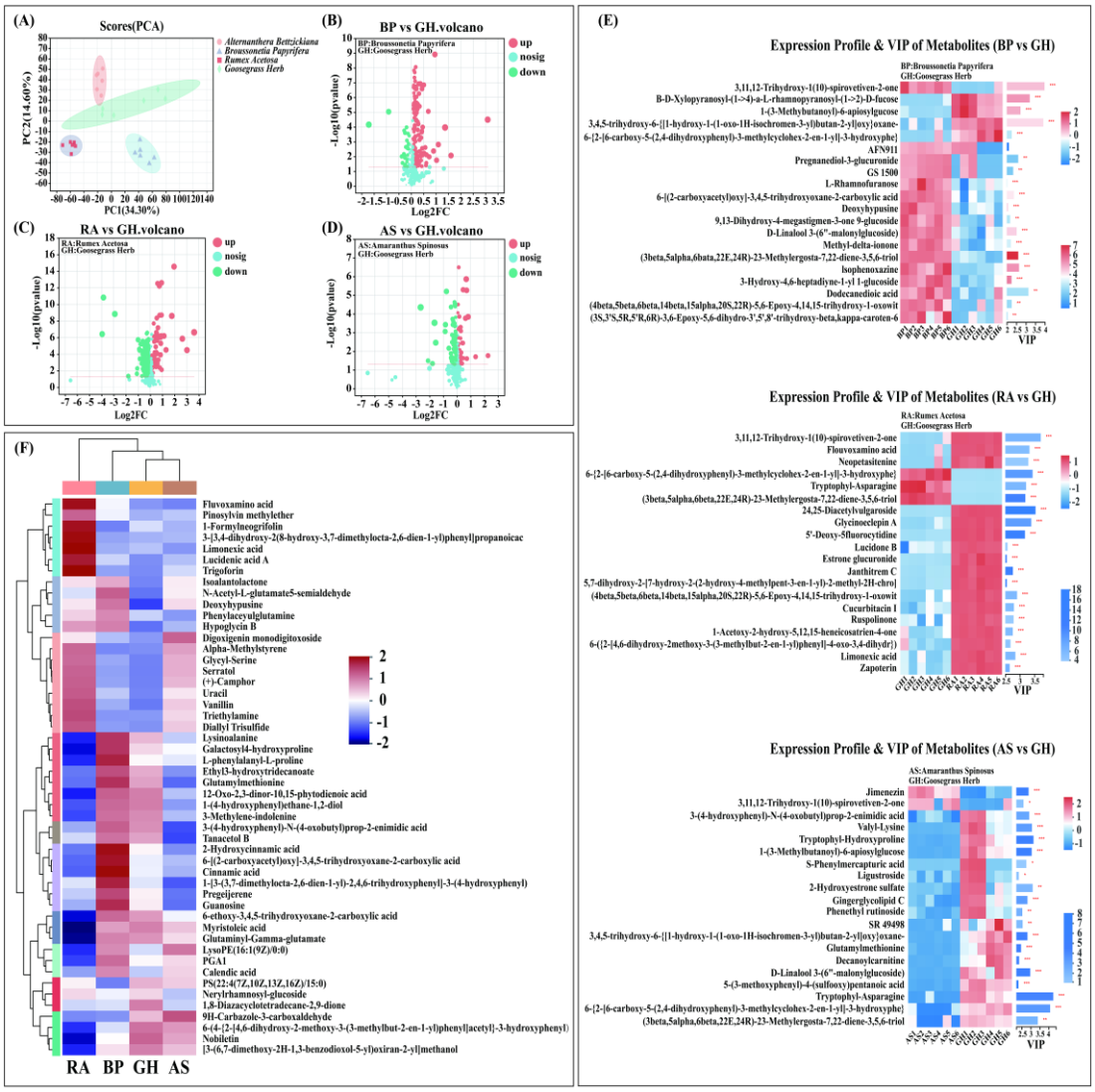

Fig. 5 Soil metabonomics analysis of typical vegetation rhizosphere in the landfill.
A: PCA scores map of typical vegetation rhizosphere soil samples(P< 0.05), B-D: volcanic difference map of typical vegetation rhizosphere soil metabolism, E: relative abundance of microbial metabolism in typical vegetation rhizosphere (significant level defined as * p < 0.05, ** p 0.01 and *** p < 0.001), F: comparison of relative abundance of different metabolites between typical vegetation rhizosphere microbial community and control group.

The correlation of differential metabolites between rhizosphere microorganisms of *Rumex Acetosa*, *Amaranthus Spinosus,* and *Broussonetia Papyrifera* vegetation and rhizosphere microorganisms was analyzed, as shown in Figure 5E. Compared with *Goosegrass Herb*, except for Asparagine A, Tryptophan-asparagine, Valine-lysine, and Neuropeptide extine, all metabolites were more in the rhizosphere microbial samples of *Rumex Acetosa* vegetation. Among them, 3,11,12-Trihydroxy-1 (10)-spirovetive-2-one, 24,25-Diacetylvulgaroside and Glycinoeclepin A significantly contributed to the differential metabolism between *Rumex Acetosa* rhizosphere microorganisms and *Goosegrass Herb* rhizosphere microorganisms. The metabolism of rhizosphere microorganisms in *Amaranthus Spinosus* and *Broussonetia Papyrifera* was significantly different from that in the rhizosphere, but the abundance of specific metabolites was not high. Thus it can be seen that the root exudates of *Rumex Acetosa* induce the production of specific metabolites of rhizosphere microorganisms, resulting in changes in the community structure and metabolic characteristics of rhizosphere microorganisms, resulting in higher methane oxidation efficiency in *Rumex Acetosa* rhizosphere soil.

3.4.3 Metabolic Pathway Analysis based on KEGG Database: The results of metabolite

classification are shown in Figure 6D and Figure 6E. A total of 14 kinds of KEGG Compounds were detected in soil samples of vegetation roots, and the corresponding statistical maps of Pathway pathways were divided into 7 categories, in which Metabolism Process accounted for the largest proportion and Cellular Process accounted for the smallest. It is inferred that the vegetation root system can effectively enhance the metabolic intensity of microorganisms in the rhizosphere and accelerate the utilization efficiency of substances in the rhizosphere microdomain. Microbial metabolites are an important medium of allelopathic effect with plants and can feedback regulate plant growth state [30-32].

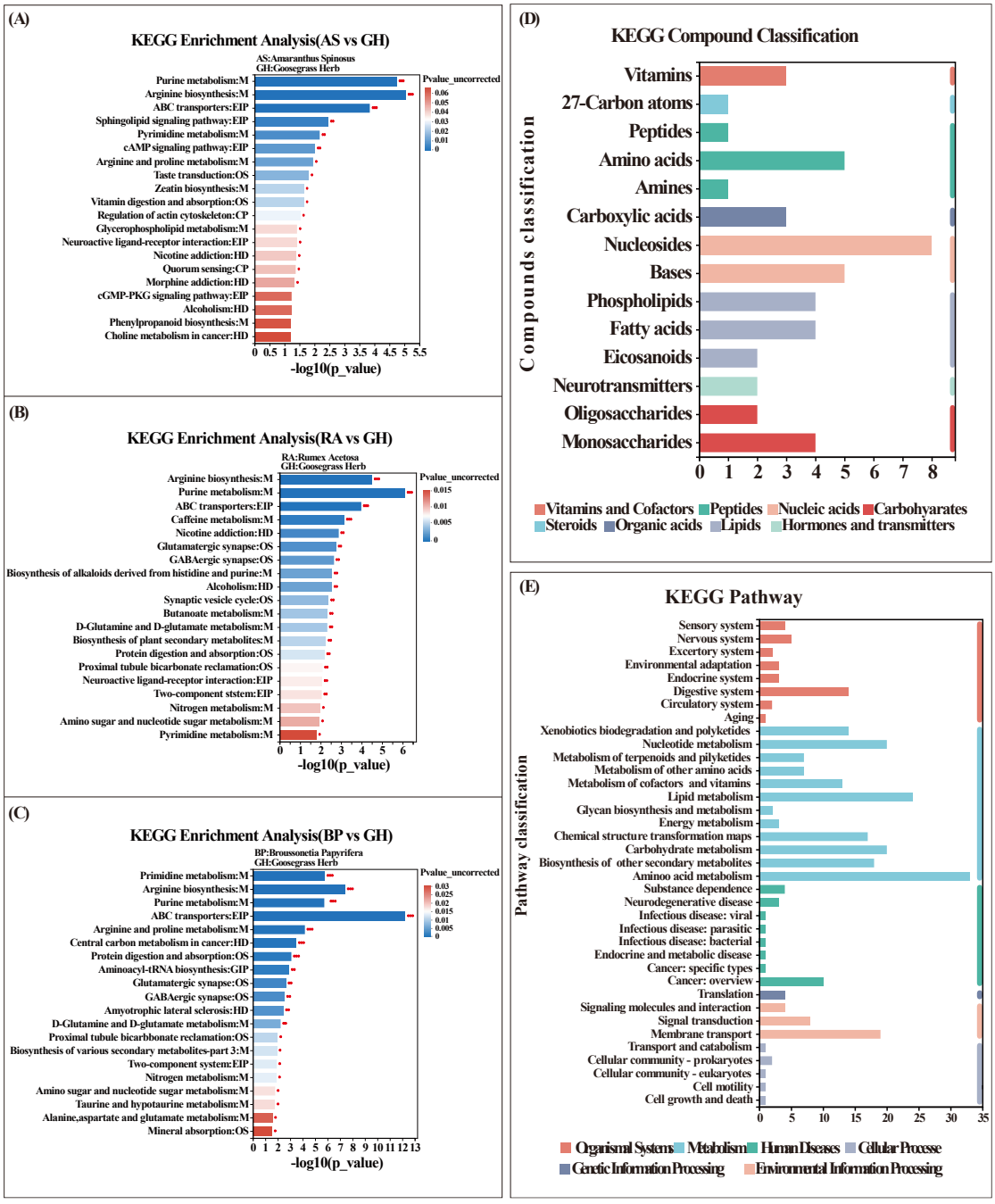

Fig. 6 Analysis of microbial metabolic pathway in the rhizosphere of typical vegetation.

A: 20 KEGG enrichment path item ratios obtained from *Rumex Acetosa*, *Amaranthus Spinosus,* and *Broussonetia Papyrifera* rhizosphere microorganisms and Rhizosphere microorganisms; D: Rhizosphere soil samples taxonomic columnar statistical chart (Note: Vertical coordinate is KEGG compound classification, Abscissa is annotated to the number of compounds of this kind; Bar color

indicates that it belongs to the first class of compounds) E: Statistical map of Pathway in rhizosphere soil samples (Note: the ordinate is the second classification of KEGG metabolic pathway, and the Abscissa is the number of compounds annotated to this pathway. KEGG metabolic pathways can be divided into seven categories: Metabolism, Genetic Information Processing, Environmental Information Processing, Cellular Processes, Organismal Systems, Human Diseases, and Drug Development. The color of the bar indicates different metabolic pathways.))

The most obvious and important metabolic or biosynthetic pathways related to metabolism were identified according to the KEGG database. The KEGG database identified 67 metabolic pathways and annotated 42 very important metabolic pathways (Table S4). The differential metabolites of four vegetation rhizosphere microorganisms are involved in the following metabolic or biosynthetic pathways: the biosynthesis of Arginine, the metabolism of Taurine and Sub-taurine, the metabolism of Alanine, Aspartic acid, and Glutamic acid, and the metabolism of Arginine and Proline.

The detailed relationship between different metabolic pathways and microorganisms was studied by comparing the results of microbial KEGG pathway enrichment in the rhizosphere of *Goosegrass Herb*. Figure 6 A-C shows 20 path items with the highest KEGG enrichment in the rhizosphere microbial communities of three kinds of vegetation. The characteristics of differential metabolites were observed in the following metabolic or biosynthetic pathways in the comparison of microbial metabolic pathways in the rhizosphere of *Amaranthus Spinosus*, *Rumex Acetosa,* and *Goosegrass Herb*: Arginine Biosynthesis: M, Purine Metabolism: M and ABC Transporters: EIP. In the comparison of microbial metabolic pathways in the rhizosphere of *Broussonetia Papyrifera* and *Goosegrass Herb* group, the characteristics of differential metabolites were observed in the following metabolic or biosynthetic pathways: Pyrimidine metabolism: M, Arginine biosynthesis: M, Purine metabolism: M, ABC Transporters: EIP, Arginine and proline metabolism: M, Central carbon metabolism in cancer: HD and Protein digestion and absorption: OS($P<0.01$). It was also found that the metabolic or biosynthetic pathways with the highest enrichment rate in each control group were the Regulation of actin cytoskeleton, Nicotinic acid, and Arginine biosynthesis. When Kateryna et al [33] studied the effect of root exudates on microbial activity, it was found that rhizosphere microorganisms preferred to eat aromatic organic acids secreted by plants (Nicotinic, Shikimic, Cinnamic acid, and Indole-3-acetic. Thus it can be seen that the nicotine contained in the root exudates of *Rumex Acetosa* promotes the metabolism or biosynthesis pathway of rhizosphere microorganisms to be enriched in the process of Nicotine, which improves the metabolic ability of rhizosphere microorganisms and obtains higher methane oxidation efficiency and this phenomenon also exists in the rhizosphere microorganisms of *Amaranthus Spinosus*.

4 CONCLUSION

Based on the investigation of landfills in Chongqing, it is found that during the operation of landfills, there are large areas of vegetation growing in covered soil areas and garbage corruption areas, and more than 22 kinds of vegetation grow well in landfills, among which herbaceous plants are the most. The methane oxidation capacity of rhizosphere soil of all vegetation was higher than that of non-rhizosphere soil, and the methane oxidation capacity of *Rumex Acetosa* root soil was the highest, which was 8.45 mg/(mL·d), which was 20 times higher than that of non-rhizosphere soil. Compared with the non-rhizosphere soil, the microbial diversity and evenness in the rhizosphere of vegetation are higher, and the difference in dominant bacteria is obvious. Under the action of vegetation, methane-oxidizing bacteria such as *Methylomicrobium*, *Methylobacter*, and *unclassified_f_Methylomonadaceae* can significantly promote the enrichment of methane-oxidizing bacteria in the rhizosphere, which is of great significance to the bio-oxidative degradation of methane in cooperation with other bacteria. *Rumex Acetosa* changed the physical and chemical properties and oxygen content of rhizosphere soil through root exudates and root oxygen transport, which could significantly induce the colonization of methane-oxidizing bacteria *Methylomicrobium* in rhizosphere microdomain, and the methane oxidation efficiency of *Rumex Acetosa* rhizosphere soil was as high as 90.32%. Limonexic acid in *Rumex Acetosa* root exudates can promote the TCA cycle of rhizosphere microorganisms, enhance the metabolic efficiency of rhizosphere microorganisms and the process of biological carbon sequestration, and its metabolites further induce the biosynthesis of plant secondary metabolites and plant hormones. Thus it can be seen that root exudates regulate the community structure and metabolic characteristics of rhizosphere microorganisms by inducing specific metabolic processes of rhizosphere microorganisms, to obtain higher methane bio-oxidation ability in rhizosphere soil. Therefore, the extensive planting of *Rumex Acetosa* and other vegetation in the landfill cover is of great significance to control the disorderly emission of landfill gas.

REFERENCES:

[1] Change Intergovernmental Panel on Climate. Climate Change 2021: The Physical Science Basis. Contribution of Working Group I to the Sixth Assessment Report of the Intergovernmental Panel on Climate Change[M]. Cambridge: Cambridge University Press, 2021

[2] Hao L M, Zhong J S, Zhang H H, et al. The release and influencing factors of ch4 in solid waste landfill spring and summer[J]. Environmental Sciences, 2009, 22(1): 83-88.

[3] Li C Y, Zhang B C. Greenhouse gas influencing global climate and research current situation of greenhouse calibration gas in our country[J]. Metrology and Measurement Technique, 2005, 32(4): 34-35.

[4] Xiaoli C, Xin Z, Ziyang L, et al. Characteristics of vegetation and its relationship with landfill gas in closed landfill[J]. Biomass and bioenergy, 2011, 35(3): 1295-1301.

[5] Reichenauer T G, Watzinger A, Riesing J, et al. Impact of different plants on the gas profile of a landfill cover[J]. Waste Management, 2011, 31(5): 843-853.

[6] Bian R, Xin D, Chai X. Methane emissions from landfill: influence of vegetation and weather conditions[J]. Environmental technology, 2019, 40(16): 2173-2181.

[7] Stralis-Pavese N, Sessitsch A, Weilharter A, et al. Optimization of diagnostic microarray for application in analyzing landfill methanotroph communities under different plant covers[J]. Environmental Microbiology, 2004, 6(4): 347-363.

[8] Zhang X Y, Tian Z Y, Zhang C, et al. Research progress on rhizosphere effect mechanism of phytoremediation of polycyclic aromatic hydrocarbons contaminated soil [J]. Soil Bulletin, 2021 (052,005).

[9] RANĐELOVIĆ D, GAJIĆ G, MUTIĆ J, et al. Ecological potential of Epilobium Dodonaea Vill. for restoration of metalliferous mine wastes[J]. Ecological Engineering，2016，95：800-810.

[10] Zu Y Q, Lu X, Zhan F D, Hu W Y, Li Y. Research progress on the role and mechanism of arbuscular mycorrhizal fungi in phytoremediation of soil contaminated by heavy metals [J]. Acta Physiologica Sinica, 2015 51 (10): 1538-1548.

[11] Shi Y F, Wang S M, Guo J N, et al. Effects of arbuscular mycorrhizal inoculation on the phytoremediation of PAH-contaminated soil: A meta-analysis[J]. Chemosphere, 2022(03), 136033,

[12] Cheng Y, Wang J H. Study on the functional difference of bacterial community in plant rhizosphere in contaminated soil [J]. Environmental Science and Technology, 2022J 45 (05): 84-91.

[13] Miao X Y, Zhou Q X. Research progress on factors affecting phytoremediation efficiency of contaminated soil [J]. Journal of Ecology, 2015, 34 (03): 870-877.

[14] Yen N C, Daniel P. S, Root exudates impact plant performance under abiotic stress[J], Trends in Plant Science, 2022, 27(01), 80-91.

[15] Charlotte V, Manhattan L, Nicolas H, et al. How does soil water status influence the fate of soil organic matter? A review of processes across scales[J], Earth-Science Reviews, 2022, 104214.

[16] Elohim B-B, Damar L-A, Thelma Y., et al. Conquering compacted soils: uncovering the molecular components of root-soil penetration[J], Trends in Plant Science, 2022, 27(08), 814-827.

[17] Yang F, Huang M B, Li C H, et al. Vegetation restoration increases the diversity of bacterial communities in deep soils[J], Applied Soil Ecology, 2022, 180,104631.

[18] Villada J C, Duran M F, Lim C K, et al. Integrative genome-scale metabolic modeling reveals versatile metabolic strategies for methane utilization in Methylomicrobium album BG8. Cold Spring Harbor Laboratory, 2021.

[19] Fu Y, Yi L, Lidstrom M. The oxidative TCA cycle operates during the methanotrophic growth of the Type I methanotroph Methylomicrobium buryatense 5GB1.[J]. Metabolic Engineering, 2017, 42:43-51.

[20] Christian, Abendroth, Sarah, et al. Complete Genome Sequence of a New Firmicutes Species Isolated from Anaerobic Biomass Hydrolysis[J]. Genome Announcements, 2017, 5(40).

[21] Subirats J, Sharpe H, Topp E. Fate of Clostridia and other spore-forming Firmicute bacteria during feedstock anaerobic digestion and aerobic composting[J]. Journal of Environmental Management, 2022, 309:114643-.

[22] Li L, Li Y C, Liu D P, et al. Research progress on biodegradation of refractory organic compounds based on methane-oxidizing bacteria [J]. Environmental Chemistry, 2020 (2): 8.

[23] Zhang H, Xing Z L, Wang J, et al. Research status, microbial metabolic characteristics and the prospect of heterotrophic assimilation degradation of chlorinated hydrocarbons [J]. Journal of Biological Engineering, 2020, 36 (6): 18.

[24] Yang L. Effects of Cinnamic Acid on Bacterial Community Diversity in Rhizosphere Soil of Cucumber Seedlings Under Salt Stress[J]. Agricultural Sciences in China, 2010.

[25] Sun H J, Wang Q. Effect of Benzoic Acid and Cinnamic Acid on Watermelon Seeding Root Cell

Protective Enzymes and Membrane Permeability[J]. Acta Agriculturae Boreali-Occidentalis Sinica, 2007.\
[26] Liang Z T, Tang T. Effects of endophytes on biosynthesis and stress resistance of plant secondary metabolites [J]. Biotechnology Bulletin, 2021, 37 (8): 11.
[27] Lv Z Y, Sun W J, Jiang R, et al. Phytohormones Jasmonic Acid, Salicylic Acid, Gibberellins, and Abscisic Acid are Key Mediators of Plant Secondary Metabolites[J]. World Journal of Traditional Chinese Medicine, 2021, 7(3):19.
[28] Christopher J, Alteri, Stephanie D, et al. Anaerobic respiration using a complete oxidative TCA cycle drives multicellular swarming in Proteus mirabilis.[J]. mBio, 2012.
[29] Ming-Hua Y, Hong-Gen D, Jiang Y, et al. GC/MS Metabonomics Analysis of Dioscorea bulbifera L. Microtubers Conserved in vitro at Low Temperature[J]. Bulletin of Botanical Research, 2018.
[30] Lin Z M, Muhammad U K, Fang C X, et al. Types of crop allelopathy: research status and prospects in China[J]. Chinese Journal of Ecological Agriculture, 2022.
[31] Troedsson U. Signalling between plants and microorganisms[J]. Cell & Organism Biology Lund University Sölvegatanb Lund Sweden, 2005.
[32] Tian J H, Rao S, Gao Y, et al. Wheat straw biochar amendment suppresses tomato bacterial wilt caused by Ralstonia solanacearum: Potential effects of rhizosphere organic acids and amino acids[J]. Journal of Integrative Agriculture, 2021, 20(9):2450-2462.
[33] Zhalnina K, Louie K B, Hao Z, et al. Dynamic root exudate chemistry and microbial substrate preferences drive patterns in rhizosphere microbial community assembly[J]. Nature Microbiology, 2018, 3(4): 470-480.

METHANE ADSORPTION OF LANDFILL COVER SOIL IMPROVED WITH HYDROPHOBIC BIOCHAR

Jingjing Mo[1,2], Xiaojie Sun[1,2*]

1.Guangxi Key Laboratory of Environmental Pollution Control Theory and Technology, Guilin University of Technology, Guilin 541004, China

2.Guangxi Collaborative Innovation Center for Water Pollution Control and Water Safety in Karst Area, Guilin University of Technology, Guilin 541004, China

Abstract: Biochar can be amended to landfill cover soils to enhance CH_4 adsorption and oxidation. However, biochar increases soil permeability, which will lead to infiltration of rainwater and increased leachate. Improving landfill cover soil with hydrophobic biochar can simultaneously achieve CH_4 reduction and prevent rainwater infiltration that increases leachate. In this study, kinetic and thermodynamic adsorption models were used to investigate the effects of different initial CH_4 concentration and different (hydrophobic) biochar addition on the CH_4 adsorption performance of the cover layer, to reveal their adsorption behaviors and patterns. The results show that the addition of hydrophobic biochar significantly improved the adsorption capacity of soil for CH_4. The pseudo-second-order equation and Freundlich isothermal adsorption model were more suitable to describe the adsorption process of CH_4 by modified soil with different (hydrophobic) biochar additions.

INTRODUCTION

Methane (CH_4) is the most abundant greenhouse gas except carbon dioxide in the atmosphere. The radiation intensity of CH_4 is 0.97W/m^2, second only to 1.68W/m^2 of CO_2, and much higher than N_2O (0.17W/m^2) and fluorinated greenhouse gases (0.18W/m^2)[1]. Also, CH_4 is a very important pollutant (ozone) precursor, and the contribution of precursor emissions to ozone pollution is 85%, of which CH_4 accounts for about 13%[2, 3]. Since the industrial revolution, the increase in CH_4 in the atmosphere means that the CH_4 of man-made emissions is 340 ±50TgCH_4/yr, contributing about 20% to climate warming[4, 5]. CH_4 emissions from landfills are the third largest anthropogenic source of emissions after agricultural production and coal mining[6]. In Europe, landfills account for 23.6% of total anthropogenic CH_4 emissions[7]. Based on a global landfill volume of 1.5 billion tons per year, the corresponding landfill CH_4 production rate is estimated at 75 billion m3, of which less than 10% is captured and utilized[8]. CH_4 released into the atmosphere has a lifetime of about 12 years [9], so reducing the level of CH_4 in the atmosphere can have an immediate effect on mitigating the greenhouse effect.

At present, the CH_4 emission reduction technologies of landfills can be divided into three categories: recycling, end control and in-situ emission reduction[10-13]. Only the large-scale sanitary landfill CH_4 has the potential of energy recovery. At the same time, due to the lack of management, the economically feasible landfill CH_4 energy recovery projects are few, the return is low, and it is difficult to implement. And end control such as flare incineration require expensive equipment and the addition of auxiliary fuels when CH_4 concentrations are insufficient[14]. China's waste is characterized by a high proportion of food waste, CH_4 production is fast and short-lived, the peak of gas production often ends quickly after landfill closure, then the release rate and concentration of CH_4 will drop significantly and the basic conditions for energy recovery and flare incineration may no longer be

available. The gas collection rate of the ongoing CH_4 recovery project in several landfills in China is estimated to be 55%-68%[15], which means that even if CH_4 gas is collected for resource utilization or end treatment, 32%-45% of CH_4 from landfills in China will still be uncontrolled released into the atmosphere, the escape emission of CH_4 is still a problem that can not be ignored[16]. In the current dual-carbon context, China is under increasing pressure to reduce greenhouse gas emissions, and reducing CH_4 emissions from landfills is crucial for countries with high greenhouse gas emissions like China. Most of the landfills in China are small and medium-sized, which do not have the conditions for energy recovery, and it is not realistic to be equipped with expensive terminal treatment facilities[17, 18].

The biochar-amended landfill cover can oxidize and adsorb CH_4[19], which can reduce landfill CH_4 gas escape and achieve in-situ emission reduction. Karhu[20] added biochar to agricultural soil and increased the adsorption capacity of CH_4 to 96%. Yaghoubi[21] obtained the maximum CH_4 adsorption capacity of 32,346,59 and 82mL/kg respectively by studying the CH_4 adsorption capacity of soil, biochar, soil containing 10% and 20% biochar, and the maximum CH_4 adsorption capacity of the cover layer increased with the increase of biochar content. The adsorption conforms to Lagergren pseudo-second-order model and Langmuir isothermal adsorption model. As a biological covering medium, biochar can not only improve the CH_4 oxidation capacity of soil, but also increase the CH_4 adsorption capacity with its large specific surface area, but the pore structure of biochar increase the permeability coefficient of soil and promote the migration and diffusion of . And affect the adsorption of CH_4 by the cover layer. The study shows that the landfill cover soil with 10%-20% moisture content has the best absorption effect of CH_4[22-24]. The large specific surface area and porosity of biochar are conducive to the transport and diffusion of CH_4 and O_2, promote CH_4 adsorption, but it increased the permeability coefficient of soil, promoted the transport and diffusion of, affected the adsorption of CH_4, and increased the leachate. Therefore, it is necessary to study the adsorption of CH_4 by hydrophobic biochar which can not only promote the diffusion of CH_4 and O_2, but also prevent from entering the coating.

To better understand the effect of hydrophobic biochar on the CH_4 adsorption properties of soil, in this study, hydrophobic biochar was added to landfill cover soil to form hydrophobic biochar modified landfill cover soil (HBS), and biochar modified landfill cover soil (BS) was used as a control. The adsorption properties of CH_4 with different initial CH_4 concentration and different amount of (hydrophobic) biochar were studied by kinetic and thermodynamic adsorption experiments. The results of the adsorption experiments were quantitatively analyzed by combining the pseudo-first-order model, pseudo-second-order model, Freundlich isothermal adsorption model and Langmuir isothermal adsorption model to reveal the adsorption behaviors and laws of CH_4 and provide a theoretical basis for the application of HBS.

EXPERIMENTAL

Materials

The cover soil used in the experiment was a silty clay soil obtained from the Shankou landfill in Guilin, which is screened by # 10 screen. Biochar, purchased from Desheng carbon Industry Co., Ltd., is made from rice straw by pyrolysis at 500 °C and screened by # 40-60 sieve. Hydrophobic biochar was modified with purchased biochar by the method of Zhang et al[25].

Prior to use for testing, soil was autoclaved at 121℃ for 30 min for two days to eliminate microbial oxidation[26, 27]. Biochar (B) and hydrophobic biochar (HB) were evenly mixed with soil (S) at mass ratios of 1:19, 1:9, 3:17 and 1:4, respectively, to obtain 5%, 10%, 15%, 20% biochar-amended soil (BS_5, BS_{10}, BS_{15}, BS_{20}) and hydrophobic biochar-amended soil (HBS_5, HBS_{10}, HBS_{15}, HBS_{20}).

Kinetics study

In this experiment, a 500 mL volumetric flask with a butyl rubber stopper was used as a CH_4 adsorption device. In this experiment, the partial pressure of adsorbent gas is changed indirectly by directly controlling the concentration of adsorbate in the system[28]. A synthetic gas was used to simulate landfill gas, consisting of 50% CH_4 and 50% CO_2[29-31].

Weigh 10 g of adsorbent material with an electronic balance and pour it into the adsorption device, cork the bottle and wrap it with tape to prevent air leakage. The initial concentrations of CH_4 of 4%, 7% and 10% were obtained by withdrawing 40, 70 and 100 mL of gas from the flask with a syringe and then injecting an equal amount of simulated gas and sealing the needle holes with a silicone pad. The experiment was carried out at room temperature (298.15-300.15K). Each group set up a blank test to check the initial concentration, and all date were subjected to the averages of triplicate experiments to ensure the experimental repeatability and improve the data accuracy[32]. The timing begins when the simulated gas is injected into the bottle by the syringe, when the gas enters the bottle and comes into contact with the test material, and the gas sample is taken with a 5mL syringe every 2, 4, 6, 10, 20, 30, 60 and 120min when the material comes into contact with the gas. The gas samples obtained were analyzed by GC-7890 gas chromatograph.

In this experiment, the adsorption process of CH_4 by improved soil with different CH_4 concentration and different addition of (hydrophobic) biochar was investigated, the adsorption speed of CH_4 by (hydrophobic) biochar modified soil was studied, and the relationship between CH_4 adsorption amount and adsorption time was clarified. The kinetic adsorption was fitted by pseudo-first-order kinetic equation and pseudo-second-order kinetic equation[33]:

$$\ln(q_e - q_t) = \ln q_e - k_1 t \quad (1)$$

$$\frac{t}{q_t} = \frac{1}{k_2 q_e^2} + \frac{1}{q_e} t \quad (2)$$

where q_e (mol/kg) is the equilibrium adsorption capacity, q_t (mol/kg) is the unit adsorption amount at time t (min), K_1 (min^{-1}) and K_2 ($kg \cdot mol^{-1} \cdot min^{-1}$) are the pseudo-first-order and the pseudo-second-order adsorption rate constant.

Isotherm study

The adsorption isotherms of CH_4 in (hydrophobic) biochar modified soils with different mass ratios (5%, 10%, 15%, 20%) were determined under low pressure, to clarify the relationship between CH_4 adsorption capacity and equilibrium pressure, and to explain the CH_4 adsorption behavior and law. The adsorption temperature is 273.15K and the adsorption pressure is 0-101kPa.

The isothermal adsorption is fitted by Langmuir equation and Freundlich equation, both of which can be applied to chemical adsorption and physical adsorption. Langmuir adsorption model is a monolayer adsorption model, which holds that the adsorbate is not adsorbed on the whole surface of the adsorbent, but on a specific point on the surface of the adsorbent[34]. Freundlich isotherm is an empirical equation. It is generally believed that the smaller 1/n the better the adsorption performance, 1/n in 0.1~0.5, it is easy to adsorb, 1/n>2 is difficult to adsorb[35]. Langmuir equation and Freundlich equation are as follows:

$$q_e = \frac{k_L q_m c_e}{1 + k_L c_e} \quad (3)$$

$$q_e = k_F c_e^{1/n} \quad (4)$$

where: q_e (mol/kg) is the equilibrium adsorption amount; q_m (mol/kg) is the saturation adsorption amount; C_e (kPa) is the equilibrium pressure; K_L (1/kPa) is the Langmuir adsorption characteristic constant; K_F and n are the Freundlich characteristic constants.

RESUIT AND DISCUSSION

CH_4 adsorption kinetics

Effect of initial CH_4 concentrations

Pseudo-first-order and pseudo-second-order kinetic

models were used to study the adsorption of S, B, HB, BS_{20} and HBS_{20} at different initial CH_4 concentrations (4%, 7% and 10%), respectively. All the adsorption curves increased sharply in a short time, followed by a slow rise to the last basically unchanged, as shown in Fig. 1 and Fig. 2.

At the initial CH_4 concentration of 4% for 2 min, the adsorption of CH_4 by S, B, HB, B_{20}, and HB_{20} was 0.25 mol/kg, 0.41 mol/kg, 0.48 mol/kg, 0.46 mol/kg, and 0.41 mol/kg, respectively, with the lowest adsorption rate of S and the highest adsorption rate of HB, followed by BS_{20}, B and HBS_{20}, which shows that HB has a faster onset adsorption rate compared to S and B. The reason may be that the hydrophilic group-OH on the surface of B is replaced by hydrophobic group, which forms an organic cover layer on the surface of biochar by chemical bonding, which reduces the agglomeration of biochar and makes its pores easier to capture adsorbate[36]. As shown in Fig. 1 (a), all the adsorption curves have basically reached a stable state when the adsorption was carried out for 60 min. The adsorption of B on CH_4 was the highest, the difference between HB, BS_{20} and HBS_{20} was not significant, and the adsorption of S was the lowest. When the initial concentration of CH_4 is 7% and 10%, each adsorption curve basically reaches a stable state at 60min. Compared with 4% CH_4 initial concentration, the adsorption capacity of S, B, HB, BS_{20} and HBS_{20} in 7% CH_4 initial concentration was increased, and the adsorption capacity of B was the highest and that of S was the lowest. Compared with the initial concentration of 7% CH_4, the adsorption capacity of B, HB, BS_{20} and HBS_{20} in the initial concentration of 10% CH_4 was increased except that the adsorption capacity of S was decreased.

The adsorption of B was the highest and S the lowest at different initial CH_4 concentrations. Both the addition of biochar and hydrophobic biochar significantly increased the adsorption capacity of soil to CH_4, with the addition of biochar having the most significant effect. As the initial concentration of CH_4 increased, the adsorption capacity of B, HB, BS_{20} and HBS_{20} on CH_4 increased accordingly, while the adsorption of S on CH_4 change little because the adsorption capacity of S on CH_4 was weak and had reached its highest point when the CH_4 concentration reached 7%, and did not change much after increasing the concentration. As seen in Table 1, Fig. 1 and Fig. 2, the pseudo-second-order model has a best correlation. Compared with other materials, the fit of S was lower, probably because the adsorption amount of S on CH_4 was smaller than 1/2 that of B, making the regularity between the measured adsorption value and adsorption time poor. The equilibrium adsorption capacity fitting value of the pseudo-second-order kinetic equation is closer to the actual equilibrium adsorption capacity measured by the experiment, so the pseudo-second-order kinetic equation is more suitable to describe the adsorption process of CH_4 on improved soil with different (hydrophobic) biochar content, which indicates that the adsorption process is mainly controlled by chemical action and its rate of CH_4 adsorption is influenced by both adsorbate concentration and adsorbent properties[37, 38]

TABLE 1 Kinetic equation parameters of the adsorption by S, B, HB, BS_{20} and HBS_{20} at different initial CH_4 concentrations

materials	initial concentrations of CH_4	Pseudo-first-order kinetics			Pseudo -second-order kinetics		
		k_1 (1/min)	q_e (mol/kg)	R^2	k_2 (kg/mol/min)	q_e (mol/kg)	R^2
S	4%	0.92	0.49	0.957	2.62	0.38	0.942
	7%	0.68	0.80	0.954	1.59	0.84	0.973
	10%	0.08	0.81	0.923	0.09	0.96	0.924

B	4%	0.38	0.69	0.987	0.92	0.73	0.992
	7%	0.92	1.29	0.980	1.63	1.33	0.994
	10%	0.37	1.92	0.972	0.28	2.06	0.984
HB	4%	0.69	0.62	0.958	2.43	0.64	0.961
	7%	0.91	1.15	0.994	2.21	1.18	0.994
	10%	0.46	1.26	0.907	0.55	1.35	0.970
BS_{20}	4%	0.61	0.61	0.976	1.95	0.64	0.990
	7%	1.16	0.89	0.973	3.02	0.92	0.989
	10%	0.61	1.57	0.992	0.82	1.63	0.974
HBS_{20}	4%	0.61	0.56	0.970	1.94	0.59	0.990
	7%	0.43	0.95	0.992	0.80	0.99	0.993
	10%	0.71	1.30	0.974	1.10	1.35	0.995

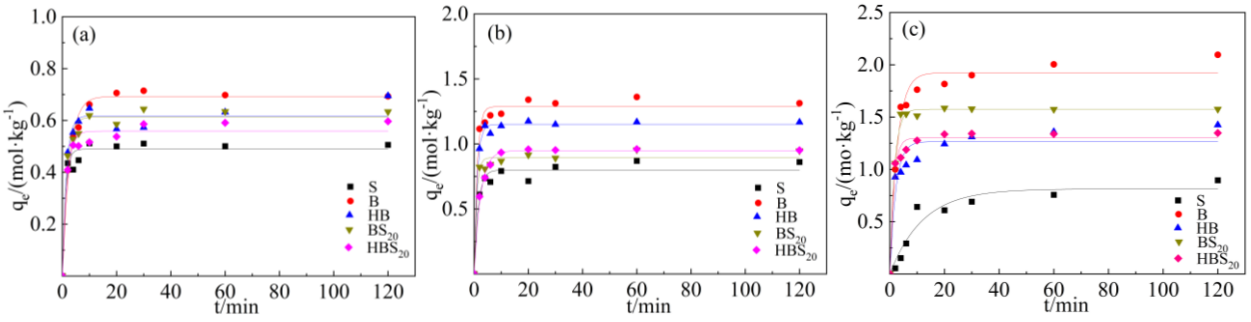

FIG. 1 Adsorption of S, B, HB, BS_{20} and HBS_{20} at different initial concentrations of CH_4 and their pseudo-first-order kinetic nonlinear fitting curves, respectively (a) 4% CH_4; (b) 7% CH_4; (c) 10% CH_4

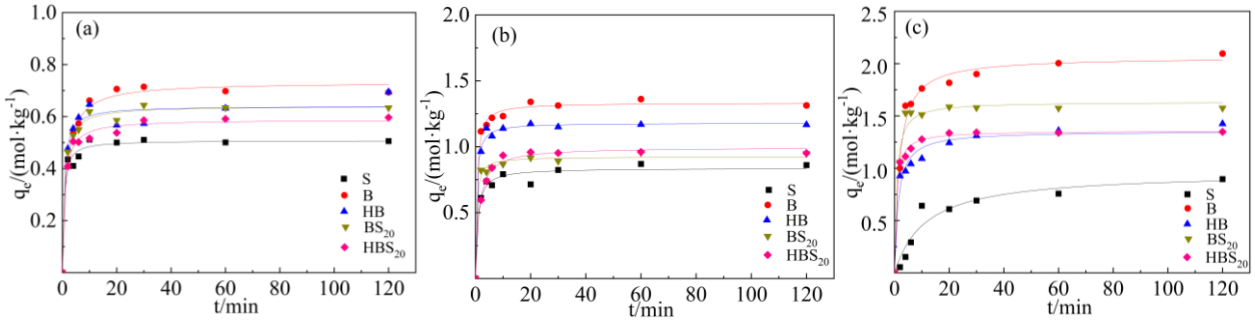

FIG. 2 Adsorption of S, B, HB, BS_{20} and HBS_{20} at different initial concentrations of CH_4 and their pseudo-second-order kinetic nonlinear fitting curves, respectively (a) 4% CH_4; (b) 7% CH_4; (c) 10% CH_4

Effect of (hydrophobic) biochar addition

In the experiment, the initial concentration of CH_4 was 4%, and biochar-amended soil (BS_5、BS_{10}、BS_{15}) and hydrophobic biochar-amended soil (HBS_5、HBS_{10}、HBS_{15}) with mass ratios of 5%, 10%, and 15% were set up to study the adsorption performance of improved soils at different additions of (hydrophobic) biochar on 4% methane. Fig. 3 show their pseudo-first-order kinetics and pseudo-second-order kinetics fitting curves, respectively.

As shown in Fig. 1 (a), and (b), all the adsorption curves in the figure follow three processes: a sharp increase in a short period of time, followed by a slow increase and finally essentially no change. The adsorption amounts of S, B and HB on CH_4 were 0.40 mol/kg, 0.70 mol/kg and 0.63 mol/kg, respectively, at an initial methane concentration of 4%. When the adsorption of BS_5 and HBS_5 is carried out for 60min, each adsorption curve has basically reached a stable state, and the adsorption amounts of BS_5 and HBS_5 on CH_4 is 0.49mol/kg and 0.52mol/kg, respectively. The addition of 5% biochar and hydrophobic biochar both improved the adsorption amount of soil on CH_4. After hydrophobic modification, the adsorption capacity of biochar to CH_4 basically unchanged, and both the addition of biochar and hydrophobic biochar can increase the adsorption capacity of soil cover, and the adsorption capacity increases with the increase of the addition[39].

As seen in Fig. 3 and Table 2, the pseudo-second-order model has a better correlation. Comparing the experimental values with the fitted values, it can be seen that the equilibrium sorption amount obtained by fitting the pseudo-secondary kinetic equation is closer to the actual equilibrium sorption amount than the pseudo-first-order kinetic equation, so the pseudo-secondary kinetic equation is more suitable to describe the adsorption process of CH_4 by (hydrophobic) biochar modified soil with content.

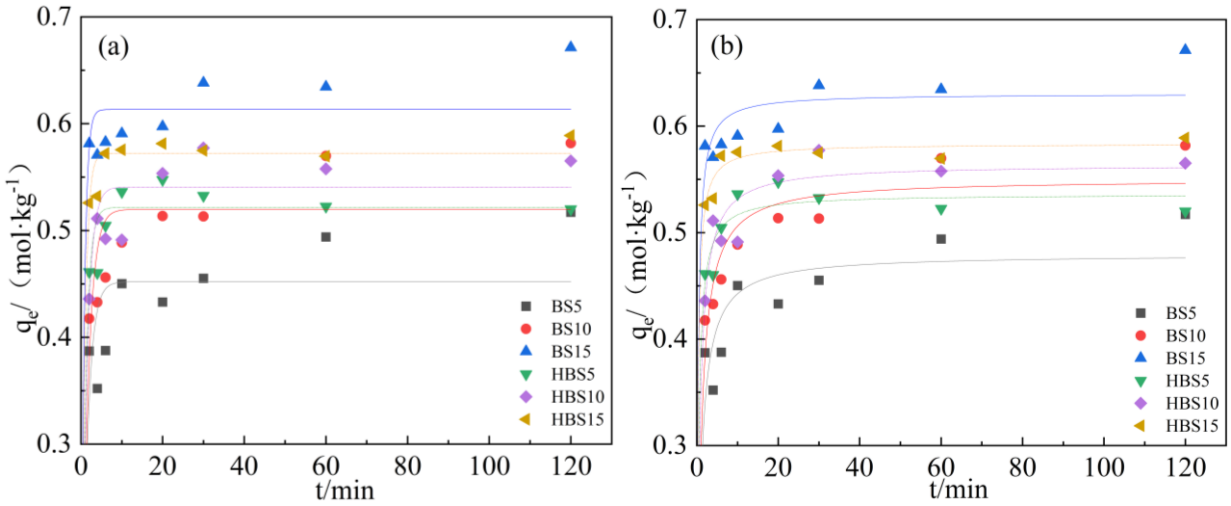

FIG. 3 CH_4 adsorption by improved soils with different (hydrophobic) biochar additions and their nonlinear kinetic fitting curves, respectively (a) pseudo-first-order; (b) pseudo-second-order;

TABLE 2 kinetic equation parameters of CH_4 adsorption by improved soil with different (hydrophobic) biochar additions

Materials	Addition amount	Pseudo-first order kinetics			Pseudo-second order kinetics		
		k_1 (1/min)	q_e(mol/kg)	R^2	k_2 (kg/mol/min)	q_e (mol/kg)	R^2
S	-	0.92	0.49	0.957	2.62	0.38	0.942
BS	5	0.70	0.45	0.897	2.50	0.48	0.949
	10	0.65	0.52	0.934	2.09	0.55	0.976
	15	1.40	0.61	0.974	5.90	0.63	0.984

	5	0.96	0.52	0.981	4.97	0.54	0.999
HBS	10	0.78	0.54	0.970	2.92	0.56	0.986
	15	1.19	0.57	0.993	7.21	0.58	0.997

Adsorption isotherms

In this experiment, the adsorption isotherms of CH_4 adsorption on soil, (hydrophobic) biochar and (hydrophobic) biochar with different mass ratios (0,5,10,15 and 20%) were tested under low pressure (0-101kPa), and the results were analyzed using the Langmuir isotherm adsorption equation and Freundlich isotherm adsorption equation. Fig. 4 (a) and (b) shows the isothermal sorption lines of CH_4 by biochar and hydrophobic biochar with different contents, respectively. It can be seen from Fig. 4 (a) and (b) that under the same temperature and pressure conditions, HB has the highest adsorption capacity for CH_4, followed by B, and S the lowest. And with the increase of (hydrophobic) biochar addition, the adsorption of CH_4 by (hydrophobic) biochar-amended soils also increased.

From the isotherm correlation coefficient R^2 in Table 3, it can be seen that the R^2 of the Freundlich isothermal sorption model was larger than that of the Langmuir isothermal sorption model, and the saturated sorption amounts fitted by the Langmuir isothermal sorption model were significantly different from those in the actual experiments, indicating that the Freundlich isothermal adsorption model can better fit the adsorption of CH_4 by different amounts of (hydrophobic) biochar modified soil. The parameter 1/n in the Freundlich isothermal adsorption model indicates the binding force or adsorption capacity of the adsorption material to the adsorbate. A smaller 1/n means better adsorption performance, and a value of 1/n between 0.1 and 0.5 means easy adsorption, while more than 2 means difficult adsorption. 1/n of the soil was 1.81, indicating its weak adsorption capacity for CH_4, while the biochar-amended soils with different additions ranged from 0.34 to 1.12 and the hydrophobic biochar-amended soils with different additions ranged from 0.35 to 1, indicating that the (hydrophobic) biochar had a weak adsorption capacity for CH_4 at low pressure, but the addition of (hydrophobic) biochar improved the adsorption capacity of the soil for CH_4.

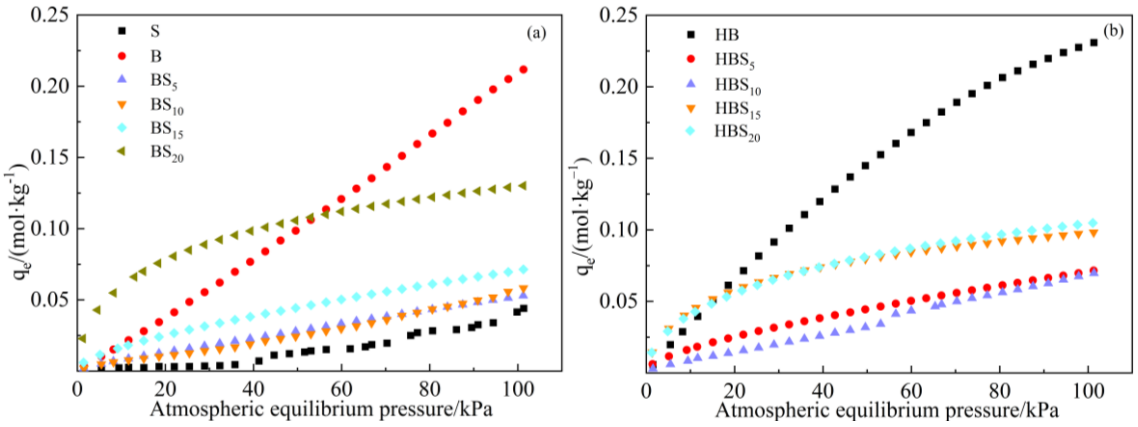

FIG. 4 Isothermal adsorption curve of CH4 by different amounts of (hydrophobic) biochar modified soil (a) biochar (b) hydrophobic biochar

TABLE 3 Isotherm parameters of CH_4 adsorption by (hydrophobic) biochar amended soils with different additions

Materials	Addition amount	Langmuir			Freundlich		
		k_L(k/Pa)	q_e(mol/kg)	R^2	k_F	1/n	R^2
S	-	-0.60×10^{-2}	-0.03	0.877	0.96×10^{-5}	1.81	0.986
BS	-	-0.10×10^{-2}	-1.74	0.999	1.50×10^{-3}	1.07	0.999
	5	0.24×10^{-2}	0.27	0.998	0.95×10^{-3}	0.87	0.999
	10	0.20×10^{-2}	-0.22	0.987	0.32×10^{-3}	1.12	0.993
	15	1.14×10^{-2}	0.13	0.988	3.70×10^{-3}	0.64	0.999
	20	6.00×10^{-2}	0.15	0.973	2.79×10^{-2}	0.34	0.994
HBS	-	0.63×10^{-2}	0.60	0.999	0.72×10^{-2}	0.76	0.994
	5	1.09×10^{-2}	0.13	0.988	3.67×10^{-3}	0.64	0.999
	10	-5.26	-13.09	0.995	0.70×10^{-3}	1.00	0.995
	15	5.51×10^{-2}	0.11	0.984	1.96×10^{-2}	0.35	0.989
	20	3.92×10^{-2}	0.13	0.982	1.62×10^{-2}	0.41	0.997

CONCLUSIONS

In this work, the effects of different CH_4 concentrations and different (hydrophobic) biochar contents on the CH_4 sorption behavior of (hydrophobic) biochar-amended soils were investigated, and the experimental results were fitted using adsorption isotherms and kinetics. The results indicate that the CH_4 adsorption onto (hydrophobic) biochar-amended soils follows pseudo-second-order kinetics and Freundlich isothermal sorption model, which is justified by kinetic and isothermal data. The addition of hydrophobic biochar significantly improved the CH_4 adsorption capacity of soil, and the adsorption amount increased with the increase of CH_4 concentration and hydrophobic biochar addition.

ACKNOWLEDGEMENTS

This work was financially supported by Guangxi innovation research team project (2018GXNSFGA281001) and Guangxi major science and technology projects (GuikeAA18118013);

REFERENCES

[1]IPCC, STOCKER T F, QIN D, et al. The physical science basis. Contribution of Working Group I to the Fifth Assessment Report of the Intergovernmental Panel on Climate Change[J]. Computational Geometry, 2013.

[2]FANG Y, MAUZERALL D L, LIU J, et al. Impacts of 21st century climate change on global air pollution-related premature mortality[J]. Climatic Change, 2013, 121(2):239-253.

[3]FANG Y, NAIK V, HOROWITZ L W, et al. Air pollution and associated human mortality: the role of air pollutant emissions, climate change and methane concentration increases from the preindustrial period to present[J]. ATMOSPHERIC CHEMISTRY AND PHYSICS, 2013, 13(3):1377-1394.

[4]KIRSCHKE S, BOUSQUET P, CIAIS P, et al. Three decades of global methane sources and sinks[J]. Nature Geoscience, 2013, 6(10):813-823.

[5]DYUPINA E, AMSTEL A V. Arctic methane[J]. Journal of Integrative Environmental Sciences, 2013.

[6]POWELL J T, TOWNSEND T G, ZIMMERMAN J B. Estimates of solid waste disposal rates and reduction targets for landfill gas emissions[J]. Nature Climate Change, 2015.

[7]AGENCY E E. Annual European Union greenhouse gas inventory 1990–2012 and inventory report 2014[J]. Renewable Energy, 2014.

[8]THEMELIS N J, ULLOA P A. Methane generation in landfills[J]. Renewable Energy, 2007, 32(7):1243-1257.

[9]BACHMANN A, BEARD V L, MCCARTY P L. Performance characteristics of the anaerobic baffled reactor[J]. Water Research, 1985, 19(1):99-106.

[10]ZHANG X, XIA J, PU J, et al. Biochar-Mediated Anaerobic Oxidation of Methane[J]. Environmental Science and Technology, 2019, 53(12).

[11]PORTEOUS A. Developments in, and environmental impacts of, electricity generation from municipal solid waste and landfill gas combustion[J]. Science Measurement & Technology Iee Proceedings A, 1993, 140(1):86-93.

[12]CHARLOTTE S, PEDERSEN G B, GIULIA C, et al. Biodegradation of Methane and Halocarbons in Simulated Landfill Biocover Systems Containing Compost Materials[J]. Journal of Environmental Quality, 2009, 38(4):1363.

[13]SCHEUTZ C, KJELDSEN P, BOGNER J E, et al. Microbial Methane Oxidation Processes and Technologies for Mitigation of Landfill gas Emissions[J]. Waste Management & Research, 2009, 27(5):409-455.

[14]FK S, BOGAN C, ROSEVEAR A, et al. Guidance on Landfill Gas Flaring[J]. 2002.

[15]DAN C, HAN M S, NANDIWARDHANA A P. Electricity generation using biogas from organic fraction of municipal solid waste generated in provinces of China: Techno-economic and environmental impact analysis[J]. Fuel Processing Technology, 2020, 203:106381.

[16]SPOKAS K, BOGNER J, CHANTON J P, et al. Methane mass balance at three landfill sites: What is the efficiency of capture by gas collection systems?[J]. Waste Management, 2006, 26(5):516-525.

[17]MOR S, DE VISSCHER A, RAVINDRA K, et al. Induction of enhanced methane oxidation in compost: Temperature and moisture response[J]. Waste Management, 2006, 26(4):381-388.

[18]STREESE J, STEGMANN R. Microbial oxidation of methane from old landfills in biofilters[J]. Waste Management, 2003, 23(7):573-580.

[19]YARGICOGLU E N, REDDY K R. Biochar-amended soil cover for microbial methane oxidation: Effect of biochar amendment ratio and cover profile[J]. Journal of Geotechnical & Geoenvironmental Engineering, 2018, 144(3):04017123.04017121-04017123.04017115.

[20]KARHU K, MATTILA T, BERGSTRM I, et al. Biochar addition to agricultural soil increased CH4 uptake and water holding capacity – Results from a short-term pilot field study[J]. Agriculture Ecosystems & Environment, 2011, 140(1):309-313.

[21]YAGHOUBI P. Development of Biochar-Amended Landfill Cover for Landfill Gas Mitigation[D];University of Illinois at Chicago.,2011.

[22]WHALEN S C, REEBURGH W S, SANDBECK K A. Rapid Methane Oxidation in a Landfill Cover Soil[J]. Applied & Environmental Microbiology, 1990, 56(11):3405-3411.

[23]BOECKX P, CLEEMPUT O V, VILLARALVO I. Methane emission from a landfill and the methane oxidising capacity of its covering soil[J]. Soil Biology & Biochemistry, 1996, 28(10-11):1397-1405.

[24]CZEPIEL P M M B, CRILL PM, ET AL. Quantifying the effect of oxidation on landfill

methane emissions[J]. Journal of Geophysical Research D: Atmospheres, 1996, 101(11):16721-16729.

[25]ZHANG M X, ZHU H X, XI B D, et al. Surface Hydrophobic Modification of Biochar by Silane Coupling Agent KH-570[J]. PROCESSES, 2022, 10(2).

[26]MUKHERJEE S, SARKAR B, ARALAPPANAVAR V K, et al. Biochar-microorganism interactions for organic pollutant remediation: Challenges and perspectives[J]. Environmental Pollution, 2022, 308:119609.

[27]BENNETT A J, LEIFERT C, WHIPPS J M. Survival of the biocontrol agents Coniothyrium minitans and Bacillus subtilis MBI 600 introduced into pasteurised, sterilised and non-sterile soils[J]. Soil Biology and Biochemistry, 2003, 35(12):1565-1573.

[28]BALA, YAMINI, SADASIVAM, et al. Adsorption and transport of methane in biochars derived from waste wood[J]. Waste Management, 2015.

[29]HARO K, OUARMA I, NANA B, et al. Assessment of CH4 and CO2 surface emissions from Polesgo's landfill (Ouagadougou, Burkina Faso) based on static chamber method[J]. Advances in Climate Change Research, 2019, 10(3):181-191.

[30]MøNSTER J, KJELDSEN P, SCHEUTZ C. Methodologies for measuring fugitive methane emissions from landfills – A review[J]. Waste Management, 2019, 87:835-859.

[31]AGHDAM E F, FREDENSLUND A M, CHANTON J, et al. Determination of gas recovery efficiency at two Danish landfills by performing downwind methane measurements and stable carbon isotopic analysis[J]. Waste Management, 2018, 73:220-229.

[32]DONG L J, SI-YING W U, SHENG-BO L I, et al. Sorption Behaviors and Mechanismsof Eu(III) on Rice Straw-derived Biochar[J]. Journal of Inorganic Materials, 2019:314.

[33]KAMATH MIYAR H, PAI A, GOVEAS L C. Adsorption of Malachite Green by extracellular polymeric substance of Lysinibacillus sp. SS1: kinetics and isotherms[J]. Heliyon, 2021, 7(6):e07169.

[34]ALI N S, JABBAR N M, ALARDHI S M, et al. Adsorption of methyl violet dye onto a prepared bio-adsorbent from date seeds: isotherm, kinetics, and thermodynamic studies[J]. Heliyon, 2022, 8(8):e10276.

[35]ROZANOV L N. Kinetic equations of non-localized physical adsorption in vacuum for Freundlich adsorption isotherm[J]. Vacuum, 2021, 189:110267.

[36]GAO M, MA Q, LIN Q, et al. Fabrication and adsorption properties of hybrid fly ash composites[J]. Applied Surface Science, 2017, 396:400-411.

[37]PéREZ-MARíN A B, ZAPATA V M, ORTUñO J F, et al. Removal of cadmium from aqueous solutions by adsorption onto orange waste[J]. Journal of Hazardous Materials, 2007, 139(1):122-131.

[38]SUN S, WANG A. Adsorption kinetics of Cu(II) ions using N,O-carboxymethyl-chitosan[J]. Journal of Hazardous Materials, 2006, 131(1):103-111.

[39]YAGHOUBI, POUPAK. Development of Biochar-Amended Landfill Cover for Landfill Gas Mitigation[J]. 2012.

MECHANISM ON METHANE OXIDATION OF LANDFILL COVER SOIL AMENDED BY BIOCHAR: A SIMULATED COLUMN EXPERIMENT

Xueshuang Lu[1, 2], Xiaojie Sun[1, 2*]

1.Guangxi Key Laboratory of Environmental Pollution Control Theory and Technology, Guilin University of Technology, Guilin 541004, China

2.Guangxi Collaborative Innovation Center for Water Pollution Control and Water Safety in Karst Area, Guilin University of Technology, Guilin 541004, China

Abstract: Application to landfill cover soils (LCS) of biochar (BC) has been widely suggested as a tool for reducing methane (CH_4) emissions from landfill. However, it is not clear whether biochar promotes methane oxidation through porous structure or nutrients of BC in BC-amended landfill cover soil (BLCS). To explore this question, a BLCS and a ceramic-amended landfill cover soil (CLCS) was prepared. A hydrophobic BC-amended landfill cover soil (HLCS) was also prepared to avoid a contradiction between the waterproofness of the ameliorated soil cover and the promotion of CH_4 oxidation. Three simulated columns were used and named RB, RH and RC based on BC, hydrophobic BC and ceramic. With the CH_4 concentration from 25% to 35%, the relative abundance of *Proteobacteria* in RB and RH was higher than that of RC. And the relative abundance of *Methylobacter* and MOB in RB was higher 10% than that of RC. The difference abundance of MOB in RC was greater between 1#, 5# and 9# sampling ports. The result suggested that CH_4 oxidation is caused by the nutrients of BC.

INTRODUCTION

Landfills become one of the main sources of CH_4 emissions (Bian et al., 2021). It is now well established from a variety of studies, that LCS can be used to reduce CH_4 emissions from landfills (Huang et al., 2020;Wang et al., 2011). MOB in the LCS can oxidize CH_4 (Huang et al. 2021; Laet al., 2018), which mainly produces CO_2, H_2O and microbial energy (Majdinasab et al., 2017), thereby decreasing it emissions from landfills. However, common landfill covering materials have shortcomings (Huang et al., 2020; Scheutz et al., 2011). For example, composting which may contribute to excessive nitrate concentration in soils can pollute the environment (Naggar et al., 2019). Therefore, better replacement materials need to be explored. BC is a product of waste biomass in the absence of oxygen and at high temperatures, and is a low-cost, environmentally friendly carbon-rich material (Campos et al., 2020;M. Zhang et al., 2022). Some researchers have found that adding BC to the LCS can improve CH_4 emissions, proving that is a kind of good alternative materials (Sadasivam et al., 2014).

BC can enhance the activity of MOB in soil, thereby improving the oxidation performance of CH_4 (Chetri et al., & Green, 2022;Weber et al., 2018). In addition, it also can help the soil retain nutrients (Xia et al., 2022). The nutrients in the modified soil were released at a relatively low rate (Mukherjee et al., 2013), which was conducive to the growth of microorganisms, especially in the newly established landfill soil with low nutrient content. BC has porous structure and high surface area (Sun et al., 2018). It is an ideal habitat and shelter for microorganisms (Huang et al., 2021;Wang et al., 2017) because they can live in pores or attach to the surface of BC (Quilliam et al., 2013). Studies have found that the addition of BC can improve the cation exchange capacity (CEC) of soil (Yao et al., 2022). This can help the growth of microorganisms because soil microorganisms absorb nutrients mainly in the form of ions (Huang et al., 2019; Weber et al., 2018). BC has also been shown to have a strong adsorption capacity and is evident in the effect of CH_4, which helps reduce CH_4 emissions (Issaka et al., 2022; Oliveira et al.,

2017;Windeatt et al., 2014).

The mechanism of BC promoting CH_4 oxidation is controversial. At present, researchers have generally maintained that both porous structure and nutrients have been influential. But some people think contribution to promoting CH_4 oxidation by porous structure (Reddy et al., 2014). (Wu et al., 2020). analysis that the porous structure of BC played an important part in capacity of CH_4 oxidation during researching the BC-amended landfill cover soil (BLCS) in compared with the conventional cover soil. Others think nutrients more responsibilities than the porous structure (Bing et al., 2015). And this study puts forward certain thought that find a substitute similar to of BC with porous structure and unable to provide nutrients. The porous ceramic material has the characteristics of high porosity, large specific surface area and low permeability resistance (Liu et al., 2016; Moritz et al., 2007). It is used to replace BC as LCS amendment in this experiment.

However, in the BLCS, investigators have examined that the permeability coefficient of LCS increased with the content of BC, which leads to the entry of rainwater and affect the CH_4 oxidation. Chen's experiment proposed that water resistance of composites by silane coupling agent (KH-570 was used) amended had been effectively improved (Chen et al., 2021). Sun et al. used this material as a hydrophobic amended for BC and it can act as a waterproof agent and change the hydrophilic soil was confirmed. (Sun et al, 2019). Therefore, CH_4 oxidation was studied by a hydrophobic BC-amended landfill cover soil (HLCS).

The comparative tests of CH_4 oxidation are conducted for the BLCS, HLCS and CLCS. The changes of microbial community structure and spatial distribution of functional microorganisms at different depths in the simulated columns of the three materials was observed. Two hypotheses are proposed: If the methane oxidation effect of BLCS is better than that of CLCS, it proves that the methane oxidation of BLCS is the result of the action of nutrients of biochar. If the methane oxidation effect of BLCS is the same or basically the same as that of CLCS, it indicates that the porous structure of biochar coating is the main reason for promoting methane oxidation. The mechanism of promoting methane oxidation by biochar can be revealed according to the similarities and differences of methane oxidation effects.

MATERIALS AND METHOD

Experimental materials

The study was conducted as a follow-up to previous study and used the same materials which BC was prepared from waste rice straw at 500℃ without oxygen and modified it with hydrophobic modifier silane coupling agent (CH2=C (CH3)COOC3H6Si (OCH3)) employed in (Zhang et al., 2022).

The soil exposed to CH_4 for the landfill experiments was obtained from landfill film overlay of Mountain pass site in Guilin, Guangxi, China. It was dried and then passed through 30 mesh sieve to remove rubbish and big stones. Silicon nitride inorganic ceramic material was also used in this experiment, which an atomic crystal prepared by the solid state reaction method and was purchased from Kurt New Material Technology Co., LTD. The properties were similar to BC of the test, with highly porous structure and high surface area (113.24 m^2/g). Besides, Total pore volume of adsorption was 0.09 cm^3/g and the average diam

TABLE 1

Physical and chemical properties of three covering materials

Proterties	BC-amended soil	Hydrophobic BC-amended soil	Silicon nitride landfill cover soil
Organic matter content/g·kg^{-1}	59.20	63.300	32.200
Porosity/g·kg^{-1}	46.12	46.310	25.860
pH	7.640	7.7400	7.5200
P/g·kg^{-1}	1.500	1.2600	1.2600
K/g·kg^{-1}	16.30	15.200	13.300
N/g·kg^{-1}	2.710	2.1600	11.600
Maximum water-holding capacity/g·kg^{-1}	530.41	410.96	344.06

Experimental setup

Three simulated columns of different cover materials (BC-amended, hydrophobic BC-amended and silicon nitride landfill cover soils） were used in this study. Those columns were named RB, RH and RC accordingly, which made of polyvinyl chloride（PVC） with 100 cm height and 15 cm diameter. The structure was constituted by permeable (15 cm), gravel (10 cm), cover (60 cm), and air (10 cm) layer from bottom to top. The gravel layer facilitated to support the cover layer and drainage. A rainfall device was in the cover layer and drainage. A rainfall device was introduced above the simulated column to mimic precipitation. When excess moisture was in the cover layer, it could be discharged through the permeable layer.Water bath cycle temperature control device was installed outside the simulated column to control the ambient temperature. No. 0 sampling port was set at the top left of the simulation column, and nine sampling ports which numbered 1 to 9 and an interval of 5 cm from top to bottom were also set in front of the cover layer.

Operation method

Them simulated landfill gas consisted of CO_2, CH_4 and N_2, which passed through a pipe with holes of uniform size and through an air inlet at the bottom of the column (Yargicoglu et al., 2017), then at a certain rate through the rotameter and humidifier evenly into the gravel layer as a buffer area, and eventually arrived the cover layer. The air was blown by a blower and entered the two instruments described above, then was sent to the simulated column through the air inlet.

The flow rates of air and simulated landfill gas controlled by the rotameter were 50 mL/min and 10-20 mL/min, respectively. The initial temperature of water bath temperature control device and moisture content was 25 ℃and 10%. There were four stages to the experiment: stage I (the rate of 15 mL/min) with CH_4 content of simulated landfill gas was 25%, stage II (the rate of 10 mL/min, 15 mL/min and 20 mL/min, respectively) with CH_4 content of simulated landfill gas was 35%, stage III (the rate of 20 mL/min) with CH_4 content was the same as in the stage II, and stage IV (the temperature was maintained at 25℃) with conditions were the same as the previous stage.

For RB, RH and RC, the samples (which were named B1.1, B1.5 and B1.9, H1.1, H1.5 and H1.9, C1.1, C1.5 and C1.9, respectively) obtained by the 1#, 5# and

9# sampling ports at the beginning of operation. At the same time, the end-stage samples were named B2.1, B2.5 and B2.9, H2.1, H2.5 and H2.9, C2.1, C2.5 and C2.9, respectively.

RESULTS AND DISCUSSION

Alpha Diversity

Variations in alpha-diversity of community obtained for analyzing at 97 % identity across different samples at the end of simulation column operation (Table 2). Alpha Diversity was estimated with the community richness indices (the Chaol and ACE index) and diversity indices (Shannon, Simpson and Good's coverage index) (Sun, et al., 2022; Zhang, Yi, & Lu, 2022). Good's coverage index represents sample library coverage and reflects whether the sequencing results present the true picture of the sample. Table 2 shows that the values Good's coverage index for all samples exceeded 0.995.

TABLE 2
Alpha Indices Statistics for different covering materials

Sample name	shannon	simpson	chao1	ACE	goods_coverage
B1.1	2.180	0.420	514.84	537.615	0.998
B1.5	1.732	0.316	430.75	445.208	0.998
B1.9	2.161	0.382	466.628	477.666	0.999
B2.1	4.639	0.861	725.082	682.229	0.997
B2.5	3.096	0.557	547.111	556.638	0.999
B2.9	2.992	0.574	512.511	532.057	0.998
H1.1	3.602	0.617	706.211	739.512	0.997
H1.5	3.304	0.601	643.554	651.088	0.997
H1.9	3.952	0.665	779.364	805.204	0.997
H2.1	4.379	0.773	770.507	811.905	0.997
H2.5	4.513	0.774	950.85	1000.6	0.995
H2.9	3.561	0.622	702.078	732.664	0.997
C1.1	4.699	0.890	568.333	565.124	0.998
C1.5	3.140	0.543	660.374	669.01	0.998
C1.9	5.611	0.899	702.202	711.96	0.998
C2.1	3.954	0.800	684.288	707.336	0.998
C2.5	2.988	0.561	568.481	576.494	0.998
C2.9	4.615	0.767	743.01	750.131	0.998

The analysis of Shannon and Simpson

The diversity of microbial community was strongly and positively correlated with the value of Shannon and Simpson, the higher value of Shannon and Simpson indicating that the the diversity was higher and the structure was more complex(Liu et al., 2021). Compared to B2.1, B2.5 and B2.9, the value of Shannon and Simpson of was increasing than that of B1.1, B1.5 and B1.9. The rising trend explained that the number of microbial species increased with the concentration of CH_4 increased from 25% to 35% in BLCS, and the adaptability of microorganisms to the environment is enhanced by adding BC. The value of 1# and 5# sampling ports of RH were also elevated but 9# were gradually decreased. However, the value of

Shannon and Simpson was almost always higher than that of RB from the beginning to the end of the simulated column operation. The circumstance suggested that hydrophobic BC contributed to diffuse smoothly for CH_4 and oxygen in HLCS, which might be favoring growth of the MOB and acclimated constantly. And other creatures were eliminated because of unable to adapt to the environment with increasing CH_4 concentration. Whereas the value of Shannon and Simpson in RC almost declined, indicating that the microbial diversity was significantly lower. It implies that CLCS could not provide optimum nutrients for advantageous bacteria growth and feasible environment for bacteria activities, which led to fail to acclimate by it.

The changes of Chaol and ACE

The value of Chaol and ACE is proportional to the distribution abundance of the community (Liu et al., 2021). From the beginning to the end of the simulated column operation, the changes of value of Chaol and ACE of 1#, 5# and 9# sampling ports progressively increased in RB. The value of 1# and 5# sampling ports also increased in RH but 9# sampling ports was reduced. The data was the same as the result of Shannon and Simpson. The decline was caused by the hydrophobic BC provided suitable moisture content and gas permeability in HLCS, which was helpful in accelerate upward diffusion of CH_4. And then caused that microorganisms made more active in the middle and upper of HLCS when CH_4 diffused upward with CH_4 concentration from 25% to 35%. The value Chaol and ACE of 1# and 9# sampling ports increased and the value of 5# sampling port decreased in RC. The data showed that the changes of value Chaol and ACE was irregularly at three sampling ports. It might be the complicated environment in CLCS and no nutrients were provided to the microbes. Eventually leading to the microbial communities was unadaptable and not evenly distributed.

COMPOSITION CHANGES OF MICROBIAL COMMUNITY STRUCTURE

The relative abundance of Phylum level

As shown in Fig. 4, *Proteobacteria* were the dominant phyla in the bacterial community occupying>50% of the total abundance (Kubaczyński et al., 2022). Because the MOBbelongs to the *Proteobacteria* (Chetri et al., 2022), which speculated that had greater methanotrophic abundance in the three simulated columns. The abundance of *Proteobacteria* of the 1#, 5#, 9# sampling part in RB goes down from 92%, 88% and 89% to 77%, 84% and 78%, respectively, with increasing CH_4 concentration (from 25% to 35%). The relative abundance of *Proteobacteria* of the 1#, 5#, 9# sampling part in RH goes down from 83%, 81% and 79% to 82%,77% and 79%, respectively. The relative abundance of *Proteobacteria* of the 1#, 5#, 9# sampling part in RC change from 54%, 82% and 61% to 52%, 82% and 71%, respectively. The relative abundance of *Proteobacteria* of the beginning and end simulated column operation in RB and RH was greater than that of RC, suggesting that *Proteobacteria* obtained a good living environment by adding BC and nutrients provided for *Proteobacteria* by BC. And the downward trend in RB and RH might be caused by the organic matter significantly decreased was due to constantly consumed in the limited column environment decreasing of the organic matter which can provide sufficient nutrients for the growth of *Proteobacteria*. Comparing the relative abundance of *Proteobacteria* of initial #1, #5 and #9 sampling parts with that of terminal #1, #5 and #9 sampling parts in RB, RH and RC, the abundance of *Proteobacteria* decreased the least in RH, illustrated that microorganisms were relatively unaffected by elevated methane concentrations. The conclusion was previously confirmed (Kubaczyński et al., 2022).

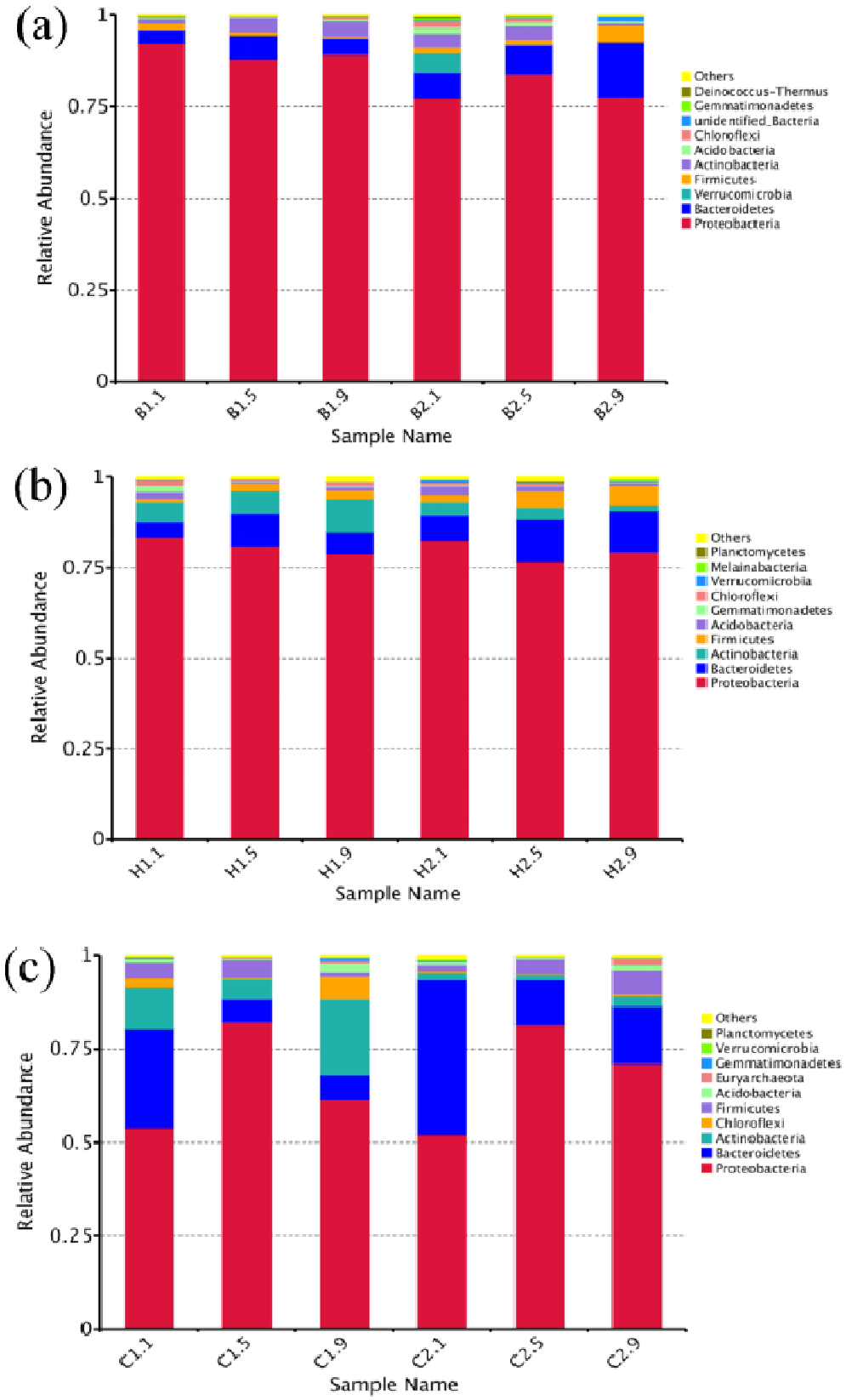

FIG. 1 Spectral relative abundance histogram at the phylum level of RB (a), RH (b) and RC (c)

The relative abundance of genus level The bacterial community structure in simulated

columns has been relatively stable with CH_4 concentration increasing from 25% to 35%. The relative abundance of samples was dominated by *Methyobacter* in the RB, RH and RC (Fig. 6). However, the relative abundance of *Methyobacter* of terminal #1, #5 and #9 sampling parts decreased than that of initial #1, #5 and #9 sampling parts in the RB, RH and RC. The relative abundance of *Methyobacter* decreased in the end because the reduction of organic matter which provided growth and reproduction of microorganism. Compared to RB and RH, the relative abundance of #1, #5 and #9 sampling parts in RC was lower and showed that have significant difference at the same concentration of CH_4. This phenomenon argued that BC addition was beneficial to the growth of *Methyobacter*.

The relative abundance of *Methyobacter* of B2.1, B2.5 and B2.9 were 32.40%, 66.23% and 64.82%, respectively. The relative abundance of *Methyobacter* of H2.1, H2.5 and H2.9 sampling ports were 46.00%, 47.24% and 61.30%, respectively. Meanwhile, the proportion of C2.1, C2.5 and C2.9 were 24.92%, 66.16% and 48.13%, respectively. The relative abundance difference of #1, #5 and #9 sampling ports in the same simulated column showed that bacterial community distribution of the upper, meddle and bottom in the RH was more evenly distributed than that of RB and RC. It indicated that *Methyobacter* was less affected by the change of CH_4 concentration than RB and RC. The average relative abundance of *Methyobacter* of RB, RH and RC was about 54.48%, 51.51% and 46.40%. By contrasting the data between RB and RC, the abundance of *Methyobacter* in #1, #5 and #9 sampling part of RB was greater 7.48%, 0.07% and 16.69% than that of RC (Figs.6 [a] and 6[c]). The data showed that the abundance of adding BC was significantly higher than that of not adding BC. The results demonstrate that the relative abundance of *Methyobacter* was significantly higher caused by BC's nutrients in RB and RH. Furthermore, the relative abundance *Methyobacter* was the most stable in RH. Meanwhile, *Sphingomonas* and *Chryseolinea* were also found more active in the upper layer of RB, RH and RC, probably because that belonged to aerobic bacteria, the results consistent with (Zhang et al., 2022; Zhao et al., 2008).

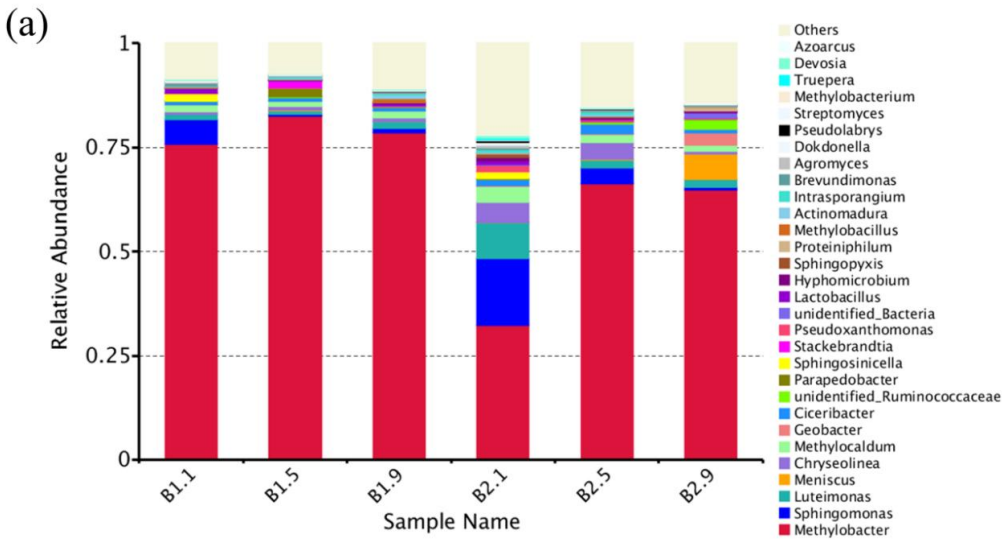

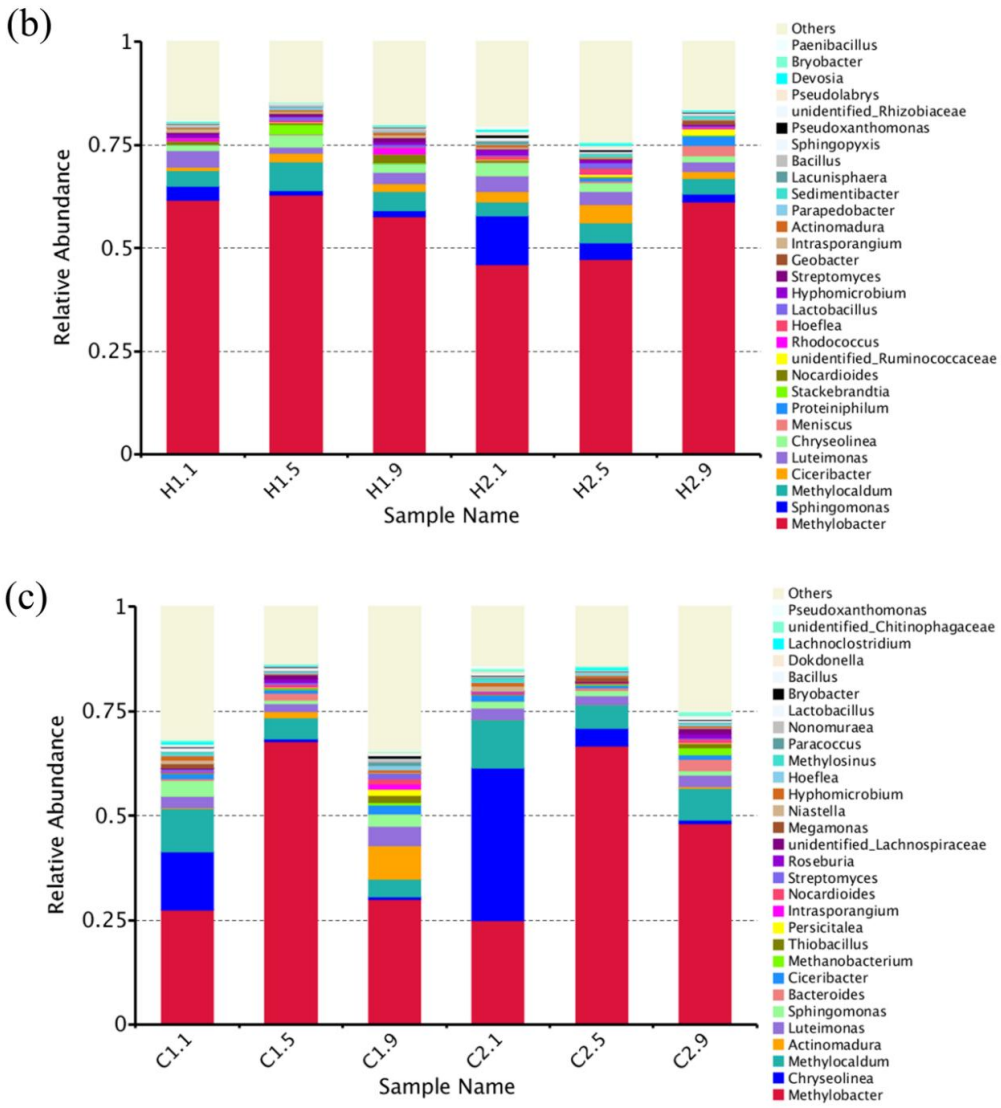

FIG. 2 Spectral relative abundance histogram at the genus level of RB (a), RH (b) and RC (c)

Conclusion

The research verified that the effect of the higher CH_4 oxidation is mainly due to nutrients of BC. With the increase of CH_4 concentration from 25% to 35% in the simulate column, the analysis of Alpha and Beta diversity exemplifies that the diversity of bacteria influenced by CH_4 concentration ranked as: RC>RB>RH. The analysis of bacterial community structure and composition of MOB showed that the largest relative abundance of bacteria categories was *Proteobacteria* and the dominant MOB was *Methylobacter* in RB, RH and RC. And the MOB distribution in RH was more evenly than RB.

ACKNOWLEDGEMENTS

This work was financially supported by Guangxi innovation research team project (2018GXNSFGA281001) and Guangxi major science and technology projects (GuikeAA18118013).

References:

Bian, R., Chen, J., Li, W., Sun, Y., Chai, X., Wang, H.,... Zhao, J. (2021). Numerical modeling of methane oxidation and emission from landfill cover soil

coupling water-heat-gas transfer: Effects of meteorological factors. *Process Safety and Environmental Protection*, 146, 647-655.

Bing-yue, L., Zhong-hui, Z., Huan-huan, T., Bing, Q., & Hong-xi, G. (2015). Methane Oxidation Capacity of Landfill Cover Biochar Amended Silt. *Science Technology and Engineering*, 15(36), 99-104

Campos, P., Miller, A. Z., Prats, S. A., Knicker, H., Hagemann, N.,... De la Rosa, J. M. (2020). Biochar amendment increases bacterial diversity and vegetation cover in trace element-polluted soils: A long-term field experiment. *Soil Biology and Biochemistry*, 150, 108014.

Chen, K., Li, P., Li, X., Liao, C., Li, X.,... Zuo, Y. (2021). Effect of silane coupling agent on compatibility interface and properties of wheat straw/polylactic acid composites. *International Journal of Biological Macromolecules*, 182, 2108-2116.

El-Naggar, A., El-Naggar, A. H., Shaheen, S. M., Sarkar, B., Chang, S. X., Tsang, D. C. W.,... Ok, Y. S. (2019). Biochar composition-dependent impacts on soil nutrient release, carbon mineralization, and potential environmental risk: A review. *Journal of Environmental Management*, 241, 458-467.

Huang, D., Bai, X., Wang, Q., & Xu, Q. (2021). Validation and optimization of key biochar properties through iron modification for improving the methane oxidation capacity of landfill cover soil. *Science of The Total Environment*, 793, 148551.

Huang, D., Yang, L., Xu, W., Chen, Q., Ko, J. H.,... Xu, Q. (2020). Enhancement of the methane removal efficiency via aeration for biochar-amended landfill soil cover. *Environmental Pollution*, 263, 114413.

Issaka, E., Fapohunda, F. O., Amu-Darko, J. N. O., Yeboah, L., Yakubu, S., Varjani, S.,... Bilal, M. (2022). Biochar-based composites for remediation of polluted wastewater and soil environments: Challenges and prospects. *Chemosphere*, 297, 134163.

Kubaczyński, A., Walkiewicz, A., Pytlak, A., Grządziel, J., Gałązka, A.,... Brzezińska, M. (2022). Biochar dose determines methane uptake and methanotroph abundance in Haplic Luvisol. *Science of The Total Environment*, 806, 151259.

La, H., Hettiaratchi, J. P. A., Achari, G., & Dunfield, P. F. (2018). Biofiltration of methane. *Bioresource Technology*, 268, 759-772.

Liu, R., Xu, T., & Wang, C. (2016). A review of fabrication strategies and applications of porous ceramics prepared by freeze-casting method. *Ceramics International*, 42(2, Part B), 2907-2925.

Liu, Z., Tang, J., Ren, X., & Schaeffer, S. M. (2021). Effects of phosphorus modified nZVI-biochar composite on emission of greenhouse gases and changes of microbial community in soil. *Environmental Pollution*, 274, 116483.

Mukherjee, A., & Zimmerman, A. R. (2013). Organic carbon and nutrient release from a range of laboratory-produced biochars and biochar – soil mixtures. *Geoderma*, 193-194, 122-130.

Oliveira, F. R., Patel, A. K., Jaisi, D. P., Adhikari, S., Lu, H.,... Khanal, S. K. (2017). Environmental application of biochar: Current status and perspectives. *Bioresource Technology*, 246, 110-122.

QINYong-li, Xiao-jie, S., Chun-lian, W., Bei-bei, W., Chen-nan, X.,... Hong-xia, Z. (2021). Methane emission reduction and biological characteristics induced by the landfill cover soil amended with biochar. *China Environmental Science*, 41(01), 254-262.

Quilliam, R. S., Glanville, H. C., Wade, S. C., & Jones, D. L. (2013). Life in the 'charosphere' – Does biochar in agricultural soil provide a significant habitat for microorganisms? *Soil Biology and Biochemistry*, 65, 287-293.

Reddy, K. R., Yargicoglu, E. N., Yue, D., & Yaghoubi, P. (2014). Enhanced microbial methane oxidation in landfill cover soil amended with biochar. *Journal*

of Geotechnical and Geoenvironmental Engineering, 140(9), 4014047

Sadasivam, B. Y., & Reddy, K. R. (2014). Landfill methane oxidation in soil and bio-based cover systems: a review. *Reviews in Environmental Science and Bio/Technology*, 13(1), 79-107.

Sarfraz, R., Yang, W., Wang, S., Zhou, B., & Xing, S. (2020). Short term effects of biochar with different particle sizes on phosphorous availability and microbial communities. *Chemosphere*, 256, 126862.

Scheutz, C., Pedicone, A., Pedersen, G. B., & Kjeldsen, P. (2011). Evaluation of respiration in compost landfill biocovers intended for methane oxidation. *Waste Management*, 31(5), 895-902.

Sun, M., Yang, Z., Fu, S., Fan, X., & Guo, R. (2018). Improved methane removal in exhaust gas from biogas upgrading process using immobilized methane-oxidizing bacteria. *Bioresource Technology*, 256, 201-207.

Wang, J., Xia, F., Bai, Y., Fang, C., Shen, D.,... He, R. (2011). Methane oxidation in landfill waste biocover soil: Kinetics and sensitivity to ambient conditions. *Waste Management*, 31(5), 864-870.

Wang, N., Chang, Z., Xue, X., Yu, J., Shi, X., Ma, L. Q.,... Li, H. (2017). Biochar decreases nitrogen oxide and enhances methane emissions via altering microbial community composition of anaerobic paddy soil. *Science of The Total Environment*, 581-582, 689-696.

Weber, K., & Quicker, P. (2018). Properties of biochar. *Fuel*, 217, 240-261.

Windeatt, J. H., Ross, A. B., Williams, P. T., Forster, P. M., Nahil, M. A.,... Singh, S. (2014). Characteristics of biochars from crop residues: Potential for carbon sequestration and soil amendment. *Journal of Environmental Management*, 146, 189-197.

Wu, B., Xi, B., He, X., Sun, X., Li, Q., Ouche, Q.,... Xue, C. (2020). Methane Emission Reduction Enhanced by Hydrophobic Biochar-Modified Soil Cover *Processes* (8, pp.).

Xia, H., Riaz, M., Liu, B., Li, Y., El-Desouki, Z.,... Jiang, C. (2022). Over two years study: Peanut biochar promoted potassium availability by mediating the relationship between bacterial community and soil properties. *Applied Soil Ecology*, 176, 104485.

Xiaojie, S., Yongli, Q., Beibei, W., Jie, L., & Chennan, X. (2019). Optimization of hydrophobic properties of biochar modified by silane coupling agent. *Environmental Science & Technology*, 42(12), 6.

Yao, R., Li, H., Yang, J., Zhu, W., Yin, C., Wang, X.,... Zhang, X. (2022). Combined application of biochar and N fertilizer shifted nitrification rate and amoA gene abundance of ammonia-oxidizing microorganisms in salt-affected anthropogenic-alluvial soil. *Applied Soil Ecology*, 171, 104348.

Yargicoglu, E. N., & Reddy, K. R. (2017). Effects of biochar and wood pellets amendments added to landfill cover soil on microbial methane oxidation: A laboratory column study. *Journal of Environmental Management*, 193, 19-31.

Zhang, J., Li, X., Lei, H., Zhao, R., Gan, W., Zhou, K.,... Li, B. (2022). New insights into thiamphenicol biodegradation mechanism by Sphingomonas sp. CL5.1 deciphered through metabolic and proteomic analysis. *Journal of Hazardous Materials*, 426, 128101.

Zhang, L., Yi, M., & Lu, P. (2022). Effects of pyrene on the structure and metabolic function of soil microbial communities. *Environmental Pollution*, 305, 119301.

Zhang, M., Zhu, H., Xi, B., Tian, Y., Sun, X., Zhang, H.,... Wu, B. (2022). Surface Hydrophobic Modification of Biochar by Silane Coupling Agent KH-570. *PROCESSES*, 10(2).

Zhao, H., Wang, L., Ren, J., Li, Z., Li, M.,... Gao, H. (2008). Isolation and characterization of phenanthrene-degrading strains Sphingomonas sp. ZP1 and Tistrella sp. ZP5. *Journal of Hazardous Materials*, 152(3), 1293-1300.

IMPACT OF HYDROPHOBIC BIOCHAR LANDFILL COVER SOIL ON METHANE OXIDATION

Qiuhong Li [1,2,3], Xiaojie Sun [1,2,3*]

1.Guangxi Key Laboratory of Environmental Pollution Control Theory and Technology, Guilin University of Technology, Guilin 541004, China

2.Guangxi Collaborative Innovation Center for Water Pollution Control and Water Safety in Karst Area, Guilin University of Technology, Guilin 541004, China

3. Guangxi Key Laboratory of Environmental Pollution Control Theory and Technology for Science and Education Combined with Science and Technology Innovation Base, Guilin University of Technology, Guilin 541004, China

Abstract: To achieve the carbon neutrality goal, the reduction of CH_4 from landfills needs to be considered. Bio soil landfill cover can achieve efficient CH_4 removal by adsorption and microbial oxidation, but in the engineering application stage, rainwater entry was found to significantly reduce CH_4 and O_2 diffusion. The air permeability and hydraulic conductivity of the landfill cover soils with the addition of hydrophobic biochar were improved and the methane reduction potential was reduced. hydrophobic biochar-amended soil cover simulation column (RH) was prepared and the biochar-amended soil cover simulation column (RB) was used as a control to study their CH_4 emission reduction characteristics. CH_4 oxidation simulation column tests manifest CH_4 oxidation enhancement on the capacity of RB and RH showed that the optimal CH_4 influx gas concentration was 35%, the optimal simulated landfill gas influx rate was 10 mL/min, and the optimal temperature was 30℃. The methane removal rate of RB can reach 99.96%. Overall, the use of hydrophobic biochar as a cover soil amendment to reduce methane emissions from landfills appears to be a promising alternative to conventional soil covers.

INTRODUCTION

Landfill disposal of municipal solid waste represents one of the largest anthropogenic global methane emission sources[1-7]. Open landfills were found to represent 91% of all landfill methane emissions[2]. These results demonstrate that open landfills need to be targeted to achieve significant near-term methane emission reductions. The main technologies for methane reduction in landfills are resource utilization, end-of-pipe control and in-situ reduction[8]. The release of methane from landfills is continuous, dispersed and unstable. Landfill gas collection systems of China have low collection efficiency (30%)[9] and methane concentrations that fail to meet resource utilization requirements. In-situ abatement technology uses adsorption and biochemical oxidation in the landfill cover system to achieve methane reduction. In-situ abatement technology is a cheaper and more effective option for older and open landfills with low CH_4 production[10].

Clay is a commonly used landfill cover material currently[11-13]. Clay has the advantages of low price, wide source, non-toxic and non-hazardous as well as easy construction, with the disadvantages of easy cracking, restriction of CH4 diffusion and lack of nutrition[10, 14-16]. To address the defects of clay, researchers used biological mulching materials such as sludge[17-20], compost[10], and mineralized waste[4, 21, 22], among which abundant microorganisms can improve the CH_4 oxidation capacity of the mulch and further promote CH_4 emission reduction. Despite the high removal

efficiency of biological mulch in laboratory studies, the formation of exopolymeric material within the mulch system clogs the pores and can impede gas diffusion and substrate availability to microorganisms, resulting in reduced methanogenic activity[23]. Therefore, the key to enhancing methane reduction is to increase the porosity of the landfill cover. It has been found that biochar amended landfill soil cover increases the porosity, permeability, specific surface area and high bioaffinity of the soil, which is conducive to microbial growth and attachment, and ultimately CH_4 adsorption and methane oxidation capacity is improved[24, 25]. Therefore, biochar has a catalytic effect on methane reduction. Biochar is a complex organic carbon solid produced by the cracking of waste biomass under anoxic or zero oxygen conditions. On the one hand, the water retained by biochar provides favorable conditions for the proliferation of methanotrophs, and the more biochar content in the cover layer, the stronger the diffusion of CH_4 and O_2, and eventually the CH_4 adsorption efficiency and oxidation reaction rate increase. On the other hand, the more biochar content in the cover layer, the higher the hydraulic conductivity of the cover material, the rainfall penetrates the cover layer into the waste pile, the rainwater occupies the pores to reduce the diffusion of CH_4 and O_2, and the CH_4 oxidation capacity decreases. The permeability of the landfill overlay is required to be less than 10^{-7}cm/s[26]. The soil permeability coefficient of 10% biochar was greater than 10^{-7}cm/s[27], and the reduction of biochar ratio would lead to the reduction of methane adsorption and oxidation performance[28]. The key, therefore, is not only to promote the diffusion of oxygen and methane, but also to prevent rainwater from entering the mulch. Therefore, a new economical landfill covering material with high porosity, high air permeability and low hydraulic conductivity should be designed to promote methane oxidation and achieve methane emission reduction in landfills.

Previously, the hydrophobic and porous structure of hydrophobic biochar has been shown to be able to account for both air permeability and hydraulic conductivity. This structure not only has a high potential for CH_4 adsorption, but also can enhance gas transport characteristics and reduce the adverse effects of pore plugging[8, 27]. In this study, the CH_4 oxidation performance of hydrophobic biochar-amended soil cover simulation column (RH) and the biochar-amended soil cover simulation column (RB) were studied in comparison. The purpose of this study is to investigate the CH_4 transport properties and optimum reaction conditions of RH and RB as landfill cover materials. The specific objectives of this study are to: (1) quantify the CH4 oxidation capacity of RB and RH at different CH_4 Influx gas concentrations (25% and 35%), different simulated landfill gas (LFG) inflow rates (10 mL/min, 15 mL/min, 20 mL/min), and different temperatures (20°C, 25°C, 30°C, 35°C, and 40°C). (2) To investigate the effect of the presence of moisture on CH4 transport and diffusion in RB and RH treated soils, simulating natural conditions under continuous rainfall weather conditions. The results from this study can help identify the potential use of Hydrophobic biochar as amendments to landfill soil with the aim of achieving cost-effective, sustained methane mitigation.

MATERIALS AND METHODS

BC and HBC

BC was obtained from Desheng Activated Carbon Company in Liyang, China. The BC was produced by burning rice straw at 500℃ under limited oxygen environments. HBC was obtained from modification at 60℃ which the above biochar as raw material and KH-570 as modifier. The contact angle with water of HBC was 143.99° . The soil was obtained from the long-term contact with biogas in the film cover of the Guilin Mountain Pass landfill (about 1 year of exposure), and it was retrieved, dried and then passed through a #30 screen to remove mixed garbage and large stones. The BC and HBC were mixed with the soil uniformly according to the volume ratio of 1:5 to obtain two different covering materials, namely, biochar modified

soil and hydrophobic biochar modified soil. Their physical and chemical properties were shown in Table 1.

TABLE 1
hysicochemical properties of three covering materials

Indicators	Unit	Material	
		Biochar modified soil	Hydrophobic biochar modified soil
Organic content	g/kg	59.2	63.3
TN	g/kg	2.71	2.16
TP	g/kg	1.5	1.26
TK	g/kg	16.3	15.2
pH	-	7.64	7.74
Specific gravity	g/cm^3	2.12	2.20
Volume density	g/cm^3	1.14	1.18
Porosity	%	46.12	46.31
Water holding capacity	g/kg	530.41	410.96
Water content	**%**	10	10

Column test device

Figure 4.1 shows the CH_4 simulated column test device for the landfill cover. The column oxidation tests were conducted to compare the oxidation characteristics of CH_4 through BC and HBC. These tests were conducted using two identical PVC columns measuring 15 cm in diameter and 100 cm in length. RB was the column filled with BC and RH was the column filled with HBC. The columns were composed of a permeable layer, a gravel layer, a cover layer and an air layer from bottom to top. The permeable layer with a height of 15 cm was used to drain excess water from the system. The gravel layer with a height of 10 cm was used to support and drain the cover layer, which was composed of pebbles with a diameter of about 1cm. The cover layer with a height of 60 cm was used to fill the cover layer material which is slightly tamped. The air layer with a height of 10 cm was mainly used to simulate atmospheric air flow. There was a rainfall simulation device at the top of the column, which could quantitatively simulate precipitation. The simulated landfill gas was introduced into the rotameter and humidifier through the PTFE tubing and then was passed into the column bottom at a pre-selected constant flow rate. A large number of small holes of the same size and uniform distribution were arranged on the annular pipe at the bottom of the column, which enabled the simulated landfill gas to enter the covering layer evenly through the buffer of the gravel layer. Air was blown into the PTFE tubing by the blower and was introduced into the top of the column through the rotameter and air humidifier. There was a water bath circulating temperature control device outside the column to control the external ambient temperature of the column. The No. 0 sampling port was set at the top air outlet. In addition, there were 9 other sampling ports with 5 cm intervals on the outer surface of the cylinder, which were numbered 1 to 9 from top to bottom. Used to collect gas and soil samples. The physical map is shown in Figure 4.2. These sampling ports were used to collect gas and soil samples.

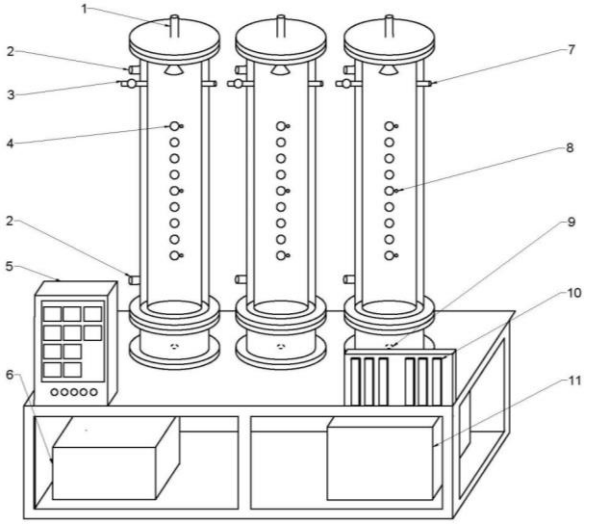

1. shower nozzle 2. Water bath circulation port 3. Air outlet 4. Sampling port 5. Electric control box 6. Water box 7. Air inlet 8. Temperature probe 9. CH_4 inlet 10. Glass rotameter 11. Water bath

FIG. 1. Schematic diagram of CH_4 oxidation simulation device for landfill cover

Column operation and sampling

The simulated landfill gas was composed of CO_2, CH_4, and N_2, where CO_2 and CH_4 had the same volume. Before the test, the device for the simulation experiment had been operating stably for one month. In order to analyze the amount of CH_4 oxidized by methane-oxidizing bacteria, it was assumed that all adsorption behaviors had reached their adsorption capacity and that any reduction in CH_4 content was the result of microbial oxidation. The air inflow rate was 50 mL/min to simulate the natural flow of the atmosphere. The inflow rate of simulated landfill gas was controlled by rotameter to be 10-20 mL/min. The initial ambient temperature of the columns were set to 25 ℃, and the initial moisture content were set to 10%. The entire test process was divided into four stages. In the first stage, the CH_4 inlet concentration of the column was 25%, and the aeration rate was 15 mL/min. In the second stage, the CH_4 inlet concentration of the column was 35%, and the aeration rate were 10 mL/min, 15 mL/min, and 20 mL/min, respectively. In the third stage, the CH_4 inlet concentration of 35% and the aeration rate of 20 mL/min were kept unchanged, and the ambient temperature of the columns were set to 20 ℃, 25 ℃, 30 ℃, 35 ℃ and 40 ℃, respectively. The fourth stage was the simulated precipitation test. Under simulated landfill gas conditions at a concentration of 35% and a rate of 20 mL/min. The column was uniformly poured with 5 L of water through the top shower for 5 consecutive days until the cover layer was completely saturated. When the seepage layer at the bottom of the column is no longer dripping, the soil sample in the column is taken to measure the water content by the weight method, and the permeability coefficient of the material in the column is measured by the ring knife method. Every two days, gas samples were collected from the #0—#9 sampling ports of the column with gas sampling bags, which were analyzed by GC-7890 gas chromatograph.

RESULTS AND DISCUSSIONR

CH_4 oxidation performance of columns

The simulation test device had been operating stably for one month beforehand. The adsorption of biochar on CH_4 can reach the adsorption capacity in a short time, so the reduction of CH_4 content in the experiment was assumed to be the result of microbial oxidation. When the CH_4 concentration in the simulated landfill gas was 25% and 35%, CH_4 content and removal rates of RB and RH varied with column depth as shown in Figure 2.

As shown in Fig 2(a) and (b), when the CH_4 concentration in the simulated landfill gas was 25%, the CH_4 content of the two columns increases as the column depth increases. The top CH_4 content of RB and RH were 0.74% and 0.22%, respectively, and the total methane removal rate were 97.05% and 99.13%, respectively. When the CH_4 concentration in the simulated landfill gas was increased to 35%, the top CH_4 content of RB and RH were 0.96% and 0.17%, respectively, the total methane removal rate was 95.80% and 99.50% (Figure 2(c)(d)), and the total methane removal rate of RH was the lowest. The CH_4 removal of RB and RH were mainly concentrated in the 50-60 cm. It could be seen that CH_4 oxidation activities mainly occured at the bottom of RB and RH. It might be that the high concentration of CH_4 at the bottom was more suitable for the self-growth and reproduction of methane oxidizing bacteria, which promoted the occurrence of methane oxidation behavior. It may be that the large specific surface area and large porosity of biochar were conducive to the diffusion of CH_4 and O_2, and the nutrients it carries led to the high rate of methane oxidation[29, 30]. After being hydrophobically modified, the modified biochar retained its original performance, and at the same time, its agglomeration was reduced and air permeability was improved, which was more suitable for the growth and reproduction of methanotrophs.

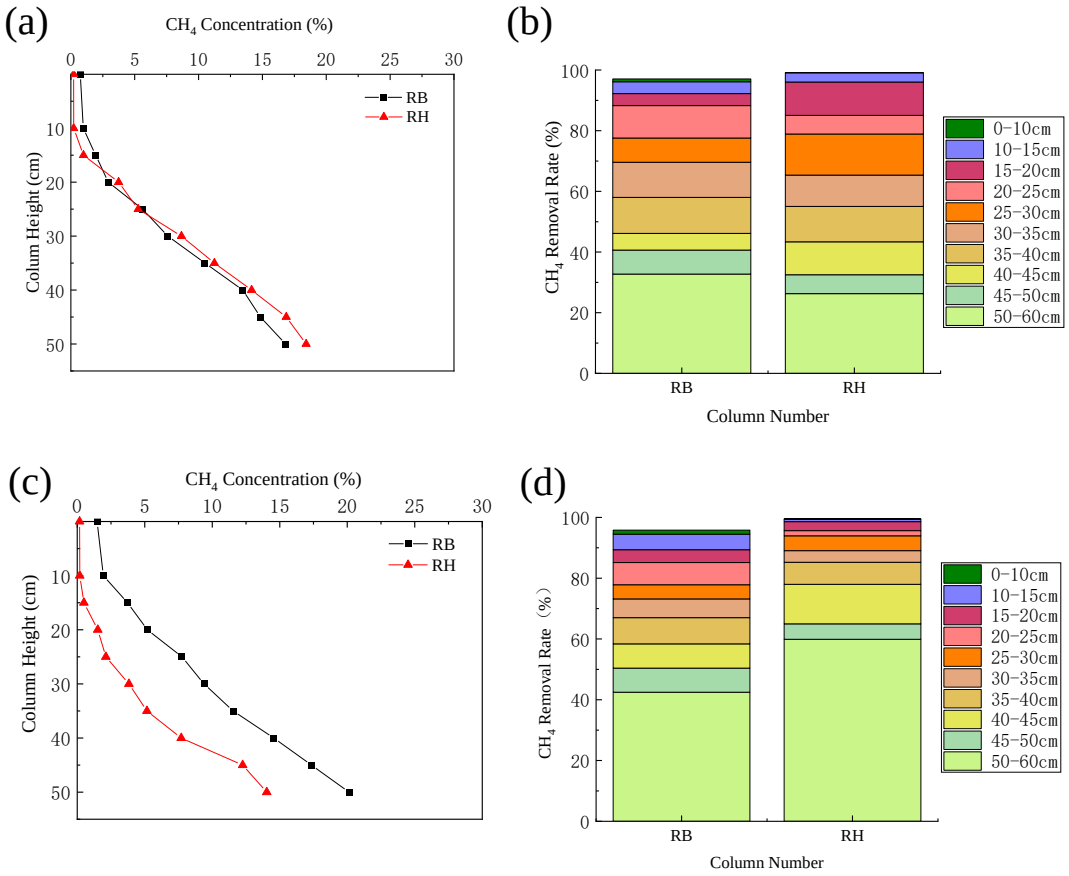

FIG. 2. Changes of CH_4 concentration and removal rate in columns with depth when CH_4 concentration is 25% (a)and(b). Changes of CH_4 concentration and removal rate in columns with depth when CH_4 concentration is 35% (c) and (d). Reaction conditions: 15 mL/min of inflow rate, 25 ℃ of ambient temperature.

Effect of CH_4 influx rate

The CH_4 influx rate affected the CH_4 oxidation. To explore the effect of influx on the change of the CH_4 oxidation, the CH_4 concentration was set to 35%, the ambient temperature was set to 25 ℃, and RB and RH were operated at three different aeration rates simultaneously. As shown in Fig. 3, as the CH_4 influx rate increased, the CH_4 content of RB and RH increased. When the CH_4 influx rate were 10, 15 and 20 mL/min, the CH_4 content on the top of RB were 0.04%, 0.96% and 2.27%, respectively, the total removal rate of CH_4 were 99.89%, 95.80% and 93.52%, respectively. The CH_4 content on the top of the RH were 0.02%, 0.17% and 0.29%, respectively, the total removal rate of CH_4 were 99.94%, 99.50% and 99.18%, respectively. In general, both RB and RH had good removal efficiency of CH_4, but RH was better, which removal rate of CH_4 had reach more than 99%.

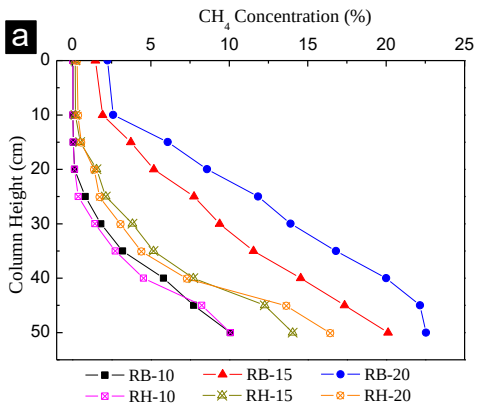

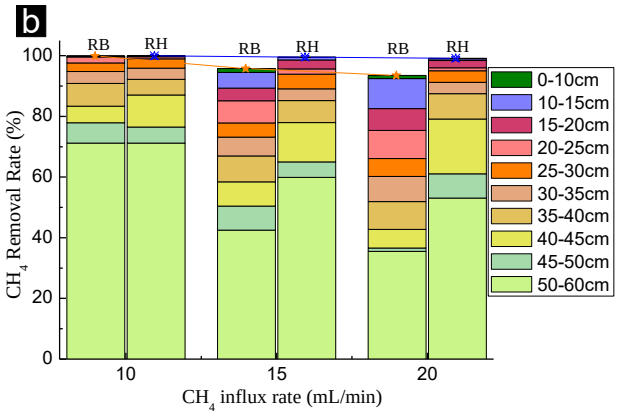

FIG. 3. Changes of CH_4 concentration in columns with depth at different CH_4 influx rate (a).
CH_4 removal rate in columns with depth at different CH_4 influx rate (b).

Effect of temperature

The ambient temperature offers significant influence in CH_4 oxidation process[10]. The CH_4 content and removal rate of RB and RH at different temperatures when CH_4 was influxed at a concentration of 35% and a rate of 20 mL/min were shown in Fig. 4. When the temperature were 20 ℃, 25 ℃, 30 ℃, 35 ℃ and 40 ℃, the top CH_4 content of RB were 2.43%, 2.27%, 1.44%, 1.58% and 2.84%, respectively, and the removal rate of CH_4 were 93.05%, 93.52%, 95.89%, 95.49% and 91.89%, respectively. The top CH_4 content of RH were 0.57%, 0.29%, 0.01%, 0.05% and 0.50%, respectively, and the removal rate of CH_4 were 98.38%, 99.18%, 99.96%, 99.86% and 98.58%, respectively. The CH_4 removal rate of RH and RB all reached the highest at 30 ℃. Some previous studies have shown that the optimum temperature for growth of methanophilic bacteria is about 30 ℃ [31-34]. When the tmperature was lower or higher than the optimum temperature, the microbial activity gradually decreases as the temperature changes, and the CH_4 removal rate also decreases. Compared with RB, RH had a better removal effect on CH_4 (99.96%), it may due to the hydrophobic modification of biochar reduced the agglomeration between particles and increased the porosity[35]. Hence, the diffusion of CH_4 and O_2 in the cover layer and the adhesion of microorganisms were promoted.

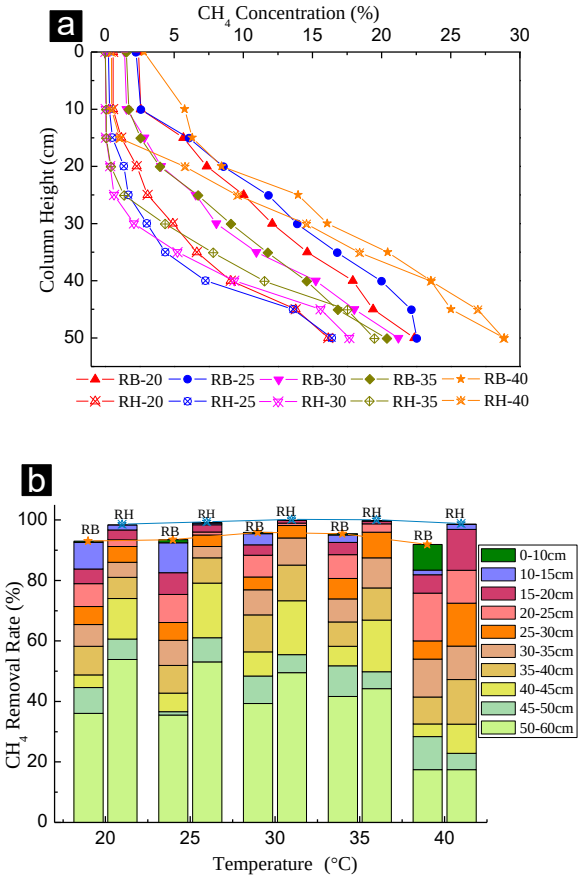

FIG. 4. Changes of CH_4 concentration in columns with depth at different temperatures (a).
CH_4 removal rate in columns with depth at different temperatures (b).

CH_4 oxidation under simulate rainfall

To study the waterproof performance and permeability of hydrophobic biochar-amended soil mulch simulated column RH by simulated rainfall experiments. The outlet CH_4 content was 9.94% and 8.05% for RB and RH, respectively, and the total CH_4 removal rate was 71.59% and 77.01%, respectively. The highest methane removal rate of biochar-amended soil cover simulation column

RB was found at column depth 15-20 cm. The hydrophobic biochar-amended soil cover simulation column RH showed the highest methane removal rate at column depths of 10-15 cm. Compared to RB, moisture has less effect on the methane removal efficiency of RH. After testing, the water contents of RB and RH were 31.22% and 22.68%, respectively, and the permeability coefficients were 1.15×10^{-7} and 7.68×10^{-8}, respectively. It shows that the hydrophobic biochar-amended soil cover simulation column RH is more waterproof than the biochar-amended soil cover simulation column RB.

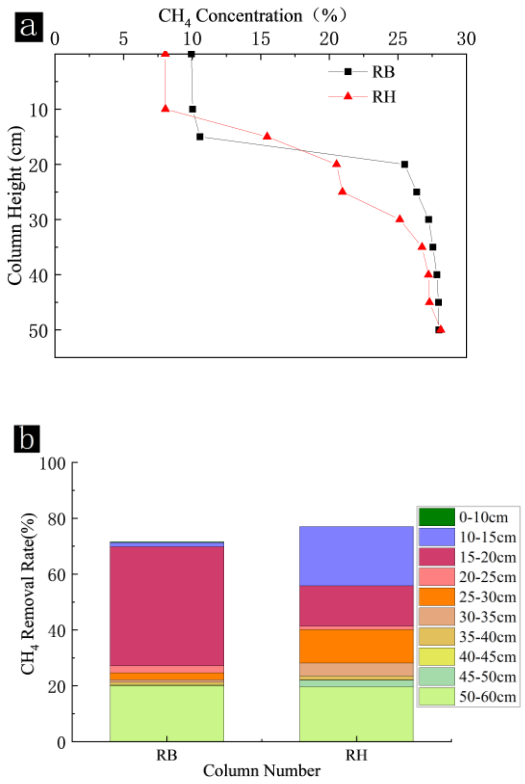

FIG. 5 Changes of CH_4 content and removal rate in columns with depth at different temperatures

SEM image analysis before and after simulated column reaction

Figure 6 (a) and (b) shows SEM images of biochar amended soil cover before and after the reaction of simulated column RB. The surface of the biochar amended soil material is clearly granular and loosely structured before the reaction. However, some mineralization and microbial residues appeared on the surface of RB after the reaction. Figure 6(c)(d) shows the SEM images of the simulated column RH before and after the reaction of the hydrophobic biochar amended soil cover. Similar to biochar, the surface of hydrophobic biochar after the reaction has numerous more agglomerated substances than before the reaction, which probably are mineralized substances and microbial residues.

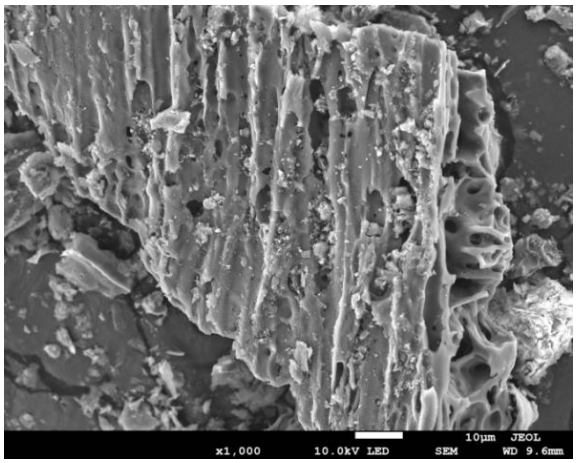

(a) Before RB reaction（10 mm）

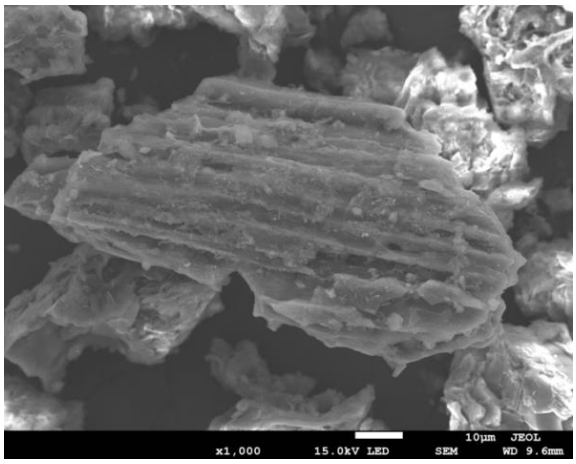

(b) After RB reaction（10 μm）

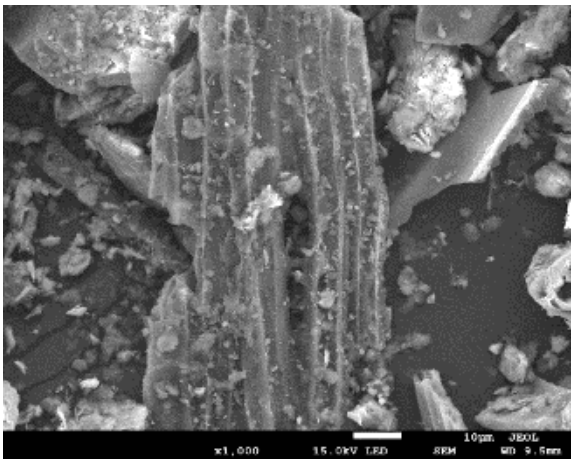

(c) Before RH reaction（10 μm）

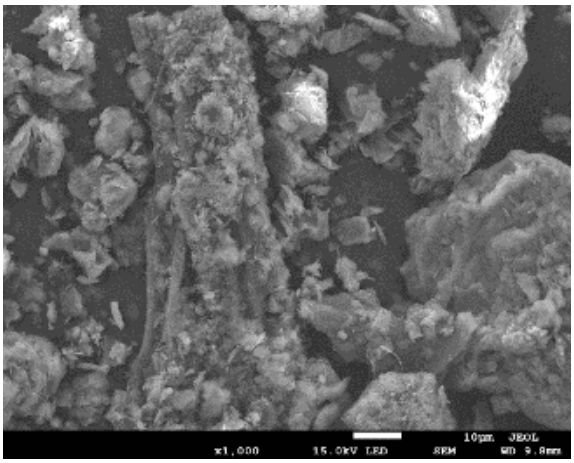

(d) After RH reaction（10 μm）

FIG. 6 SEM images before and after RB and RH reactions

CONCLUSION

The oxidative removal of CH_4 by RH was very satisfactory, with a removal rate of 99.13%, which was higher than that of 97.05% by RB. Methane removal by both RB and RH occurred mainly at depths of 50-60 cm. The removal rate of CH_4 for both RB and RH decreased with increasing simulated landfill gas influx rate. However, the buffering capacity of RH was better than that of RB when the simulated landfill gas influx rate was increased. The optimum temperature for methane removal was 30°C for both RB and RH, at which the removal rates were 95.89% and 99.96%, respectively.

Under simulated precipitation conditions, RH had better water repellency and better removal of CH_4 than RB. SEM image characterization indicates that mineralized and microbial residues were observed in both RB and RH after the simulated landfill reaction. Therefore, the oxidation of CH_4 is due to the combined effect of the porous structure of hydrophobic biochar and nutrients.

ACKNOWLEDGEMENTS

This work was financially supported by Guangxi innovation research team project (2018GXNSFGA281001) and Guangxi major science and technology projects (GuikeAA18118013).

REFERENCES

[1] Purmessur B, Surroop D. Power generation using landfill gas generated from new cell at the existing landfill site[J]. Journal of Environmental Chemical Engineering, 2019,7(3):103060.

[2] Powell J, Townsend T, Zimmerman J. Estimates of solid waste disposal rates and reduction targets for landfill gas emissions[J]. Nature Climate Change, 2015,6.

[3] Haro K, Ouarma I, Nana B, et al. Assessment of CH4 and CO2 surface emissions from Polesgo's landfill (Ouagadougou, Burkina Faso) based on static chamber method[J]. Advances in Climate Change Research, 2019,10(3):181-191.

[4] Han D, Zhao Y, Xue B, et al. Effect of bio-column composed of aged refuse on methane abatement – A novel configuration of biological oxidation in refuse landfill[J]. Journal of Environmental Sciences, 2010,22(5):769-776.

[5] Rees-White T C, Mønster J, Beaven R P, et al.

Measuring methane emissions from a UK landfill using the tracer dispersion method and the influence of operational and environmental factors[J]. Waste Management, 2019,87:870-882.

[6] Bogner J, Pipatti R, Hashimoto S, et al. Mitigation of global greenhouse gas emissions from waste: conclusions and strategies from the Intergovernmental Panel on Climate Change (IPCC) Fourth Assessment Report. Working Group III (Mitigation)[J]. Waste Management & Research, 2008,26(1):11-32.

[7] Scheutz C, Kjeld A, Fredenslund A M. Methane emissions from Icelandic landfills – A comparison between measured and modelled emissions[J]. Waste Management, 2022,139:136-145.

[8] Wu B B, Xi B D, He X S, et al. Methane Emission Reduction Enhanced by Hydrophobic Biochar-Modified Soil Cover[J]. PROCESSES, 2020,8(2).

[9] Xie H, Wang Q, Bouazza A, et al. Analytical model for vapour-phase VOCs transport in four-layered landfill composite cover systems[J]. Computers and Geotechnics, 2018,101:80-94.

[10] Chetri J K, Reddy K R. Advancements in Municipal Solid Waste Landfill Cover System: A Review[J]. Journal of the Indian Institute of Science, 2021,101(4):557-588.

[11] Das P, Bharat T V. Kaolin based protective barrier in municipal landfills against adverse chemo-mechanical loadings[J]. Scientific Reports, 2021,11(1):10354.

[12] Rajesh S, Khan V. Characterization of water sorption and retention behavior of partially saturated GCLs using vapor equilibrium and filter paper methods[J]. Applied Clay Science, 2018,157:177-188.

[13] Dutta J, Mishra A K. Consolidation behaviour of bentonites in the presence of salt solutions[J]. Applied Clay Science, 2016,120:61-69.

[14] Divya P V, Viswanadham B V S, Gourc J P. Influence of geomembrane on the deformation behaviour of clay-based landfill covers[J]. Geotextiles and Geomembranes, 2012,34:158-171.

[15] Sathiyamoorthy R, Viswanadham B V S, P. V. D, et al. Influence of randomly distributed geofibers on the integrity of clay-based landfill covers: A centrifuge study[J]. Geosynthetics International, 2011,18:255-271.

[16] Albright W H, Benson C H, Gee G W, et al. Field performance of a compacted clay landfill final cover at a humid site[J]. JOURNAL OF GEOTECHNICAL AND GEOENVIRONMENTAL ENGINEERING, 2006,132(11):1393-1403.

[17] Lo I M C, Zhou W W, Lee K M. Geotechnical characterization of dewatered sewage sludge for landfill disposal[J]. Canadian Geotechnical Journal, 2002,39(5):1139-1149.

[18] O Kelly B C. Sewage Sludge to Landfill: Some Pertinent Engineering Properties[J]. Journal of the Air & Waste Management Association, 2005,55(6):765-771.

[19] Diliunas J, Dundulis K, Gadeikis S, et al. Geotechnical and hydrochemical properties of sewage sludge[J]. BULLETIN OF ENGINEERING GEOLOGY AND THE ENVIRONMENT, 2010,69(4):575-582.

[20] Li Y L, Liu J W, Chen J Y, et al. Reuse of dewatered sewage sludge conditioned with skeleton builders as landfill cover material[J]. International Journal of Environmental Science and Technology, 2014,11(1):233-240.

[21] Zhang Y, Zhang H, Jia B, et al. Landfill CH4 oxidation by mineralized refuse: Effects of NH4+ - N incubation, water content and temperature[J]. The Science of the total environment, 2012,426:406-413.

[22] Warmadewanthi I D A A, Chrystiadini G,

Kurniawan S B, et al. Impact of degraded solid waste utilization as a daily cover for landfill on the formation of methane and leachate[J]. Bioresource Technology Reports, 2021,15:100797.

[23] Parsaeifard N, Sattler M, Nasirian B, et al. Enhancing anaerobic oxidation of methane in municipal solid waste landfill cover soil[J]. Waste Management, 2020,106:44-54.

[24] Chavan D, Kumar S. Reduction of methane emission from landfill using biocover as a biomitigation system: A review[J]. INDIAN JOURNAL OF EXPERIMENTAL BIOLOGY, 2018,56(7):451-459.

[25] Reddy K R, Yargicoglu E N, Chetri J K. Effects of Biochar on Methane Oxidation and Properties of Landfill Cover Soil: Long-Term Column Incubation Tests[J]. JOURNAL OF ENVIRONMENTAL ENGINEERING, 2021,147(1).

[26] Ministry Of Housing And Urban-Rural Development P. Technical specifications for sanitary landfill treatment of domestic waste（GB 50869-2013）[EB/OL]. [2022-09-28]. https://www.mohurd.gov.cn/gongkai/fdzdgknr/tzgg/201308/20130820_224784.html.

[27] Zhang M X, Zhu H X, Xi B D, et al. Surface Hydrophobic Modification of Biochar by Silane Coupling Agent KH-570[J]. PROCESSES, 2022,10(2).

[28] Wu H, Chen T, Wang H, et al. Field air permeability and hydraulic conductivity of landfilled municipal solid waste in China[J]. Journal of Environmental Management, 2012,98:15-22.

[29] Liu W J, Jiang H, Yu H Q. Development of Biochar-Based Functional Materials: Toward a Sustainable Platform Carbon Material[J]. CHEMICAL REVIEWS, 2015,115(22):12251-12285.

[30] Reddy K R, Yargicoglu E N, Yue D B, et al. Enhanced Microbial Methane Oxidation in Landfill Cover Soil Amended with Biochar[J]. JOURNAL OF GEOTECHNICAL AND GEOENVIRONMENTAL ENGINEERING, 2014,140(9).

[31] Boeckx P, VanCleemput O, Villaralvo I. Methane emission from a landfill and the methane oxidising capacity of its covering soil[J]. SOIL BIOLOGY & BIOCHEMISTRY, 1996,28(10-11):1397-1405.

[32] Stein V B, Hettiaratchi J. Methane oxidation in three Alberta soils: Influence of soil parameters and methane flux rates[J]. ENVIRONMENTAL TECHNOLOGY, 2001,22(1):101-111.

[33] WHALEN S C, REEBURGH W S, SANDBECK K A. RAPID METHANE OXIDATION IN A LANDFILL COVER SOIL[J]. APPLIED AND ENVIRONMENTAL MICROBIOLOGY, 1990,56(11):3405-3411.

[34] Scheutz C, Kjeldsen P, Bogner J E, et al. Microbial methane oxidation processes and technologies for mitigation of landfill gas emissions[J]. WASTE MANAGEMENT & RESEARCH, 2009,27(5):409-455.

[35] Wang L L, Li R M, Wang C L, et al. Surface grafting modification of titanium dioxide by silane coupler KH570 and its influences on the application of blue light curing ink[J]. DYES AND PIGMENTS, 2019,163:232-237.

STABILIZATION OF THE MUNICIPAL SOLID WASTE BY USING OF *EX SITU* SND AND *IN SITU* DENITRIFICATION BIOREACTOR LANDFILL IN A LONG-TERM OPERATION

Muxi Zhang[1,2,3], Xiaojie Sun[1,2,3*]

1.Guangxi Key Laboratory of Environmental Pollution Control Theory and Technology, Guilin University of Technology, Guilin 541004, China

2.Guangxi Collaborative Innovation Center for Water Pollution Control and Water Safety in Karst Area, Guilin University of Technology, Guilin 541004, China

3. Guangxi Key Laboratory of Environmental Pollution Control Theory and Technology for Science and Education Combined with Science and Technology Innovation Base, Guilin University of Technology, Guilin 541004, China

Abstract: The objective of this research was to investigate and compare stabilization of the municipal solid waste of *ex situ* simultaneous nitrification denitrification (SND)/*in situ* denitrification and *ex situ* nitrification/*in situ* denitrification bioreactor landfill in the long-term operations. Based on previous studies of 78 weeks, the two sets of laboratory-scale bioreactor landfill systems (an *ex situ* nitrification/*in situ* denitrification bioreactor and an *ex situ* SND/*in situ* denitrification bioreactor) continued to run up to weeks 105. The concentrations of NH_4^+-N, NO_3^--N, NO_2^--N, TN and COD in leachate were analyzed and monitored by standard methods. The results showed that *ex situ* SND/*in situ* denitrification was better than *ex situ* nitrification/*in situ* denitrification in the removal of NH_4^+-N, NO_3^--N, TN and COD. The average effluent NH_4^+-N concentration in F1 was 12.02 mg/L, and F2 was 8.20 mg/L. The average effluent NO_3^--N concentration in F1 was 542.80 mg/L, and F2 was 513.12mg/L. The average effluent TN concentrations in F1 was 555.27 mg/L, and F2 was 522.47 mg/L. The average effluent COD concentrations of F1 and F2 reached 153.10 mg/L and 116.99 mg/L. The concentrations of NH_4^+-N and COD could meet the discharge standard established in the Standard for Pollution Control on the Landfill Site of Municipal Solid Waste (GB16889-2008), the COD concentration of F1 and F2 met the discharge standard (less than 100 mg/L) at week 104 and 100, respectively. But TN could not reach discharge standard because low NO_3^--N removal rate caused by the lack of carbon sources. Therefore, other effective measures or processes need to be adopted in order to remove NO_3^--N from landfill leachate.

INTRODUCTION

Landfill is one of the main treatment methods of domestic waste[1]. However, the traditional landfill technology has some problems, such as long stabilization time, complex and difficult treatment of leachate components, low landfill gas production rate and difficult recycling[2-4]. In view of the problems existing in traditional landfill, the bioreactor landfill technology with leachate recirculation as the main control measure came into being in the 1970s[5]. Nitrogen removal bioreactor landfill technology that can solve the problem of high ammonia nitrogen concentration of leachate from the source has attracted attention in the field of landfill and leachate treatment[6-8].

One of the treatment scenarios for nitrogen removal was *ex situ* nitrification/*in situ* denitrification bioreactor landfill. The *ex situ* nitrification of leachate can be performed by various wastewater nitrification processes, such as SBR[9-11], aerobic activated-sludge reactor[12,13], and aged refuse bioreactor[14,15]. The nitrified leachate is then recycled into the fresh-refuse bioreactor for

denitrification[16]. Sun et al.[17] combined the process of *ex situ* nitrification and *in situ* denitrification to remove nitrogen from municipal landfill leachate. The results showed that the average effluent ammonia concentration was 49 mg N L^{-1}, TN concentration was 93 ± 13 mg N L^{-1} in landfill bioreactor. Wang et al.[18] used the combined process of *ex situ* nitrification in an aged refuse bioreactor and *in situ* denitrification in a fresh refuse bioreactor, and found that after 146 days of operation, the effluent concentration of COD and NH_4^+-N in fresh refuse bioreactor were 613 mg/L and 97.34 mg/L, respectively. The results of Zhong et al.[19] showed that the COD gradually decreased to about 2000 mg/L, effluent ammonia of the denitrification column was higher than 300 mg N L^{-1}about 250 days. The above researches indicated that *ex situ* nitrification/*in situ* denitrification bioreactor landfill has good nitrogen removal effect. But the COD, NH_4^+-N or TN did not meet the discharge standards (less than 100, 25 or 40) at the end of the experiment. Therefore, *ex situ* nitrification/*in situ* denitrification should continue to be studied for a long time. Meanwhile, it has been reported that the high concentration nitrate produced in *ex situ* nitrification phase inhibit the methane production of refuse *in situ* denitrification bioreactor.

In order to solve the above problems, *ex situ* simultaneous nitrification denitrification (SND)/*in situ* denitrification bioreactor landfill process has been conducted[20,21]. The results showed that the *ex situ* SND/*in situ* denitrification process obtained a better leachate removal performance compared with the *ex situ* nitrification/*in situ* denitrification process, and the *ex situ* SND process can reduce the energy costs. Based on the experimental data from week 4 to week 30, it is predicted that NH_4^+-N concentration would reach less than 25 mg/L after 63 weeks in *ex situ* nitrification/*in situ* denitrification (in F1) and 40 weeks in *ex situ* SND/*in situ* denitrification (in F2), the COD concentrations of leachate in F1 and F2 were expected to meet the discharge standard (less than 100 mg/L) after weeks 41 and 34, respectively[20]. Effluent TN concentrations of leachate in F1 and F2 were expected to meet the discharge standard (less than 40 mg/L) after weeks 54 and 35, respectively [21]. However, the NH_4^+-N concentration in F1 and F2 reached 52.71 mg/L and 54.74 mg/L at the predicted time. The COD concentration in FRBs failed to reach below 100 mg/L, F1 and F2 was about 696.96 mg/L and 396 mg/L at the predicted time, respectively. Although the TN concentration in FRBs reach below 40 mg/L, F1 and F2 was about 39.16 mg/L and 20.06 mg/L at the predicted time, respectively, TN concentration fluctuated in this stage and did not reach the standard discharge at week 78[21]. Since the concentration of COD and NH_4^+-N did not reach the standard in the previous studies, the experiment has been continued.

In this study, *ex situ* SND and in situ denitrification bioreactor landfill was investigated in a long-term operation lasted for 105 weeks based on previous study. The purpose is: (1) to investigate whether and when the effluent can meet the discharge standard established in the Standard for Pollution Control on the Landfill Site of Municipal Solid Waste (GB16889-2008). (2) Evaluate and compare the effects of *ex situ* nitrification/*in situ* denitrification and *ex situ* SND /*in situ* denitrification on landfill leachate.

MATERIALS AND METHODS

Fresh and aged refuse

Fresh refuse was obtained from a waste transfer station near Guilin University of Technology, Guilin, Guangxi, China. Sample compositions were adjusted based on the investigations of average composition of MSW made in Guilin City. These compositions comprised (by wet weight) organics (51.13%), paper (14.99%), plastic (4.45%), metal (0.14%), glass (2.84%), wood (2.30%), and others (24.16%). The large samples were cut into approximately 2-5 cm and were then mixed uniformly.

The 10-years old aged refuse utilized was obtained from the Chongkou Sanitary Landfill in Guilin, Southwest China. Non-biodegradable materials, such as stones, metals, glass, and plastic bags, were removed.

The fine fraction resembling soil with diameters of 4 -10 mm was selected because this refuse is an ideal bioreactor material. The properties of the fresh refuse and aged refuse were the same as those used in Sun et al. and Li et al.[20,21].

Experimental setup

A schematic diagram of the experimental setup is presented in Fig. 1(a). Two fresh refuse bioreactors (FRBs), namely, F1 and F2, were made of a stainless steel cylinder with an inner diameter of 340 mm and height of 650 mm. Two aged refuse bioreactors (ARBs), namely, A1 and A2, were made of a polyvinyl chloride cylinder with an inner diameter of 390 mm and a height of 1000 mm. F1 and F2 were loaded from bottom to top with 50 mm gravel (<10 mm in diameter) followed by 400 mm fresh refuse and topped with 50 mm gravel (<10 mm in diameter). Meanwhile, A1 and A2 were loaded from bottom to top with 50 mm gravel (<10 mm in diameter) followed by 800 mm aged refuse and topped with 50 mm small gravel (<10 mm in diameter).

A combined process comprising *ex situ* nitrification (or SND) in an aged refuse bioreactor and *in situ* denitrification in a fresh refuse bioreactor was constructed. The leachate from F1 and F2 was introduced into A1 and A2, while the effluent from A1 and A2 was recirculated into F1 and F2 once per day, respectively. F1 and A1 constituted the *ex situ* nitrification and *in situ* denitrification process (Fig. 1(b)), while F2 and A2 constituted the *ex situ* SND and *in situ* denitrification process (Fig. 1(c)).

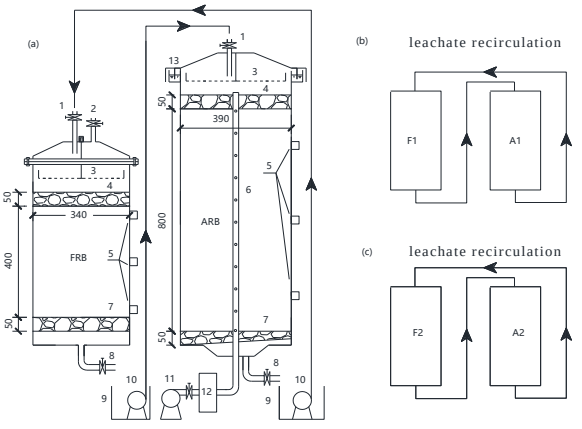

FIG. 1 The schematic of bioreactor landfill for nitrogen removal

1. leachate inlet 2. gas valve 3. liquid distributor 4. gravel layer 5. sample collection 6. perforated vent pipe 7. gravel layer 8. outlet valve 9. storage water tank 10. water pump 11. air compressor 12. gas flowmeter 13. sealing cover

Experimental operations

In this experiment, F1 and F2 were operated as *in situ* denitrification reactors. To secure the anaerobic conditions, the sealing cover was placed on top of the FBRs and the outlet valve at the bottom was closed. A1 was operated as an *ex situ* nitrification reactor. Based on the aeration rate of 2.01 $m^3/(m^3$ refuse·d)and aeration time of 8 h per day in the preliminary experiment [22], the aeration rate of A1 in this study was set to 6.03 $m^3/(m^3$ aged refuse·d) for aeration time extended three times and was 24 h per day to guarantee the nitrification condition. The airflow rate of ARBs was measured by using the rotor flowmeter (LZB-3WB, KEDE Instrument Ltd., China) with a range of 40 ml/min to 400 ml/min, which was regularly calibrated with a soap bubble flowmeter (GILIBRATOR-2, Sensidyne LP., American). A2 was operated as an *ex situ* SND reactor. Based on the effluent leachate quality and aeration rate in our previous experiment[20,21], the aeration rate was set to 0.09 $m^3/(m^3$ aged refuse·d) and the aeration time was set to 3 h.

Experimental analysis

Leachate samples of approximately 50 mL were used for the analysis every week. The NH_4^+-N, NO_3^--N, NO_2^--N, and COD of the leachate samples were analyzed according to the standard methods set by standard for pollution control on the landfill site of MSW (Ministry of Environmental Protection of the People's Republic of China, 2008). NH_4^+-N was measured by using the Nessler's reagent spectrophotometric method, NO_3^--N was measured by using the ultraviolet spectrophotometric method, and NO_2^--N was measured by using the spectrophotometric method. COD was

measured by using the potassium dichromate volumetric method. The samples were stored in glass bottles at temperatures below 4 °C. The leachate samples were then filtered by using a qualitative filter paper, and the filtered samples were measured in triplicate.

RESULTS AND DISCUSSIONR

The data for weeks 1 to 30 of the experiment were obtained from the operation of bioreactors in the early study[20]. The data for weeks 31 to 78 of the experiment were obtained from the operation of bioreactors in the mid-stage study[21]. This experiment was conducted for weeks 85 to 105 as a late study.

NH_4^+-N

Fig. 2 shows the changes of leachate NH_4^+-N concentration during the operation of the bioreactor landfill system. According to the leachate NH_4^+-N concentration were fitted based on weeks 4 to 30, the NH_4^+-N concentrations of leachate in F1 and F2 were expected to meet the discharge standard (less than 25 mg/L) after weeks 63 and 40, respectively[20]. However, the NH_4^+-N concentration in F1 and F2 exceeded emission standards and reached 52.71 mg/L and 54.74 mg/L at the predicted time, respectively[21]. The NH_4^+-N concentration only met the standard for pollution control on the landfill site of MSW (Ministry of Environmental Protection of the People's Republic of China, 2008) in F1 at weeks 49-52 and had an average effluent value of 19.29 mg/L, while the NH_4^+-N concentration in F2 cannot reach below 25 mg/L and obtained a minimum value of 28.01 mg/L in week 49. According to Fig. 2(a), at the end of 78 week, the effluent concentration of NH_4^+-N in FRBs did not meet the discharge standard, F1 was 48.03mg /L, F2 was 53.11mg /L. Fig. 2 (b) summarize the changes of NH_4^+-N concentration reactor in this experiment. The concentrations of NH_4^+-N in F1 and F2 during 85-105 weeks were both less than 25 mg/L, which met the landfill pollution control standards (Ministry of Environmental Protection of the People's Republic of China, 2008). The average effluent NH_4^+-N concentration in F1 was 12.02 mg/L, while that of F2 was 8.20 mg/L. The NH_4^+-N concentration in F2 was 5.57 mg/L, which was lower than that in F1 (3.85 mg/L) at the end of the experiment. The results suggested that *ex situ* SND/*in situ* denitrification was more effective than *ex situ* nitrification/*in situ* denitrification in eliminating ammonia.

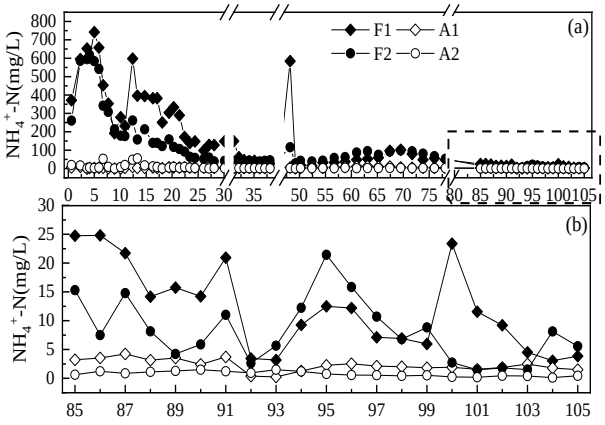

FIG. 2 Removal performance of NH_4^+-N from leachates.

NO_3^--N

The changes of NO_3^--N concentration during the operation is shown in Fig.3. NO_3^--N in the FRBs were relatively stable within 50-78 weeks, and the concentration was less about 30mg/L. The results showed that the FRBs had an excellent denitrification effect. Compared with week 50-78, the NO_3^--N concentration of the A reactor in 85-105 week increased significantly. This may be that the leachate contained high concentration of NH_4^+-N in the early stage of the test, and the aged refuse adsorbed a large amount of NH_4^+-N and converted into NO_3^--N. With the progress of the test, the NH_4^+-N concentration in the influent of the aged refuse reactor gradually decreased, and the saturated aged refuse desorbed, resulting in the increase of NO_3^--N concentration in the effluent of the aged refuse reactor. At the end of the experiment, the average effluent NO_3^--N concentration in reactor A2 was 533.41

mg/L, which was significantly lower than that of A1 (712.82 mg/L). Nitrogen removal by biological methods was divided into two stages, namely aerobic nitrification of ammonia to nitrate or nitrite and anaerobic/anoxic denitrification of nitrate to nitrogen[10]. Due to the denitrification of A2 under low aeration conditions, NO_3^--N produced by nitrification was reduced, so that the NO_3^--N concentration of A2 was lower than A1. The average effluent NO_3^--N concentration in reactor F2 was 513.12mg/L, which was lower than that of F1 (542.80 mg/L). This may be due to the lack of carbon sources leading to the difficulty of denitrification of NO_3^--N from ARBs, resulting in the increase of NO_3^--N concentration in FRBs [23,24]. This was also the reason for the increase in TN concentration in Fig. 5.

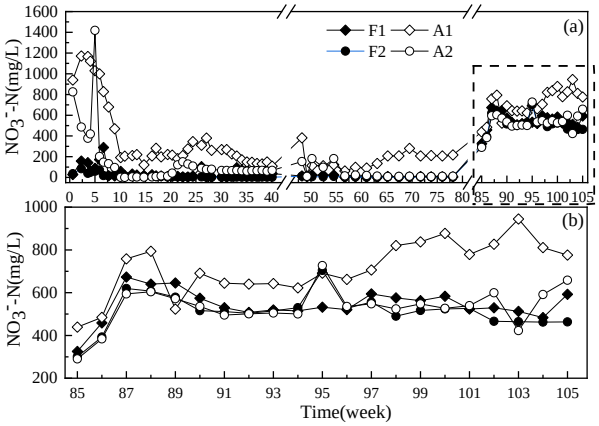

FIG. 3 Variation of NO_3^--N concentration in leachate

NO_2^--N

The changes of NO_2^--N concentration during the operation of the bioreactor is shown in Fig.4. The effluent NO_2^--N concentration of A1 and A2 reactors remained at a low level during 50-78 weeks. The concentration of NO_2^--N in this experiment was also relatively low compared with that at 50-78 weeks. At the end of the experiment, the concentration of NO_2^--N in A2 was slightly higher than that in A1, the average concentration of NO_2^--N in A1 was 0.69 mg/L, and that in A2 was 0.85mg/L. These findings can be attributed to the short-cut denitrification of A2 under low aeration conditions[25]. The average concentration of NO_2^--N in F1 was 0.45 mg/L, and that in F2 was 1.14mg/L. Nag et al. [26]believed that the formation of nitrite was confirmed in the process of denitrification, which could stimulate the conversion of NO_3^--N to N_2 gas under low aeration conditions.

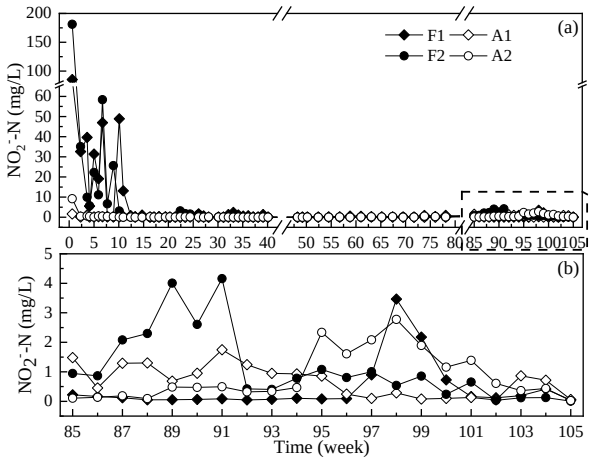

FIG. 4 Variation of NO_2^--N concentration in leachate

TN

The variation of TN concentration in leachate during the entire operation of the bioreactor is shown in Fig. 5. TN could meet the 25 mg/L standard of the Chinese Emission Standards for pollution control on MSW landfill sites (GB16889-2008) at the predicted time. Specifically, F1 and F2 were 39.16 and 20.06 mg/L after 54 and 35 weeks, respectively. However, TN concentration fluctuated and did not reach the emission standards for a long time. The effluent TN concentration of leachate in ARBs was higher than that of influent in 85-105 week. These findings may be due to organic matter reaching adsorption saturation at this stage, and some pollutants were washed away[27]. At the end of the test, the average effluent TN concentrations of F1 and F2 reached 555.27 mg/L and 522.47 mg/L, respectively. Sufficient carbon source was the key for denitrifying

bacteria to remove nitrogen efficiently[28-30]. The poor removal effect of TN may be because the ammonia nitrogen in the influent generates nitrite and nitrate in ARBs, but only a small part of nitrogen was metabolized by microorganisms, and most of it was still retained in the leachate. Nitrate cannot be denitrified due to the lack of carbon source after recirculation to the FRBs, resulting in nitrate accumulation. This can be verified from Fig.3.

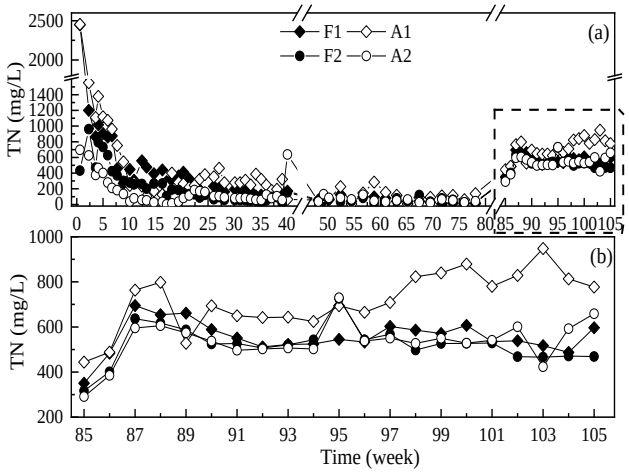

FIG. 5 Removal performance of TN concentration in leachate

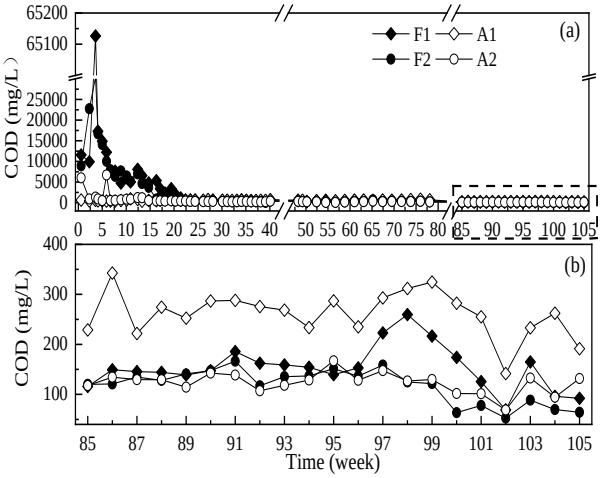

FIG. 6 Removal performance of COD in leachate

COD

The change of leachate COD concentration during the whole operation of the bioreactor is shown in Fig. 6. The COD concentration of ex situ SND/in situ denitrification was significantly lower than that of ex situ nitrification/in situ denitrification. From week 1 to 30, The COD concentration of each bioreactor landfill showed a trend of fluctuation and decline. At 31-105 weeks, COD concentration is basically around 100-300 mg/L in FRBs (Fig. 5). Although the COD concentration in F1 and F2 failed to reach the discharge standard at the expected time after weeks 41 and 34[21], the COD concentration of F1 and F2 can meet the discharge standard (less than 100 mg/L) in the Standard for Pollution Control on the Landfill Site of Municipal Solid Waste (GB16889-2008) at week 104 and 100, respectively. The average effluent COD concentrations of F1 and F2 reached 153.10 mg/L and 116.99 mg/L, respectively. At week 105, the COD concentration of F1 and F2 reached 92.11 mg/L and 64.32 mg/L, respectively. Results of the experiment indicate that the COD concentrations of leachate from F2 decreased more rapidly than that those from F1. Therefore, *ex situ* SND/*in situ* denitrification can accelerate the degradation of the refuse.

CONCLUSION

Compared with the *ex situ* nitrification/*in situ* denitrification process, the *ex situ* SND/*in situ* denitrification process obtained lower concentrations of NH_4^+-N, NO_3^--N, TN and COD in the experiment. The NH_4^+-N concentration in F2 was 5.57 mg/L, which was lower than that in F1 (3.85 mg/L) at the end of the experiment. The COD concentration in F2 was 64.32 mg/L, which also was lower than that in F1 (92.11 mg/L). *Ex situ* SND/*in situ* denitrification process could effectively remove the NH_4^+-N and COD concentration in leachates. The NH_4^+-N and COD concentrations could meet the discharge standard established in the Standard for Pollution Control on the Landfill Site of Municipal Solid Waste (GB16889-2008). *Ex situ* nitrification/*in*

situ denitrification and *ex situ* SND/*in situ* denitrification could accelerate the stabilization of refuse, and *ex situ* SND/*in situ* denitrification was better. However, the treatment performance of TN this process was unsatisfactory. Further research is required to develop effective measures or processes that can effectively treat leachates with low high concentrations of NO_3^--N.

ACKNOWLEDGEMENTS

This work was financially supported by Guangxi innovation research team project (2018GXNSFGA281001) and Guangxi major science and technology projects (GuikeAA18118013).

REFERENCES

[1] Ding, Y., Zhao, J., Liu, J.-W., et al. A review of China's municipal solid waste (MSW) and comparison with international regions: Management and technologies in treatment and resource utilization[J]. Journal of Cleaner Production, 2021, 293 (126144.

[2] Han, Z., Liu, Y., Zhong, M.,et al. Influencing factors of domestic waste characteristics in rural areas of developing countries[J]. Waste Management, 2018, 72 (45-54.

[3] Chen, W., Zhang, A., Jiang, G.,et al. Transformation and degradation mechanism of landfill leachates in a combined process of SAARB and ozonation[J]. Waste Management, 2019, 85 (283-294.

[4] Dang, Y., Lei, Y., Liu, Z.,et al. Impact of fulvic acids on bio-methanogenic treatment of municipal solid waste incineration leachate[J]. Water research: A journal of the international water association, 2016, 106 (Dec.1): 71-78.

[5] Benson, C. H., Barlaz, M. A..Lane, D. T. Practice review of five bioreactor/recirculation landfills[J]. Waste Management, 2007, 27 (2): 13-29.

[6] He, P. J., Shao, L. M., Guo, H. D.,et al. Nitrogen removal from recycled landfill leachate by ex situ nitrification and in situ denitrification[J]. Waste Management, 2006, 26 (8): 838-845.

[7] Shao, L.-M., He, P.-J..Li, G.-J. In situ nitrogen removal from leachate by bioreactor landfill with limited aeration[J]. Waste Management, 2008, 28 (6): 1000-1007.

[8] A.Q.Burton, S..A.Watson-Craik, I. Ammonia and nitrogen fluxes in landfill sites: applicability to sustainable landfilling[J]. Waste Management & Research, 1998, 16 (1): 41-53.

[9] Spagni, A..Marsili-Libelli, S. Nitrogen removal via nitrite in a sequencing batch reactor treating sanitary landfill leachate[J]. Bioresource Technology, 2009, 100 (2): 609-614.

[10] Bucci, P., Coppotelli, B., Morelli, I.,et al. Micronutrients and COD/N ratio as factors influencing granular size and SND in aerobic granular sequencing batch reactors operated at low organic loading[J]. Journal of Water Process Engineering, 2022, 46 (102625.

[11] Krishna Mohan, T. V., Nancharaiah, Y. V., Venugopalan, V. P.,et al. Effect of C/N ratio on denitrification of high-strength nitrate wastewater in anoxic granular sludge sequencing batch reactors[J]. Ecological Engineering, 2016, 91 (441-448.

[12] He, R., Liu, X.-w., Zhang, Z.-j.,et al. Characteristics of the bioreactor landfill system using an anaerobic–aerobic process for nitrogen removal[J]. Bioresource Technology, 2007, 98 (13): 2526-2532.

[13] Fall, C., Barrón-Hernández, L. M., Gonzaga-Galeana, V. E.,et al. Ordinary heterotrophic organisms with aerobic storage capacity provide stable aerobic granular sludge for C and N removal[J]. Journal of Environmental Management, 2022, 308 (114662.

[14] Sun, X. J., Sun, Y. J., Zhao, Y. C.,et al. Leachate recirculation between alternating aged refuse bioreactors and its effect on refuse decomposition[J]. ENVIRONMENTAL TECHNOLOGY, 2014, 35 (7): 799-807.

[15] Sun, Y., Sun, X..Zhao, Y. Comparison of semi-aerobic and anaerobic degradation of refuse with recirculation after leachate treatment by aged refuse bioreactor[J]. Waste Management, 2011, 31 (6): 1202-1209.

[16] Bae, W., Kim, S., Lee, J.,et al. Effect of leachate circulation with ex situ nitrification on waste decomposition and nitrogen removal for early

stabilization of fresh refuse landfill[J]. Journal of Hazardous Materials, 2019, 371 (721-727.
[17] Sun, F., Sun, B., Li, Q.,et al. Pilot-scale nitrogen removal from leachate by ex situ nitrification and in situ denitrification in a landfill bioreactor[J]. Chemosphere, 2014, 101 (77-85.
[18] Wang, Y.-n., Sun, Y.-j., Wang, L.,et al. N2O emission from a combined ex-situ nitrification and in-situ denitrification bioreactor landfill[J]. Waste Management, 2014, 34 (11): 2209-2217.
[19] Zhong, Q., Li, D., Tao, Y.,et al. Nitrogen removal from landfill leachate via ex situ nitrification and sequential in situ denitrification[J]. Waste Management, 2009, 29 (4): 1347-1353.
[20] Sun, X., Zhang, H..Cheng, Z. Use of bioreactor landfill for nitrogen removal to enhance methane production through ex situ simultaneous nitrification-denitrification and in situ denitrification[J]. Waste Management, 2017, 66 (97-102.
[21] Li, J., Wu, B., Li, Q.,et al. Ex situ simultaneous nitrification-denitrification and in situ denitrification process for the treatment of landfill leachates[J]. Waste Management, 2019, 88 (301-308.
[22] Sun, X., Zhang, H., Cheng, Z.,et al. Effect of low aeration rate on simultaneous nitrification and denitrification in an intermittent aeration aged refuse bioreactor treating leachate[J]. Waste Management, 2017, 63 (410-416.
[23] Zhong, Q., Li, D..Tao, Y. Nitrogen removal from landfill leachate via ex situ nitrification and sequential in situ denitrification[J]. Waste Management, 2009, 29 (4): 1347-1353.
[24] Zhang, X., Wu, P., Ma, L.,et al. A novel simultaneous partial nitrification and denitratation (SPND) process in single micro-aerobic sequencing batch reactor for stable nitrite accumulation under ambient temperature[J]. Chemical Engineering Journal, 2021, 425 (130646.
[25] Price, G. A., Barlaz, M. A..Hater, G. R. Nitrogen management in bioreactor landfills[J]. Waste Management, 2003, 23 (7): 675-688.
[26] Nag, M., Shimaoka, T..Komiya, T. Impact of intermittent aerations on leachate quality and greenhouse gas reduction in the aerobic–anaerobic landfill method[J]. Waste Management, 2016, 55 (71-82.
[27] Long, Y., Guo, Q.-W., Fang, C.-R.,et al. In situ nitrogen removal in phase-separate bioreactor landfill[J]. Bioresource Technology, 2008, 99 (13): 5352-5361.
[28] Fu, X., Hou, R., Yang, P.,et al. Application of external carbon source in heterotrophic denitrification of domestic sewage: A review[J]. Science of The Total Environment, 2022, 817 (153061.
[29] Guo, Y., Guo, L., Jin, C.,et al. Comparison of primary and secondary sludge carbon sources derived from hydrolysis or acidogenesis for nitrate reduction and denitrification kinetics: Organics utilization and microbial community shift[J]. Environmental Research, 2022, 212 (113403.
[30] Wang, C., Zhao, Y., Xie, B.,et al. Nitrogen removal pathway of anaerobic ammonium oxidation in on-site aged refuse bioreactor[J]. Bioresource Technology, 2014, 159 (266-271.